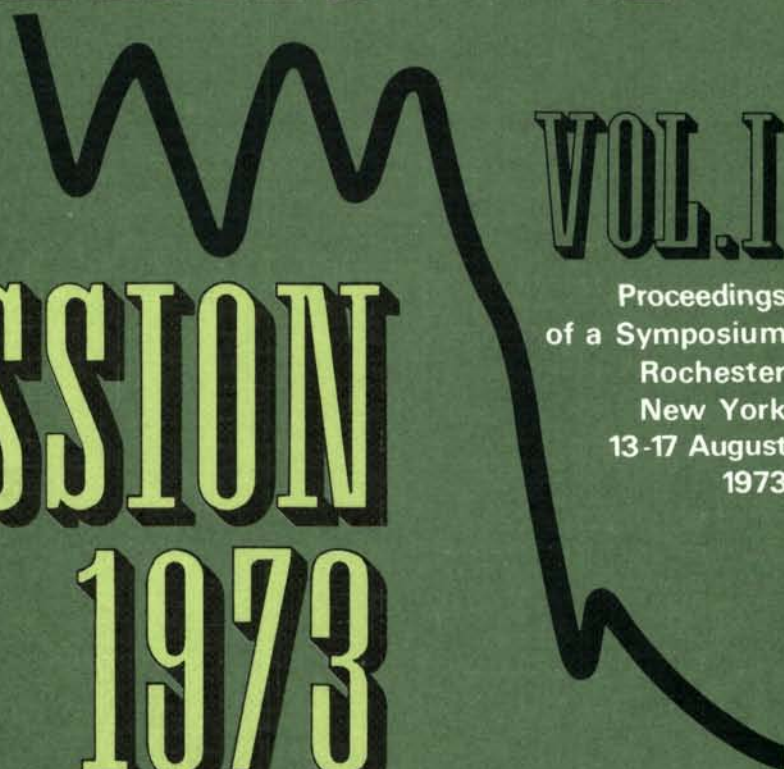


73ROCH

INDC SPECIAL 1

PHYSICS AND CHEMISTRY OF FISSION 1973



VOL. I

Proceedings
of a Symposium
Rochester
New York
13-17 August
1973



INTERNATIONAL ATOMIC ENERGY AGENCY, VIENNA, 1974

PHYSICS AND CHEMISTRY OF FISSION 1973

VOL. I

The following States are Members of the International Atomic Energy Agency:

AFGHANISTAN	HAITI	PAKISTAN
ALBANIA	HOLY SEE	PANAMA
ALGERIA	HUNGARY	PARAGUAY
ARGENTINA	ICELAND	PERU
AUSTRALIA	INDIA	PHILIPPINES
AUSTRIA	INDONESIA	POLAND
BANGLADESH	IRAN	PORTUGAL
BELGIUM	IRAQ	ROMANIA
BOLIVIA	IRELAND	SAUDI ARABIA
BRAZIL	ISRAEL	SENEGAL
BULGARIA	ITALY	SIERRA LEONE
BURMA	IVORY COAST	SINGAPORE
BYELORUSSIAN SOVIET SOCIALIST REPUBLIC	JAMAICA	SOUTH AFRICA
CAMEROON	JAPAN	SPAIN
CANADA	JORDAN	SRI LANKA
CHILE	KENYA	SUDAN
COLOMBIA	KHMER REPUBLIC	SWEDEN
COSTA RICA	KOREA, REPUBLIC OF	SWITZERLAND
CUBA	KUWAIT	SYRIAN ARAB REPUBLIC
CYPRUS	LEBANON	THAILAND
CZECHOSLOVAK SOCIALIST REPUBLIC	LIBERIA	TUNISIA
DENMARK	LIBYAN ARAB REPUBLIC	TURKEY
DOMINICAN REPUBLIC	LIECHTENSTEIN	UGANDA
ECUADOR	LUXEMBOURG	UKRAINIAN SOVIET SOCIALIST REPUBLIC
EGYPT, ARAB REPUBLIC OF	MADAGASCAR	UNION OF SOVIET SOCIALIST REPUBLICS
EL SALVADOR	MALAYSIA	UNITED KINGDOM OF GREAT BRITAIN AND NORTHERN IRELAND
ETHIOPIA	MALI	UNITED STATES OF AMERICA
FINLAND	MEXICO	URUGUAY
FRANCE	MONACO	VENEZUELA
GABON	MONGOLIA	VIET-NAM
GERMAN DEMOCRATIC REPUBLIC	MOROCCO	YUGOSLAVIA
GERMANY, FEDERAL REPUBLIC OF	NETHERLANDS	ZAIRE, REPUBLIC OF
GHANA	NEW ZEALAND	ZAMBIA
GREECE	NIGER	
GUATEMALA	NIGERIA	
	NORWAY	

The Agency's Statute was approved on 23 October 1956 by the Conference on the Statute of the IAEA held at United Nations Headquarters, New York; it entered into force on 29 July 1957. The Headquarters of the Agency are situated in Vienna. Its principal objective is "to accelerate and enlarge the contribution of atomic energy to peace, health and prosperity throughout the world".

PROCEEDINGS SERIES

PHYSICS AND CHEMISTRY OF FISSION
1973

PROCEEDINGS OF THE THIRD IAEA SYMPOSIUM
ON THE
PHYSICS AND CHEMISTRY OF FISSION
HELD BY THE
INTERNATIONAL ATOMIC ENERGY AGENCY
IN ROCHESTER, NEW YORK, 13-17 AUGUST 1973

In two volumes

VOL. I

INTERNATIONAL ATOMIC ENERGY AGENCY
VIENNA, 1974

PHYSICS AND CHEMISTRY OF FISSION 1973
IAEA, VIENNA, 1974
STI/PUB/347

FOREWORD

This third international Symposium on the Physics and Chemistry of Fission, held in Rochester, N. Y., from 13 to 17 August 1973, was a worthy successor to the important symposia held in Salzburg (1965) and in Vienna (1969). Although there may not have been in Rochester quite the excitement that prevailed in Vienna (where the beautiful verification of the structured fission barrier provided by the Strutinsky calculations was presented), the present meeting reaped the benefits of this revolutionary discovery. The first direct experimental verifications of the deformed fission isomers have also only recently been achieved.

The present Symposium, somewhat more than previous ones, concentrated on theoretical concepts and calculations concerning the fission process itself, and only on those new experimental results most pertinent to the theoretical development. Contained in these two volumes are the full texts and discussions of the 62 papers presented at the Symposium, and abstracts of those contributions that, because of time limitations, could not be presented.

These Proceedings of course do not represent the *last* word on this obviously complex topic. It is apparent that even the liquid drop features of the fission process have not yet been fully, or even adequately, worked out, the most obvious deficiency still being a reliable treatment of the dynamics, where a better knowledge of the 'viscosity' is obviously needed. The importance of quantum mechanical, single particle effects in the fission process is emphasized in these Proceedings, and a number of advances in microscopic calculations are included.

It is clear, in view of the large participation and the quality of the work presented, that scientists throughout the world find these meetings a valuable international forum for the exchange of information and welcome the Agency's initiative in promoting this continuing series of symposia.

EDITORIAL NOTE

The papers and discussions incorporated in the proceedings published by the International Atomic Energy Agency are edited by the Agency's editorial staff to the extent considered necessary for the reader's assistance. The views expressed and the general style adopted remain, however, the responsibility of the named authors or participants.

For the sake of speed of publication the present Proceedings have been printed by composition typing and photo-offset lithography. Within the limitations imposed by this method, every effort has been made to maintain a high editorial standard; in particular, the units and symbols employed are to the fullest practicable extent those standardized or recommended by the competent international scientific bodies.

The affiliations of authors are those given at the time of nomination.

The use in these Proceedings of particular designations of countries or territories does not imply any judgement by the Agency as to the legal status of such countries or territories, of their authorities and institutions or of the delimitation of their boundaries.

The mention of specific companies or of their products or brand-names does not imply any endorsement or recommendation on the part of the International Atomic Energy Agency.

CONTENTS OF VOL. I

FISSION BARRIERS AND RESONANCE FISSION: EXPERIMENT (Session I)

Experimental fission barriers for actinide nuclei (IAEA-SM-174/201)	3	Ø
B. B. Back, Ole Hansen, H. C. Britt, J. D. Garrett, B. Leroux		
Fission barriers for doubly even actinide nuclei from (t, pf), (³ He, df) (p, p'f) and (t, αf) studies (IAEA-SM-174/27)	25	Ø
B. B. Back, Ole Hansen, H. C. Britt, J. D. Garrett		
Discussion	37	
The structure of the fission transition nucleus ²²⁷ Ra (IAEA-SM-174/81)	39	y
H. Groening, W. Loveland		
Discussion	52	
Subbarrier photofission of ²³⁸ U (IAEA-SM-174/36)	55	y
A. Alm, T. Kivikas, L. J. Lindgren		
Discussion	68	
Etude de la réaction ²³¹ Pa(n, f) induite par neutrons rapides (IAEA-SM-174/40)	71	Alain
A. Sicre, G. Barreau, R. Chastel, T. P. Doan, B. Leroux, J. C. Sageaux		
Discussion	83	
Determination of spins of intermediate structure resonances in subthreshold fission (IAEA-SM-174/65)	85	y
G. A. Keyworth, J. R. Lemley, C. E. Olson, F. T. Seibel, J. W. T. Dabbs, N. W. Hill		
Discussion	97	

FISSION BARRIERS: THEORY (STATIC) (Session II)

Review Paper:		
Calculation of fission barriers (IAEA-SM-174/202)	103	Ø
P. Möller, J. R. Nix		
Discussion	140	
Calculation of fission barriers for heavy neutron-rich nuclei (IAEA-SM-174/60)	145	Ø
W. M. Howard, J. R. Nix		
Discussion	158	

Modified definition of the surface energy in the liquid drop formula (IAEA-SM-174/12)	159	Ø
H.J. Krappe, J.R. Nix		
Discussion	175	
Fission barriers for heavy elements with quadrupole, hexadecapole, and axially asymmetric distortions taken into account simultaneously (IAEA-SM-174/06)	177	
S.E. Larsson, G. Leander		
Discussion	202	
On the treatment of shell and pairing energies when the liquid drop parameters are refitted to reproduce the experimental barrier heights (IAEA-SM-174/07)	203	Ø
R. Bengtsson		
Hartree-Fock calculations of the fission barriers of plutonium isotopes (IAEA-SM-174/38)	221	
H. Flocard, P. Quentin, D. Vautherin, A.K. Kerman		
Discussion	230	
Test of Strutinsky's method using Hartree-Fock results (IAEA-SM-174/98)	231	
M. Brack, P. Quentin		
Discussion	248	

FISSION ISOMERS (Session III)

Review paper:		
Fission isomer systematics (IAEA-SM-174/203)	251	Y
R. Vandenbosch		
Discussion	269	
Gamma branch of the ²³⁸ U shape isomer (IAEA-SM-174/96)	271	Ø
P.A. Russo, J. Pedersen, R. Vandenbosch		
Fragment anisotropy in isomeric fission (IAEA-SM-174/19)	285	Ø
H.J. Specht, E. Konecny, J. Weber, C. Kozhuharov		
Discussion	296	
Delayed fission fragment angular distributions in some <u>alpha</u> - particle-induced reactions (IAEA-SM-174/15)	297	Ø
D. Galeriu, N. Marinescu, D. Poenaru, I. Vîlcov, N. Vîlcov, Yu.P. Gangrsky, P.Z. Hien, N.C. Khan		
Discussion	304	
Spontaneous-fission decay constant of ²³⁵ U (IAEA-SM-174/05)	305	Ø
A. Grüttler, H.R. von Gunten, V. Herrnberger, B. Hahn, U. Moser, H.W. Reist, G. Sletten		
Discussion	315	
Half-life systematics of fission isomers in even-even Pu isotopes (IAEA-SM-174/26)	317	Ø
V. Metag, E. Liukkonen, O. Glomset, A. Bergman		
Discussion	325	

FISSION BARRIERS: THEORY (THERMODYNAMICS)
(Session IV)

Review paper:

Fission probabilities in lighter nuclei: A theoretical and experimental investigation of the shell and pairing effects in fissioning nuclei (IAEA-SM-174/204)	329
L.G. Moretto	
Discussion	365

Review paper:

Role of symmetry of the nuclear shape in rotational contributions to nuclear level densities (IAEA-SM-174/205)	367
S. Bjørnholm, A. Bohr, B.R. Mottelson	
Discussion	373
Single particle effects on fission barriers and statistical interpretation of fragment anisotropies and mass division in fission (IAEA-SM-174/10)	375
S.S. Kapoor, V.S. Ramamurthy	
Discussion	388
Fission of ^{238}U , ^{209}Bi and ^{197}Au with intermediate-energy ^4He ions (IAEA-SM-174/85)	391
V.E. Viola, Jr., M.M. Minor, C.T. Roche, R.G. Clark	
Discussion	408
Statistical calculation of the mass distribution in fission (IAEA-SM-174/28)	409
A.S. Jensen, T. Døssing	
Discussion	419
Potential energy surfaces and dependence of fission mass asymmetry on the internal excitation energy of the fissioning nucleus (IAEA-SM-147/73)	421
H.W. Schmitt, M.G. Mustafa	
Discussion	428
Prompt and delayed neutron yields from low-energy photofission of ^{232}Th , ^{235}U , ^{238}U and ^{239}Pu (IAEA-SM-174/100)	431
J.T. Caldwell, E.J. Dowdy, G.M. Worth	
Discussion	444
Energy dependence of Γ_f/Γ_n for the nucleus ^{216}Rn (IAEA-SM-174/56)	447
H. Freiesleben, H.C. Britt, J.R. Huizenga	
Discussion	458

FISSION PROCESS: THEORY (DYNAMIC)
(Session V)

Review paper:

The dynamics of fission in the subbarrier region of deformation (IAEA-SM-174/206)	463
H.C. Pauli, T. Ledergerber	
Discussion	497

Viscosity in the fission process (IAEA-SM-174/210)	503	Ø
G. Schütte, L. Wilets		
Discussion	513	
Conservation of single particle quantum numbers in fission (IAEA-SM-174/22)	515	Ø
Y. Boneh, Z. Fraenkel, Z. Paltiel		
Discussion	522	
First estimates of the nuclear viscosity constant from the damping of the fission dynamics and from the widths of β -vibrations and giant dipole resonances (IAEA-SM-174/02)	523	Ø
R. Wieczorek, R.W.Hasse, G. Süssmann		
Discussion	532	Ø
Compressibility in nuclear collective dynamics (IAEA-SM-174/58)...	533	
J.J. Griffin, K.-K. Kan		
Discussion	544	
Unified theory of low-energy fission and fission models (IAEA-SM-174/24)	547	Ø
W. Nörenberg		
Discussion	566	
The asymmetric two-centre shell model and mass distributions in fission (IAEA-SM-174/102)	569	Ø
J. Maruhn, W. Greiner, P. Lichtner, D. Drechsel		
Discussion	577	
Chairmen of Sessions and Secretariat of the Symposium	579	

FISSION BARRIERS AND RESONANCE FISSION:
EXPERIMENT

(Session I)

Chairman: J. R. Huizenga (*United States of America*)

EXPERIMENTAL FISSION BARRIERS FOR ACTINIDE NUCLEI*

B.B. BACK, Ole HANSEN

Los Alamos Scientific Laboratory, University of California, USA

H.C. BRITT

Los Alamos Scientific Laboratory, University of California, and
Nuclear Structure Research Laboratory, University of Rochester, USA

J.D. GARRETT

Los Alamos Scientific Laboratory, University of California, and
Brookhaven National Laboratory, USA

B. LEROUX

Los Alamos Scientific Laboratory, University of California, USA, and
University of Bordeaux, France

Abstract

EXPERIMENTAL FISSION BARRIERS FOR ACTINIDE NUCLEI.

Fission probability distributions are measured for a number of isotopes of Th, Pa, U, Np, Pu, Am, Cm and Bk using (d,pf), (t,pf), (^3He ,df), (p,p'f), (^3He , α f) and (t, α f) reactions. The results, together with previous data available from (d,pf) and (n,f) studies, are analysed with a statistical model and estimates are obtained for the heights, E_A and E_B , and curvatures, $h\omega_A$ and $h\omega_B$, of the two peaks of the fission barrier for a wide range of actinide nuclei. The statistical model used for the analysis of odd A and odd-odd nuclei includes competition between fission, neutron emission and gamma-ray de-excitation in the decay of the compound nucleus. The results suggest that fission widths which are greater by about a factor of 4 than those calculated are necessary to reproduce the magnitude of the measured fission probabilities. The results show that E_A is roughly constant throughout this region and E_B decreases with increasing Z. An exception to the approximate constancy of E_A is in Cm where E_A drops by 1.0 MeV from ^{248}Cm to ^{250}Cm . In some cases an odd-even fluctuation of 0.30-0.50 MeV is observed in the experimental E_A values.

1. INTRODUCTION

At the last IAEA conference on the Physics and Chemistry of Fission^[1] in 1969 many of the exciting new developments were related to the investigation of the qualitative implications of the effects of deformed nuclear shells on the potential energy surfaces associated with the fission process and the wide variety of experiments that had recently confirmed the major predictions of this new theory. At that conference experimental results were presented on the existence of fission isomers in a wide range of actinide nuclei, intermediate structure resonances in subbarrier

*

Work supported by the US Atomic Energy Commission.

Permanent addresses of the authors are: B. B. Back, Niels Bohr Institute, Denmark (supported by Staten naturvidenskabelige forskningsrad, Denmark); Ole Hansen, Niels Bohr Institute, Denmark; H. C. Britt, Los Alamos Scientific Laboratory, USA; J. D. Garrett, Brookhaven National Laboratory, USA; B. Leroux, University of Bordeaux, France. The present address of H. C. Britt is: Nuclear Structure Research Laboratory, University of Rochester, USA.

neutron fission, and gross structure resonances in (n,f) and (d,pf) studies. All of these experimental phenomena were found to be consistent with the concept of a two-peaked fission barrier that resulted theoretically from fluctuations in the shell corrections to the single-peaked fission barrier predicted by the liquid drop model.

Since the last conference there has been considerable activity both theoretically and experimentally directed toward trying to quantitatively determine the characteristics of the potential energy surface involved in fission and to try to understand how these complex potential energy surfaces affect some aspects of the fission process. In other papers at this symposium both the current status of potential energy calculations and recent theoretical efforts to qualitatively understand the more difficult problems of fission dynamics will be reviewed [2,3]. In our paper we will present a review of current efforts to try to experimentally determine fission barrier characteristics for actinide elements with particular emphasis on recent direct reaction fission results from Los Alamos. In general, the fission barrier properties that can be most readily compared with theoretical calculations are the energies of the two saddle points and the secondary minimum relative to the ground

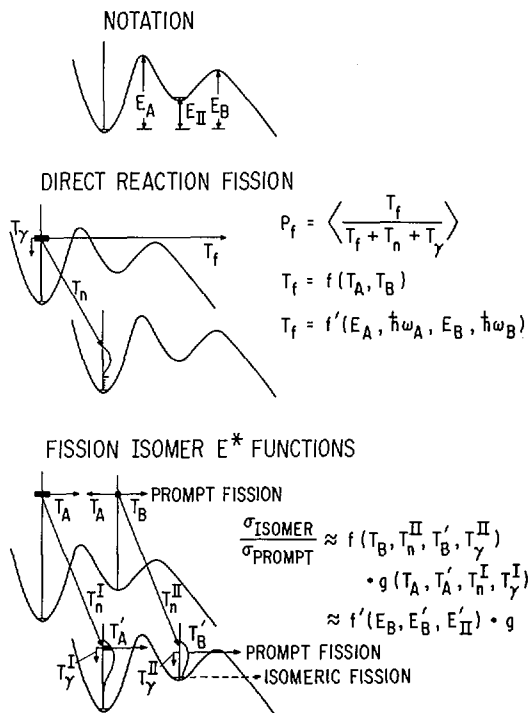


FIG.1. Schematic illustration of the major features of the direct reaction fission and fission isomer population processes.

state. We will concentrate on these properties although in some cases the experiments also yield information on barrier curvatures.

Figure 1 illustrates schematically the two types of experiment which have been used to obtain most of the current information on fission barrier heights. In a direct reaction fission experiment a direct reaction (or neutron capture reaction) is used to produce a residual nucleus at a particular excitation energy and the branching ratio for decay by fission relative to neutron or gamma deexcitation (or the fission cross-section) is measured. This type of experiment gives information primarily on the height and curvature of the highest peak in the fission barrier. However, in some cases resonances are observed which can be associated with vibrations near the top of the second well and a detailed analysis of the experimental results gives information on both peaks. The results and analysis for even-even fissioning nuclei where these resonance structures are observed will be presented in another paper [4]. Figure 1 also illustrates schematically the population of a shape isomeric state in the second well following the evaporation of a neutron. In most cases of experimental interest the isomeric states are populated following the subsequent evaporation of two or three neutrons but qualitatively the data analysis is the same [5]. In practice, fission isomer excitation functions have been analyzed using E_A values from other sources and the experimental data is used to determine E_B and E_{II} . Thus, in the

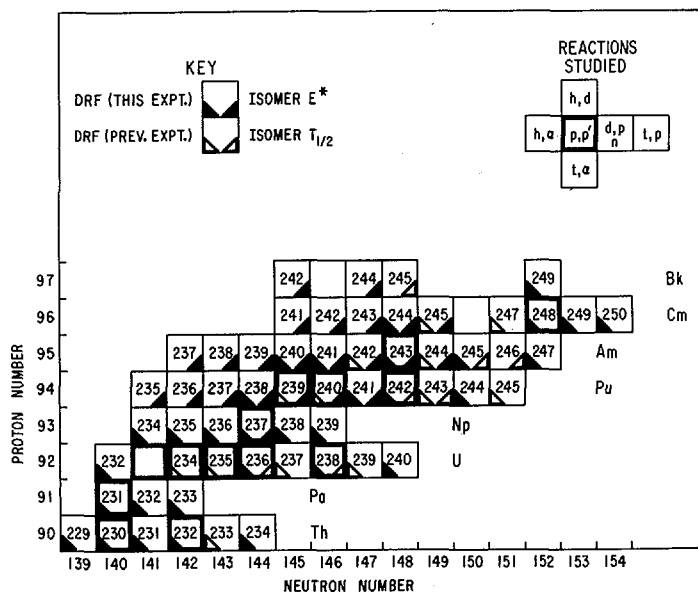


FIG.2. Actinide nuclei for which data are currently available from direct reaction fission or (n,f) cross-section measurements, DRF, and fission isomer excitation functions and half-lives. Heavily outlined boxes indicate nuclei that were used as targets in the present DRF studies.

heavy actinides where $E_A > E_B$, the direct-reaction fission and the fission isomer excitation function measurements are complementary. In addition, intermediate structure resonances from subbarrier neutron fission experiments can in some cases be used to estimate E_{II} [5,6]. Finally, the half-lives for fission decay from the ground and isomeric states give information on the curvatures and/or average mass parameters and these aspects will be discussed in other contributions at this conference.

The actinide nuclei which have been studied either by direct-reaction fission or fission isomer techniques are indicated in Figure 2. It is seen that the current direct-reaction fission results plus earlier (d,pf) [7] and (n,f) [8] results provide a rather extensive survey of the actinide region. For several plutonium, americium and curium isotopes complementary information is available from both types of experiment.

In the current direct-reaction fission studies a variety of reactions including (d,p), (t,p), (^3He ,d), (p,p'), (^3He , α) and (t, α) have been used so that a large number of fissioning nuclei could be investigated starting from the limited number of available target species. Of particular interest is the (^3He ,df) reaction which allows the investigation of many odd-Z nuclei starting from the relatively plentiful even Z targets. In general, it was found that cross-sections for exciting nuclei to energies near the top of the fission barrier were quite adequate for (d,p), (t,p) and (^3He ,d) reactions but the other reactions tried were of limited usefulness.

In the remainder of this paper we will present:

1) some of the general features of the experimental setup and results, 2) a discussion of techniques used to analyze the data for odd-A and odd-odd residual nuclei and 3) a survey of the experimental information currently available on the barrier heights E_A and E_B for actinide elements. A discussion of resonance phenomena and the analysis of data from even-even fissioning nuclei will be given in Paper IAEA-SM-174/27 (see Ref. [4]).

2. EXPERIMENTAL RESULTS

The setup used in the direct-reaction fission studies is illustrated schematically in Fig. 3. The outgoing

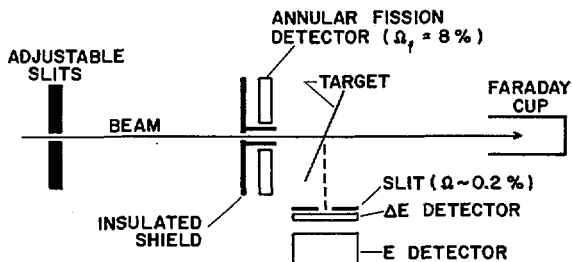


FIG.3. Schematic diagram of the experimental setup for the direct reaction fission experiments.

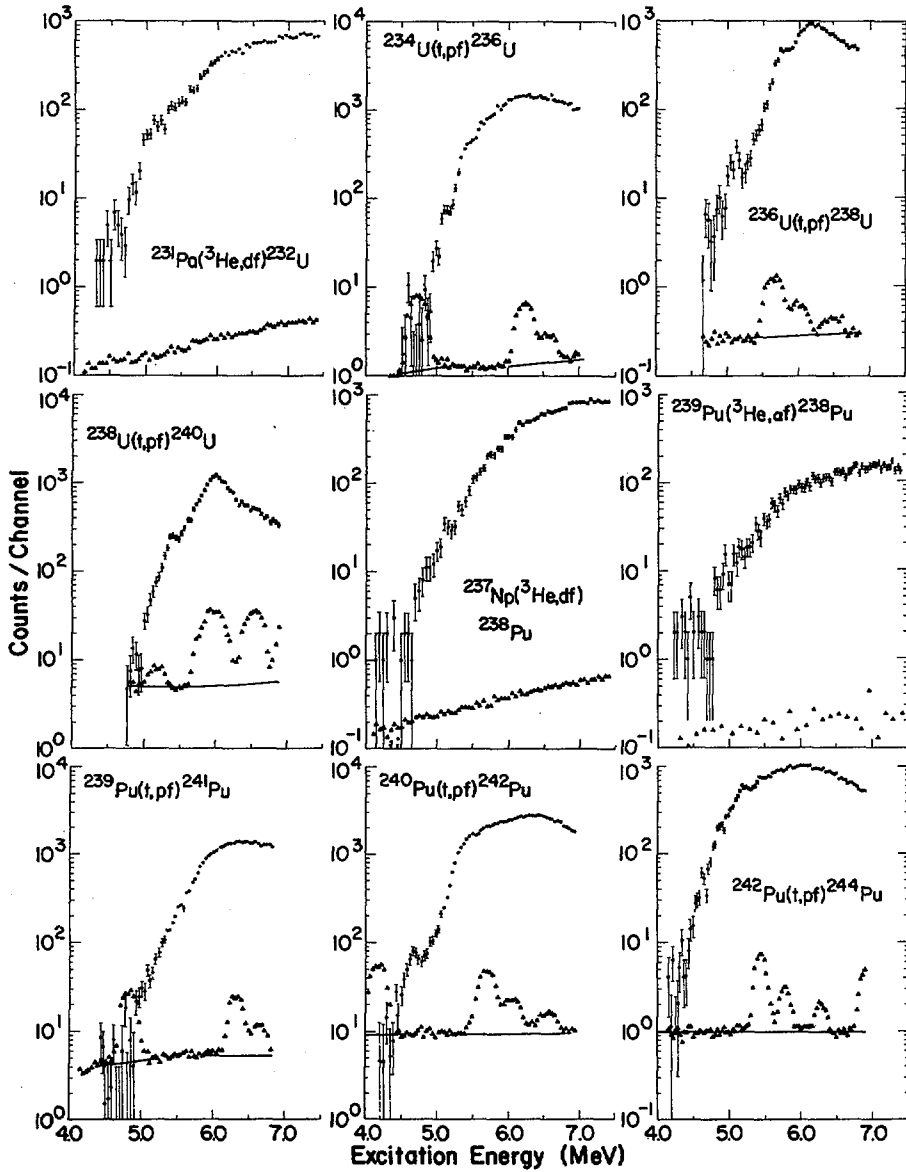


FIG. 4. Measured coincidence (circles) and singles (triangles) spectra for a variety of reactions. Solid lines indicate interpolated singles cross-sections for the target element. Singles spectra have been normalized to the level of the accidental contributions in the coincidence spectrum.

reaction particle is identified and its energy measured with a resolution of 40-100 keV in a standard ΔE -E counter telescope placed at an angle near 90° . For each event the excitation energy of the residual nucleus can be determined from the kinetic energy of the outgoing reaction particle. In the experiment the spectrum of reaction particles are measured both in a configuration where a coincidence is required with a large annular fission detector (coincidence spectrum) and in a configuration where no coincidence is required (singles spectrum). Using a measured solid angle for the fission detector and assuming that the coincident fission fragments are isotropically distributed, the ratio of coincidence to singles spectra can be transformed to a distribution of fission probability as a function of excitation energy in the residual nucleus. The absolute energy scales are determined from known Q values [9] and a calibration of the counter telescope with known energy lines [10] from appropriate reactions on lead targets.

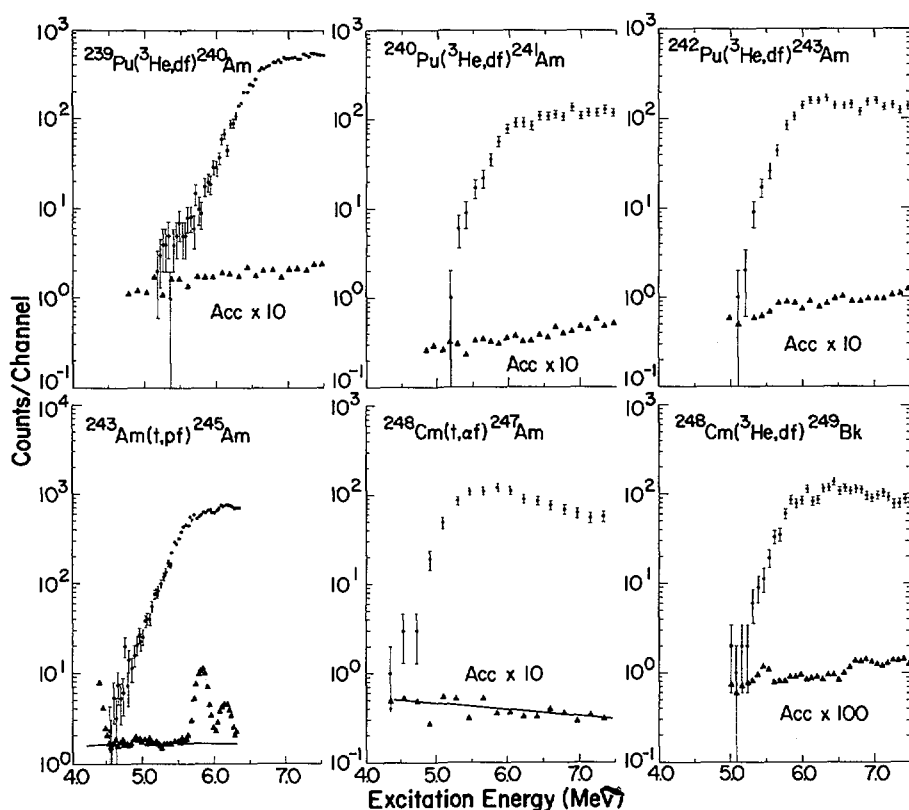


FIG. 5. Measured coincidence (circles) and singles (triangles) spectra for a variety of reactions. Solid lines indicate interpolated singles cross-sections for the target element. Singles spectra have been normalized to the level of the accidental contributions in the coincidence spectrum. In some cases the accidental contributions have been multiplied by factors of 10 or 100.

Absolute excitation energies determined in this manner are believed to be accurate to ± 50 keV. Systematic errors in the absolute fission probabilities are believed to be less than $\pm 20\%$ for ($^3\text{He}, \text{df}$) cases, $< \pm 30\%$ for (t, pf) cases, and $< \pm 40\%$ for (t, af), ($^3\text{He}, \text{af}$) and ($\text{p}, \text{p}'\text{f}$) cases. For (d, pf) reactions to excitation energies above the neutron binding energy, systematic uncertainties in the fission probabilities are estimated to be less than $\pm 30\%$ with part of this estimate being due to uncertainties in the corrections for protons coming from deuteron breakup reactions. The targets used in this experiment were all oxides vacuum-evaporated on carbon backings. This experimental setup is similar to previous experiments [7, 11] and will be described in detail in a more comprehensive report on these results [12].

Typical coincidence and singles spectra are shown in Figs 4 and 5. In the (t, pf) reactions the peaks come from reactions on carbon and oxygen in the target and the solid lines represent extrapolated estimates of the singles counting rate from the actinide element. For ^3He reactions the Q values and kinematics are such that light element contaminants do not appear in this excitation energy range at 90° . The absence of light element contamination in the singles spectrum for ($^3\text{He}, \text{d}$) reactions allows a more reliable determination of the fission probability distribution for these cases. The singles spectra have been normalized to show the magnitude of the accidental corrections in the coincidence measurements. It is seen that in most cases the accidental corrections are negligible. For (t, pf) and (d, pf) reactions the angle of the proton detector was varied in the range 70° - 100° in order to minimize the accidental contributions in the threshold region.

The results for typical even-even nuclei (Fig. 4) show pronounced resonance structure characteristic of the sub-barrier resonant penetration of the two peaks of the fission barrier. These resonances come from the enhanced fission penetrability when the excitation energy overlaps the energy of a vibrational state in the second well. The general characteristics of these resonances will be discussed in Paper IAEA-SM-174/27 [4]. In contrast the odd A and odd-odd nuclei (Fig. 5) do not show subbarrier resonant structure, which we interpret as being due to increased mixing (or damping) of the vibrational states in the second well with other types of compound excitations. The damping for the odd nuclei is expected to be greater than for even-even nuclei because of the increased density of compound levels in well II at the top of the barrier.

Previous comparisons [13] of (t, pf), (d, pf) and (n, f) reactions for the same residual nuclei have shown that for excitation energies above the neutron binding energy a significant fraction of the singles protons from (d, p) reactions come from breakup of the deuteron without the corresponding excitation of the residual nucleus. This effect leads to low estimates for the fission probabilities from (d, pf) reactions for energies above the neutron binding energy. In the current analysis of experimental data we have corrected all (d, pf) fission probabilities by multiplying by a function of $(E^* - B_n)$ taken from Britt and Cramer [13].

3. STATISTICAL MODEL FOR ANALYSIS OF EXPERIMENTAL RESULTS

From the experimental results it is seen that there are significant differences in the requirements for a statistical model which will reproduce the results from direct reaction fission experiments involving even-even residual nuclei and those involving odd-A or odd-odd nuclei. In particular the even-even nuclei show resonant penetration of the two barriers, but to help in simplifying the problem only a few vibrational and rotational excitations are involved in the fission penetrability near threshold. The excitation energies of these vibrations can be estimated from previous angular correlation measurements^[11]. In addition, the fission thresholds for even-even actinide nuclei are usually well below the neutron binding energy so that in the region of most interest only fission and gamma ray deexcitation can compete.

For the odd nuclei, since in most cases resonances are not observed in the fission probability distributions, the complete damping approximation which considers the penetration of the two barriers separately can be used. However, for odd nuclei the competition from neutron emission as well as gamma decay must be included and estimates of the

FISSION PROBABILITY IN COMPLETE DAMPING LIMIT

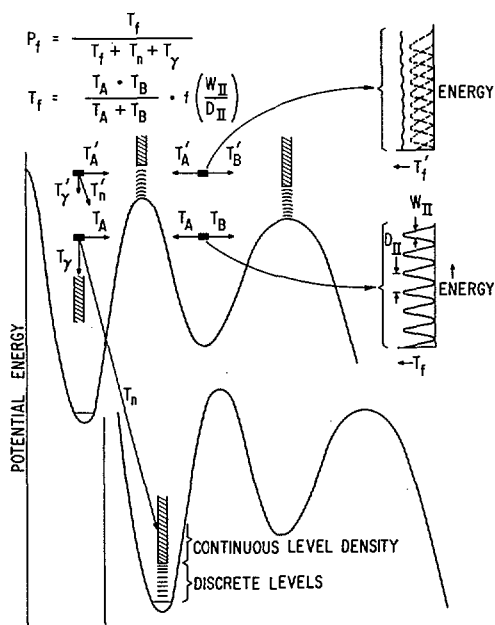


FIG.6. A schematic illustration of the statistical model used to fit the experimental fission probability distribution of odd residual nuclei. W_{II} is the width of the levels in the second well and D_{II} is the average level spacing in the second well.

fission penetrabilities involve summations over distributions of transition states about which there is no experimental information.

The different requirements of the two cases have led us to develop two rather different statistical models. The model used to fit the even-even nuclei will be discussed in Paper IAEA-SM-174/27 [4]. The model used to describe the fission of odd-A and odd-odd residual nuclei is detailed below in general terms and will be described in quantitative detail in a subsequent more comprehensive paper [14].

The statistical model we have used to describe the fission of odd residual nuclei is shown diagrammatically in Fig. 6. The transmission coefficients T_f are calculated in the complete damping limit where the transmission through the two peaks are treated separately. In this limit:

$$T_f = \frac{T_A \cdot T_B}{T_A + T_B} \cdot f\left(\frac{W_{II}}{D_{II}}\right)$$

where f is a correction factor that takes into account the finite width of the compound levels in the second minimum through which the fission is coupled. If the levels in the second well are assumed to be equispaced then it can be shown [12] that the fission probability is given by

$$P_f = (1 + a^2 + 2a \coth(t/2))^{-1/2}$$

where

$$a = (T_\gamma + T_n) \cdot (T_A + T_B) / (T_A \cdot T_B)$$

and

$$t = 4\pi W_{II}/D_{II} = T_A + T_B$$

In the limit where $t \gg 1$ (i.e. levels in second well strongly overlap) this expression reduces to the more usual expression:

$$P_f = \frac{T_f}{T_f + T_n + T_\gamma}$$

where

$$T_f = T_A \cdot T_B / (T_A + T_B)$$

The calculation of the fission probability now reduces to a calculation of the transmission coefficients T_A , T_B , T_n , and T_γ . The calculation of these transmission coefficients involves estimating the distribution of residual levels available for neutron and gamma deexcitation and the distribution of saddle point transition states for T_A and T_B . At the deformation of the first well, (T_n and T_γ calculations) the residual levels were assumed to be discrete for excitation energies less than 1 MeV and a continuous level density was used for excitation energies greater than 1 MeV. For odd-odd nuclei a continuous level density was used at all energies. The continuous level density was obtained from calculated single particle levels as described previously [5]. For odd-A nuclei the discrete levels were taken as rotational bands built on the one quasi-particle states obtained from calculated single particle levels [5,15,16] with the appropriate shifts due to pairing. For even-even nuclei the discrete levels were obtained from a composite spectrum based on

experimental measurements in the uranium-curium region. Then T_Y and T_N were estimated from expressions given previously [5] except that optical model transmission coefficients were used in the T_N calculations. The T_Y values were normalized so that calculated values of T_Y reproduce measured values at the neutron binding energy for odd Pu isotopes.

The level spectra used in the T_A and T_B calculations were obtained in a similar manner except that single particle levels appropriate to the first saddle and second asymmetric saddle were used. The transmission coefficients were calculated as a sum of penetrabilities through parabolic barriers with curvatures $\hbar^2\omega_A$ and $\hbar^2\omega_B$.

The level spectra used in these calculations are shown in Fig. 7 where solid lines indicate energy regions where continuous level densities were used and the triangles represent the average total density of the discrete levels for a given case. At the first saddle, discrete levels from Bosterli et al. [15] and Tsang [16] are compared and it is seen that the average densities are similar. Figure 8 shows that below 1 MeV the continuous level density calculation seriously underestimates the total number of levels. This discrepancy is due to the inadequacy at low excitation energies of the saddle point approximation [5] used in estimating the continuous level density.

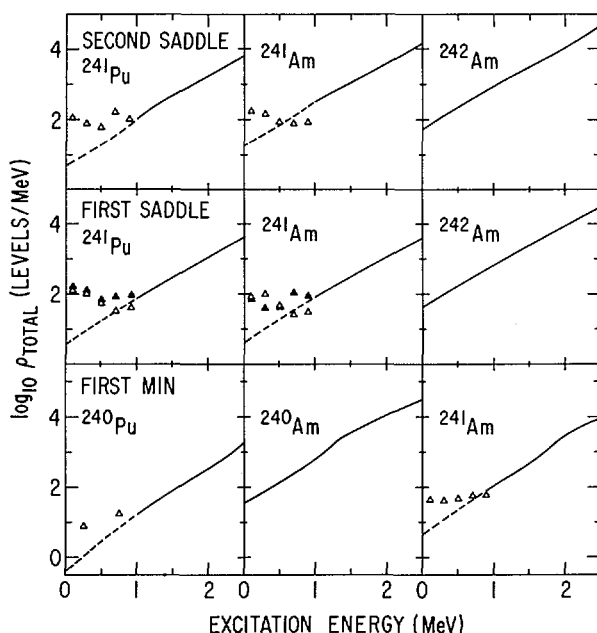


FIG. 7. Calculations of the total level density as a function of excitation energy. Solid and dashed lines show results obtained using the saddle point integration method. Open and closed triangles show estimates of the total density of discrete levels from the single particle spectra of Bolsterli et al. [15] and Tsang [16], respectively.

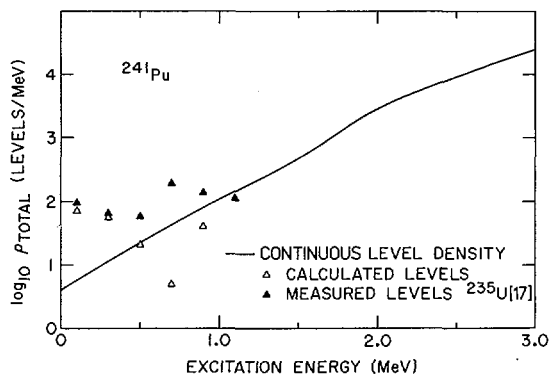


FIG.8. Calculations of the total level density using the saddle point integration method (solid line) compared with calculated discrete levels from Bolsterli et al. [15] and the experimentally observed levels of Rickey et al. [17].

Figure 8 compares the density of calculated one-quasiparticle states with the continuous level density for ^{241}Pu . The continuous level density is normalized to the measured value for $1/2^+$ states at the neutron binding energy. Also shown in fig. 8 are the density of measured levels [17] for ^{235}U and it is seen that the calculated density of one-quasiparticle states is in reasonable agreement with measurements.

4. FITS TO EXPERIMENTAL RESULTS

Using the statistical model described in the previous section, experimental fission probability distributions for odd-A and odd-odd nuclei were fit in order to systematically determine properties of the fission barrier for actinide nuclei. In these fits different procedures were used for nuclei in the region Pu-Bk and for the Pa-Np region.

As we pointed out in the introduction, for many isotopes of Pu, Am and Cm there is considerable data available from fission isomer studies which can be used to estimate E_{II} , E_B and $\hbar\omega_B$. Therefore, in fitting the direct reaction fission data in this region we have fixed E_B and $\hbar\omega_B$ to the values determined from fission isomer studies or in cases where no data is available to values that were extrapolated from nearby nuclei. The experimental data were then fit by varying E_A , $\hbar\omega_A$ and a normalization factor to get the correct plateau value for the fission probability. For the odd Pu and Cm isotopes and the odd-odd Am isotopes this normalization factor was an adjustable constant (G_n) multiplying the function Γ_n/Γ_f . For the odd Am isotopes where the fission threshold is below the neutron binding energy the adjustable constant (G_γ) multiplied Γ_γ/Γ_f . In addition to the results obtained in the present experiment, data from previous (d,pf) [7] and (n,f) [6,18] studies were also fit to obtain a consistent set of barriers. The published (n,f) cross-sections were converted to fission probabilities as described

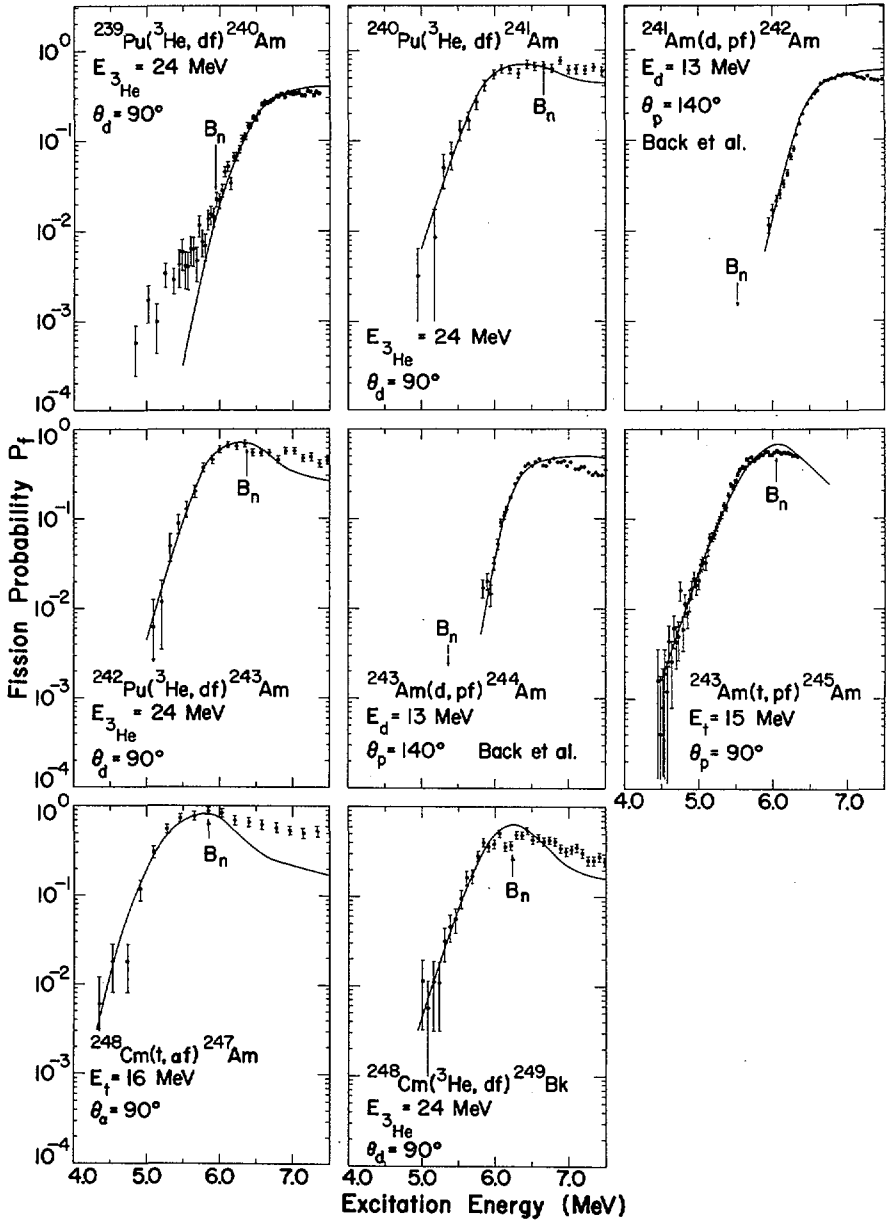
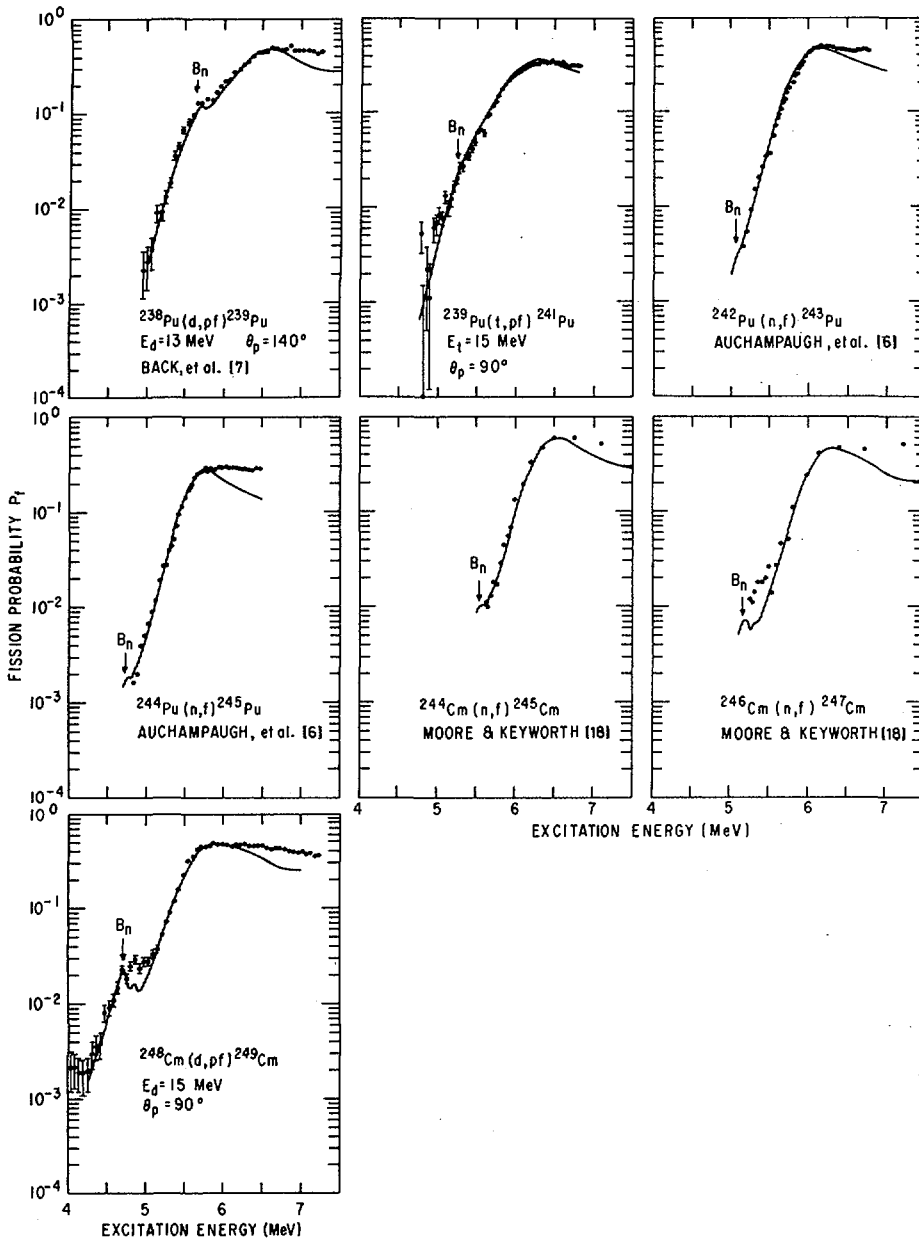


FIG. 9. Fission probabilities for Am and Bk nuclei. Solid curves indicate best fits with the statistical model described in the text. Data for ^{242}Am and ^{244}Am were taken from Back et al. [7].



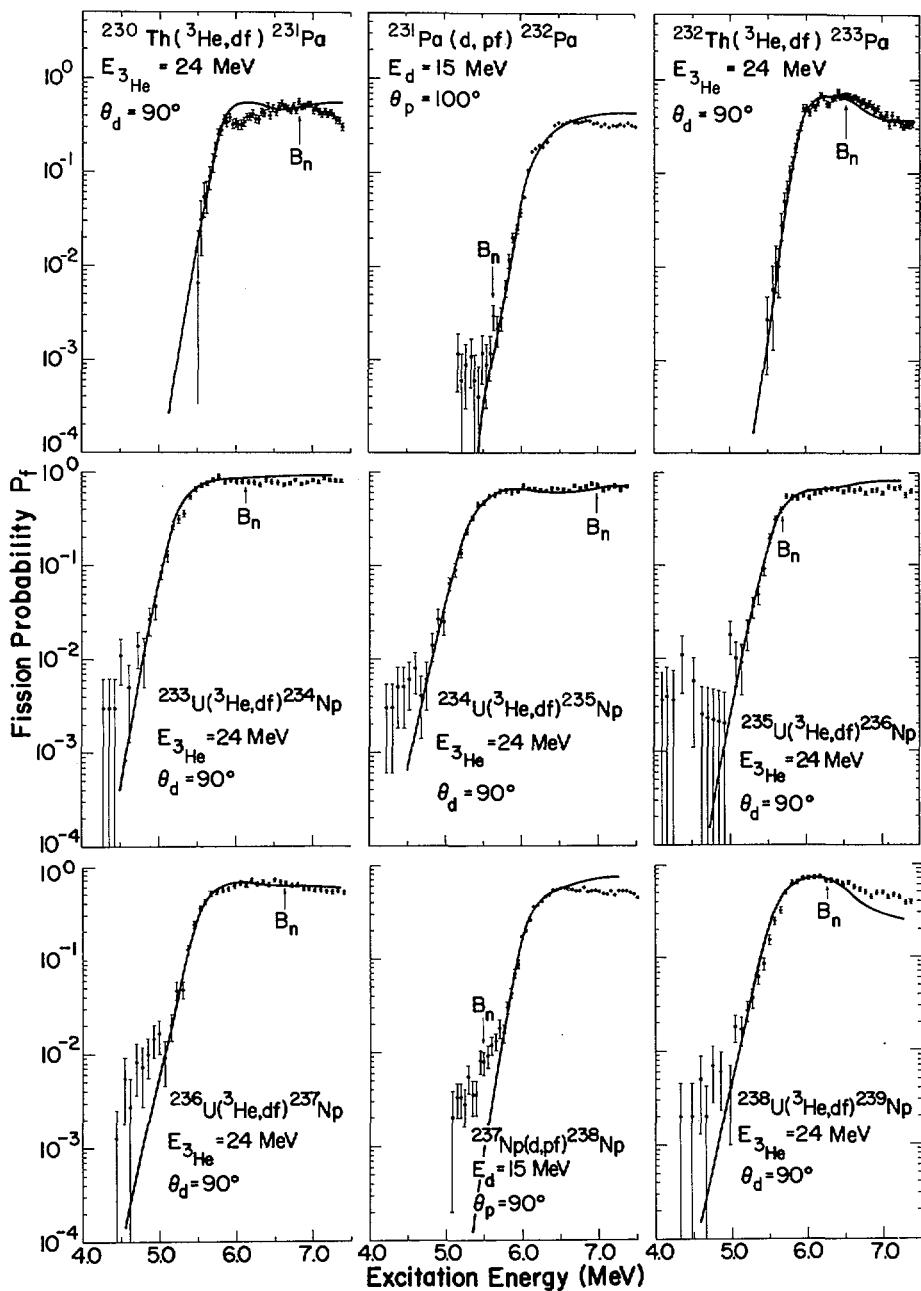


FIG.11. Fission probabilities for Pa and Np isotopes. Solid curves indicate best fits with the statistical model described in the text.

TABLE I. ESTIMATED BARRIERS FOR ODD A AND ODD-ODD NUCLEI

Values given in parentheses were estimated as described in text and held fixed during fitting of data. For Pa, U, and Np nuclei, values for G_n and G_γ not in parentheses were obtained from fitting the magnitude of P_f but the values are not unique and depend also on values of some of the other parameters that were held fixed. The values of E_A , E_B , $\hbar\omega_A$, $\hbar\omega_B$ are given in MeV.

Nucleus	E_A	E_B	$\hbar\omega_A$	$\hbar\omega_B$	G_n	G_γ
^{231}Pa	5.75 ± 0.30	5.85 ± 0.30	(0.8)	(0.45)	(0.3)	3.6
^{232}Pa	5.75 ± 0.30	6.10 ± 0.30	(0.6)	(0.45)	0.45	(3.6)
^{233}Pa	5.85 ± 0.30	6.00 ± 0.30	(0.8)	(0.40)	(0.3)	1.8
^{235}U	6.10 ± 0.30	5.65 ± 0.30	(0.85)	(0.50)	(0.3)	(2.5)
^{237}U	6.35 ± 0.30	5.95 ± 0.30	(0.85)	(0.55)	0.12	(2.5)
^{239}U	6.55 ± 0.30	6.30 ± 0.30	(0.90)	(0.65)	0.05	(2.5)
^{234}Np	5.35 ± 0.30	5.00 ± 0.30	(0.6)	(0.42)	(0.3)	2.6
^{235}Np	5.60 ± 0.30	5.20 ± 0.30	(0.8)	(0.55)	(0.3)	3.6
^{236}Np	5.70 ± 0.30	5.20 ± 0.30	(0.6)	(0.42)	(0.3)	2.5
^{237}Np	5.70 ± 0.30	5.50 ± 0.30	(0.8)	(0.55)	(0.3)	2.8
^{238}Np	6.00 ± 0.30	6.00 ± 0.30	(0.6)	(0.42)	.04	(1.8)
^{239}Np	5.85 ± 0.30	5.50 ± 0.30	(0.8)	(0.55)	(0.3)	1.8
^{239}Pu	6.43 ± 0.20	(5.50)	1.00 ± 0.10	(0.55)	0.30 ± 0.15	0.77 ± 0.12
^{241}Pu	6.25 ± 0.20	(5.50)	1.10 ± 0.10	(0.55)	0.30 ± 0.15	1.15 ± 0.40
^{243}Pu	6.05 ± 0.20	(5.60)	0.80 ± 0.10	(0.55)	0.15 ± 0.08	(1.2)
^{245}Pu	5.72 ± 0.20	(5.45)	0.90 ± 0.10	(0.55)	0.40 ± 0.15	(1.2)
^{240}Am	6.35 ± 0.20	(4.80)	0.60 ± 0.10	(0.42)	$0.70 \pm .20$	(1.2)
^{241}Am	6.00 ± 0.20	(4.80)	0.80 ± 0.10	(0.55)	(0.3)	1.8 ± 0.9
^{242}Am	6.38 ± 0.20	(4.80)	0.50 ± 0.10	(0.42)	$0.08 \pm .05$	(1.2)
^{243}Am	5.98 ± 0.20	(4.80)	0.75 ± 0.10	(0.55)	(0.3)	1.8 ± 0.9
^{244}Am	6.18 ± 0.20	(4.80)	0.50 ± 0.10	(0.42)	$0.15 \pm .07$	(1.2)
^{245}Am	5.88 ± 0.20	(4.80)	0.85 ± 0.10	(0.55)	(0.3)	1.8 ± 1.0
^{247}Am	5.60 ± 0.20	(4.80)	0.90 ± 0.10	(0.55)	(0.3)	$1.8 \pm_{1.8}^4$
^{245}Cm	6.38 ± 0.20	(4.20)	0.65 ± 0.10	(0.55)	0.20 ± 0.13	(0.4)
^{247}Cm	6.20 ± 0.20	(4.20)	0.70 ± 0.10	(0.55)	0.20 ± 0.10	(0.4)
^{249}Cm	5.80 ± 0.20	(4.20)	0.75 ± 0.10	(0.55)	0.15 ± 0.08	0.38 ± 0.12
^{249}Bk	6.05 ± 0.20	(4.20)	0.80 ± 0.10	(0.55)	(0.3)	$1.8 \pm .65$

previously [13]. The fits obtained to the experimental data are shown in Figures 9 and 10. It is seen that using the three adjustable parameters the shapes of the distributions can be reasonably well reproduced near threshold but at energies above the peak P_f value the calculations from odd-A nuclei decrease sharply whereas the data show a plateau. This result indicates that the functional form for Γ_n/Γ_f obtained from the present statistical model is not adequate. This point will be discussed in more detail in the next section.

For the Pa and Np nuclei there is no independent information available (e.g. from fission isomers) so that the parameters E_A , $\hbar\omega_A$, E_B , $\hbar\omega_B$, and the normalization factors G_n , or G_γ are all unknown. In general, fits to the experimental fission probability distributions were not capable of uniquely determining all of these parameters. Therefore, the experimental results were fit by fixing $\hbar\omega_A$ and $\hbar\omega_B$ to average values determined from the heavier nuclei and then varying E_A , E_B , and G_n or G_γ . In most cases G_n values were held fixed to average values determined from the Pu-Bk results. In addition to the Pa and Np results, fission probabilities obtained [13] from (n,f) cross-sections for ^{235}U , ^{237}U and ^{239}U were also analyzed. Due to the lack of independent information on E_B and $\hbar\omega_B$ and because $E_A \approx E_B$, the uncertainties on the barrier parameters determined for the Pa-Np region are greater than for the Pu-Bk nuclei. The results of these fits are shown in Figure 11. For ^{231}Pa and ^{232}Pa there appears to be some resonant structure which cannot be reproduced in the complete damping approximation used in our statistical model. This resonant structure may be analogous to the more pronounced structure observed in ^{231}Th .

The barrier parameters obtained from analysis of all the odd nuclei are given in Table I. Results for even-even nuclei are tabulated in Paper IAEA-SM-174/27 [4].

5. EXPERIMENTAL vs CALCULATED DECAY WIDTHS

Within the context of the statistical model described in Section 3, the widths for neutron and fission decay are calculated on an absolute basis and the adjustable normalization in the gamma decay width was fixed by normalizing to experimental data. Therefore, it was initially expected that the normalization factors G_n and G_γ should each be equal to 1 except for fluctuations due to systematic uncertainties in the absolute experimental fission probabilities. The results from the fits indicate that this is not the case, as is shown in Fig. 12.

Except for ^{249}Cm the values of G_γ are generally consistent with 1 although the Am and Bk nuclei are better fit with a value of ~ 2 and the Pa and Np isotopes (Table I) show a preference for values of 3-4. In contrast, the G_n values are definitely not consistent with 1 and a value of $G_n = 0.2-0.3$ gives the best average representation of all the results. Furthermore, the underestimates of the fission probabilities at high energies with the current statistical model suggests that the value of G_n is even less at energies of 1-2 MeV above the fission threshold.

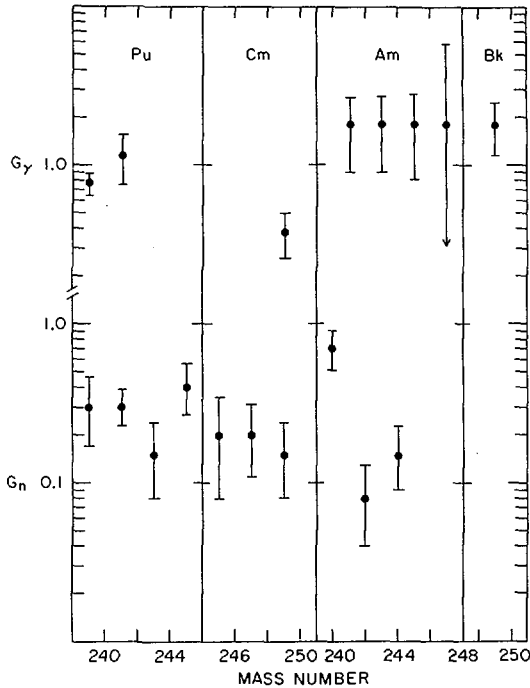


FIG.12. Factors G_n and G_γ obtained from fits to the fission probabilities for Pu-Bk nuclei.

The Γ_n and Γ_f calculations involve only an estimate of the spectrum of states available for de-excitation in the first well (Γ_n) and across the two saddle points (Γ_f). For nuclei in the region Pu-Bk the transmission across the first saddle point is of major importance in estimating Γ_f . Since average properties of the level spectra involved in the Γ_n calculation can be checked against experiment at low energy and the continuous level densities are normalized to experimental values at high energies it seems most reasonable to connect the low values of G_n with an underestimate of Γ_f . By using a single normalization factor for all the high energy level densities and treating the discrete levels in similar ways at the first minimum and the saddle points we have effectively assumed that the enhancement of the level densities due to coupling with low-lying collective excitations is the same at the minima and the saddle points. The low and possibly energy-dependent value we obtain for G_n may indicate that the level densities at the saddle points are enhanced by coupling to additional low-lying collective excitations. The theoretical justification for such an effect will be discussed in detail in other contributions to this conference[19,20].

This connection of low G_n values with an underestimate of the level density at the saddle point is, however, not consistent with the higher values obtained for G_γ . If the

Γ_n and Γ_γ calculations are correct and the main difficulty is in calculating Γ_f then G_n and G_γ should be roughly equal and this is not the case. Therefore, it appears that there are still unsolved problems in the attempts to calculate relative values of Γ_f , Γ_n , Γ_γ .

6. EXPERIMENTAL FISSION BARRIERS

The barrier heights E_A and E_B extracted from the experimental data for Pu-Bk isotopes are shown in Fig. 13. Figure 13 includes results from the analysis of odd-A and odd-odd nuclei as described earlier in this paper, results from the analysis of data from even-even nuclei described in Paper IAEA-SM-174/27[4] and estimates of E_B from the analysis of fission isomer excitation functions[5]. For the two cases where there is overlap, ^{238}Pu and ^{240}Pu , the E_B values estimated from the analysis of fission isomer data agree well with values obtained from these direct reaction fission experiments.

In the discussion below we will concentrate on some of the general trends for the barrier heights in actinide nuclei and in another paper[2] in these Proceedings, these barrier heights will be compared with various theoretical predictions.

The outstanding characteristics of the fission barriers for nuclei in the Pu-Bk region are:

1. The values for E_A show a decrease with increasing neutron number but do not seem to vary significantly with proton number. This trend is contrary to

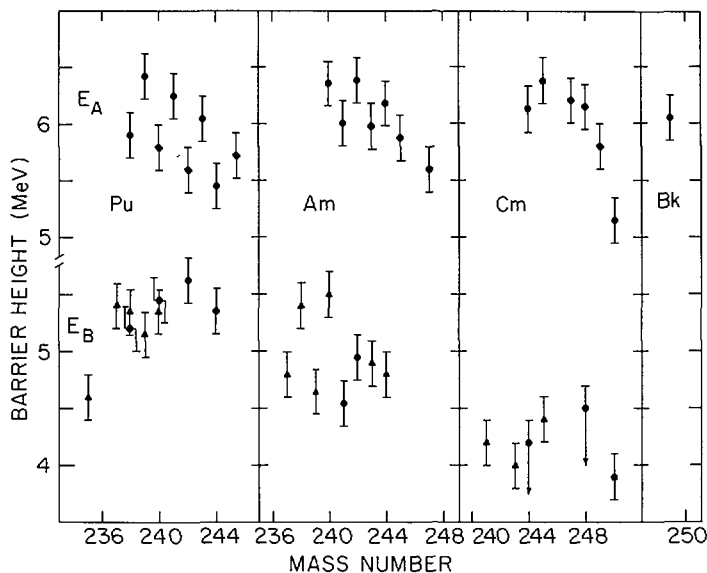


FIG.13. Heights of the fission barriers for Pu-Bk nuclei obtained from fits to experimental fission probabilities. Solid triangles show values obtained from the previous analysis of fission isomer data [5].

- most theoretical calculations which show E_A increasing with proton number.
2. The values of E_B do not seem to show a consistent trend with neutron number but decrease strongly with increasing proton number. These trends are qualitatively similar to theoretical predictions.
 3. The E_A values for Pu and Am isotopes and possibly the E_B values for Am isotopes show an apparent odd-even fluctuation with E_A being 0.3-0.5 MeV higher for odd-neutron than for even-neutron nuclei. This result would be consistent with a larger pairing gap at the saddle point and can be compared to an average value $\Delta_{\text{saddle}} - \Delta_{\text{ground state}} \approx 0.23$ MeV obtained from recent theoretical calculations [15] which assume that the pairing strength is independent of deformation. The apparent experimental odd-even fluctuations should be viewed with some caution, however, because the even-N nuclei involve competition between fission and gamma emission near threshold whereas the odd-N nuclei have fission thresholds above the neutron binding energy. Therefore, systematic errors in the estimates of Γ_γ relative to Γ_n could lead to spurious odd-even effects. At present we believe that the ± 0.2 MeV uncertainties in E_A for these nuclei are realistic but as noted in the previous section the normalizations of the various decay widths are not completely understood.
 4. The E_A values for Cm isotopes show a decrease of ~ 1.0 MeV in going from ^{248}Cm ($N=152$) to ^{250}Cm ($N=154$). This decrease seems to be significantly greater than the additional binding of ~ 0.6 MeV [21,22] attributed to the $N = 152$ shell for the equilibrium shape of ^{248}Cm and is not apparent

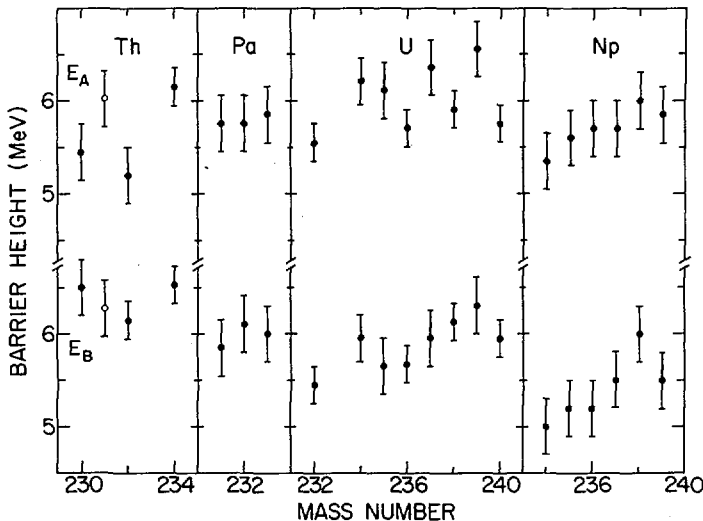


FIG.14. Heights of the fission barriers for Th-Np nuclei obtained from fits to experimental fission probabilities.

in the E_B estimates. The results suggest that there is an additional increase of ~ 0.4 MeV in the binding at the first saddle point between ^{248}Cm and ^{250}Cm when measured relative to a liquid drop mass surface.

The experimental barrier parameters for Th-Np nuclei are shown in Fig. 14. The barrier parameters for ^{231}Th are taken from reference 23. The uncertainties in the estimated barrier heights for odd-A and odd-odd nuclei are somewhat greater than in the Pu-Bk region because of the lack of fission isomer results to tie down the E_B and $\hbar\omega_B$ values. The results again show E_A relatively constant and E_B decreasing with increasing proton number. The dependence on neutron number and possible odd-even effects do not seem as prominent as for the Pu-Bk region but details are obscured by the larger uncertainties on the estimated barrier heights.

7. CONCLUSION

In this paper we have presented a summary of the new data from direct reaction fission experiments which when coupled with previous (d,pf) and (n,f) data and analyzed with a realistic statistical model lead to a self-consistent set of fission barriers for a large number of actinide nuclei from Th (Z=90) through Bk (Z=97). These results along with systematic results from fission isomer studies form a set of experimental barriers which can be used to test current theoretical estimates of fission barrier properties. How well the theories stand the test of experiment will be shown in the theoretical chapter of this story in Paper IAEA-SM-174/202 [2].

ACKNOWLEDGEMENTS

We are grateful to J. Lerner at Argonne National Laboratory for producing the ^{248}Cm target. It is a pleasure to acknowledge useful discussions with S. Bjørnholm, A. Bohr, J.R. Huizenga, J.E. Lynn, B. Mottelson, S.G. Nilsson, J.R. Nix, and R. Vandenbosch. We would like to thank the Neutron Cross-Section Group at Brookhaven National Laboratory for providing tabulations of current (n,f) cross-section data for many of the isotopes of interest.

REFERENCES

- [1] Proceedings of the Second International Atomic Energy Agency Symposium on Physics and Chemistry of Fission, Vienna, 1969 (International Atomic Energy Agency, Vienna, 1969).
- [2] J.R. NIX and P. MÖLLER, Paper IAEA/SM-174/202, these Proceedings, Vol.1.
- [3] H.C. PAULI and T. LEDERGERBER, Paper IAEA/SM-174/206, these Proceedings, Vol.1.
- [4] B.B. BACK, H.C. BRITT, J.D. GARRETT and OLE HANSEN, Paper IAEA/SM-174/27, these Proceedings, Vol.1.

- [5] H.C. BRITT, M. BOLSTERLI, J.R. NIX and J.L. NORTON, Phys. Rev. C7(1973)801; H.C. BRITT, S.C. BURNETT, B.H. ERKKILA, J.E. LYNN and W.E. STEIN, Phys. Rev. C4(1971)1444.
- [6] G.F. AUCHAMPAUGH, J.A. FARRELL and D.W. BERGEN, Nucl. Phys. A171(1971)31.
- [7] B.B. BACK, J.P. BONDORF, G.A. OTROSHENKO, J. PEDERSEN, and B. RASMUSSEN, Nucl. Phys. A165(1971)449.
- [8] See, for example, J.R. STEHN, et.al., Brookhaven National Laboratory Report, BNL325, Second Edition, Supplement No.2(1965); References to specific (n,f) cross-section data used in this paper are given in the analysis section where appropriate.
- [9] A.H. WAPSTRA and N.B. GOVE, Nuclear Data Tables 9, (1971)265.
- [10] M.J. MARTIN, Nuclear Data Sheets, Section B5(1971)287; M.B. LEWIS, Nuclear Data Sheets, Section B5(1971)601.
- [11] J.D. CRAMER and H.C. BRITT, Phys. Rev. C2(1970)2350; J.D. CRAMER, Los Alamos Scientific Laboratory Report, LA-4198, 1969 (unpublished).
- [12] B.B. BACK, OLE HANSEN, H.C. BRITT, J.D. GARRETT, (to be published).
- [13] H.C. BRITT and J.D. CRAMER, Phys. Rev. C2(1970)1758.
- [14] B.B. BACK, OLE HANSEN, B. LEROUX, H.C. BRITT and J.D. GARRETT, (to be published).
- [15] M. BOLSTERLI, E.O. FISET, J.R. NIX, and J.L. NORTON, Phys. Rev. C5(1972)1050.
- [16] C.F. TSANG, private communication; S.G. NILSSON, C.F. TSANG, A. SOBICZEWSKI, A. SZYMANSKI, S. WYCECH, C. GUSTAFSSON, I.L. LAMM, P. MOLLER, and B. NILSSON, Nucl. Phys. A131(1969)1.
- [17] F.A. RICKEY, E.T. JURNEY and H.C. BRITT, Phys. Rev. C6(1972)2072.
- [18] M.S. MOORE and G.A. KEYWORTH, Phys. Rev. C3(1971)1656.
- [19] L.G. MORETTO, Paper IAEA/SM-174/204, these Proceedings.
- [20] S. BJØRNHOLM, A. BOHR, B.R. MOTTELSON, Paper IAEA/SM-174/205, these Proceedings, Vol.1.
- [21] N.B. GOVE and A.H. WAPSTRA, Nucl. Data Tables 11(1972)127.
- [22] S. BJØRNHOLM, private communication; S. BJØRNHOLM and J.E. LYNN, Rev. Mod. Phys. (to be published).
- [23] G.D. JAMES, J.E. LYNN, and L.G. EARWAKER, Nucl. Phys. A189(1972)225.

FISSION BARRIERS FOR DOUBLY EVEN ACTINIDE NUCLEI FROM (t, pf), (^3He , df), (p, p'f) and (t, α f) STUDIES*

B.B. BACK, Ole HANSEN
Los Alamos Scientific Laboratory,
University of California, USA,
and
The Niels Bohr Institute,
University of Copenhagen, Denmark

H.C. BRITT⁺, J.D. GARRETT⁺⁺
Los Alamos Scientific Laboratory,
University of California, USA

Abstract

FISSION BARRIERS FOR DOUBLY EVEN ACTINIDE NUCLEI FROM (t, pf), (^3He , df), (p, p'f) AND (t, α f) STUDIES.

Fission probability distributions have been measured for $^{230,232,234}\text{Th}$, $^{232,236,238,240}\text{U}$, $^{238,242,244}\text{Pu}$ and $^{244,248,250}\text{Cm}$ using (t, pf), (^3He , df), (p, p'f) and (t, α f) reactions. In general, resonance structures are observed in the fission probability distributions near threshold. The results are analyzed with a statistical model which incorporates resonant penetration through the two-peaked fission barrier and damping in the second well. From the analysis, estimates are obtained for the heights and curvatures of the two peaks of the fission barrier (E_A , $\hbar\omega_A$, E_B , $\hbar\omega_B$). The results give a value ~ 6 MeV for the height E_A of the first peak for most nuclei, whereas the height of the second peak E_B decreases from ~ 6 MeV to ~ 4 MeV in going from Th to Cm isotopes. A major exception to the apparent constancy of E_A occurs between $N=152$ and $N=154$ where for ^{248}Cm , $E_A=6.2$ MeV, while for ^{250}Cm , $E_A=5.1$ MeV. Comparison with ground state mass systematics suggests that only about one half of the change in E_A between ^{248}Cm and ^{250}Cm is due to the $N=152$ shell at the equilibrium deformation.

1. INTRODUCTION

Since the last IAEA conference in Vienna in 1969) (1) there has been an intensive interest in shell effects on the nuclear deformation potential. Probably the most spectacular result of this type of investigation is the prediction of super-heavy elements in the region of $Z \sim 114$ and $N \sim 184$ (2), but at the same time it has cast light on many other observations related to nuclear fission, like the mass asymmetry in the actinide region (3), the systematic occurrence of fission isomers (4), gross structures in (n,f) compound resonances (5) and vibrational resonances observed in direct reaction fission experiments (6). Qualitatively the Strutinsky prescription (7) for calculating the potential energy surface has been very successful in explaining these observations.

* Work supported by the US Atomic Energy Commission.

⁺ Presently on leave at the Nuclear Structure Research Laboratory, University of Rochester, USA;

⁺⁺ Present address: Brookhaven National Laboratory, Upton, N.Y., USA.

In this work we present measurements of some properties of the potential energy surface, especially saddle point energies and curvatures, for 15 doubly even actinide nuclei, ranging from ^{230}Th to ^{250}Cm , which can be used for a more quantitative test of the theoretical calculations in this region. We shall mainly discuss the results of direct reaction induced experiments interpreted within a double-humped fission barrier model.

This work is an integral part of the extensive program reported by Dr. Britt in the previous paper (8), but the results for the doubly even nuclei are analyzed with a different model due to the existence of subbarrier fission resonances in the experimental fission probability distributions. The experimental procedure is fairly standard and has been reported in the previous paper (8).

In the remainder of this paper we shall discuss: 1) the main features of the statistical model used in the analysis of the results for doubly even nuclei, 2) the agreement between calculated and experimental fission probability distributions and 3) the systematics of the extracted fission barrier parameters.

2. MAIN FEATURES OF THE STATISTICAL MODEL

In this section we discuss some of the main assumptions underlying the statistical model used in the analysis of the experimental data. First, it is assumed that the direct reaction induced fission process proceeds in two steps, namely the formation of a compound nucleus through the direct reaction and the subsequent decay of the compound states through various channels (fission, γ -radiation and neutron emission). In the doubly even nuclei studied here, the fission threshold E_f is lower than the neutron binding energy B_n and we can therefore study the fission decay in competition with γ -deexcitation only, which allows a simpler derivation of the fission barrier from the experimental results.

A. Formation

Since we measure the fission probability $P_f(E)$, it is not of primary interest to calculate the absolute magnitude of the formation cross-section, but only its relative spin-parity composition. We calculate the relative cross-sections using the formula (9)

$$\alpha(J^\pi) = N_0 \rho(J^\pi) \sum_{j=|J-I_0|}^{J+I_0} \frac{\sigma(j^\pi)}{J+I_0-|J-I_0|+1} \quad (1)$$

where N_0 is a normalization constant determined by

$$\sum_{J^\pi} \alpha(J^\pi) = 1 \quad (2)$$

J^π denotes the spin and parity of the final state reached in the direct reaction from the target state of spin I_0 .
 j^π is the transferred spin and parity and

$$\rho(J^\pi) = \frac{1}{2}(2J+1) \exp\left\{-\frac{(J+\frac{1}{2})^2}{2\sigma^2}\right\} \quad (3)$$

is the statistical spin density (10). The factor $\frac{1}{2}$ stems from the assumption of equal density of positive and negative parity states. The single particle transfer cross-sections $\sigma(j^\pi)$ are obtained from DWBA calculations using the computer code DWUCK (11).

We estimate that the approximation of an energy-independent relative spin parity distribution $\alpha(J^\pi)$ is fulfilled for all the reactions studied here, except possibly the (d,pf) reaction. This limitation of the present model is not considered serious, because the (d,pf) reaction is analyzed in only one case.

B. Decay

As mentioned earlier, we need only to consider decay by fission and γ -emission below the neutron binding energy B_n for the doubly even nuclei. The partial width for γ -radiation is calculated from a statistical expression taking only electric dipole radiation into account (12). The resulting partial width for γ -decay is nearly independent of the spin of the compound state and varies slowly with excitation energy. A normalization constant in the expression ensures that the observed value of $\Gamma_\gamma \sim 30$ -40 meV at the neutron binding energy is reproduced.

For the calculation of the fission width, we employ the formula (13)

$$\Gamma_f = \frac{D}{2\pi} \sum_v T_v \quad (4)$$

Here D is the average energy spacing of compound states of the appropriate spin and parity, and T_v is the penetrability factor for the fission channel v . The characteristics of the fission barrier enter into the calculation through this penetrability factor. The central assumption of a two-humped fission barrier will produce resonances in the penetrability function $T_f(E)$ corresponding to quasistationary β -vibrational (i.e. stretching-type) states in the second well. These resonances also appear in the fission probability

$$P_f = \sum_{J^\pi} \left\{ \alpha(J^\pi) < \frac{\Gamma_f(J^\pi)}{\Gamma_f(J^\pi) + \Gamma_\gamma(J^\pi)} > \right\} \quad (5)$$

as it is observed experimentally.

The shape of the fission barrier is approximated by three smoothly joined parabolic sections, Fig.1, defined by six parameters, namely three heights E_A , E_{MIN} and E_B and

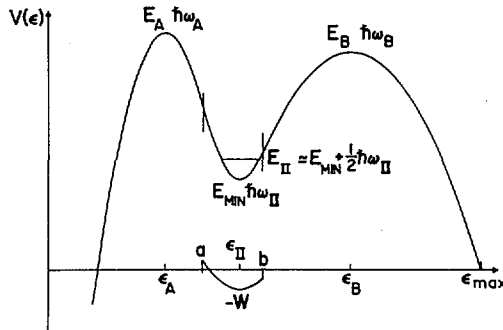


FIG.1. The fission barrier approximated by three smoothly joined parabolic sections parametrized by the heights E_A , E_{MIN} , E_B and the curvatures $\hbar\omega_A$, $\hbar\omega_{II}$ and $\hbar\omega_B$. The positions of the first maximum, the second minimum and the second maximum are denoted ϵ_A , ϵ_{II} and ϵ_B , respectively. ϵ_{MAX} denotes the position where the potential drops down to the ground state energy. W is the strength of the imaginary potential.

three curvatures $\hbar\omega_A$, $\hbar\omega_{II}$ and $\hbar\omega_B$. At the position of the second well we have also included an imaginary part of the potential which simulates the damping of the vibrational strength into the underlying "continuum", in the same manner as described in ref.(14). The tunneling probability through this potential is calculated analytically using parabolic cylinder functions (15).

The effect of statistical fluctuations of Γ_f on the mean value of the branching ratio is taken into account through a fluctuation factor, again following the prescription in ref.(14). As pointed out by E.Lynn (16), the existence of the second well also influences the statistical distribution of Γ_f . We have not included this effect in the calculations because it is estimated to be small in the cases of doubly even nuclei, where the damping in the second well is moderate.

It should be kept in mind that the parameters E_A , $\hbar\omega_A$, E_B and $\hbar\omega_B$ that can be extracted from a comparison to experimental fission probability distributions have a meaning only to the extent that the fission motion can be regarded as one-dimensional and that the shape of the fission barrier can be approximated by three smoothly joined parabolic sections as we have done. Failures to fit the experimental data could stem from deviations from these assumptions. Furthermore we have for simplicity assumed that the shape of the fission barrier is the same for all fission channels. This is equivalent to assuming that the excitation energy for a specific internal mode is independent of deformation. Theoretical calculations have shown that for most actinides the system preferentially assumes an octupole type shape at the second maximum (3) which reduces the internal energy of the $K^\pi = 0^-$ band, and for the heavier actinides the nucleus has an instability towards non-axial symmetric shapes at the first maximum (17) which tends to lower the $K^\pi = 2^+$ band. In the present analysis these effects are not taken into account.

Even in the case where the fission barrier is inadequately described by the adopted potential, the parameters extracted would still on the average describe the shape close to the barrier tops, but maybe not further down the potential.

3. FITS TO EXPERIMENTAL DATA

The experimentally measured fission probabilities and the fits obtained are shown in Fig.2 for Th and U isotopes and in Fig.3 for Pu and Cm isotopes.

The ^{230}Th results are poor in detailed structure due to the very small cross-section for the (t,α) reaction, but they suffice to determine the height of the fission barrier. The ^{232}Th data have indications of a resonance at $E = 5.0$ MeV, but it is not significant statistically. We have therefore chosen to fit the data without a resonance at this point. The ^{232}Th data are fundamentally different from the ^{234}Th results which show a strong resonance structure in the region $E = 5.5$ - 5.8 MeV. This difference manifests itself as a significant discontinuity in the extracted barrier parameters, see Fig.4. Several trial runs aimed at removing this discontinuity have been unsuccessful.

The ^{232}U results obtained from a $(^3\text{He},d)$ reaction show weak indications of a resonance at $E = 5.1$ MeV. In the fit we have assumed such a resonance to be present and obtained good agreement. The ^{234}U data are taken from the (d,pf) study described in ref.(14). It shows a resonance at $E = 5.0$ MeV which is reproduced in the fit, but just above this energy there is some discrepancy. For this reason we assign a larger uncertainty to the barrier parameters in this case. The ^{236}U fission probability is somewhat steeper than for the other U isotopes. This manifests itself through smaller $\hbar\omega$ -values. The calculated curve follows the overall trend and reproduces the resonance structure at $E = 5.15$ MeV. The ^{238}U results show resonance structures at $E = 5.15$ MeV and $E = 5.80$ MeV. Both are reproduced by the calculation. A fission resonance is apparent at $E = 5.4$ MeV in the ^{240}U data and is also reproduced by the calculated curve. Just below this resonance there is some discrepancy. Experimentally the fission probability increases very slowly, but with the present model this behaviour is not reproduced.

The fission probability of ^{238}Pu , shown in Fig.3, increases fairly gently in the threshold region and there is an indication of a resonance at $E = 5.10$ MeV which is reproduced by the calculation. The measurement of the second barrier depends strongly on the existence of the resonance at $E = 5.1$ MeV, and we therefore assign a larger uncertainty to E_B in this case. The ^{240}Pu data were taken from ref.(18) and show the classical resonance at $E = 5.0$ MeV. The theoretical curve gives an acceptable fit in the whole threshold region. A resonance is also observed at $E = 4.65$ MeV in ^{242}Pu and the calculated curve gives good agreement up to $E = 5.3$ MeV. Above this energy there are some deviations. The theoretical model fails to give a detailed fit to the experimental data of ^{244}Pu , but follows the general trend. It is reasonable to connect the difficulties in reproducing the results of ^{242}Pu and ^{244}Pu

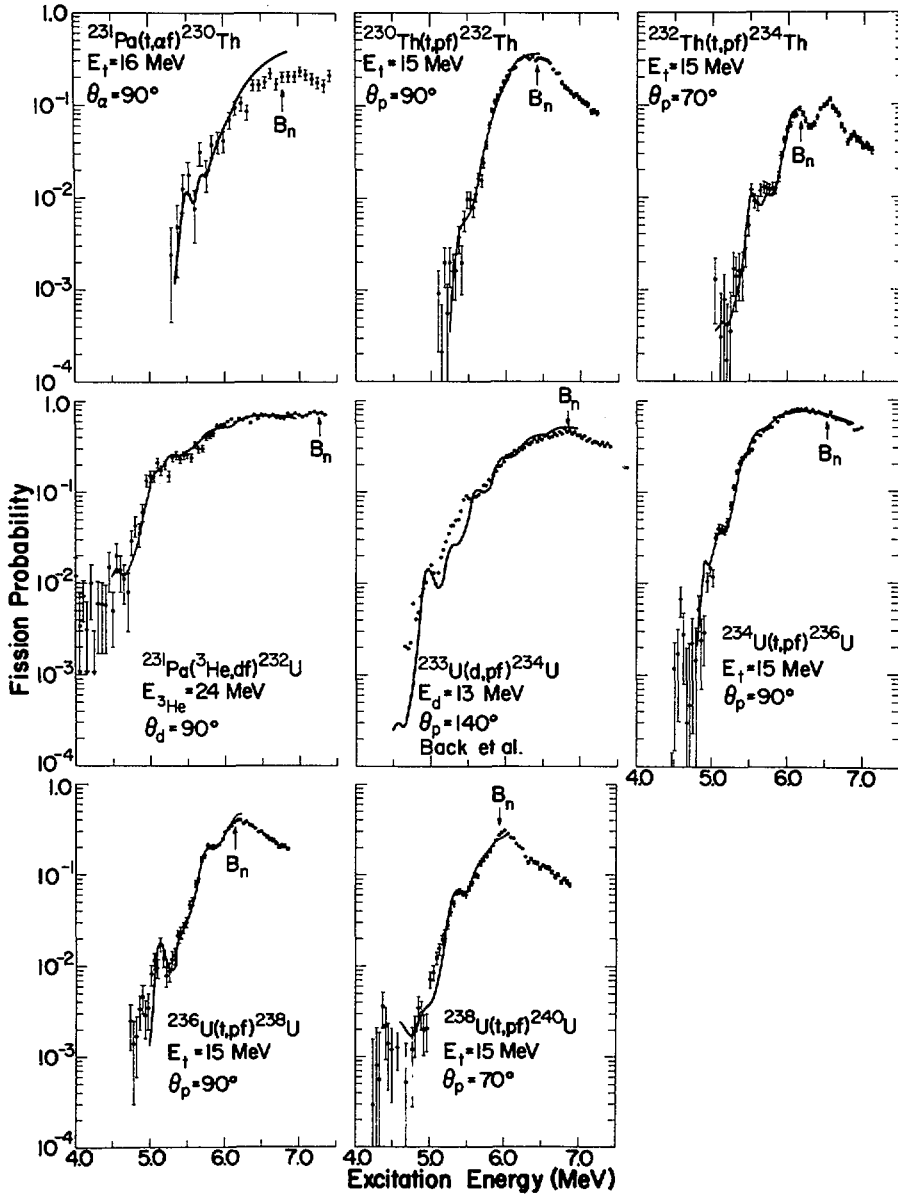


FIG. 2. Experimental fission probabilities vs. excitation energy for 230 , 232 , 234 Th and 232 , 234 , 236 , 238 , 240 U (points with error bars) and fitted curves extracted from model calculations. B_n indicates the neutron binding energy. The 234 U data are taken from Ref. [14].

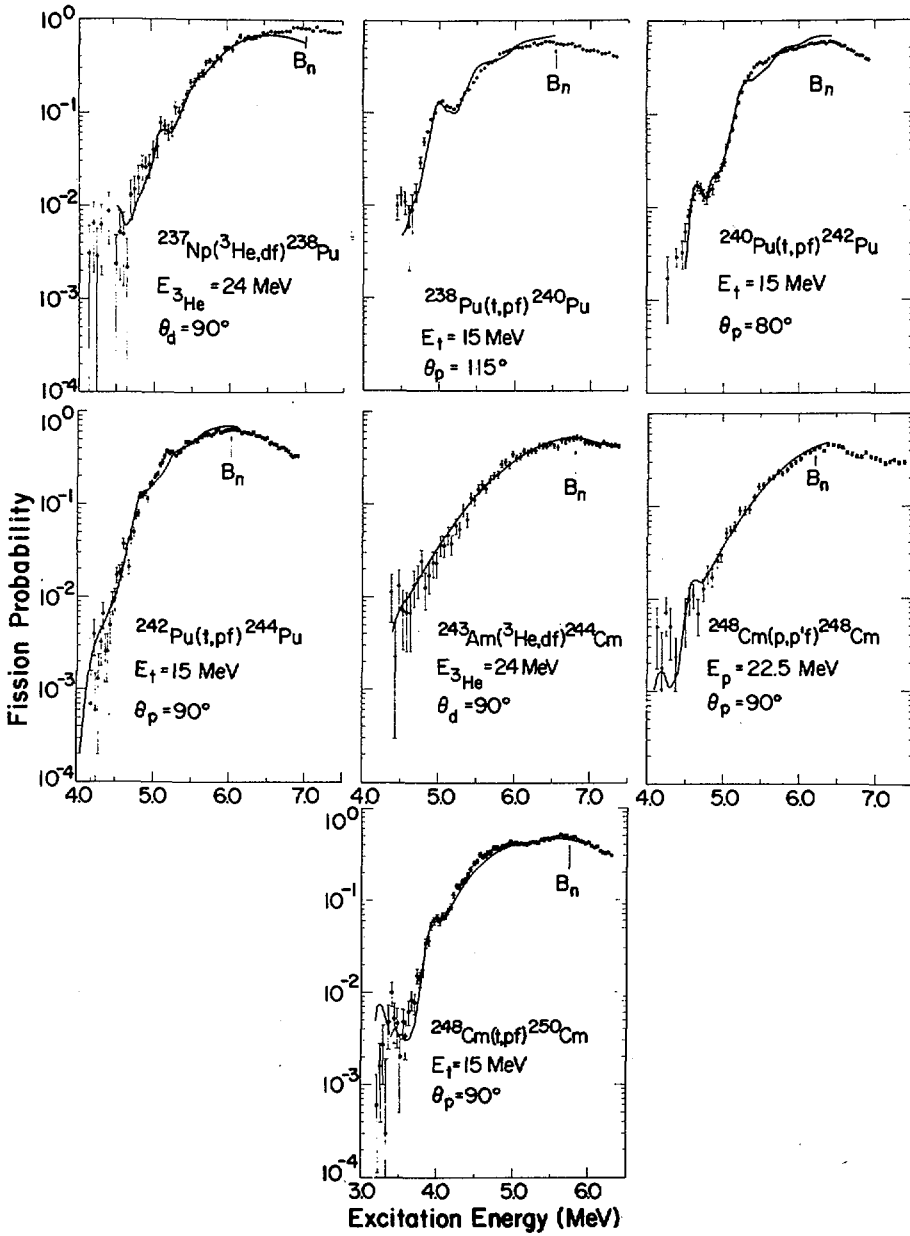


FIG. 3. Experimental fission probabilities vs. excitation energy for $^{238}, ^{240}, ^{242}, ^{244}\text{Pu}$ and $^{244}, ^{248}, ^{250}\text{Cm}$ (points with error bars) and fitted curves extracted from model calculations. B_n indicates the neutron binding energy. The ^{240}Pu data are taken from Ref. [18].

with the instability towards non-axial symmetric shapes at the inner barrier, which is predicted to be especially strong for these nuclei. This is probably also the reason why attempts to reproduce previously measured angular distributions of fission fragments (18) with the present model have been successful for U-isotopes, but problematic for Pu-isotopes.

The fission probability of ^{244}Cm rises very gently without any resonance structure above noise level in the threshold region, and it is described by a theoretical curve without any assumed resonance structure. The ^{248}Cm data are very similar to the ^{244}Cm data with the exception of a possible structure at $E = 4.6$ MeV, which is reproduced in the theoretical curve. As mentioned earlier, the fission threshold of ^{250}Cm is shifted to lower energy by approximately 1.0 MeV, and we observe a shoulder at $E = 4.0$ MeV which is reproduced by the calculation.

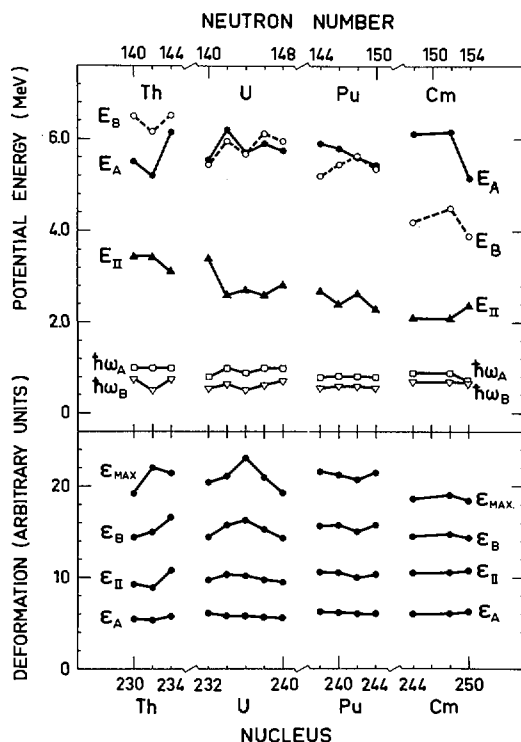


FIG.4. The height of the first maximum E_A (filled circles connected with full drawn lines), the height of the second maximum E_B (open circles connected with dotted lines), the isomer energy E_{II} (filled triangles), the curvature of the first barrier $\hbar\omega_A$ (open squares) and the curvature of the second barrier $\hbar\omega_B$ (open triangles) are displayed in the upper part of the figure. In the lower part of the figure the deformations of the first maximum ϵ_A , the second minimum ϵ_{II} , the second maximum ϵ_B , and ϵ_{MAX} (see text) are plotted in arbitrary units. (The mass parameter is assumed to be constant in this calculation.)

TABLE I. FISSION BARRIER PARAMETERS

Nucleus	E_A (MeV)	E_B (MeV)	$\hbar\omega_A$ (MeV)	$\hbar\omega_B$ (MeV)
^{230}Th		6.5 ± 0.3		
^{232}Th		6.15 ± 0.20		0.50 ± 0.10
^{234}Th	6.15 ± 0.20	6.52 ± 0.20	1.00 ± 0.10	0.75 ± 0.10
^{232}U	5.54 ± 0.20	5.45 ± 0.20	0.80 ± 0.10	0.55 ± 0.10
^{234}U	6.20 ± 0.25	5.95 ± 0.25	1.00 ± 0.10	0.65 ± 0.10
^{236}U	5.70 ± 0.20	5.68 ± 0.20	0.90 ± 0.10	0.50 ± 0.10
^{238}U	5.90 ± 0.20	6.12 ± 0.20	1.00 ± 0.10	0.62 ± 0.10
^{240}U	5.75 ± 0.20	5.95 ± 0.20	1.00 ± 0.10	0.70 ± 0.10
^{238}Pu	5.90 ± 0.20	5.20 ± 0.30	0.80 ± 0.10	0.55 ± 0.10
^{240}Pu	5.80 ± 0.20	5.45 ± 0.20	0.82 ± 0.10	0.60 ± 0.10
^{242}Pu	5.60 ± 0.20	5.63 ± 0.20	0.82 ± 0.10	0.59 ± 0.10
^{244}Pu	< 5.6	5.35 ± 0.20		0.57 ± 0.10
^{244}Cm	6.12 ± 0.20	< 4.9	0.90 ± 0.10	
^{248}Cm	6.15 ± 0.20	< 4.6	0.90 ± 0.10	
^{250}Cm	5.15 ± 0.20	3.90 ± 0.30	0.72 ± 0.10	0.69 ± 0.10

4. BARRIER PARAMETERS

The barrier parameters used to reproduce the experimental results are shown in Fig.4. Albeit determined with varying accuracy, these parameters show that the experimental data are in agreement with fairly smooth systematic trends (and also with parameters determined from other sources).

The most accurate information is obtained in the cases where fission resonances are observed (^{234}Th , ^{232}U , ^{234}U , ^{236}U , ^{238}U , ^{240}U , ^{238}Pu , ^{240}Pu , ^{242}Pu , ^{250}Cm). Here the parameters E_A , $\hbar\omega_A$, E_B and $\hbar\omega_B$ are well-determined. In the other cases (^{230}Th , ^{232}Th , ^{244}Pu , ^{244}Cm , ^{248}Cm) the height and curvature of the least transparent barrier is well determined and one can set upper limits for the other barrier (see Table I). The height and curvature of the secondary minimum are less uniquely determined and are therefore omitted from Table I*. Systematic investigations have shown that equally good fits can be obtained with parameters differing in some cases by as much as 200 keV for the heights E_A and E_B and 100 keV for the curvatures $\hbar\omega_A$ and $\hbar\omega_B$. We therefore generally assign uncertainties of this magnitude to the resulting parameters. The observed deviations from smooth trends are significant since attempts aimed at eliminating these deviations resulted in unacceptable fits to the experimental data. The results of the present analysis can therefore be summarized in Table I.

* Generally we have assumed values for E_{II} and $\hbar\omega_{II}$ that agree with values obtained from other sources (19) and follow smooth systematic trends.

The height of the inner barrier shows relatively small variations from ^{230}Th to ^{244}Pu around a mean value of $E_A \sim 5.8$ MeV. For ^{244}Cm and ^{248}Cm , E_A is as high as ~ 6.2 MeV, dropping to ~ 5.1 MeV for ^{250}Cm . With constant shell corrections the liquid drop properties would lead to a steady decrease of the fission barrier in going from Th to Cm. The shell structure has the effect of keeping the first barrier constant or even increasing it, as in ^{244}Cm and ^{248}Cm . Since the barrier height is measured relative to the ground state energy, shell effects acting at the ground state shape and at the shape of the first barrier may both contribute to the variations. Careful analysis of the results indicates that both effects play a role. The well-known $N = 152$ shell gives rise to a discontinuity in the ground state mass occurring between $N = 152$ and $N = 154$ (20), while the positive shell correction at barrier A appears to have a pronounced peak also for $N = 152$ (see Fig.5). The two effects enhance each other and contribute equally to the resulting drop of 1.0 MeV in the first barrier in going from ^{248}Cm to ^{250}Cm .

Although the first peak (E_A) is fairly constant from Th to Pu there are still significant fluctuations; especially in the U isotopes where we have high barriers for $N = 142$ and 146 and low barriers for $N = 140$, 144 and 148. This trend seems to be paralleled by the second maximum.

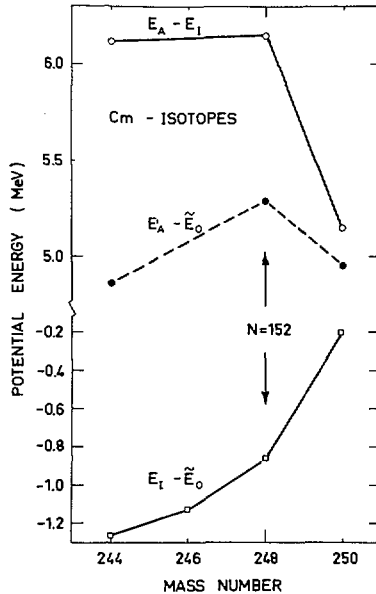


FIG.5. The height of the first maximum relative to the ground state energy $E_A - E_I$ (open circles), the height of the first maximum relative to the spherical liquid drop energy $E_A - E_O$ (black dots) and the ground state energy relative to the spherical liquid drop energy $E_I - E_O$ (open squares) are displayed for ^{244}Cm , ^{248}Cm and ^{250}Cm . The spherical liquid drop energies E_O are taken from Ref. [20].

In general, the second maximum follows a trend that would be expected from the liquid drop model, namely that it decreases steadily from $E_B \sim 6.4$ MeV in Th to $E_B \sim 3.9$ MeV in ^{250}Cm . This explains the gradual shift in the relative height of the two peaks in the sense that in the Th isotopes the second maximum is the higher and therefore dominating fission in the threshold region, in the U isotopes the two peaks are of comparable height, in the Pu isotopes the inner barrier is higher for the light isotopes and of almost equal height for the heavier isotopes. Finally, the second maximum drops 1-2 MeV below the first one in the Cm isotopes.

Assumptions about the depth of the secondary minimum are rather uncritical in reproducing the measurements. It is nevertheless nice to see that this depth follows a very regular decreasing pattern going from Th to Cm.

The curvatures $\hbar\omega_A$ and $\hbar\omega_B$ of the two barriers are fairly constant through the region investigated with $\hbar\omega_A \simeq 0.90 \pm 0.10$ MeV and $\hbar\omega_B \simeq 0.62 \pm 0.10$ MeV.

In Fig. 4 is also plotted the deformation of four points of the fission barrier relative to the ground state deformation namely the position of the first maximum ϵ_A , second minimum ϵ_{II} , second maximum ϵ_B and the intersection between the potential and ground state energy ϵ_{MAX} (see Fig. 1). Theoretically one would expect the position of the secondary minimum ϵ_{II} to be constant, since the shell structure causing it occurs at a very definite prolate deformation, namely where the ratio between the two axes is 2:1. We see that, with our parameters, this expectation is fulfilled within ± 10 per cent. Also the positions of the two maxima are constant within $\pm 10\%$ limits, whereas ϵ_{MAX} fluctuates more, especially for U isotopes. It has a decreasing trend going from Th to Cm as could be expected from theoretical considerations.

5. CONCLUSION

The two-peaked fission barrier model appears adequate for the analysis of direct reaction induced fission in the region from ^{230}Th to ^{250}Cm . In general, the resulting barrier parameters show smooth trends throughout the region with the exception of the 1.0-1.2 MeV drop in the height of the first barrier occurring from ^{248}Cm to ^{250}Cm . Half of this is due to the $N = 152$ shell at the equilibrium deformation and the other half of it is due to an antishell at the first maximum occurring for $N = 150-152$.

ACKNOWLEDGEMENTS

We gratefully acknowledge discussions with A. Bohr, B. Motelson, S. Bjørnholm, J. E. Lynn, J. R. Nix and J. Pedersen. We are grateful to J. Lerner at Argonne National Laboratory, U.S.A. for producing the ^{248}Cm target. One of us (B.B.B.) is indebted to Statens naturvidenskabelige forskningsråd, Denmark, for financial support.

REFERENCES

- (1) Second Symposium on the Physics and Chemistry of Fission, IAEA - Vienna, 1969.
- (2) H.Meldner, Arkiv för Fysik 36 (1967) 593 and W.D.Myers and W.J.Swiatecki, Nucl.Phys. 81 (1966) 1.
- (3) P.Möller and S.G.Nilsson, Phys.Lett. 31B (1970) 283.
- (4) H.C.Britt, Nuclear Data Tables, 1973 (to be published).
- (5) E.Migneco and J.P.Theobald, Nucl.Phys. A112 (1968) 603 and A.Fubini, J.Blons, A.Michaudon and D.Paya, Phys.Rev. Lett. 20 (1968) 1373.
- (6) J.Pedersen and B.D.Kuzminov, Phys.Lett. 29B (1969) 176.
- (7) V.M.Strutinsky, Nucl.Phys. A122 (1968) 1 and Yad.Fiz. 3 (1966) 614, (Sov.J.Nucl.Phys. 3 (1966) 449).
- (8) B.B.Back, H.C.Britt, J.D.Garrett, Ole Hansen and B. Leroux, Paper IAEA/SM-174/201, these Proceedings, Vol. 1.
- (9) H.C.Britt, F.A.Rickey, Jr. and W.S.Hall, Phys.Rev. 175 (1968) 1525.
- (10) A.Gilbert and A.G.W.Cameron, Can.J.Phys. 43 (1965) 1446.
- (11) P.D.Kunz, unpublished.
- (12) H.C.Britt, S.C.Burnett, B.H.Erkkila, J.E.Lynn and W.E.Stein, Phys.Rev. C4 (1971) 1444.
- (13) J.M.Blatt and V.F.Weisskopf, Theoretical Nuclear Physics, John Wiley & Sons, p.389.
- (14) B.B.Back, J.P.Bondorf, G.A.Otroschenko, J.Pedersen and B.Rasmussen, Nucl.Phys. A165 (1971) 449.
- (15) J.D.Cramer and J.R.Nix, Phys.Rev. C2 (1970) 1048.
- (16) J.E.Lynn, private communication, March 1973.
- (17) S.E.Larsson, I.Ragnarsson and S.G.Nilsson, Phys.Lett. 38B (1972) 269.
- (18) J.D.Cramer and H.C.Britt, Phys.Rev. C2 (1970) 2350.
- (19) H.C.Britt, M.Bolsterli, J.R.Nix and J.L.Norton, Phys.Rev. C7 (1973) 901.
- (20) S.Bjørnholm and J.E.Lynn, private communication, March 1973.

DISCUSSION

Papers IAEA-SM-174/201 and IAEA-SM-174/27

J. B. WILHELMY: How well do you know the outer barriers when no resonances are seen (i. e. in the case of Cm isotopes, for which you say the outer barrier is ~ 1 MeV below the inner barrier)?

B. B. BACK: In cases where no resonances are observed we can measure only the higher of the two barriers. In the case of ^{244}Cm and ^{248}Cm , where no prominent resonance structure is observed, we have extrapolated from values of E_B extracted from the fission isomer excitation functions obtained by Mr. Britt and his colleagues. In the case of ^{250}Cm we do measure E_B due to the resonance structure at $E = 4.0$ MeV.

L. WILETS: How did you obtain the deformations quoted? Did you assume a constant mass parameter?

B. B. BACK: The deformations are given in arbitrary units relative to the equilibrium deformation, and the mass parameter is assumed to be independent of Z , N , and deformation. Under these assumptions the deformations derive directly from the adopted parametrization of the fission barrier and the quoted barrier parameters.

S. BJØRNHOLM: H. C. Pauli and co-workers have discussed theoretically the occurrence of an anti-shell for $N = 152$ at the barrier. Could Mr. Pauli tell us how this fits with Mr. Back's observation?

H. C. PAULI: There is a shell at $N = 152$. The detailed results for the barriers, however, depend on the shell effect at the ground state and at the barrier.

THE STRUCTURE OF THE FISSION TRANSITION NUCLEUS ^{227}Ra

H. GROENING*, W. LOVELAND

Oregon State University

Corvallis, Oregon,

United States of America

Abstract

THE STRUCTURE OF THE FISSION TRANSITION NUCLEUS ^{227}Ra .

From experimental data for the $^{226}\text{Ra}(n, f)$ reaction, the height of the fission barrier and the character of the low-lying single particle level scheme for the fission transition nucleus ^{227}Ra have been deduced. The analysis involved simultaneously fitting the energy variation of the fission cross-section and angular distributions in the neutron energy range $3.6 \leq E_n \leq 9.0$ MeV using a Hauser-Feshbach formalism. The free parameters determined in fitting the data were the number, position, and (K, π) of the low-lying single particle states at the fission barrier and the density and K_0^2 value of the higher-lying states. Neutron emission widths for the calculation were taken from experimental data. Fission widths were calculated assuming, as suggested by theoretical calculations, a single-humped shape for the fission barrier and a Hill-Wheeler barrier penetrability expression. The best fit to the experimental data gave a fission barrier height of 3.7 MeV (relative to the neutron binding energy) and a single particle state sequence at the barrier of $3/2^-, 1/2^+, 5/2^+, 1/2^+$ for the odd-A transition nucleus ^{227}Ra . The level densities at higher energies were characterized by K_0^2 values of 8-10 for $4 \leq E_n \leq 7$ MeV and a_f values that increased with decreasing excitation energy. Evidence for a value of the gap parameter, $2\Delta_f$, of 2.7 MeV for the ^{227}Ra transition nucleus is presented. Comparison with theoretical predictions is made.

I. Introduction

Recently there has been a great deal of interest in and success in calculating various features of the fission barrier structure in heavy nuclei using the Strutinsky shell-correction method [1]. Recent calculations involving the use of P_3 and P_5 nuclear deformations have suggested that the fission mass distributions may be determined by asymmetric distortions at the fission saddle point [2]. While these fission barrier calculations appear to describe reasonably well the experimental data on spontaneously fissioning isomeric states, they have not, in general, been rigorously tested as to how well they predict the low energy single particle level spacings at the saddle point, and few if any tests have been made concerning predictions of fission barrier structure in nuclei with $Z < 90$.

The fission transition nucleus ^{227}Ra (formed in the reaction $^{226}\text{Ra} + n$) is a fascinating place to check out many of these points. Firstly, calculations [2,3,4,5,6,7] predict that, for all intents and purposes, the fission barrier is effectively single-humped for this system. (For example, the height of the inner barrier for ^{228}Ra has been estimated to be 2.4 MeV compared to an outer barrier height of 8.2 MeV [6].) Thus, deduction of the parameters describing the barrier shape is much easier and more meaningful than similar attempts for heavier nuclei with double-humped fission barriers. Secondly, the fission of nuclei in the Ra region has shown many

* On leave from Instituto Venezolano de Investigaciones Cientificas, Caracas, Venezuela.

unusual features, particularly with regard to the occurrence of triple-humped mass distributions and sharp changes in the mass distribution with small changes in excitation energy [8,9,10].

Recently Babenko and co-workers [11,12,13] have reported some very unusual data concerning the ^{227}Ra transition nucleus. Their published data on the energy variation of the fission cross-section and angular distributions is shown in Figures 1, 2 and 3. Note the sharp changes in the fission fragment angular distribution during the first smooth rise in the fission cross-section from 3.5 to 4.1 MeV neutron bombarding energy. Also of interest is the plateau in the fission cross-section between 4.0 and 4.7 MeV, while there appears to be a violent change in the fragment anisotropy in this region. An additional interesting feature is the further rise in the fission cross-section beyond 4.7 MeV. Since the neutron binding energy in ^{227}Ra is ~ 4.5 MeV and the fission barrier is $\sim 8-9$ MeV high, we can safely deduce that none of the low energy structure is due to second-chance fission effects.

We have performed calculations using a Hauser-Feshbach formalism to fit the energy variation of the fission cross-section and fragment angular distributions for the $^{226}\text{Ra}(n,f)$ reaction in the energy range $3.6 \leq E_n \leq 9.0$ MeV. Parameters in the calculation such as the number of single particle states in the transition nucleus and the values of K , π , E_0 and $\hbar\omega$

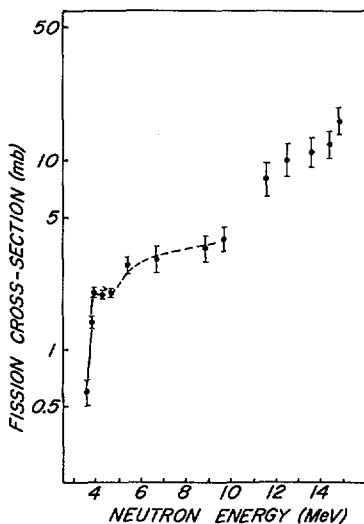


FIG. 1. Fission cross-section versus neutron bombarding energy for the $^{226}\text{Ra}(n,f)$ reaction. Data taken from Refs [11-13]. Solid line shows our "best fit" calculation using discrete single particle levels in the transition nucleus while the dashed line represents a statistical description of the transition nucleus.

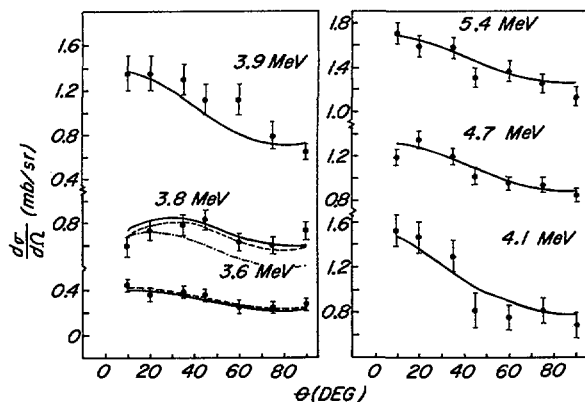


FIG.2. Fission fragment angular distributions for the $^{226}\text{Ra} (n, f)$ reactions for incident neutron energies of 3.6, 3.8, 3.9, 4.1, 4.7 and 5.4 MeV. Data from Refs [11-13]. For neutron energies of 3.6, 3.8, and 3.9 MeV, the solid curves represent our "best fit" to all of the angular distributions using a symmetric saddle point shape and the dashed curves show the best fit using an asymmetric saddle point shape. Dot-dash curve for the 3.8 MeV data represents the best fit omitting 5/2 states from the single particle spectrum. For the higher neutron energies, the solid curves represent our best fit using a statistical description of the transition nucleus.

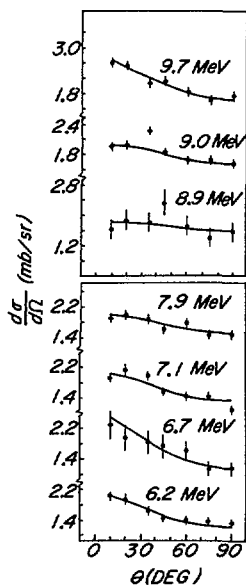


FIG.3. Fission fragment angular distributions for the $^{226}\text{Ra} (n, f)$ reaction for incident neutron energies of 6.2, 6.7, 7.1, 7.9, 8.9, 9.0, and 9.7 MeV. Data from Refs [11-13]. The solid curves represent our "best fit" calculations.

which characterize these states or the level density parameter a_f and the K_0^2 value were determined by choosing the values of these parameters which gave the best fit to the experimental data of Babenko and co-workers [11,12,13] shown in Figures 1, 2 and 3.

II. Theoretical Framework of Calculations

The general theoretical formalism used in the calculations was the same as that outlined by Huizenga et al. [14]. The cross-section for neutron-induced fission of an even-even nucleus through a specific state of the transition nucleus of given (K, J, π) is

$$\sigma_f(K, J, \pi) = \pi \chi^2 \frac{(2J+1)}{2} T_{\ell J}(E_n) \frac{2T_f(K, J, \pi)}{\sum_K 2T_f(K, J, \pi) + T_\gamma(E, J, \pi) + \sum_{E', \ell, J'} T_{\ell, J'}(E')}$$

where E_n is the incident neutron energy, χ the reduced wavelength of the neutron, T_f , T_γ , and $T_{\ell J}$ are the transmission coefficients for fission, γ -ray emission and neutrons of orbital angular momentum ℓ populating a state of total angular momentum J , respectively. The factor of 2 multiplies T_f because of the double degeneracy of all $K \neq 0$ states. The total fission cross-section, σ_f^{total} , is then given as

$$\sigma_f^{\text{total}} = \sum_{K, J, \pi} \sigma_f(K, J, \pi)$$

The fragment angular distributions were given then by the expression

$$W_K(\theta) = \sum_{J, K, \pi} \sigma_f(J, K, \pi) W_{KM}^J(\theta)$$

where the fragment angular distribution associated with fission through a given transition state, $W_{KM}^J(\theta)$, has been described previously [14].

For $E_n \leq 3.9$ MeV, the fission transmission coefficients, T_f , were calculated from the Hill-Wheeler expression for the penetrability of an inverted parabolic fission barrier as

$$T_f(J, K, \pi, E) = \{1 + \exp[2\pi(E_f(J, K, \pi) - E_n)/\hbar\omega]\}^{-1},$$

where $E_f(J, K, \pi)$ is the fission barrier height (relative to the neutron binding energy) associated with the state (J, K, π) of the transition nucleus, and $\hbar\omega$ is the barrier curvature. The barrier height $E_f(J, K, \pi)$ was calculated using the expression

$$E_f(J, K, \pi) = E_0 + (\hbar^2/2\mathcal{J}_1) [J(J+1) - \alpha(-1)^{J+\frac{1}{2}}(J+\frac{1}{2})\delta_{K, \frac{1}{2}}]$$

where E_0 is a constant corresponding to the base of the rotational band, \mathcal{I}_1 is the effective moment of inertia about an axis of rotation perpendicular to the nuclear symmetry axis, α is the familiar decoupling constant for the $K = \frac{1}{2}$ band, and $\delta_{K,J}$ is the Kronecker δ . The values of K, π chosen for each state of the transition nucleus govern the allowed values of J in the rotational band and the allowed values of ℓ , the orbital angular momentum, to reach a given J . We wish to emphasize that this choice of an inverted parabolic shape for the fission barrier is a special assumption made for the ^{227}Ra nucleus based upon theoretical estimates of an extremely small inner barrier and this choice would not, in general, be expected to be valid for heavier nuclei.

As recently pointed out by Vandenbosch [15], the choice of the values of (J, π) in the rotational band associated with a given K state is somewhat ambiguous. If the transition nucleus has a reflection symmetric shape, then one would expect the usual form of the allowed values of (J, π) for a rotational band, i.e., $0+, 2+, 4+, 6+ \dots$ or $3/2-, 5/2-, 7/2-, \dots$. However, if, as predicted by calculations [2,6], the transition nucleus ^{227}Ra has an asymmetric shape, then the number of levels in the rotational bands are doubled. For example, asymmetric e-e nucleus rotational bands have the form $0+, 1-, 2+, 3-, 4+, 5-, \dots$ while odd-A nucleus rotational bands have the form $3/2\pm, 5/2\pm, 7/2\pm, \dots$. In the odd-A case, levels of both parity are degenerate due to the lack of reflection symmetry in the nucleus. Thus, each (K, J) level is four-fold degenerate, i.e., \pm parity and $\pm K$ value. Although some theoretical predictions favor an asymmetric shape for the ^{227}Ra transition nucleus, we do not feel that we can a priori rule out the symmetric transition nucleus. We have therefore carried out calculations using both assumptions for $E_n \leq 3.9$ MeV.

For $E_n \geq 4.1$ MeV, insufficient experimental data is available to allow a statistically significant specification of the single particle states of the transition nucleus. For these energies, a statistical description of the level density of the transition nucleus was used. Specifically, one calculated T_f as

$$T_f(K, J, \pi, E) = \frac{U - B_f \int_0^{\infty} \rho_f(E, K, J, \pi) T_f'(E) dE}{\sum_{K=-I_{\max}}^{I_{\max}} \exp[-K^2/2K_0^2]}$$

where $\rho_f(E, K, J)$ is the density of levels with quantum numbers K, J and π at energy E . The compound nucleus excitation energy is U and the fission barrier height is B_f . $T_f'(E)$ represents a Hill-Wheeler penetrability factor. The level density was parameterized in Fermi gas form as

$$\rho_f(E, K, J) = \frac{1}{24\sqrt{2}} \frac{(2J+1)}{a_f^{1/4} E^{5/4} \sigma^3} \exp(2\sqrt{aE} - \frac{(J+1/2)^2}{2\sigma^2} - \frac{K^2}{2K_0^2})$$

where a_f , the level density parameter, and K_0^2 are varied as free parameters to give the best fit simultaneously to the energy variation of the fission cross-section and angular distribution. The total level density $\rho_f(E, K, J)$ was assumed to consist of equal numbers of positive and negative parity levels.

In specifying the parameters to be used in the above equations $\hbar\omega$ was assumed to be 0.4 MeV, while the spin cutoff parameter, σ , was calculated from the expression

$$\sigma^2 = \frac{\mathcal{J}_1 T}{\hbar^2}$$

where \mathcal{J}_1 was taken from the estimates of Brack et al. [6] ($\frac{\hbar^2}{2\mathcal{J}_1} \approx 2$ keV). The nuclear temperature, T , was calculated using the expression

$$\frac{1}{T} = \sqrt{\frac{af}{E}} - \frac{3}{2E}$$

The γ -ray transmission coefficients, $T_\gamma(E, J, \pi)$, for γ -ray decay of the compound nuclear state with total angular momentum J , parity π and excitation energy, U , were calculated using the formalism outlined previously by others [16,14].

The procedure which we decided to follow in order to account for the residual nucleus is to treat these residual levels in a nondiscrete, statistical manner, accounting for every $J\pi$ value individually. The overall effect of this assumption is that outgoing neutron transmission coefficients are now replaced by "compound transmission coefficients". The neutron channel summation in the denominator of the Hauser-Feshbach expression would then be replaced in the following way

$$\sum_{E'} \sum_{\ell' j'} T_{\ell' j'}(E') \rightarrow \sum_{J\pi} \sum_{\ell' j'} \int_0^E n_{T_{\ell' j'}}(E_k) \rho_{I\pi}(E_n - E_k) dE_k$$

where $\rho(E_n - E_k)$ is the level density at an excitation energy equal to the incident neutron kinetic energy minus that of the outgoing neutron.

No attempt was made in the calculations to account for level width fluctuation effects [16] because to do so would be inconsistent with use of neutron transmission coefficients based on optical model search codes not incorporating the Moldauer theory. Individual neutron transmission coefficients were taken from the compilation by Meldner and Lindner [17] corresponding to $A = 232$, the only tabulated value in this region. A check upon the appropriateness of these transmission coefficients was made by using them to calculate the energy variation of the total reaction cross-section for $^{232}\text{Th} + n$. Quite good agreement was obtained between the calculations and the experimental data of Batchelor et al. [18]. Level densities for the residual nucleus were calculated using the Gilbert and Cameron level density expressions [19] with some notable changes. The Gilbert and

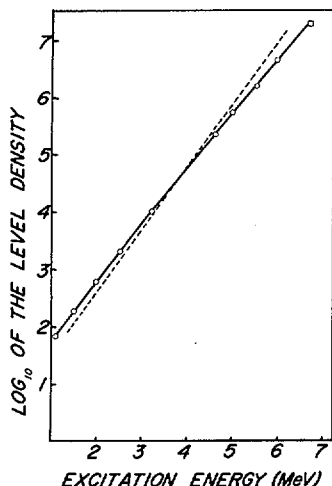


FIG.4. Level density of the residual nucleus ^{226}Ra as a function of excitation energy. Solid line represents our best fit to the experimental data (circles) for ^{232}Th , the dashed line represents the Gilbert and Cameron [19] prediction.

Cameron constants, E_0 and T , in the constant temperature portion of the level density expression and the level density parameter, a , in the Fermi gas portion of the level density expression were determined in a fit to the experimental data [18,20] on level densities for ^{232}Th . Furthermore, the transition between the constant temperature and Fermi gas forms of the level density was assumed to take place at 3.0 MeV excitation energy. A spin dependence was added to the level density expression below 3.0 MeV. The fit of the modified Gilbert and Cameron formula to the experimental level density data is shown in Figure 4 and was found to be quite good. The level density parameter a_n was found to vary strongly with energy as shown in Figure 5. The best values for the other constants were determined to be $T = 0.422$ MeV and $E_0 = -0.397$ MeV. The calculated values of the (n,γ) cross-section agreed well with experimental values of this cross-section [21] in the energy range tested, $3.6 \leq E_n \leq 6.4$ MeV.

III. Results of the Calculations

We have attempted to fit the energy variation of the total fission cross-section and fragment angular distributions in the energy region from $E_n = 3.6$ MeV to $E_n = 11.6$ MeV. Using the theory described above and after an extensive search of the possible number of accessible states of the transition nucleus and the possible values of the free parameters, K , π , E_0 and $\hbar\omega$ for each state, we have concluded that the experimental data in the energy region from $E_n = 3.6$ MeV to $E_n = 3.9$ MeV can be fitted by assuming the ^{227}Ra transition nucleus single particle spectrum shown in Figure 6 and Table I. The best fits to the data in this region are shown in Figures 1 and 2.

TABLE I. PARAMETERS DESCRIBING THE LOW-LYING SINGLE PARTICLE STATES IN THE ^{227}Ra TRANSITION NUCLEUS

Symmetric Saddle Point Deformation			
State No.	(K, π)	E_0 (MeV)	$\hbar\omega$ (MeV)
1	3/2-	3.65	0.4
2	1/2+	3.68	0.75
3	5/2 \pm	3.8	0.4
4	1/2 \pm	3.88	~ 0.15
Asymmetric Saddle Point Deformation			
State No.	K	E_0 (MeV)	$\hbar\omega$ (MeV)
1	3/2	3.76	0.6
2	5/2	3.83	0.5
3	1/2	3.92	1.0

To guide us in a quantitative evaluation of the agreement between theory and experiment, we used the χ^2 criterion to reject unsatisfactory hypotheses. Each hypothesis tested consisted of two parts, the calculational framework described above and a particular choice of the free parameters K, E_0 , $\hbar\omega$, and π . Unsatisfactory hypotheses were rejected at the 0.05 level of significance. Although we reached reasonable choices of K, E_0 , $\hbar\omega$, and π , we made only a limited search of different forms of the calculational framework. In particular, we found that a $\pm 10\%$ variation in Γ_n , and a factor of two change in the decoupling constant α and in the rotational constant $\frac{\hbar^2}{2I}$ had a negligible effect upon the calculated transition state spectrum. Therefore, we are saying that using the theoretical approximations described above as a basis for calculation, we can reject all unsatisfactory values of the free parameters with only one chance in twenty of being in error.

In making our search for acceptable hypotheses to describe the data, we have assumed that we should use the minimum number of accessible states of the transition nucleus at any given energy. This assumption, made for simplicity and precision in the determination of the free parameters, means that there may be many hypotheses involving weakly excited states (i.e., high spin states) which will fit the data. We simply cannot say anything about them.

Examining the data in Figures 1 and 2, we can see qualitatively the 3.6 MeV angular distribution shows the characteristic pattern of fission through a $K = 1/2$ band. The parity of the $K = 1/2$ state was found to be + rather than - because the required $K = 3/2$ and $K = 5/2$ strength needed to fit the 3.8 MeV data would not be achieved if a very strongly excited $K = 1/2^-$ state were present. The 3.8 MeV angular distribution shows an intermediate angle peaking characteristic of $K > 1/2$ states. The peak at $\sim 45^\circ$ in the angular distribution requires more than a $K = 3/2$ state to reproduce it. Significant $K = 5/2$ strength must be present to cause peaking at such angles as shown in Figure 2. The parity of the $K = 3/2$ state was chosen to be - to allow the necessary strength for this fission channel to fit the angular distribution and cross-section data. It was found that both $K = 5/2^-$ and $K = 5/2^+$ states would allow statistically significant fits to the data, so the parity of the $K = 5/2$ state has not been determined. The 3.9 MeV angular distribution data show the signature of a $K = 1/2$ state whose parity could not be determined in a statistically significant manner. For $E_n \geq 4.1$ MeV, the quantity and quality of the data is not sufficient to sustain statistically significant further analysis in terms of the single particle levels of the ^{227}Ra nucleus.

Many detailed searches for best fits to the data have indicated that the positions of the single particle states given in Table I should be regarded as uncertain to $\leq \pm 0.1$ MeV for the symmetric case and $\leq \pm 0.05$ MeV for the asymmetrically deformed case. The values of the barrier curvature $\hbar\omega$ should be regarded as uncertain to ± 0.2 MeV. Assuming a neutron binding energy of 4.5 MeV for ^{227}Ra , this calculation places an upper limit on the fission barrier of ~ 8.2 MeV.

The analysis of the higher energy data was carried out using the statistical description of the transition state nucleus described earlier. The fission level density parameter, a_f , and K_0^2 parameter were determined for each energy by determining the best fit to the available cross-section and angular distribution data. Once again, a χ^2 criterion was used to judge the statistical significance of the results and to assign uncertainties to the K_0^2 values. The best fits to the cross-section and angular distribution data are shown in Figures 1, 2 and 3. The values of a_f determined in the fitting are shown in Figure 5, while the values of K_0^2 are shown in Figure 7. Some checks were made of the sensitivity of the calculated values of a_f and K_0^2 to changes in the barrier curvatures, $\hbar\omega$, and the spin cutoff parameter, σ . The effect of a 0.2 MeV change in $\hbar\omega$ was to produce a 0.5% change in a_f , while a 50% change in σ^2 produced an $\sim 13\%$ change in a_f and no change in K_0^2 . Since second-chance fission should become energetically possible for $E_n \approx 9$ MeV, the a_f and K_0^2 results for energies of this magnitude and higher should be considered with this in mind. In fact, the rise K_0^2 at 9 MeV can be taken as secondary evidence for the correctness of the assignment of the fission barrier height of ~ 3.7 MeV for ^{227}Ra .

IV. Discussion of Results

The available data on fission barrier heights for the lighter fissioning elements is summarized in Table II along with many calculations of these quantities. The fission barrier height of 8.2 ± 0.1 MeV deduced for the

TABLE II. CALCULATED AND EXPERIMENTAL VALUES OF FISSION BARRIER HEIGHTS (in MeV) FOR THE LIGHTER FISSIONING ELEMENTS

Nucleus	Inner Barrier	Outer Barrier (Symmetric)	Outer Barrier (Asymmetric)	Expt'l	Reference
^{226}Ra	-	-	-	8.5 ± 0.5	Zhagrov et al. [22]
	~ 4.5	~ 10	~ 10	-	Adeev et al. [4]
	4.2	10.5	9.0	-	Moller [2]
	3.7	10.7	-	-	Mosel & Schmitt [23]
		10.2	10.2	-	Pauli [7]
^{227}Ra	-	-	-	8.2 ± 0.1	This work
^{228}Ra	2.4	-	8.2		Brack et al. [6]
	4.2	11.3	8.7	-	Moller [2]
^{230}Th	-	-	-	6.1 inner 6.5 outer	James et al. [24]
	4.0	6.9	9.4	-	Moller [2]
^{232}Th	-	-	-	5.9 inner 6.1 outer	Bjornholm [7]
	3.9	-	6.8	-	Brack et al. [6]
	4.6	10.1	6.7	-	Moller [2]
	3.4	-	6.6	-	Pauli [7]

^{227}Ra transition nucleus agrees well with the value of 8.5 ± 0.5 MeV found by Zhagrov et al. [22] for ^{226}Ra in photofission studies. (Throughout this discussion, we shall assume that odd-even effects, i.e., "specialization energies", are small for these nuclei and will thus compare e-e and odd-A nuclei.) The value of 8.2 ± 0.1 MeV for the ^{227}Ra fission barrier height is ~ 1 -2 MeV lower than most calculations of fission barrier heights in this region (with the exception of the calculations of Brack et al. [6] who predict a fission barrier height of 8.2 MeV for ^{228}Ra). In comparing the agreement between theory and experiment for Ra and Th isotopes, one may be seeing systematic theoretical overestimation of fission barriers as the (Z,A) of the fissioning system decreases, i.e. as the

transition state nucleus becomes more deformed. One may speculate that this difference between theory and experiment is due to the fact that ground state shell corrections in this region may be positive (as indicated by neutron level density data discussed later) while the calculations indicate negative ground state shell corrections.

Figure 6 shows the spectrum of single particle states found for the ^{227}Ra transition nucleus along with various theoretical predictions of the expected neutron single particle state ordering in ^{227}Ra . The "predictions" represent our best deductions based upon the single particle level schemes shown in References [2,5,25]. The best agreement between the deduced single particle levels and those predicted by various authors appears to occur with the single particle level scheme of Bolsterli et al. [25], although some similarities can be found between prediction and experiment in all the level schemes. In the calculations by Bolsterli et al., the average positions and relative orderings of the levels appear to be well-reproduced although the level spacings are not well-reproduced.

Figure 7 shows the values of K_0^2 deduced in this work compared with the calculated values of K_0^2 based upon single particle level schemes and the agreement between theory and experiment seems to be good. The rise in the theoretically calculated value of K_0^2 at an excitation energy relative to the fission barrier of ~ 3.3 MeV is due to the formation of the three quasi-particle state. From this rise in K_0^2 , which seems to be verified by the data, one can infer a value of the energy gap parameter for the ^{227}Ra transition nucleus, $2\Delta_f$, of ~ 2.7 MeV as compared to the equilibrium value, $2\Delta_0 = 1.5$ MeV.

Figure 5 shows the values of the level density parameters, a_n and a_f , for the residual ^{226}Ra nucleus and the transition nucleus ^{227}Ra , respectively, as a function of excitation energy, along with the a_f/a_n ratio. The increase of a_f and a_n at the lowest excitation energies can be attributed to positive shell corrections for both the transition nucleus and the residual nucleus [27]. Such positive shell corrections are associated with a greater than average single particle level density near the Fermi energy.

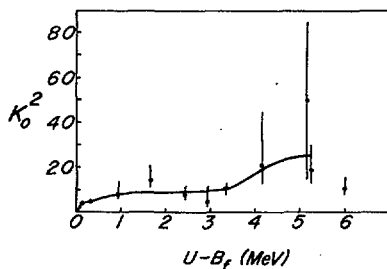


FIG. 7. Deduced values of K_0^2 versus excitation energy above the fission barrier ($B_f = 3.7$ MeV) for ^{227}Ra . Solid curve represents calculation of Ippolitov and co-workers [26].

As the excitation energy increases, single particle states further away from the Fermi energy begin to play a greater role and the values of a_f and a_n decrease. The magnitude of the a_f/a_n ratio is not as large as that observed for other fissioning systems because of the apparent positive shell correction for the residual nucleus ^{226}Ra ground state deformation. Usually the residual nucleus ground state deformation has a negative shell correction, a lower than average single particle level density and a decrease in a_n at the lowest excitation energies. It is interesting (and quite speculative) to note that the apparent leveling off of the a_f/a_n ratio occurs at an excitation energy above the fission barrier corresponding to the three-quasi-particle excitation threshold. The plateau in the cross-section between 4.1 and 4.7 MeV is apparently due to a momentary constancy in Γ_f/Γ_n in this region, which is made possible by the fact that a_f and a_n both increase at low excitation energies.

The data of Nobles and Leachman [10] show that in the energy region $4 \leq E_n \leq 10$ MeV the fragment mass distribution (as inferred from their fragment kinetic energy spectra) for ^{226}Ra (n, f) changes from one of predominantly asymmetric character, to equal amounts of symmetric and asymmetric fission, to a distribution in which symmetric fission dominates. In our analysis of the structure of the ^{227}Ra transition nucleus in this energy region, we see no apparent unusual changes in the structure of the transition nucleus.

REFERENCES

- [1] NIX, J.R., Calculations of fission barriers for heavy and superheavy nuclei, *Ann. Rev. Nucl. Sci.* 22 (1972) 65.
- [2] MÖLLER, P., *Nucl. Phys.* A192 (1972) 529.
- [3] MÖLLER, P., NILSSON, S.G., *Phys. Lett.* 31B (1970) 283.
- [4] ADEEV, G.D., GAMALYA, I.A., CHERDANTSEV, P.A., *Sov. J. Nucl. Phys.* 14 (1972) 637.
- [5] PASHKEVICH, V.V., Twentieth Annual Conference on Nuclear Spectroscopy, Leningrad, 1970 (as cited in Ref.[26]).
- [6] BRACK, M., DAMGAARD, J., JENSEN, A., PAULI, H., STRUTINSKY, V., WONG, C., *Rev. Mod. Phys.* 44 (1972) 320.
- [7] PAULI, H. *Phys. Rep.* 7 (1973) 35.
- [8] PERRY, D.G., FAIRHALL, A.W., *Phys. Rev.* C4 (1971) 977.
- [9] KONECNY, E., SPECHT, H.J., WEBER, J., Paper IAEA-SM-174/20, these Proceedings, Vol.2.
- [10] NOBLES, R.A., LEACHMAN, R.B., *Nucl. Phys.* 5 (1958) 211.
- [11] BABENKO, Y.A., NEMILOV, Y.A., SELITSKII, Y.A., FUNSHTEIN, V.B., *Sov. J. Nucl. Phys.* 7 (1968) 186.

- [12] BABENKO, Y.A., IPPOLITOV, V.T., NEMILOV, Y.A., SELITSKII, Y.A., FUNSHTEIN, V.B., Sov. J. Nucl. Phys. 10 (1969) 133.
- [13] BABENKO, Y.A., NEMILOV, Y.A., PLESKACHEVSKII, L.A., SELITSKII, Y.A., FUNSHTEIN, V.B., Sov. J. Nucl. Phys. 11 (1970) 560.
- [14] HUIZENGA, J.R., BEHKAMI, A.N., ROBERTS, J.H., Physics and Chemistry of Fission, IAEA, Vienna (1969) 403.
- [15] VANDENBOSCH, R., private communication.
- [16] LOVELAND, W., HUIZENGA, J.R., BEHKAMI, A.N., ROBERTS, J.H., Phys. Lett. 24B (1967) 666.
- [17] MELDNER, H., LINDNER, A.Z., Z. Physik 180 (1964) 362.
- [18] BATCHELOR, R., GILBOY, W.B., TOWNLE, J.H., Nucl. Phys. 65 (1965) 236.
- [19] GILBERT, A., CAMERON, A.G.W., Can. J. Phys. 43 (1965) 1446.
- [20] VOROTNIKOV, P.E., Sov. J. Nucl. Phys. 9 (1969) 179.
- [21] HUGHES, D.J., SCHWARTZ, R.B., USAEC Rep. BNL-325 (1958).
- [22] ZHAGROV, E.A., NEMILOV, Y.A., SELITSKII, Y.A., Sov. J.
- [23] MOSEL, U., SCHMITT, H.W., Nucl. Phys. A165 (1971) 73.
- [24] JAMES, G.D., LYNN, J.E., EARWACKER, L.G., Nucl. Phys. 189 (1972) 225.
- [25] BOLSTERLI, M., FISET, E.O., NIX, J.R., NORTON, J.L., Phys. Rev. C5 (1972) 1050.
- [26] IPPOLITOV, V.T., NEMILOV, Y.A., SELITSKII, Y.A., FUNSHTEIN, V.B., Sov. J. Nucl. Phys. 14 (1972) 526.
- [27] VANDENBOSCH, R., MOSEL, U., Phys. Rev. Lett. 28 (1972) 1726

DISCUSSION

J.R. NIX: Although most calculations do not reproduce both symmetric and asymmetric saddle points for nuclei in this region, the potential energy surface for ^{227}Ra probably contains both types of saddle points. Would the simultaneous introduction of symmetric and asymmetric saddle points complicate your analysis?

W. LOVELAND: No, it certainly would be possible to include simultaneous symmetric and asymmetric saddle point deformations in our analysis. I do not think, however, that our results would be significantly different in that case, since we obtain similar results for the single particle spacings and spins using the two forms of the rotational bands of the transition nucleus.

J. R. HUIZENGA: In making your comparison between the experimental and theoretical single particle levels at the saddle, have you taken into account the effects of the Coriolis interaction? These forces will perturb considerably the experimental spectrum.

W. LOVELAND: Except for the usual effects of the $K = \frac{1}{2}$ bands, we have neglected the effect of Coriolis coupling in our analysis. The effect of such coupling (between states of $\Delta K = 0, \pm 1$) might shift the overall positions of the single particle states by a small amount but should not affect, to any great extent, our general conclusions concerning the fission barrier height and transition-nucleus single particle level ordering.

H. C. BRITT: Since the experimental barriers for Th isotopes indicate equal-height barriers as compared to theoretical calculations, which predict the second barrier to be much higher, it seems possible that a similar effect might be present in radium. Would this seriously affect your calculations?

W. LOVELAND: Yes, our analysis is predicated on the premise that the outer barrier is so much higher than the inner barrier that the inner barrier can be neglected in the calculations. However, if the barriers were of similar height, this would imply a very serious failure of the theoretical calculations inasmuch as Brack and co-workers, for example, predict an inner-barrier height of 2.8 MeV compared to an outer-barrier height of 8.2 MeV for nuclei in this region.

H. J. SPECHT: What is the explanation for the apparent plateau in the fission cross-section between 4.1 and 4.7 MeV?

W. LOVELAND: This plateau is apparently due to a momentary constancy in Γ_f/Γ_n in this region, which is made possible by the fact that a_f and a_n both increase at low excitation energies.

H. J. SPECHT: Would you then expect it to be influenced by the angular momentum distribution of the reaction? As reported¹ in Paper IAEA-SM-174/20, we have studied the ^{226}Ra (d, pf) reaction leading to the same fissioning compound nucleus and we do not observe this structure at all.

W. LOVELAND: I am frankly surprised that you do not see this plateau in the ^{226}Ra (d, pf) reaction. I would not have expected the difference in reaction mechanism between the (d, pf) and (n, f) reactions to cause the disappearance of the plateau. As far as the impact of such a finding upon our analysis goes, the absence of a plateau in this region would merely decrease slightly the values of a_f in this energy region.

¹ KONECNY, E., SPECHT, H. J., WEBER, J., Paper IAEA-SM-174/20, these Proceedings, Vol. 2.

SUBBARRIER PHOTOFISSION OF ^{238}U

A. ALM, T. KIVIKAS, L.J. LINDGREN

Institute of Physics,
University of Lund,
Lund, Sweden

Abstract

SUBBARRIER PHOTOFISSION OF ^{238}U .

Experimental yield curves for symmetric and asymmetric photofission of ^{238}U in the subbarrier energy region are analysed in the framework of a double-hump fission model, where the potential energy is described by three parabolas. In the model, the outer fission barrier is assumed to depend on the type of deformation of the nucleus, thus leading to a coupling between symmetric and asymmetric fission. It is shown that the model reproduces well the experimental data in an energy region where the fission cross-section varies by 5 orders of magnitude. The asymmetric yield can be described by one dominant $1^-,0$ channel with a resonance at 4.6 MeV and one $2^+,0$ channel. The information about the symmetric fission is however very limited, except that a strong resonance at about 5.8 MeV is clearly observed. The maximum at 6 MeV in the valley-to-peak ratio is interpreted as an effect of this resonance in the symmetric yield and not as an effect of neutron competition.

INTRODUCTION

During the past seven years great advances in our understanding of the physics connected with the fission process have been made. These advances have been triggered by new theoretical means of calculating the potential energy of a nucleus as a function of its shape and particle number. According to Strutinski [1], the potential energy for deformation of a nucleus in the actinide region is given by a "double-hump" barrier, i.e. there exists a secondary minimum with a deformation greater than that of the ground state. Approximate one-dimensional calculations with this model explain the occurrence of long-lived fission isomers, as well as certain types of resonances in the fission cross-section. Because of this, the Strutinski theory has been widely accepted in the interpretation of experimental fission data. More detailed calculations with the Strutinski theory, in which account is taken of several deformation coordinates, have yielded three-dimensional surfaces [2] (see fig 1). In these calculations, the deformation coordinates have been divided into two groups, symmetric and asymmetric. This leads to the result that the outer deformation barrier is considerably higher for symmetric fission than for asymmetric. It has also been demonstrated that the inner barrier is common to asymmetric and symmetric fission.

The purpose of this paper is to see to what extent it is possible to find agreement between low-energy fission yield curves for asymmetric and symmetric photofission of ^{238}U and model calculations performed with a somewhat refined model based on these recent theoretical advances.

EXPERIMENTAL PROCEDURE AND RESULTS

The experiment [3] was performed with bremsstrahlung photons produced in a 6.5-MeV microtron. The irradiations took place in the vacuum tank of the microtron. The average current was 20-50 μA and, as target, samples of natural uranium were used. The fission yields have been determined by β -counting of chemically separated isotopes characterizing symmetric and asymmetric fission yields. The activities of ^{115}Cd , ^{117}Cd giving symmetric

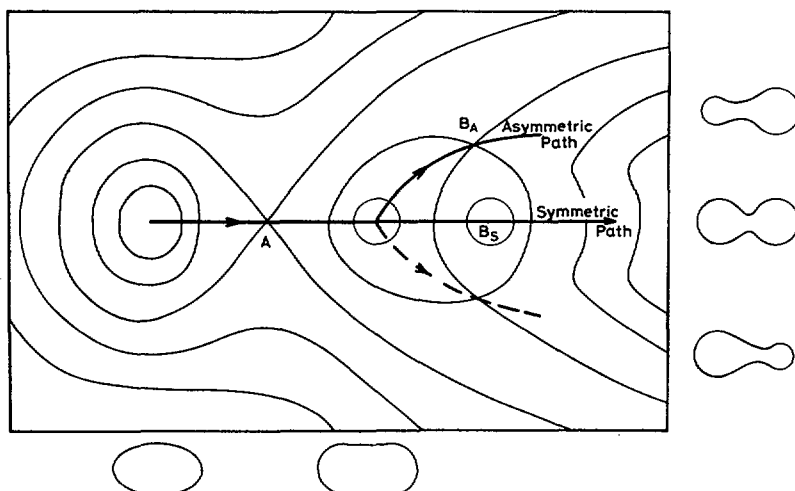


FIG.1. Schematic plot of a deformation energy surface showing the paths for asymmetric and symmetric fission. A indicates the common inner fission barrier, B_A and B_S are the outer fission barrier for asymmetric and symmetric fission respectively.

fission yield were measured for incident electron energies between 5.0 MeV and 6.5 MeV and the activity of ^{139}Ba giving the asymmetric fission yield was measured between 4.6 MeV and 6.5 MeV. The yield curves are shown in figures 2 and 3.

PHOTOFISSION AT LOW ENERGIES

The photofission process at low energies is assumed to be a two-step process. The nucleus absorbs a photon and the compound nucleus thus created decays by fission or by gamma deexcitation or neutron emission

Photo-absorption

It was pointed out by Bohr [4] that the low-energy fission channels for an even-even nucleus should be describable in terms of collective excitations similar to the known collective bands of an actinide nucleus in its ground state deformation. Thus, for ^{238}U we assume that the fission process takes place mainly through 1^- and 2^+ fission channels.

A great drawback when analysing photofission data is the absence of direct, reliable data on the cross-sections for dipole and quadrupole absorption. One has in general to rely mainly on the electrodynamical estimate $(R/\lambda)^2 \approx 1/50$ for the ratio $\sigma_{\gamma\text{abs}}^{2^+}/\sigma_{\gamma\text{abs}}^{1^-}$, where $2\pi\lambda$ is the wavelength of the photon and R is the nuclear radius. For the energy dependence, the best one can do in the absence of direct data is to extrapolate absorption cross-sections from data at higher energies, keeping the ratio constant. We have simply assumed the approximately exponential energy-dependence given by Khan and Knowles [5] and used the formula

$$\sigma_{\gamma\text{abs}}^{2^+} \approx \left(\frac{R}{\lambda}\right)^2 \sigma_{\gamma\text{abs}}^{1^-}$$

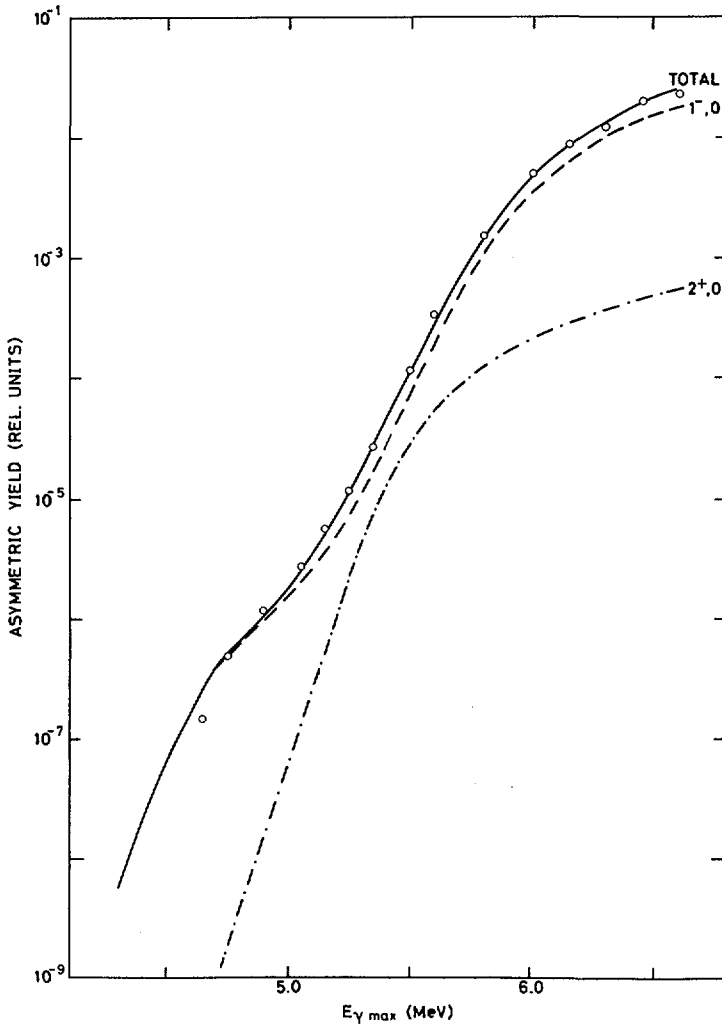


FIG.2. The calculated asymmetric yield curve (solid line) with its channel decomposition compared with the experimental data.

The explicit formula is

$$\sigma_{\gamma \text{ abs}}^{1-} = 1.65 \cdot 10^{-3} \exp (.72 E_{\gamma})$$

Competing decay channels

The possible decay modes of the compound nucleus apart from fission are gamma deexcitation and neutron emission.

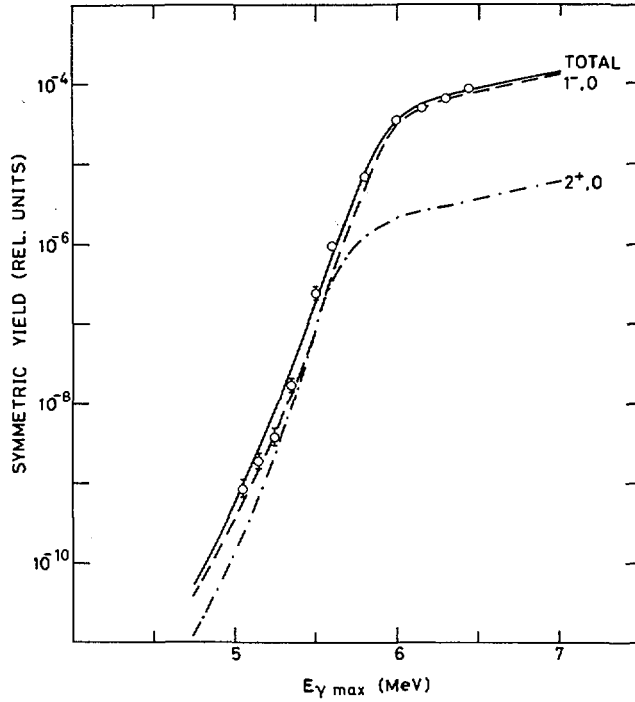


FIG.3. The calculated symmetric yield (solid line) curve with its channel decomposition compared with the experimental data.

The gamma radiation width $\Gamma_Y^{I^\pi}$ is taken from Huizenga and Britt [6]. For the neutron emission width

$$\Gamma_n^{I^\pi} = \frac{D^{I^\pi}}{2\pi} \sum_{\alpha l j} T_{lj}$$

is used, where D^{I^π} is the average distance between levels in the compound nucleus with spin and parity I^π , and T_{lj} is the transmission coefficient for emission of a neutron with angular momentum l and channel spin j . The summation is performed over all combinations of j , l and all available levels α in the ^{237}U nucleus provided that total angular momentum and parity are conserved. The transmission coefficients are taken from Emmerich [7]. At low neutron energies the energy dependence of the transmission coefficient is given by

$$T_{lj} \sim K_{lj} (E_Y - S_n - E_\alpha)^{\frac{2l+1}{2}}$$

Here S_n is the neutron binding energy, E_α is the excitation energy of the ^{237}U nucleus and K_{lj} is a constant.

The fission model

The model is developed on the assumption that the fission process is governed only by barrier transmission. The two-step fission cross-section formula is given by

$$\sigma_f(E_Y) = \sum_I \sigma_{Yabs}^{I\pi} \frac{\sum_K \Gamma_f^{I\pi K}}{\sum_K \Gamma_f^{I\pi K} + \Gamma_Y^{I\pi} + \Gamma_n^{I\pi}}$$

where $I = 1, 2$, π is the parity and the symbols $\Gamma_f^{I\pi K}$, $\Gamma_Y^{I\pi}$ and $\Gamma_n^{I\pi}$ denote, respectively, the widths for fission, γ -deexcitation and neutron emission, the only decay modes possible.

K-mixing is not included in our analysis since our experimental yields can be described mainly by $K = 0$ channels.

According to Bohr-Wheeler [8] the average fission width of a channel is

$$\Gamma^I = \frac{D^I}{2\pi} P^I$$

where D^I is the average distance between compound levels with the same spin and P^I is the barrier penetration.

The expression for barrier penetration [9] is

$$P(E_Y) = \frac{P_A P_B}{4} f$$

where

$$f = \left\{ \cos^2 x \left[\cosh y + \sinh y \frac{P_A + P_B}{4} \right]^2 + \sin^2 x \left[\sinh y + \cosh y \frac{P_A + P_B}{4} \right]^2 \right\}^{-1}$$

P_A and P_B are the penetration of the inner and outer fission barriers respectively and are, according to Hill-Wheeler [10], for a parabolic barrier given by

$$P_A(E_Y) = \left[1 + \exp\left(\frac{2\pi}{\hbar\omega_A}(E_Y - E_A)\right) \right]^{-1}$$

where E_A is the barrier height and $\hbar\omega_A$ is the barrier transparency with

$$\omega_A = \sqrt{\frac{C}{B}}$$

where C is the curvature and B is the mass parameter. In the analysis, a double-hump fission barrier in the form of three conjugate parabolas has been used. $P_A P_B / 4$ is known as P_{min} , the penetration in the absence of resonances. The factor f in the $P(E_Y)$ -expression is due to the fact that

in the double-hump description one expects resonances. If there was no coupling between fission and other degrees of freedom, one would, according to the WKB-approximation, have $f = \{\sin^2 x + \cos^2 x\}^{-1}$, where

$$x(E_Y) = \text{Re } \varphi(E_Y)$$

with

$$\varphi(E_Y) \approx \frac{\pi}{\hbar\omega_{II}} (E_Y - E_{II} + iW_{II})$$

Here, E_{II} is the energy above the ground state of the secondary minimum and $\hbar\omega_{II}$ is the curvature of the parabola describing the secondary minimum.

We get resonances for the values

$$x(E_Y) = \pi(n + \frac{1}{2}) \quad n = 0, 1, 2, \dots$$

However energy can "leak" from fission to other degrees of freedom and this is taken care of by the complex part

$$y(E_Y) = \text{Im } \varphi(E_Y)$$

in the potential, which results in damping and broadening of the resonances.

The fission cross-section is further split into two parts, one asymmetric $\sigma_f^a(E_Y)$ and one symmetric $\sigma_f^s(E_Y)$, and we get the final expressions

$$\sigma_f^a(s)(E_Y) = \sum_{I^\pi} \sigma_{Yabs}^{I^\pi} \frac{\Gamma_f^{I^\pi a(s)}}{\Gamma_f^{I^\pi a} + \Gamma_f^{I^\pi s} + \Gamma_n^{I^\pi} + \Gamma_Y^{I^\pi}} \quad (K = 0)$$

In the model, it is assumed that the inner barrier is common to the symmetric and the asymmetric channels with the same spin and parity and that the fission path is split at the passage of the outer barrier, as indicated in figure 1, in agreement with the calculations of Möller [2].

The asymmetric (symmetric) cross-section can be written

$$\sigma_f^a(s)(E_Y) = \sum_{I^\pi} \sigma_{Yabs}^{I^\pi} \frac{P_f^{I^\pi a(s)} \cdot F^{I^\pi}}{P_f^{I^\pi a} + P_f^{I^\pi s} + P_n^{I^\pi} + P_Y^{I^\pi}}$$

where F^{I^π} is the level density fluctuation factor, which is assumed to be equal to 1.

METHOD OF ANALYSIS

Taking into consideration the fact that the γ -source is a bremsstrahlung beam, the fission yield $Y(E_{\gamma\max})$ as a function of maximum bremsstrahlung energy $E_{\gamma\max}$ is given by

$$Y(E_{\gamma\max}) = C' \int_0^{E_{\gamma\max}} \sigma_f(E_\gamma) n(E_\gamma, E_{\gamma\max}) dE_\gamma$$

where $\sigma_f(E_\gamma)$ is the fission cross-section, $n(E_\gamma, E_{\gamma\max})$ is the bremsstrahlung spectrum giving the number of photons of energy E_γ for incident electron energy $E_{\gamma\max}$ and C' is a constant.

Comparison of the experimental results and the theoretical calculations can be based on either the fission cross-sections or the fission yield curves. We have chosen to make use of the latter approach by performing a theoretical model calculation for $\sigma_f(E_\gamma)$, folding in the bremsstrahlung spectrum to obtain the fission yield for comparison with experimental yields. With this method, we can avoid ambiguous solutions when the fission cross-sections are evaluated from the integral equation by a photo-difference method.

For the bremsstrahlung spectrum, the thin target form of Schiff [11] has been used because an accurate thick target spectrum describing a particular experimental set-up is difficult to calculate. Although we in our experiment have definitely had a thick target bremsstrahlung spectrum which should be somewhat softer than the Schiff spectrum, no serious changes in the form of calculated yield curves in the subbarrier energy region were obtained by changing the form of the bremsstrahlung spectrum in order to represent better a thick target spectrum. This effect reflects the very rapid rise of the fission cross-section with excitation energy, thus limiting the useful region of the bremsstrahlung spectrum to a very narrow part at the upper end.

Since our experimental data are insufficient to enable us to make self-consistent calculations with the model described, it is necessary to make some simplifying assumptions, and to make extensive use of other experimental and theoretical information in order to reduce the number of parameters in the model. We have therefore restricted ourselves to considering only the lowest channels in symmetric and asymmetric fission.

In the case of symmetric fission we have limited ourselves to discussing different possibilities of explaining the fission yield.

Information about the second well is contained only in the resonant part of the yield curve. The location of the resonances on the energy scale is determined by the depth and curvature of the second well. However, it is not possible, from experimental data, to determine the sequential number of a resonance counted from the bottom of the well, since only resonances not too far from the barrier are observed. Therefore, very little is known of the parameters describing the second well. Furthermore, different types of vibrations might have different well parameters. Therefore we have used a theoretical well depth [2] and chosen a curvature that reproduces our resonant effects, assuming that only two resonances are present in the well.

Asymmetric fission yield

According to theory [2], the outer barrier for ^{238}U is asymmetric in shape and is about 6 MeV high. At this deformation the 0^- and 0^+ bands are degenerate in energy [12]. Recent theoretical calculations including non-axial deformations [13] give a value of 5.6 MeV for the inner ground

state barrier. The lowest $2^+,0$ state is expected to be a few hundred keV below the lowest-lying $1^-,0$ state [6].

Measurements of the angular distributions and total fission yields in bremsstrahlung-induced photofission of ^{238}U [14] indicate that the asymmetric fission goes predominantly through a $1^-,0$ channel in the energy region from 5.5 MeV to 6.0 MeV. As a consequence of the above-mentioned facts we expect the fission process in the subbarrier energy region to be described mainly by $K = 0$ channels. With these assumptions our experimental yield curve for asymmetric photofission is analyzed.

Symmetric fission yield

Very little is known about the character of the symmetric fission barrier. There exists no experimental evidence as to which spin and parity values characterize the exit channels. This lack of knowledge leads to considerable ambiguities in the calculations. It is therefore necessary to limit our discussions to different analysis possibilities and to find the minimum number of channels necessary to reproduce the experimental yield curves.

Some facts can be stated:

1. The theory gives an outer symmetric fission barrier of about 9 MeV height, which is unstable against ϵ_3 and ϵ_5 distortions [2]. This greatly diminishes the possibility of a symmetric 1^- channel in the static description.
2. Some experiments indicate resonance structures in the total fission cross-section of ^{238}U at 5.2 MeV and 5.8 MeV.
3. Since the inner barrier is common to asymmetric and symmetric fission, the symmetric yield must be analyzed jointly with the asymmetric yield.

In order to obtain agreement between calculations with a high symmetric barrier, and experimental data, the swift rise of the experimental yield must be reproduced by a strong resonant effect. This is so, since the nonresonant penetrability.

$$P_{\min} \sim \exp \left[\frac{2\pi}{\hbar\omega_A} (E_Y - E_A) \right] \cdot \exp \left[\frac{2\pi}{\hbar\omega_B} (E_Y - E_B) \right]$$

influences the magnitude of the valley-to-peak ratio to a large extent. The higher the barrier, the greater the curvature parameter. The inverse curvature $(\hbar\omega_B)^{-1}$ influences the energy dependence of P_{\min} and a high barrier E_B will give a weak energy dependence. The steep rise in the yield curve must then be due to a strong resonance. The strength has to be so great that the resonance necessarily must be subbarrier, and can therefore hardly be of $2^+,0$ type, since the inner $2^+,0$ barrier is expected to be less than 5.7 MeV [13]. The strength has to be greater, the higher the barrier. In this connection it may be worth pointing out that it is possible to reproduce the low energy part of the symmetric fission yield curve by pure barrier penetration, but it is then necessary to choose an outer barrier height of 5.8 MeV and a curvature of 0.5 MeV. These parameter values are however in violent disagreement with theory. We have therefore in our calculations assumed a high symmetric barrier. The calculations show that it is impossible to explain the symmetric fission yield curve by making use of only one symmetric channel. In this case, only one resonance is possible between 5.3 and 5.8 MeV, and the form of the yield curve

demands a resonance too broad and too strong to be consistent with our calculations. The inclusion of a second resonance channel greatly improves the agreement between the model calculations and the experimental data.

RESULTS OF MODEL CALCULATIONS

The fit of the asymmetric yield was made with the assumption of a dominant $1^{-},0$ channel. The best fit was obtained with $E_A + E_B = 12.15$ MeV. The curve was found to be rather insensitive to small changes in the relative magnitude of the barrier heights. We have used the values $E_A = 6.1$ MeV and $E_B = 6.05$ MeV, as reported also by [14]. In order to reproduce the yield curve in the deep subbarrier region, it was found necessary to include a resonance at 4.6 MeV with a damping of about 0.05, in agreement with [14].

The effective curvature $(\hbar\omega_{\text{eff}}) = (1/\hbar\omega_A + 1/\hbar\omega_B)^{-1}$ appeared to have a strong influence on the asymmetric yield curve, and we found the value 0.47 MeV to represent our data best. For simplicity, the curvatures of the single barriers were put equal. The influence of resonances between 5 MeV and 6 MeV is expected to be small, due to considerable damping found in other experiments.

Since the outer $1^{-},0$ and $2^{+},0$ barriers are expected to be degenerate in energy in the asymmetric case, the outer $2^{+},0$ barrier height was found immediately. The inner $2^{+},0$ barrier was assumed to be about 5.6 MeV in agreement with recent theoretical calculations [13]. The curvature was

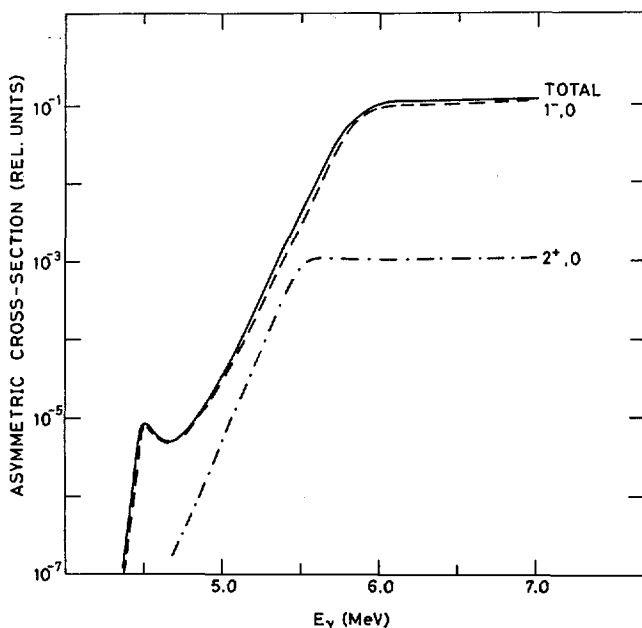


FIG. 4. The asymmetric fission cross-section.

assumed to be about equal to that of the $1^-_{\gamma},0$ channel, with the same simplifying assumption of equality between inner and outer barriers (i.e. $\hbar\omega_B = \hbar\omega_A$). The quadrupole channel thus determined influenced the yield only below 5.5 MeV.

The results of the calculations and a comparison with the experimental yield curve are shown in fig 2. In fig 4 the cross-section for asymmetric fission is shown.

As mentioned above, information about the character of the symmetric barrier is scarce and the calculations are restricted to some typical cases. The outer barrier is known to be about 9 MeV high and the inner barrier is the same as that of the asymmetric case. Starting from this, the symmetric yield was calculated, using one or two channels.

In the one channel approximation, we considered pure quadrupole and pure dipole fission. According to the calculations by Möller [2], the symmetric barrier is unstable against ϵ_3 and ϵ_5 deformations, which makes it hard to understand the existence of a symmetric $1^-_{\gamma},0$ channel. The symmetric quadrupole case however is not restricted in that way. The inner barrier height of 5.6 MeV makes it difficult to obtain resonances strong enough to reach agreement between model calculations and experimental data. Our calculations show that a barrier height of at least 6.0 MeV is needed to produce such resonances. Therefore, the question of the character of the symmetric fission exit channel seems to remain open.

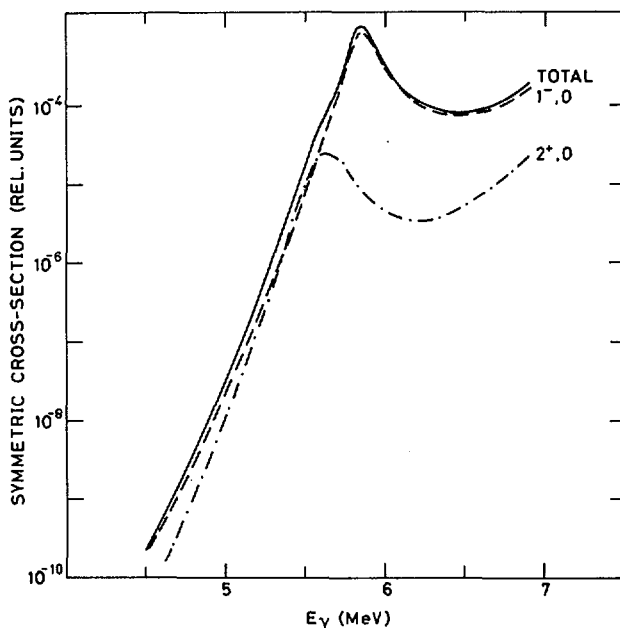


FIG. 5. The symmetric fission cross-section.

TABLE I. BARRIER PARAMETERS FOR THE TWO-HUMPED BARRIER ^a

channel I^π, K parameter (MeV)	$1^-, 0$				$2^+, 0$			
	Asym.	Sym.				Asym.	Sym.	
		1	2	3	4		1	2
E_A	6.10	6.10	6.10		6.10	5.7		6.0
$\hbar\omega_A$	1.0	1.0	1.0		1.0	0.9		0.9
E_B	6.05	8.15	9.2		8.15	6.05		7.5
$\hbar\omega_B$	0.9	1.5	2.0		1.5	0.9		1.5
E_{II}	2.90	2.25	2.25		2.25			2.8
$\hbar\omega_{II}$	3.20	2.40	2.40		2.40			2.0
W_{II}	-0.05	-0.06	-0.01		-0.06			-0.05

^a For the different cases considered in the text, where a detailed definition of the quantities may also be found. In the symmetric analysis, the cases 1 and 2 refer to the pure dipole, 3 refers to a pure quadrupole and 4 to the combined dipole-quadrupole.

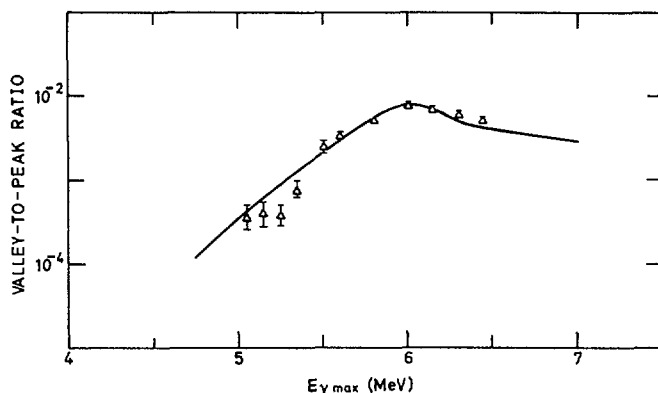


FIG.6. The calculated valley-to-peak ratio for the fission yield curve compared with the experimental data.

In the calculations, a dipole barrier of 9.2 MeV height and curvature of 2.0 MeV gave a reasonable fit to experimental data, using a resonance damping of -0.01 . An equally good fit was however obtained with a lower barrier, 8.2 MeV a smaller curvature, 1.5 MeV and larger damping, -0.05 . To obtain agreement between symmetric quadrupole fission in the one channel approximation and the valley-to-peak ratio, we had to use an inner barrier not less than 6 MeV and an outer barrier of about 7.5 MeV with a curvature of 1.5 MeV. These parameters gave as good an agreement as the dipole case.

However, for the one channel approximation, it was difficult to reproduce properly the behaviour of the symmetric yield between 5.3 MeV and 5.8 MeV. The influence of only one resonance gives too steep an ascent to the curve. Therefore we joined two channels with resonances separated about 0.25 MeV. We have arbitrarily used one $1^-,0$ and one $2^+,0$ channel, which gave a much better agreement between model and experiment. It thus seems probable that the symmetric fission process is at least a two channel process, strong resonant effects being associated with it. The results of the calculations and a comparison with the experimental data is shown in fig 3. Fig 5 shows the cross-section of symmetric fission. In table 1 we give the parameter values giving the best fits to experimental yield curves.

Neutron emission does not seem to compete to any significant degree with the resonant effects, and the maximum at 6 MeV, observed in the valley-to-peak ratio as shown in fig 6, seems to originate from the resonant effects of the fission yield together with a local saturation of the fission channel due to the passage of the inner fission barrier.

CONCLUSIONS

On the basis of what has been said, we can draw the following conclusions:

- 1) In the subbarrier region the symmetric and asymmetric yields can be interpreted in terms of penetration of double-hump barriers.

- 2) In order to obtain agreement between the theoretically predicted high symmetric barrier and our experimental data, it is necessary to introduce strong resonances between 5 MeV and 6 MeV. The most significant resonance is the one located at about 5.8 MeV. The maximum at 6 MeV observed in the valley-to-peak ratio is reproduced clearly by the effects of this resonance.
- 3) Neutron competition appears to be unimportant in our model, compared to barrier- and resonance effects. When the neutron threshold is below the fission threshold, the importance of neutron competition is increased. However, in the "penetration" model with a high symmetric barrier, neutron competition can not possibly reproduce the maximum at 6 MeV in the valley-to-peak ratio of ^{238}U .

REFERENCES

- [1] Strutinsky, V.M., Nucl. Phys. A95 (1967) 420.
- [2] Möller, P., Nucl. Phys. A192 (1972) 529.
- [3] Alm, A., Kivikas, T., Nuclear Physics Report LUNP 7302, Lund 1973; Submitted to Nuclear Physics.
- [4] Bohr, A., Int. Conf. peaceful uses atom. Energy (Proc. Conf. Geneva, 1956) 2, UN, New York (1956) 151.
- [5] Khan, A.M., Knowles, J.W., Nucl. Phys. A179 (1972) 333.
- [6] Huizenga, J.R., Britt, H.C., "Threshold Photofission: theory and experiment", Photonuclear Reactions and Applications (Proc. Int. Conf. Asilomar, Cal., 1973), 1, Lawrence Livermore Laboratory, Univ. of California, Livermore (1973) 833.
- [7] Emmerich, W.S., "Fast Neutron Physics, Part II", ch. II A, (Marion, J.B., Fowler, J.L., Eds.) Wiley, New York (1963).
- [8] Bohr, N., Wheeler, J.A., Phys. Rev. 56 (1969) 426.
- [9] Gai, E.V., Ignatiuk, A.V., Rabotnov, N.S., Smirenkin, G.N., Yad. Fiz. 10 (1969) 542; Sov. Journ. Nucl. Phys. 10 (1970) 311 (English Translation).
- [10] Hill, D.L., Wheeler, J.A., Phys. Rev. 89 (1953) 1102.
- [11] Schiff, L.I., Phys. Rev. 83 (1951) 252.
- [12] Brack, M., Damgaard, J., Jensen, A.S., Pauli, H.C., Strutinsky, V.M., Wong, C.Y., Rev. Mod. Phys. 44, (1972) 320; Möller, P., Nilsson, S.G., Phys. Lett. 31B (1970) 283; Nix, J.R., Annu. Rev. Nucl. Sci. 22 (1972) 65.
- [13] Larsson, S.E., Leander, G., Paper IAEA-SM-174/06, these Proceedings, Vol. 1.
- [14] Ignatiuk, A.V., Rabotnov, N.S., Smirenkin, G.N., Soldatov, A.S., Tsipeniuk, Yu. M., Sovj. Phys. JETP 34, 3 (1972) 684.

DISCUSSION

J.R. NIX: Did you find a difference in the mass distribution at a resonance in the cross-section compared to the average mass distribution?

J.R. HUIZENGA (Chairman): Perhaps I could respond to that question. Some 15 years ago Schmitt and Duffield measured the valley-to-peak ratio for photofission of ^{238}U with low-energy bremsstrahlung. This experiment showed a peak in this ratio at $E_{\text{max}} \approx 6$ MeV, indicating that the mass distribution may change at a resonance.

J.R. NIX: The data of Duffield and Schmitt you mention can be interpreted to give the relative penetrabilities of the second asymmetric peak and the first (symmetric) peak in the barrier. This is done by using the WKB expression for the penetrability through a two-peaked barrier. The result is that the second asymmetric peak is more penetrable than the first peak.

T. GOZANI: I would like to make an observation which pertains both to Mr. Back's paper¹ and Mr. Alm's paper². When one compares the available photofission cross-sections for ^{232}Th and ^{238}U with the fission cross-section of the equivalent residual nuclei from charged particle interaction (e. g. $^{230}\text{Th}(t, \text{pf})^{232}\text{Th}$ and $^{236}\text{U}(t, \text{pf})^{238}\text{U}$), one observes the following: the structure in the ^{232}Th cross-section appears in both data at about the same excitation energy, namely 5.6 to 5.8 MeV. It seems however that the structure is more pronounced in the photofission data. On the other hand, the structure in ^{238}U , especially above about 5.3 MeV, which appears clearly in the charged particle data (see Fig. 2, paper IAEA-SM-174/27), hardly appears in the photofission data. Since the experimental uncertainties (mostly energy resolution problems) in the latter are practically the same for both isotopes, I wonder if the difference between the charged particle data and the photofission data reflects the possible excitation of many more angular momentum states in the former as compared to a rather limited number of states (i. e. one or two) which can be excited in this energy range in the photofission process.

B.S. BHANDARI: Mr. Alm, do you take into account any coupling between states in the second well and those in the primary well at corresponding excitation energies?

A. ALM: No. Since our calculations are very phenomenological, we have not dealt with any considerations of that kind.

B.S. BHANDARI: Could this 5.8-MeV resonance be explained in terms of a doorway state?

A. ALM: It possibly could.

H.C. BRITT: I would just point out that there is a strong resonance at 5.8 MeV from $^{236}\text{U}(t, \text{pf})^{238}\text{U}$. This is presumably a resonance in the second well which could be considered a "doorway state".

C.D. BOWMAN: Essentially all photofission measurements have been carried out at energies above 5 MeV and much significant information has been obtained from these measurements. However, I would like to point out that measurements at much lower energies are possible and that interesting results on barrier parameters can be obtained.

¹ BACK, B.B., HANSEN, O., BRITT, H.C., GARRETT, J.D., Paper IAEA-SM-174/27, these Proceedings, Vol.1.

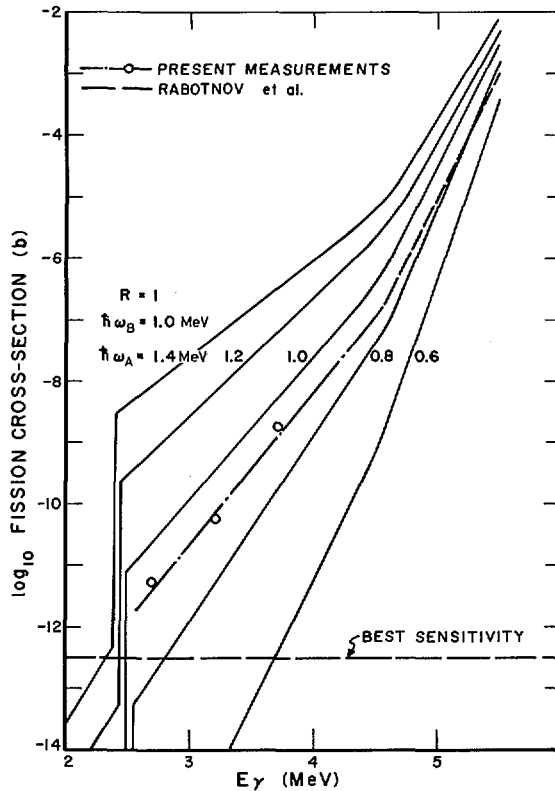


FIG. A. Comparison of subbarrier ^{238}U photofission measurements and calculations.

As the energy of the gamma ray exciting the nucleus decreases, the gamma-ray decay in the second well competes successfully with fission through the outer barrier. As $\Gamma_{\gamma\text{II}}$ becomes greater than Γ_{fission} , the photofission cross-section is dominated by isomeric fission. In this region the photofission cross-section is dependent only on penetration of the inner barrier. The cross-section, therefore, drops less rapidly with energy in this region, and a shelf appears on the photofission cross-section. The cross-section can be analysed for $\hbar\omega_A$ and $\hbar\omega_B$, radiation and fission widths in the second well and other parameters of interest.

Dr. I. Schroder, C. Dick and myself have carried out measurements on ^{238}U down to 2.8-MeV gamma-ray energy and the results are shown in Fig. A. The solid lines represent calculations of the fission cross-section using a method which is an extension of Lynn's very weak coupling formation. The height for both barriers is taken to be 6 MeV and the outer barrier curvature is taken to be $\hbar\omega_B = 1.0$ MeV. The various curves are calculated for different values of $\hbar\omega_A$. The dashed line above 4.5 MeV shows the photofission results of Rabotnov and co-workers. We have measured the cross-section at 3.8, 3.3 and 2.8 MeV using the bremsstrahlung from the 4-MeV electron Van de Graaff accelerator at the National Bureau of Standards.

The dot-dashed line through the points is a straight line fit by eye to our data. The statistical uncertainty in the points is less than $\pm 20\%$. Systematic errors could be as large as a factor of two. A shelf in the cross-section is clearly visible.

We believe that these results confirm our prediction² that measurements in this region are feasible and that such measurements can probably be a useful source of information on fission barrier parameters.

M.S. MOORE: Mr. Bowman, are you suggesting that the dramatic change in valley-to-peak ratio reported by Mr. Alm is related to the change from prompt to isomeric fission as the bremsstrahlung energy is reduced?

C.D. BOWMAN: No. The two effects are entirely unrelated. Alm has shown that low-energy photofission is dominated by asymmetric fission. Since we do not distinguish between symmetric and asymmetric fission, essentially all the fission cross-section and effects we see are concerned with asymmetric fission.

² BOWMAN, C.D., et al., in *Photonuclear Reactions and Applications*, (Proc. Int. Conf. Asilomar, Cal., 1973); Lawrence Livermore Laboratory, University of California, Livermore (1973).

ETUDE DE LA REACTION $^{231}\text{Pa}(n, f)$ INDUITE PAR NEUTRONS RAPIDES*

A. SICRE, G. BARREAU, R. CHASTEL,
T.P. DOAN, B. LEROUX, J.C. SAGEAUX
Centre d'études nucléaires de Bordeaux-Gradignan,
Université de Bordeaux I,
Le Haut-Vigneau, Gradignan, France

Abstract-Résumé

STUDY OF THE $^{231}\text{Pa}(n, f)$ REACTION INDUCED BY FAST NEUTRONS.

The excitation function of the $^{231}\text{Pa}(n, f)$ reaction has been measured from 100 keV to 1.3 MeV with 10-15 keV energy resolution. The neutrons were produced by the $^7\text{Li}(p, n)$ reaction, and the fission fragments were detected in 2π geometry by polycarbonate resin detectors. The cross-sections are calibrated by comparison with $^{235}\text{U}(n, f)$ and $^{238}\text{U}(n, f)$ cross-sections. The excitation function shows two resolved resonance structures around 200 keV and 330 keV, and other structures at higher energy. Fission barrier parameters are obtained from the analysis of this excitation function with a statistical model which takes into account the competition between the different decay channels and assumes a complete damping in the two wells. Fission fragment angular distributions have been measured in the vicinity of the resonances and structures. Using a statistical model including resonance penetration through the double humped barrier, it has not been possible to interpret the 200 keV and 330 keV resonances as pure vibrational resonances.

ETUDE DE LA REACTION $^{231}\text{Pa}(n, f)$ INDUITE PAR NEUTRONS RAPIDES.

La fonction d'excitation de la réaction $^{231}\text{Pa}(n, f)$ a été mesurée de 100 keV à 1,3 MeV avec une résolution en énergie de 10 à 15 keV. Les neutrons sont produits par la réaction $^7\text{Li}(p, n)$, et les fragments de fission sont détectés dans une géométrie 2π à l'aide de détecteurs visuels plastiques. Les sections efficaces sont normalisées par comparaison avec les sections efficaces des réactions $^{235}\text{U}(n, f)$ et $^{238}\text{U}(n, f)$. La fonction d'excitation présente deux résonances bien résolues autour de 200 keV et de 330 keV, ainsi que plusieurs structures à plus haute énergie. La forme de la barrière de fission est obtenue par l'analyse de cette fonction d'excitation à l'aide d'un modèle statistique qui rend compte de la compétition entre les différentes voies de sortie et suppose un amortissement («damping») complet dans les deux puits. La distribution angulaire des fragments de fission a été mesurée au voisinage des résonances et des structures. En utilisant un modèle statistique incluant la pénétration résonnante à travers la barrière à deux maximums il n'a pas été possible d'interpréter les résonances à 200 keV et 330 keV en tant que résonances de vibration pures.

1. Introduction

Récemment encore, les structures observées dans les fonctions d'excitation des réactions (n, f) et dans les probabilités de fission mesurées en réactions directes étaient attribuées à la compétition entre les différentes voies de sortie possibles [1] ; l'ouverture successive de voies de fission et de voies de neutron permettrait en effet d'expliquer l'existence des plateaux observés. Par contre certaines résonances très marquées observées sous le seuil de fission, par exemple la résonance observée à 720 keV dans la réaction $^{230}\text{Th}(n, f)$, ne pouvaient guère être expliquées par cette compétition.

La notion de barrière de fission à deux maxima qui résulte de l'introduction des effets de couche dans le calcul de l'énergie potentielle du noyau [2] a permis d'attribuer ces résonances à l'existence d'états de vibration β quasi stationnaires dans le second puits de potentiel [3, 4] .

* Travail partiellement effectué sous contrat CEA.

De telles résonances de vibration ont été observées et étudiées dans de nombreux noyaux pairs-pairs [5], ainsi que dans plusieurs noyaux de masse impaire [6] ; le noyau ^{232}Pa est l'un des seuls noyaux impair-impair pour lesquels on a pu observer des résonances de ce type [7,8]. Nous avons donc étudié la réaction $^{231}\text{Pa}(n, f)$ pour tenter de déterminer les caractéristiques de ces résonances.

2. Description de la méthode expérimentale

La fonction d'excitation, ainsi que les distributions angulaires des fragments de fission ont été mesurées auprès de l'accélérateur Van de Graaff de 4 MeV du C.E.N.B.G. à Bordeaux. Les neutrons incidents sont produits à l'aide de la réaction $^7\text{Li}(p, n)$ sur une cible de lithium naturel obtenue par évaporation sous vide sur un support d'or de 0,5 mm d'épaisseur. Le faisceau de protons est défocalisé et diaphragmé de telle sorte que son impact sur la cible forme une tache uniforme d'environ 25mm^2 ; de plus le support de la cible est refroidi par une circulation d'eau, afin d'absorber l'énergie dissipée par le faisceau dont l'intensité était voisine de $15\text{ }\mu\text{A}$.

Un détecteur de neutrons (compteur BF3 entouré de paraffine) placé à 1 mètre de la cible de lithium, dans la direction des protons incidents, sert de moniteur pour contrôler le flux de neutrons.

La calibration en énergie du faisceau de protons est obtenue par la mesure du seuil de la réaction $^7\text{Li}(p, n)$, qui a été pris égal à 1,881 MeV, et vérifiée grâce à la résonance $^{13}\text{C}(p, \gamma)$ à 1,747 MeV.

L'épaisseur des cibles de lithium est mesurée avant et après utilisation, à partir de la courbe de production de neutrons, au voisinage du seuil de la réaction $^7\text{Li}(p, n)$.

2.1 Mesure de la fonction d'excitation de la réaction $^{231}\text{Pa}(n, f)$

Pour mesurer la fonction d'excitation de la réaction $^{231}\text{Pa}(n, f)$, nous avons utilisé le dispositif représenté schématiquement sur la figure 1.

La cible de ^{231}Pa est constituée par un dépôt d'oxyde de protactinium de $2\text{mg}/\text{cm}^2$ d'épaisseur, et de 2 cm de diamètre supporté par un disque d'aluminium de 0,024 mm d'épaisseur ; la cible contient 93,5% de ^{231}Pa , et 6,5% de descendants du ^{231}Pa .

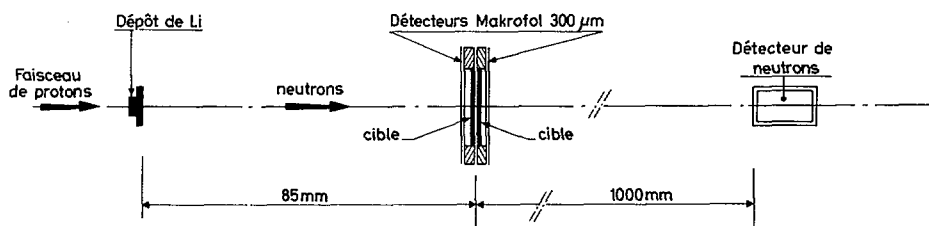


FIG. 1. Dispositif expérimental utilisé pour la mesure de la fonction d'excitation de $^{231}\text{Pa}(n, f)$ au moyen de détecteurs plastiques visuels.

Les fragments de fission issus de la cible de ^{231}Pa sont détectés à l'aide d'un détecteur visuel plastique constitué par un disque de Makrofol de 300 μ d'épaisseur, ayant le même diamètre que le support de cible (2,54 cm). Le détecteur est maintenu face au dépôt de ^{231}Pa , à une distance de 1 mm.

Pour permettre la normalisation de la fonction d'excitation, une cible de ^{235}U (ou ^{238}U) et son détecteur associé sont placés contre les éléments précédents. Le sandwich ainsi formé est placé perpendiculairement au faisceau de neutrons, à une distance de 8,5 cm de la cible de lithium.

La résolution en énergie des neutrons incidents dépend de plusieurs facteurs :

- la résolution en énergie du faisceau de protons (≈ 1 keV)
- l'épaisseur du dépôt de lithium (≈ 10 keV pour une cible de lithium de 60 $\mu\text{g}/\text{cm}^2$)
- l'angle d'ouverture du faisceau de neutrons atteignant les cibles (cette dispersion en énergie, due à la cinématique, introduit une dispersion en énergie croissant de 2 keV à 9 keV lorsque l'énergie des neutrons passe de 85 keV à 2,3 MeV).

Au cours de nos expériences, la résolution en énergie globale était comprise entre 10 et 15 keV.

Après irradiation, les détecteurs plastiques sont soumis à l'action d'un bain de NaOH 6N à 50°C pendant 100 minutes. Le comptage des traces se fait alors au microscope optique en lumière transmise ; pour éviter les effets de bord, seule la zone centrale du détecteur est dépouillée sur une surface de 144 mm².

2.2 Mesure des distributions angulaires des fragments de fission

Le dispositif expérimental utilisé pour la mesure des distributions angulaires est représenté sur la figure 2 ; il est constitué d'une chambre à vide formée de 2 cônes accolés par leur base, permettant de réaliser éventuellement 2 mesures simultanées. Le dépôt de ^{231}Pa occupe le centre de la base commune des 2 cônes, et son centre est fixé à 8,5 cm de la cible de lithium. Une feuille de Makrofol de 10 μ d'épaisseur est fixée sur la face interne de la chambre. L'axe commun des 2 cônes est incliné à 45° par rapport à la direction des neutrons incidents pour permettre la détection des fragments de fission de 0 à 90°.

Après irradiation, la feuille de Makrofol est soumise à l'action d'un bain de NaOH 6N à 70°C pendant 20 minutes.

En raison de la grande surface du détecteur (190 cm²) nous avons utilisé pour visualiser les traces la méthode développée par Repnow (9) pour la mise en évidence des isomères de fission. La feuille de Makrofol est placée entre une plaque de cuivre et une feuille de plastique aluminisée dont la couche d'aluminium est portée à la haute tension ; les claquages qui se produisent à travers les traces détruisent la couche d'aluminium, permettant ainsi de visualiser une image des traces sur la feuille aluminisée sous la forme de petits cercles transparents. La surface dépouillée est divisée radialement et angulairement en zones élémentaires d'environ 1 cm² dans chacune desquelles on mesure le nombre de traces. Seule est exploitée la région du détecteur dans laquelle les traces proviennent de fragments de fission dont la direction d'émission fait un angle $> 30^\circ$ par rapport à la surface de la cible.

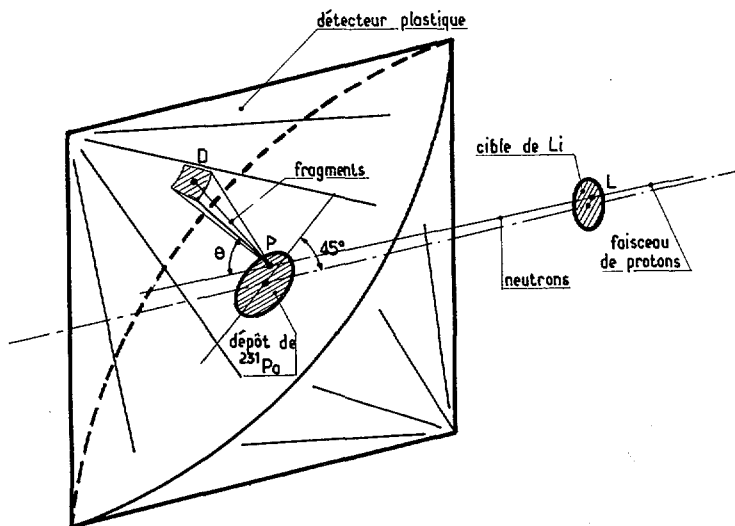


FIG. 2. Dispositif expérimental utilisé pour la mesure des distributions angulaires des fragments de fission.

Compte tenu de la dimension relativement importante de la cible de ^{231}Pa par rapport à la distance entre la cible et le détecteur, la distribution angulaire est obtenue sous la forme :

$$W(\theta) = \sum_{n=0}^3 \alpha_{2n} P_{2n}(\cos\theta)$$

où les coefficients α_{2n} sont obtenus à partir d'un calcul de moindres carrés entre la répartition des traces mesurées sur le détecteur plastique et les répartitions calculées pour chacune des composantes $P_{2n}(\cos\theta)$ à l'aide d'un calcul de simulation dans lequel la surface d'impact des protons sur la cible de lithium et la surface de la cible de ^{231}Pa sont divisées chacune en 100 zones élémentaires.

La précision sur les coefficients α_{2n} est obtenue en supposant que le nombre de traces mesurées dans chacune des zones élémentaires du détecteur plastique suit une loi de distribution de Poisson.

Afin de vérifier la validité de cette méthode, nous avons irradié un détecteur plastique à l'aide d'une source de ^{252}Cf ayant la même dimension que la cible de ^{231}Pa , et nous avons bien obtenu une distribution angulaire isotrope.

3. Résultats expérimentaux

La fonction d'excitation que nous avons obtenue pour la réaction $^{231}\text{Pa}(n, f)$ est représentée sur la figure 3 ; les barres d'erreur correspondent uniquement aux fluctuations statistiques sur le nombre de traces détectées, et ne tiennent pas compte d'erreurs systématiques éventuelles.

La valeur absolue de la section efficace est obtenue par comparaison avec une cible ^{235}U jusqu'à 1,2 MeV et avec une cible ^{238}U de 0,9 à 1,2 MeV.

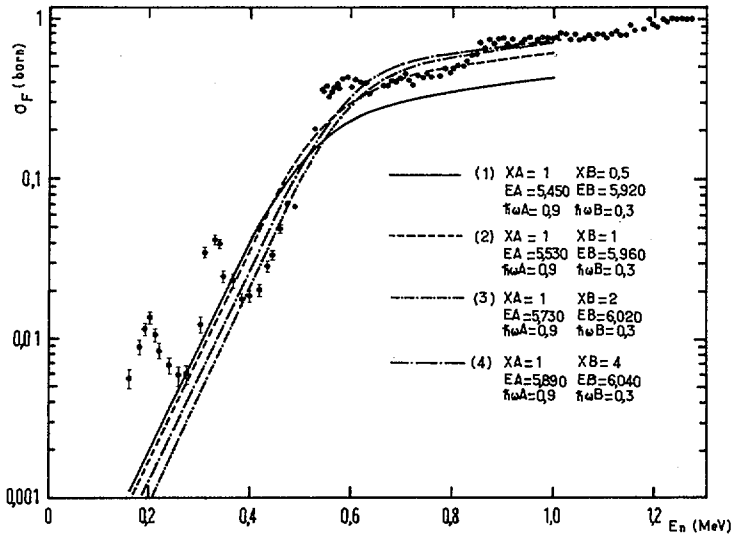


FIG. 3. Fonction d'excitation de la réaction $^{231}\text{Pa}(n, f)$ et interprétation au moyen du modèle avec « damping » complet dans les deux puits.

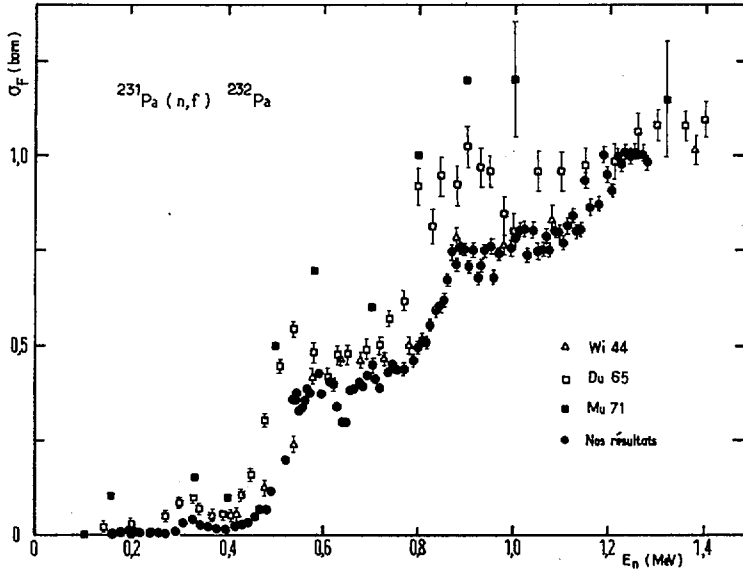


FIG. 4. Section efficace de $^{231}\text{Pa}(n, f)$ comparée aux résultats de Williams [11], de Dubrovina et Shigin [7] et à quelques points caractéristiques de Muir et Veese [8].

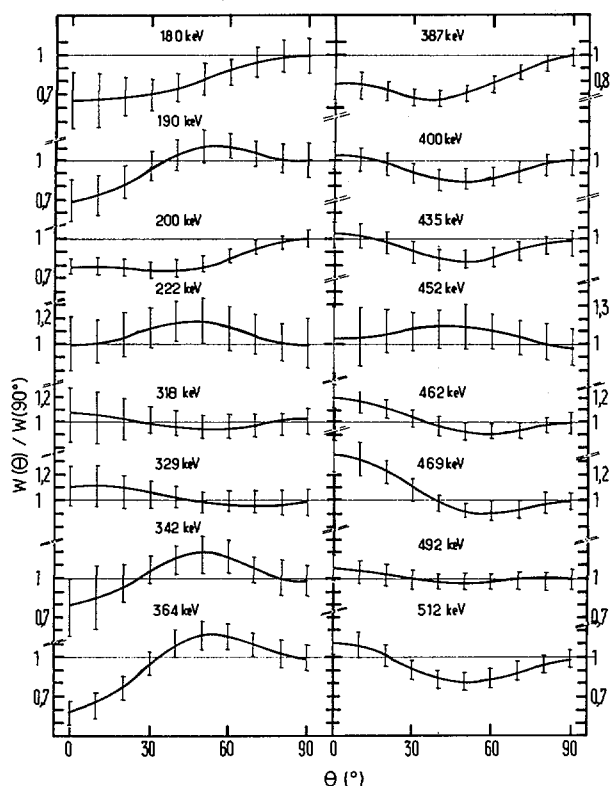


FIG. 5a. Distributions angulaires des fragments de fission de $^{231}\text{Pa}(n, f)$ de 180 keV à 512 keV.

Les valeurs des sections efficaces des réactions $^{235}\text{U}(n, f)$ et $^{238}\text{U}(n, f)$ ont été extraites de la compilation de Davey [10].

Comme le montre la figure 4, nous retrouvons à 200 keV la résonance observée à 160 keV par Veesser et Muir [8], nous retrouvons à 330 keV la résonance observée pour la première fois par Dubrovina et Shigin [7]; nous trouvons ensuite un groupe de structures au voisinage de 600 keV, une structure vers 700 keV et une autre structure au voisinage de 880 keV.

De 400 keV à 1 MeV, la section efficace croît en 2 larges marches séparées d'environ 310 keV. La position de ces marches, qui est en bon accord avec les résultats de Williams [11] et les résultats obtenus par Britt [12] en (d, pf) , est légèrement décalée par rapport aux résultats de Dubrovina et Shigin [7] et de Veesser et Muir.

En ce qui concerne la valeur absolue de la section efficace, tous les résultats concordent vers 1,3 MeV, mais nos sections efficaces, qui sont compatibles avec celles de Williams, sont nettement plus faibles que celles de Dubrovina et Shigin aux faibles énergies.

Les résonances à 200 et 330 keV présentent respectivement des largeurs à mi-hauteur de 50 keV et 60 keV; avec la résolution en énergie utilisée, elles ne présentent pas de sous-structure.

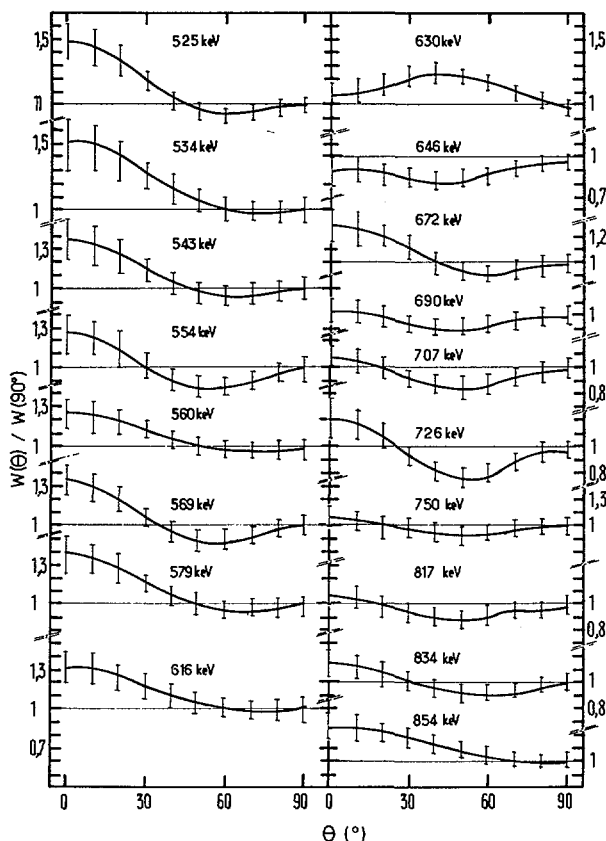


FIG. 5b. Distributions angulaires des fragments de fission de $^{231}\text{Pa}(n, f)$ de 525 keV à 854 keV.

La forme des distributions angulaires, normalisées à 1 à 90° , est présentée sur la figure 5 ; l'anisotropie de ces distributions angulaires est comparée sur la figure 6 avec les résultats obtenus par Vorotnikov et ses collaborateurs [13].

4. Interprétation des résultats expérimentaux.

4.1 Analyse de l'allure générale de la fonction d'excitation

L'un de nos objectifs consistant à obtenir des informations sur la forme de la barrière de fission, nous avons tout d'abord tenté d'interpréter la fonction d'excitation à l'aide du modèle statistique présenté au cours de ce symposium par BRITT [12].

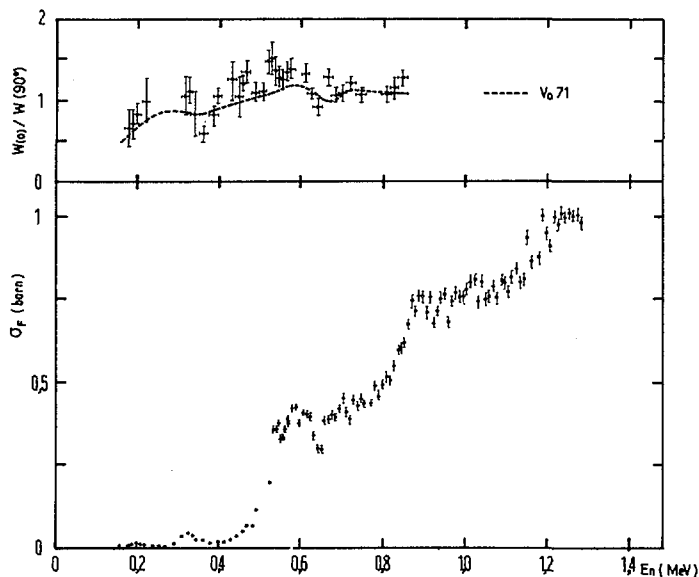


FIG. 6. Variation de $W(0^\circ)/W(90^\circ)$ en fonction de l'énergie des neutrons comparée aux résultats de Vorotnikov et coll. [13].

Rappelons que ce modèle repose essentiellement sur les deux hypothèses suivantes :

1) La réaction peut être décrite à l'aide d'un mécanisme en deux étapes successives : formation d'un noyau composé faiblement déformé, puis désexcitation de ce noyau composé suivant l'un des différents modes de désexcitation possibles (émission d'un rayonnement gamma, émission d'un neutron, ou fission du noyau).

2) Il y a un amortissement complet (complete damping) des mouvements collectifs associés à la voie de fission dans le premier et dans le second puits ; de telle sorte que la transmission à travers chacune des deux barrières peut être traitée indépendamment.

La section efficace obtenue dans le cadre de ce modèle peut s'écrire sous la forme :

$$\sigma_f(E) = \sum_{J\pi} \sigma_c(J, \pi, E) \cdot (1 + a^2 + 2a \coth(t/2))^{-\frac{1}{2}}$$

$$\text{avec } a = \frac{(T_n + T_\gamma)(T_A + T_B)}{T_A \cdot T_B} \quad \text{et} \quad t = T_A + T_B$$

où T_A , T_B , T_n et T_γ sont respectivement les coefficients de transmission associés à la traversée de la première barrière, à la traversée de la deuxième barrière, à l'émission d'un neutron, et à l'émission d'un rayonnement gamma (seules les transitions E_1^- ont été considérées). Chacun de ces coefficients de transmission est calculé pour chaque valeur de

J et π en fonction de l'énergie E par sommation sur les différentes transitions possibles, ce qui implique l'utilisation des densités de niveaux des noyaux ^{231}Pa et ^{232}Pa dans le premier puits, et l'utilisation des densités des états de transition du ^{232}Pa au niveau des deux barrières ; nous avons utilisé les densités proposées par BRITT et NIX [14] normalisées sur la valeur expérimentale de la densité de niveaux mesurée dans le premier puits du ^{232}Pa à l'énergie de liaison du neutron [15] :

$$\rho(E^* = 5,652 \text{ MeV}, J\pi = 1^- \text{ et } 2^-) = (1,0 \pm 0,2) 10^6 \text{ MeV}^{-1}$$

La section efficace de formation du noyau composé $\sigma_c(J, \pi, E)$ et les coefficients $T_n(J, \pi, E)$ ont été calculés en utilisant les coefficients de transmission de neutrons $T_{\ell}^{\pm 1/2}$ obtenus par Perey et Buck [16] à l'aide d'un potentiel optique non local.

Les coefficients T_γ sont normalisés de telle sorte que l'on retrouve la valeur de la largeur partielle d'émission gamma mesurée pour le ^{232}Pa à l'énergie de liaison du neutron [15] :

$$\Gamma_\gamma(E^* = 5,652 \text{ MeV}, J\pi = 1^- \text{ et } 2^-) = 51 \pm 5 \text{ meV}.$$

Les 4 paramètres qui seuls devraient intervenir dans ce modèle sont les hauteurs des 2 barrières : E_A et E_B , et les courbures de ces barrières : $\hbar\omega_A$ et $\hbar\omega_B$; nous avons fait varier systématiquement $\hbar\omega_A$ entre 0,5 et 0,9 MeV et $\hbar\omega_B$ entre 0,3 et 0,7 MeV, les valeurs de E_A et E_B étant alors déterminées par un calcul de moindres carrés sur la fonction d'excitation expérimentale.

Naturellement, ce modèle ne permet pas d'interpréter les résonances et les structures observées dans la fonction d'excitation mesurée ; de plus, comme dans le cas de la réaction $^{231}\text{Pa}(d, p)^{232}\text{Pa}$ [12], nous avons pu observer que la fonction d'excitation théorique croissait trop lentement ; cette croissance trop lente peut être corrigée si l'on augmente d'un facteur voisin de 2 la densité des états de transition utilisés au niveau de la seconde barrière ; cette augmentation pourrait être associée au fait que la seconde barrière prévue par les calculs les plus récents, est asymétrique.

La figure 3 représente la fonction d'excitation théorique obtenue pour différentes valeurs du facteur XB par lequel nous avons multiplié la densité des états de transition associés à la seconde barrière.

Les meilleurs résultats sont obtenus avec une première barrière étroite ($\hbar\omega_A \approx 0,8 - 0,9 \text{ MeV}$) et une seconde barrière large ($\hbar\omega_B \approx 0,3 - 0,4 \text{ MeV}$) ; la hauteur de la seconde barrière s'est avérée peu sensible à la variation des autres paramètres ($E_B = 6,0 \pm 0,15 \text{ MeV}$) ; la hauteur obtenue pour la première barrière est beaucoup plus sensible aux différents paramètres car son influence sur le résultat est moins importante ($E_A = 5,8 \pm 0,3 \text{ MeV}$). Ces résultats sont en bon accord avec les résultats obtenus en (d, pf).

4.2 Analyse des résonances

Si l'on admet les hypothèses suivantes :

- la réaction (n, f) peut être décrite à l'aide d'un mécanisme comportant deux étapes successives et indépendantes, comme dans le modèle précédent,

- la projection K du moment angulaire total J du noyau composé sur l'axe de déformation du noyau est un bon nombre quantique au cours du processus de fission,

- les fragments de fission sont émis le long de l'axe de déformation du noyau,

la section efficace différentielle de la réaction (n, f) peut s'écrire sous la forme :

$$d\sigma_f(\theta, E) = \sum_{J\pi} \sum_{M=-J}^{+J} \sigma_c(J, \pi, M, E) \cdot \frac{\sum_{K=0}^J T_f^{KJ\pi}(E)}{\sum_{K=0}^J T_f^{KJ\pi}(E) + T_n^{J\pi}(E) + T_\gamma^{J\pi}(E)} \cdot F.$$

$$\frac{2J+1}{4} (|d_{MK}^J(\theta)|^2 + |d_{M-K}^J(\theta)|^2) \sin\theta d\theta$$

Dans cette expression, σ_c est la section efficace de formation du noyau composé, T_f , T_n et T_γ sont les coefficients de transmission associés aux différents modes de désexcitation du noyau composé, F est un facteur de fluctuations, généralement voisin de 1, et les fonctions $d_{MK}^J(\theta)$ sont les fonctions d'onde de la toupie symétrique [17].

Pour chaque état de transition (K, J, π), nous avons calculé le coefficient de transmission T_f en considérant une barrière de fission à une seule dimension constituée par trois paraboles jointives, avec une partie imaginaire dans le second puits pour rendre compte d'un "damping" éventuel dans le second puits [5, 18, 19].

Ce coefficient de transmission T_f présente des résonances lorsque l'énergie disponible dans la voie de fission coïncide avec l'énergie des états de vibration β dans le second puits.

A l'aide de ce modèle, nous avons essayé de voir si les résonances à 200 keV et 330 keV pouvaient être interprétées comme étant des résonances de vibration pures, analogues à la résonance de 720 keV observée dans la réaction $^{230}\text{Th}(n, f)$, et attribuée à un état de vibration couplé à la bande de rotation construite sur l'état intrinsèque $K=1/2$ [6]; si tel était le cas, la forme de ces résonances et la forme des distributions angulaires au voisinage de ces énergies devraient être caractéristiques des nombres quantiques K et π définies par la structure interne des états de vibration du second puits responsables de ces résonances. Notons que, selon les calculs de Nilsson [20], l'état intrinsèque de plus faible énergie du ^{232}Pa devrait être, pour une déformation correspondant au second puits, un état $K\pi=2^-$ provenant du couplage du niveau de proton $[633] 7/2^+$ avec le niveau de neutron $[512] 3/2^-$.

La seule comparaison entre la forme des distributions angulaires expérimentales au voisinage de 200 keV et 330 keV, et les formes calculées pour différentes valeurs de K, J et π , et présentées sur la figure 7 (la forme de ces distributions angulaires théoriques varie peu avec l'énergie des neutrons incidents) montre qu'aucune de ces deux résonances ne peut être considérée comme une résonance de vibration pure.

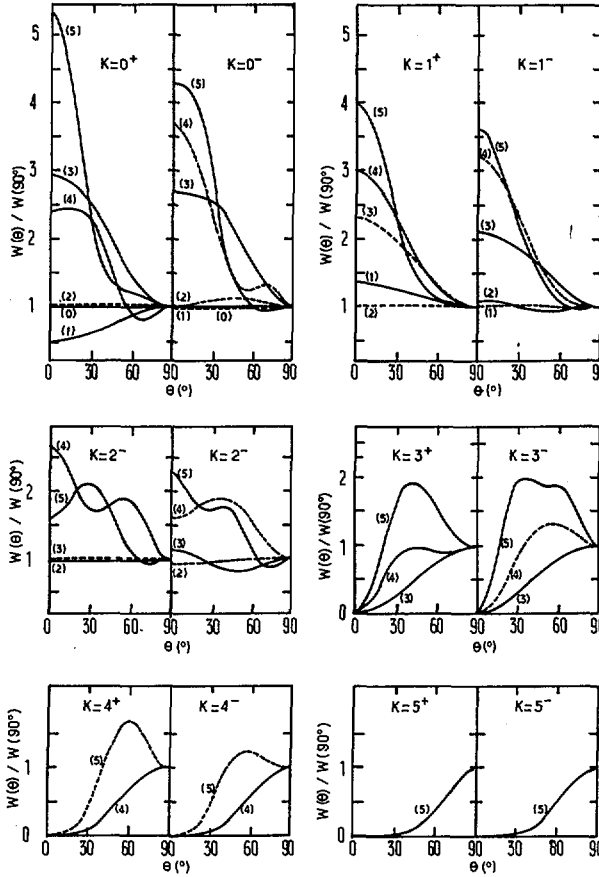


FIG. 7. Distributions angulaires théoriques.

Ce résultat est en accord avec un travail effectué par Holmberg[21], dans lequel la forme des résonances à 200 keV et 330 keV, mesurées avec une très bonne résolution en énergie, semble comporter une sous-structure.

En utilisant des paramètres raisonnables pour décrire la forme de la barrière de fission : E_A et $E_B \simeq 6$ MeV, $\hbar\omega_A \simeq 0,9$ MeV et $\hbar\omega_B \simeq 0,5$ MeV, $\hbar\omega_{II} \simeq 0,9$ MeV et $E_{II} \simeq 3,1$ MeV et en considérant que chacune de ces 2 résonances peut être attribuée à la superposition des contributions de 2 à 3 bandes, il semble possible de retrouver la forme de la section efficace différentielle jusqu'à 400 keV.

5. Conclusion

Au cours de ce travail, nous avons précisé la forme de la fonction d'excitation, et mesuré la forme des distributions angulaires au voisinage

des résonances et des structures observées. L'analyse de la fonction d'excitation nous a permis d'extraire la forme des deux barrières de fission.

Les deux résonances observées à 200 keV et à 330 keV ne sont pas des résonances de vibration pure.

REMERCIEMENTS

Nous tenons à remercier tout particulièrement MM. B. B. Back, S. Bjornholm, H. C. Britt, K. Dietrich, J. D. Garrett et J. R. Nix de l'intérêt qu'ils ont bien voulu accorder à ce travail; les informations qu'ils ont eu l'amabilité de nous communiquer nous ont beaucoup aidés dans l'analyse des résultats.

REFERENCES

- [1] WHEELER, J. A., Fast Neutron Physics (Marion, J. B., Fowlers, J. L., Eds), Wiley, New York (1963) 2051.
- [2] STRUTINSKY, V. M., Nucl. Phys. A95 (1967) 420.
- [3] BJORNHOLM, S., STRUTINSKY, V. M., Nucl. Phys. A136 (1969) 143.
- [4] LYNN, J. E., in Physics and Chemistry of Fission (C. r. Coll. Vienne, 1969), AIEA, Vienne (1969) 249; UKAEA Rep. AERE-M-2505 (1971).
- [5] SPECHT, H. J., FRASER, J. S., MILTON, J. C. D., DAVIES, W. G., in Physics and Chemistry of Fission (C. r. Coll. Vienne, 1969), AIEA, Vienne (1969) 363;
BRITT, H. C., BURNETT, S. C., CRAMER, J. D., Ibid., p. 375;
BACK, B. B., BONDORF, J. P., OTROSHENKO, G. A., PEDERSEN, J., RASMUSSEN, B., Ibid., p. 351.
- [6] JAMES, G. D., LYNN, J. E., EARWAKER, L. G., Nucl. Phys. A189 (1972) 225;
BEHKAMI, A. N., HUIZENGA, J. R., ROBERTS, J. H., Nucl. Phys. A118 (1968) 65;
VOROTNIKOV, P. E., Sov. J. Nucl. Phys. 5 (1967) 415.
- [7] DUBROVINA, S. M., SHIGIN, V. A., Sov. Phys. - Dokl. 9 7 (1967) 579.
- [8] MUIR, D. W., VEESER, L. R., Proc. Conf. Neutron Cross Sections and Technology (Knoxville, March 1971), USAEC Rep. Conf-710301 1 (1971) 292.
- [9] REPNOW, R., METAG, V., FOX, J. D., Von BRENTANO, P., Nucl. Phys. A147 (1970) 183.
- [10] DAVEY, W. G., Nucl. Sci. Eng. 32 (1968) 35.
- [11] WILLIAMS, J. H., LA-150 (1944).
- [12] BACK, B. B., BRITT, H. C., GARRETT, J. D., HANSEN, O., LEROUX, B., « Experimental fission barriers for actinide nuclei », ces comptes rendues, IAEA-SM-174/201.
- [13] VOROTNIKOV, P. E., DUBROVINA, S. M., OTROSHCHENKO, G. A., SHIGIN, V. A., Sov. J. Nucl. Phys. 10 (1970) 280.
- [14] BRITT, H. C., BOLSTERLI, M., NIX, J. R., NORTON, J. L., Phys. Rev. C7 (1963) 801.
- [15] LYNN, J. E., The Theory of Neutron Resonance Reactions, Clarendon, Oxford (1968).
- [16] PEREY, F., BUCK, B., Nucl. Phys. 32 (1962) 353;
AUERBACH, E. H., PEREY, F. G. J., BNL-765 (1962).
- [17] BEHKAMI, A. N., Tables of rotational wave functions d_{MK}^I , Nuclear Data Tables 10 (1971) 1.
- [18] CRAMER, J. D., NIX, J. R., Phys. Rev. C2 (1970) 1048.
- [19] BACK, B. B., HANSEN, O., BRITT, H. C., GARRETT, J. D., « Fission barriers for doubly even actinide nuclei from (t, pf), (^3He , df), (p, p'f) and (t, α f) studies », ces comptes rendus, IAEA-SM-174/27.
- [20] NILSSON, S. G., TSANG, C. F., SOBICZEWSKI, A., SZYMANSKI, Z., WYCECH, S., GUSTAFSON, C., LAMM, I. L., MOLLER, P., NILSSON, B., Nucl. Phys. A131 (1969) 1.
- [21] JAMES, G. D., Communication privée.

DISCUSSION

R. W. HASSE: As I understand your analysis of the widths of the resonances in the excitation function, you assumed complete damping in the first minimum. However, as Back and co-workers (Nucl. Phys. A165 (1970) 449) showed, the assumption of incomplete damping is more compatible with experimental data which they could not explain by complete damping¹. Can you comment on this disagreement?

B. LEROUX: In both Back's analysis and our own, complete damping is assumed in the first well. Back also assumed some damping in the second well, in order to account for the width of the resonances in his data. In our case we do not need any damping in the second well and the reason is that the excitation energy of the nucleus in the vicinity of the resonances is about the same as the height of the first barrier, which is relatively thin and lower than the broad second barrier; as a result, the coupling width of the second-well vibrational states through the first barrier is large enough to account for the width of our resonances.

¹ BACK, B. B., et al., "Analysis of resonances observed in (d,pf)-reactions", Physics and Chemistry of Fission (Proc. Symp. Vienna, 1969), IAEA, Vienna (1969) 351.

DETERMINATION OF SPINS OF INTERMEDIATE STRUCTURE RESONANCES IN SUBTHRESHOLD FISSION*

G. A. KEYWORTH, J. R. LEMLEY[†], C. E. OLSEN, F. T. SEIBEL
Los Alamos Scientific Laboratory,
University of California,
Los Alamos, N. Mex.

J. W. T. DABBS, N. W. HILL
Oak Ridge National Laboratory,
Oak Ridge, Tenn.,
United States of America

Abstract

DETERMINATION OF SPINS OF INTERMEDIATE STRUCTURE RESONANCES IN SUBTHRESHOLD FISSION.

The appearance of prominent intermediate structure in subthreshold fission is currently ascribed to coupling between the normal (Class I) compound nuclear states and Class II states belonging to the second minimum in a double-humped fission barrier. This explanation requires that only Class I resonances of a single spin state be enhanced through coupling to a Class II state of the same spin. To verify this explanation, the fission (σ_f) and total (σ_t) cross-sections of ^{237}Np for resonance energy neutrons have been measured with a polarized neutron beam and polarized target, using time-of-flight methods. Neutrons from the Oak Ridge Electron Linear Accelerator were polarized by transmission through a dynamically pumped proton sample. The ^{237}Np was polarized in a ferromagnetic medium cooled by a ^3He - ^4He dilution refrigerator. The individual fine-structure resonances comprising the Class II structure at 40-eV incident neutron energy were determined to have the same spin, $J^\pi = 3^+$. Spins of 14 other Class II structures below 1 keV were also determined, although the fine structure is unresolved. Comparison of these results with earlier data on the angular distribution of fission fragments from aligned ^{237}Np reveals an apparent admixing of transition states, as evidenced by nonintegral values of the projection quantum number, K .

1. INTRODUCTION

In order to proceed to a detailed understanding of fission systematics, it is necessary to measure the spins of resonances in fissionable nuclei. In particular, the properties of the transition states in fissioning nuclei remain somewhat obscure without determination of the channel spin.

Previous attempts to determine spins of compound nuclear levels in fissionable nuclei have primarily involved indirect methods, such as observing deexcitation capture gamma rays, relative gamma-ray multiplicities, and combination of total and partial cross-sections. The more direct method utilizing a polarized neutron beam and polarized target has previously been limited to low neutron energies, < 10 eV, where polarizing the neutron beam is a relatively simple matter. Because of the inconsistencies in those published spin assignments for fissionable nuclei, it was decided in 1968 at the Los Alamos Scientific Laboratory to undertake an experimental program to develop the equipment and techniques to polarize a wide range of fissionable targets and a neutron beam over a wide energy range.

* Work performed under the auspices of the US Atomic Energy Commission.

[†] Now at the International Atomic Energy Agency, Vienna.

The determination of narrow intermediate structure in the fission cross-section of ^{237}Np was first reported by Paya et al. [2]. Although the total cross-section is characteristic of other odd-odd heavy elements, with an s-wave level spacing of ~ 0.7 eV, the fission cross-section is composed of numerous structures whose mean spacing is ~ 60 eV. The explanation of this intermediate structure in terms of a double-humped fission barrier [3] requires that the individual resonances in each group or structure have the same spin, that of the "parent" state in the second well. Thus, the choice of ^{237}Np as a target nucleus was an obvious one to demonstrate this technique of spin determination and to verify the presence of intermediate structure resulting from coupling of states in the second well, Class II, to the normal, Class I, compound nuclear states.

The ^{237}Np nucleus has ground state spin and parity $5/2^+$, and the compound system ^{238}Np resulting from absorption of s-wave neutrons has $J^\pi = 3^+$ states for the target and neutron polarization parallel and 2^+ for the antiparallel case. The ratio of observed cross-sections is approximated by

$$R = \frac{\sigma_{\text{par}}}{\sigma_{\text{anti}}} = \frac{1 + f_I f_N}{1 - f_I f_N} \quad (1)$$

where f_N is the target polarization, f_n the neutron polarization, and $f_I = I/I+1$ for $J = I+1/2$ and $f_I = -1$ for $J = I-1/2$. Thus, in ^{238}Np , the ratio $R > 1$ for $J^\pi = 3^+$ resonances and $R < 1$ for those with $J^\pi = 2^+$.

2. EXPERIMENTAL

The technique of neutron polarization used in this experiment was first reported by Shapiro [4] in 1965. This method utilizes the strong spin dependence of the neutron-proton interaction where the cross-section for scattering through the singlet state of the system is ~ 20 times larger than that for the triplet state. Thus an unpolarized neutron beam becomes polarized when filtered through a sample of polarized protons. Since the cross-sections for singlet and triplet scattering vary little over the range 10 eV to 50 keV, the polarization of the transmitted beam is essentially constant over this range.

The method of dynamic nuclear polarization [5] is used to polarize the protons in the water of hydration of single crystals of $\text{La}_2\text{Mg}_3(\text{NO}_3)_{12} \cdot 24\text{H}_2\text{O}$ (LMN). A series of LMN crystals are placed in a microwave cavity at a temperature of 1.15°K located in a homogeneous magnetic field of ~ 20 kOe in a superconducting coil. The system of free electrons and protons in the paramagnetic LMN is then "pumped" by microwaves, whereby simultaneous electron and proton spin flips are induced. Owing to their long relaxation times, the protons remain flipped, resulting in a net bulk proton polarization. In this experiment, a neutron polarization of $\sim 55\%$ with a transmission through the LMN of 18% was realized. The difficulty of this technique arises primarily from the fact that the "pumped" transition is forbidden and, hence, narrow. High stabilization of the microwave source and high homogeneity of the magnetic field are required over long periods of time. In addition, the large size of the cryogenic and vacuum equipment, coupled with a fast nuclear magnetic resonance system to monitor the polarization, makes the equipment complex.

The method used to polarize the fissionable target involves thermal equilibrium techniques. The simplest of the thermal equilibrium techniques is the brute-force method, whereby the interaction between an externally applied magnetic field with the nuclear magnetic moment at low temperature

results in a net polarization. With currently available magnetic fields and attainable temperatures, polarization of $< 1\%$ are achieved by this method. However, by choosing a suitable ferromagnetic system containing the desired target, the large hyperfine fields may result in high polarization.

In this experiment, a target of NpA2 was fabricated and attached to a ^3He - ^4He dilution refrigerator. This dilution refrigerator, which utilizes the fact that the dissolving of ^3He in ^4He is a heat-absorbing process, is capable of maintaining a temperature of $< 0.01^\circ\text{K}$, with no external heat input. The natural radioactivity of the 2.5 g of ^{237}Np used here resulted in an operating temperature of 0.135°K , however. This target was also placed in a superconducting coil whose field was parallel to the LMN magnetic field. In order to reduce eddy-current heating in the sample, the entire cryogenic apparatus was suspended from a 2300-kG marble slab supported by pneumatic pistons.

The fission neutrons were detected in 12 liquid scintillator cells, each 5 in. x 5 in. Pulse shape discrimination techniques were used to reduce the gamma-ray background.

The Oak Ridge Electron Linear Accelerator (ORELA) was used as a pulsed source of neutrons.

3. EXPERIMENTAL RESULTS

The relative fission cross-section has been measured from 1-1000 eV by detecting fission neutrons at 0° and 90° relative to the incident beam. In addition, the transmission has been measured from 1-102 eV. The target was located 13.4 meters from the source and the transmission detector was positioned at 15.2 meters. The ORELA was operated at a repetition rate of 1000 pps with a pulse length of 30 ns, resulting in an average power of 50 kW. With these parameters, the useful energy range of the fission data was determined by the signal-to-background ratio, whereas the transmission data were limited by resolution.

The data are composed of four pairs of runs, each run of approximately 24-h duration. Each pair is composed of one run with the beam and target polarization parallel and another with the direction of polarization antiparallel. The polarization of the neutron beam only was reversed; this was achieved by pumping transitions of electron-proton pairs which are parallel rather than those which are antiparallel. This reversal only required a change in magnetic field or, equivalently, in microwave pumping frequency, of $\sim 0.2\%$. Thus, no substantial change in operating conditions resulted from neutron polarization reversal.

In processing the data, each pair of runs was treated identically in order to preserve the normalization. An average background was subtracted from both runs in each pair, rather than a separate one for each run. After initial processing, the data were integrated over each resonance and the ratio, R , of the integrals for the parallel and antiparallel geometries was determined. This resulted in four independent measurements of J for each resonance.

The resonances observed in fission are listed in Table I. The quantities $R_\mu = \langle R \rangle$ are the mean ratios determined from the four pairs of runs. The two columns of errors represent the standard deviations from the mean and the statistical errors. The J values indicated are determined from the R_μ .

TABLE I. FISSION MEASUREMENTS

E_o (eV)	$R_\mu = \left\langle \frac{R_{\text{par}}}{R_{\text{anti}}} \right\rangle$	σ_μ	Statistical Error	J
26.6	1.259	$\pm .060$	0.131	3
30.4	1.086	.074	0.042	3
37.1	1.163	.064	0.060	3
38.9	1.091	.031	0.034	3
39.2	1.134	.036	0.047	3
39.9	1.169	.023	0.017	3
41.3	1.201	.041	0.036	3
46.0	1.160	.035	0.066	3
50.4	1.409	.084	0.154	3
119	1.207	.046	0.042	3
188	0.467	.153	0.243	2
195	0.818	.080	0.079	2
201	1.160	.036	0.035	3
207	1.393	.176	0.292	3
229	0.721	.218	0.150	2
234	0.839	.133	0.080	2
253	1.316	.091	0.098	3
283	0.946	.140	0.073	(2)
370	0.804	.143	0.119	2
373	0.745	.151	0.084	2
427	1.514	.284	0.158	3
476	0.819	.160	0.132	2
668	1.459	.616	0.437	3
718	1.918	.409	0.449	3
808	1.984	.306	0.240	3
873	0.810	.209	0.116	2
884	1.182	.078	0.146	3

The single uncertainty in extracting J values from such data is knowledge of the target polarization relative to the applied magnetic field. Either the magnetic moment of the target nucleus may be negative or the hyperfine field may be opposite to the impressed field. In the data presented here, the evidence appears to be conclusive that the target polarization is parallel to the applied field and, hence, that for $R_\mu > 1$, $J = 3$. The strongest evidence arises from the factor f_I in Eq. (1). This predicts a greater deviation from unity of R_μ for a resonance with $J = I - 1/2 = 2$ than for one with $J = I + 1/2 = 3$. Knowing the neutron beam polarization, f_N , Eq. (1) may be solved for f_N .

TABLE II. J ASSIGNMENTS FROM TRANSMISSION

E_0 (eV)	J	E_0 (eV)	J	E_0 (eV)	J
1.47	2	22.9	3	52.6	2
1.96	3	23.7	3	53.9	2
3.07	(3)	24.0	2	55.0	3
3.85	3	25.0	3	56.1	(2)
4.26	2	26.2	3	58.4	3
4.86	2	26.6	3	59.5	2
5.76	3	28.5	2	60.0	3
6.36	3	28.9	(2)	61.0	3
6.65	2	29.5	(2)	61.7	3
7.18	(2)	30.4	3	62.5	3
7.42	3	31.3	3	62.9	3
8.29	3	33.4	3	65.0	(3)
8.96	3	33.9	2	65.7	3
9.28	2	34.7	3	66.7	3
10.2	2	35.2	2	67.5	3
10.7	3	36.4	3	68.0	2
10.8	3	37.1	3	68.7	3
11.1	2	38.2	3	70.3	3
12.2	(3)	38.9	3	71.1	3
12.6	2	39.2	3	74.4	(2)
13.1	(3)	39.9	3	78.4	3
15.8	(3)	41.3	3	79.2	2
16.1	2	43.6	2	80.7	3
16.8	2	45.7	2	82.2	3
17.6	3	46.0	3	86.5	3
18.9	2	46.3	3	87.7	2
19.1	3	47.3	2	90.9	3
19.9	(3)	48.8	2	93.4	2
20.4	2	49.8	3	97.9	2
21.1	3	50.4	3	98.6	2
22.0	2	52.2	2	100.3	3
				101.1	2

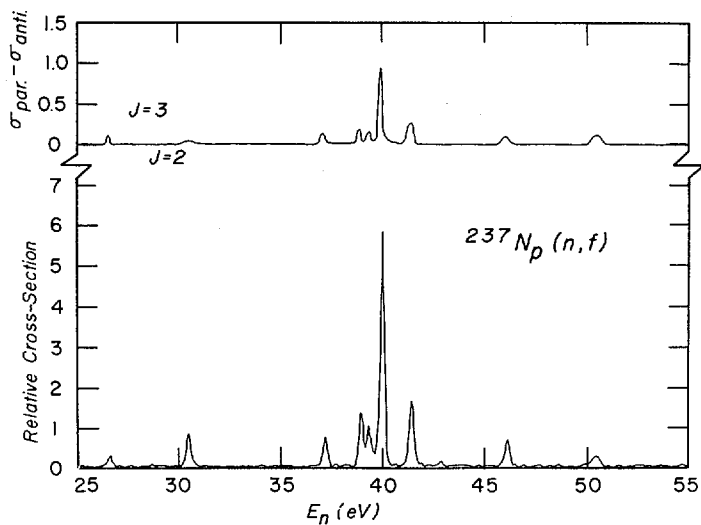


FIG. 1. Fission data in the region of the group at 40 eV. The upper curve, representing the difference between the cross-sections measured with beam and target polarization parallel and antiparallel, is consistently greater than unity over each of the nine individual resonances, indicating $J = 3$ in each case.

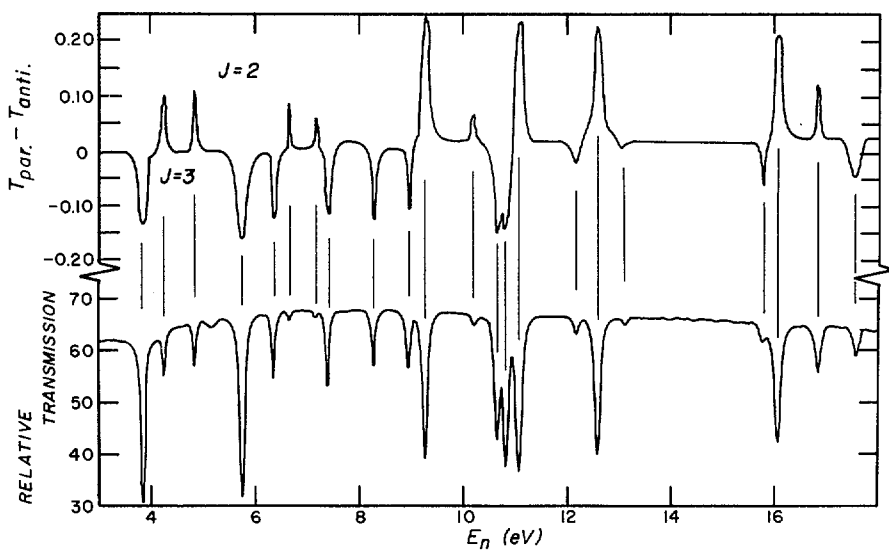


FIG. 2. A sample of the transmission data. The upper curve dips below zero for resonances with $J = 3$ and protrudes above zero for those with $J = 2$.

From Table I, the average R_M for resonances with $J = 3$ indicated in the table is 1.17 ± 0.02 and 0.79 ± 0.04 . From Eq. (1), one arrives at $f_N = 0.20$ from the $J = 3$ resonances and $f_N = 0.21$ from the $J = 2$ resonances. If, however, the assumption is made that the polarization is antiparallel to the applied field, then one determines $f_N = 0.30$ for the $J = 3$ states and $f_N = 0.14$ for those with $J = 2$. Clearly, the former assumption appears more valid. As supporting evidence, calculations [6] of hyperfine fields in actinide compounds based on systematic interpretation of Mössbauer effect data indicate that, for a hyperfine field of the magnitude of that observed in NpAl_2 , the sign must be positive. Further evidence relies upon the assumption that the level density, where no nonstatistical mechanism is present, should vary according to $2J + 1$. In Table II, the resonances observed in transmission are listed with the spins determined in this experiment. Of these 94 resonances, 57 are assigned $J = 3$ and 37 are assigned $J = 2$. Although the error is large on this sampling, the $2J + 1$ dependence is supported with these assignments and strongly violated for the opposite spin assignments.

The fission data in the region of the 40-eV structure are shown in Fig. 1. The enhancement of the compound nuclear levels is distributed over nine individual resonances. The curve labeled $\sigma_{\text{par}} - \sigma_{\text{anti}}$ is consistently greater than unity over each individual fine structure resonance, indicating that each resonance has the same spin, $J = 3$. A sample of the transmission data is shown in Fig. 2, over the range 4-18 eV. Here the plot of $T_{\text{par}} - T_{\text{anti}}$ demonstrates the clear distinction between resonances of different spin.

4. DISCUSSION

The inherent difficulty in determining spins by methods less direct than that employed in this experiment are well-known. Preliminary results of an experiment on ^{235}U using the equipment and techniques reported here are given in Table III. Comparison of spin assignments determined here and those assignments resulting from indirect methods are quite poor. Although some individual measurements are consistent, no single technique involving indirect methods appears to be at all reliable. For example, the results of Corvi et al. [7] are in excellent agreement, whereas the results of Weigmann et al., [8] using a similar technique, are in agreement on only 44% of the resonances studied. Although far less effort has been expended on the system $^{237}\text{Np} + n$, comparison of J assignments from the data presented here and from a measurement [9] of the total, scattering, and capture cross-sections further demonstrates the ambiguity of indirect spin determination. As shown in Table IV, the two sets of spin assignments are in no better than random agreement. Not only do the assignments for the resonances belonging to the group at 40 eV differ, but those below 26 eV are in agreement in only four out of nine cases.

Reference 9 also indicates a possible spin dependence of the mean capture width for resonances in each spin state. In that work, $\langle \Gamma_\gamma \rangle = 47$ meV for those resonances assigned $J = 3$ and $\langle \Gamma_\gamma \rangle = 57$ meV for those assigned $J = 2$. However, as Table V demonstrates, when the spin assignments from the experiment described here are applied to the capture widths of Ref. 9, the mean width is the same for both spin states. Similarly, examining a total of 62 resonances whose reduced neutron widths are compiled in Ref. 16 and whose J values are determined here, no spin dependence is observed, within the sizeable errors. The average values, $\langle \Gamma_n^0 \rangle$, for each J value are also given in Table V.

However, interpretation of the results of Kuiken, Pattenden, and Postma [1] with the J values assigned here is somewhat enlightening. In that experiment, the angular distribution of fission fragments from an aligned

TABLE III. ^{235}U J-ASSIGNMENTS

E_0 (eV)	PRESENT WORK	POLARIZATION [10]	CAPTURE [11]	CAPTURE [8]	CAPTURE [7]	CAPTURE [12]	γ -MULTIPLICITY [13]	SCATTERING [14]	SYMMETRY [15]
1.13	4	4	-	-	-	-	3	-	-
2.04	3	3	3	-	3	3	4	-	-
3.14	3	3	-	-	-	-	3	-	-
3.61	4	4	-	-	-	-	3	-	-
4.84	4	4	-	-	4	4	4	-	-
6.17	3	-	-	-	-	-	-	-	-
6.38	4	4	-	4	4	3	4	-	-
7.07	4	4	-	3	-	-	3	-	-
8.73	4	4	-	-	-	-	3	3	-
9.27	4	-	-	3	-	-	3	-	-
10.2	4	-	-	-	-	-	3	-	-
11.7	4	4	4	-	4	-	4	4	-
12.4	3	3	3	4	3	-	4	3	-
12.9	4	-	-	-	-	-	-	-	-
14.2	3	-	-	-	-	-	-	-	-
14.6	3	-	3	-	3	-	-	-	-
15.4	4	-	-	3	4	-	3	-	4
16.1	4	-	4	3	4	-	4	-	4
16.7	4	-	-	3	-	-	3	-	4
18.1	3	-	-	-	-	-	3	-	-
19.0	4	-	-	-	-	-	-	-	-
19.3	4	-	-	4	-	-	4	4	4
20.7	4	-	-	-	-	-	-	-	-
21.1	4	-	-	3	4	-	-	-	4
22.9	4	-	-	3	4	-	3	-	4
23.4	4	-	-	4	4	-	-	4	-

TABLE III. (continued)

E_0 (eV)	PRESENT WORK	POLARIZATION [10]	CAPTURE [11]	CAPTURE [8]	CAPTURE [7]	CAPTURE [12]	γ -MULTIPLICITY [13]	SCATTERING [14]	SYMMETRY [15]
23.6	3	-	-	-	-	-	-	-	4
24.2	3	-	-	-	3	-	-	-	3
25.6	3	-	-	-	-	-	-	-	3
27.8	4	-	-	4	-	-	3	-	4
29.7	4	-	-	-	-	-	-	-	-
30.6	3	-	-	-	-	-	-	-	-
30.9	4	-	-	3	4	-	-	-	4
32.0	4	-	3	4	-	-	4	4	4
33.5	4	-	-	4	-	-	4	4	4
34.4	4	-	-	3	-	-	4	4	3
34.9	3	-	-	-	-	-	-	-	4
35.2	4	-	-	4	-	-	4	4	-
35.3	3	-	-	-	-	-	-	-	-
38.4	4	-	-	-	-	-	-	-	3
39.4	4	-	-	4	-	-	4	3	3
40.5	4	-	-	-	-	-	-	-	4
41.9	3	-	-	-	3	-	-	3	4
44.0	4	-	-	-	-	-	-	-	4
44.6	4	-	-	-	-	-	-	-	3
45.9	4	-	-	-	-	-	-	-	4
48.0	4	-	-	-	-	-	-	-	4
48.3	3	-	-	-	-	-	-	-	-
48.8	3	-	-	-	-	-	-	-	4
49.5	4	-	-	-	-	-	-	-	3
51.3	4	-	-	-	-	-	-	4	4
55.1	4	-	-	-	-	-	-	4	-
56.6	4	-	-	-	-	-	-	3	4
PERCENT AGREEMENT		100	83	44	100	67	50	78	67

TABLE IV. COMPARISON OF J ASSIGNMENTS

E_0 (eV)	Present Work J	Poortmans et al.[9] J
5.76	3	3
10.8	3	3
11.1	2	2
12.6	2	3
16.1	2	2
20.4	2	3
22.0	2	3
23.7	3	3
25.0	3	2
26.6	3	2
30.4	3	2
46.0	3	(3)
47.3	2	(3)
50.4	3	2
43% Agreement		

TABLE V. J DEPENDENCE - AVERAGE WIDTHS

J = 2	J = 3
$\langle \Gamma_Y \rangle = 51.7 \pm 3.2 \text{ meV}$	$\langle \Gamma_Y \rangle = 52.3 \pm 1.7 \text{ meV}$
$\langle \Gamma_n^o \rangle = 0.019 \pm 0.007 \text{ meV}$	$\langle \Gamma_n^o \rangle = 0.018 \pm 0.006 \text{ meV}$

^{237}Np target was studied. For the experimental conditions realized in the alignment experiment, the angular distribution of fission fragments may be expressed as

$$\omega(\theta) = 1 + A_2 f_2 P_2(\cos \theta) \quad (2)$$

where f_2 is the alignment parameter and A_2 is given by

$$A_2 = \frac{15}{4} \frac{I}{I+1} \left\{ \frac{3K^2}{J(J+1)} - 1 \right\} \quad (3)$$

The intent of the experiment was to glean information about the K-quantum number, the projection of J on the nuclear symmetry axis. However, this task is made difficult by the lack of knowledge of the J values for each resonance studied.

The nature of the deformation barriers and the possible effects upon the observed K values is discussed by Kuiken et al. Current evidence in the form of a broad low peak under the 40 eV group, observed by Paya et al., [2] and the lack of lines in the gamma-ray spectrum corresponding to transitions between intermediate levels in the second well, indicate very weak coupling between the compound nuclear levels and the intermediate levels. This corresponds to a situation where the second barrier, at higher deformation, is lower than the first barrier. In this case, there may be some admixing of higher transition states, although Kuiken et al. assume this admixing to be small.

In Table VI, a list of those resonance groups observed in both the present work and by Kuiken et al. is given, along with the J assignments, the measured A_2 values, and the theoretical A_2 values. Poor resolution averages several of the A_2 values over more than a single fine structure resonance, in the 40-eV group, or over more than a single group, at higher energies. Using the assignment from Ref. 9 of $J = 2$ for the resonances in the group at 40 eV, Kuiken et al. concluded that the evidence was consistent with an integral K value, $K = 2$, for those resonances. However, the present assignment of $J = 3$ to this group makes this interpretation less tenable and implies an admixture of $K = 3$ and $K = 2$ components. For most of the resonances in the 40-eV group, the $K = 3$ component seems predominant, although alone insufficient to explain many of the measured A_2 values. Interpretation of the alignment results becomes more ambiguous at higher energies, owing to larger statistical errors. The structure at 119 eV has a measured A_2 value in between that expected for a resonance with $(J:K) = (3:3)$ and one with $(3:2)$. Similarly, the A_2 values for the three structures at 231, 283, and 370 eV, all of which are assigned $J = 2$, are most consistent with a mixture of $K = 2$ and $K = 1$ components. The pairs of structures near 200 and 870 eV were unresolved in the alignment data and, since the members of these pairs are of opposite spin, are difficult to interpret. The remaining structures appear to be consistent with integral K assignments of $(J:K) = (3:2)$.

Some conclusions may be deduced from the mean A_2 values for each spin state, shown in Table VI. In both cases, $K = 0$ transition states appear to be unavailable. The observed $\langle A_2 \rangle$ values are consistent with the explanation that the $K = 2$ channel is generally preferred with $(J:K) = (2:1)$ and $(3:3)$ partially open. The mean A_2 value for the $J = 3$ resonances would imply that the $K = 3$ channel is preferred for resonances of this spin, but this is primarily a result of the small errors on the individual resonances in the 40-eV structure. These resonances in the 40-eV group appear to preferentially decay through $K = 3$ transition states, whereas the remaining $J = 3$ structures prefer $K = 2$ channels.

TABLE VI. J vs. A_2 PARAMETERS

E_0 (eV)	J	A_2 [1]
26.6	3	2.98 ± 1.21
30.4	3	3.50 ± 0.47
37.1	3	0.62 ± 0.97
38.9	3	$*1.82 \pm 0.45$
39.2	3	
39.9	3	2.73 ± 0.26
41.3	3	2.36 ± 0.46
46.0	3	1.57 ± 1.00
50.7	3	3.25 ± 1.06
119	3	2.56 ± 0.21
193	2	$*-0.13 \pm 0.57$
203	3	
231	2	1.84 ± 1.45
253	3	-0.02 ± 1.30
283	(2)	0.57 ± 1.72
371	2	1.47 ± 1.34
427	3	-0.37 ± 1.87
873	2	$*1.86 \pm 1.74$
884	3	

THEORETICAL A_2 VALUES			
(J:K)	A_2	(J:K)	A_2
(2:0)	-2.679	(3:0)	-2.679
(2:1)	-1.339	(3:1)	-2.009
(2:2)	+2.679	(3:2)	0
		(3:3)	+3.348

MEAN OBSERVED A_2 VALUES	
$J = 2$	$J = 3$
$\langle A_2 \rangle = 1.38 \pm 0.35$	$\langle A_2 \rangle = 2.42 \pm 0.24$
	40-eV group $\langle A_2 \rangle = 2.56 \pm 0.24$
	Other groups $\langle A_2 \rangle = 0.76 \pm 0.50$

*Unresolved.

5. CONCLUSION

From the experimental results described here, several conclusions may be deduced. The Strutinsky theory of a double-humped fission barrier is substantiated as the mechanism by which intermediate structure in subthreshold fission is explained. The coupling of the Class II states in the second potential minimum to the compound nucleus states in the first minimum selects resonances of a single-spin state, that of the "parent" Class II state. From correlation of existing data on the angular distribution of fission fragments from aligned ^{237}Np with the data presented here, it is concluded that, at least in the odd-odd system $^{237}\text{Np}+n$, there is a substantial admixing of transition states, evidenced by nonintegral values of the projection quantum number, K . Although all values of K from zero to J are allowed, the value $K = 2$ appears to be predominant for resonances of both $J = 2$ and $J = 3$, with contribution from $K = 3$, $J = 3$ and $K = 1$, $J = 2$ states.

In contrast to the fission results, the total cross-section shows no intermediate structure with a $2J+1$ distribution of level densities. Similarly, no nonstatistical spin dependence is observed in the capture or neutron widths.

REFERENCES

- [1] KUIKEN, R., PATTENDEN, N. J., POSTMA, H., Nucl. Phys. A196 (1972) 389.
- [2] PAYA, D., DERRIEN, H., FUBINI, A., MICHAUDON, A., RIBON, P., "Nuclear data for reactors", (IAEA, Vienna, 1967) II, p. 128.
- [3] STRUTINSKY, V. M., Nucl. Phys. A95 (1967) 420.
- [4] SHAPIRO, F. L., Nuclear Structure Study with Neutrons, North-Holland Pub. Co., Amsterdam (1966) 223.
- [5] JEFFRIES, C. D., Dynamic Nuclear Orientation, Interscience Publishers, New York (1963).
- [6] DUNLAP, B. D., KALVIUS, G. M., Inter. J. Magnetism 2 (1972) 231.
- [7] CORVI, F., STEFANON, M., COCEVA, C., GIACOBBE, P., Nucl. Phys. A203 (1973) 145.
- [8] WEIGMANN, H., WINTER, J., HESKE, M., Nucl. Phys. A134 (1969) 535.
- [9] POORTMANS, F., CEULEMANS, H., THEOBALD, J., MIGNECO, E., (Proc. 3rd Conf. on Neutron Cross Sections and Technology, Knoxville, 1971) CONF-710301, Vol. 2, p. 667.
- [10] REDDINGIUS, E. R., POSTMA, H., OLSEN, C. E., RORER, D. C., SAILOR, V. L., Nucl. Phys. (submitted for publication).
- [11] GRAVES, R. D., CHRIEN, R. E., GARBER, D. I., COLE, G. W., WASSON, O. A., Phys. Rev. (submitted for publication).
- [12] KANE, W. R., Phys. Rev. Lett. 25 (1970) 953.
- [13] ASGHAR, M., MICHAUDON, A., PAYA, D., Phys. Lett. 26B (1968) 664.
- [14] POORTMANS, F., CEULEMANS, H., MIGNECO, E., THEOBALD, J. P., 2nd Inter. Conf. on Nuclear Data for Reactors, Helsinki (I.A.E.A., Vienna, 1970) 449.
- [15] COWAN, G. A., BAYHURST, B. P., PRESTWOOD, R. J., GILMORE, J. S., KNOBELOCH, G. W., Phys. Rev. 62 (1970) 615.
- [16] STEHN, J. R., GOLDBERG, M. D., WIENER-CHASMAN, R., MUGHABGHAB, S. F., MAGORNO, B. A., MAY, V. M., Neutron Cross Sections, Brookhaven National Laboratory report BNL-325, 2nd ed., Suppl. No. 2 (1965), (TID-4500, 42nd ed).

DISCUSSION

R. C. BLOCK: Raymond Reed at the Rensselaer Polytechnic Institute has just compared his prompt $\bar{\nu}$ results for ^{235}U with your spin assignments.

TABLE A. ^{235}U SPIN VALUES AND TERNARY TO BINARY (T/B) FISSION RATIOS

E (eV)	Spin preference as given by Milton in summing-up of the 1969 Vienna Symp.	Spin values of Keyworth et al. in full agreement with Corvi et al. and Reddingius et al.	T/B-classification Wagemans and Deruytter [Nucl. Phys. A194 (1972) 657] ^a
32.05		4	H : 4
30.84 } 30.6 }		4 } $\Gamma_f = 18 \pm 5$ meV 3 } $\Gamma_f = 70 \pm 20$ meV	(L) : (3) ^b
21.1	3	4	H : 4
19.3	4	4	H : 4
18.05	3	3	H : 4 wrong
16.67	3	4	(H) : (4)
16.10	3	4	U
15.45	3	4	H : 4
14.53		3	L : 3
14.0		3	L : 3
13.7		3	L : 3
12.39	4	3	L : 3
11.67	4	4	(H) : (4)
8.79	3	4 (30% : 3 Reddingius)	L : 3 wrong ^c
7.08	3	4	H : 4
6.39	4	4 } 3 }	(L) : (3) ^d
6.17			

^a H stands for high, L for low and U for uncertain T/B values. Brackets indicate that the statistical error is too large to be conclusive.

^b The largest contribution to σ_f comes from the 3^- resonance, so our assignment is justified.

^c The measurements of Reddingius and co-workers clearly indicate the presence of a doublet for the 8.79-eV resonance. They claim it might be a doublet, of which one component with about 30% of the total strength has spin 3^- .

^d The assignment L : 3 for this resonance is strongly influenced by the underlying cross-section of the 6.17-eV resonance of spin 3.

The $\bar{\nu}$ results do vary from resonance to resonance and they seem to cluster into two groups. However, there appears to be no correlation between $\bar{\nu}$ and the J assignments from your experiment.

G. A. KEYWORTH: We have also examined this question with both the Rensselaer Institute's and other $\bar{\nu}$ data and arrived at the same conclusion. Perhaps the paper by Fréhaut and Shackleton¹ may shed some light on a possible correlation of $\bar{\nu}$ with some quantity other than spin.

A. J. DERUYTTER: The very remarkable and excellent measurements of Keyworth and co-workers show the danger of indirect measurements of spin values, even if there are many such experiments available. In his

¹ FREHAUT, J., SHACKLETON, D., Paper IAEA-SM-174/47, these Proceedings, Vol. 2.

summing-up of the 1969 IAEA fission symposium, J.C.D. Milton used six such experiments and arrived at completely different values, as shown in Table A. Our T/B measurements for ^{235}U are shown in the last column. The really disturbing value here is the 8.79-eV resonance, because it makes a large contribution to the low-energy fission integral and should have been one of the best cases for comparison.

However, assuming the Keyworth values to be correct, we made only two incorrect assignments out of 18. Only the discrepancy at the 18.05-eV resonance seems to have no explanation. We do not however consider this proof that a perfect correlation between spin and T/B exists.

FISSION BARRIERS: THEORY (STATIC)
(Session II)

Chairman: J.J. Griffin (United States of America)

Review Paper

CALCULATION OF FISSION BARRIERS*

P. MÖLLER, J. R. NIX
 Los Alamos Scientific Laboratory,
 University of California,
 Los Alamos, N. Mex.,
 United States of America

Abstract

CALCULATION OF FISSION BARRIERS.

Recent advances in the calculation of the nuclear potential energy of deformation, including both self-consistent microscopic methods and the macroscopic-microscopic method are reviewed. Particular attention is paid to the steps that are involved in calculating the potential energy according to the latter method. These steps include specifying the nuclear shape, calculating the macroscopic (liquid-drop) energy, generating the single-particle potential, solving the Schrödinger equation, and calculating the microscopic (shell and pairing) corrections.

In the second part of the paper the results of the new calculations that have been performed recently at Los Alamos are presented and compared. In the first calculation, the nuclear shapes are specified in terms of smoothly joined portions of three quadratic surfaces of revolution, which permits the calculation of the potential energy all the way to the scission point. The extrema in the potential-energy surfaces are determined by varying independently three of the coordinates in this parametrization; the ground-state energy is determined also by use of an alternative parametrization. The macroscopic energy is calculated from the droplet model of Myers and Swiatecki, which includes higher-order terms in $A^{-1/3}$ and in $[(N-Z)/A]^2$ than are retained in the liquid-drop model. The microscopic shell and pairing corrections are calculated by means of Strutinsky's method from the single-particle levels of a diffuse-surface folded Yukawa single-particle potential. A new set of potential parameters is used, which was obtained from adjustments to experimental single-particle levels in heavy deformed nuclei and from statistical calculations. The second new calculation is performed with the modified oscillator potential and is similar to a previous calculation with this potential except that the droplet model is used in place of the liquid-drop model.

These and earlier calculations provide an understanding and unification of many varied phenomena associated with nuclear shape changes: nuclear ground-state masses and deformations, second minima in the fission barriers of actinide nuclei, fission-barrier heights, and fission-fragment mass distributions. For the lighter actinide nuclei, the asymmetric second saddle point is split into two individual saddle points separated by an asymmetric third minimum, which possibly resolves the thorium anomaly. The calculated energies of the local minima and saddle points in the potential-energy surfaces reproduce the experimental values to within an accuracy of about 1 MeV, although larger systematic errors are still present in some cases. The calculated properties of the saddle points also reproduce qualitatively the main features of experimental fission-fragment mass distributions.

1. INTRODUCTION

You probably have followed the renaissance that has taken place in our understanding of fission since the first IAEA fission symposium in Salzburg eight years ago. At that symposium we still thought that the fission barrier of a nucleus was a monotonically increasing function of deformation until it reached its maximum value and then a monotonically decreasing function of deformation. But it soon became clear that instead of this smooth behavior the fission barrier contains large fluctuations as a function of

* This work was supported by the US Atomic Energy Commission and the Swedish Atomic Research Council.

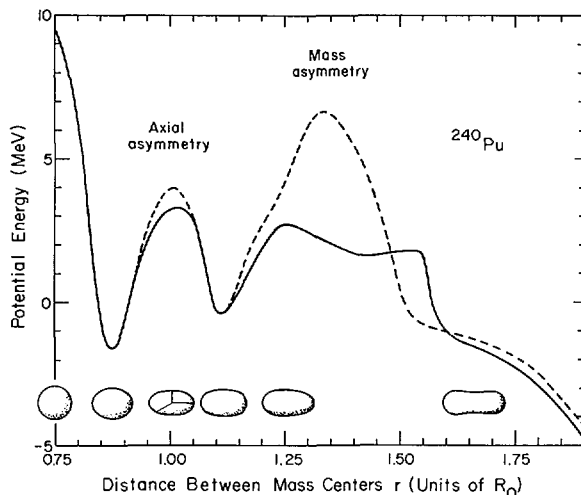


FIG. 1. Effect of axial asymmetry and mass asymmetry on the fission barrier of ^{240}Pu . The dashed curve (which sometimes coincides with the solid curve) gives the potential energy for symmetric deformations as a function of the distance r between the centers of mass of the two nascent fragments. The solid curve gives the potential energy along a path that leads over the axially asymmetric first saddle point and over the mass-asymmetric second saddle point. The lower portion of the figure shows the nuclear shapes corresponding to selected points along this path, namely the sphere, four equilibrium points, and the point of emergence from the barrier in spontaneous fission. The results for axially symmetric shapes are calculated with the folded Yukawa potential and the droplet model by use of methods to be described later. The reduction in energy at the first saddle point is taken from Ref. [1].

both nuclear shape and particle numbers. For some nuclei, these fluctuations lead to a fission barrier that contains two peaks separated by a second minimum, as illustrated in Fig. 1 for ^{240}Pu .

By the time of the second IAEA fission symposium in Vienna four years ago, we were able to calculate such a barrier for symmetric deformations in terms of nonuniformities in the single-particle levels near the Fermi surface. We could also understand three new experimental discoveries--spontaneously fissioning isomers, broad resonances in fission cross-sections, and narrow intermediate structure in fission cross-sections--in terms of this second minimum.

But three major puzzles remained. First, for most actinide nuclei the calculated height of either the first peak or the second peak was several MeV higher than the experimental value. Second, the calculated fission barriers were all stable with respect to mass-asymmetric deformations, which violated the well-established preference of heavy nuclei to divide asymmetrically at low excitation energy. And third, the calculated heights of the first peak and second minimum for isotopes of thorium were substantially lower than the experimental values.

Since Vienna two of these puzzles have largely disappeared. We now know that in most actinide nuclei the second peak is unstable with respect to mass asymmetry and that in the heavier actinide nuclei the first peak is unstable with respect to axial asymmetry (gamma deformations). Instabilities of this type lower the calculated barrier heights and also provide a

mechanism for an asymmetric mass division. These instabilities arise because of single-particle effects similar to those responsible for a deformed ground-state minimum and second minimum in the fission barrier. The third puzzle is not definitely solved, but we suggest later a possible resolution in terms of single-particle effects near the asymmetric second saddle point.

Our plan is first to review the various approaches that are taken in the calculation of fission barriers and second to present some new results that we have obtained at Los Alamos. We do not have space here to review everyone's contributions but instead concentrate on recent results that best illustrate the physical principles involved. Exhaustive references to other work, as well as to the mathematical details, can be found in four recent review articles [2-5]. We then compare the calculated energies of the local minima and saddle points in the barriers with experimental results, some of which are described in this symposium by Britt, Vandenbosch, and others [6,7]. We also discuss the extent to which experimental fission-fragment mass distributions can be understood in terms of the calculated properties of the saddle-point shapes. We conclude with an assessment of our present ability to calculate fission barriers.

2. SELFCONSISTENT MICROSCOPIC METHODS

There are two general approaches for calculating the nuclear potential energy of deformation—selfconsistent microscopic methods and the macroscopic-microscopic method. In the microscopic methods, one usually starts with a given nucleon-nucleon potential and solves the many-body Schrödinger equation by means of the Hartree-Fock approximation. This can be done either with a realistic potential that is adjusted to reproduce fundamental data such as two-nucleon scattering data, or with an effective interaction that is adjusted to reproduce gross nuclear properties.

The realistic potentials of course lead to equations that are more difficult to solve. If the potential has a hard core, then the infinities associated with it must be removed by means of the approximations introduced by Brueckner. The resulting Brueckner-Hartree-Fock equations are so complicated that they have been solved so far only for spherical nuclei [8,9].

The equations are simpler for a soft-core potential, where the ordinary Hartree-Fock method can be applied. At deformations away from a local minimum the potential energy is calculated by applying an external field and solving the resulting constrained Hartree-Fock equations. In this way the potential energy has now been computed as a function of the quadrupole moment for some medium-weight nuclei such as ^{108}Ru [10]. However, computational difficulties have prevented the extension of these calculations to heavy nuclei. For heavy spherical nuclei the calculated total binding energies are substantially smaller than the experimental values [11]. Although the agreement would be improved somewhat by including the second-order correction to the Hartree-Fock energy [12], this correction has not yet been calculated for deformed nuclei.

A major difficulty associated with the use of realistic potentials is the necessity to calculate the exchange terms in the Hartree-Fock equations. This difficulty can be eliminated by choosing an effective interaction for which the exchange terms are easy to calculate. Or alternatively, the exchange effects can be absorbed into the effective interaction [13,14]. With either approach the higher-order corrections to the first-order energy are absorbed into the interaction through a readjustment of its parameters.

Although several effective interactions have been proposed, the only one that is used in practice for the calculation of fission barriers is Skyrme's interaction [15] as simplified by Vautherin and Brink [16]. This interaction is easy to use because most of its terms contain delta functions and because saturation is achieved by means of a three-body term. The six adjustable parameters of the interaction are related loosely to the coefficients of the five dominant terms in the semiempirical nuclear mass formula (corresponding to the volume, surface, Coulomb, volume-asymmetry, and surface-asymmetry energies) and to the spin-orbit interaction strength.

The Skyrme interaction has now been used by Flocard, Quentin, Kerman, and Vautherin to compute the potential energy as a function of the quadrupole moment for several isotopes of cerium [17] and more recently for ^{240}Pu [18]; we will learn about such calculations later in this session from Quentin [19]. The calculated height of the second peak in the barrier for ^{240}Pu is 19 MeV, which is substantially higher than the experimental value of 5.35 MeV [20]. This large discrepancy probably arises from a combination of three factors: (1) The results have not converged as a function of the basis size. (2) The parameters of the Skyrme interaction yield a surface energy that is too large compared to the Coulomb energy. (3) Mass-asymmetric deformations are not included. When these three points are taken care of we can expect such calculations to reproduce experimental fission barriers with satisfactory accuracy. This is the most promising of the microscopic approaches, and perhaps four years from now at the fourth IAEA fission symposium a substantial fraction of the fission barriers discussed will be computed selfconsistently in terms of such an effective interaction.

3. MACROSCOPIC-MICROSCOPIC METHOD

But at present nearly all fission barriers are calculated by means of the second approach—the macroscopic-microscopic method. This method synthesizes the best features of two complementary approaches: The smooth trends of the potential energy (with respect to particle numbers and deformation) are taken from a macroscopic model, and the local fluctuations are taken from a microscopic model. The method in its present form was developed in 1966 by Strutinsky [21] and has since revolutionized the calculation of fission barriers. The idea of a macroscopic-microscopic method had been introduced earlier by Swiatecki [22] and others.

In this method, which is suitable for treating nuclear systems that contain a large number of particles, the total nuclear potential energy of deformation is written as the sum of two terms,

$$V = V_{\text{macroscopic}} + \Delta V_{\text{microscopic}}$$

The first term is a smoothly varying macroscopic energy that reproduces the broad trends of the potential energy. In a heavy nucleus it accounts for about 99.5% of the 2000 MeV total binding energy and for about 95% of the 200 MeV variation in energy during fission. The second term contains oscillating microscopic corrections that arise because of the discreteness of the individual particles. The most important of these purely microscopic contributions are the shell and pairing corrections. For a tightly bound nucleus in its ground state the total microscopic correction is over 10 MeV in magnitude, but in other situations it is usually somewhat less.

The nuclear potential energy of deformation is calculated by means of the macroscopic-microscopic method in five steps: (1) The overall geometrical shape of the nucleus is first specified, and (2) the macroscopic part of the energy is calculated for this shape. (3) The single-particle potential felt by a neutron or proton is generated, and (4) the Schrödinger equation is solved for the single-particle energies. (5) These energies are then used to calculate the microscopic (shell and pairing) corrections. The total potential energy is given finally by the sum of the macroscopic energy calculated in step 2 and the microscopic corrections calculated in step 5. These steps have received considerable study, and several methods have evolved for handling each of them.

3.1. Nuclear shapes

In fission, as well as in the related areas of heavy-ion reactions and nuclear ground-state masses and deformations, at least four collective coordinates are required to describe the most important shapes that arise. These are (1) a separation coordinate, which specifies the overall separation of the mass centers of the two nascent or separated fragments or colliding ions, (2) a mass-asymmetry coordinate, which specifies the amount of mass in one fragment relative to the other, (3) a fragment elongation coordinate, which specifies the overall elongation of the fragments, or alternatively the radius of the neck between them, and (4) an axial-asymmetry (γ) coordinate, which specifies the flattening of the shape about its symmetry axis. Because of computational difficulties the latter coordinate is not included in most studies in fission. Our discussion is therefore sometimes restricted to axial symmetry, but the generalization to axially asymmetric shapes is straightforward.

The methods for describing such shapes fall into two major classes. The first class is an expansion about some basic shape, such as a sphere, a spheroid, or a Cassinian oval. For example, shapes close to a sphere are described conveniently by expanding the radius vector to the nuclear surface in a series of spherical harmonics. If the shape is elongated it is better to absorb some of the deformation into the basic shape and expand about a spheroid (ellipsoid of revolution). This can be done either by means of the coordinates e_1 used by Nilsson and others [1, 2, 23-29], or by writing ρ^2 as a polynomial in z , which is the method used by Lawrence, Hasse, Strutinsky, Pauli and others [3, 5, 30-35]. If the shape has already developed an appreciable neck it is sometimes advantageous to expand about a Cassinian oval, which can absorb some of the necking as well as elongation into the basic shape; this method is used by Cherdantsev and co-workers [36] and by Pashkevich [37].

The second class of methods describes the shape in terms of two bodies rather than a single body. In these two-center parametrizations each end of the nucleus is usually represented by a portion of a spheroid. In the most simple version the two spheroids intersect in an undesirable cusp [38], but this cusp may be removed by connecting portions of the two end spheroids smoothly with a third function that describes the neck region. In the method used by Greiner, Mosel, and their co-workers [39-43], precisely one-half of each end spheroid is used in forming the shape, which unfortunately prevents the description of diamond-like nuclear ground-state deformations and some important shapes that arise in heavy-ion reactions. In another method [44-52], arbitrary portions of the two end spheroids are connected smoothly by a quadratic neck function.

Because an expansion method is usually better for describing nuclear ground-state deformations and the early stages of fission, whereas a two-center method is usually required for describing the later stages of fission

and heavy-ion reactions, it is desirable to define the collective coordinates in some parametrization-independent way that permits a connection to be made between the various methods. Of course the ideal choice would be to define the coordinates so that the resulting inertia matrix is everywhere diagonal and constant. This is in general impossible to accomplish, and the best that we can achieve at present is to define the coordinates in terms of physically measurable quantities.

For symmetric shapes a good choice involves the use of successive central moments of one-half of the mass distribution [53]. Then the separation coordinate is simply the distance between the centers of mass of the two nascent or separated fragments, and the fragment elongation coordinate is the root-mean-square extension of a fragment about its center of mass. As Sierk will discuss later in the symposium, this choice has already proved useful for displaying dynamical paths in fission and heavy-ion reactions [51]. The mass-asymmetry coordinate may be defined conveniently (and unambiguously) as the difference between the masses to either side of the point midway between the ends of the shape [3, 5, 33]. For shapes with a well-defined neck a more pleasant choice would involve the masses to either side of the neck, but in practice the two definitions are approximately equivalent because in such cases the volume in the neck region is small.

3.2. Macroscopic energy

Once the nuclear shape is specified, the macroscopic energy must be calculated for this shape. This usually is done by expanding the nuclear energy in powers of $A^{-1/3}$ and $[(N-Z)/A]^2$. Truncating the expansion at the $A^{2/3}[(N-Z)/A]^2$ term leads to the liquid-drop model, where the two shape-dependent terms are the cohesive surface energy and the disruptive Coulomb energy.

The inclusion of higher-order terms in the expansion leads to the droplet model, which takes into account effects that are associated with the finite size of nuclei, such as nuclear compressibility [54-56]. Myers and Swiatecki have now determined a preliminary set of constants for the droplet model [56] from adjustments to nuclear ground-state masses and fission-barrier heights and from statistical calculations. The resulting curvature-energy constant is zero. The effective surface-asymmetry constant, which regulates how rapidly fission barriers are lowered with the addition of neutrons, is significantly larger for heavy nuclei than the value in their earlier liquid-drop model [57]. As Howard will describe in the next paper [50], this makes it unlikely that superheavy nuclei can be formed by multiple neutron capture.

The condition that must be satisfied in order for the nuclear energy to be expanded in this way is that the surface diffuseness be small compared to the extension of the neighboring volume region. This condition breaks down for light nuclei and for shapes with small necks, for example near the scission point in fission and near the point of first contact in heavy-ion reactions. When calculating the energy of such shapes it is necessary to take into account the finite range of the nuclear force.

This could be done by treating an effective nucleon-nucleon interaction in some statistical approximation such as the Thomas-Fermi method [54, 58, 59]. However, in practice such calculations have been limited either to small deformations [60] or to two light spherical nuclei specified by a single separation coordinate [61, 62].

A simpler method has been developed recently for including finite-range effects. In this method the nuclear macroscopic energy is calculated in

terms of a double volume integral over a Yukawa function. As Krappe will discuss later in this session [63], this leads to several important consequences, such as a reduction in the stiffness of light nuclei with respect to deformation. This lowers the fission barriers of nuclei near silver by about 10 MeV relative to those calculated with the liquid-drop model and shifts the critical Businaro-Gallone point (where stability against mass asymmetry is lost) to $Z^2/A \approx 23$, in approximate agreement with recent experimental evidence. The reduced stiffness also leads to a secondary minimum in the potential energy of ^{40}Ca and certain other light nuclei, which provides a natural interpretation of the rotational states observed in these nuclei. In addition, experimental interaction-barrier heights for systems ranging from $^{40}\text{Ca} + ^{16}\text{O}$ and $^{208}\text{Pb} + ^4\text{He}$ to $^{238}\text{U} + ^{84}\text{Kr}$ are reproduced to within 5% accuracy. This method also provides a way to calculate the nuclear macroscopic energy corresponding to the inner surface of a bubble nucleus [64].

3.3. Single-particle potential

Once the nuclear shape is specified and the macroscopic energy is calculated, the next step is to generate the single-particle potential for this shape. We know of course that the true potential is nonlocal and that it would require a selfconsistent calculation for its determination. But the great virtue of the macroscopic-microscopic method is that single-particle effects can be extracted approximately from a local static potential that is not generated selfconsistently.

Figure 2 illustrates our qualitative expectations concerning the spin-independent part of the nuclear potential. Because the single-particle potential arises from the interaction of a nucleon with its close neighbors,

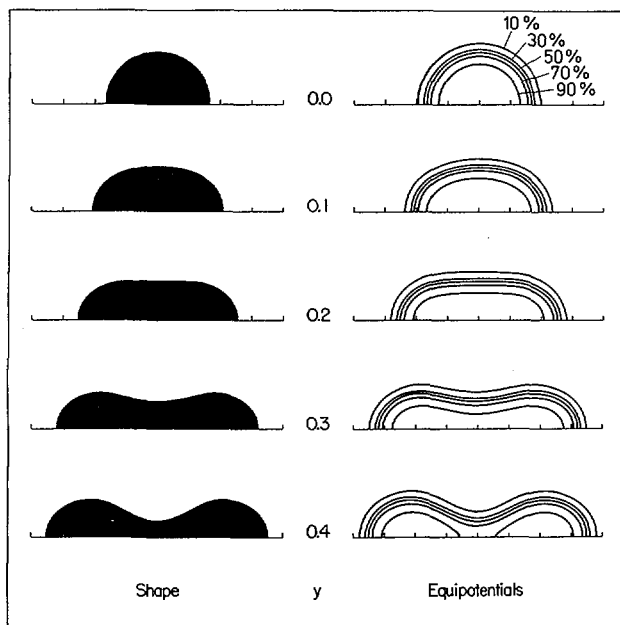


FIG. 2. Nuclear shapes described by the fission coordinate y , and the corresponding spin-independent nuclear single-particle potentials for a diffuse-surface folded Yukawa potential [45, 47, 49]. The equipotential curves are shown for 10, 30, 50, 70 and 90% of the well depth.

it is roughly constant in the nuclear interior and rises to zero within a surface region whose thickness is approximately independent of nuclear size and position on the surface. For separated nuclei the potential has similar features concentrated in each of the individual nuclei. This means that near the scission point in fission, or near the point of first touching in heavy-ion reactions, the potential is roughly constant in the interior of each nucleus and is elevated somewhat in the neck region. The overall geometrical shape of the potential follows closely that of the nucleus.

The potentials that have been developed for approximating this behavior fall into two general classes: modified oscillator potentials that rise to infinity at large distances, and diffuse-surface potentials that go to zero at large distances. Modified oscillator potentials are usually obtained by starting with a potential that rises parabolically to infinity from either one or two centers. An angular-momentum correction term proportional to ℓ^2 is then added, which in effect makes the potential rise more slowly near the center and faster near the nuclear surface. In an ordinary (one-center) potential, which has been studied extensively by Nilsson and others [1, 2, 21, 23-29, 32, 65, 66], the minimum of the original oscillator potential always occurs at the nuclear center. However, for sufficiently large deformations it is possible that the ℓ^2 correction term leads to a potential that in effect has two centers [67]. In the potential commonly referred to as a two-center potential, which has been used by Cherdantsev, Greiner, Mosel, and others [36, 39-43, 52], two separate minima occur in the original oscillator potential itself. At first sight this may seem clearly preferable. However, when the fragment centers separate, the two-center potential rises several times as rapidly in the neck region as would be expected from fundamental considerations. This leads to the possibility that some of the conclusions based on this potential are associated with this spurious feature.

There are also two major types of diffuse-surface potentials. The first type is obtained by generalizing a spherical Woods-Saxon potential to deformed shapes. In the generalization used by Pashkevich, Strutinsky, Pauli, and others [3, 5, 32-35, 37, 68], the potential's normal diffuseness is to first order constant over the surface. The resulting generalized Woods-Saxon potential is satisfactory for most shapes, but contains unphysical features when the neck radius is smaller than the diffuseness parameter. It therefore cannot be used to describe shapes near the scission point in fission or near the point of first touching in heavy-ion reactions.

The second type of diffuse-surface potential is generated by folding a Yukawa function over a uniform sharp-surface generating potential whose shape corresponds to the given nuclear shape [45-50]. In other words, a finite square-well potential of the appropriate depth and geometrical shape is converted into a diffuse-surface potential by folding a Yukawa function over it; the range of this function is chosen to reproduce the desired surface diffuseness. For small deformations the resulting potential is very close to a generalized Woods-Saxon potential. The major advantage of this folding procedure is that it can be used to generate easily a potential for any conceivable shape, including the transition for shapes with small necks to a potential concentrated in each of two individual nuclei, or vice versa. The potentials shown in Fig. 2 were generated in this way.

Besides the spin-independent part of the potential, there is an additional potential arising from the interaction between the nucleon spin and orbital angular momentum. Finally, protons feel a Coulomb potential, which is calculated easily by assuming that the nuclear charge is distributed uniformly within the nuclear surface or within the nuclear generating potential.

However, in studies with oscillator potentials the Coulomb potential usually is not included explicitly, but its effects are absorbed by readjusting the parameters of the nuclear part of the potential.

Irrespective of how it is generated, the final potential usually contains about six parameters that effectively describe the depth, radius, diffuseness, and spin-orbit strength of the potentials for neutrons and protons. In studies with oscillator potentials these parameters are usually determined from adjustments to experimental single-particle levels in heavy deformed nuclei. For diffuse-surface potentials some of the parameters can be obtained from statistical calculations [69]; the remainder are usually determined from adjustments to experimental single-particle levels in either heavy spherical or heavy deformed nuclei.

3.4. Solution of Schrödinger equation

Once the potential appropriate to a given shape is generated, the next step is to solve the Schrödinger equation for the single-particle energies. There are two general methods for doing this: expansion in basis functions and finite-difference methods. The expansion methods are usually several times as fast as the finite-difference methods for calculating single-particle energies with comparable accuracy [46, 47]. For most applications in fission the preferred choice is to expand the wave function in a set of deformed harmonic-oscillator basis functions.

3.5. Microscopic corrections

Once the single-particle energy levels are solved for, the microscopic corrections to the potential energy must be extracted from them. The two most important of these corrections are the shell correction and the pairing correction,

$$\Delta V_{\text{microscopic}} = \Delta V_{\text{shell}} + \Delta V_{\text{pairing}}$$

They arise because of fluctuations in the actual distribution of levels relative to a smooth distribution.

These fluctuations are especially dramatic for a pure harmonic-oscillator potential, as shown in Fig. 3. For a shape of high symmetry, such as a sphere or a spheroid whose major axis to minor axis is in the ratio of two small integers, the levels group into highly degenerate shells [70]. For such a shape, the energy of the system is relatively lower for particle numbers that complete a shell than for intermediate particle numbers. At other deformations, the levels are distributed more uniformly. In an actual nucleus similar fluctuations in the single-particle levels give rise to microscopic corrections that oscillate with deformation and particle numbers. These are the oscillations that are responsible for deformed ground states, second minima in fission barriers, and asymmetric saddle-point shapes.

The primary theoretical justification for extracting the shell correction from single-particle energies is provided by the stationary property of the Hartree-Fock solution: To first order in the deviation of the actual nuclear density from a smooth density, the total Hartree-Fock energy is equal to the sum of single-particle energies

$$\sum_{n=1}^N \epsilon_n$$

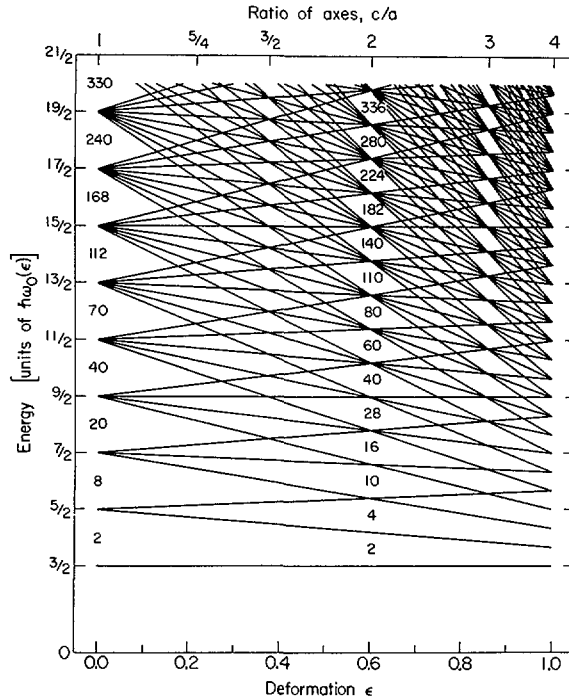


FIG. 3. Energy levels of a harmonic-oscillator potential for prolate spheroidal deformations [49]. The particle numbers of the closed shells are indicated for a sphere and for a spheroid whose major axis is twice its minor axis.

calculated from a smooth single-particle potential, plus a smoothly varying term [3, 5, 9, 10, 65, 71, 72]. Therefore, to first order in nuclear density deviations, the fluctuations that we want to isolate are contained in this sum of single-particle energies. As Brack will discuss later in this session [71], second-order effects in the shell correction [72] are expected in general to be about 1 MeV in magnitude, but could be somewhat larger for spherical nuclei. These second-order effects are probably responsible for some of the remaining discrepancies between calculated and experimental results.

The extraction of the shell correction from the single-particle energies has a simple geometric interpretation, as illustrated in Fig. 4. First plot the energies ϵ_n at a given deformation vs the single-particle number n . For a macroscopic system without single-particle effects all the energies would lie on a smooth curve, but the discreteness of the single particles causes some fluctuations about a monotonically increasing function of n . The discrete energies ϵ_n can be regarded as a staircase function formed by horizontal and vertical lines through the points. Next remove the local fluctuations of the staircase function while retaining its long-range behavior by passing a smooth curve $\bar{\epsilon}(n)$ through it. Then the shell correction for a specified number of particles N is given simply by the difference between the areas under the staircase curve and the smooth curve up to N ; that is,

$$\Delta V_{\text{shell}} = \sum_{n=1}^N \epsilon_n - \int_0^N \bar{\epsilon}(n) \, dn$$

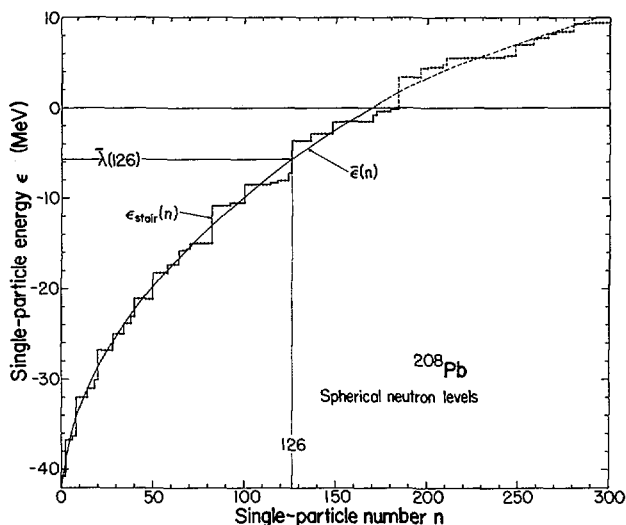


FIG. 4. Extraction of the shell correction from single-particle energies [47, 49]. The neutron levels in a spherical ^{208}Pb nucleus are shown by solid points and define a staircase function $\epsilon_{\text{stair}}(n)$. The smooth curve $\bar{\epsilon}(n)$ removes the local fluctuations of the solid points but retains their long-range behavior. The Fermi surface $\bar{\lambda}$ of the smooth distribution of levels is illustrated for 126 neutrons. The corresponding shell correction is given by the difference between the areas under the staircase curve and the smooth curve up to $n = 126$.

A variety of methods have been proposed for determining the smooth curve $\bar{\epsilon}(n)$. Unfortunately, most of these methods work only for certain simple potentials and cannot be used, for example, with potentials that contain a spin-orbit term. For realistic potentials of arbitrary shape, the most satisfactory way at present to determine $\bar{\epsilon}(n)$ is by use of Strutinsky's method [21], which was described to us at the second IAEA fission symposium by Strutinsky himself [32]. We need not repeat the technical details of his method here.

An alternative method has been studied for calculating the shell correction from the high-temperature dependence of the entropy of the single-particle system on excitation energy [73-77]. For heavy nuclei the results obtained by use of this method agree with those obtained by use of Strutinsky's method to within about 0.5 MeV. Perhaps this method will be discussed during the session on thermodynamic properties of nuclei.

The second type of single-particle correction—the pairing correction—arises from the short-range interaction of correlated pairs of nucleons moving in time-reversed orbits. This is the most important and easily treated of the many residual interactions felt by a nucleon. Relative to the energy without pairing, this interaction always lowers the energy. But relative to the pairing energy of a smooth distribution of levels representing an average nucleus, the pairing correction can have either sign. The lowering in energy is larger when more pairs of nucleons are able to interact, which occurs when the level density near the Fermi surface is high. This is opposite to the behavior of the shell correction, and this leads to a partial cancellation of the two corrections. Because the shell correction is larger, it determines the main trends of the total single-particle correction.

The essential features of the pairing correction can be described in terms of a constant pairing interaction between a given number of pairs of particles. Then a standard pairing calculation in the BCS approximation gives the lowering in energy for the actual levels. A similar calculation for the same number of particles distributed smoothly according to $\bar{\epsilon}(n)$, or in practice distributed uniformly, gives the lowering for an average nucleus. The difference between the lowering for the actual levels and the lowering for the smooth levels is the pairing correction.

Once the fluctuating shell and pairing corrections are calculated, the final step is to add them to the smooth macroscopic energy calculated in step 2 to obtain the total potential energy.

These methods have now been used by several groups to calculate the fission barriers for dozens of nuclei [1-5, 24-28, 32-37, 41-43, 47-50, 52, 65, 66, 68]. In most instances the results obtained by the different groups are qualitatively similar, although some differences exist. Rather than trying to review all of this work, we would like to describe instead some new results that we have obtained recently at Los Alamos.

4. NEW CALCULATIONS

We have performed two separate new calculations: one with the folded Yukawa potential and the other with the modified oscillator potential. Both of these calculations are limited to even nuclei. In the former calculation, there are three main differences compared to previous studies with this potential. First, we now use the droplet model in place of the liquid-drop model for calculating the macroscopic energy. The constants of the droplet model are a preliminary set determined by Myers and Swiatecki in January 1973 [56]. We may therefore regard the present results as one step in the complex iteration that is required for a final determination of these constants.

Second, we now investigate a larger part of the deformation space when determining the extrema of the potential-energy surfaces. Our exact procedure is described in the appendix, but the idea is that in the region that includes the first and second saddle points and the second minimum we minimize the potential energy calculated in the three-quadratic-surface parametrization with respect to a necking coordinate. During this minimization the eccentricities of the two ends of the nucleus and the distance between the centers of mass of the two nascent fragments are held fixed at the values corresponding to the y family of shapes [45, 47]. In the region of the ground state a somewhat different constraint on the three-quadratic-surface parametrization is used. The ground-state energy is also calculated by use of the two coordinates ϵ and ϵ_4 in Nilsson's perturbed-spheroid parametrization [1, 2, 23-29], which for most deformed nuclei yields a lower energy. In the region somewhat beyond the second saddle point down to scission the potential energy is no longer minimized (because the nucleus is on the side of a steep hill), but is calculated instead for shapes along the most probable idealized liquid-drop-model dynamical path for fissility parameter $x = 0.8$ [44, 51] and for asymmetric perturbations about these shapes. The fissility parameter is defined as the ratio of the Coulomb energy of a spherical sharp-surface drop to twice the spherical surface energy.

In all regions the final potential energy is displayed in terms of a fission coordinate r , defined as the distance between the mass centers of the two halves of the dividing nucleus, and a mass-asymmetry coordinate $(M_1 - M_2)/M_0$, defined as the difference between the masses to either side of the point midway between the ends of the shape. For computational convenience the fission coordinate for an asymmetric shape is chosen equal to the fission coordinate for the corresponding symmetric shape.

The third difference is that we are now using a new set of parameters for the single-particle potential. Our original set of parameters was determined from statistical calculations and from adjustments to experimental single-particle levels in the heavy spherical nucleus ^{208}Pb [47]. In the new set, which has been determined in collaboration with Nilsson, we have re-determined the range of the Yukawa folding function (which regulates the surface diffuseness of the potential) and the spin-orbit interaction strengths for neutrons and protons from adjustments to experimental single-particle levels in heavy deformed nuclei. The resulting values of these constants are

$$a = 0.8 \text{ fm}$$

$$\lambda_n = 36$$

and

$$\lambda_p = 34$$

the well depths for neutrons and protons and the radius of the spherical generating potential remain unchanged [47]. The potential's surface is now 11% thinner than previously, and the spin-orbit interactions for neutrons and protons are now stronger by 12% and 6%, respectively. These differences arise mainly from requiring the calculated single-particle levels to reproduce the observed gap at $N = 152$ in the experimental neutron levels. With these new parameters, the experimental levels in ^{208}Pb are reproduced slightly less accurately than before. It appears extremely difficult to find a single set of parameters that reproduces satisfactorily the experimental levels in both spherical and deformed nuclei.

In the new calculation with the modified oscillator potential, the only difference compared to a previous study with this potential [28] is the replacement of the liquid-drop model by the droplet model; we therefore omit the intermediate results calculated with this potential and present only the final comparison with experimental data.

We show in Fig. 5 the barriers that are calculated with the folded Yukawa potential for a group of actinide nuclei. The dashed curves give the potential energy for symmetric deformations and illustrate what we believed about fission barriers four years ago in Vienna. At that time we thought that a second minimum existed between two peaks in the barrier and that it was responsible for shape isomers and intermediate structure in fission cross-sections.

This second minimum occurs because of special degeneracies in the single-particle energies for shapes of high symmetry. In particular, when the nucleus is approximately twice as long as it is wide, the energy is lowered substantially for particle numbers that correspond to actinide nuclei. Because of this—and because the macroscopic contribution to the energy is close to its saddle point and hence relatively flat at this deformation—the resulting fission barriers of most actinide nuclei contain a second minimum.

But in Vienna we still could not understand why the calculated barrier heights reproduced the experimental values so poorly, or why actinide nuclei usually divide asymmetrically. Shortly thereafter several calculations [2-5, 26-28, 33-37, 42, 47, 49] indicated that the second saddle point in the fission barriers of the lighter actinide nuclei is lowered by several MeV when mass-asymmetric deformations are introduced, as indicated in Fig. 5 by the solid curves. For the heavier actinide nuclei the energy of the second saddle point is reduced much less by mass-asymmetric deformations.

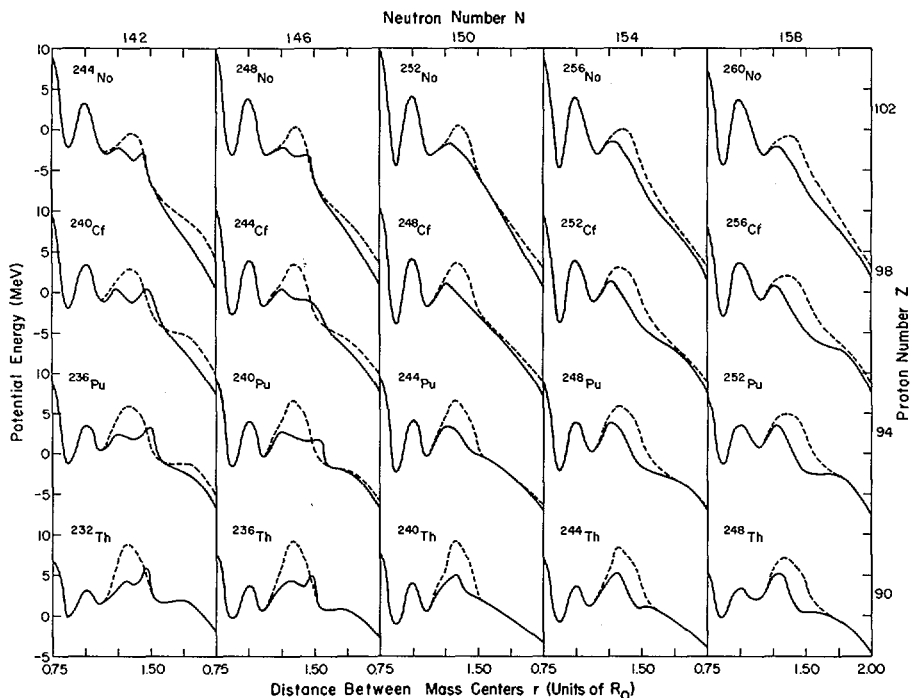


FIG. 5 Fission barriers for actinide nuclei, calculated with the folded Yukawa potential and the droplet model. The dashed curves (which sometimes coincide with the solid curves) give the potential energy for symmetric deformations as a function of the distance r between the centers of mass of the two nascent fragments. The solid curves give the potential energy along a path that leads over the mass-asymmetric second saddle point. This path is usually determined by minimizing the potential energy with respect to mass asymmetry for fixed values of r . However, when such a path jumps discontinuously from one valley to another without passing over the asymmetric saddle point, the path in this region is determined by the method of steepest descent. This explains why the solid curves sometimes lie above the dashed curves. The potential energy for each nucleus is calculated with single-particle levels for ^{250}Cf .

The first peak is found to be stable with respect to mass asymmetry. However, studies by Larsson, Pashkevich, Pauli, and others [1, 66, 68] have demonstrated that for the heavier actinide nuclei the first peak is unstable with respect to axial asymmetry (γ deformations); this lowers the energy by over 2 MeV in some cases.

The variation of the calculated heights of the equilibrium points with neutron number arises primarily from single-particle effects. However, the variation of the heights with proton number is associated also with large changes in the macroscopic energy. Increasing the proton number Z pulls in the maximum of the macroscopic energy to make the first peak higher than the second. Conversely, decreasing Z pushes out the macroscopic maximum to make the second peak higher than the first.

We come finally to a new observation that is apparent in Fig. 5: For small neutron numbers (below about 146 in these calculations), the asymmetric second saddle point is actually split into two individual saddle points

separated by a third minimum! Such a splitting is possibly responsible for the broad resonance observed in the fission cross-sections of the compound nuclei ^{231}Th , ^{232}Th , and ^{234}Th [78, 79]. These data have always been interpreted as implying that the first saddle point and second minimum in the barrier are substantially higher than the calculated values. But it now appears likely that these experimental values refer instead to the middle saddle point and third minimum in the barrier, which offers a simple resolution of the thorium anomaly. These third minima are associated with a shift in the location of the asymmetric second saddle point from a large distortion r to a smaller distortion as the neutron number increases. Similar third minima are also present in some previous calculations for thorium isotopes with both the generalized Woods-Saxon potential [37] and the modified oscillator potential [28], but the possible significance of these minima was not realized until now. It is conceivable that such third minima are a spurious feature of limited shape parametrizations, but this can be checked through further work. The possibility of this additional complexity in the vicinity of the asymmetric second saddle point means that great care should be taken when determining barrier heights from fission cross-sections [6], when calculating spontaneous-fission half-lives [35, 80, 81], and when correlating the properties of fission isomers [7].

Some of these points are appreciated better in a contour map where the mass-asymmetry coordinate is included explicitly. Two such maps are shown in Fig. 6: one for ^{236}U , where the experimental most probable mass division is asymmetric at low excitation energy, and the other for ^{258}Fm , where the most probable mass division is symmetric. We may think of the ground states of these nuclei as lakes that are separated from the regions to the right by mountain ranges. Each range contains one or more peaks, additional lakes, and passes (saddle points), although in other respects they are different in character. For example, the ^{258}Fm range is significantly narrower than the ^{236}U range; this arises because of the larger Coulomb force in ^{258}Fm .

For each nucleus the first lake, first pass, and second lake occur for symmetric shapes. (Axially asymmetric distortions, which are not considered here, would lower the first pass by about 0.3 MeV for ^{236}U and by about 2 MeV for ^{258}Fm [1].) Because of its high elevation the symmetric peak for ^{236}U is snow-capped. However, it is not necessary to go over this forbidding peak in order to fission: the asymmetric route around this mountain is 3.7 MeV lower. In addition, the asymmetric lake that separates the two asymmetric passes provides a convenient resting place. Beyond this lake, the asymmetric route for ^{236}U divides. One branch leads over an asymmetric pass down into another small lake in the symmetric valley. The second branch leads over a slightly higher and more asymmetric pass into an asymmetric valley. These two valleys are separated by an asymmetric snow-capped peak. We have not yet investigated these valleys in detail, but if a similar topology occurs for nuclei near radium it could possibly be responsible for the experimentally observed three-peaked mass distributions for these nuclei. In contrast, the symmetric peak for ^{258}Fm is relatively low in elevation, and only 1.2 MeV is gained by taking the asymmetric route around this mountain.

Apart from the equilibrium points, such potential-energy surfaces are not invariant under a change of coordinates. It is well-known that valleys can be transformed into ridges, and vice versa, by coordinate transformations [82]. We therefore do not attach a great deal of significance to the apparent valleys or ridges on the steep hillside between the saddle and scission regions. The answer to the motion in this region must await a proper dynamical calculation; some aspects of dynamics will be discussed later in the symposium by Pauli, Sierk, and others [35, 51].

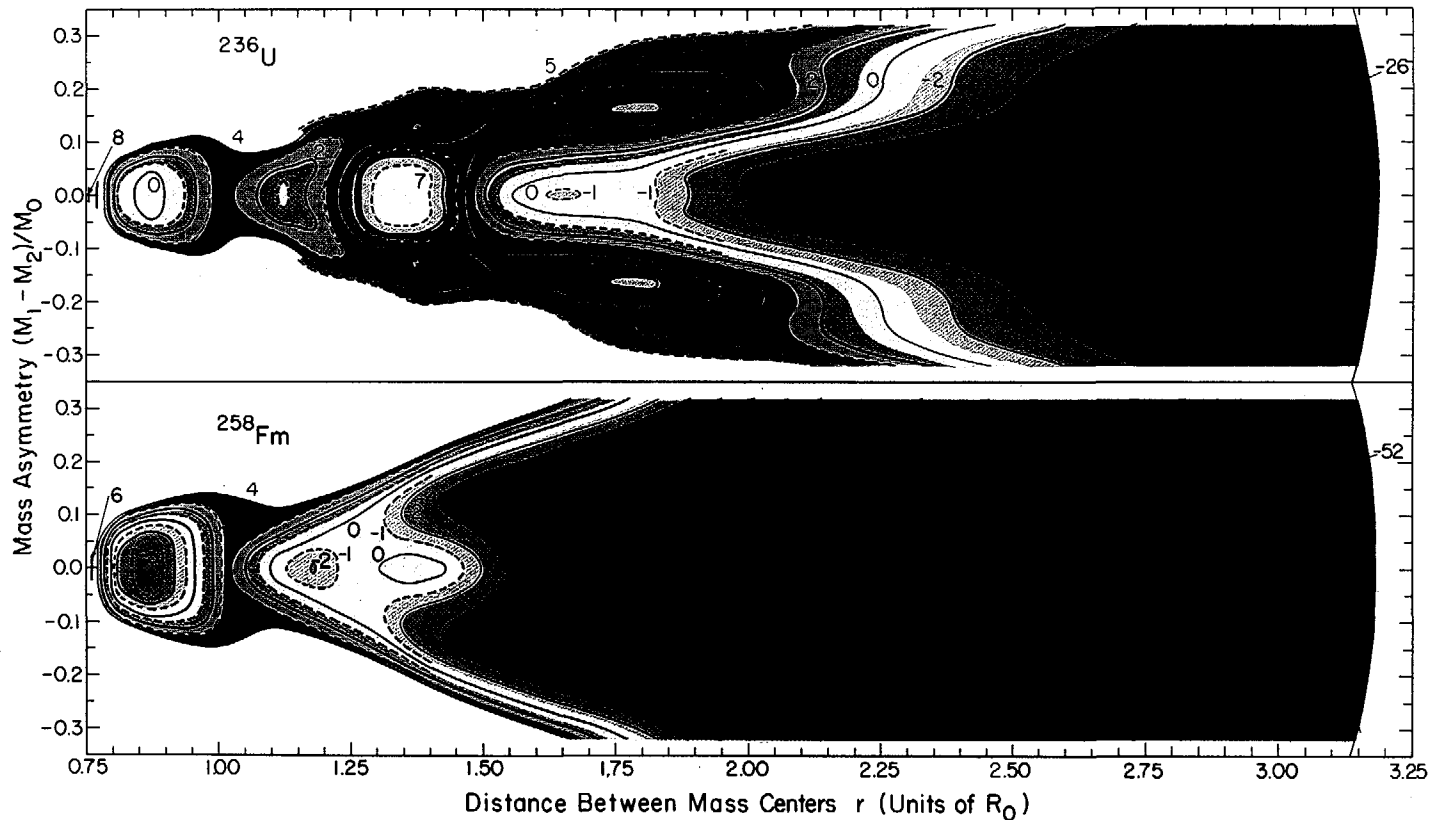


FIG. 6. Potential energy of ^{236}U and ^{258}Fm , calculated with the folded Yukawa potential and the droplet model. For each nucleus, contours of constant potential energy are plotted as functions of the distance between mass centers r and the mass-asymmetry coordinate $(M_1 - M_2)/M_0$. The contours are labelled by the energy (in MeV) relative to the spherical droplet-model energy. The solid curves are spaced at intervals of 2 MeV; dashed curves are used for intermediate values. The distortions included vary from a sphere (at $r = 0.75 R_0$) all the way to scission, which is indicated by the slightly curved dot-dashed line. The potential energy for each nucleus is calculated with single-particle levels for ^{250}Cf .

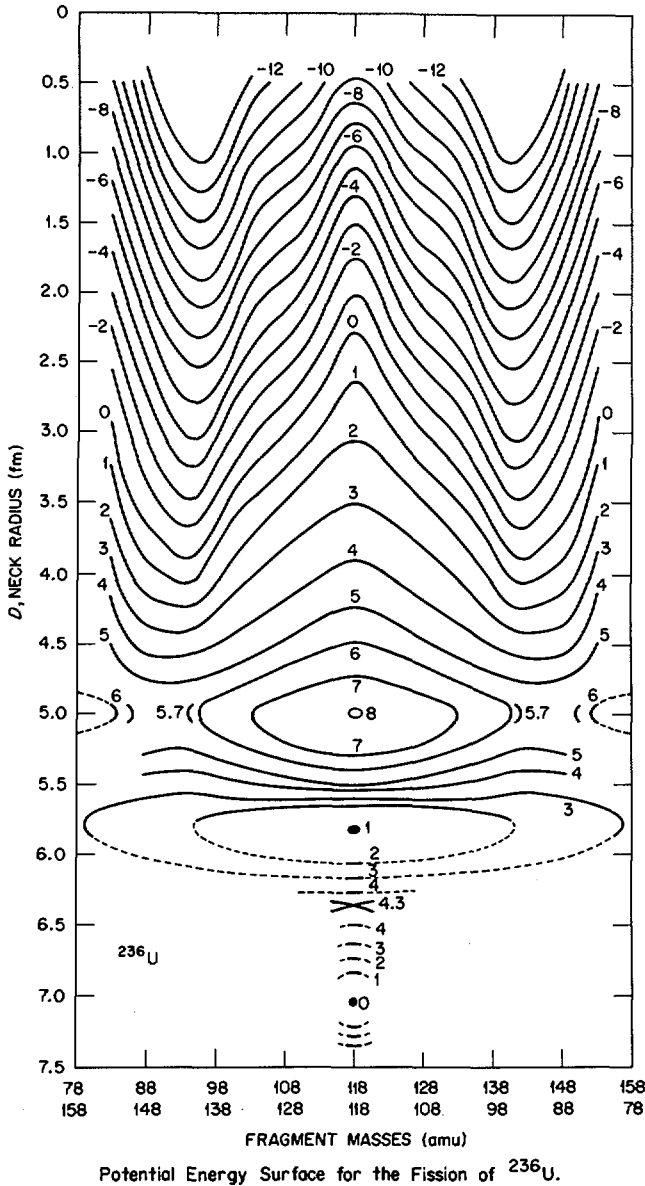


FIG. 7. Potential energy of ^{236}U , calculated by Mustafa, Mosel, and Schmitt with a modified two-center oscillator potential [42]. Contours of constant potential energy are plotted as functions of the neck radius D and the masses of the two nascent fragments. The contours are spaced at intervals of 1 MeV and are labelled by the energy (in MeV) relative to the ground-state minimum potential energy; an additional contour is included near each saddle point. The dashed lines represent interpolated or extrapolated values.

We do note, however, that beyond the last saddle point the apparent stability shifts between symmetric and asymmetric shapes. Such shifts arise from oscillations in the single-particle corrections. From fundamental considerations one expects these oscillations to continue well past the saddle-point region provided that the nucleus continues to elongate as it does along the path chosen in Fig. 6.

However, the opposite result was obtained recently by Mustafa, Mosel, and Schmitt in some calculations with the modified two-center oscillator potential [41-43]. Figure 7 shows their calculated potential-energy surface for ^{236}U , which is obtained by minimizing the potential energy with respect to overall elongation and with respect to the difference in the transverse semi-axes of the nascent fragments. Note the apparent valley that extends from the scission region all the way back to the second saddle point.

Part of the difference between these two results for ^{236}U stems from the use of different single-particle potentials, as illustrated in Fig. 8. Whereas the folded Yukawa potential is practically constant along the symmetry axis, the two-center oscillator potential is 5 MeV higher in the middle than in the center of either nascent fragment, even though this particular two-center saddle-point shape does not contain an indented neck! This early rise of the two-center potential in the neck region contributes somewhat to an early formation of shell structure associated with the fragments.

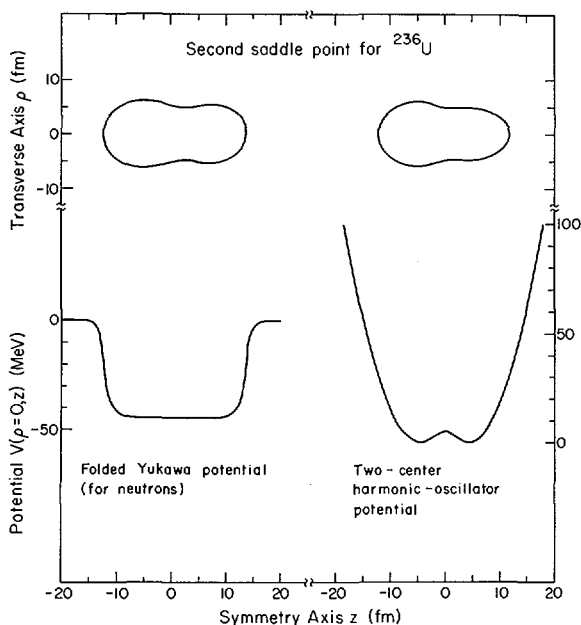


FIG. 8. Comparison of the folded Yukawa potential with the two-center oscillator potential at the asymmetric second saddle point for ^{236}U . The upper portion of the figure shows the saddle-point shapes, and the lower portion shows the corresponding potentials along the symmetry axis. The folded Yukawa potential is 0.19 MeV higher in the neck than in the center of the larger nascent fragment and is 0.04 MeV higher in the neck than in the center of the smaller nascent fragment. The two-center oscillator potential [42] is 5 MeV higher in the middle than in the center of either nascent fragment.

But the main difference arises because different shapes are considered. In our calculations the distance between the fragment mass centers increases continuously, whereas Mustafa, Mosel, and Schmitt minimize the potential energy with respect to this coordinate. This makes it possible for the nucleus to adjust its length as its neck radius is decreased in order to remain in a local asymmetric valley. Similar local valleys are evident in the potential-energy surfaces calculated by Pauli with a generalized Woods-Saxon potential and the liquid-drop model [5]. These valleys are aligned approximately along fixed values of the distance between mass centers r . With increasing r the nucleus passes from one valley into another, which is the situation in Fig. 6. When the nucleus adjusts its length to remain in an asymmetric valley, it arrives at the scission region with a more compact shape; this partially explains why the scission energy is higher in Fig. 7 than in Fig. 6.

5. ENERGIES OF THE LOCAL MINIMA AND SADDLE POINTS

We turn now to a comparison between calculated and experimental energies of the equilibrium points in the potential-energy surfaces.

5.1. Folded Yukawa potential

Figure 9 compares the calculated and experimental ground-state masses of heavy even nuclei; both spherical nuclei near ^{208}Pb and deformed actinide nuclei are included. The calculations reproduce the general trends of the experimental results, but some systematic discrepancies remain, as shown in the lower portion of the figure. Similar discrepancies have been observed previously [2-5, 24, 28, 29, 57]. When viewed over a broad region of nuclei, the discrepancy in the ground-state masses oscillates with particle number. The maximum error occurs for ^{222}Th , where it is 2.6 MeV in magnitude. For the isotopes of a given actinide element, the minimum in the calculated ground-state single-particle correction is always at neutron number $N = 152$. This is because the parameters of the single-particle potential are adjusted to reproduce the gap at $N = 152$ in the experimental single-particle levels of ground-state nuclei. However, this minimum in the ground-state single-particle correction is observed experimentally only for the heavier actinide nuclei ($Z \geq 100$). For the isotopes of a given actinide element, the difference between the experimental and calculated masses is an increasing function of neutron number.

Provided that it does not affect the potential energy at larger deformations in the same way, such an error in the calculated ground-state mass can propagate into the calculated heights of the saddle points and remaining minima in the potential-energy surface. This is illustrated in Fig. 10 for even actinide nuclei between thorium and fermium. The solid curves give the appropriate theoretical height relative to the calculated ground-state energy, and the dashed curves give the corresponding height relative to the experimental ground-state energy. The difference between the solid and dashed curves is therefore simply the error in the calculated ground-state energy. On the other hand, an error in a term that is independent of deformation, such as the volume energy [28], would not affect the calculated heights of the remaining extrema.

The first column of Fig. 10 compares the theoretical and experimental heights for the first saddle point. The theoretical results do not include the effects of axially asymmetric deformations, which would lower somewhat the calculated heights for the heavier nuclei [1]. When allowance is made for this lowering, the theoretical heights (relative to either the calculated

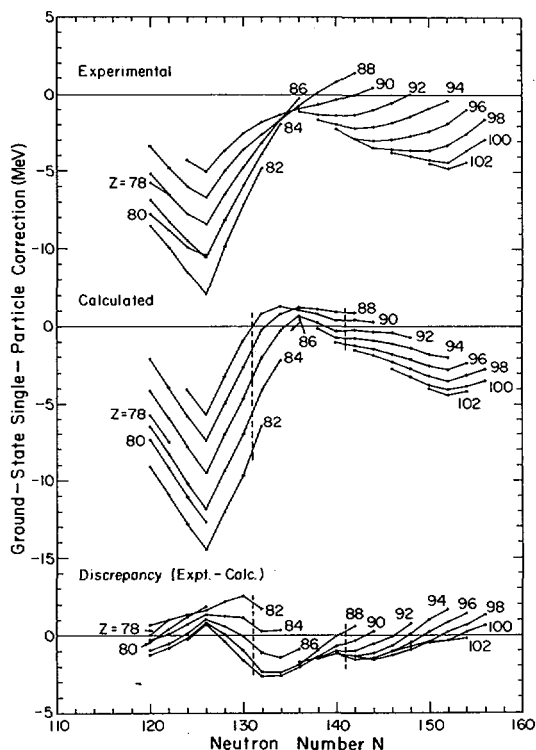


FIG. 9. Comparison of experimental ground-state single-particle corrections for even nuclei with values calculated by use of the folded Yukawa potential and the droplet model. The ground-state single-particle correction is the nuclear ground-state mass relative to the spherical macroscopic energy, which is calculated here from the 1973 droplet model of Myers and Swiatecki [50, 55, 56]. The experimental masses are taken from Ref. [83]. The calculated masses are obtained by minimizing the potential energy with respect to a separation coordinate and a necking coordinate in two different shape parametrizations, as discussed in the appendix. Single-particle levels for ^{208}Pb , ^{224}Ra , and ^{250}Cf are used to calculate the potential energy for each nucleus in the left-hand, middle, and right-hand regions, respectively; these regions are indicated by the dashed vertical lines. A constant ground-state zero-point energy of 0.5 MeV is included for each nucleus. The lower portion of the figure gives the discrepancy between the experimental and calculated masses.

or experimental ground-state energies) are slightly lower than the experimental heights. The second column is a similar comparison for the height of the second minimum. Apart from the results for thorium, the theoretical and experimental values are in approximate agreement, although both the solid and dashed theoretical curves show a stronger dependence on neutron number than is observed experimentally.

For isotopes of thorium the calculated second minima are about 3 MeV lower than the experimental values commonly attributed to this minimum. This large discrepancy—together with a similar discrepancy at the first saddle point—constitutes the thorium anomaly [34, 78, 79]. We suggest that a possible resolution of this anomaly is the third asymmetric minimum in the barrier, whose calculated heights agree with the experimental values to within 0.5 MeV. The discrepancies for thorium that are evident in the first

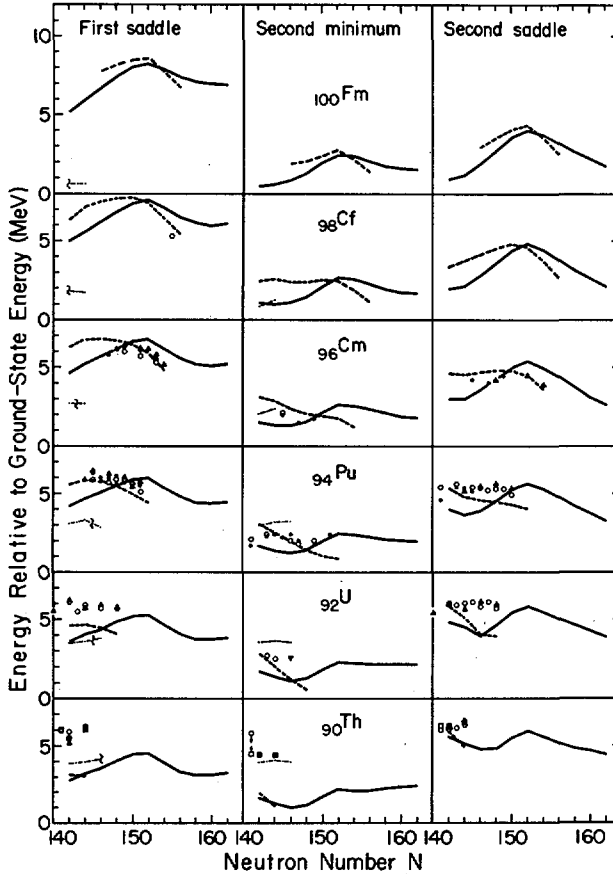


FIG. 10. Heights of the first saddle point, second minimum, and asymmetric second saddle point, as functions of neutron number N . The solid curves give the heights calculated with the folded Yukawa potential and the droplet model relative to the calculated ground-state energy, and the dashed curves give the corresponding height relative to the experimental ground-state energy. The lightweight dot-dashed lines in the first column give the height of the lower of the two asymmetric saddle points that surround the asymmetric third minimum (relative to the calculated ground-state energy). To the left of the wavy vertical line the lower saddle point occurs before the minimum, and to the right it occurs after the minimum. The height of this third minimum is given in the second column by the lightweight dot-dashed lines. A constant zero-point energy of 0.5 MeV is included for each nucleus at its ground state, second minimum, and third minimum. The potential energy for each nucleus is calculated with single-particle levels for ^{250}Cf . The calculations are performed for even nuclei only, but odd-neutron nuclei are also included in the experimental data, which are given by solid circles [20], open circles [84], solid squares [79], open squares [78], solid upward-pointing triangles [6], and a solid downward-pointing triangle [85].

column are reduced somewhat when the experimental heights that are commonly attributed to the first saddle point are compared instead with the calculated heights for the lower of the two asymmetric saddle points that surround the asymmetric third minimum. But these calculated heights are still lower than the experimental ones by about 2 MeV.

For plutonium the experimental heights of the second minimum are systematically lower by about 0.2 MeV for odd-neutron isotopes than for even isotopes. As pointed out by Nilsson [67], this implies that the pairing gap is smaller by this amount at the second minimum than at the ground state. This arises because the single-particle levels have a larger shell at the second minimum—where the shape has a ratio of axes of approximately 2/1—than at the ground state. Such odd-particle fluctuations in the height of the second minimum are evident in the calculations of Ref. [20].

The third column of Fig. 10 compares the theoretical and experimental heights of the second saddle point. For thorium and uranium both the solid and dashed theoretical curves are somewhat lower than the experimental values and show a more rapid variation with neutron number. For plutonium and curium the dashed curves are in approximate agreement with the experimental values, but the solid curves vary too rapidly with neutron number.

In some calculations of fission-barrier heights [34, 80, 86], the values of two constants in the liquid-drop model are adjusted in order to reproduce optimally the experimental heights of the second saddle point. Because the calculated heights are affected to an unknown extent by the poorly understood systematic error in the calculated ground-state energies, great care must be exercised when attempting to determine liquid-drop-model constants in this way. As an extreme example, had experimental rather than calculated ground-state energies been used in the previous studies [34, 80, 86], the resulting values of the surface-asymmetry constant κ would have been substantially lower.

At present we are calculating the fission barriers for a broad region of lighter nuclei. The calculated barrier height for ^{210}Po is 23.3 MeV relative to the calculated ground-state energy, and is 22.0 MeV relative to the experimental ground-state energy. These theoretical heights are to be compared with 21.4 and 20.5 MeV obtained in two different experiments [87], and with the value of 24.7 MeV calculated by Mosel with the modified two-center oscillator potential and the liquid-drop model [41].

5.2. Modified oscillator potential

In the next three figures we present some analogous results obtained with the modified oscillator potential. In Fig. 11 we see the effect of axially asymmetric (gamma) distortions at the first saddle point; this will be discussed in greater detail later in this session by Larsson [1]. We note the excellent agreement with experimental results that is achieved for the heavier nuclei by including axially asymmetric distortions. However, there are some significant deviations between the calculated and experimental results for the lighter isotopes of thorium and uranium.

The results shown in Figs. 12 and 13 for the second minimum and the second saddle point, respectively, are calculated in the same way as those of Ref. [28] with two exceptions: We now use the droplet model for the macroscopic energy and include a zero-point energy of 0.5 MeV at the ground state and second minimum. The strength of the pairing interaction is taken to be independent of deformation. In Fig. 12 we see that although the experimental and calculated heights of the second minimum are in approximate agreement, the

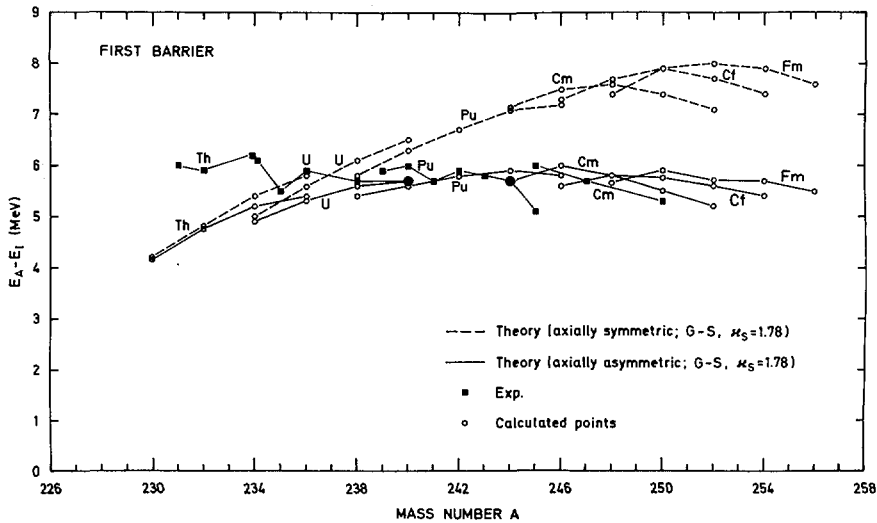


FIG. 11. Reduction in the height of the first saddle point due to axially asymmetric deformations, as a function of mass number A . The open circles connected by the dashed lines give the heights calculated with a modified oscillator potential and the liquid-drop model for shapes that are restricted to axial symmetry [28]; the open circles connected by the solid lines give the corresponding heights calculated by Larsson and Leander for axially asymmetric shapes [1]. The strength of the pairing interaction is assumed to be proportional to the surface area; the liquid-drop-model constants are taken from Ref. [57]. No zero-point energy is included at the ground state. The calculations are performed for even nuclei only, but odd-neutron nuclei are also included in the experimental data, which are given by the solid squares [84].

calculated values depend more strongly on neutron number than do the experimental values. In particular, the calculated values contain a minimum at $N = 144$ and a maximum at $N = 152$, whereas the experimental values are approximately independent of neutron number (apart from the odd-particle fluctuations discussed earlier).

As seen in Fig. 13, the calculated heights of the second saddle point for uranium and plutonium are fairly constant as functions of neutron number and are in excellent agreement with the experimental results. The agreement is also very good for curium, whereas for thorium the calculated values are about 1 MeV higher than the experimental values and vary somewhat too rapidly with neutron number.

For the heavier actinide nuclei there are no experimental measurements on the height of the second saddle point. However, the spontaneous-fission half-life for ^{258}Fm is unexpectedly short compared to that of the neighboring nucleus ^{256}Fm . In particular, the half-life of 380 μs for ^{258}Fm is only 4×10^{-8} times that for ^{256}Fm [88, 89]. This may indicate that for ^{258}Fm the second saddle point is lower than the ground state [80]. This could also be true for ^{244}Fm , which has a short spontaneous-fission half-life of 3.3 ms [90]. This indirect evidence therefore suggests that the heights of the second saddle points for ^{244}Fm and ^{258}Fm are about zero. This is reproduced approximately by the calculations shown in Fig. 13.

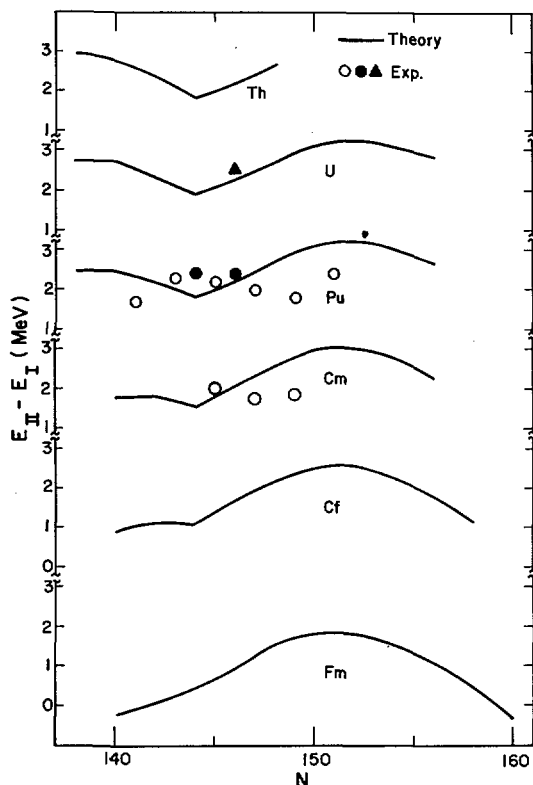


FIG. 12. Height of the second minimum, as a function of neutron number N . The curves are calculated with the modified oscillator potential and the droplet model for even nuclei. The experimental data are given by circles [20] and a triangle [85]. Solid symbols are used for even nuclei, and open symbols are used for odd-neutron nuclei.

5.3. Comparison of folded Yukawa and modified oscillator potentials

For both the folded Yukawa potential and the modified oscillator potential, the present calculations agree better with experimental results than previous calculations with these potentials [20, 28, 47, 49]. Of particular importance, the rapid variation of the height of the second saddle point with neutron number that was predicted by the old calculations but is not observed experimentally is reduced substantially. For the modified oscillator potential this improved agreement stems from the use of the droplet model for the macroscopic energy. For the folded Yukawa potential the introduction of additional shape coordinates and the use of different parameters for the single-particle potential also contribute. Unfortunately we are not able to answer the delicate question of whether the improved agreement arises because of the higher-order terms in the droplet model or simply because of a better set of constants for the leading terms.

In carrying out this study we have come to appreciate the remarkable similarity in the results calculated for actinide nuclei by use of potentials that at first sight seem radically different. Similarities near the ground

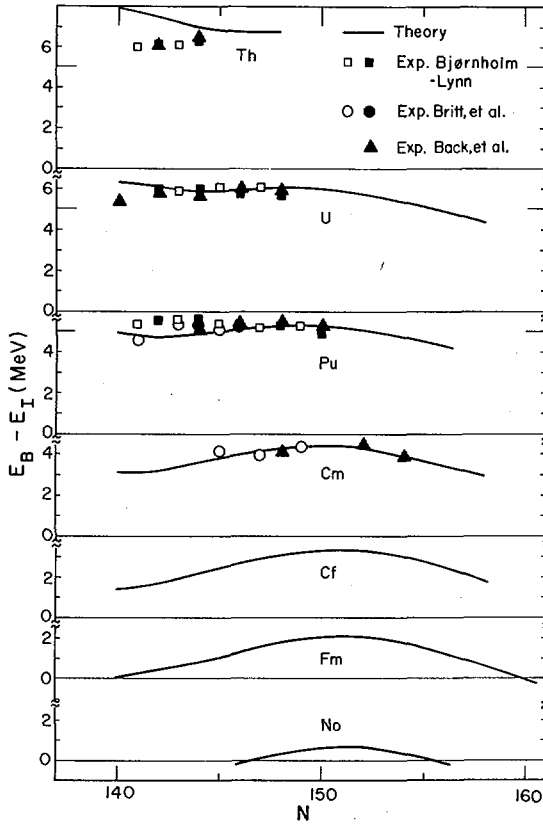


FIG. 13. Height of the asymmetric second saddle point, as a function of neutron number N . The curves are calculated with the modified oscillator potential and the droplet model for even nuclei. A constant ground-state zero-point energy of 0.5 MeV is included for each nucleus. The experimental data are given by squares [84], circles [20], and triangles [6]. Solid symbols are used for even nuclei, and open symbols are used for odd-neutron nuclei.

state are understood easily because we adjust the parameters of each potential to reproduce the same experimental single-particle levels in heavy deformed nuclei. But in addition the two calculations yield similar results at the second saddle point for detailed questions: For example, for which isotope does the maximum decrease in energy due to asymmetric distortions occur? And, for which isotope does the location of the asymmetric second saddle point shift from a large distortion r to a smaller distortion? The two calculations answer both these questions in the same way to within an accuracy of ± 2 neutrons for all even nuclei between thorium and fermium. This suggests that the dependence of single-particle effects on deformation arises primarily from the overall geometrical shape of the potential rather than from fine details associated with it. This agrees with the conclusions obtained by Balian and Bloch on the basis of closed stationary paths in potentials [91].

But of course there are some differences in the results calculated with the two potentials. For example, compare the rapid increase in the height of the second saddle point with increasing neutron number just below 152 in the

folded Yukawa calculations with the relatively constant behavior in the modified oscillator calculations. This difference comes about from effects both at the ground state and at the second saddle point. As an example, for plutonium the ground-state energy calculated with the folded Yukawa potential decreases by 1.1 MeV between $N = 144$ and $N = 152$ and the saddle-point energy increases by 1.0 MeV, which increases the height of the second saddle point by 2.1 MeV. In the modified oscillator calculations the corresponding values are 0.19 MeV and 0.02 MeV, which increases the height by only 0.21 MeV. At the ground state the differences arise because the single-particle level density near neutron number $N = 144$ is slightly higher for the folded Yukawa potential than for the modified oscillator potential (even though both potentials are meant to reproduce the same experimental levels).

We find that the levels at the second saddle point are much less sensitive to changes in the parameters of the single-particle potential than are those near the ground state. The major differences at the second saddle point seem to arise because in the folded Yukawa calculations we vary the necking coordinate σ_2 independently of the separation and asymmetry coordinates, whereas in the modified oscillator calculations the necking coordinate ϵ_4 has a prescribed dependence on the other coordinates.

Another difference is that the heights of the second saddle point do not decrease as rapidly with increasing proton number in the folded Yukawa calculations as in the modified oscillator calculations. This arises primarily because the second saddle point for heavy nuclei near ^{252}Fm , for example, occurs near the macroscopic saddle point with the folded Yukawa potential, whereas with the modified oscillator potential it occurs at a somewhat larger deformation, where the macroscopic contribution is about 2 MeV lower. The main reason that the second saddle occurs at a smaller deformation with the folded Yukawa potential is that the single-particle levels cross earlier.

In order to permit a better choice between the available single-particle potentials, and in order to determine the constants of these potentials more precisely, we need more direct experimental information at large deformations. This includes the determination of the nuclear shape and the identification of the single-particle states at the second minimum, for which some notable first steps have been taken [92-94].

We again stress that, despite these minor differences, the two potentials yield remarkably similar results for the fission barriers of actinide nuclei. It is therefore disconcerting to note the relatively large differences in the predictions for superheavy nuclei based on the two potentials [24, 25, 47-49]. In particular, the modified oscillator potential predicts that the eastern side of the island of superheavy nuclei (i.e., the side with neutron number greater than 184) is more stable than the western side, whereas the folded Yukawa potential (as well as the Woods-Saxon potential) predicts that the western side is more stable.

We had originally thought that part of this difference was caused by having used experimental single-particle levels in ^{208}Pb to determine the parameters of the folded Yukawa potential and single-particle levels in heavy deformed nuclei to determine the parameters of the modified oscillator potential. But now that we use levels in heavy deformed nuclei for both potentials the differences are even greater [50]! This comes about because the surface-diffuseness parameter for the folded Yukawa potential is now smaller, which makes this potential more like a square-well potential. We conclude that although satisfactory agreement with experimental results may be achieved for a limited region of nuclei through the adjustment of parameters in the single-particle potential, great care must be exercised when extrapolating the potential to new regions of nuclei.

6. FISSION-FRAGMENT MASS DISTRIBUTIONS

We come finally to the puzzle that has intrigued physicists ever since the discovery of fission: the preference of most actinide nuclei at low excitation energy to divide asymmetrically. We now understand this preference—as well as the preference in other situations for nuclei to divide symmetrically—in terms of single-particle effects superimposed on a smooth macroscopic background.

6.1. Origin of asymmetric instabilities

Let us examine these two contributions individually. As illustrated in Fig. 14, the saddle-point shapes for the macroscopic portion of the energy are stable against mass-asymmetric deformations for nuclei heavier than about silver and are unstable for lighter nuclei. Because the quantity plotted is equal to the stiffness against mass asymmetry divided by the corresponding inertia, the effective macroscopic stiffness against mass asymmetry increases sharply for heavier nuclei. In order for an asymmetric mass division to occur, a possible single-particle preference for asymmetry must be sufficiently strong to overcome this macroscopic preference for stability. Because the

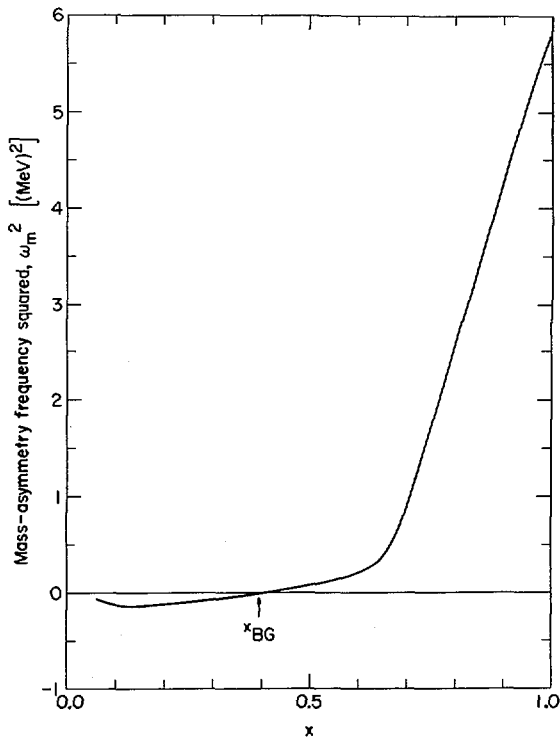


FIG. 14. Square of the frequency of mass-asymmetric oscillations of an idealized liquid drop about its saddle-point shape, as a function of fissility parameter x . The results are shown for nuclei along the valley of beta stability [44]. The critical Businaro-Gallone point [95] is denoted by the arrow. To the right of this point the liquid-drop-model saddle-point shape is stable against mass asymmetry, and to the left it is unstable.

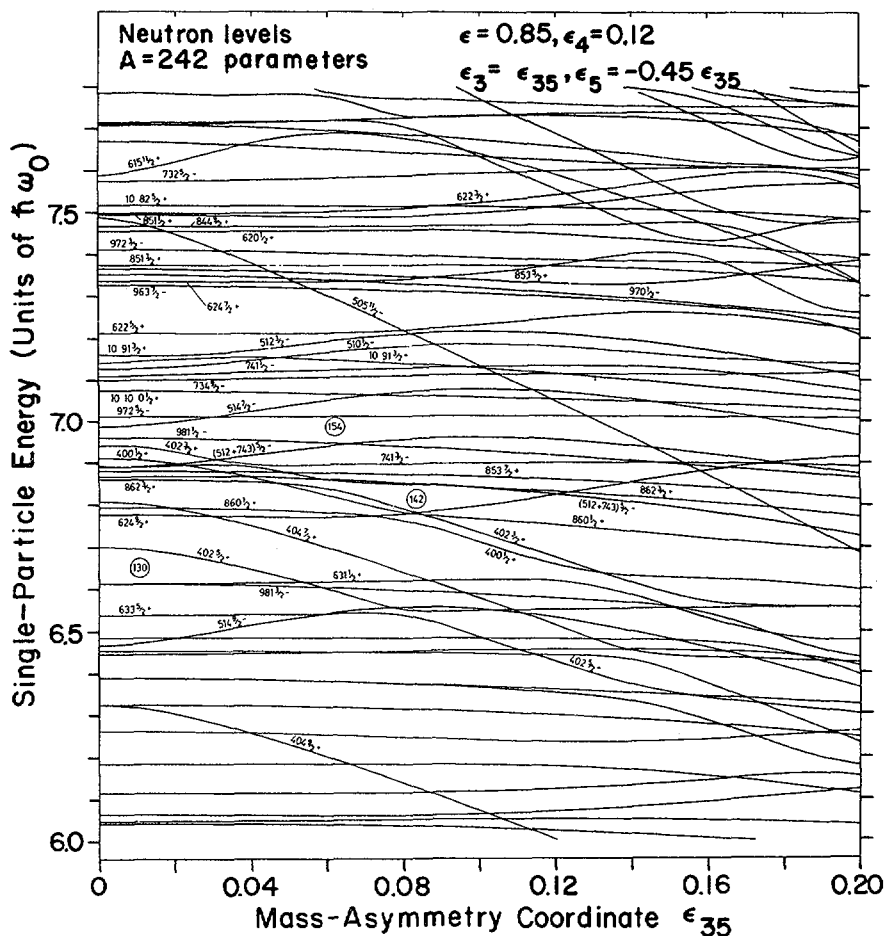


FIG. 15. Single-neutron levels near the second saddle point of an actinide nucleus, as functions of the mass-asymmetry coordinate ϵ_{35} . The levels are calculated with the modified oscillator potential for asymmetric distortions defined by $\epsilon_3 = \epsilon_{35}$ and $\epsilon_5 = -0.45 \epsilon_{35}$ [27]. The levels are labelled by the asymptotic quantum numbers $[Nn_z\Lambda\Omega]$ and by the parity for the corresponding symmetric shape.

magnitude of single-particle effects remains approximately constant with increasing mass number, this increase in the stiffness of the macroscopic contribution suggests that sufficiently heavy nuclei will always prefer to divide symmetrically. Some recent calculations with the modified two-center oscillator potential support this observation [43].

We have already seen that the addition of single-particle effects to the macroscopic energy can lead to a high and sharp peak in the total potential energy as a function of the symmetric fission coordinate. This peak is caused by an unusually high single-particle level density near the Fermi surface for this particular shape. Any type of deformation that reduces this high level density leads to a decrease in the single-particle correction.

Whereas the single-particle levels depend linearly upon symmetric deformations, they are to first order independent of asymmetric deformations. For large asymmetric deformations many levels remain practically constant, whereas some specific levels vary strongly [27]. When these specific levels are near the Fermi surface, asymmetric deformations can reduce the single-particle correction. Then, provided that the macroscopic energy does not increase too rapidly, the total potential energy should have an asymmetric path of lower energy leading around the symmetric peak [27, 96].

Two near-lying levels are affected strongly by an asymmetric perturbation when the matrix element of the perturbation between them is large. The matrix element of a mass-asymmetric perturbation is large between two states of opposite parity that have similar transverse and azimuthal wave functions and that have 0 and 1 node, respectively, in their wave functions along the symmetry axis z . This is illustrated in Fig. 15, where the neutron levels near the second saddle point of an actinide nucleus are shown as functions of mass asymmetry. These results are calculated with the modified oscillator potential. In terms of the asymptotic quantum numbers $[Nn_z\Lambda\Omega]$, the levels that are affected most by mass asymmetry are $[40\Lambda\Omega]$ and $[51\Lambda\Omega]$. Four orbitals of each type occur between neutron number 130 and 170 at the second saddle point; it is the presence of these eight mass-asymmetry-favoring orbitals near the Fermi surface that leads to mass-asymmetric second saddle points in actinide nuclei. These same orbitals are also responsible for mass asymmetric saddle points in calculations with the folded Yukawa potential and with the generalized Woods-Saxon potential [5].

As the nucleus continues to deform past the saddle point, the development of the neck and ultimately the rise of the potential in the neck cause all levels to group into nearly degenerate pairs of levels of opposite parity. This occurs because the squeezing at the neck raises the energy of a state without a node at $z = 0$ more than it raises the energy of a state with a node. As stressed by Andersen [97], these pairs of levels finally become the levels in the two individual fragments after scission. In this limit every level is affected by a change in mass asymmetry. However, because of the difficulty of mass transfer near scission, the mass split must be decided somewhat before this point. But in this way we see the connection between the effects of shell structure in the fragments and at the saddle point.

At the first symmetric saddle point of actinide nuclei the single-particle level density near the Fermi surface is also high, but such shapes are stable against mass asymmetry because the mass-asymmetry-favoring orbitals are not as close to each other there. On the other hand, axial-asymmetry-favoring orbitals are present near the Fermi surface at the first saddle point of the heavier actinide nuclei, which leads to axially asymmetric first saddle points in these nuclei.

6.2. Saddle-point properties

Although a few mysteries still remain, the main features of experimental fission-fragment mass distributions are now understood in terms of the calculated properties of the saddle points. At low excitation energy, most heavy nuclei ($Z \geq 90$) divide primarily into one large fragment and one small fragment. For these nuclei, the second saddle point is calculated to be reflection-asymmetric in shape. Figure 16 shows for actinide nuclei the correlation that exists between the experimental most probable mass asymmetries and the values calculated at the second saddle point with the folded Yukawa potential.

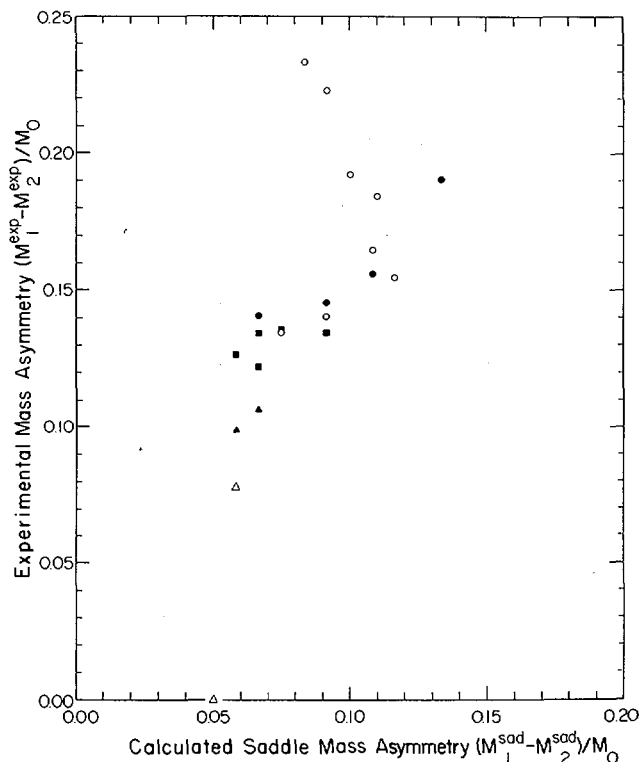


FIG. 16. Correlation of experimentally most probable fission-fragment mass asymmetries with values calculated at the asymmetric second saddle point by use of the folded Yukawa potential and the droplet model, for even actinide compound nuclei. The experimental data are given by circles [98], triangles [99], and squares [100]. Solid symbols are used for spontaneous fission, and open symbols are used for neutron-induced fission.

If the mass distribution is determined at the second saddle point, then the experimental peak-to-valley ratio should be related exponentially to the difference between the energies of the second symmetric saddle point and the second asymmetric saddle point [101]. Such a correlation is presented in Fig. 17 for actinide nuclei; the folded Yukawa potential is used to calculate the differences in the energies of the saddle points.

What happens to the nucleus after it passes over the asymmetric second saddle point? It has two main choices: It can adjust its overall length in order to remain in an asymmetric valley of low potential energy created by the single-particle effects [5, 42, 43]. Or alternatively, it can increase its overall length in accordance with the preference of the macroscopic part of the energy. If this occurs, it moves out of the asymmetric valley of low potential energy onto another part of the multidimensional deformation space [5]. These two possible alternatives are illustrated by the potential-energy maps in Figs. 7 and 6, respectively. Perhaps some information on which alternative a nucleus chooses could be obtained from a careful examination of experimental fission-fragment kinetic energies. But it is more likely that we will have to wait for a proper dynamical calculation to provide the answer to this important question.

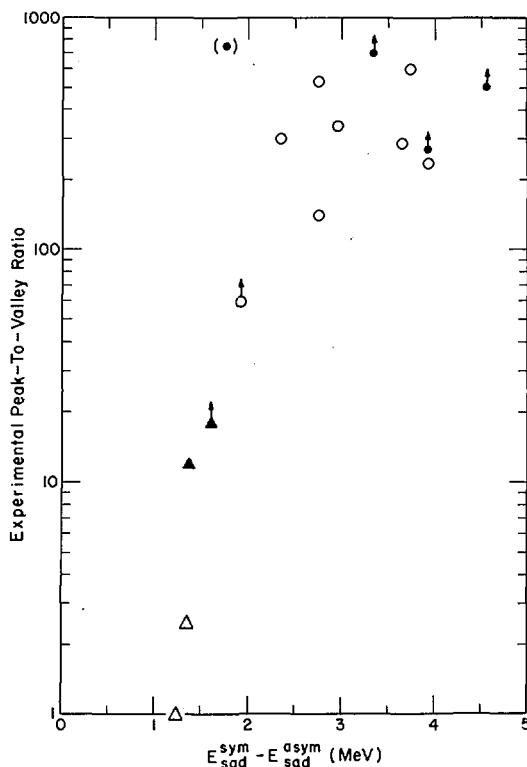


FIG. 17. Correlation of the peak-to-valley ratio in experimental fission-fragment mass distributions with the difference between the energies of the symmetric and asymmetric second saddle points, for even actinide compound nuclei. The energy differences are calculated with the folded Yukawa potential and the droplet model. The experimental data are given by circles [98] and triangles [99]. Solid symbols are used for spontaneous fission, and open symbols are used for neutron-induced fission.

Experimental fission-fragment mass distributions for nuclei in the vicinity of radium ($84 < Z < 90$) have three peaks; one corresponds to division into equal fragments and the others correspond to division into unequal fragments. Still lighter nuclei ($Z \leq 84$) divide primarily into two equal fragments at all excitation energies for which the mass distributions are known. More recent experiments show that the mass asymmetry also decreases strongly for very heavy nuclei [102, 103]. In particular, the most probable mass split in the thermal-neutron-induced fission of ^{257}Fm ($Z = 100$) is symmetric [103].

In our new calculations with the folded Yukawa potential, the saddle point for ^{226}Ra is slightly asymmetric [$(M_1 - M_2)/M_0 = 0.075$] and is 2.3 MeV lower in energy than the corresponding symmetric saddle point; this agrees qualitatively with most of the other calculations for radium isotopes [5, 28, 33, 47, 49]. We have not yet investigated the potential-energy surface for ^{226}Ra for large distortions beyond the saddle point or for large mass asymmetry, but it is possible that an asymmetric valley similar to the one shown in Fig. 6 for ^{236}U will appear. If so, the presence of such an additional

valley may be responsible for the three-peaked mass distributions observed experimentally for nuclei near radium. On the other hand, odd-particle effects may be partially responsible, because the experimental mass distributions are for compound nuclei such as ^{227}Ac and ^{228}Ac , which contain one or more odd particles [104, 105].

For ^{210}Po we find in our new calculations with the folded Yukawa potential that the potential energy is extremely flat near the saddle point. Although the small differences in potential energy in this region are comparable to the numerical accuracy of the calculations, the results taken at face value yield an asymmetric saddle point [at $(M_1 - M_2)/M_0 = 0.092$] that is 0.25 MeV lower than the symmetric saddle point. The peak that separates them is only 0.25 MeV higher than the symmetric saddle point. Although the total potential energy is flat near the saddle point, the single-particle levels themselves vary strongly with deformation. Because the single-particle levels at the saddle point influence such quantities as fission-fragment angular distributions, the proper measurement and analysis of these quantities provide valuable information concerning the saddle-point shape [106].

For heavier actinide nuclei, the second saddle point decreases in height relative to the first, and these nuclei begin their descent with a shape corresponding to the first saddle point, which is reflection symmetric. In addition, the asymmetric second saddle point is only slightly lower than the corresponding symmetric one and occurs at a relatively small mass asymmetry (for ^{258}Fm these values are 1.2 MeV and 0.050, respectively, in our folded Yukawa calculations). This is at least partially responsible for the transition to symmetric divisions in the thermal-neutron-induced fission of ^{257}Fm .

As the excitation energy increases, the probability for division into two equal fragments increases, until at high energies the experimental mass distribution for all nuclei is peaked about a division into two equal fragments. This transition is probably associated with the decrease in relative importance of single-particle effects at high excitation energies, where the nucleons are distributed randomly over a large number of single-particle levels. This effectively destroys the influence of the shells, and—in a loose manner of speaking—the system divides in accordance with the smooth macroscopic contribution to the energy, which prefers an equal-mass split. This will be discussed later in the symposium by Jensen [107].

The phenomena that we are able to understand qualitatively in terms of the calculated saddle-point symmetry properties are thus the mass asymmetry in the low-energy fission of most actinide nuclei, and the transitions to symmetric divisions for both lighter and heavier nuclei and at high excitation energy. The calculated saddle-point properties do not reproduce the exact locations of the transitions to symmetric divisions and do not reproduce the expected symmetric and asymmetric saddle points for nuclei such as radium in the transition region. A more quantitative study of fission-fragment mass distributions would require a dynamical calculation to determine the motion beyond the second saddle point.

7. CONCLUDING COMMENTS

We have discussed recent advances in the calculation of the nuclear potential energy of deformation, with primary emphasis on the macroscopic-microscopic method. As specific examples of this method we have presented some new results obtained recently at Los Alamos with the folded Yukawa and modified oscillator single-particle potentials; the macroscopic energy is calculated by use of the droplet model.

A variety of phenomena associated with nuclear shape changes can be understood on the basis of this two-part approach. The macroscopic part gives the smooth trends, and the microscopic part gives the fluctuations that arise from single-particle effects. In this way such varied phenomena as nuclear ground-state masses and deformations, second minima in the fission barriers of actinide nuclei, fission-barrier heights, and fission-fragment mass distributions are seen to have a common origin.

From comparisons with experimental results we have seen that the present accuracy with which we are able to calculate the nuclear potential energy of deformation is about 1 MeV, although larger systematic errors are still present in some cases. Some of these errors are associated with imperfect determinations of the constants of both the macroscopic energy and the single-particle potential. Numerical inaccuracies arise from calculating shell and pairing corrections for a region of nuclei from single-particle levels for one central nucleus; numerical inaccuracies are also present in the extraction of the shell correction from a given set of single-particle levels. Some of the errors could arise from an inadequate treatment of zero-point energies. Perhaps we are using the wrong functional form for either the macroscopic energy or the single-particle potential. But probably the major errors stem from an inherent limitation of the macroscopic-microscopic method itself, such as the neglect of terms that are second order in the deviation of the actual nuclear density from a smooth density. These second-order effects will be discussed later in this session by Brack [71].

When these same general methods are applied to superheavy nuclei, we find the result shown in Fig. 18: An island of nuclei in the vicinity of 114 protons and 184 neutrons is expected to be relatively stable against spontaneous fission, alpha decay, and beta decay. As is true for any island, there are two general ways by which the island of superheavy nuclei may conceivably be reached--by sea and by air. In the next talk Howard will discuss the approach by sea, where one would reach the southeastern, or neutron-rich shore of the island through the multiple capture of neutrons [50].

APPENDIX. SHAPE CONSTRAINTS

The ground-state energy is determined by minimizing the potential energy with respect to an elongation coordinate and a necking coordinate in two different shape parametrizations. We use first a constrained version of the three-quadratic-surface parametrization, which contains the six deformation coordinates $\sigma_1, \sigma_2, \sigma_3, \alpha_1, \alpha_2$, and α_3 [44-51]. The first three coordinates describe symmetric deformations, and the last three describe asymmetric deformations. For specifying ground-state deformations, we eliminate one of the three symmetric coordinates by relating the eccentricity of the middle spheroid to that of the two end spheroids. This is done by requiring that the relative quadrupole moment of the middle spheroid be equal in magnitude but of opposite sign to the relative quadrupole moment of either end spheroid. The two remaining symmetric coordinates are chosen to be the quadrupole moment Q_2 and hexadecapole moment Q_4 of the shape [50]. We find that this parametrization describes very poorly the shapes of nuclei with large positive hexadecapole moments (light isotopes of thorium, uranium, and plutonium). In particular, the generated shapes have a large curvature near $z = 0$, which results in an unphysically large surface energy. For this reason we also

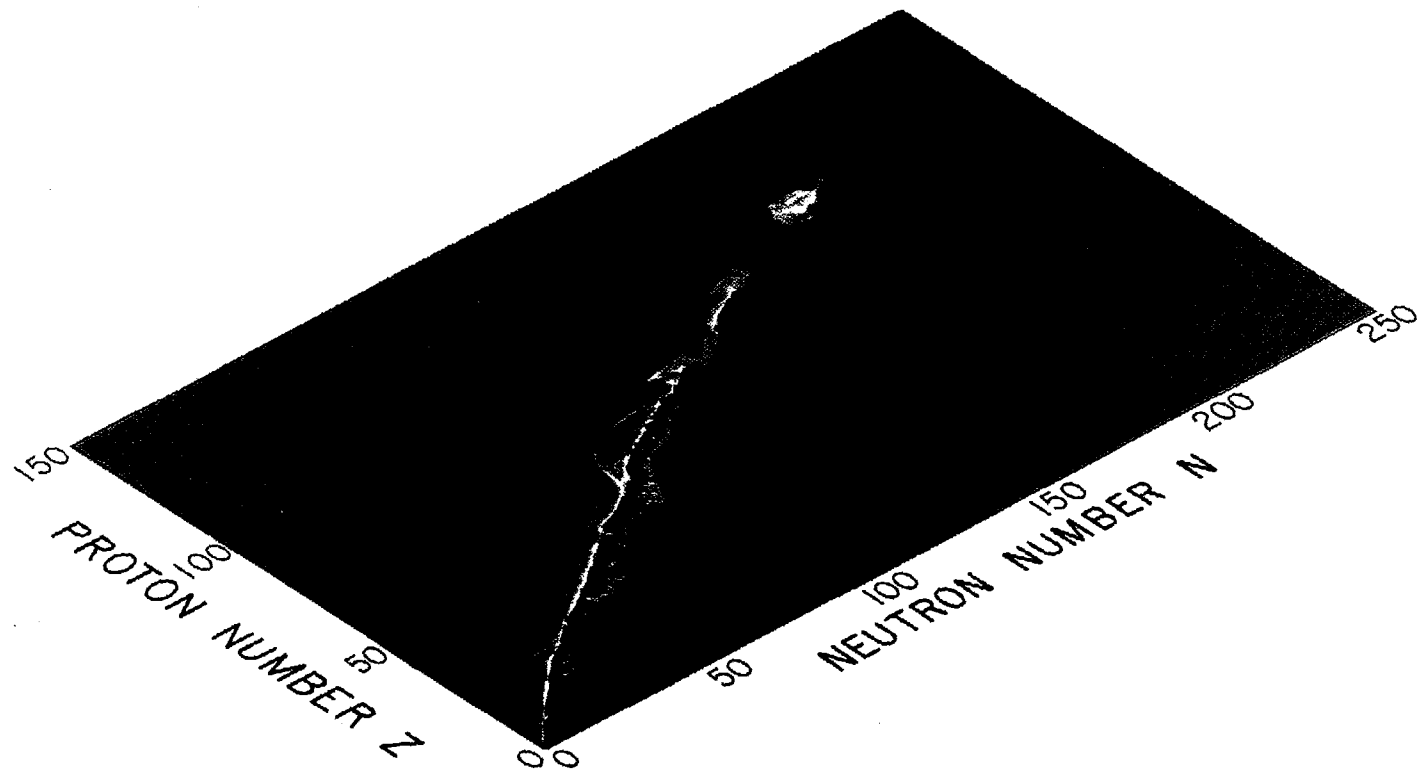


FIG. 18. Location of the predicted island of superheavy nuclei relative to the peninsula of observed nuclei. The nuclei included in the island have calculated total half-lives longer than about 5 min [48].

study the potential energy near the ground state as a function of the coordinates ϵ and ϵ_4 in Nilsson's perturbed-spheroid parametrization [1, 2, 23-29]. For most nuclei the use of this parametrization results in a lower ground-state energy (by up to 1.2 MeV for ^{226}Th). However, for several nuclei with neutron number N close to 152 the energy calculated in the constrained version of the three-quadratic-surface parametrization is lower (by up to 0.4 MeV for ^{250}Cf). For each nucleus we use the lower ground-state energy calculated with these two parametrizations.

The remaining fission barrier extrema are determined by use of the three-quadratic-surface parametrization only. (For comparison we are currently re-determining them by use of Nilsson's perturbed-spheroid parametrization.) In this determination three coordinates are varied independently: the distance between mass centers r , the necking coordinate σ_2 , and the asymmetry coordinate α_2 . The coordinate α_3 is always set equal to 0, and α_1 is used to keep the center of mass fixed at the origin. When σ_2 is varied, the coordinate σ_1 which specifies the separation of the end-spheroid centers is determined so that the distance r between the actual nascent-fragment mass centers remains fixed. The fragment-eccentricity coordinate σ_3 is taken equal to its value for the y-family shape [45, 47] that has the same value of r . For asymmetric shapes ($\alpha_2 \neq 0$), r is chosen to be the same as for the corresponding symmetric shape. Because a large change in α_2 sometimes leads to a small change in the actual shape, we define the mass-asymmetry coordinate as $(M_1 - M_2)/(M_1 + M_2) = (M_1 - M_2)/M_0$. Here M_1 is the mass on one side of the point midway between the ends of the shape, and M_2 is the mass on the other side.

The asymmetric saddle points are determined in the following way: We consider seven values of r in the vicinity of the second saddle point. With r fixed we vary σ_2 and the mass-asymmetry coordinate independently; we use five values for each of the last two coordinates, which makes a total of 25 grid points. For each mass asymmetry we minimize the energy with respect to σ_2 . In this way we obtain for each value of r the energy as a function of mass asymmetry; these energies are then used to construct contour maps as functions of r and mass asymmetry. From these contour maps the asymmetric saddle points are then determined. In our contour maps all distortion coordinates ($\sigma_1, \sigma_2, \sigma_3, \alpha_1, \alpha_2, \alpha_3$) are continuous functions of r and mass asymmetry, thus insuring that we do not "tunnel through" a mountain ridge when minimizing with respect to σ_2 and consequently obtain a spurious saddle point of lower energy.

When determining the first saddle point and second minimum, only r and σ_2 are varied because in this region the potential energy is stable against mass-asymmetric distortions (or in a few cases only slightly unstable). Therefore, in the two contour diagrams displayed in Fig. 6 the potential energy for asymmetric shapes is minimized with respect to σ_2 only in the vicinity of the second saddle point. In other regions asymmetric distortions are generated from the corresponding symmetric shape by making $\alpha_2 \neq 0$. In the region preceding the second saddle point these symmetric shapes are those for the ground state, first saddle point, and second minimum for the particular nucleus under consideration. Beyond the second saddle point the symmetric shapes correspond to those along the most probable idealized liquid-drop-model dynamical path from saddle to scission [44,51] for fissility parameter $x = 0.8$.

ACKNOWLEDGMENTS

Our greatest debt concerning this work is owed to our friend and colleague S. G. Nilsson, who collaborated with us in redetermining the parameters of the folded Yukawa single-particle potential and who—through our near-daily

interactions during the past six months—has provided new insight into most of the points discussed here. We are also grateful to R. W. Hasse, W. M. Howard, M. G. Mustafa, W. D. Myers, A. J. Sierk, and W. J. Swiatecki for their contributions to this work.

REFERENCES

- [1] LARSSON, S. E., LEANDER, G., Paper IAEA-SM-174/6, these Proceedings.
- [2] JOHANSSON, T., NILSSON, S. G., SZYMANSKI, Z., Ann. Phys. (Paris) 5 (1970) 377.
- [3] BRACK, M., DAMGAARD, J., JENSEN, A. S., PAULI, H. C., STRUTINSKY, V. M., WONG, C. Y., Rev. Mod. Phys. 44 (1972) 320.
- [4] NIX, J. R., Ann. Rev. Nucl. Sci. 22 (1972) 65.
- [5] PAULI, H. C., Phys. Rep. 7 (1973) 35.
- [6] BACK, B. B., BRITT, H. C., GARRETT, J. D., HANSEN, O., LEROUX, B., Paper IAEA-SM-174/201, these Proceedings; BACK, B. B., HANSEN, O., BRITT, H. C., GARRETT, J. D., Paper IAEA-SM-174/27, these Proceedings.
- [7] VANDENBOSCH, R., Paper IAEA-SM-174/203, these Proceedings.
- [8] DAVIES, K. T. R., MCCARTHY, R. J., Phys. Rev. C 4 (1971) 81.
- [9] BETHE, H. A., Ann. Rev. Nucl. Sci. 21 (1971) 93.
- [10] BASSICHIS, W. H., KERMAN, A. K., TSANG, C. F., TUEPPE, D. R., WILETS, L., Magic Without Magic: John Archibald Wheeler (KLAUDER, J. R., Ed.), Freeman, San Francisco (1972) 15.
- [11] BASSICHIS, W. H., KERMAN, A. K., Phys. Rev. C 6 (1972) 370.
- [12] KERMAN, A. K., PAL, M. K., Phys. Rev. 162 (1967) 970.
- [13] MELDNER, H. W., Phys. Rev. 178 (1969) 1815.
- [14] KÖHLER, H. S., Nucl. Phys. A170 (1971) 88.
- [15] SKYRME, T. H. R., Nucl. Phys. 9 (1959) 615.
- [16] VAUTHERIN, D., BRINK, D. M., Phys. Rev. C 5 (1972) 626.
- [17] FLOCARD, H., QUENTIN, P., KERMAN, A. K., VAUTHERIN, D., Nucl. Phys. A203 (1973) 433.
- [18] QUENTIN, P., Orsay Preprint (1973).
- [19] FLOCARD, H., QUENTIN, P., VAUTHERIN, D., KERMAN, A. K., Paper IAEA-SM-174/38, these Proceedings.
- [20] BRITT, H. C., BOLSTERLI, M., NIX, J. R., NORTON, J. L., Phys. Rev. C 7 (1973) 801.
- [21] STRUTINSKY, V. M., Yad. Fiz. 3 (1966) 614; Sov. J. Nucl. Phys. 3 (1966) 449.
- [22] SWIATECKI, W. J., Nuclidic Masses (Proc. Conf. Vienna, 1963), Springer-Verlag (1964) 58.
- [23] GUSTAFSSON, C., LAMM, I. L., NILSSON, B., NILSSON, S. G., Ark. Fys. 36 (1967) 613.
- [24] NILSSON, S. G., TSANG, C. F., SOBICZEWSKI, A., SZYMAŃSKI, Z., WYCECH, S., GUSTAFSSON, C., LAMM, I. L., MÖLLER, P., NILSSON, B., Nucl. Phys. A131 (1969) 1.
- [25] TSANG, C. F., NILSSON, S. G., Nucl. Phys. A140 (1970) 289.
- [26] MÖLLER, P., NILSSON, S. G., Phys. Lett. 31B (1970) 283.
- [27] GUSTAFSSON, C., MÖLLER, P., NILSSON, S. G., Phys. Lett. 34B (1971) 349.
- [28] MÖLLER, P., Nucl. Phys. A192 (1972) 529.
- [29] SEEGER, P. A., Atomic Masses and Fundamental Constants (Proc. Conf. Teddington, 1971), Plenum, London (1972) 255.
- [30] LAWRENCE, J. N. P., Phys. Rev. 139 (1965) B1227.
- [31] HASSE, R. W., Nucl. Phys. A128 (1969) 609.
- [32] STRUTINSKY, V. M., PAULI, H. C., Physics and Chemistry of Fission (Proc. Symp. Vienna, 1969), IAEA, Vienna (1969) 155.
- [33] PAULI, H. C., LEDERGERBER, T., BRACK, M., Phys. Lett. 34B (1971) 264.
- [34] PAULI, H. C., LEDERGERBER, T., Nucl. Phys. A175 (1971) 545.
- [35] PAULI, H. C., LEDERGERBER, T., Paper IAEA-SM-174/206, these Proceedings.

- [36] ADEEV, G. D., GAMALYA, I. A., CHERDANTSEV, P. A., *Yad. Fiz.* 13 (1971) 1180; *Sov. J. Nucl. Phys.* 13 (1971) 679.
- [37] PASHKEVICH, V. V., *Nucl. Phys.* A169 (1971) 275.
- [38] NIX, J. R., SWIATECKI, W. J., *Nucl. Phys.* 71 (1965) 1.
- [39] MARUHN, J., GREINER, W., *Z. Phys.* 251 (1972) 431.
- [40] MARUHN, J., et al., Paper IAEA-SM-174/102, these Proceedings, Vol.1.
- [41] MOSEL, U., *Phys. Rev. C* 6 (1972) 971.
- [42] MUSTAFA, M. G., MOSEL, U., SCHMITT, H. W., *Phys. Rev. C* 7 (1973) 1519.
- [43] MUSTAFA, M. G., SCHMITT, H. W., Oak Ridge Preprint (1973).
- [44] NIX, J. R., *Nucl. Phys.* A130 (1969) 241.
- [45] BOLSTERLI, M., FISET, E. O., NIX, J. R., *Physics and Chemistry of Fission (Proc. Symp. Vienna, 1969)*, IAEA, Vienna (1969) 183.
- [46] FISET, E. O., NIX, J. R., BOLSTERLI, M., Los Alamos Rep. LA-4735-MS (1971).
- [47] BOLSTERLI, M., FISET, E. O., NIX, J. R., NORTON, J. L., *Phys. Rev. C* 5 (1972) 1050.
- [48] FISET, E. O., NIX, J. R., *Nucl. Phys.* A193 (1972) 647.
- [49] NIX, J. R., Warsaw Rep. INR-P-1447/I/PL (1972) 299.
- [50] HOWARD, W. M., NIX, J. R., Paper IAEA-SM-174/60, these Proceedings, Vol.1.
- [51] SIERK, A. J., NIX, J. R., Paper IAEA-SM-174/74, these Proceedings, Vol.2.
- [52] ANDERSEN, B. L., DICKMANN, F., DIETRICH, K., *Nucl. Phys.* A159 (1970) 337.
- [53] KOONIN, S. E., unpublished (1972).
- [54] MYERS, W. D., SWIATECKI, W. J., *Ann. Phys. (New York)* 55 (1969) 395.
- [55] MYERS, W. D., SWIATECKI, W. J., Berkeley Rep. UCRL-19543 (1970).
- [56] MYERS, W. D., SWIATECKI, W. J., Berkeley Preprint LBL-1957 (1973).
- [57] MYERS, W. D., SWIATECKI, W. J., *Ark. Fys.* 36 (1967) 343.
- [58] BETHE, H. A., *Phys. Rev.* 167 (1968) 879.
- [59] BRUECKNER, K. A., BUCHLER, J. R., CLARK, R. C., LOMBARD, R. J., *Phys. Rev.* 181 (1969) 1543.
- [60] BRUECKNER, K. A., CLARK, R. C., LIN, W., LOMBARD, R. J., *Phys. Rev. C* 1 (1970) 249.
- [61] BRUECKNER, K. A., BUCHLER, J. R., KELLY, M. M., *Phys. Rev.* 173 (1968) 944.
- [62] SCHEID, W., GREINER, W., *Z. Phys.* 226 (1969) 364.
- [63] KRAPPE, H. J., NIX, J. R., Paper IAEA-SM-174/12, these Proceedings, Vol.1.
- [64] NILSSON, S. G., NIX, J. R., MÖLLER, P., Los Alamos Preprint (1973).
- [65] STRUTINSKY, V. M., *Nucl. Phys.* A122 (1968) 1.
- [66] PASHKEVICH, V. V., *Nucl. Phys.* A133 (1969) 400.
- [67] NILSSON, S. G., private communication (1973).
- [68] GÖTZ, U., PAULI, H. C., JUNKER, K., *Phys. Lett.* 39B (1972) 436.
- [69] MYERS, W. D., *Nucl. Phys.* A145 (1970) 387.
- [70] GEILIKMAN, B. T., *Yad. Fiz.* 9 (1969) 894; *Sov. J. Nucl. Phys.* 9 (1969) 521.
- [71] BRACK, M., QUENTIN, P., Paper IAEA-SM-174/98, these Proceedings, Vol.1.
- [72] BUNATIAN, G. G., KOLOMIETZ, V. M., STRUTINSKY, V. M., *Nucl. Phys.* A188 (1972) 225.
- [73] RAMAMURTHY, V. S., KAPOOR, S. S., *Phys. Lett.* 42B (1972) 399.
- [74] RAMAMURTHY, V. S., KAPOOR, S. S., Abstract IAEA-SM-174/09, these Proceedings, Vol.2.
- [75] RAMAMURTHY, V. S., KAPOOR, S. S., *Int. Conf. Nuclear Physics (Proc. Conf. Munich, 1973)* I, North-Holland, Amsterdam (1973).
- [76] WILLIAMS, F. C., Jr., CHAN, G., HUIZENGA, J. R., *Nucl. Phys.* A187 (1972) 225.
- [77] BENGTSSON, R., *Nucl. Phys.* A198 (1972) 591.
- [78] JAMES, G. D., LYNN, J. E., EARWAKER, L. G., *Nucl. Phys.* A189 (1972) 225.
- [79] BACK, B. B., BRITT, H. C., GARRETT, J. D., HANSEN, O., *Phys. Rev. Lett.* 28 (1972) 1707.
- [80] RANDRUP, J., TSANG, C. F., MÖLLER, P., NILSSON, S. G., LARSSON, S. E., Berkeley Preprint (1973).

- [81] RANDRUP, J., Abstract IAEA-SM-174/29, these Proceedings, Vol.2.
- [82] WILETS, L., Theories of Nuclear Fission, Clarendon, Oxford (1964) 46.
- [83] WAPSTRA, A. H., GOVE, N. B., Nucl. Data Tables 9 (1971) 265.
- [84] BJØRNHOLM, S., LYNN, J. E., unpublished (1970).
- [85] RUSSO, P. A., PEDERSEN, J., VANDENBOSCH, R., Paper IAEA-SM-174/96, these Proceedings, Vol.1.
- [86] BENGTSSON, R., Paper IAEA-SM-174/7, these Proceedings, Vol.1.
- [87] MORETTO, L. G., THOMPSON, S. G., ROUTTI, J., GATTI, R. C., Phys. Lett. 38B (1972) 471.
- [88] HULET, E. K., WILD, J. F., LOUGHEED, R. W., EVANS, J. E., QUALHEIM, B. J., NURMIA, M., GHIORSO, A., Phys. Rev. Lett. 26 (1971) 523.
- [89] PHILLIPS, L., GATTI, R. C., CHESNE, A., MUGA, L., THOMPSON, S. G., Phys. Rev. Lett. 1 (1958) 215.
- [90] NURMIA, M., SIKKELAND, T., SILVA, R., GHIORSO, A., Phys. Lett. 26B (1967) 78.
- [91] BALIAN, R., BLOCH, C., Ann. Phys. (New York) 69 (1972) 76.
- [92] SPECHT, H. J., WEBER, J., KONECNY, E., HEUNEMANN, D., Phys. Lett. 41B (1972) 43.
- [93] SOBICZEWSKI, A., BJØRNHOLM, S., POMORSKI, K., Nucl. Phys. A202 (1973) 274.
- [94] VANDENBOSCH, R., RUSSO, P. A., SLETTEN, G., MEHTA, M., Seattle (Univ. of Washington) Preprint (1973).
- [95] BUSINARO, U. L., GALLONE, S., Nuovo Cim. 5 (1957) 315.
- [96] SWIATECKI, W. J., unpublished (1969).
- [97] ANDERSEN, B. L., Phys. Lett. 42B (1972) 307.
- [98] VON GUNTEN, H. R., Actinides Rev. 1 (1969) 275.
- [99] HOFFMAN, D. C., Los Alamos Rep. LA-DC-72-898 (1972).
- [100] BRANDT, R., THOMPSON, S. G., GATTI, R. C., PHILLIPS, L., Phys. Rev. 131 (1963) 2617.
- [101] TSANG, C. F., WILHELMY, J. B., Nucl. Phys. A184 (1972) 417.
- [102] BALAGNA, J. P., FORD, G. P., HOFFMAN, D. C., KNIGHT, J. D., Phys. Rev. Lett. 26 (1971) 145.
- [103] JOHN, W., HULET, E. K., LOUGHEED, R. W., WESOLOWSKI, J. J., Phys. Rev. Lett. 27 (1971) 45.
- [104] KONECNY, E., SPECHT, H. J., WEBER, J., Phys. Lett., to be published.
- [105] KONECNY, E., SPECHT, H. J., WEBER, J., Paper IAEA-SM-174/20, these Proceedings, Vol.2.
- [106] FREIESLEBEN, H., BRITT, H. C., HUIZENGA, J. R., Paper IAEA-SM-174/56, these Proceedings, Vol.1.
- [107] JENSEN, A. S., DØSSING, T., Paper IAEA-SM-174/28, these Proceedings, Vol.1.

DISCUSSION

M.G. MUSTAFA: Have you carried out your calculation all the way to scission and did you have any problems?

J.R. NIX: Our calculations were carried out all the way to scission; the slightly curved dot-dashed line near the right-hand edge of Fig.6 indicates scission. Our shape parametrization permits a smooth transition from pre-scission to post-scission shapes and no problems were encountered in this region.

M.G. MUSTAFA: I would like to add to your statement about two possible paths to scission. We, too, have seen two possible paths in our two-centre model calculations. I think that in the Pb region and in the heavy actinides one of the paths dominates, but in Ra the two paths are perhaps

equally possible. Thus the mass distribution in the Pb region and in the actinides would show a double hump, but in Ra it would be expected to have a triple hump.

S.S. KAPOOR: Does one have to carry out calculations of shell correction energy as a function of smoothing parameters p and γ for each shape for which calculations are carried out, in order to ensure the constancy of the shell correction with respect to these parameters, or is it sufficient to determine p and γ for a few shapes and use this for all the shapes?

J.R. NIX: It is sufficient to determine best values for the order p and the smoothing range γ of the shell correction for several selected shapes and then use those values for all shapes.

S.S. KAPOOR: With regard to the different mass distributions occurring with spontaneous fission of ^{256}Fm and thermal neutron fission of ^{257}Fm , is it not possible that a symmetric mass distribution can occur in the second case, because the excitation energy tends to wipe out shell effects?

J.R. NIX: The thermal-neutron-induced fission of ^{255}Fm has now been studied by R.C. Ragaini, E.K. Hulet and R.W. Loughheed¹. According to their results, the most probable mass division for the fission of an excited ^{256}Fm nucleus is slightly asymmetric (whereas it is symmetric for ^{258}Fm).

U. MOSEL: I would like to support Nix's statement that the difference between the potential-energy surface for ^{236}U , as calculated in his method, and the one calculated by Mustafa, Schmitt and myself is indeed due to the different choice of shape parameters. It is highly probable that one misses the essential parts of the potential energy surface entirely when following a liquid drop model dynamic path, as was done in Nix's calculations. After all, the shell corrections amount to several MeV and may change this path quite a bit. In our case the shell corrections at scission favour shorter, less deformed shapes than in Nix's calculations. A final answer to this problem can, of course, be obtained only in dynamic calculations.

There is also another reason why the asymmetric valley should actually run from the saddle to scission. As was pointed out by Nix, the asymmetry at the barrier is due to the presence of two types of specific levels at the Fermi surface. These levels are there because of the final fragment structure. Therefore this grouping has to become stronger with decreasing neck radius, thus favouring a continuous valley out to scission.

J.R. NIX: Near the second saddle point only levels of the type $[\text{Nnz}\Lambda\Omega] = [40\Lambda\Omega]$ and $[51\Lambda\Omega]$ are affected strongly by asymmetric perturbations. As the nucleus deforms towards scission, other levels begin to be affected. Beyond scission, all levels are affected. But of course the mass division must already be decided somewhat before scission because of the difficulty of transferring mass through shapes with small necks.

H.C. PAULI: You report a local minimum for thorium in the symmetric-asymmetric plane. We have observed a similar behaviour in some nuclei, but, if we include the second symmetric degree (like h), the minimum is unstable. Minimizing with respect to some one deformation may also lead to spurious results.

J.R. NIX: We have indicated that the third minimum in the potential-energy surface may be a spurious feature of limited shape parametrizations. Similar minima have appeared in two independent calculations. We have

¹ Paper IAEA-SM-174/72, these Proceedings, Vol. 2.

minimized the potential energy in this region with respect to a necking co-ordinate, but need to make further minimizations to check that this minimum does not disappear.

H.C. PAULI: The interpretation of the thorium anomaly as being due to a third minimum interests me and I wonder if any of our experimentalists could tell us whether such a shallow minimum could produce such a sharp resonance as that observed?

H.C. BRITT: The analysis of the ^{231}Th resonance by Lynn indicates a shallow minimum which is qualitatively in agreement with the concept of a third minimum. However, both our and Lynn's analyses of the data indicate $\hbar\omega_A$ and $\hbar\omega_B$ values that are similar to those found in heavier actinide nuclei. I wonder whether the normal second peak in Th nuclei could break up into two peaks which are as broad as that.

H.C. PAULI: Next, I should like to ask the authors whether the instability due to axially asymmetric deformation is calculated for a spheroid or at the real (static) barrier?

P. MÖLLER: In the calculations, which are discussed by S.E. Larsson², who performed them, both spheroidal (ϵ) and hexadecapole (necking or P_4) distortions were taken into account simultaneously.

H.C. PAULI: I do not understand why the peak-to-valley ratio in the fragment mass distribution should be correlated at all with the lowering of the outer barrier due to asymmetry.

J.R. NIX: The reason for the correlation of the peak-to-valley ratio of the fission-fragment mass distribution with the difference in energy between the second symmetric and asymmetric saddle points has been given by C.F. Tsang and J.B. Wilhelmy (Nucl. Phys. A184 (1972) 417). Basically, the reason is that in spontaneous fission the penetrabilities through the symmetric and asymmetric portions of the barrier depend exponentially upon the barrier heights and curvatures. In induced fission, the probabilities for proceeding over the symmetric and asymmetric saddle points depend exponentially upon the barrier heights and the nuclear temperature.

R. VANDENBOSCH: It has been suggested that the relative prominence of the two valleys from near saddle to scission is dependent on whether one minimizes the energy with respect to mass asymmetry for liquid-drop-like elongations, as was done by Möller and Nix, or whether one also minimizes with respect to necking-in as in the case of Mustafa, Mosel and Schmitt. I believe there is experimental evidence that can help us distinguish which valley is being followed. The origin of the shell effects resulting in the asymmetric valley to scission is the single-particle degeneracies of the final fragments. These are particularly strong for the double-magic spherical $A = 132$ fragment. We know that the fragment neutron yield and hence the excitation energy and scission deformation for fragments with $A \approx 132$ is very small. I believe this observation is inconsistent with following the Möller-Nix valley which is associated with larger elongations near scission.

I would also like to comment on the more general question regarding the relation between the stability of the saddle point with respect to asymmetric distortions and the experimental mass distributions. It has been suggested that the qualitative features of the dependence of mass asymmetry on mass number can be understood from the saddle properties. I would remind you, however, that there are now a number of calculations

² LARSSON, S. E., LEANDER, G., Paper IAEA-SM-174/06, these Proceedings, Vol. 1.

(Pashkevich; Mustafa, Mosel and Schmitt; Möller and Nix) which show that the asymmetric saddle is from 0.25 to 2 MeV lower than the symmetric saddle for nuclei in the lead region, whereas the experimental mass yield distributions are symmetric. I believe we should not be over-eager to try to relate all observations to static properties such as saddle shapes. One of the characteristic features of nuclear fission, as contrasted with other nuclear reactions, is the large shape change which occurs. I believe that a complete understanding of fission will require a consideration of the dynamics of nuclear distortions.

CALCULATION OF FISSION BARRIERS FOR HEAVY NEUTRON-RICH NUCLEI*

W.M. HOWARD, J.R. NIX
Los Alamos Scientific Laboratory,
University of California,
Los Alamos, N. Mex.,
United States of America

Abstract

CALCULATION OF FISSION BARRIERS FOR HEAVY NEUTRON-RICH NUCLEI.

A study is made of the possible production of superheavy nuclei by the multiple capture of neutrons in the astrophysical r-process, the conventional thermonuclear explosion, and the multi-step explosions proposed by Meldner. This is done by calculating the fission barriers and neutron separation energies for the appropriate region of heavy neutron-rich nuclei. An improved version of the macroscopic-microscopic method is used. The macroscopic energy is calculated according to the droplet model of Myers and Swiatecki, with constants they determined in January 1973 by adjustments to experimental nuclear ground state masses and fission-barrier heights and by statistical calculations. The microscopic corrections to the energy are calculated from a diffuse-surface single particle potential of the folded Yukawa type. The potential radius is taken from the statistical calculations of Myers; the potential well depths and diffuseness and the spin-orbit interaction strengths are adjusted to reproduce experimental single particle levels in heavy nuclei.

The calculated fission barriers are displayed as functions of the distance between the centers of mass of the two nascent fragments. The actual shapes considered are the sequence of idealized liquid-drop-model saddle point shapes (the so-called γ family of shapes) for distortions up to the vicinity of the saddle point. For larger distortions the most probable idealized liquid-drop-model dynamical path is used. The neutron separation energies are calculated from ground state masses that are determined by minimizing the potential energy with respect to the nuclear quadrupole moment Q_2 and hexadecapole moment Q_4 .

For a broad region of heavy neutron-rich nuclei the calculated fission barriers are less than the calculated neutron separation energies. This stems primarily from the predicted rapid decrease in the effective surface tension of a nucleus with increasing neutron excess. Therefore, the capture of a neutron should excite the nucleus above the top of the fission barrier and consequently terminate the neutron-capture process before any superheavy nuclei are produced.

1. INTRODUCTION

The prediction of the possible existence of superheavy nuclei has led to attempts to produce them in the laboratory and to searches for them in nature. Calculations of the nuclear properties of such nuclei by Myers and Swiatecki [1], Nilsson and his coworkers [2], and more recently by other workers [3,4] have predicted half-lives as long as 10^9 yr. Thus, if these nuclei are produced in astrophysical environments, they should be detectable on the earth and in the cosmic rays impinging on the earth. Thus far, efforts to produce superheavy nuclei in the laboratory or to find them in nature have failed.

In this paper, we study the effectiveness of the mechanism that nature would use to produce them as well as the mechanism that man might use if he employed nuclear explosions. In particular, we study the astrophysical r-process, the conventional thermonuclear explosion, and the multistep process

* Work performed under the auspices of the US Atomic Energy Commission.

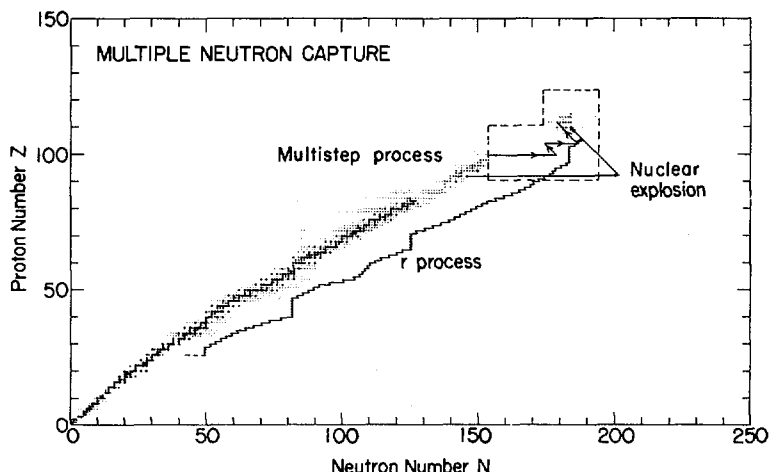


FIG. 1. Plot of known and predicted nuclei as a function of neutron number N and proton number Z . The three possible ways to reach the island of superheavy nuclei by the multiple capture of neutrons are illustrated.

proposed by Meldner [5]. Neutron-induced fission plays the critical role in terminating these processes; we therefore calculate the fission barriers and neutron separation energies for a broad region of heavy neutron-rich nuclei.

Figure 1 is a plot of known and predicted nuclei as a function of the neutron number N and proton number Z . The heaviest points represent stable nuclei, the medium-size points nuclei with half-lives greater than one year, and the lightest points nuclei with half-lives less than one year. Nuclei with predicted half-lives greater than about five minutes are included in the island of superheavy nuclei [4]. The dashed lines outline the region of nuclei where we calculate fission barriers and nuclear ground-state masses. Our fission-barrier calculations are limited to even nuclei. The solid lines indicate the approximate regions of heavy neutron-rich nuclei through which the various processes occur.

In Sec. 2 we discuss the method of calculation, in Sec. 3 our results, in Sec. 4 the significance of our results to these various neutron-capture processes, and in Sec. 5 our conclusions.

2. METHOD OF CALCULATION

The potential energy surfaces for these heavy neutron-rich nuclei are calculated by use of the macroscopic-microscopic method as described in the previous review paper on the calculation of fission barriers [6]. The macroscopic energy is calculated according to the droplet model of Myers and Swiatecki [7,8], with constants they determined in January 1973 by adjustments to experimental nuclear ground-state masses and fission-barrier heights and from statistical calculations. The droplet model takes into account terms of order $A^{1/3}$ in the nuclear energy as well as a more precise dependence of the effective surface energy on the neutron excess. The microscopic corrections to the energy are calculated from a diffuse-surface single-particle potential of the folded Yukawa type. The potential radius is taken from the statistical calculations of Myers [9]; the potential well

depths are adjusted to reproduce experimental single-particle levels in heavy spherical nuclei and the diffuseness and spin-orbit interaction strengths in heavy deformed nuclei [6]. This macroscopic-microscopic method is consistent with experimental fission barriers and ground-state masses in the actinide region as well as with information from conventional nuclear explosions in the neutron-rich region.

The neutron separation energies are calculated from ground-state masses that are determined by minimizing the potential energy with respect to the nuclear quadrupole moment Q_2 and the hexadecapole moment Q_4 . The nuclear shapes are described in terms of smoothly joined portions of three quadratic surfaces of revolution [10,11]. One of the three symmetric coordinates that define such shapes is eliminated by requiring that the relative quadrupole moment of the middle spheroid be equal in magnitude but of opposite sign to the relative quadrupole moment of either end spheroid. The two remaining coordinates are chosen to be the quadrupole moment Q_2 and hexadecapole moment Q_4 of the shape.

For the droplet-model mass excess we use the following form [7,8], where it is understood that all energies and masses are in MeV and that all lengths are in fm:

$$\begin{aligned}
 M(Z,A; \text{shape}) = & 8.07169 (A-Z) + 7.28922 Z \\
 & + (-a_1 + J\bar{\delta}^2 - \frac{1}{2}K\bar{\epsilon}^2 + \frac{1}{2}M\bar{\delta}^4) A \\
 & + (a_2 + \frac{9}{4}[\frac{J}{Q}]\bar{\delta}^2) A^{2/3} B_s \\
 & + a_3 A^{1/3} B_k + C_1 Z^2 A^{-1/3} B_c - C_2 Z^2 A^{1/3} B_r \\
 & - C_3 Z^2 A^{-1} - 2^{-1/3} C_4 Z - C_5 Z^2 B_w \\
 & + 30|I| + \frac{11}{\sqrt{A}}\delta' + \frac{30}{A}\delta''
 \end{aligned} \tag{1}$$

where

$$I = \frac{A-2Z}{A} \tag{2}$$

$$\bar{\delta} = \frac{(I + \frac{3}{16}[\frac{C_1}{Q}]ZA^{-2/3}B_v)}{(1 + \frac{9}{4}[\frac{J}{Q}]A^{-1/3}B_s)} \tag{3}$$

$$\bar{\epsilon} = (-2a_2 A^{-1/3} B_s + L\bar{\delta}^2 + C_1 Z^2 A^{-4/3} B_c)/K \tag{4}$$

$$C_1 = \frac{3}{5} \frac{e^2}{r_0} \tag{5}$$

$$C_2 = \frac{C_1^2}{168} (\frac{1}{2J} + \frac{9}{K}) \tag{6}$$

$$C_3 = \frac{5}{2} C_1 \left(\frac{H}{r_0} \right)^2 \quad (7)$$

$$C_4 = \frac{5}{4} \left(\frac{3}{2\pi} \right)^{2/3} C_1 \quad (8)$$

$$C_5 = \frac{C_1^2}{64Q} \quad (9)$$

$$\delta' = \begin{cases} +1, & \text{odd nuclei} \\ 0, & \text{odd-particle nuclei} \\ -1, & \text{even nuclei} \end{cases} \quad (10)$$

$$\delta'' = \begin{cases} 1, & \text{odd nuclei with } A = 2Z \\ 0, & \text{otherwise} \end{cases} \quad (11)$$

The six relative energies B_i are functions only of the nuclear shape and are defined so as to have the value unity for a sphere. The quantities B_s and B_c are the relative surface and coulomb energies of the liquid-drop model, B_k is the relative curvature energy, B_r is the relative coulomb redistribution energy in the nuclear volume, and B_v and B_w are two types of relative coulomb redistribution energy in the nuclear surface. The reader is referred to Ref. [7] for the relevant equations to calculate these shape-dependent terms. From a combination of statistical calculations and adjustments to nuclear ground-state masses and fission-barrier heights, values for the constants that appear are determined to be [8]: $a_1 = 15.986$, $a_2 = 20.760$, $a_3 = 0$, $J = 36.5$, $Q = 17$, $r_0 = 1.175$, $K = 240$, $L = 100$, $M = 0$, and $H = 0.99$. Notice that the coefficient of the curvature term is identically zero. The difference in Eq. (1) relative to what appears in Ref. [7] for the coulomb term multiplying C_4 arises because the substitution $A = 2Z$ has been made.

There is much interest in the value of the surface-asymmetry constant κ in liquid-drop-model mass formulas because it has an important bearing on the fissility of neutron-rich nuclei. In the droplet-model the shape dependence of the potential energy is more complicated than in the liquid-drop model, and the constant κ no longer enters. However, by neglecting the relatively small influence of the four new shape-dependent energies, the more complicated dependence of the droplet model on the surface and coulomb energies can be described approximately in terms of an effective value of κ which would yield the same saddle point as the liquid-drop model [12]. The result is

$$\kappa_{\text{eff}} = \frac{\frac{9}{4} \left(\frac{J^2}{Q} \right)}{a_2 \left(1 + \frac{9J\hat{B}_s}{4QA^{1/3}} \right)^2} \quad (12)$$

where \hat{B}_s is the relative surface energy of the saddle-point shape. Thus, unlike in the liquid-drop model, this effective value of κ depends on the mass number and the saddle-point shape. For the neutron-rich nucleus ^{280}Pu , where the macroscopic saddle-point shape is close to $y = 0.10$, we obtain $\kappa_{\text{eff}} = 2.8$. This is significantly higher than the frequently used value of $\kappa = 1.7826$ in the liquid-drop model [13]. Thus, in the droplet model the effective surface tension decreases much more rapidly with neutron excess than in the liquid-drop model of Myers and Swiatecki.

The fission barriers are calculated for the sequence of idealized liquid-drop-model saddle-point shapes (the so-called γ family of shapes) for distortions up to the vicinity of the saddle point. For larger distortions we use the most probable idealized liquid-drop-model dynamical path [10,11]. The barrier heights that we calculate should be considered upper limits since we have not included mass-asymmetric or axially asymmetric (γ) distortions. As shown in the previous paper [6] inclusion of these effects could lower our calculated barriers by 1 or 2 MeV.

3. RESULTS OF CALCULATION

Figure 2 is a comparison of the experimental ground-state single-particle correction for nuclei in the lead, rare-earth, and actinide regions with our calculated values. The discrepancies oscillate with particle number and are as large as 4 MeV for nuclei close to ^{226}Th . Part of the error for these nuclei arises because the constrained version of the three-quadratic-surface parametrization that we are using does not describe adequately shapes with large positive hexadecapole moments: the generated shapes have a large curvature near the equator, which increases substantially the surface energy. The error for these nuclei can be reduced (by up to 1.2 MeV for ^{226}Th) by use [6] of the coordinates ϵ and ϵ_4 in Nilsson's perturbed-spheroid parametrization [2]. However, for several nuclei with neutron number N close to 152, the energy calculated by use of the coordinates

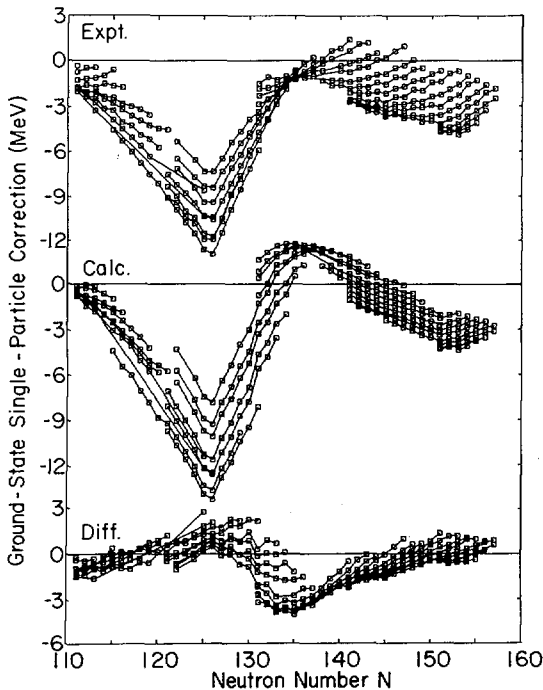


FIG.2. Comparison of experimental and calculated ground state single-particle corrections. The difference between the experimental and calculated values is given in the lower portion of the figure. The ground state single-particle correction is the nuclear mass excess relative to the spherical droplet-model energy.

Q_2 and Q_4 is lower (by up to 0.4 MeV for ^{252}Cf). Comparing this figure with the results of Ref. [6], different conventions are adopted here concerning two separate points. First, our calculated values do not include any zero-point energy. Second, they are relative to the pairing convention of Myers and Swiatecki [8,13], in which an odd-particle nucleus rather than an even nucleus has zero pairing energy. The combined effects of these two differences increase our calculated values by 0.2 to 0.3 MeV relative to those in Ref. [6].

Figures 3, 4, and 5 show some of our calculated barriers as functions of the distance between the centers of mass of the two nascent fragments. We note that the droplet-model contribution to the potential energy is greatly reduced for an increased neutron excess; this is because the effective surface-asymmetry constant for these nuclei is relatively large ($\kappa_{\text{eff}} \approx 2.8$). The barriers are also greatly reduced with increasing proton number due to the strong dependence of the fissility on the disruptive coulomb force. The large second peaks on the barriers of ^{248}U , ^{252}U , and ^{256}U should be reduced by at least 1 or 2 MeV when mass-asymmetric distortions are taken into account.

Our calculated barriers for superheavy nuclei are displayed in Fig. 5; they are very similar to those calculated by Bolsterli et al. [3]. There are three differences in these two calculations: (1) we employ the full droplet model for the macroscopic energy instead of the liquid-drop model, (2) we adjust the surface diffuseness and the spin-orbit interaction strengths to

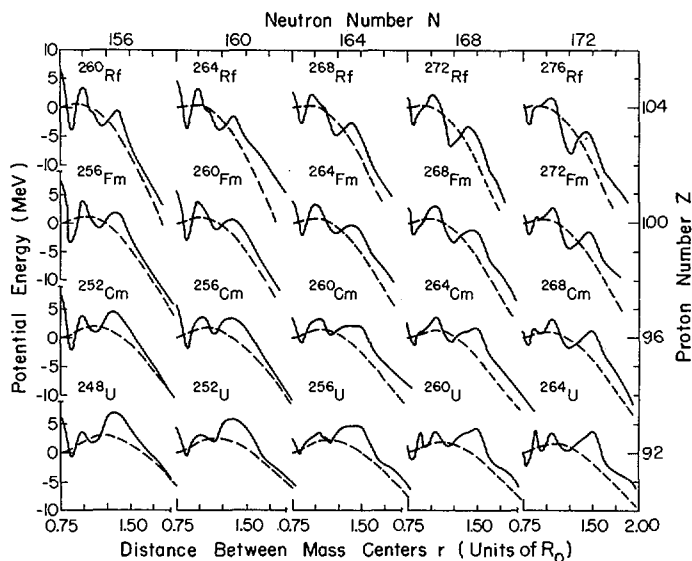


FIG. 3. Fission barriers for nuclei as functions of the distance between the mass centers of the nascent fragments. The dashed curves give the droplet-model contributions and the solid curves the total potential energies. These barriers are calculated by use of the γ family of shapes out to the distortion $\gamma = 0.2$ and the most probable liquid-drop-model dynamical path for fissility parameter $x = 0.8$ for larger distortions. The microscopic contributions to the barriers are calculated with the single-particle levels for ^{264}Fm .

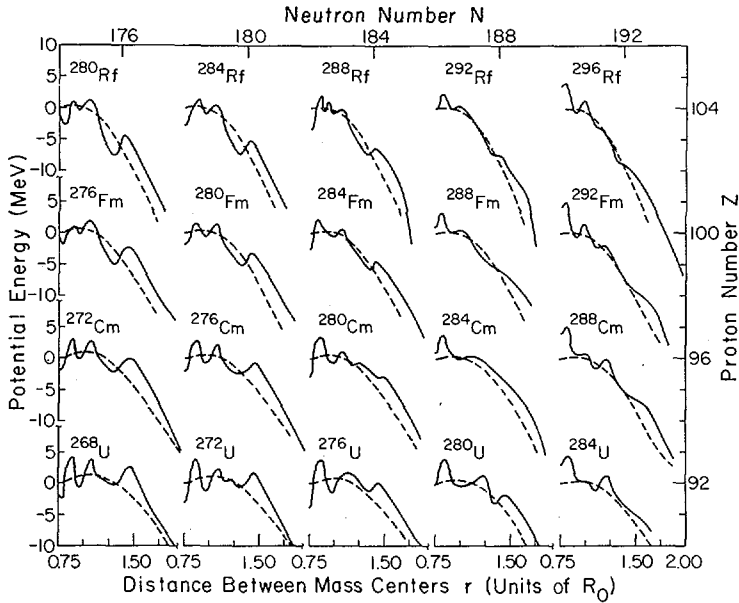


FIG. 4. These barriers are calculated by use of the γ family of shapes out to the distortion $\gamma = 0.1$ and the most probable liquid-drop-model dynamical path for fissility parameter $x = 0.9$ for larger distortions. The microscopic contributions to the barriers are calculated with the single-particle levels for ^{284}Fm . Dashed and solid curves have the same meaning as in Fig. 3.

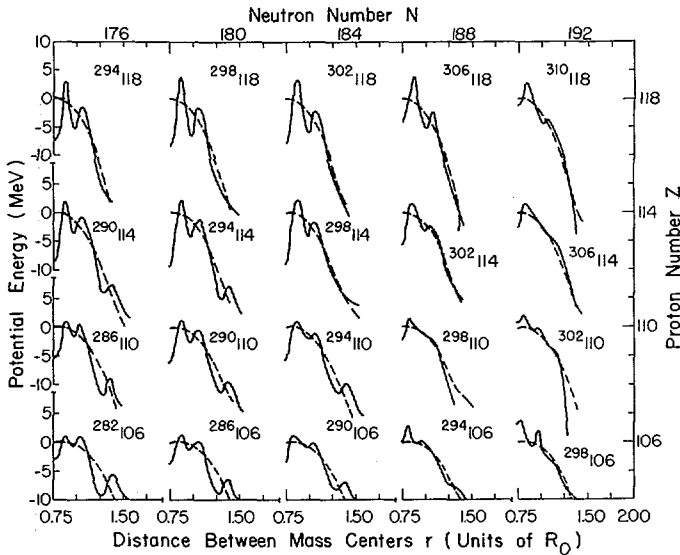


FIG. 5. These barriers are calculated by use of the most probable liquid-drop-model dynamical path for fissility parameter $x = 1.0$. The microscopic contributions to the barriers are calculated with the single-particle levels for $^{298}\text{114}$. Dashed and solid curves have the same meaning as in Fig. 3.

reproduce experimental single-particle levels in the rare-earth and actinide nuclei instead of in ^{208}Pb , and (3) beyond the vicinity of the saddle point we use the liquid-drop-model dynamical path instead of the γ -family sequence of shapes.

The barriers for $^{294}_{118}$, $^{298}_{118}$, $^{302}_{118}$, $^{290}_{114}$, $^{294}_{114}$, and $^{298}_{114}$ are all over 10 MeV high. The barrier for $^{298}_{114}$ is slightly lower than in the previous calculation [3,4]; however, in our calculation the barriers for $^{294}_{114}$ and $^{298}_{118}$ (at $N = 180$) are larger than the barriers for $^{298}_{114}$ and $^{302}_{118}$ (at $N = 184$). As in the previous calculations, when neutrons are added beyond $N = 184$, the barrier height decreases dramatically. We predict the superheavy island to be somewhat more stable in the neutron-deficient direction than has been predicted by previous calculations. This is due to the increased spin-orbit interaction strengths and the decreased surface-diffuseness parameter [6] that we use. This change has the effect of decreasing the neutron level density below $N = 180$, which increases the binding of nuclei with neutron numbers near $N = 180$.

Figure 6 is a contour plot of the calculated fission-barrier height for even nuclei. We include a zero-point energy of 0.5 MeV for motion in the fission direction. Figure 7 is a contour plot of the calculated neutron separation energy for even nuclei, and Fig. 8 is a contour plot of the difference between the calculated fission-barrier height and the calculated neutron separation energy for even nuclei. We will employ these three figures in evaluating where neutron-induced fission will terminate the various multiple-neutron-capture processes. We have not performed any spontaneous-fission half-life calculations.

4. APPLICATION OF RESULTS TO MULTIPLE-NEUTRON-CAPTURE PROCESSES

4.1 Astrophysical r-process

The astrophysical r-process [14] is the multiple capture of neutrons on heavy nuclei on a time scale that is much shorter than beta-decay half-lives for heavy neutron-rich nuclei. In some catastrophic supernova events the high-density matter is thermalized to an energy of order 200 keV, so that neutron capture is impeded by neutron photodisintegration at a low neutron separation energy. The neutron-capture flow thus proceeds far to the neutron-rich side of the valley of beta stability. Neutron separation energies decrease dramatically immediately after a closed shell of neutrons, which tends to halt temporarily the capture flow. When beta decays increase the proton number sufficiently, neutron separation energies again become large enough to allow the capture flow to continue. Figure 1 shows a typical r-process capture path. Since the nuclei along the path are in statistical equilibrium with respect to the exchange of photons and neutrons, the r-process path is determined by the neutron separation energies of the neutron-rich nuclei and, in fact, follows a path of essentially constant neutron separation energy.

There has been much interest as to whether superheavy nuclei can be produced in the r-process, which is known to produce many of the naturally occurring neutron-rich nuclei between germanium and bismuth and all of the naturally occurring nuclei heavier than bismuth. Two groups [15,16] have studied in some detail the fission properties of heavy neutron-rich nuclei in regard to the production of superheavy nuclei by use of the macroscopic-microscopic approach. Boleu et al. [15] have calculated the nuclear potential-energy surface with the modified harmonic-oscillator potential and the liquid-drop model of Myers and Swiatecki [13]. They conclude that even with a low surface asymmetry constant ($\kappa = 1.7826$) superheavy nuclei cannot be produced by the conventional r-process.

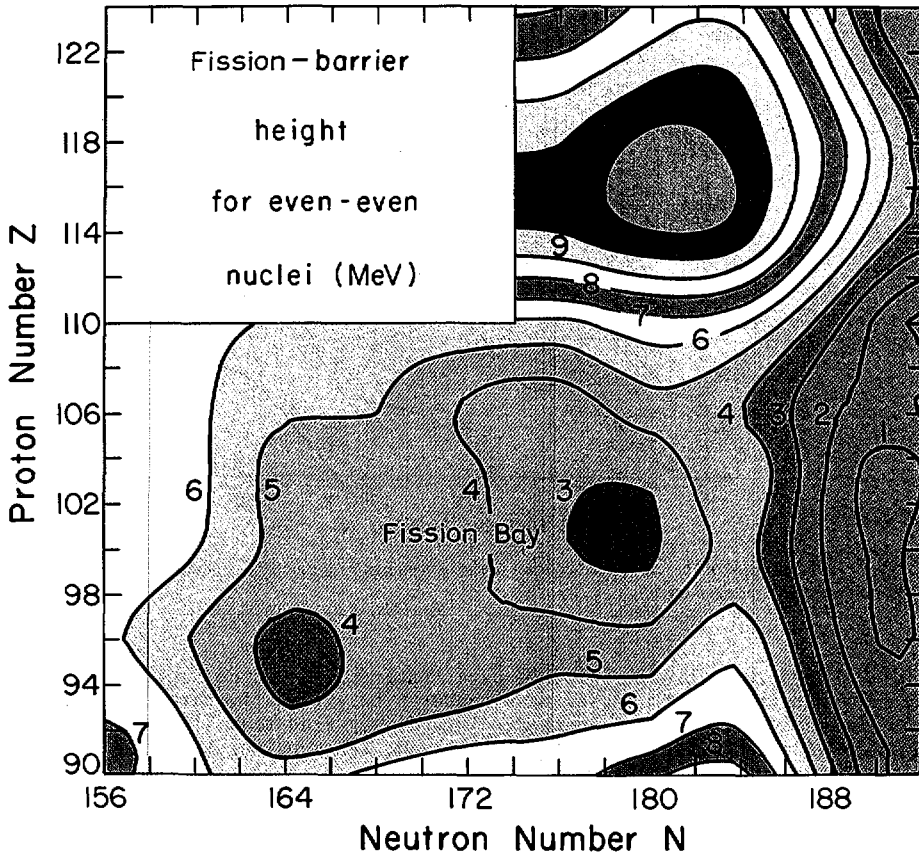


FIG. 6. Contour plot of the calculated fission barrier height as a function of neutron number N and proton number Z for even nuclei.

They find that the r -process would be terminated by neutron-induced fission at approximately $Z = 98$ and $N = 186$. However, these calculations are performed with a pairing strength proportional to the surface area, which reduces the barrier with increasing distortion. According to Ref. [4], the lightest super-heavy nucleus with an astrophysically significant half-life is $A = 291$ ($Z = 110$, $N = 181$).

Schramm and Fiset [16] also use the Myers and Swiatecki [13] liquid-drop model for the macroscopic contribution to their barriers and the diffuse-surface single-particle potential of the folded Yukawa type [3] for the microscopic corrections to the energy. In addition, they studied the dependence of the results on the value of the surface-asymmetry constant κ . The neutron separation energies were calculated from the 1966 mass formula of Myers and Swiatecki [1], which included an empirical microscopic-energy correction. However, their neutron separation energies are similar to those that we calculate. They predict the neutron-induced-fission cutoff to be near $Z = 100$ and $N = 190$ (for $\kappa = 1.7826$). Since the Myers-Swiatecki mass

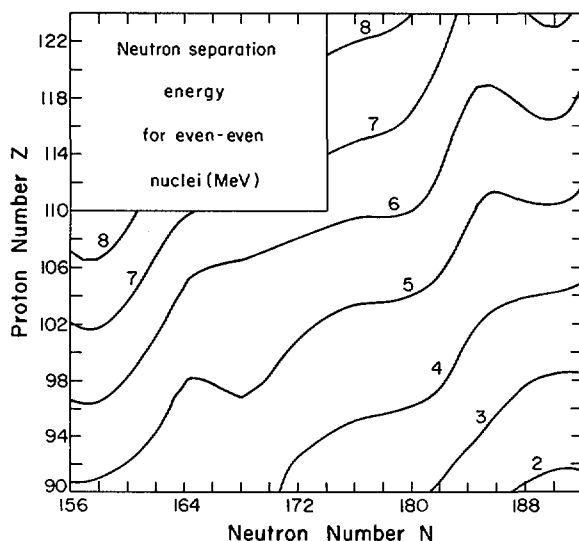


FIG. 7. Contour plot of the calculated neutron separation energy as a function of neutron number N and proton number Z for even nuclei.

formula predicts a broad r -process path, material below the neutron-induced-fission cutoff but with higher mass number A survives. By carefully following the decay back to the superheavy island they find that significant amounts of nuclei with $A = 290, 291, 292$, and 293 survive, depending on what is included for the zero-point energy.

For a given determination of the neutron separation energy for neutron-rich nuclei, the r -process path can be determined approximately without carrying out a full r -process calculation. When calculating neutron-induced fission on the approach to the superheavy island, it is important to know where the r -process path will occur in this region.

There exist two peaks in the solar system abundance distribution of r -process nuclei, at $A = 130$ and $A = 195$. These peaks are due to an accumulation of material along the r -process path at the neutron closed shells $N = 82$ and $N = 126$. The second peak extends through the region $185 \leq A \leq 200$; the r -process path must therefore pass through the same mass region at $N = 126$. The neutron separation energies in the region where the path enters and leaves the neutron closed shell at $N = 126$ therefore determine the values of the neutron separation energy that the r -process path follows.

We calculate the neutron separation energies in this region to be $B_n = 3 \pm 1$ MeV. We therefore find from a study of Figs. 7 and 8 that the neutron-induced-fission cutoff is $Z = 96$ and $N = 186$; this is somewhat lower than the estimates by Boleu et al. [15] and Schramm and Fiset [16].

Thus, we predict that nuclei with mass number $A = 281$ will be the last to survive in the r -process before neutron-induced fission terminates the path. According to the results of Ref. [4], nuclei with mass number 281 would spontaneously fission with half-lives of the order of 1 sec after a few beta decays. In order for superheavy nuclei to be observed in cosmic

rays, their half-lives would need to be at least 10^6 yr. This would require the production of nuclei with mass number $A \geq 291$, which is 10 mass units higher than the heaviest yield that we predict. This lower neutron-induced-fission cutoff is due primarily to the rapid decrease predicted by the drop-let model of the surface energy with the addition of neutrons.

Schramm and Fiset [16] suggest that a small fraction of the material at the neutron-closed shell $N = 184$ could climb along this closed shell during the freeze-out of the r-process neutron flux and reach the superheavy island. However, as seen in Fig. 8, such nuclei would reach Cape Farewell [17] somewhere between $Z = 98$ and 102 and suffer neutron-induced fission before reaching the superheavy island.

4.2 Conventional nuclear explosions

Conventional nuclear explosions yield neutron exposures similar to those in the astrophysical r-process; however, the time duration is so short ($\Delta t \lesssim 10^{-6}$ sec) that there is no time for beta decays during the neutron-capture process. The thermal photon temperature is much less than that in the r-process. The neutron captures therefore proceed to a lower neutron separation energy, which extends into a more neutron-rich region. In nuclear explosions to date, targets of various actinide nuclei have been irradiated with intense neutron sources. Independent of the target used or the intensity of the neutron irradiation, the heaviest nucleus recovered from the debris has been ^{257}Fm [18].

We can understand this failure to produce heavier nuclei in terms of our results. From Fig. 8 we see that neutron-induced fission terminates the neutron-capture chain on the U isotopes at mass number $A = 256$. Actually, neutron-induced fission should occur somewhat before this because we overestimate the barrier for U isotopes in this region by 1 or 2 MeV by not including mass-asymmetric distortions. Thus, we conclude that conventional nuclear explosions have even less hope for producing superheavy nuclei than the r-process.

From Fig. 8 we see that if a lighter target (such as ^{227}Ac , ^{226}Ra , or ^{222}Rn) were used, the neutron capture could proceed well beyond $A = 256$. The results of Fig. 6 show that subsequent beta-decay products would have barriers lower than 4.5 MeV and would therefore spontaneously fission with short half-lives. We have not performed spontaneous-fission half-life calculations for these nuclei, but perhaps some odd-mass chains could survive spontaneous fission and produce nuclei that live long enough ($\gtrsim 6$ h) to be detected in the debris. Neutron exposure experiments on targets of Ac, Ra, or Rn could yield valuable information about the spontaneous-fission half-lives in this region of nuclei. This broad region of nuclei with fission barriers lower than 4.5 MeV (here referred to as the "Fission Bay") is also found in the calculations of Boleu et al. [15].

4.3 Multistep process

The failure of conventional nuclear explosions to produce superheavy nuclei has led Meldner [5] to propose a multistep explosive process that would allow beta decays between subsequent explosions. However, his process seems fraught with the same difficulties encountered in the r-process and in conventional nuclear explosions. Certainly odd-mass capture chains would have to be utilized as well as a target lighter than Th to avoid initial termination of the process by neutron-induced fission. It would then be re-

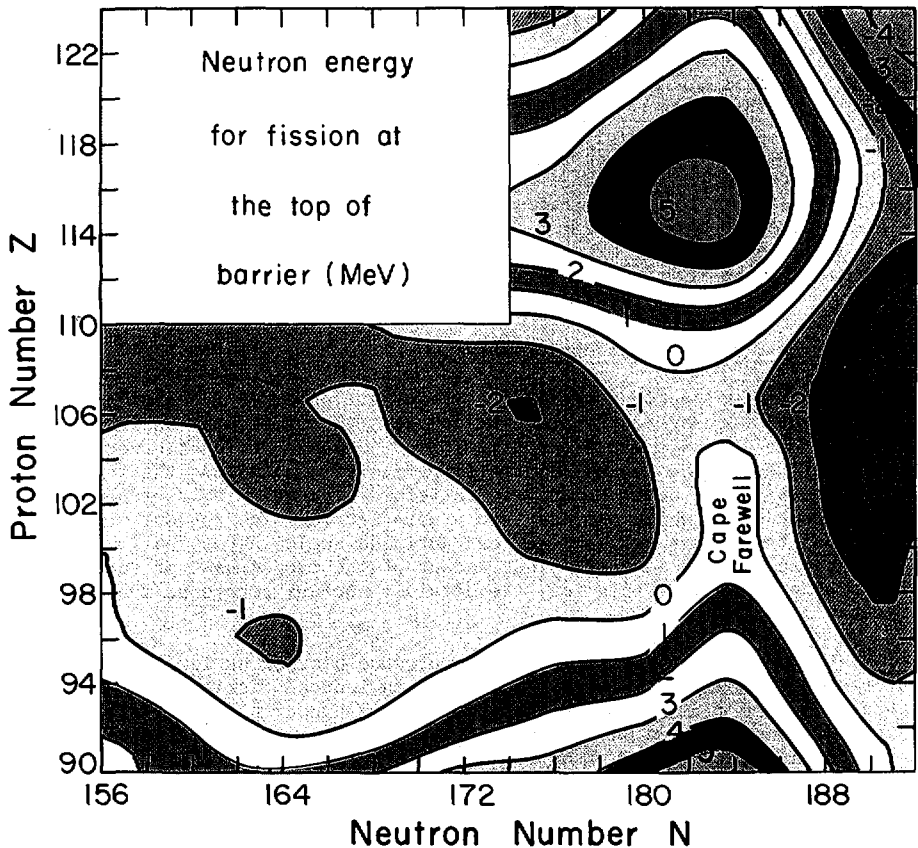


FIG.8. Contour plot of the difference between the fission barrier height and the neutron separation energy for even nuclei. When this difference is less than about 1 MeV, the capture of a neutron leads to immediate fission.

quired that beta decay lead to a region of stability against neutron-induced fission before the next neutron burst.

Meldner would like to take advantage of neutron capture along odd-proton chains where the fission barrier could be enhanced relative to the barrier heights of even nuclei. In the actinide region the spontaneous-fission half-lives of odd-particle nuclei are systematically about 10^3 times as long as those of neighboring even nuclei [19]. These hindrances arise from an increase either in the height of the barrier or in the inertia (or in both). If this hindrance factor is assumed to arise only from an increase in the barrier height, then the barriers for odd-particle nuclei are raised by about 0.5 MeV relative to those for even nuclei [1].

An examination of Fig. 8 reveals that after an initial neutron burst and subsequent beta decay into the Fission Bay, the nuclei would be in a

region where a second neutron burst would initiate neutron-induced fission. This conclusion also applies for odd-proton capture chains. We conclude therefore that the multistep process has little chance of reaching the super-heavy island.

5. CONCLUSIONS

We have used an improved version of the macroscopic-microscopic method to calculate fission barriers and neutron separation energies for a broad region of heavy neutron-rich nuclei. On the basis of these calculations we conclude that neutron-induced fission terminates the three possible multiple-neutron-capture processes well before the superheavy island is reached. However, it is possible that the use of somewhat lighter targets in conventional nuclear explosions could lead to the production of slightly heavier nuclei than are obtained at present.

ACKNOWLEDGMENTS

We are grateful for stimulating discussions with G. A. Cowan, S. E. Koonin, H. W. Meldner, P. Möller, W. D. Myers, S. G. Nilsson, D. N. Schramm, P. A. Seeger, and A. J. Sierk.

REFERENCES

- [1] MYERS, W. D., SWIATECKI, W. J., Nucl. Phys. 81 (1966) 1.
- [2] NILSSON, S. G., TSANG, C. F., SOBIĆZEWSKI, A., SZYMAŃSKI, Z., WYCECH, S., GUSTAFSSON, C., LAMM, I. L., MÖLLER, P., NILSSON, B., Nucl. Phys. A131 (1969) 1.
- [3] BOLSTERLI, M., FISET, E. O., NIX, J. R., NORTON, J. L., Phys. Rev. C 5 (1972) 1050.
- [4] FISET, E. O., NIX, J. R., Nucl. Phys. A193 (1972) 647.
- [5] MELDNER, H. W., Phys. Rev. Lett. 28 (1972) 975.
- [6] MÖLLER, P., NIX, J. R., Paper IAEA-SM-174/202, these Proceedings, Vol.1.
- [7] MYERS, W. D., SWIATECKI, W. J., Berkeley Preprint UCRL-19543 (1970).
- [8] MYERS, W. D., SWIATECKI, W. J., unpublished work (1973).
- [9] MYERS, W. D., Nucl. Phys. A145 (1970) 387.
- [10] NIX, J. R., Nucl. Phys. A130 (1969) 241.
- [11] SIERK, A. J., NIX, J. R., Paper IAEA-SM-174/74, these Proceedings, Vol.2.
- [12] SEEGER, P. A., Atomic Masses and Fundamental Constants (Proc. Conf. Teddington, 1971), Plenum, London (1972) 255.
- [13] MYERS, W. D., SWIATECKI, W. J., Ark. Fys. 36 (1967) 343.
- [14] SEEGER, P. A., FOWLER, W. A., CLAYTON, D. D., Astrophys. J. Suppl. 11 (1965) 121.

- [15] BOLEU, R., NILSSON, S. G., SHELINE, R. K., TAKAHASHI, K., Phys. Lett. 40B (1972) 517.
- [16] SCHRAMM, D. N., FISET, E. O., Ap. J. 180 (1973) 551.
- [17] NILSSON, S. G., private communication (1973).
- [18] ECCLES, S. F., Symposium on Engineering with Nuclear Explosions (Proc. Symp. Las Vegas, 1970), CONF-700101, USAEC Division of Technical Information, Springfield, Mass. (1970) 1269.
- [19] HYDE, E. K., The Nuclear Properties of the Heavy Elements, Vol. III: Fission Phenomena, Prentice-Hall, Englewood Cliffs (1964) 50.

DISCUSSION

C. F. TSANG: Can you give a quantitative indication as to how sensitive your results are to the effective surface symmetry coefficient? What would its value have to be for your Fission Bay to disappear?

W. M. HOWARD: If you are willing to accept a chi-square value for the fit to the ground state masses and fission barrier heights that is 10% larger than its minimum value, then the effective value for the surface symmetry coefficient can vary from 2.6 to 3.3. For the value 2.6, the fission barriers in the Fission Bay can be raised by about 1 MeV. The barriers near the neutron closed shell $N = 184$ remain unaffected. However, one must remember that this increase in the barrier height affects the second barrier peak and therefore one should also take into account mass-asymmetry distortions which could lower that second peak by 1 or 2 MeV.

MODIFIED DEFINITION OF THE SURFACE ENERGY IN THE LIQUID DROP FORMULA*

H.J. KRAPPE**

Lawrence Berkeley Laboratory,
University of California,
Berkeley, Calif.

J.R. NIX

Los Alamos Scientific Laboratory,
University of California,
Los Alamos, N. Mex.,
United States of America

Abstract

MODIFIED DEFINITION OF THE SURFACE ENERGY IN THE LIQUID DROP FORMULA.

When calculated in the liquid drop model, the deformation energy of strongly necked in fission or fusion configurations shows a spuriously strong dependence on the details of the shape in the neck region. This is a consequence of the assumed sharp surface in the liquid drop model. This model can be improved by replacing the surface-energy term by the self-energy of a drop caused by a short-range two-particle interaction. For a Yukawa function the self-energy integral can be evaluated analytically for a few important special configurations, and it can be transformed into a three-dimensional integral for arbitrary axially symmetric shapes. A numerical calculation is therefore only slightly more complicated than the usual treatment of the Coulomb energy.

In addition to the parameters in the conventional liquid drop model, the new definition of the nuclear part of the deformation energy contains a parameter to specify the range of the Yukawa function. Parameters for the new definition are determined from fission barrier heights and interaction barrier heights throughout the periodic table.

The influence of the proposed change in the liquid drop formula on the stiffness of spherical nuclei, the ground state deformation and the existence of shape isomeric states in light nuclei is discussed. Fission barrier heights and saddle point shapes are determined for nuclei along the line of beta stability, and the static interaction potential between heavy ions is calculated.

1. INTRODUCTION

Considerable progress has been made in calculating the nuclear potential energy of deformation as a function of the nuclear shape and the mass and charge numbers by splitting it into a slowly varying function of these quantities and a rapidly fluctuating part. The latter is usually calculated according to a prescription given by Strutinsky [1]. Here we will deal only with the smooth part. It is usually expressed in terms of a Bethe-Weizsäcker type of expansion in powers of $A^{-1/3}$ and I^2 , for example [2-4]

$$E_{LD} = -C_V A + C_S A^{2/3} B_s(\xi_V) + \frac{3}{5} \frac{e^2 Z^2}{r_0 A^{1/3}} \left[B_c(\xi_V) - \frac{5}{6} \pi^2 \frac{d^2}{r_0^2 A^{2/3}} - \frac{0.7636}{Z^{2/3}} \right] \quad (1)$$

* This work was supported by the US Atomic Energy Commission and the German Academic Exchange Service.

** Hahn-Meitner Institut für Kernforschung, Berlin, Fed. Rep. of Germany, visitor at the Lawrence Berkeley Laboratory, Apr. 1972 - Sep. 1973.

where

$$C_v = a_v (1 - \kappa_v I^2)$$

$$C_s = a_s (1 - \kappa_s I^2)$$

and

$$I = (N - Z)/A$$

The quantity d is the surface-thickness parameter in a Fermi function that specifies the charge distribution. The shape-dependent function $B_s(\xi_v)$ is the ratio of the surface area of the deformed nucleus to that of the spherical nucleus, and $B_c(\xi_v)$ is the ratio of the Coulomb energy of the deformed equivalent sharp-surface nucleus to that of the spherical nucleus. Such a leptodermous expansion [2] is valid only if all geometrical dimensions of the drop are large compared to the surface thickness. This condition is not satisfied for strongly necked-in configurations with neck radii smaller than about 2 fm, for example around the scission region in fission or the point of first contact in heavy-ion reactions.

One could overcome this difficulty by going back to a constrained self-consistent microscopic calculation for such configurations. But that would be a rather involved program from a numerical point of view. Therefore, it is desirable to construct a generalization of the liquid-drop formula - still on a purely phenomenological basis - which satisfies the following conditions:

(1) For spherical configurations it should give practically the same result as the old liquid-drop formula (except for very light nuclei).

(2) In contrast to the usual surface energy it should not be sensitive to high-multipole wiggles on the surface of the drop. The liquid-drop formula yields a spurious and undesirable sensitivity of calculated fission barriers on unphysical fine details of the shape in the neck region.

(3) Between two separated fragments there should be an attractive nuclear interaction energy besides the Coulomb repulsion. The range of that force should extend beyond the equivalent sharp radius by roughly the range of the nucleon-nucleon interaction.

(4) It should be possible to calculate the new expression for general shapes with reasonable computational effort.

We will show that one can satisfy these conditions by replacing the surface energy term $C_s A^{2/3} B_s(\xi_v)$ by

$$E = - \frac{V_0}{4\pi a^3} \int d^3r d^3r' \frac{e^{-\frac{|\vec{r}-\vec{r}'|}{a}}}{\frac{|\vec{r}-\vec{r}'|}{a}} \quad (2)$$

with the two phenomenological parameters V_0 and a instead of the single liquid-drop parameter C_s and allowing for a renormalization of the volume-energy coefficient C_v . The six-fold integral is to be taken over the volume

of the equivalent sharp-surface nucleus whose shape can be parametrized by any suitable set of deformation parameters; this volume is specified by the nuclear-radius parameter r_0 .

2. SPECIAL CONFIGURATIONS

We will discuss the results of this replacement for a sequence of shapes of increasing complexity and show that these four conditions are fulfilled.

2.1. Spherical shape

A straightforward calculation of the integral (2) in spherical coordinates yields

$$E = V_0 \left[-\frac{4\pi}{3} R_0^3 + 2\pi a R_0^2 - 2\pi a^3 + 2\pi a (R_0 + a)^2 e^{-2R_0/a} \right]$$

where $R_0 = r_0 A^{1/3}$ is the equivalent sharp radius. For $a/R_0 \ll 1$ the last two terms are negligible. The second term yields the surface energy if the interaction strength V_0 is related to the semi-empirical surface-energy constant C_s by

$$C_s = a_s (1 - \kappa_s I^2) = 2\pi V_0 a r_0^2$$

The first term gives a contribution to the volume energy and has to be compensated for by a renormalization of C_v . This way we meet the first of the four requirements on E . The limit $a \rightarrow 0$ yields the usual liquid-drop model.

2.2. Bubble nucleus

For a bubble nucleus with inner radius R_1 and outer radius R_2 one gets from (2)

$$\begin{aligned} E = & - \left(\frac{a}{r_0} \right)^2 C_s \left[\frac{2}{3} \left(\frac{R_2}{a} \right)^3 - \frac{2}{3} \left(\frac{R_1}{a} \right)^3 - \left(\frac{R_2}{a} \right)^2 - \left(\frac{R_1}{a} \right)^2 + 2 - \left(\frac{R_1}{a} + 1 \right)^2 \exp(-2R_1/a) \right. \\ & + 2 \left(\frac{R_1}{a} - 1 \right) \left(\frac{R_2}{a} + 1 \right) \exp \left(-\frac{R_2 - R_1}{a} \right) + 2 \left(\frac{R_1}{a} + 1 \right) \left(\frac{R_2}{a} + 1 \right) \exp \left(-\frac{R_1 + R_2}{a} \right) \\ & \left. - \left(\frac{R_2}{a} + 1 \right)^2 \exp(-2R_2/a) \right] \end{aligned}$$

Recently the bubble-nucleus model has been discussed for $R_1 \approx a$ [5]. In this case the application of the usual liquid-drop formula (1) is doubtful and should be replaced by this formula.

2.3. Small distortions about a spherical shape

If the shape is parametrized by the normal coordinates for harmonic vibrations around the spherical shape,

$$R = R_0 \left(1 + \sum_{\substack{\ell \geq 2 \\ m}} \beta_{\ell m} Y_{\ell m}(\Omega) + \beta_{\text{corr}} \right) \quad (3)$$

where

$$\beta_{\text{corr}} = -\frac{1}{4\pi} \sum_{\substack{\ell \geq 2 \\ m}} |\beta_{\ell m}|^2$$

the deformation energy to second order in $\beta_{\ell m}$ is given by

$$E(\beta_{\ell m}) - E(0) = \frac{C_s}{4\pi} A^{2/3} \sum_{\substack{\ell \geq 2 \\ m}} |\beta_{\ell m}|^2 c_\ell \quad (4)$$

where

$$c_\ell = \left(\frac{R_0}{a} + 1 \right) \left[\frac{R_0}{a} - 1 + \left(\frac{R_0}{a} + 1 \right) \exp(-2R_0/a) \right] - 2 \left(\frac{R_0}{a} \right)^3 I_{\ell+1/2} \left(\frac{R_0}{a} \right) K_{\ell+1/2} \left(\frac{R_0}{a} \right)$$

Here $I_{\ell+1/2}$ and $K_{\ell+1/2}$ are modified Bessel and Hankel functions, respectively [6]

The simplest way to derive this formula is to use the expansion

$$\begin{aligned} \int d\Omega \int_0^{R(\Omega)} r^2 f(|\vec{r}-\vec{r}'|) dr &= \int d\Omega \left[\int_0^{R_0} r^2 f(|\vec{r}-\vec{r}'|) dr \right. \\ &\quad + R_0^3 f(|\vec{r}-\vec{r}'|)_{r=R_0} \left(\sum_{\ell, m} \beta_{\ell m} Y_{\ell m}(\Omega) + \beta_{\text{corr}} \right) \\ &\quad \left. + \frac{R_0^2}{2} \frac{\partial}{\partial r} r^2 f(|\vec{r}-\vec{r}'|)_{r=R_0} \left(\sum_{\ell, m} \beta_{\ell m} Y_{\ell m}(\Omega) \right)^2 \right] \end{aligned} \quad (5)$$

for the integration with respect to r and a similar one for the integration with respect to r' . Integrals of the type

$$\int_{-1}^1 dx P_\ell(x) \frac{\exp\left(-\frac{1}{a} \sqrt{r_1^2 + r_2^2 - 2r_1 r_2 x}\right)}{\frac{1}{a} \sqrt{r_1^2 + r_2^2 - 2r_1 r_2 x}}$$

are evaluated by use of the addition theorem for modified Bessel functions [6]

$$\frac{\exp\left(-\frac{1}{a}\sqrt{r_1^2+r_2^2-2r_1r_2x}\right)}{\frac{1}{a}\sqrt{r_1^2+r_2^2-2r_1r_2x}} = \sum_{\ell=0}^{\infty} (2\ell+1) P_{\ell}(x) \frac{a}{\sqrt{r_1r_2}} I_{\ell+1/2}\left(\frac{r_1}{a}\right) K_{\ell+1/2}\left(\frac{r_2}{a}\right) \quad (6)$$

An expansion of Eq. (4) in powers of $A^{-1/3}$ yields for the stiffness constant for multipole vibrations of order ℓ the result

$$\begin{aligned} \frac{c_s}{4\pi} A^{2/3} c_{\ell} &= \frac{c_s}{8\pi} \left\{ [\ell(\ell+1)-2] A^{2/3} - \frac{3}{4} (\ell-1)\ell(\ell+1)(\ell+2) \left(\frac{a}{r_0}\right)^2 \right\} \\ &+ O\left(\frac{a^4}{r_0^4} A^{-2/3}\right) + O[\exp(-2R_0/a)] \end{aligned}$$

The first term is the well-known contribution of the surface energy in the liquid-drop formula. There is no term proportional to $A^{1/3}$, which means physically that the contribution to the energy from the curvature of the nuclear surface is identically zero. This $A^{1/3}$ term is absent also for more general shapes [7], provided that the smallest curvature radius is large compared to the range a . The term of order A^0 reduces the stiffness for finite values of the range a ; this reduction becomes relatively more important for light nuclei. The last two terms are negligible for low multipole orders ℓ , provided that the nuclear radius R_0 is large compared to a . For higher multipoles, the expression (4) for the stiffness constant becomes independent of multipole order, because for large v

$$I_v(z) K_v(z) \longrightarrow \frac{1}{2v}$$

This is to be contrasted to the quadratic increase with multipole order for the stiffness constant calculated with the usual liquid-drop model. It shows the insensitivity of the modified liquid-drop formula to unphysical fine wiggles of the surface. Therefore also the second of the four requirements on E is satisfied by (2).

The fissility parameter x is defined as the ratio of the Coulomb energy $E_c^{(0)}$ of a spherical sharp-surface drop to twice the spherical surface energy $E_s^{(0)} = c_s \cdot A^{2/3}$. The value of the critical fissility x_{crit} for which the sphere loses stability against fission corresponds to the point where the restoring force for P_2 vibrations vanishes. Addition of the Coulomb contribution to the deformation energy (4) yields for $\ell=2, m=0$ the result

$$\delta E = \frac{E_s^{(0)}}{4\pi} \beta_{20}^2 \left[2 - 2x - 9 \frac{a^2}{R_0^2} + O(e^{-2R_0/a}) \right]$$

This leads to

$$x_{\text{crit}} = 1 - \frac{9}{2} \left(\frac{a}{R_0}\right)^2 + O(e^{-2R_0/a}) \quad (7)$$

instead of the usual value 1.

2.4. Two non-overlapping spheres

The nuclear interaction energy of two non-overlapping spheres of radii R_1 and R_2 and center-of-mass distance $D \geq R_1 + R_2$ follows from straightforward integration of (2):

$$E_{\text{int}} = -4 \left(\frac{a}{r_0} \right)^2 C_s \left(\frac{R_1}{a} \cosh \frac{R_1}{a} - \sinh \frac{R_1}{a} \right) \left(\frac{R_2}{a} \cosh \frac{R_2}{a} - \sinh \frac{R_2}{a} \right) \frac{e^{-D/a}}{D/a} \quad (8)$$

For R_1/a and $R_2/a \gg 1$ this reduces to

$$E_{\text{int}} = -4 \pi \gamma \frac{R_1 R_2}{R_1 + R_2} a e^{-l/a} + O\left(\frac{a}{R_1}, \frac{a}{R_2}, \frac{1}{R_1 + R_2}\right)$$

where l is the distance between the two sharp surfaces and $\gamma = \frac{C_s}{4\pi r_0^2}$ is the surface tension.

This formula is a special case of a general theorem [8] which states that to order $\frac{a}{R}$ the interaction energy between two arbitrarily shaped objects interacting via a short range force (short compared to all curvature radii) can always be expressed in the form

$$E_{\text{int}}(l) = \frac{2\pi}{\sqrt{D_{xx} D_{yy}}} \int_1^\infty e(\xi) d\xi + O\left(\frac{a}{R}\right)$$

The first factor is purely geometrical and in the case of two spheres is equal to $2\pi R_1 R_2 / (R_1 + R_2)$. The quantity $e(\xi)$ is the interaction energy per unit area of two parallel infinite surfaces at distance ξ . Obviously $e(0) = -2\gamma$. A Thomas-Fermi calculation [8] of the function $e(\xi)$ yields a result that can be approximated roughly by an exponential function of range $a = 1.4$ fm, that is,

$$e(\xi) \approx -2\gamma e^{-\xi/(1.4 \text{ fm})}$$

2.5. Non-overlapping spherical nucleus and slightly deformed nucleus

The generalization of Eq. (8) to the interaction energy between a spherical nucleus with radius R_1 and a deformed nucleus with radius

$R = R_2 \left[1 + \beta_{\text{corr}} + \sum_{\ell, m} \beta_{\ell m} Y_{\ell m}(\Omega) \right]$ is given to second order in $\beta_{\ell m}$ by

$$E_{\text{int}} - E_{\text{int}}^{\text{sph}} = -2C_s \left(\frac{a}{r_0} \right)^2 \left(\frac{R_1}{a} \cosh \frac{R_1}{a} - \sinh \frac{R_1}{a} \right) \left(\frac{R_2}{a} \right)^3 \times \left[\sum_{\ell, m} \sqrt{\frac{4\pi}{2\ell+1}} Y_{\ell m}(\theta, \psi) \left(\beta_{\ell m} A_\ell + \sum_{\ell', \ell'', m'} \beta_{\ell' m'} \beta_{\ell'' m-m'} C_{\ell, \ell', \ell'', m, m'} \right) \right] \quad (9)$$

Here θ and ψ are the angular coordinates of the vector joining the centers of mass of the two nuclei in a coordinate system whose origin is at the center of the deformed nucleus. The deformation parameters β_{lm} refer to the same system of reference. The other quantities are given by

$$A_{\ell} = \sqrt{\frac{2\ell+1}{\pi}} \frac{a}{\sqrt{R_2 D}} I_{\ell+1/2}\left(\frac{R_2}{a}\right) K_{\ell+1/2}\left(\frac{D}{a}\right)$$

$$C_{\ell, \ell', \ell'', m, m'} = \left[\frac{(2\ell'+1)(2\ell''+1)}{4\pi(2\ell+1)} \right]^{1/2} (\ell' m' \ell'' m - m' | \ell m) (\ell' 0 \ell'' 0 | \ell 0) \frac{1}{2R_2} \frac{\partial}{\partial R_2} (R_2^2 A_{\ell})$$

$$\beta_{00} = \sqrt{4\pi} \beta_{\text{corr}}$$

and $E_{\text{int}}^{\text{sph}}$ is the expression (8) for the spherical case. This formula is obtained easily by use of the expansions (5) and (6).

3. DETERMINATION OF PARAMETERS

The shape-dependent terms of the nuclear macroscopic energy calculated according to Eq. (1) contain a total of four parameters: the equivalent sharp-surface nuclear-radius parameter r_0 , the range a of the Yukawa function, the surface-energy constant a_s for equal numbers of neutrons and protons, and the surface-asymmetry constant κ_s . The equivalent sharp-surface nuclear-radius parameter r_0 is known accurately from analyses of electron-scattering data; its value is therefore not adjusted but is taken instead to be 1.16 fm from these studies [9].

Interaction-barrier heights depend mainly on r_0 and the range a and more weakly on a_s and κ_s . Therefore, once r_0 is fixed, the range a is determined by adjusting to experimental interaction-barrier heights [10-25]. The resulting value of 1.4 fm is the same as the range determined from the above-mentioned Thomas-Fermi calculations [8].

Once both r_0 and a are known, the final two parameters a_s and κ_s are determined by adjusting to experimental fission-barrier heights [26-28]. Because these two parameters are highly correlated, their individual values are determined poorly. For example, the value of 4.0 determined for κ_s is uncertain by at least ± 1.0 .

The resulting value of 24.7 MeV for a_s is significantly higher than the value of about 18 MeV obtained in the usual liquid-drop model by adjusting to fission barrier heights [2,3]. It is on the other hand only slightly larger than values obtained by adjusting to nuclear ground-state masses alone [4]. The difference between our value and the values of Refs. [2,3] arises because the finite range of the nuclear force reduces the effective stiffness with respect to deformations. It is therefore possible that the surface-energy constant is indeed larger than previously believed.

To summarize, the preliminary values chosen for the four parameters are

$$\left. \begin{aligned} r_0 &= 1.16 \text{ fm} \\ a &= 1.4 \text{ fm} \\ a_s &= 24.7 \text{ MeV} \\ \kappa_s &= 4.0 \end{aligned} \right\} \quad (10)$$

No attempt has been made so far to redetermine the parameters in the shape-independent terms of Eq. (1) after replacing the surface term by the integral (2).

4. INTERACTION BARRIERS

The combined action of the Coulomb and the nuclear forces usually yields a maximum in the interaction-energy as a function of the distance between two ions. For symmetric configurations this interaction barrier disappears for a critical fissility of the combined system of $x = 6/5$, at which point the

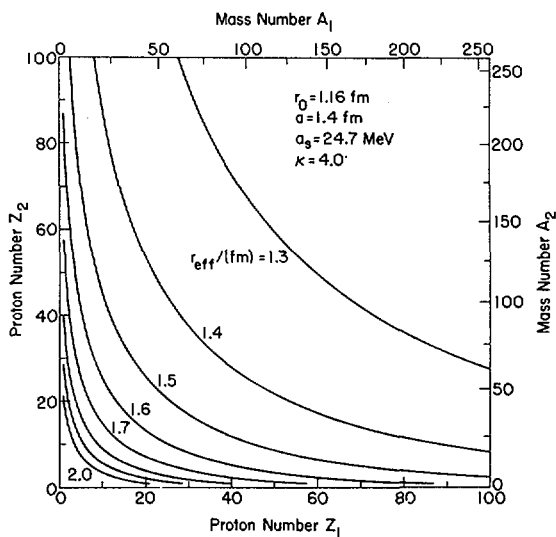


FIG. 1. Contour diagram of the effective nuclear radius parameter r_{eff} as a function of the charge numbers of the colliding ions for nuclei along the valley of beta stability (defined by Green's formula $N-Z = 0.4 A^2/(A+200)$; see Ref. [29]).

Coulomb repulsion can no longer be counter-balanced by the nuclear force even for two touching spheres. Below this critical value of x the height of the barrier is often represented in the form

$$E_{\text{int}}^{\text{max}} = \frac{Z_1 Z_2 e^2}{r_{\text{eff}} (A_1^{1/3} + A_2^{1/3})} \quad (11)$$

Figure 1 shows r_{eff} as a function of the charges Z_1 and Z_2 of the two colliding ions for nuclei along Green's approximation to the line of beta-stability [29]. Equation (11) can be rewritten in the form

$$E_{\text{int}}^{\text{max}} = \frac{Z_1 Z_2 e^2}{R_1 + R_2 + a + d} \quad (12)$$

where d is the distance between the two nuclear surfaces at which the total interaction energy has its maximum. The value of d is determined easily by iteration from the equations

$$\left. \frac{d}{dD} \left(\frac{e^2 Z_1 Z_2}{D} + E_{\text{int}}(D) \right) \right| = 0$$

$$D = r_0 (A_1^{1/3} + A_2^{1/3}) + d$$

where $E_{\text{int}}(D)$ is inserted from Eq. (8). A contour plot of $d(Z_1, Z_2)$ for nuclei along the line of beta-stability is given in Fig. 2.

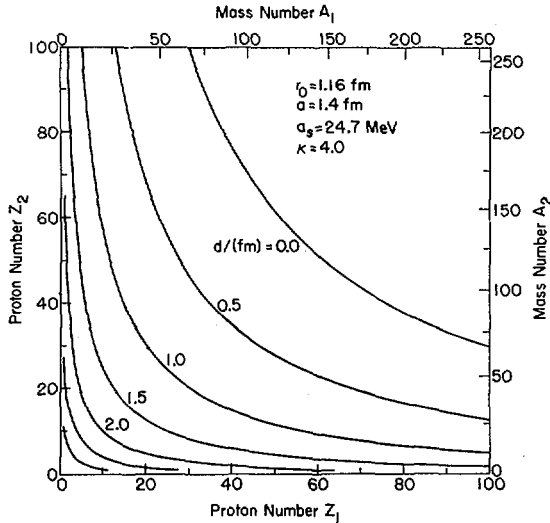


FIG.2. Contour diagram of the distance d between the equivalent sharp surfaces of two spherical nuclei of charges Z_1 and Z_2 at the peak of the interaction potential. The results are for nuclei along the valley of beta stability. Beyond the line defined by $d = 0$ the interaction barrier has no maximum.

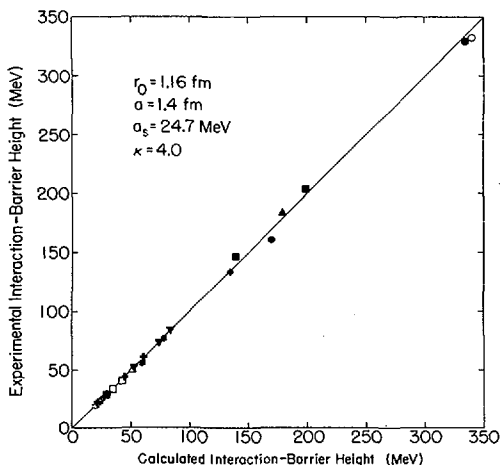


FIG. 3. Comparison of experimental and calculated interaction-barrier heights. The solid points are experimental values derived from excitation functions (solid circle [10], solid square [11], solid diamond [12], solid upward-pointing triangle [13, 14], solid downward-pointing triangle [13, 15], solid hexagon [16], solid plus sign [17], and solid star [18]); the open points are experimental values derived from elastic scattering data (open circle [19], open square [20], open diamond [20, 21], open upward-pointing triangle [20, 22], open downward-pointing triangle [20, 23], open hexagon [20, 24], open plus sign [24], and open star [25]).

In Fig. 3 experimental Coulomb barriers from reaction cross-section measurements [10-18] and from elastic scattering experiments are compared with the predictions of this theory. The deviations from the calculated values are smaller than $\pm 5.4\%$ or 9 MeV in absolute units. The data used in Fig. 3 include the deformed nuclei ^{238}U [13-15, 19], ^{232}Th [10], and ^{164}Dy [12]. For these deformed nuclei Eq. (9) is used with $\beta_{20} = 0.277$, 0.248, and 0.319, respectively [30]. The orientation angles θ and ψ are taken equal to zero, which gives the minimum interaction barrier. We have not taken into account any shell effects on interaction barriers because the influence of one potential well on the level density around the Fermi surface in the other well is supposed to be very small at the point of geometrical contact or even farther out.

The distance between the two centers of mass is the only degree of freedom that we have considered in calculating interaction barriers. We are thus disregarding the coupling of the relative motion to the neck-formation or any intrinsic degrees of freedom of the two ions. Elastic-scattering data on the other hand are usually analyzed in terms of optical potentials. Only the tail regions of these potentials are determined unambiguously, which often excludes the maximum. Moreover the optical potential reflects the coupling of intrinsic degrees of freedom to the relative motion in an average way, whereas these effects are completely neglected in our model.

Information on interaction barriers is also extracted from fusion reaction cross-sections. They are mostly analyzed in terms of transmission coefficients calculated by assuming transmission of a real parabolic potential barrier. This amounts to assuming an ingoing-wave boundary condition inside the potential barrier. It has been shown [31] that optical-model potentials

are not necessarily identical with potentials to be used with an ingoing-wave boundary condition, especially when the imaginary part is neglected or not determined in the latter method.

To overcome the problems connected with the ambiguity in potential fits it is advisable to determine the critical angular momentum $\Lambda(E)$ as a function of energy from a phase-shift analysis of elastic or reaction scattering data [32]. Using the relation

$$\Lambda(\Lambda+1) = (kR_r)^2 \left(1 - \frac{V(R_r)}{E} \right)$$

for several energies, one can extract the pair of values $V(R_r)$ and R_r , i.e. the interaction potential at the reaction radius R_r , independent of where the maximum of that potential might be. Of course, the assumption has been made that the interaction can be described by an energy-independent, local potential and that the process is purely diffractive.

5. GENERAL SHAPES

The integral (2) can be reduced to the double surface integral

$$E = \frac{V_0 a}{4\pi} \iint d\vec{S} \cdot (\vec{r} - \vec{r}') d\vec{S}' \cdot (\vec{r} - \vec{r}') \left[\frac{|\vec{r} - \vec{r}'|}{a} + \left(2 + \frac{|\vec{r} - \vec{r}'|}{a} \right) e^{-\frac{|\vec{r} - \vec{r}'|}{a}} - 2 \right] \times |\vec{r} - \vec{r}'|^{-4} \quad (13)$$

by using the identity

$$\vec{\nabla}_{\vec{r}} \cdot (\vec{r} - \vec{r}') \vec{\nabla}_{\vec{r}'} \cdot (\vec{r} - \vec{r}') \left[\frac{|\vec{r} - \vec{r}'|}{a} + \left(2 + \frac{|\vec{r} - \vec{r}'|}{a} \right) e^{-\frac{|\vec{r} - \vec{r}'|}{a}} - 2 \right] \left(\frac{|\vec{r} - \vec{r}'|}{a} \right)^{-4} \\ = - \frac{e^{-\frac{|\vec{r} - \vec{r}'|}{a}}}{\frac{|\vec{r} - \vec{r}'|}{a}}$$

and applying Gauss's theorem with respect to \vec{r} and \vec{r}' . For systems with cylindrical symmetry (13) reduces to the three-dimensional integral in cylindrical coordinates

$$E = - \frac{V_0}{2a^3} \int dz \int dz' \int_0^{2\pi} d\psi R(z) [R(z) - R(z') \cos \psi - \frac{dR(z)}{dz}(z-z')] R(z') \\ \times [R(z') - R(z) \cos \psi - \frac{dR(z')}{dz'}(z'-z)] \frac{[d + (2+d)e^{-d} - 2]}{d^4} \quad (14)$$

where

$$d = \frac{1}{a} [R^2(z) + R^2(z') - 2R(z) R(z') \cos \psi + z^2 + z'^2 - 2zz']^{1/2}$$

The function $R(z)$ gives the shape in cylindrical coordinates. The z integrations are taken between the zeros of $R(z)$. The three-fold integral (14) in general must be evaluated numerically, but this is only slightly more complicated than the evaluation of the integral for the Coulomb energy.

6. FISSION BARRIERS

Figure 4 shows the maximum and minimum radii of saddle-point shapes as functions of the fissility parameter x for various values of the range a . The remaining constants are held fixed at the values determined in Ref. [3] on the basis of the liquid-drop model, that is, for zero range. The saddle points are calculated by use of the methods of Ref. [33], with the surface energy replaced by Eq. (14). The class of shapes investigated is that of two spheroids connected smoothly by a quadratic surface of revolution [33]. There is a clear tendency to more compact saddle-point shapes with increasing a for fixed values of the other constants. The shift of x_{crit} to values smaller than 1 as given by (7) to second order in $\frac{a}{R_0}$ is also clearly seen. The critical Businaro-Gallone point (where stability against mass asymmetry is lost) [34] first moves to slightly larger values of the fissility x with

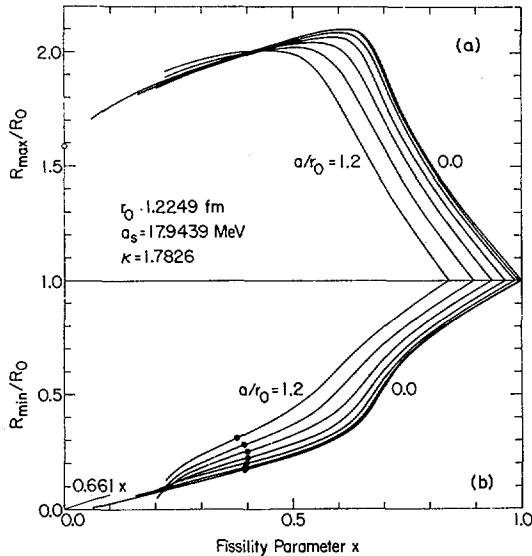


FIG. 4. Saddle point shapes as functions of the fissility parameter $x = \frac{E_C^{(0)}}{[2E_S^{(0)}]}$ for liquid-drop-model parameters from Ref. [3] and $a/r_0 = 0.0(0.2)1.2$. (a) gives the largest radius of the saddle point shape in units of the radius of the sphere with equal volume; (b) gives the smallest radius. The solid points give the location of the Businaro-Gallone point.

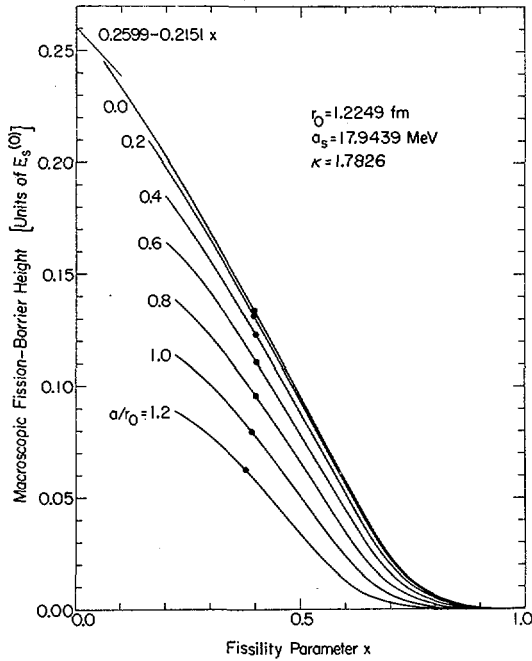


FIG. 5. Fission-barrier height in our model as a function of the fissility parameter x and the range a/r_0 for liquid-drop-model parameters from Ref.[3]. The solid points mark the Businaro-Gallone point.

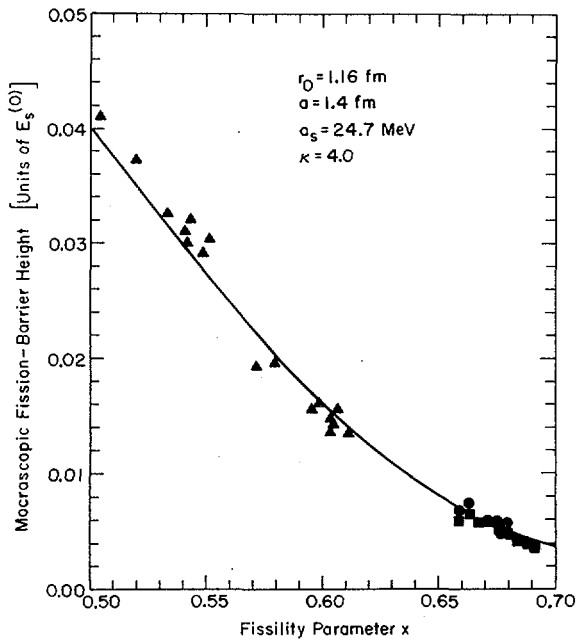


FIG. 6. Comparison of theoretical fission-barrier heights (solid line) calculated with the parameters (10) and experimental barrier heights corrected for single particle effects. The circles [26] and squares [27] are reduced fission-barrier heights for actinide nuclei, and the triangles [28] are shell-corrected fission barrier heights for lighter nuclei.

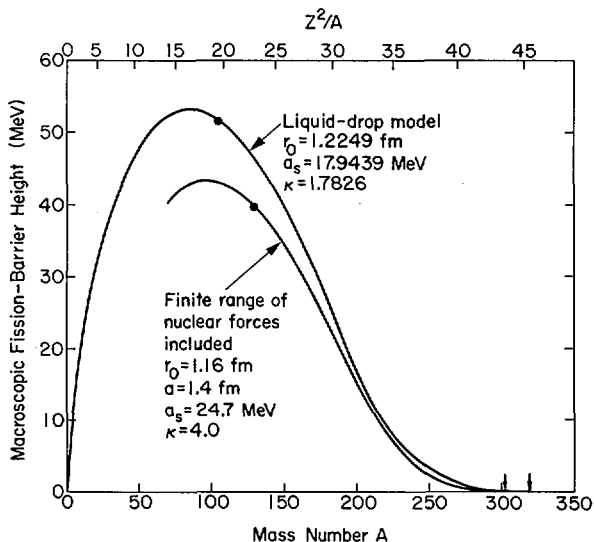


FIG. 7. Comparison of macroscopic barrier heights calculated in our model with the parameters (10) and in the liquid drop model with parameters from Ref. [3] for nuclei along the line of beta stability. The solid points indicate the Businaro-Gallone point. The arrows show the mass numbers at which the system would lose stability against fission if shell corrections were not present.

increasing range a . It reaches a maximum at $a/r_0 \approx 0.7$ and then it moves back to smaller values of x . Figure 5 gives the fission-barrier height as a function of the fissility parameter x for various values of the range a , again for fixed values of the other constants. The barrier heights are seen to decrease drastically with increasing range.

Figure 6 compares the calculated macroscopic contribution to the fission-barrier height with experimental values. The curve is calculated with the parameters of Eq. (10), and the experimental data represent both reduced fission-barrier heights for actinide nuclei [26,27] and shell-corrected fission-barrier heights for lighter nuclei [28]. In the region of fissility parameter x between 0.50 and 0.55 the experimental values are systematically somewhat higher than the calculated curve. It would be very desirable to have experimental data for still lighter nuclei with fissility parameter smaller than 0.5.

Figure 7 shows the difference between the predicted barrier height in the liquid-drop model with the parameter set from Ref. [3] and in our model with the parameters (10) along the line of beta-stability. The finite range of the nuclear force lowers the fission barriers of nuclei near silver by about 10 MeV relative to those calculated with the liquid-drop model and shifts the critical Businaro-Gallone point to $Z^2/A = 23$, in approximate agreement with recent experimental evidence [35].

7. POTENTIAL-ENERGY SURFACES OF LIGHT NUCLEI

The general trend to decrease the stiffness of nuclei with increasing range of the interaction Eq. (10) shows up especially for light nuclei where the

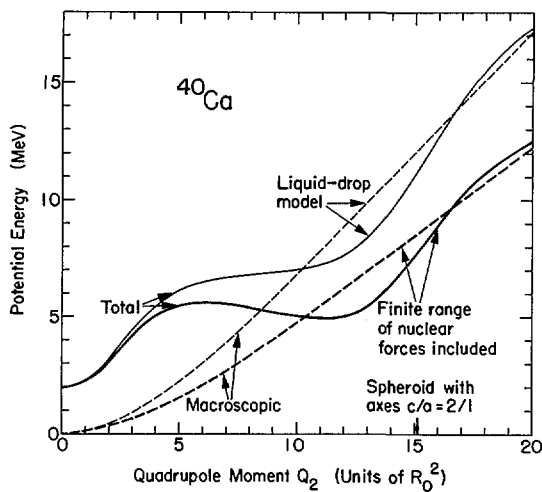


FIG. 8. Deformation energy of ^{40}Ca . The dashed lines show the macroscopic contribution to the deformation energy in our model and in the conventional liquid-drop model. The solid curves give the total deformation energy including single particle corrections; these corrections are calculated by use of the methods and parameters of Ref. [36].

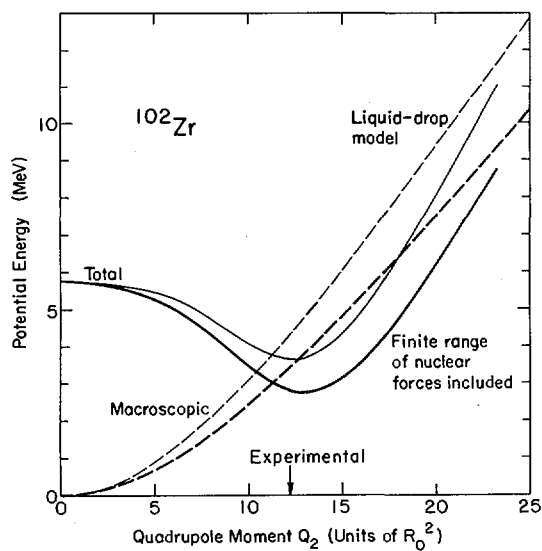


FIG. 9. Analogous diagram to Fig. 8 for ^{102}Zr ; the single particle corrections are calculated by use of the methods and parameters of Ref. [39].

radius is no longer an order of magnitude larger than a . A calculation of the deformation energy of ^{40}Ca as a function of the quadrupole deformation shows that the shell correction is more effective in producing a second minimum with our expression for the macroscopic part of the energy than with the conventional liquid-drop model, as seen in Fig. 8. This provides a natural interpretation of the rotational states observed in this nucleus and certain other light nuclei [37]. A similar study for ^{102}Zr shows that its calculated ground-state quadrupole moment is shifted towards slightly larger values by the finite-range model. Within the experimental uncertainty this agrees with the most recent measurement of the quadrupole moment [38]. This result is shown in Fig. 9.

8. SUMMARY

We have redefined the surface term in the liquid-drop formula so that it can be used for configurations in which the size of a curvature radius of the nuclear surface becomes comparable to the surface thickness. We have shown that the new version of the liquid-drop formula yields a weaker dependence of the deformation energy on surface wiggles of high multipole order than the old model and generally results in a smaller nuclear stiffness. As a consequence the shell correction produces a larger ground-state deformation especially of some light nuclei, and there seems to appear a second minimum in the deformation-energy curve of ^{40}Ca .

Saddle-point shapes have been calculated, and they are less necked-in than in the usual liquid-drop model. The dependence of the Businaro-Gallone point on the range parameter of our model has been studied. We have derived an explicit expression for the nuclear interaction energy between two non-overlapping ions and have calculated interaction-barrier heights. For very heavy systems the maximum in the interaction energy transforms into a point of inflection and the interaction energy increases monotonically with decreasing distance between the ions.

We determined the parameters of our model so that the reduced fission barrier heights for fissility values larger than 0.5 and experimental interaction-barrier heights are reproduced on the average. The fission barriers for nuclei with a smaller fissility parameter are predicted to be lower than they are in the old version of the liquid-drop formula with parameters from Ref. [3].

ACKNOWLEDGMENTS

We are indebted to W. J. Swiatecki and W. D. Myers for suggestions and discussions throughout this work and to S. E. Koonin for writing the computer program to evaluate the three-dimensional integral for the nuclear macroscopic energy. We also thank J. Randrup for making his calculations available prior to publication.

REFERENCES

- [1] BRACK, M., DAMGAARD, J., JENSEN, A.S., PAULI, H.C., STRUTINSKY, V.M., WONG, C.Y., *Rev. Mod. Phys.* **44** (1972) 320.
- [2] MYERS, W.D., SWIATECKI, W.J., *Nucl. Phys.* **81** (1966) 1.
- [3] MYERS, W.D., SWIATECKI, W.J., *Ark. Fys.* **36** (1967) 343.
- [4] SEEGER, P.A., *Atomic masses and fundamental constants* (Proc. Fourth Conf. Teddington, 1971), Plenum, London (1972) 255.

- [5] WONG, C.Y., Phys. Letters 41B (1972) 451.
- [6] ABRAMOWITZ, M., STEGUN, I.A., Eds., Handbook of mathematical functions, National Bureau of Standards, Washington, D. C. (1964).
- [7] TSANG, C.F., Berkeley Report, UCRL-18899 (1969).
- [8] RANDRUP, J., SWIATECKI, W.J., to be published.
- [9] MYERS, W.D., Berkeley Preprint, LBL-1259 (1972).
- [10] BIMBOT, R., GAUVIN, H., LE BEYEC, Y., LEFORT, M., PORILE, N.T., TAMAIN, B., Nucl. Phys. A189 (1972) 539.
- [11] GAUVIN, H., LE BEYEC, Y., LEFORT, M., DEPRUN, C., Phys. Rev. Letters 28 (1972) 697.
- [12] LE BEYEC, Y., LEFORT, M., VIGNY, A., Phys. Rev. C 3 (1971) 1268.
- [13] WONG, C.Y., Oak Ridge Preprint (1972).
- [14] SIKKELAND, T., Ark. Fys. 36 (1967) 539.
- [15] VIOLA, V.E., SIKKELAND, T., Phys. Rev. 128 (1962) 767.
- [16] BIMBOT, R., GARDES, D., RIVET, M.F., Phys. Rev. C 4 (1971) 2180.
- [17] BLANN, M., Bull. Am. Phys. Soc. 18 (1973) 31; slightly revised final values are given in GUTBROD, H.H., WINN, W.G., BLANN, M., Rochester Preprint, C00-3494-8 (1972).
- [18] LE BEYEC, Y., LEFORT, M., SARDA, M., Nucl. Phys. A192 (1972) 405.
- [19] LEFORT, M., NGÔ, C., PETER, J., TAMAIN, B., Nucl. Phys. A197 (1972) 485.
- [20] OBST, A.W., McSHAN, D.L., DAVIS, R.H., Phys. Rev. C 6 (1972) 1814.
- [21] ORLOFF, J., DAEHNICK, W.W., Phys. Rev. C 3 (1971) 430.
- [22] ROBERTSON, B.C., SAMPLE, J.T., GOOSMAN, D.R., NAGATANI, K., JONES, K.W., Phys. Rev. C 4 (1971) 2176.
- [23] FLETCHER, N.R., WEST, L., KEMPER, K.W., Bull. Am. Phys. Soc. 16 (1971) 1149.
- [24] BERTIN, M.C., TABOR, S.L., WATSON, B.A., EISEN, Y., GOLDRING, G., Nucl. Phys. A167 (1971) 216.
- [25] GOLDRING, G., SAMUEL, M., WATSON, B.A., BERTIN, M.C., TABOR, S.L., Phys. Letters 32B (1970) 465.
- [26] PAULI, H.C., LEDERGERBER, T., Nucl. Phys. A175 (1971) 545.
- [27] RANDRUP, J., TSANG, C. F., MÖLLER, P., NILSSON, S. G., LARSSON, S. E., Berkeley Preprint (1973).
- [28] MORETTO, L.G., THOMPSON, S.G., ROUTTI, J., GATTI, R.C., Phys. Letters 38B (1972) 471.
- [29] GREEN, A.E.S., Nuclear Physics, McGraw-Hill, New York (1955) 185, 250.
- [30] LÖBNER, K.E.G., VETTER, M., HONIG, V., Nucl. Data Tab. A7 (1970) 495.
- [31] RAWITSCHER, G.H., Nucl. Phys. 85 (1966) 337.
- [32] McINTYRE, J.A., BAKER, S.D., WANG, K.H., Phys. Rev. 125 (1962) 584.
- [33] NIX, J.R., Nucl. Phys. A130 (1969) 241.
- [34] BUSINARO, U.L., GALLONE, S., Nuovo Cim. 5 (1957) 315.
- [35] METHASIRI, T., JOHANSSON, S.A.E., Nucl. Phys. A167 (1971) 97.
- [36] MÖLLER, P., NIX, J.R., Paper IAEA-SM-174/202, these Proceedings, Vol.1.
- [37] SETH, K.K., SAHA, A., GREENWOOD, L., Northwestern University Preprint (1973).
- [38] JARED, R.C., NIFENECKER, H.A., THOMPSON, S.G., Paper IAEA-SM-174/62, these Proceedings, Vol.2.
- [39] BOLSTERLI, M., FISET, E.O., NIX, J.R., NORTON, J.L., Phys. Rev. C 5 (1972) 1050.

DISCUSSION

P. QUENTIN: You commence with the direct part of the interaction energy. Have you made an estimate of the exchange part of this interaction energy in some approximation (e. g. of the Slater type), especially for the case where there are two nascent fragments?

H. J. KRAPPE: I would like to stress that the use of a Yukawa potential in the six-dimensional integral does not imply that it represents the total

potential energy of the nucleus calculated microscopically with an effective two-body interaction. The integral has rather to account for the finite range of the nuclear forces as well as for the surface diffuseness on a purely phenomenological basis.

S. BJÖRNHOLM: Have you tried to fit ground state masses with your approach?

H. J. KRAPPE: So far only deformation energies have been investigated. Therefore we have not yet tried to fit ground state masses. As the six-dimensional integral contributes to the volume-energy term, a considerable renormalization of the volume-energy constant is to be expected when the surface-energy term is replaced by the integral.

R. W. HASSE: Unfortunately, you did not show a slide with the potential energy (Coulomb plus Krappe surface energies) plotted versus the distance between the surfaces of the two nuclei, say ℓ . Since the long-range Coulomb energy behaves like $1/(R_1 + R_2 + \ell)$ and the short-range nuclear interaction energy like $-e^{-\ell/a}$, where a is some constant and R_1, R_2 are the radii of the nuclei, the potential energy at scission should exhibit a minimum or, at any rate, should be very flat. Is this behaviour of the potential energy supported by your results as it is by the results of microscopic calculations, e. g. with a molecular potential¹ or with the two-nucleus shell model²?

H. J. KRAPPE: Except for very heavy nuclei, the interaction energy between two ions reaches a maximum at a distance d between the two sharp surfaces. For ℓ values smaller than d the interaction potential decreases with decreasing distance between the nuclei, until the two nuclei touch. The interaction potential is still decreasing at this point. Where it finally reaches its minimum for centre-of-mass distances $D < R_1 + R_2$ depends on detailed assumptions about the compressibility and the coupling to other degrees of freedom, as for instance the "neck-healing". This is beyond the scope of the present investigation.

¹ Nörenberg, W., Z. Phys. 197 (1966) 246.

² Hasse, R. W., Abstract IAEA-SM-174/1, these Proceedings, Vol. 2.

FISSION BARRIERS FOR HEAVY ELEMENTS WITH QUADRUPOLE, HEXADECAPOLE AND AXIALLY ASYMMETRIC DISTORTIONS TAKEN INTO ACCOUNT SIMULTANEOUSLY

S.E. LARSSON, G. LEANDER

Department of Mathematical Physics,
Lund University,
Lund, Sweden

Abstract

FISSION BARRIERS FOR HEAVY ELEMENTS WITH QUADRUPOLE, HEXADECAPOLE AND AXIALLY ASYMMETRIC DISTORTIONS TAKEN INTO ACCOUNT SIMULTANEOUSLY.

Nuclear potential energy surfaces have been calculated on the basis of the modified oscillator model by means of the Strutinsky shell correction method. The deformation energies of nuclei in the actinide region have been investigated. The nuclear shapes of the studied nuclei have been described in terms of quadrupole (ϵ_2), hexadecapole (ϵ_4) and axially asymmetric (γ) deformations. The effect of the γ degree of freedom on the fission barriers has been studied in detail. Special emphasis has been put on the calculations of the simultaneous effect of γ -deformations and hexadecapole deformations on saddle-point deformations for the inner barrier of the two peak barriers. The height of the inner barrier for heavy actinide elements is found to be reduced by up to 2.3 MeV. As a consequence, the lifetimes will also be reduced by inclusion of the γ degree of freedom. Lighter elements such as Th and those lighter than Th seem, however, to be unaffected by axially asymmetric distortions. Furthermore both the ground state and the isomeric state for the studied nuclei are stable with respect to axially asymmetric deformations.

A large part of the emphasis of the present study is on an accurate evaluation of the Coulomb energy with ϵ_4 and γ simultaneously taken into account, which has not been done up to now.

In the general case with axially asymmetric nuclear shapes, the Coulomb energy can be expressed as a six-dimensional integral. However, this six-dimensional volume integral can be reduced to a four-dimensional integral over the surface by the use of Gauss' divergence theorem. The four-dimensional integral has been evaluated by numerical methods.

1. INTRODUCTION

Recently, the effect of reflection asymmetric degrees of freedom along the fission barrier has been studied by e. g. Möller and Nilsson [1, 2], using the modified oscillator model and the Strutinsky shell correction method. It turns out that degrees of freedom of this type, introduced in terms of $P_3 + P_5$ -multipoles in the nuclear potential, are very important in the actinide region, because they lower the second peak in the barrier by several MeV.

In this paper we discuss another type of asymmetry, namely axial asymmetry or γ -deformation, together with quadrupole and hexadecapole deformations. The effect of the γ -degree of freedom on the fission barrier was first studied by Pashkevich [3] and later by Schultheiss and co-workers [4, 5], Larsson and co-workers [6, 7] and Götz and co-workers [8-10]. We will now extend the calculations to include γ -deformations simultaneously with ϵ and ϵ_4 , which has not been studied before. Special care has been taken to calculate the Coulomb energy accurately in the entire $(\epsilon, \epsilon_4, \gamma)$ -space relevant to the fission barrier problem. The entire dynamical problem including the character of the static energy surface in terms of the coordinates

β and γ was formulated in the early papers of Bohr [11] and Bohr and Mottelson [12]. In the rare-earth region very extensive dynamical calculations including axially asymmetric shapes have been performed by Kumar and Baranger on the basis of a pairing-plus-quadrupole model of nuclear interactions (Refs [13-15]). These latter calculations are, however, limited to the vicinity of the ground state minimum. For the fission problem, the inclusion of reflection asymmetric (Refs [1, 2]) and axially asymmetric degrees of freedom leads to a considerable lowering of both the first and the second saddle points (see Fig. 1). This improves considerably the agreement with experimental barrier data, which are now available for several actinide nuclei. The calculations (see below) bear out that the barrier heights for neutron-rich actinide elements are reduced by 2 MeV or more when axial asymmetry is included.

2. THE NUCLEAR ONE-BODY POTENTIAL

As a starting point we use the modified oscillator model (Refs [16-18]) and represent the effective nucleon-nucleon interaction by the deformed single particle potential

$$V = V_{\text{osc}} + V_{\text{corr}}$$

where

$$V_{\text{osc}} = \frac{1}{2} \hbar \omega_0 \cdot \rho^2 \left[1 - \frac{2}{3} \epsilon \sqrt{\frac{4\pi}{5}} \cos \gamma \cdot Y_{20} + 2 \epsilon_4 P_4 + \frac{2}{3} \epsilon \sqrt{\frac{4\pi}{5}} \cdot \frac{\sin \gamma}{\sqrt{2}} \cdot (Y_{22} + Y_{2-2}) \right]$$

and

$$V_{\text{corr}} = - \kappa \cdot \hbar \omega_0 \cdot \left[2 \vec{l}_t \cdot \vec{s} + \mu (\vec{l}_t^2 - \langle \vec{l}_t^2 \rangle) \right]$$

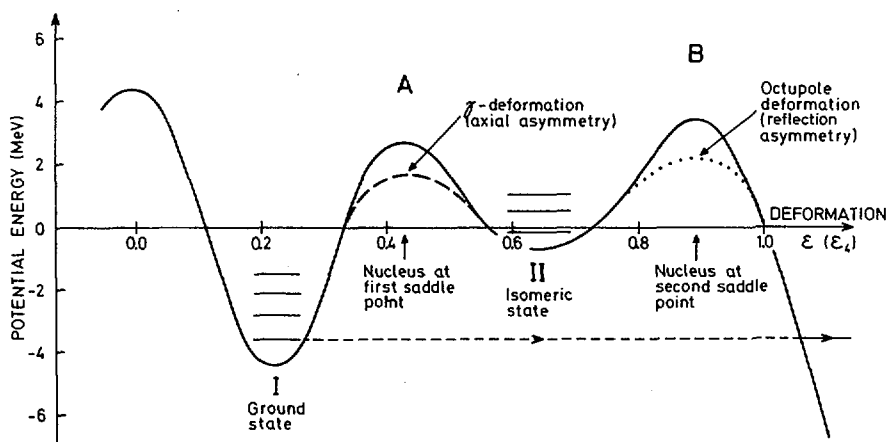


FIG. 1. Sketch showing the effect on the fission barrier of the two types of asymmetry coordinates, the reflection asymmetry (P_3+P_5) and the axial asymmetry (γ). The first saddle point is stable with respect to reflection asymmetry. The solid curve corresponds to symmetric fission.

TABLE I. VALUES OF κ AND μ USED IN THE CALCULATION OF SINGLE PARTICLE LEVELS

Protons		Neutrons	
κ_p	μ_p	κ_n	μ_n
0.0577	0.650	0.0635	0.325

The term V_{corr} contains the familiar spin-orbit term and an \vec{l}^2 -term. The \vec{l}^2 -term makes the oscillator potential more square-well-like. The potential parameters κ and μ have been determined to optimally reproduce the experimental level order of single particle states in the actinide region (Refs [19, 20]). The (κ, μ) -values employed are given in Table I.

Thus the nuclear shapes studied here can be generated in terms of three coordinates, which are

- (1) ϵ , representing nuclear elongation
- (2) ϵ_4 , representing waist-line development (or its opposite)
- (3) γ , representing axial asymmetry

We restrict our discussion here primarily to these three coordinates. They are the most important at the first barrier of the two-peak barrier, since it is borne out by Ref. [2] that the inner barrier is in almost all cases unaffected by the reflection asymmetry coordinates (represented by $P_3 + P_5$ - deformations).

All quantities are expressed in triaxially stretched coordinates

$$\left\{ \begin{array}{l} \xi = x \cdot \left[\frac{M\omega_x}{\hbar} \right]^{1/2} \\ \eta = y \cdot \left[\frac{M\omega_y}{\hbar} \right]^{1/2} \\ \zeta = z \cdot \left[\frac{M\omega_z}{\hbar} \right]^{1/2} \end{array} \right.$$

We introduce ρ as the radius vector length in the stretched coordinates, i. e.

$$\rho^2 = \xi^2 + \eta^2 + \zeta^2$$

The frequencies are defined by

$$\left\{ \begin{array}{l} \omega_x = \omega_0(\epsilon, \epsilon_4, \gamma) \left[1 - \frac{2}{3}\epsilon \cdot \cos\left(\gamma + \frac{2\pi}{3}\right) \right] \\ \omega_y = \omega_0(\epsilon, \epsilon_4, \gamma) \left[1 - \frac{2}{3}\epsilon \cdot \cos\left(\gamma - \frac{2\pi}{3}\right) \right] \\ \omega_z = \omega_0(\epsilon, \epsilon_4, \gamma) \left[1 - \frac{2}{3}\epsilon \cdot \cos\gamma \right] \end{array} \right.$$

The triaxially stretched coordinates have the advantage of transforming away coupling terms of $\rho^2 Y_{20}$ and $\rho^2(Y_{22} + Y_{2-2})$ between oscillator shells N and $N \pm 2$ (Refs [7, 16]). The matrix elements of the multipole operators occurring in the potential are easily obtained in terms of Clebsch-Gordan coefficients. The presence of the term proportional to $\rho^2(Y_{22} + Y_{2-2})$ gives rise to a coupling between states $\Omega \rightarrow \Omega \pm 2$.

3. CONDITION OF VOLUME CONSERVATION

To simulate approximately the saturation properties of nuclear matter reflecting the short-range character of nuclear forces, we have to impose the condition of conservation of the nuclear volume under any deformation. Thus we conserve the nuclear volume enclosed by an equipotential, which at least for equilibrium shapes is also equivalent to the shape of the nuclear density distribution. The condition of volume conservation can be simply fulfilled by a scaling of ω_0 for the main part of the potential.

$$\left[\frac{\omega_0}{\bar{\omega}_0} \right]^3 = \frac{1}{4\pi} \cdot \frac{1}{\sqrt{\left[1 - \frac{2}{3}\epsilon \cdot \cos(\gamma + \frac{2\pi}{3})\right] \cdot \left[1 - \frac{2}{3}\epsilon \cdot \cos(\gamma - \frac{2\pi}{3})\right] \cdot \left[1 - \frac{2}{3}\epsilon \cdot \cos\gamma\right]}} \times \int_0^\pi \int_0^{2\pi} \frac{\sin\theta \, d\theta \, d\phi}{\left[1 - \frac{2}{3}\epsilon \cdot \cos\gamma \cdot P_2(\theta) + 2\epsilon_4 P_4(\theta) + \frac{2}{3}\epsilon \sqrt{\frac{4\pi}{5}} \frac{\sin\gamma}{\sqrt{2}} \cdot (Y_{22} + Y_{2-2})\right]^{3/2}}$$

In this formulation (see Ref. [18]) we have ignored the spin- and angular-momentum-dependent terms in the nuclear potential. In the special case $\epsilon_4 = 0$, the integral can be evaluated analytically, giving the result

$$\left[\frac{\omega_0}{\bar{\omega}_0} \right]^3 = \frac{1}{\left[1 - \frac{2}{3}\epsilon \cdot \cos(\gamma + \frac{2\pi}{3})\right] \cdot \left[1 - \frac{2}{3}\epsilon \cdot \cos(\gamma - \frac{2\pi}{3})\right] \cdot \left[1 - \frac{2}{3}\epsilon \cdot \cos\gamma\right]}$$

If $\epsilon_4 \neq 0$ the integral has to be evaluated numerically.

Furthermore we have assumed

$$(\hbar\omega_0)_n^p = \frac{41.0}{A^{1/3}} \cdot \left[1 + \frac{1}{3} \frac{N-Z}{A}\right] \quad (\text{MeV})$$

where the isospin dependence on $I = (N - Z)/A$ is such as to ensure that the proton and neutron distributions have equal radii.

4. SINGLE PARTICLE STATES

The single particle states are obtained by solving the Schrödinger equation. This has been done by expanding the wave functions in the basis of

eigenstates of the isotropic harmonic oscillator. As is easily seen, the projection Ω (or K) of the single particle total angular momentum on the z -axis is not a constant of the motion, while obviously parity is conserved. The conservation of parity ensures that the single particle states of even and odd parity can be calculated separately. The inclusion of the complete couplings between states $|N'\Omega'\rangle$ and $|N\Omega\rangle$, with the coupling rules $\Omega' = \Omega \pm 2$, $N' = N, N \pm 2, \dots$, would give rise to very large matrices, actually as large as 308×308 for the odd parity case with $N_{\max} = 13$. In this work, however, we have ignored the coupling between different oscillator shells (apart from what is absorbed by the use of the stretched representation, in which there are no matrix elements for $N' = N \pm 2$) on account of computer storage limitations. The neglected coupling between energy shells N' and N is expected to change the single particle level spacings only very slightly.

5. PAIRING EFFECTS

The most important of the residual interactions is the pairing interaction (Refs [21,22]). The correction to the ground state energy, due to the short-range interaction of correlated pairs of nucleons moving in time-reversed orbits, is treated in the BCS formalism (Ref. [23]). The simple summation of single particle energies is replaced by the standard BCS expression

$$E_{\text{BCS}} = \sum_v 2\epsilon_v v_v^2 - G \left(\sum_v u_v v_v \right)^2 - G \sum_v v_v^4 + G \sum_v 1$$

where ϵ_v are the single particle energies and u_v and v_v are the usual pairing factors. The last term, $G \sum_v 1$, with summation over occupied states only, represents the subtraction of the diagonal pairing energy so that only the strict correlation energy remains.

The pairing matrix element, or the pairing strength, G , is taken to be isospin dependent as

$$(G \times A)_n^p = g_0 \pm g_1 \frac{N-Z}{A}$$

with

$$\begin{cases} g_0 = 19.2 \text{ MeV} \\ g_1 = 7.4 \text{ MeV} \end{cases}$$

where the plus sign holds for protons and the minus sign for neutrons. Furthermore the pairing matrix element is assumed to grow proportionally to the nuclear surface area S (Ref. [18], cf. Ref. [24]).

To reproduce the phenomenological $A^{-1/2}$ -dependence of even-odd mass differences, the number of levels included in the BCS calculation are taken as $\sqrt{15N}$ levels for neutrons above and below the Fermi level and $\sqrt{15Z}$ levels for protons (Ref. [18]).

6. COULOMB AND SURFACE ENERGIES

The additional Coulomb potential acting between protons is not included explicitly in the nuclear potential, but its effects are absorbed by the re-adjustment of the potential parameters of the nuclear single particle potential. In the calculations of the total energy, the Coulomb and surface energies represent the macroscopic part, or the smooth background part.

The quantum mechanical expression for the Coulomb energy is

$$E_{\text{Coul}} = \frac{1}{2} \sum_{i \neq j} \langle \psi(\vec{r}_1, \vec{r}_2, \dots, \vec{r}_Z) | \frac{e^2}{r_{ij}} | \psi(\vec{r}_1, \vec{r}_2, \dots, \vec{r}_Z) \rangle$$

where $|\psi(\vec{r}_1, \vec{r}_2, \dots, \vec{r}_Z)\rangle$ is the Slater determinant built from single particle states in the nuclear single particle potential given above, and $r_{ij} = |\vec{r}_i - \vec{r}_j|$. The exchange term, as derived by Bethe and Bacher [25], can be seen to represent essentially a volume energy and is consequently independent of the shape. Thus, if we neglect the antisymmetrization condition and replace $|\psi\rangle$ by a simple unsymmetrized product of single particle wave functions, we get

$$E_{\text{Coul}} = \frac{1}{2} \sum_{i \neq j} \iint \rho_i(\vec{r}_i) \frac{e^2}{r_{ij}} \rho_j(\vec{r}_j) d^3\vec{r}_i d^3\vec{r}_j$$

where ρ_i denotes the single particle density

$$\rho_i = |\psi_i|^2$$

As a further simplification in the spirit of the liquid-drop model, we assume the total charge Ze to be homogeneously distributed over a nuclear volume with a sharp surface, S , defined by

$$r = r(\theta, \phi; \epsilon, \epsilon_4, \gamma)$$

The validity of the sharpness assumption has been demonstrated by Swiatecki [26, 27] by means of an expansion of the Coulomb energy in increasing powers of the ratio of a small surface "thickness" to the radius. The first term of the expansion is identical with the energy obtained with a sharp surface and the second term, which provides the first-order correction due to surface diffuseness, turns out to be exactly independent of shape. Thus we have

$$E_{\text{Coul}} = \frac{1}{2} \iiint_{V_1} \iiint_{V_2} \frac{\rho}{r_{12}} d^3\vec{r}_1 d^3\vec{r}_2$$

where the radius vectors \vec{r}_1 and \vec{r}_2 vary independently over the volume of the nucleus. For clarity of notation the indices 1 and 2 will be used to distinguish between \vec{r}_1 - and \vec{r}_2 -space.

When the nuclear shape is axially symmetric, this six-dimensional integral presents no difficulty, being easily reduced to a two-dimensional integral in terms of complete elliptic integrals (Refs [28, 29]). Also, Lawrence [30]

has derived a three-dimensional integral, which has the advantage of a simple integrand. For the triaxially ellipsoidal shapes generated by our (ϵ, γ) -parametrization, the first triple integral was evaluated by Dirichlet [31] (for a modern reference see Ref. [32]) and the second one is elementary.

The resulting expression for an ellipsoid with semiaxes $a < b < c$ may be written in the simple form (Ref. [33])

$$E_{\text{coul}} = \frac{3}{5} (Ze)^2 \cdot \frac{1}{\sqrt{c^2 - a^2}} \cdot F(k, \phi)$$

where $F(k, \phi)$ is an elliptic integral of the first kind and

$$\begin{cases} k^2 = \frac{b^2 - a^2}{c^2 - a^2} \\ \sin \phi = \frac{\sqrt{c^2 - a^2}}{c} \end{cases}$$

An equivalent formula is obtained in Ref. [8].

For the case of arbitrary nuclear shapes and in particular those including hexadecapole deformations ($\epsilon_4 \neq 0$), we will now derive a four-dimensional integral with a very simple integrand. The surface of V is denoted by S and its unit normal by \hat{n} . Starting from the six-dimensional expression above, Gauss' divergence theorem is applied successively in \vec{r}_2 - and \vec{r}_1 -space. Use of the obvious identities

$$\frac{1}{|\vec{r}_1 - \vec{r}_2|} = -\vec{\nabla}_2 \cdot \left[\frac{1}{2} \frac{\vec{r}_1 - \vec{r}_2}{|\vec{r}_1 - \vec{r}_2|} \right]$$

and

$$\frac{1}{2} \frac{\vec{r}_1 - \vec{r}_2}{|\vec{r}_1 - \vec{r}_2|} \cdot \hat{n}_2 = -\vec{\nabla}_1 \cdot \left[\frac{1}{6} \frac{(\vec{r}_1 - \vec{r}_2)(\vec{r}_2 - \vec{r}_1) \cdot \hat{n}_2}{|\vec{r}_1 - \vec{r}_2|} \right]$$

leads to the desired form

$$E_{\text{coul}} = \frac{1}{12} \rho^2 \oint_{S_1} \oint_{S_2} \frac{[(\vec{r}_1 - \vec{r}_2) \cdot \hat{n}_1][(\vec{r}_2 - \vec{r}_1) \cdot \hat{n}_2]}{|\vec{r}_1 - \vec{r}_2|} dS_1 dS_2$$

One may note in passing that if S_1 and S_2 enclose two different, spatially disconnected bodies, this formula may be used to evaluate their interaction energy.

For a sphere of unit radius the integration is easily performed, giving

$$E_{\text{coul}} = \frac{16\pi^2}{15} \rho^2$$

In practice it was sufficient to use a nine-point Gaussian quadrature three times in each of the four dimensions to evaluate the Coulomb energy for the

saddle-point deformations to a relative accuracy of the order of 10^{-6} (1 keV). For certain deformations, e.g. the diamond shapes of negative ϵ_4 , the Coulomb energy is highly sensitive even to small distortions and a finer lattice is necessary.

The surface energy, being proportional to the surface area of the nucleus, is given by a two-dimensional integral which, for ellipsoidal shapes, may be expressed in terms of two elliptic functions.

In summary, the shape-dependent part of the liquid-drop contribution to the total energy is

$$E_{LD} = (B_C - 1) \cdot a_c \cdot \frac{Z^2}{A^{1/3}} + (B_S - 1) \cdot a_s \cdot (1 - \kappa_s \cdot I^2) A^{2/3}$$

where the functions B_C and B_S are the relative Coulomb and surface energies.

Furthermore, the isospin-dependent term, containing $I = (N - Z)/A$ to second order, accounts for the decrease in surface energy with increasing neutron excess (Ref. [27]). The values used for a_c , a_s and the surface symmetry coefficient κ_s are equal to those given by Myers and Swiatecki in 1967 [34].

$$\begin{cases} a_c = 0.70531 & (\text{or } r_0 = 1.2249 \text{ fm}) \\ a_s = 17.9439 \\ \kappa_s = 1.7826 \end{cases}$$

The droplet-model mass formula of Myers and Swiatecki [34, 35] also includes shape-dependent terms stemming from the unequal distribution of neutrons and protons in the nucleus and curvature effects. The contribution of these terms to our axially asymmetric saddle-point shapes is now being investigated.

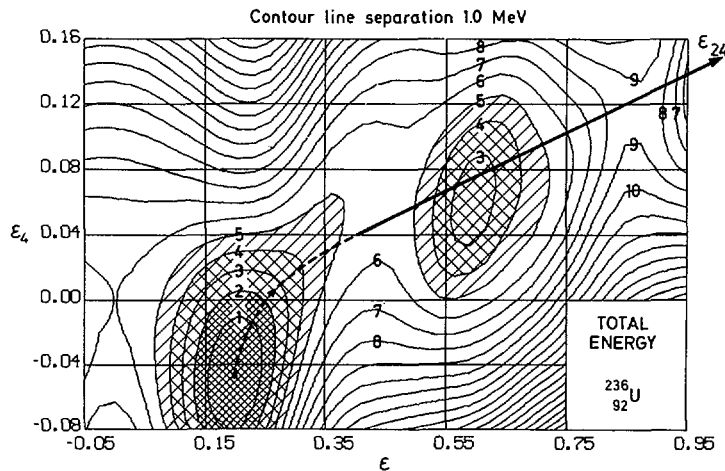


FIG. 2. Potential-energy surface in (ϵ, ϵ_4) -space for the nucleus $^{236}_{92}\text{U}$. The set of ϵ and ϵ_4 values, defined by the solid arrow, defines roughly a fission coordinate ϵ_{24} for actinide nuclei. (Figure taken from Ref. [1]).

7. POTENTIAL-ENERGY SURFACES AND CALCULATIONAL RESULTS

To calculate the total-energy surface we have employed the Strutinsky method of renormalization of the average behaviour of the total energy to that of the liquid-drop model (Refs [23, 36, 37]). The total energy is given by

$$\mathcal{E}_{\text{tot}} = (\delta E_{\text{shell}})_{p+n} + (\delta E_{\text{pair}})_{p+n} + E_{\text{LD}}$$

where the liquid-drop contribution, E_{LD} , has been discussed above. Shell and pairing corrections for protons and neutrons are calculated separately as

$$\delta E_{\text{shell}} + \delta E_{\text{pair}} = \sum_{\nu} 2\epsilon_{\nu} v_{\nu}^2 - G \left(\sum_{\nu} u_{\nu} v_{\nu} \right)^2 - G \left(\sum_{\nu} v_{\nu}^4 - \sum_{\nu} 1 \right) - E(g)$$

where

$$E(g) = \int_{-\infty}^{\lambda} 2e \cdot g(e) de$$

based on the smoothed level density

$$g(e) = \frac{1}{\gamma_s \sqrt{\pi}} \sum_{\nu} f_{\text{corr}} \cdot e^{-\left(\frac{e - \epsilon_{\nu}}{\gamma_s}\right)^2}$$

Text continues on page 197.

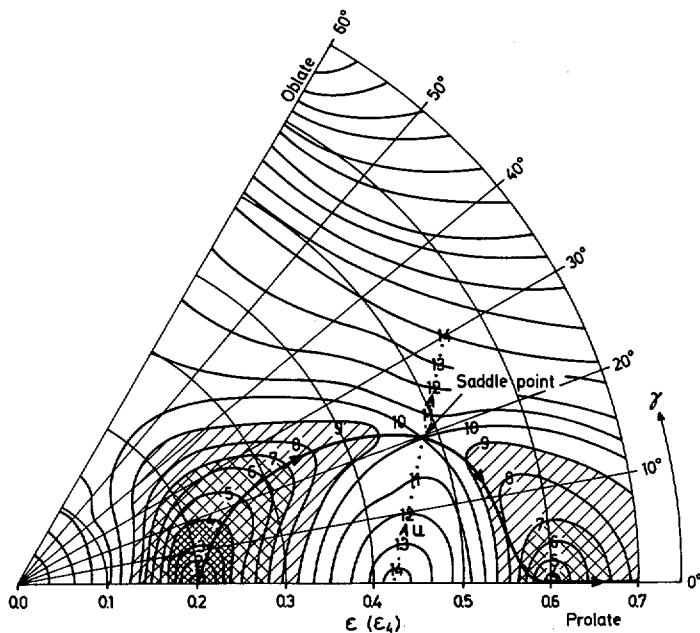


FIG.3. Sketch showing the structure of the potential energy surfaces obtained in the calculations. Note that the ground state and the isomeric state are both stable with respect to axial asymmetry, while the first saddle point is moved out into the γ -plane.

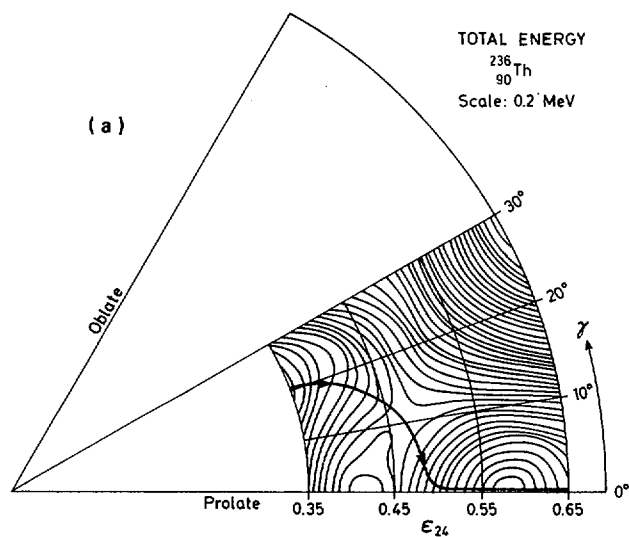


FIG.4a. Total-energy surface in the (ϵ_{24}, γ) -space for the nucleus $^{238}_{90}\text{Th}$, calculated with $G \propto S$, $\kappa_s = 1.78$. Scale = 0.2 MeV, which means that between each line on the diagram there is an 0.2-MeV energy separation.

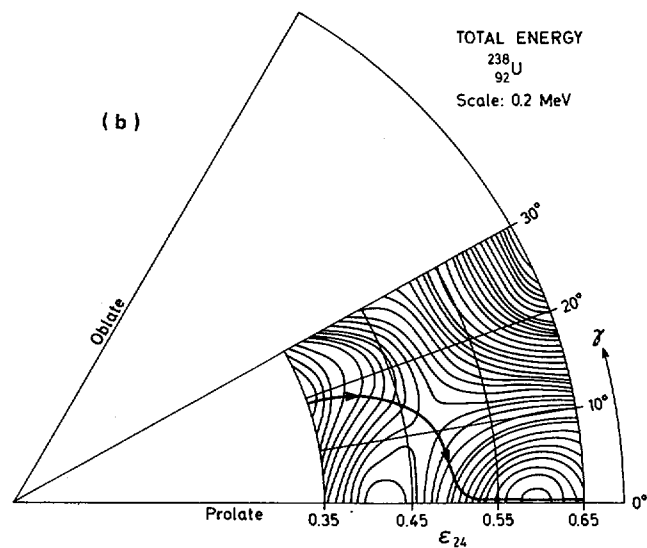
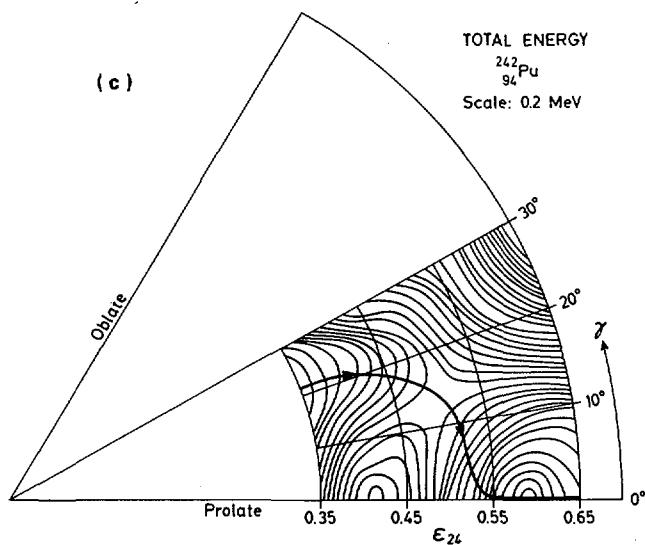
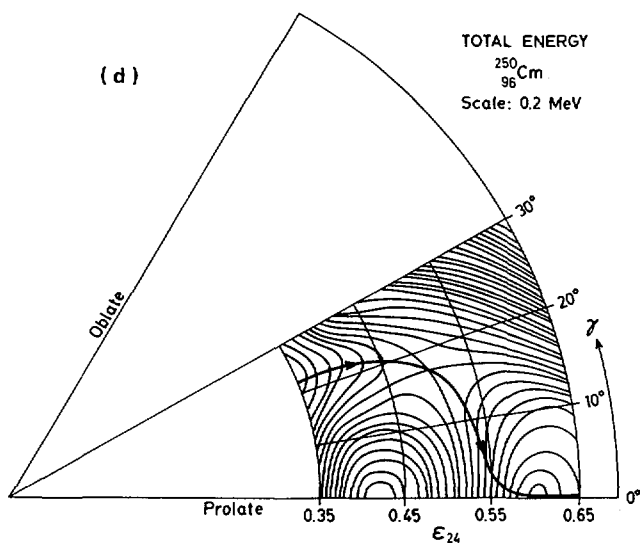
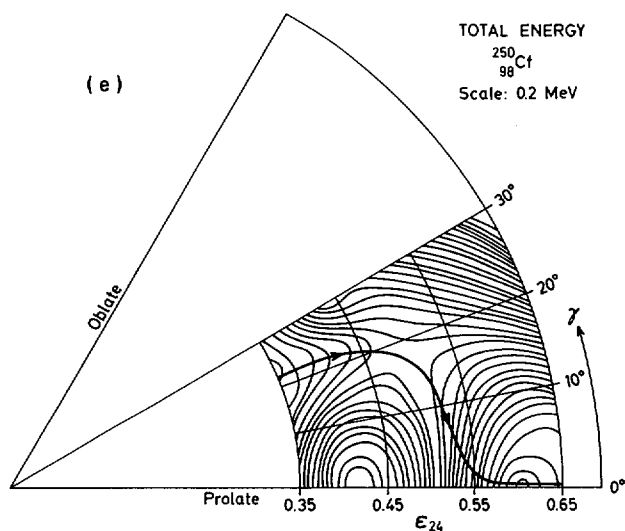
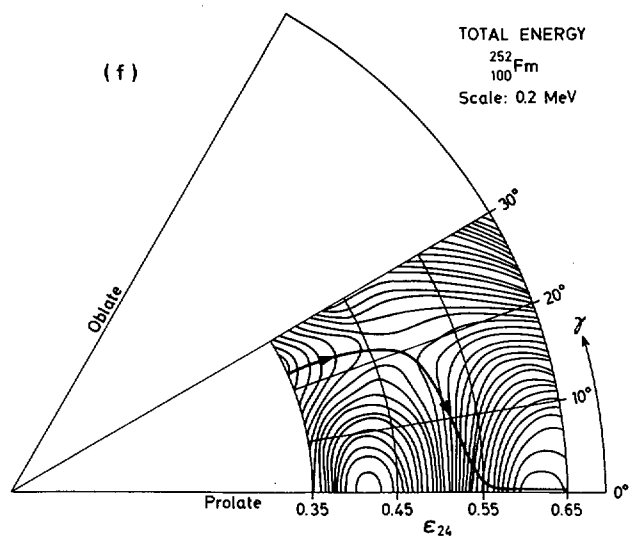
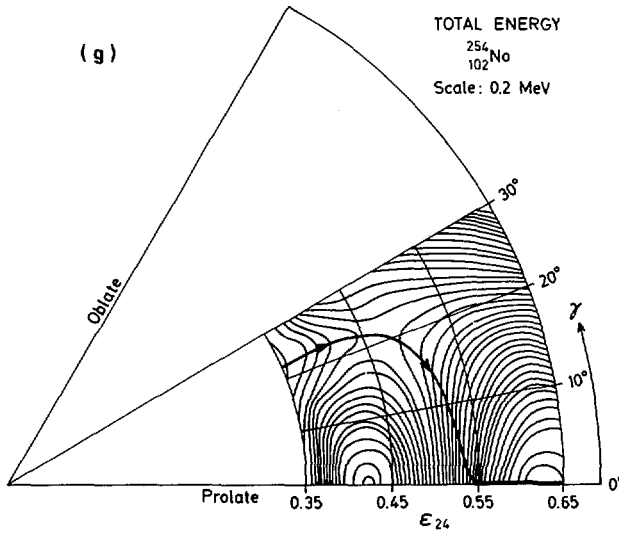
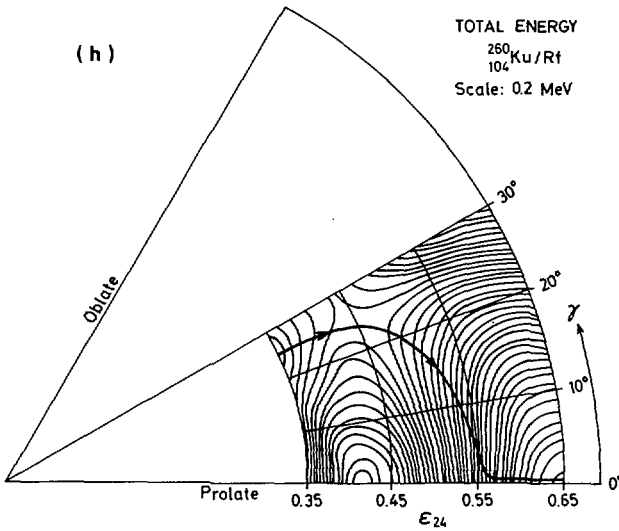


FIG.4b. Same as Fig.4a for $^{238}_{92}\text{U}$.

FIG.4c. Same as Fig.4a for $^{242}_{94}\text{Pu}$.FIG.4d. Same as Fig.4a for $^{250}_{96}\text{Cm}$.

FIG. 4e. Same as Fig. 4a for $^{250}_{98}\text{Cf}$.FIG. 4f. Same as Fig. 4a for $^{252}_{100}\text{Fm}$.

FIG.4g. Same as Fig.4a for $^{254}_{102}\text{No}$.FIG.4h. Same as Fig.4a for $^{260}_{104}\text{Ku/Rf}$.

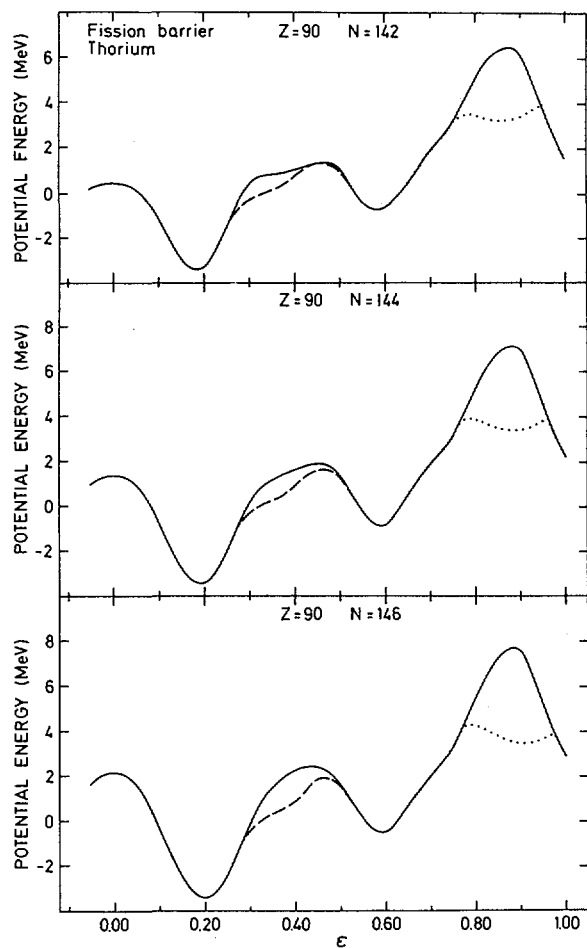


FIG. 5a. Energy projection along the ϵ -axis for Th isotopes. Each point along the curve corresponds to an energy along the paths defined in Figs 4a-h.

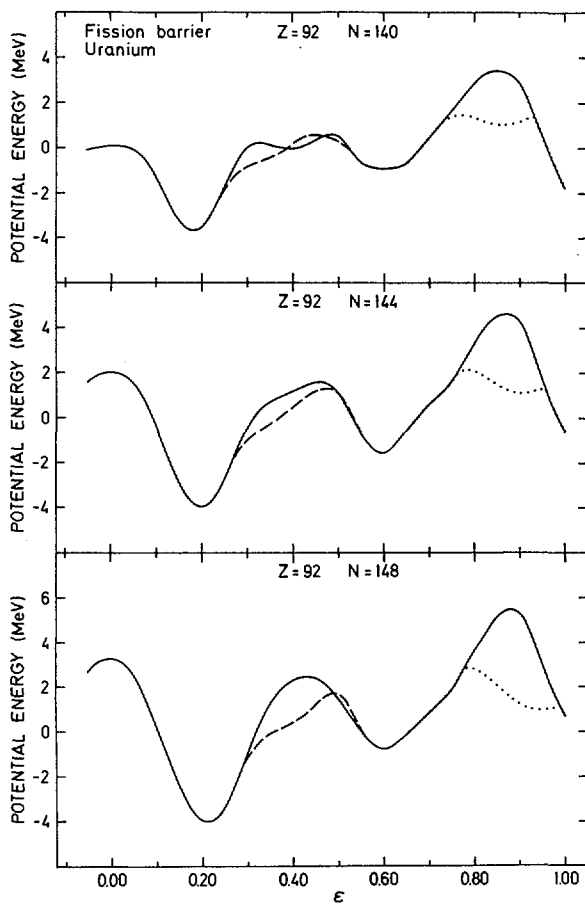


FIG. 5b. Same as Fig. 5a for isotopes of U.

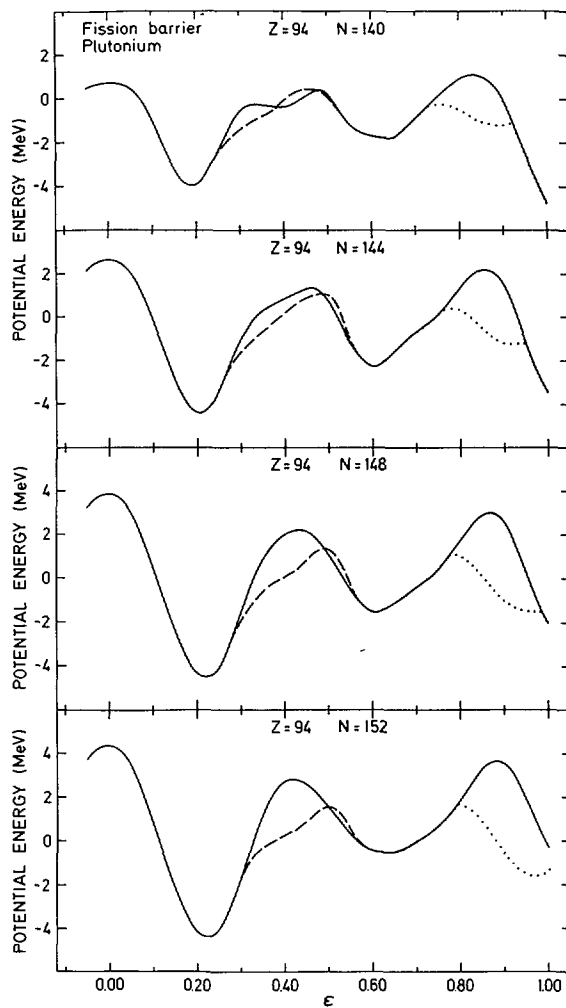


FIG.5c. Same as Fig.5a for isotopes of Pu.

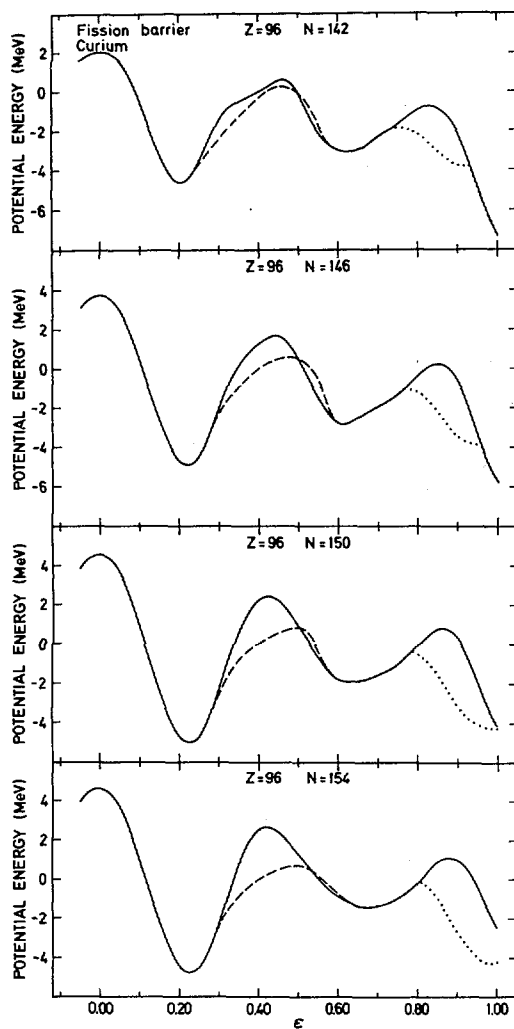


FIG.5d. Same as Fig.5a for isotopes of Cm.

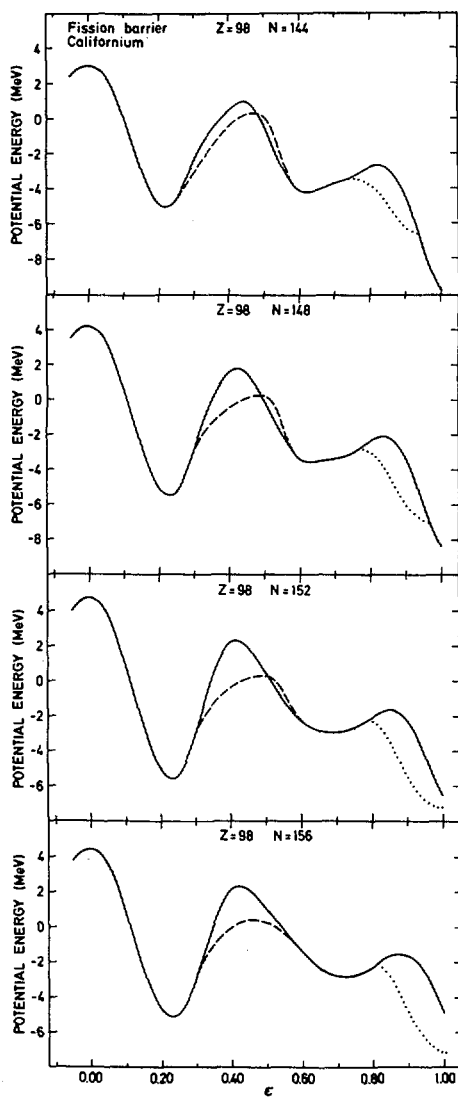


FIG. 5e. Same as Fig. 5a for isotopes of Cf.

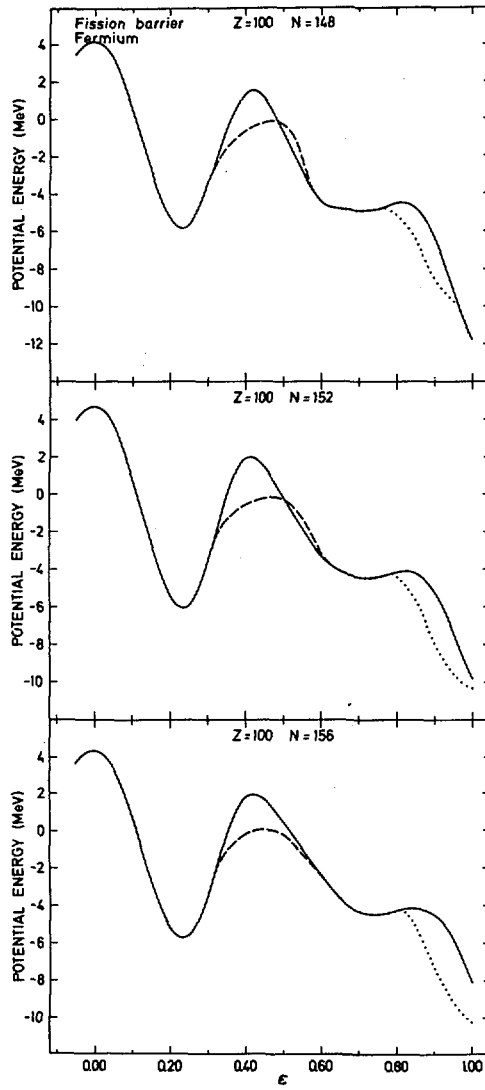


FIG. 5f. Same as Fig. 5a for isotopes of Fm.

TABLE II. FISSION BARRIER PARAMETERS AT THE FIRST SADDLE AND CORRESPONDING DISTORTIONS CALCULATED WITH $G \sim S$, $\kappa_s = 1.78$

Nucleus		First saddle			
Z	A	ϵ	γ ($^\circ$)	$E_A^a - E_1$ (MeV)	$\Delta E_\gamma = E_A^s - E_A^a$ (MeV)
90	230	0.42	0	4.0	0.0
	232	0.43	0	4.3	0.0
	234	0.45	9	5.2	0.2
	236	0.47	10	5.3	0.5
92	232	0.42	0	4.3	0.0
	234	0.45	7	5.0	0.1
	236	0.47	10	5.3	0.3
	238	0.48	11	5.6	0.5
	240	0.49	12	5.7	0.8
94	232	0.43	0	3.4	0.0
	234	0.43	0	4.3	0.0
	236	0.46	9	5.0	0.1
	238	0.48	12	5.4	0.4
	240	0.49	12	5.6	0.7
	242	0.50	13	5.8	0.9
	244	0.50	14	5.9	1.2
	246	0.51	14	5.8	1.4
96	238	0.48	13	4.9	0.3
	240	0.49	14	5.2	0.7
	242	0.50	15	5.6	1.0
	244	0.51	15	5.8	1.3
	246	0.51	15	5.9	1.6
	248	0.51	16	5.8	1.8
	250	0.51	17	5.5	1.9
	252	0.48	19	5.2	1.9
98	242	0.50	18	5.1	0.9
	244	0.50	18	5.4	1.3
	246	0.50	18	5.5	1.6
	248	0.50	18	5.8	1.9
	250	0.50	19	5.8	2.1
	252	0.48	20	5.6	2.1
	254	0.46	21	5.4	2.0

TABLE II. (cont.)

Nucleus		First saddle			
Z	A	ϵ	γ ($^\circ$)	$E_A^a - E_I$ (MeV)	$\Delta E_\gamma = E_A^s - E_A^a$ (MeV)
100	248	0.50	21	5.7	1.7
	250	0.49	21	5.9	2.0
	252	0.48	21	5.7	2.3
	254	0.47	22	5.7	2.2
	256	0.45	23	5.5	2.1

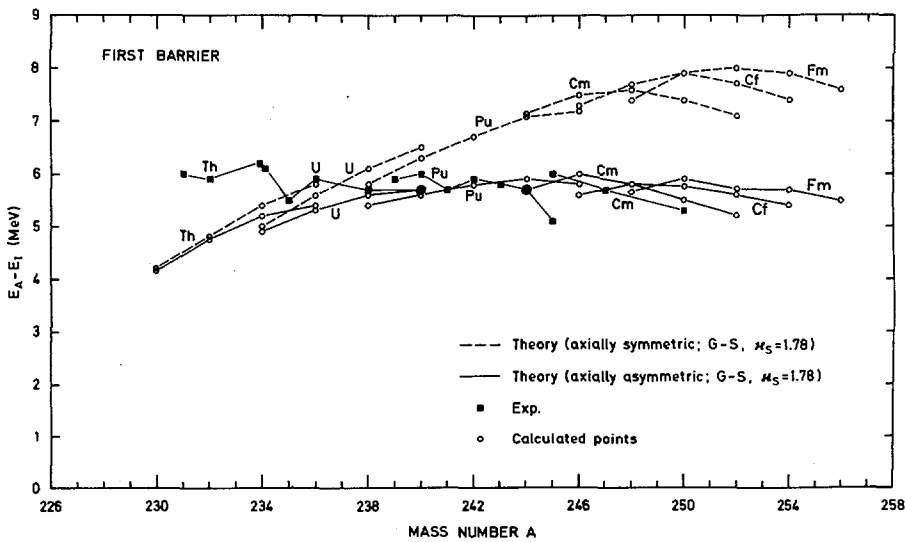


FIG. 6. Calculated barrier heights for the first barrier peak in terms of symmetric (ϵ and ϵ_4) (solid lines) and asymmetric deformations (ϵ , ϵ_4 and γ) (dashed lines), compared with the experimental barrier heights. The errors in the experimental data are estimated to be ± 0.3 MeV. Note the good agreement between theory and experiment except for Th.

Furthermore we have used the smearing parameter $\gamma_s = 1.2 \hbar \omega_0$ and a sixth-order corrective polynomial as suggested in Ref. [18].

In the following calculations we have limited ourselves to doubly even nuclei. Special emphasis has been put on saddle-point deformations for the first barrier peak. The first saddle point and a path to fission in the (ϵ, ϵ_4) -space was determined earlier, for example by Möller [2], see also Fig. 2. A set of (ϵ, ϵ_4) -values defining a coordinate ϵ_{24} in the fission direction is determined by calculating for each ϵ the ϵ_4 -value which minimizes the energy. The resulting fission path is roughly independent of Z and N.

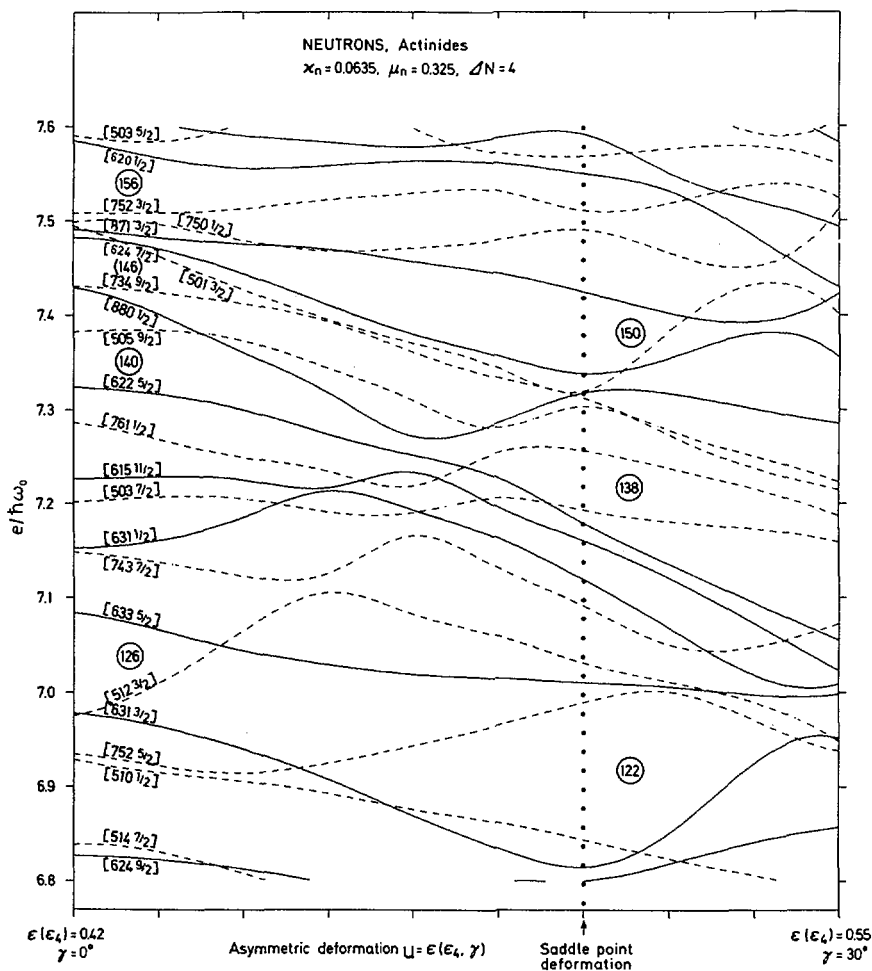


FIG. 7. Single-neutron orbitals relevant to the actinide region. The plot represents a cut in the (ϵ_{24}, γ) -plane along the path \cup indicated in Fig. 3. Orbitals are labelled by their asymptotic quantum numbers $[Nn_2\Lambda\Omega]$. Full lines correspond to even parity and dashed lines to odd parity.

A typical example of the potential-energy surface obtained with the γ degree of freedom included is shown in Fig. 3, where one axis corresponds to the fission coordinate path ϵ_{24} described above in terms of ϵ and ϵ_4 , while the γ coordinate is represented in terms of an angle $0^\circ \leq \gamma \leq 60^\circ$.

The results of the calculations of the total energy for a number of nuclei in the vicinity of the first barrier peak are presented in Figs 4a-h. Apparently, the first saddle point is moved out into the γ -plane, simultaneously reducing the barrier height relative to the ground state. For heavy actinide nuclei, the saddle points show an asymmetry of up to $\gamma \approx 20^\circ$. Probable fission paths are shown in Figs 4a-h. The dashed curves in Figs 5a-f display

the energy along these paths, plotted as a function of ϵ . The solid curves in Figs 5a-f represent the fission barriers calculated in Ref. [18] taking only P_2 - and P_4 -distortions into account. At the second peak the dotted line shows the resulting barrier when reflection asymmetric P_3 - and P_5 -distortions are included in the calculations [2]. The fission barrier parameters for the first saddle are given in Table II.

As seen from Fig. 6, the theoretical barrier heights relative to the ground state are in excellent agreement with experimental results (Ref. [38]), except for Th.

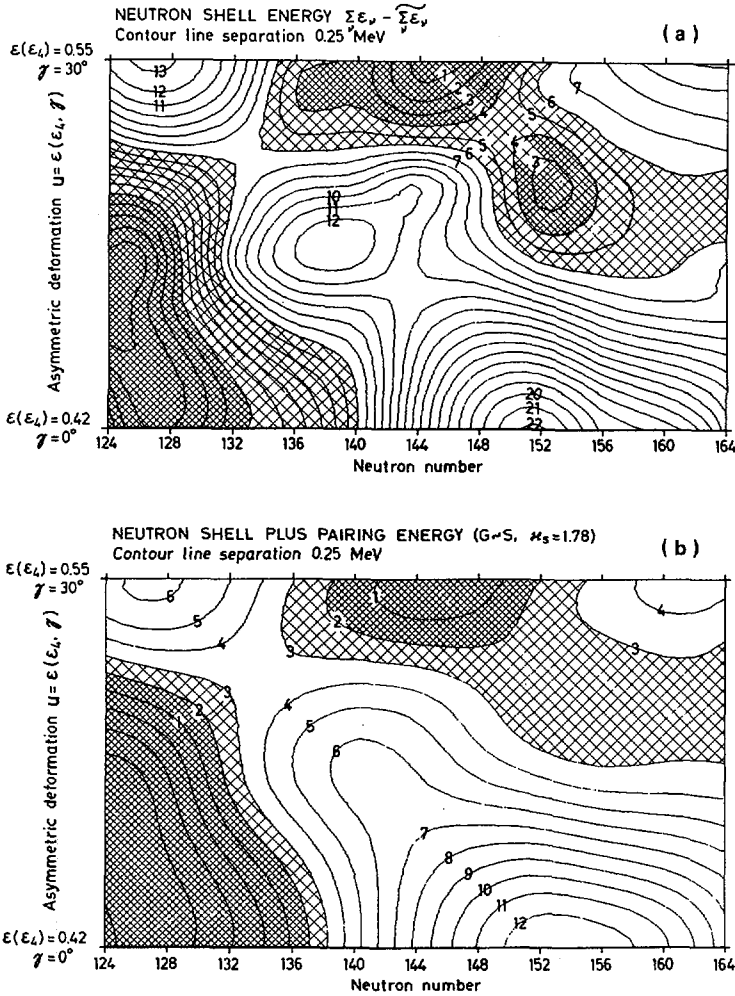


FIG. 8. Shell correction energy (a) and shell correction plus pairing energy (b) for neutrons, calculated from the level diagram in Fig. 7, as a function of neutron number and the distortions defined by the path u in Fig. 3. Note the strong preference for axially asymmetric nuclear shapes at neutron numbers around $N = 152$.

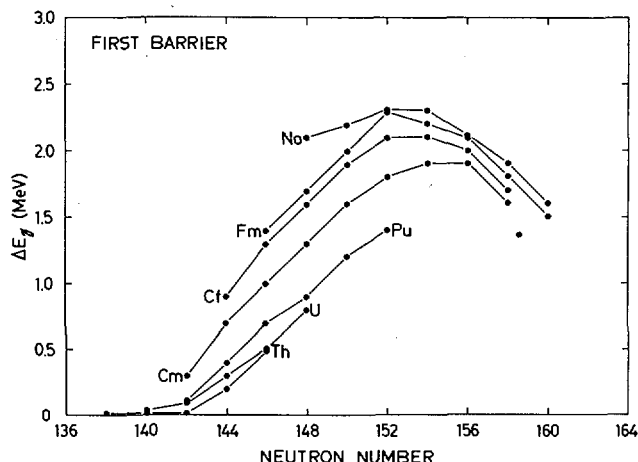


FIG. 9. The energy reduction due to axial asymmetry at the first saddle point as a function of the neutron number. Note that the maximal energy reduction for heavy actinides occurs around $N = 152$. This reflects the large decrease, with increasing γ , of the level density at the Fermi surface (as seen in Fig. 7) for these neutron numbers.

To understand the single particle effects on the nuclear potential-energy surface, the single particle levels have been plotted along a dotted path u , as indicated in Fig. 3. The level scheme along this path is exhibited in Fig. 7. The high level density around neutron number $N = 152$ at $\epsilon = 0.42$, $\epsilon_4 = 0.03$, corresponding to the saddle point under the restriction $\gamma = 0^\circ$, is changed over into a low level density at $\epsilon = 0.50$, $\epsilon_4 = 0.0$ and $\gamma \approx 20^\circ$. The degree of bunching and thinning-out of single particle levels near the Fermi surface is highly decisive for the shell energy. In Figs 8a, b the neutron shell and the shell plus pairing energies have been plotted as functions of the asymmetric deformation path u (in Fig. 7) and the neutron number. The gain in the shell plus pairing energy, due to the γ -instability, is seen to be at most 2.3 MeV for neutron number $N = 152$. Obviously, the instability of the potential energy is due almost entirely to the neutron shell correction energy. The barrier reduction due to the instability towards γ distortions is shown in Fig. 9 for a number of nuclei. From this picture it turns out that the greatest barrier reduction is associated with the neutron number $N = 152$.

8. SUMMARY AND CONCLUSION

For those transuranium elements that we have studied we find that nuclei with $N > 144$ are axially asymmetric at the first barrier peak. The asymmetry reaches its maximum value near the neutron number $N = 152$, where the first barrier is lowered by several MeV because of axial asymmetry. The agreement between theoretical results and experimental data on the fission barriers is very much improved when axial asymmetry and hexadecapole deformations are simultaneously included in the calculations of the Coulomb energy.

A further investigation of the influence of axial asymmetry on the fission barrier in the region of superheavy elements is presently in progress.

ACKNOWLEDGEMENTS

The authors would like to thank S.G. Nilsson for guidance and many stimulating discussions. Thanks are also due to our colleagues in the Lund group, in particular P. Möller for supplying us with unpublished results, and to our skilful draftsman L. Nilsson. Valuable comments on the manuscript were also made by J.R. Nix.

REFERENCES

- [1] MÖLLER, P., NILSSON, S.G., Phys. Lett. 31B (1970) 283.
- [2] MÖLLER, P., Nucl. Phys. A192 (1972) 529.
- [3] PASHKEVICH, V.V., Nucl. Phys. A133 (1969) 400.
- [4] SCHULTHEISS, H., SCHULTHEISS, R., Phys. Lett. 34B (1971) 245.
- [5] SCHULTHEISS, H., SCHULTHEISS, R., Phys. Lett. 35B (1971) 296.
- [6] LARSSON, S.E., RAGNARSSON, I., NILSSON, S.G., Phys. Lett. 38B (1972) 269.
- [7] LARSSON, S.E., Phys. Scr. 8 (1973) 17.
- [8] GÖTZ, U., PAULI, H.C., ALDER, K., Nucl. Phys. A175 (1971) 481.
- [9] GÖTZ, U., PAULI, H.C., ALDER, K., Phys. Lett. 38B (1972) 274.
- [10] GÖTZ, U., PAULI, H.C., ALDER, K., JUNKER, K., Nucl. Phys. A192 (1972) 1.
- [11] BOHR, A., K. Dan. Vidensk. Selsk., Mat.-Fys. Medd. 26 (1952) No.14.
- [12] BOHR, A., MOTTELSON, B., K. Dan. Vidensk. Selsk., Mat.-Fys. Medd. 27 (1953) No.16.
- [13] KUMAR, K., BARANGER, M., Nucl. Phys. A62 (1965) 113.
- [14] KUMAR, K., BARANGER, M., Nucl. Phys. A110 (1968) 490.
- [15] KUMAR, K., BARANGER, M., Nucl. Phys. A110 (1968) 529.
- [16] NILSSON, S.G., K. Dan. Vidensk. Selsk., Mat.-Fys. Medd. 29 (1955).
- [17] GUSTAFSSON, C., LAMM, I.L., NILSSON, S.G., NILSSON, B., Ark. Fys. (1967).
- [18] NILSSON, S.G., TSANG, C.F., SOBICZEWSKI, A., SZYMAŃSKI, Z., WYCECH, S., GUSTAFSSON, C., LAMM, I.L., MÖLLER, P., NILSSON, B., Nucl. Phys. A131 (1969) 1.
- [19] NILSSON, S.G., NIX, J.R., SOBICZEWSKI, A., SZYMAŃSKI, Z., WYCECH, S., GUSTAFSSON, C., MÖLLER, P., Nucl. Phys. A115 (1968) 545.
- [20] RAGNARSSON, I., NILSSON, S.G., Progress Report on Experimental and Theoretical Studies, Colloquium on Intermediate Nuclei, 30 Jun. - 2 Jul. 1971, Orsay.
- [21] BOHR, A., MOTTELSON, B.R., PINES, D., Phys. Rev. 110 (1958) 936.
- [22] BELIAEV, S.T., K. Dan. Vidensk. Selsk., Mat.-Fys. Medd. 31 (1959) No.11.
- [23] BRACK, M., DAMGAARD, J., PAULI, H.C., JENSEN, A.S., STRUTINSKY, V.M., WONG, C.Y., Rev. Mod. Phys. 44 (1972) 320.
- [24] KENNEDY, R.C., Phys. Rev. 144 (1966) 804.
- [25] BETHE, H.A., BACHER, R.F., Rev. Mod. Phys. 8 (1936) 193.
- [26] SWIATECKI, W.J., Nuclidic Masses (Proc. 2nd Int. Conf., Vienna, 1963), Springer, Vienna (1964).
- [27] MYERS, W.D., SWIATECKI, W.J., Nucl. Phys. 81 (1966) 1.
- [28] NIX, J.R., Further Studies in the Liquid-Drop Theory of Nuclear Fission, Appendix, Univ. of Calif., Lawrence Radiation Rep. UCRL-17958 (July 1968).
- [29] HILL, D.L., WHEELER, J.A., Phys. Rev. 89 (1953) 1102.
- [30] LAWRENCE, J.P., Phys. Rev. 139 (1965) B1227.
- [31] DIRICHLET, P., Journal de Crelle 32 (1846).
- [32] BECKER, R., SAUTER, F., Electromagnetic Fields and Interactions, 1, Blaisdell, Waltham, Mass. (1964) 104.
- [33] LANDAU, L.D., LIFSHITZ, E.M., The Classical Theory of Fields, 2, Pergamon Press, London (1961).
- [34] MYERS, W.D., SWIATECKI, W.J., Ark. Fys. 36 (1967) 343.
- [35] MYERS, W.D., SWIATECKI, W.J., Nucl. Phys. 55 (1969) 395; HASSE, R., Ann. Phys. (N.Y.) 68 (1971) 2.
- [36] STRUTINSKY, V.M., Nucl. Phys. A95 (1967) 420.
- [37] STRUTINSKY, V.M., Nucl. Phys. A122 (1968) 1.
- [38] BJÖRNHOLM, S., LYNN, J.E., unpublished (1970).

DISCUSSION

M. G. MUSTAFA: Is there a physical reason why there is a preference for axial asymmetry at the first barrier but not at the second minimum?

S. E. LARSSON: The strong preference for axial asymmetry in heavy actinide nuclei is mainly a neutron single-particle effect. The axial asymmetry at the first barrier is almost entirely due to a development of a "N = 152-shell", when the γ degree of freedom is taken into account.

S. BJÖRNHOLM: When are we going to see a study of the γ stability of the pear shapes characteristic of the outer barrier?

S. E. LARSSON: In principle, this is a straightforward calculation, except for one thing, namely the solving of the Schrödinger equation to obtain the single-particle energies. The complicated coupling rules would give rise to energy matrices of the order of 680×680 . Because of computer storage limitations this cannot be done in Lund at present. However, the outer barrier is stable to γ deformations when ϵ_3 (and ϵ_5) are neglected. This is probably also the case when ϵ_3 (and ϵ_5) are taken into account, because the liquid-drop energy will kill all other effects.

ON THE TREATMENT OF SHELL AND PAIRING ENERGIES WHEN THE LIQUID DROP PARAMETERS ARE REFITTED TO REPRODUCE THE EXPERIMENTAL BARRIER HEIGHTS

R. BENGTSOON

Department of Mathematical Physics,
Lund Institute of Technology,
Lund, Sweden

Abstract

ON THE TREATMENT OF SHELL AND PAIRING ENERGIES WHEN THE LIQUID DROP PARAMETERS ARE REFITTED TO REPRODUCE THE EXPERIMENTAL BARRIER HEIGHTS.

Some less satisfactory aspects of the microscopic-macroscopic nuclear model are discussed and alternative ways for treating some details in the model are suggested. The dominating procedure for calculating shell energies, i. e. the Strutinsky procedure, but also the recently developed temperature-entropy method, both require that a great number of excited states are known. Many of these only appear in the theoretical model but do not exist as bound states in real nuclei, and are thus not relevant. An alternative method is presented here which exploits a smoothing of the occupied levels only, over a large number of deformations. The result of this procedure is a set of "smooth" single particle levels for each of the considered deformations. The shell energy, which for each deformation is calculated as the sum of the energies of the occupied original levels minus the sum of the "smooth" levels, does not, according to preliminary calculations, deviate much from the Strutinsky shell energy. A similar procedure is applied to the pairing energy, prescribing that from the pairing energy a "smoothed" deformation-dependent mean value of the pairing energy should be subtracted. The most frequently used assumptions about the pairing strength, namely $G = \text{const.}$ and $G \sim \text{nuclear surface}$, give a smooth pairing energy, which is either constant or has the form of a surface energy. The advantage of subtracting a smooth pairing energy is that the macroscopic (liquid drop) energy becomes the same, independent of the assumption about the pairing strength, a desired effect which cannot be obtained otherwise. The rightness of introducing a smooth pairing energy is discussed by means of refitted liquid drop parameters.

1. INTRODUCTION

The study of different modifications of the deformed modified harmonic oscillator potential, involving models which contain deformation-dependent spin-orbit and ℓ^2 -terms such as the one proposed by Bohr and Mottelson[1], has led to a point where a major interest is concentrated on pure single particle properties, such as the deformation dependence of the single particle levels, which is drastically revealed in the sum of single particle energies (Fig. 1).

Two variants of the modified harmonic oscillator potential are considered in this report. They can both be written in the general form

$$V = \frac{1}{2} \hbar \omega_0 \rho^2 \left(1 - \frac{2}{3} \epsilon P_2 + 2 \sum_v \epsilon_v P_v \right) + V_{\text{corr}} \quad (1.1)$$

Using

$$V_{\text{corr}} = -2\kappa \hbar \omega_0 \left(\bar{\ell}_t \cdot \bar{s} + \frac{1}{2} \mu (\ell_t^2 - \langle \ell_t^2 \rangle_N) \right) \quad (1.2)$$

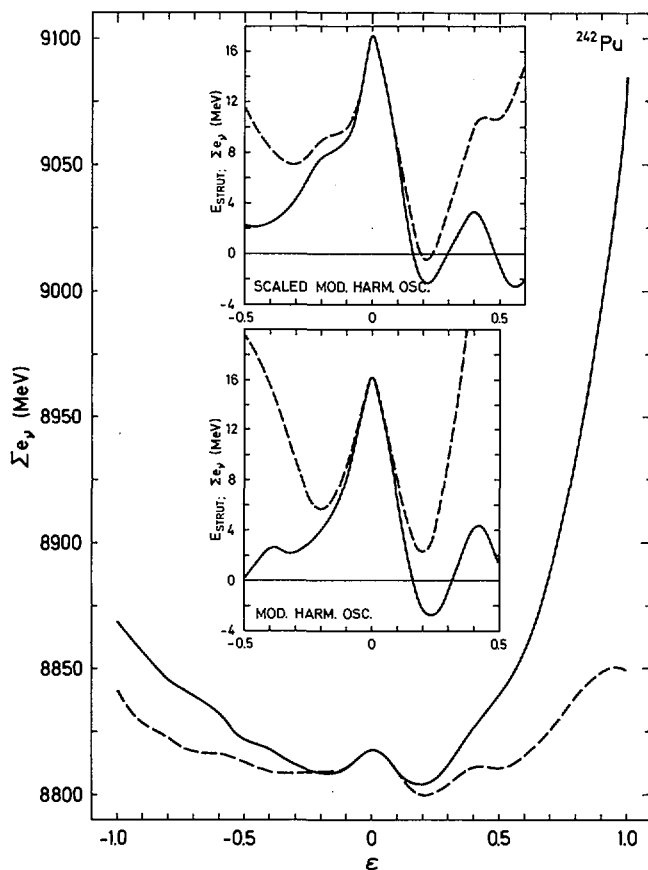


FIG. 1. Sum of single particle energies (protons + neutrons) for ^{242}Pu . Solid line is used for the modified harmonic oscillator, Eq. (1.2), and dashed line for the scaled modified harmonic oscillator, Eq. (1.3). The small diagrams show a comparison with the Strutinsky shell energy (solid lines). The curves have been adjusted to coincide at zero deformation.

gives the potential described in Ref. [2] while

$$\begin{aligned}
 V_{\text{corr}} = & -2 \kappa \hbar \omega_0 \left\{ \frac{\sqrt{\omega_1 \omega_2}}{\omega_0} \left[\bar{\ell}_t \cdot \bar{s} + \sqrt{\frac{\omega_1}{\omega_2}} - 1 \right) \ell_\zeta \cdot s_\zeta \right] \right. \\
 & \left. + \frac{1}{2} \mu \left[\frac{\omega_1 \cdot \omega_2}{\omega_0^2} (\ell_t^2 + (\frac{\omega_1}{\omega_2} - 1) \ell_\zeta^2) - \langle \ell_t^2 \rangle n_1 n_2 \right] \right\}
 \end{aligned}
 \quad (1.3)$$

gives the modification proposed by Bohr and Mottelson [1, 3].

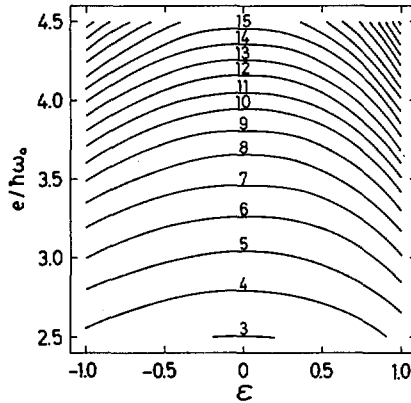


FIG. 4. The final version of the fitted smooth levels. To get this level scheme a smoothing has been done also over ν (cf. Eq.(3.11)).

The smooth set of single particle levels, \tilde{e}_ν , can be used to define a shell correction energy

$$E_{\text{shell}} = \sum e_\nu - \sum \tilde{e}_\nu \quad (1.4)$$

where e_ν is the original set of Nilsson levels (Fig. 2). Using the redefined volume conservation condition mentioned above for redefining the value of $\hbar\omega$, the shell energy can be written in the more compact form

$$E_{\text{shell}} = \sum e_\nu - \text{const.} \quad (1.5)$$

since with the redefined value of $\hbar\omega$, $\sum \tilde{e}_\nu$ does not depend on deformation.

As the fitting procedure gives a complete set of smooth single particle levels, these can be used not only to determine a value of the shell energy but also to determine an average value of the pairing energy \tilde{E}_{pair} , which consequently is defined as the value of the pairing energy that a BCS calculation gives when applied to the set of smooth single particle levels. The pairing energy \tilde{E}_{pair} , which might be dependent on N , Z and deformation, should replace the usually used constant value -2.3 MeV (Refs [2, 4]).

In accordance with the above idea, the total microscopic energy can be written

$$E_{\text{micr}} = \sum e_\nu - \sum \tilde{e}_\nu + E_{\text{pair}} - \tilde{E}_{\text{pair}} \quad (1.6)$$

As it turns out, this way of calculating E_{micr} has two advantages over previously used prescriptions (Refs [2, 4-8]), which are:

- (a) The shell correction energy can be calculated without using any levels above the Fermi energy.
- (b) The definition of \tilde{E}_{pair} ensures that the macroscopic (liquid drop) energy becomes independent of the choice of pairing strength.

2. FITTING OF A SET OF SMOOTH SINGLE PARTICLE LEVELS

The basis of the calculations is the derivation of a set of smooth single particle levels from a usual Nilsson diagram (Fig. 2). The diagram is first redefined in such a way that the levels are not connected according to the quantum numbers but only according to the number index ν , determined by numbering the levels from the lowest energy ($\nu=1$) to the highest one. This gives Fig. 3, which is nothing but a Nilsson diagram drawn under the assumption that there is a coupling between all states (the matrix elements, however, vanishing in most cases). Then to each level $e_\nu(\epsilon)$ is fitted a smooth level $\tilde{e}_\nu(\epsilon)$, which together build up a smooth single particle scheme (Fig. 4), which is assumed to have the general form

$$\tilde{e}_\nu(\epsilon) = A_\nu \cdot f_\nu(\epsilon) \hbar \omega_0 \quad (2.1)$$

where A_ν are the smooth levels for a spherical nucleus and $f_\nu(\epsilon)$ is a factor which contains the deformation dependence. This might be different for different levels, therefore the index ν is used.

An approximate estimate of $\tilde{e}_\nu(\epsilon)$ can be made from a Thomas-Fermi model. Putting $V_{\text{corr}} = 0$ in the potential (1.1) gives

$$N = \frac{E_N^3}{3\hbar^3} \cdot \frac{\int_0^\pi \left(\frac{1}{2} \cdot \sin\theta \cdot d\theta \right)}{\left(1 - \frac{2}{3}\epsilon P_2 + 2 \sum_\nu \epsilon_\nu P_\nu \right)^{3/2}} = \frac{E_N^3}{3\hbar^3 \omega_0^3} \quad (2.2)$$

where the last equality comes from the volume conservation condition (Ref. [2])

$$\left(\frac{\omega_0}{\omega_0} \right)^3 = \frac{1}{\left(1 + \frac{\epsilon}{3} \right) \left(1 - \frac{2\epsilon}{3} \right)^{1/2}} \int_0^\pi \frac{\frac{1}{2} \sin\theta \, d\theta}{\left(1 - \frac{2}{3}\epsilon P_2 + 2 \sum_\nu \epsilon_\nu P_\nu \right)^{3/2}} \quad (2.3)$$

In Eq. (2.2) N is the number of particles with energy less than or equal to E_N .

In the case of pure quadrupole deformations Eq. (2.3) transforms to

$$\left(\frac{\omega_0}{\omega_0} \right)^3 = \frac{1}{\left(1 + \frac{\epsilon}{3} \right)^2 \left(1 - \frac{2}{3}\epsilon \right)} \quad (2.4)$$

leading to a simplification of Eq. (2.2), which becomes

$$E_N = \sqrt[3]{3N} \cdot \sqrt[3]{1 - \frac{1}{3}\epsilon^2 - \frac{2}{27}\epsilon^3} \cdot \hbar \omega_0 \quad (2.5)$$

Since in the following calculations only P_2 -deformations are considered, it is assumed that the smooth levels can be written as a generalization of Eq. (2.5):

$$\tilde{e}_\nu(\epsilon) = \sqrt[3]{a_{\nu 0}} \cdot \nu \cdot \sqrt[3]{1 + a_{\nu 1}\epsilon + a_{\nu 2}\epsilon^2 + a_{\nu 3}\epsilon^3 + a_{\nu 4}\epsilon^4} \cdot \hbar \omega_0 \quad (2.6)$$

where the coefficients $a_{\nu i}$ depend on ν . This equation defines A_ν and $f_\nu(\epsilon)$ as

$$A_\nu = \sqrt[3]{a_{\nu 0} \cdot \nu} \quad (2.7)$$

$$f_\nu(\epsilon) = \sqrt[3]{1 + a_{\nu 1}\epsilon + a_{\nu 2}\epsilon^2 + a_{\nu 3}\epsilon^3 + a_{\nu 4}\epsilon^4} \quad (2.8)$$

Notice that $\nu = N/2$ because of the doubly degenerate levels, and therefore $a_{\nu 0}$ is about 6. The addition of the ϵ and ϵ^4 terms is essential to get a good fit.

The fitting of the coefficients is done by fitting a fourth degree polynomial to reproduce the cubed original level, $e_\nu^3(\epsilon)$. However, this gives coefficients which depend quite a lot on ν , at least for the lowest levels ($\nu \leq 25$), while Eq. (2.5) indicates that there is no ν -dependence, or if there really is such a dependence for the complete potential (Eqs (1.2) or (1.3)) it should be very weak. In fact the reason for the fluctuations is found in the very strong shell effects for the spherical nuclei, cf. Fig. 5 showing $a_0/2$, which should be 3 according to Eq. (2.5). The magic numbers 8, 20, 28, 50, 82 and 126 are clearly seen. This effect can of course be more or less washed out by considering an even greater number of deformations than in Figs 2-4, but the same effect can more easily be reached by just neglecting deformations with $|\epsilon| \lesssim 0.1$ in the fitting. This is preferable since deformations greater than $|\epsilon| \gtrsim 1.0$ are seldom of interest. However, some shell-structure-like fluctuations can still be found in the fitted coefficients. How this disadvantage can be avoided is discussed in the next section.

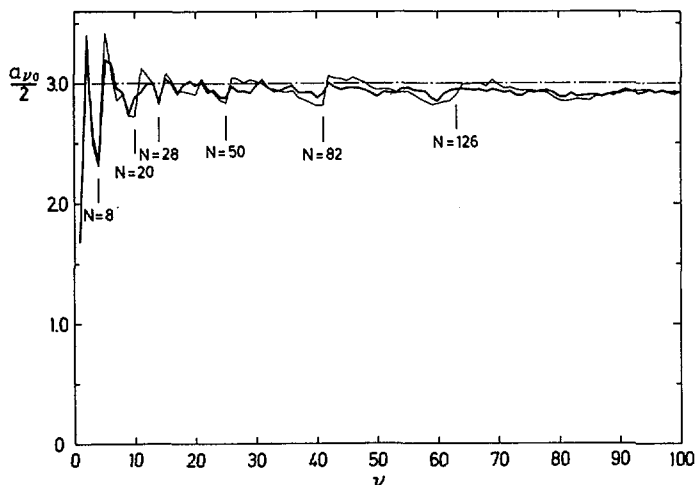


FIG. 5. The parameter $a_{\nu 0}/2$ as a function of the number of the energy level, ν . The thin curve is for the case where all deformations $|\epsilon| \leq 1.0$ are used for the fit. Notice that the shell structure of the spherical nucleus is clearly seen. The thick curve is for the case where deformations with $|\epsilon| \leq 0.1$ have been omitted.

3. CALCULATION OF THE SHELL CORRECTION ENERGY AND A REDEFINED VOLUME CONSERVATION CONDITION

There exists a number of possible methods for calculating shell energies. Some of the more relevant are discussed by Bohr and Mottelson [1]. The most successful one is the widely used Strutinsky procedure [9]. However, recent calculations by several authors (Refs [10-12]) have shown that another method, which exploits the statistical behaviour of nuclei at high temperatures, can be used to calculate shell energies with the same precision as the Strutinsky method. A third method involves a smoothing procedure over large deformations. Such a smoothing has in fact been done in Section 2, and it seems reasonable to define the shell energy as

$$E_{\text{shell}} = 2 \sum_{\nu=1}^{N/2} e_{\nu} - 2 \sum_{\nu=1}^{N/2} \tilde{e}_{\nu} \quad (3.1)$$

This corresponds to the Strutinsky formula except that the continuous level density used by Strutinsky is replaced by the discrete levels \tilde{e}_{ν} . However, the methods of fitting the smooth density and levels respectively are quite different. Strutinsky's method, as well as the statistical method, uses the levels for one deformation and smoothes over ν , using levels high above the Fermi surface, which is a complication when using e. g. a Woods-Saxon potential, which gives a limited number of bound excited states. In the present model the smoothing is done over different deformations. As will be shown later, smoothing also over ν improves the results somewhat, but only levels below the Fermi surface have to be used. Since only physically relevant levels and deformations are used, the method can be applied to any potential without complications.

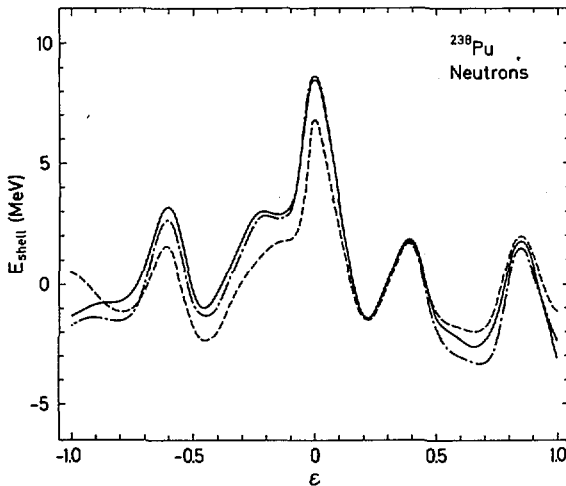


FIG. 6. Neutron shell correction energy for ^{238}Pu . The solid curve is calculated with the Strutinsky procedure. The dashed curve is calculated using the direct fitted levels of Eq. (2, 6), while the dot-dashed curve is obtained after a smoothing also over ν (cf. Eq. 3, 11).

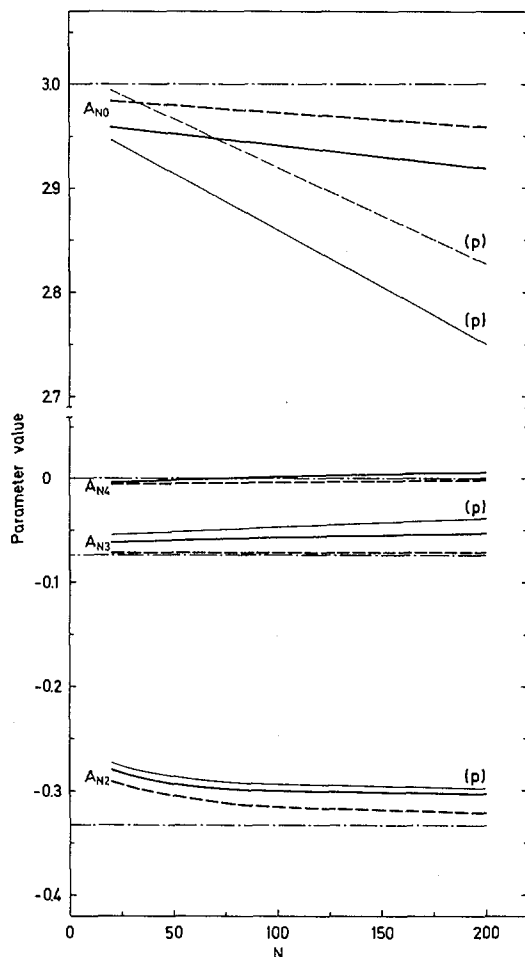


FIG. 7. The parameters A_{Ni} appearing in Eqs (3.5) and (3.7) as functions of the neutron (or proton) number N . The solid curves give the appropriate parameters for the potential (1.2) and the dashed curves give the parameters for the potential (1.3). Separate curves for protons (thin lines, (p)) are given only when they deviate by more than 0.0025 from the corresponding neutron curves. The parameter A_{N1} has been omitted since it would not have been separable from zero in the scale of this diagram. Dot-dashed lines show the values obtained from Eq. (2.5).

Although the smooth energies are differently fitted in the two procedures the resulting shell energies are very much alike as is seen from Fig. 6.

The calculation of the shell energy can be carried out in a somewhat different way. In Eq. (2.1) $f_v(\epsilon)$ takes different values for every value of v . The variation however is small, and Eq. (2.1) might be rewritten as

$$\tilde{\epsilon}'_v(\epsilon) = A_v \cdot F_N(\epsilon) \cdot \hbar\omega_0 \quad (3.2)$$

if $F_N(\epsilon)$ is chosen in a suitable way. For example, if the shell energy is not to change, the following relation must hold

$$F_N(\epsilon) = \frac{\sum_{\nu=1}^{N/2} A_\nu f_\nu(\epsilon)}{\sum A_\nu} \quad (3.3)$$

Thus $F_N(\epsilon)$ is a mean value of $f_\nu(\epsilon)$, $\nu \leq N/2$, and for a given nucleus $F_N(\epsilon)$ has the same value for all levels independent of the value of ν . For heavier nuclei $f_\nu(\epsilon)$ and $F_N(\epsilon)$ come very close to each other, and the corresponding single particle level schemes (Eqs (2.1) and (3.2)) differ significantly only for the lowest 20 or 30 levels.

Using the function $F_N(\epsilon)$, the shell energy can be written

$$E_{\text{shell}} = 2 \sum_{\nu=1}^{N/2} e_\nu - 2\hbar\omega_0 F_N(\epsilon) \sum_{\nu=1}^{N/2} A_\nu \quad (3.4)$$

where

$$F_N(\epsilon) = \sqrt[3]{1 + A_{N1}\epsilon + A_{N2}\epsilon^2 + A_{N3}\epsilon^3 + A_{N4}\epsilon^4} \quad (3.5)$$

The average behaviour of the coefficients A_{Ni} is given in Fig. 7 for neutrons in the potential (1.2). If the Eqs (3.2) and (2.5) are compared it is evident that $(F_N(\epsilon))^3$ directly corresponds to the volume conservation condition (2.4), which might be redefined as

$$\frac{\omega'_0}{\omega_0} = \frac{1}{F_N(\epsilon)} \quad (3.6)$$

This quantity is slightly different for different nuclei because of the N dependence of $F_N(\epsilon)$. The prime is used to distinguish ω'_0 from the corresponding value in Eq. (2.4).

Introducing $A_{N0} = a_{\nu 0}/2$ ($\nu = N/2$) the modified volume conservation gives

$$N = \frac{E_N^3}{A_{N0} \hbar^3 \omega_0^3} = \text{const.} \quad (3.7)$$

for all deformations in correspondence to Eq. (2.2). Here $E_N = e_\nu$ is the energy of particle N. It also follows that

$$E_{\text{shell}} = 2 \sum_{\nu=1}^{N/2} e_\nu - 2\hbar\omega_0 \sum_{\nu=1}^{N/2} A_\nu = 2 \sum_{\nu=1}^{N/2} e_\nu - \text{const.} \quad (3.8)$$

Equations (3.6) and (2.4) explain the behaviour of the curves in Fig. 1. As the V_{corr} part of the potential (1.1) leads to different values of $F_N(\epsilon)$ for the two alternatives of V_{corr} given by Eqs (1.2) and (1.3) respectively, the use of Eq. (2.4) gives the summed energy $\sum e_\nu$ a smooth trend, which

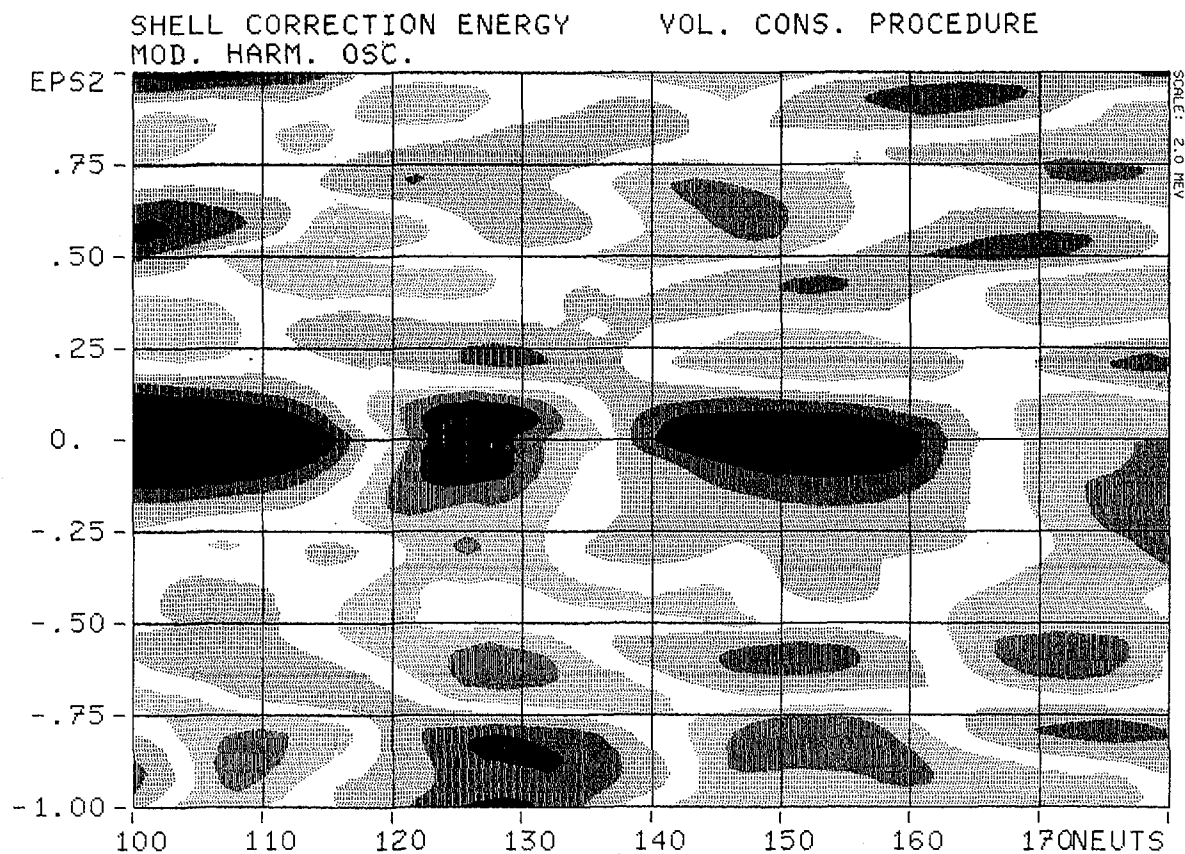


FIG. 8. Shell correction energy for neutrons as a function of deformation and neutron number, calculated as $\Sigma \epsilon_{\nu} - \Sigma \tilde{\epsilon}_{\nu}$, where $\tilde{\epsilon}_{\nu}$ has been determined after a smoothing also over ν . The regions marked with blue and green colours have negative shell energies, while the red and violet colours stand for positive shell energies. In the yellow region, $-1.0 \text{ MeV} < E_{\text{shell}} < 1.0 \text{ MeV}$. Each colour extends over 2.0 MeV.

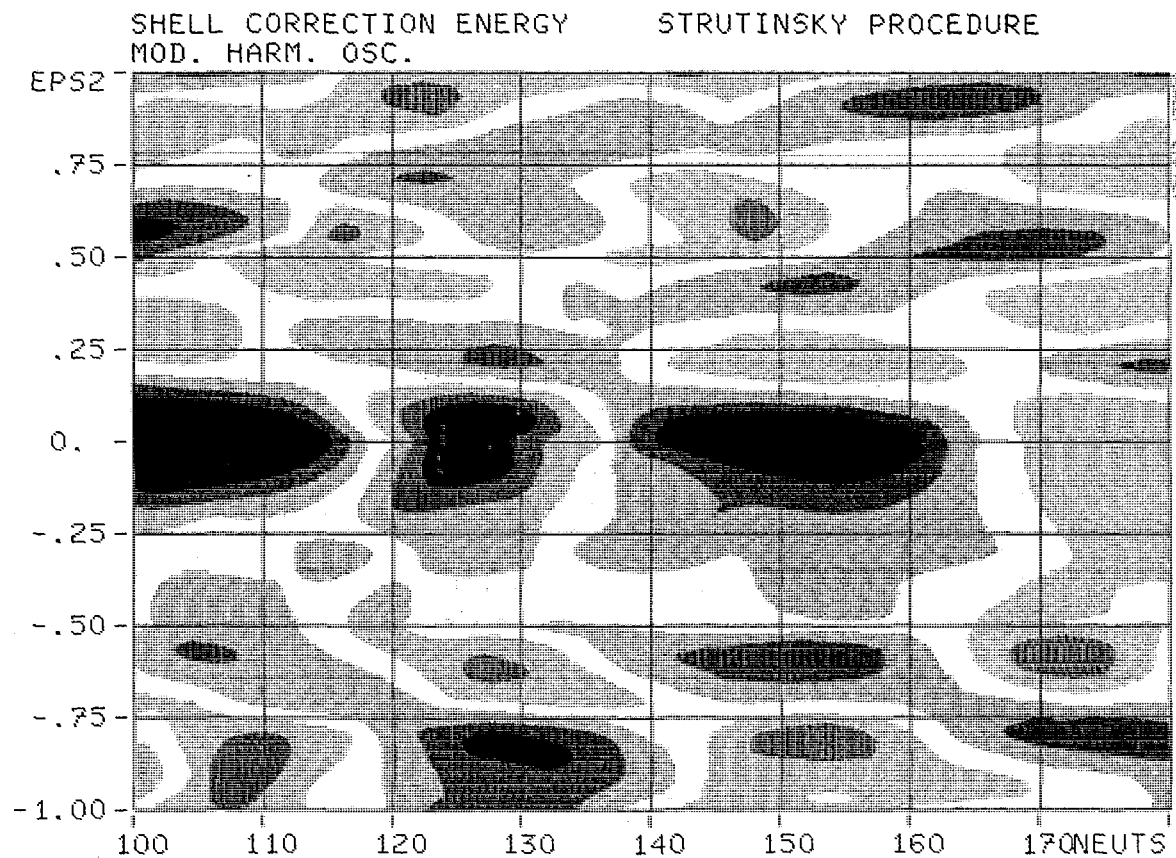


FIG. 9. Same as Fig. 8, but E_{shell} is calculated with the Strutinsky procedure.

is determined by the quotient ω_0/ω_0^i . Although this quotient is close to one it affects the sum Σe_ν by some hundred MeV, because the sum itself is of the order of 10 000 MeV in the actinide region. However, the alternative use of ω_0^i in Eq. (3.4) does not change E_{shell} by more than a tenth of an MeV or less, which is negligible. Notice that, with the version (1.3) of the potential, the sum Σe_ν reproduces the shell energy comparatively well also without redefining ω_0 . This is in fact quite natural, since the volume conservation condition is determined from the P_2 -deformation, and for the potential (1.3) this deformation has been considered also in V_{corr} , which might imply that ω_0^i for this potential should be much closer to ω_0 than it is for the potential (1.2). This is confirmed by Fig. 7, which shows the coefficients appearing in the expression for ω_0^i (Eqs. (3.5) and (3.6)) and for ω_0 (Eqs (2.4) or (2.5)). Note that the $A=242$ values of the parameters κ and μ (see Refs [2, 3]) appearing in Eqs (1.2) and (1.3) have been used in all the calculations. Consideration also of the variations with mass number in κ and μ might change the curves in Fig. 7 somewhat.

The method of calculating shell energies by redetermining the volume conservation condition has been studied by Hillman [13] who presumes that Σe_ν should also contain the surface energy as given by Myers and Swiatecki [14]. This gives of course a different value of ω_0 .

Of great interest are also the attempts to determine the shell energy by smoothing Σe_ν over the nucleon number A (protons or neutrons) assuming that

$$\Sigma e_\nu = C_0 A + C_1 A^{2/3} + C_2 A^{1/3} + \dots + E_{\text{shell}} \quad (3.9)$$

Here $C_0 A$ is identified as a volume term, $C_1 A^{2/3}$ as a surface term and $C_2 A^{1/3}$ as a curvature term. Higher terms might be included. By letting A become very large (of the order of several thousand) it is possible to determine the constants. A preliminary calculation has been done in Lund by Thegerström [15], who finds that $C_0 = 44.03$ MeV for a spherical nucleus. The other constants are difficult to fit, but Siemens and Sobiczewski [16] seem to have succeeded well. For a pure harmonic oscillator it can be shown analytically that $C_0 = (3^{4/3}/4) \times 41.0$ MeV, $C_2 = 0.0$ MeV, and $C_3 = (3^{2/3}/8) \times 41.0$ MeV. The surface term is thus zero. In fact, C_0 can be derived from Eq. (2.6). If it is assumed that $a_{\nu 0} = \text{const.}$, one finds

$$C_0 \approx \frac{3}{4} \cdot \left(\frac{a_{\nu 0}}{2} \right)^{1/3} \cdot 41.0 \text{ MeV} \quad (3.10)$$

which for $a_{\nu 0} = 5.90$ gives $C_0 = 44.10$, in good agreement with Thegerström. It is then assumed¹ that $\hbar\omega_0 = 41.0 A^{-1/3}$ MeV. As is seen from Fig. 5, $a_{\nu 0}$ depends on ν (and thus also on N). If this dependence could be determined it might be possible to estimate also C_1 and C_2 . However, $a_{\nu 0}$ contains some fluctuations caused by the remaining small shell effects. The same

¹ This is really not correct since A in this case stands for the proton (or neutron) number. In a more serious calculation a more proper value must be used.

is the case for A_{Ni} ($i=1, \dots, 4$). In an attempt to improve the calculations, the smooth curves shown in Fig. 7 were fitted to A_{Ni} . The ν dependence is, however, very weak and the magnitude of the fluctuations decreases rapidly to zero for higher ν -values. Thus, except for very light nuclei, nothing is gained by considering levels above the Fermi surface, so the conclusions drawn in the beginning of Section 3 still hold. The shell energies calculated after such a smoothing remain somewhat more about the Strutinsky shell energies, as is seen from Fig. 6. Figure 8 also shows shell energies calculated after smoothing over ν ($\nu \leq N/2$), which should be compared with the Strutinsky shell energies in Fig. 9.

It must be emphasized that the above method for calculating shell energies is not developed to the same degree of precision as the Strutinsky procedure. Consequently no recommendations can be made, for example, about how many deformations one has to include. At any rate, $-1.0 < \epsilon < 1.0$ is insufficient to smooth out the shell effects completely, as is seen from Fig. 5. If on the other hand the smooth quantities resulting from the Strutinsky procedure are studied as functions of the deformation they behave very smoothly. For example, the Fermi energy follows Eq. (2.6) within 0.02% with coefficients which agree well with those found in the fitting of \tilde{e}_ν .

Considerations of this kind lead to a more general approach to the calculation of shell energies. Any quantity such as e_ν , Σe_ν etc. is a function of a number of independent variables, e.g. $e_\nu = e_\nu(N, (Z), \nu, \epsilon, \epsilon_3, \epsilon_4, \dots)$. The same is true for the corresponding smooth quantities \tilde{e}_ν , $\Sigma \tilde{e}_\nu$ etc. It must be required that the smooth quantities really behave smoothly in all the variables. To determine if this is the case it is necessary to compare the results of smoothing prescriptions exploiting different variables, some examples being given in this section. A more general investigation of this kind ought to give a good evaluation of the reliability and accuracy of different prescriptions for calculating shell energies.

Note that the smooth energy levels of Fig. 4 are calculated when $f_\nu(\epsilon)$ is replaced with $\tilde{f}_n(\epsilon)$, where

$$\tilde{f}_{n+1}(\epsilon) = \tilde{F}_{N+2} + \frac{\tilde{F}_{N+2} - \tilde{F}_N}{A_{n+1}} \sum_{\nu=1}^n \tilde{A}_\nu \quad (3.11)$$

and $\tilde{F}_N(\epsilon)$ is the smooth version of $F_N(\epsilon)$ and $n = N/2$. It is preferable to do the smoothing in $F_N(\epsilon)$ since this function fluctuates less than $f_\nu(\epsilon)$.

4. THE PAIRING ENERGY

One of the more uncertain factors in the calculation of the pairing energy is whether the pairing force

$$G = \frac{1}{A} \left(g_0 + g_1 \frac{N-Z}{A} \right) \quad (4.1)$$

(plus sign is for protons) is constant or dependent on the nuclear surface area, i.e. g_0 and g_1 should be deformation dependent. The later assumption

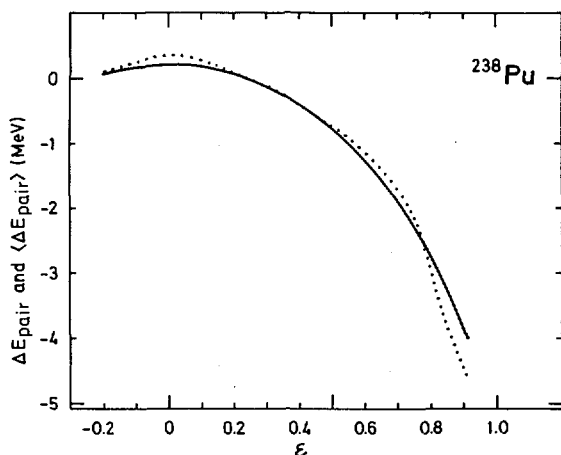


FIG. 10. The difference in the pairing energy between the cases $G \sim S$ and $G = \text{const.}$ (dotted curve), compared with the difference between the corresponding smooth pairing energies calculated from Eq. (4.3) (solid curve).

is based on the fact that it is only the orbitals located near the surface which contribute to the pairing energy, and G is simply postulated to be proportional to the nuclear surface.

It is also known (Refs [4, 7, 17]) that the different assumptions about G necessitate different parameter values in the liquid-drop energy formula. While the case $G \sim S$ agrees with the Myers-Swiatecki formula (Ref. [14]), a revised formula has to be used in the case $G = \text{const.}$ if the fission barriers are to be correctly reproduced. For example, one could change the surface asymmetry constant from the value 1.7826 given by Myers and Swiatecki to 2.53 (Ref. [4]). This means that the pairing energy contains a certain smooth "liquid-drop-like" part. In this section this part will be determined.

Denoting the smooth part of the pairing energy by $\langle E_{\text{pair}} \rangle$, the quantity $\langle E_{\text{pair}} \rangle_{G \sim S} - \langle E_{\text{pair}} \rangle_{G = \text{const.}}$ can be determined as the difference between the liquid-drop energies for the two cases, since the liquid-drop formula was changed just to compensate for the average change in pairing energy.

To get the best possible value of $\langle E_{\text{pair}} \rangle_{G \sim S} - \langle E_{\text{pair}} \rangle_{G = \text{const.}}$ the liquid-drop energies are refitted according to Pauli and Ledergerber [18]. For the modified harmonic oscillator one gets (see also Fig. 10)

$$\begin{aligned} & \langle E_{\text{pair}} \rangle_{G \sim S} - \langle E_{\text{pair}} \rangle_{G = \text{const.}} \\ &= E_{\text{liq. drop}}|_{G = \text{const.}} - E_{\text{liq. drop}}|_{G \sim S} = \langle \Delta E_{\text{pair}} \rangle \end{aligned} \quad (4.2)$$

where

$$\langle \Delta E_{\text{pair}} \rangle = -a_1(1-a_2 I^2) A^{2/3} \left[B_s(\epsilon) - B_s(\epsilon_0) \right]$$

$$a_1 = 0.490 \text{ MeV}$$

$$a_2 = 1.38 \quad (4.3)$$

$$\epsilon_0 = 0.25$$

$$I = \frac{N-Z}{A}$$

B_s is the relative surface area.

The constants are determined at the second saddle point using the calculations by Möller [4], and the formula is relevant only for the lighter actinides and to the extent that it is assumed that the difference in pairing energy can be approximated with a surface energy. For the details of the fitting see Ref. [19]. This calculation does not give any values of $\langle E_{\text{pair}} \rangle_{G \sim S}$ or $\langle E_{\text{pair}} \rangle_{G=\text{const}}$. However, $\langle E_{\text{pair}} \rangle_{G=\text{const}}$ can be estimated to be about -2.3 MeV (Ref. [2]).

However, the use of the smooth levels of either Eq. (3.2) or Eq. (3.11) makes it possible to calculate $\langle E_{\text{pair}} \rangle$. If it is assumed that the levels just above the Fermi surface also are described either by Eq. (3.2) or Eq. (3.11) it is simple to calculate what pairing energy the smooth levels give. It is natural to identify this energy as $\langle E_{\text{pair}} \rangle$. This energy has been calculated both for $G = \text{const.}$ and $G \sim S$. The results confirm within a quarter of an MeV those given by Eq. (4.3). This is also illustrated in Fig. 11. To give an idea of the numerical results, it can be mentioned that $\langle E_{\text{pair}} \rangle_{G=\text{const}}$ for the potential (1.2) is about -2.35 MeV for mass numbers around 175 and decreases slightly with A to about -2.50 MeV for $A \sim 250$. This decrease is dependent on the decrease of $a_{\nu 0}$. Since ω_0/ω'_0 increases with deformation, $\langle E_{\text{pair}} \rangle_{G=\text{const}}$ becomes dependent on deformation and, for $\epsilon = 0.95$, is about -1.95 MeV for $A \sim 175$ and -2.05 MeV for $A \sim 250$. For the potential (1.3) $\langle E_{\text{pair}} \rangle_{G=\text{const}}$ is about -2.20 MeV for $A \sim 175$ and about -2.35 MeV for $A \sim 250$. The variation with the deformation is negligible in this case. For comparison, Jensen and Damgaard [20] obtained fluctuating values in the interval -1.4 to -1.9 MeV for a Woods-Saxon potential using a continuous level density $g(\epsilon)$ as determined by the Strutinsky procedure.

At any rate, the introduction of a consistently determined smooth pairing energy makes it possible to separate that part of the total energy

$$E_{\text{Tot}} = E_{\text{shell.dep.}} + E_{\text{shell.indep.}} \quad (4.4)$$

which depends on shell effects, namely

$$E_{\text{shell.dep.}} = 2 \left(\sum_{\nu=1}^{N/2} \epsilon_{\nu} - \sum_{\nu=1}^{N/2} \tilde{\epsilon}_{\nu} \right) + E_{\text{pair}} - \langle E_{\text{pair}} \rangle \quad (4.5)$$

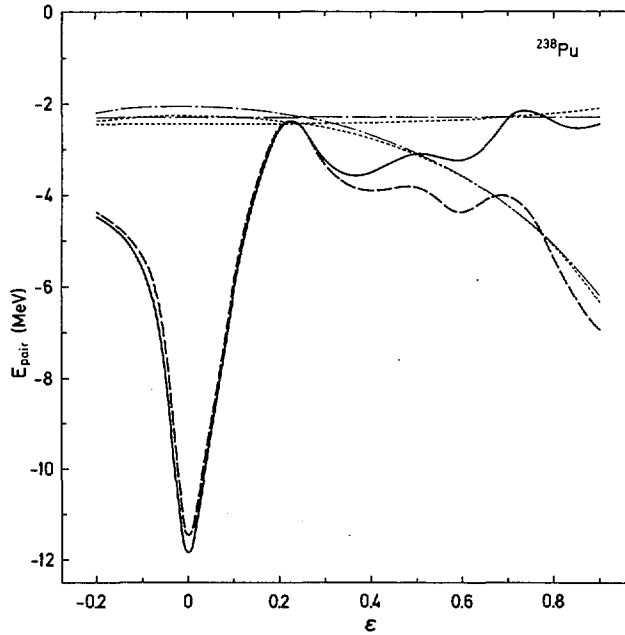


FIG. 11. Total pairing energy (protons + neutrons) for ^{238}Pu . The solid curve is for the case $G=\text{const.}$, and the dashed curve is for the case $G\sim S$. The corresponding smooth energies, $\langle E_{\text{pair}} \rangle_{G=\text{const.}} = -2.3 \text{ MeV}$ and $\langle E_{\text{pair}} \rangle_{G\sim S}$, calculated from Eq.(4.3), are also shown (dot-dashed curves). The apparent bad agreement is because the smooth curves are the result of a fit using many nuclei. For some other nuclei the smooth curves lie almost entirely below the real curves. The dotted curves show the smooth pairing energy (for $G=\text{const.}$ and $G\sim S$ respectively) calculated from the smooth set of energy levels \tilde{e}_ν .

This is in fact the microscopic energy given in Eq.(1.6). However, the name shell-dependent energy is preferred, because $E_{\text{shell dep.}}$ indicates how much the energy of a real nucleus deviates from the energy of a corresponding nucleus without any shell structure. The remaining part of the total energy is then independent of the shell structure and equal to the total energy of the shell-structureless nucleus.

The shell-dependent part of the energy fluctuates around zero. (See e. g. the figures in Ref. [21]). Different prescriptions for the pairing strength essentially cause a change of the magnitude of the fluctuations.

Since Eqs (4.) and (4.5) ensure that all smooth energy contributions must be contained in the shell-independent energy, $E_{\text{shell indep.}}$, this becomes independent of the specific choice of the pairing strength, which in fact is the content of Eq.(4.2). It is evident that $E_{\text{shell indep.}}$ must be equal to the Myers-Swiatecki liquid drop energy (or any equivalent energy) plus the smooth surface-dependent pairing energy if it is assumed that $G\sim S$. Recent calculations by Sobiczewski and co-workers [22] give some support to this assumption. If on the other hand it is assumed that $G=\text{const.}$,

$E_{\text{shell indep.}}$ must still have the same numerical value. This is true since $E_{\text{shell indep.}}$ should reproduce the smooth trend of a number of experimental data, and insofar as no particular single particle model has been used to optimize the parameters (which in fact Pauli and Ledergerber do), $E_{\text{shell indep.}}$ is determined only by the experimental data. However, the macroscopic and microscopic theories must agree in the sense that if in the microscopic theory a surface-dependent pairing force is used, this must also be the case in the macroscopic theory, etc. However, different macroscopic models might reproduce the experimental data more or less well. For example, the surface-dependent pairing energy behaves very much like a surface energy due to deformation but not due to mass number. Thus the equivalence between the pairing and surface energy stated in Eq. (4.2) might be used successfully for the description of the fission barriers, but not for calculating nuclear masses. In this latter case the Myers-Swiatecki mass formula combined with a surface-dependent pairing energy reproduces the experimental masses. The revised liquid drop formula (with $k_s = 2.53$), which reproduces the barriers in connection with a constant pairing energy, fails to reproduce the masses. However, it must be required that any reliable macroscopic mass formula reproduces the experimental masses at least as well as the one given by Myers and Swiatecki [14]. Thus, in a theory using a constant pairing force, $E_{\text{shell indep.}}$ must contain some correction terms in addition to the terms of the type given by Myers and Swiatecki, in order to bring the masses back to the experimental values, which do not allow for much variation; i. e. the value of $E_{\text{shell indep.}}$ must not change although it is described by different formulas.

The simple expression for the surface energy (with $k_s = 2.53$) used previously (Refs[2,4]) in connection with a constant pairing force is in fact not even good for describing the fission barriers. The difference in the calculated barriers (of the order 1 MeV) between the two cases of pairing

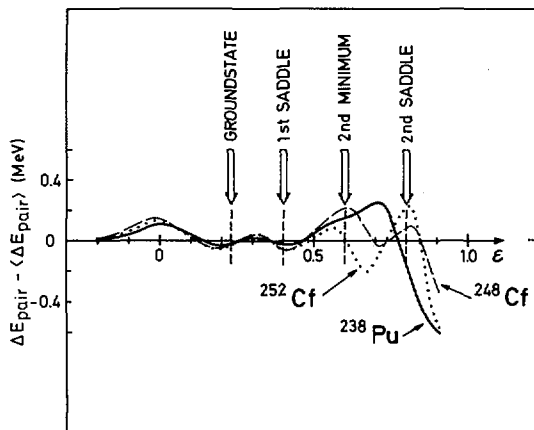


FIG. 12. Resulting total energy change caused by the change of the pairing strength from $G = \text{const.}$ to $G \sim S$.

force mainly reflects the fact that the liquid drop formulas used do not fulfil Eq. (4.2). If Eq. (4.2) is fulfilled, the remaining difference between the two cases of pairing is the one illustrated in Fig. 12, which means that the choice of pairing strength is not so important as has been thought (Refs [2, 4, 8, 17]). The difference is in fact less than 0.5 MeV at the second barrier.

5. SUMMARY

A convenient tool for calculating the shell correction energy has been obtained by introducing the smooth single particle levels. By separating the shell correction energy (which includes the shell-dependent part of the pairing energy) from the smooth energy, a more well-defined value of the smooth energy is obtained which hopefully could be used as a guide in the attempts to determine an improved liquid drop formula. However, more work has to be done to bring down the errors in the numerical calculations. It is also necessary to include more general deformations.

REFERENCES

- [1] BOHR, A., MOTTELSON, B., Nuclear Structure, Vol. 2, Benjamin, New York, to be published.
- [2] NILSSON, S.G., TSANG, C.F., SOBICZEWSKI, A., SZYMAŃSKI, Z., WYCECH, S., GUSTAFSSON, C., LAMM, I.L., MÖLLER, P., NILSSON, B., Nucl. Phys. A131 (1969) 1.
- [3] BENGTTSSON, R., BOLEU, R., to be published.
- [4] MÖLLER, P., Nucl. Phys. A192 (1972) 529.
- [5] LIN, W., Phys. Rev. C2 (1970) 871.
- [6] BOLSTERLI, M., FISET, E.O., NIX, J.R., NORTON, J.L., Phys. Rev. C5 (1972) 1050.
- [7] BRACK, M., DAMGAARD, J., JENSEN, A.S., PAULI, H.C., STRUTINSKY, V.M., WONG, C.Y., Rev. Mod. Phys. 44 (1972) 320.
- [8] MOSEL, U., Phys. Rev. C6 (1972) 971.
- [9] STRUTINSKY, V.M., Nucl. Phys. A95 (1967) 420.
- [10] WILLIAMS, F.C., Jr., CHAN, G., HUIZENGA, R., Nucl. Phys. A181 (1972) 225.
- [11] BENGTTSSON, R., Nucl. Phys. A198 (1972) 591.
- [12] RAMAMURTHY, V.S., KAPOOR, S.S., Phys. Lett. 42B (1972) 399.
- [13] HILLMAN, M., Brookhaven preprint BNL-1763 (1973).
- [14] MYERS, W.D., SWIATECKI, W.H., Nucl. Phys. 81 (1966) 1.
- [15] THEGERSTRÖM, C., Private communication.
- [16] SIEMENS, Ph.J., SOBICZEWSKI, A., Phys. Lett. 41B (1972) 16.
- [17] BRITT, H.C., BOLSTERLI, M., NIX, J.R., NORTON, J.L., Phys. Rev. C7 (1973) 801.
- [18] PAULI, H.C., LEDERGERBER, T., Nucl. Phys. A175 (1971) 545.
- [19] RANDRUP, J., TSANG, C.F., MÖLLER, P., NILSSON, S.G., LARSSON, S.E., Berkeley preprint (1973).
- [20] JENSEN, A.S., DAMGAARD, J., Nucl. Phys. A203 (1973) 578.
- [21] NILSSON, S.G., DAMGAARD, J., Phys. Scr. 6 (1972) 81.
- [22] SOBICZEWSKI, A., BJØRNHOLM, S., POMORSKI, K., Nucl. Phys. A202 (1973) 274.

HARTREE-FOCK CALCULATIONS OF THE FISSION BARRIERS OF PLUTONIUM ISOTOPES

H. FLOCARD, P. QUENTIN*, D. VAUTHERIN

Division de Théorie,
Laboratoire associé au C.N.R.S.,
Institut de Physique Nucléaire,
Orsay, France

A. K. KERMAN**

Laboratory for Nuclear Science and
Department of Physics,
Massachusetts Institute of Technology,
Cambridge, Mass., USA

Abstract

HARTREE-FOCK CALCULATIONS OF THE FISSION BARRIERS OF PLUTONIUM ISOTOPES.

Complete self-consistent calculations with a constraint on the quadrupole moment have been performed to obtain the deformation energy curve of ^{240}Pu beyond the second barrier. Preliminary calculations of the excitation energy of the isomeric state and the first barrier height of ^{238}Pu and ^{244}Pu are also presented.

These calculations were done using a phenomenological effective interaction introduced by Skyrme and used extensively in Hartree-Fock calculations by Vautherin and Brink. This force has been supplemented with the standard pairing interaction. Within the framework of this parametrization of the effective force, an improved set of parameters has been determined which gives total nuclear binding energies within an accuracy of less than 8 MeV for the whole chart of nuclides and reproduces within $\pm 3\%$ the quadrupole moments of permanently deformed nuclei.

The solution of the Hartree-Fock equations is obtained by expanding the Hartree-Fock states into deformed harmonic oscillator eigenstates. A deformation-dependent prescription for the truncation of the oscillator basis is used. Particular attention has been paid to insure the independence of our results with respect to basis parameters. However, for very large deformations such as those occurring near the second fission barrier of heavy nuclei like ^{240}Pu , the basis used here (which would correspond in the spherical case to 13 major shells) appears to be nearly sufficient. Owing to the complexity of numerical calculations, axial symmetry and left-right reflection symmetry have been assumed so far.

Two different prescriptions have been used to introduce pairing correlations. The first consists in keeping a gap constant as a function of deformation for both protons and neutrons. The second introduces a pairing force proportional to the surface.

For the height of the first barrier E_A as well as for the excitation energy E_I of the isomeric states a reasonable agreement with experiments ($E_A \approx 9.0$ MeV, $E_I \approx 3.0$ MeV in ^{240}Pu) is obtained. However, this is no longer the case for the second fission barrier ($E_B \approx 13.0$ MeV in ^{240}Pu). This may be due to the force but there are also errors due to the imposed symmetries and to the lack of numerical convergence at large deformations.

1. INTRODUCTION

One of the most striking successes of the phenomenological calculations using the Strutinsky prescription [1] has been the prediction of doubly humped fission barriers for some actinide [2-6] nuclei. On the other hand, microscopic calculations using the Skyrme effective interaction [7, 8] have already

* Guest scientist from the Department of Theoretical Physics, CEA, Saclay.

** Work supported in part through funds provided by the US Atomic Energy Commission under Contract AT(11-1)-3069.

been shown to give the experimental deformation properties for light and medium nuclei [8-12] and to be very close to phenomenological predictions in these regions of the mass table. It is then interesting to see if a self-consistent calculation of the fission energy curve of heavy elements using a nucleon-nucleon effective interaction leads to the same kind of agreement with experimental data. We present here a calculation performed at Orsay for a typical nucleus of the actinide region, ^{240}Pu , and some preliminary results concerning two neighbouring nuclei, ^{238}Pu and ^{244}Pu .

2. METHOD OF CALCULATION

We have used the Skyrme effective interaction, which consists of a two-body short-range potential and a three-body zero-range interaction, to simulate a linear dependence on density with the set of parameters SIII displayed in Table I. This set of parameters has been fitted to the nuclear binding energies over the whole mass table [11].

In Fig. 1 the error in the total binding energies is shown for more than 100 nuclei covering the periodic table. The calculations are made within a spherical self-consistent formalism including an approximate treatment of pairing. Center-of-mass motion has also been taken into account in an approximate way. For nuclei which do not belong to deformed regions one sees that the mean error in the total binding energy is less than 5 MeV. In the rare-earth region, where the decrease of total energy due to deformation is known to be very important, we have done deformed self-consistent calculations [12]. Once the deformation correction is properly taken into account, it appears that the deviation from experimental masses is again less than 5 MeV. We have particularly insisted upon a precise reproduction of nuclear masses, because numerous works [13-14] have shown that the liquid drop parameters, which are determined by a broad fit to the masses, are strongly correlated with good prediction of fission barriers heights.

TABLE I. PARAMETERS OF THE SKYRME INTERACTION SIII USED IN THESE CALCULATIONS

Notation is that of Ref. [7], i. e. the two-body matrix elements in momentum space are given by

$$\langle \vec{k} | v | \vec{k}' \rangle = t_0(1 + x_0 P_0) + \frac{1}{2}t_1(\vec{k}^2 + \vec{k}'^2) + t_2 \vec{k} \cdot \vec{k}' + iW_0(\vec{\sigma}_1 + \vec{\sigma}_2) \cdot (\vec{k} \times \vec{k}')$$

and the three-body force is chosen to be $t_3 \delta(\vec{r}_1 - \vec{r}_2) \delta(\vec{r}_2 - \vec{r}_3)$

t_0 (MeV · fm ³)	t_1 (MeV · fm ⁵)	t_2 (MeV · fm ⁵)	t_3 (MeV · fm ⁶)	x_0	W_0 (MeV · fm ⁵)
-1123.75	395.0	-95.0	14000.0	0.45	120.0

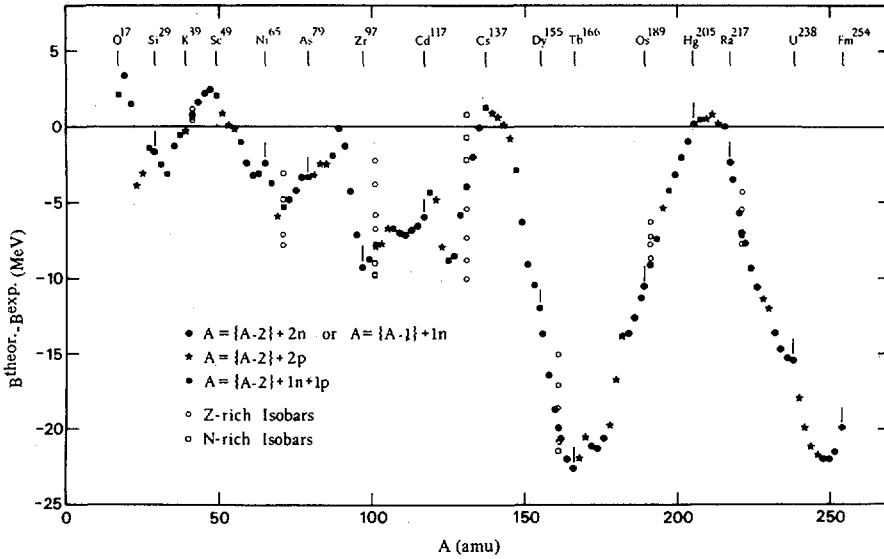


FIG.1. Error in total binding energies using the SIII interaction, as a function of the mass number A . Calculations are made in the spherical formalism (Ref.[7]). The results must be corrected by deformation energies in the rare earth and actinide regions. The path in the chart of the nuclides is defined as follows. Black dots correspond to calculations of nuclei with the addition of one or two neutrons with respect to the neighboring lighter calculated nucleus. Black stars correspond to the addition of two protons, and black squares to the simultaneous addition of one proton and one neutron.

The solution of self-consistent field equations with the Skyrme interaction is equivalent to the minimization of a functional \mathcal{H}' depending on the density ρ and the kinetic density τ [8] defined as

$$\rho = \sum_i v_i^2 |\Phi_i|^2 \quad \text{and} \quad \tau = \sum_i v_i^2 |\Phi_i|^2$$

where the Φ_i represent the individual single particle states, and the pairing effects are contained in the usual B.C.S. quantities u_i and v_i . The functional [8,9] \mathcal{H}' is given in terms of the hamiltonian [7] \mathcal{H} by

$$\mathcal{H}' = \mathcal{H} - f(u_i, v_i)$$

In \mathcal{H} the Coulomb exchange contribution is included within the Slater approximation. We have used two different forms for the function f

$$(A) \quad f(u_i, v_i) = \Delta \Sigma u_i v_i$$

where Δ represents the energy gap; its value has been extracted from odd-even differences in the experimental mass table and has been kept constant along the deformation path [9] (constant gap)

$$(B) \quad f(u_i, v_i) = \frac{G}{2} (\sum u_i v_i)^2$$

where G is the usual pairing interaction strength. Its value has been adjusted to reproduce experimental quasi-particle energies at the ground state deformation. Phenomenological calculations [2] using the same kind of pairing interaction have shown that it is necessary to make G proportional to the liquid drop surface in order to reproduce correct fission barrier heights. In a microscopic self-consistent calculation, the surface of the nucleus is not geometrically well-defined; therefore we have taken G proportional to the surface of an ellipsoidal liquid drop with the quadrupole moment of the self-consistent solution (surface pairing).

In this paper we present calculations of fission curves corresponding to both prescriptions A and B.

For technical reasons we have restricted ourselves to axially symmetric shapes. In addition we have also imposed left-right reflection symmetry. These two restrictions are of great importance for the case of ^{240}Pu , where phenomenological calculations have shown that $\gamma \sim 10^\circ$ for the first barrier [15] and that the second barrier is not left-right symmetric [3, 16]. We shall discuss the possible implications of these restrictions in Section 3.

To describe the fission energy curve it is necessary to constrain the nucleus away from its minima. We have adopted a constraint on the quadrupole moment (Q). Since the necking phenomenon, which requires more moments than Q , is expected to occur beyond the second barrier, it is probably reasonable to use a quadrupole constraint (excluding hexadecapole or higher multipole constraints) up to the second saddle point. To obtain deformation energy curves exhibiting inflection points we have chosen a quadratic form for the constraint [9]. We expand the individual single particle wave functions in eigenvectors of a deformed oscillator well [8, 17]. These eigenvectors are characterized by four quantum numbers: the axial quantum number n_z , the perpendicular quantum number n_\perp , the projection Λ of angular momentum on the symmetry axis of the nucleus, and the spin projection Σ on the same axis. The oscillator well is defined by the two frequencies ω_z and ω_\perp , or equivalently

$$b = \sqrt{m\omega_0/\hbar} \quad \text{with} \quad \omega_0^3 = \omega_z \omega_\perp^2 \quad \text{and} \quad q = \frac{\omega_\perp}{\omega_z}$$

At a given deformation we select all the eigenvectors satisfying the condition:

$$\hbar\omega_z(n_z + \frac{1}{2}) + \hbar\omega_\perp(n_\perp + 1) \leq \hbar\omega_0(N + 2)$$

The number N characterizes the size of the basis. We have made our calculations with $N = 12$, which at the spherical point corresponds to 13 oscillator shells. We have also checked the convergence of our results by calculations with $N = 14$ for the maxima and minima of the fission curve.

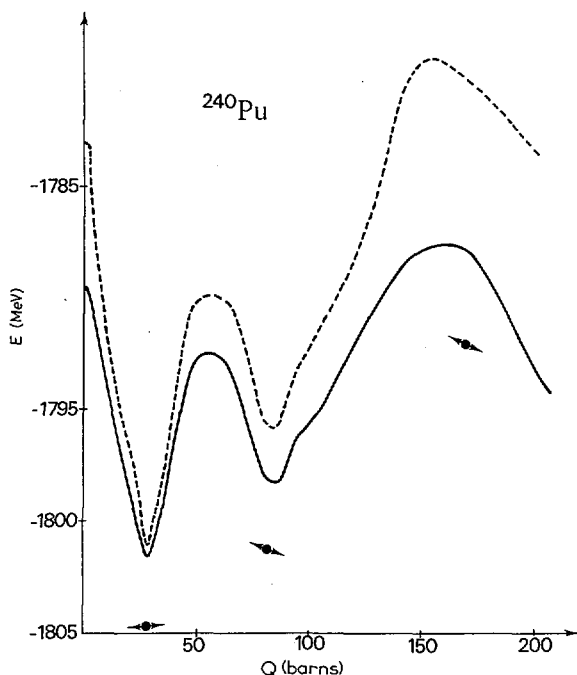


FIG. 2. Calculated deformation energy curves over the fission barrier (with $N=12$). Dashed and solid curves correspond to constant-gap and surface-pairing calculations, respectively. Energies are expressed in MeV. Mass quadrupole moments are given in barns. Three calculated points with a larger basis ($N=14$) are also shown. Double arrows represent calculated slopes of the tangents to the deformation energy curve (for $N=14$) (Ref.[9]).

Special attention has been devoted to a precise estimation of integrals occurring throughout the calculation. Indeed, the high degree of the basis polynomial wave functions corresponding to $N = 12$ or 14 requires a large mesh of integration points. Therefore we have used a 16-point Gauss-Hermite mesh for z integration and a 15-point Gauss-Laguerre mesh for the perpendicular space. Finally we have determined and used at each deformation the parameters b and q which minimize the energy functional as discussed in Ref.[9].

3. RESULTS

Deformation energy curves for both constant-gap and surface pairing calculations are plotted on Fig. 2.

The calculated ground state deformations are in good agreement with experiment. For example, in the surface pairing calculation we have obtained for charge quadrupole (Q) and hexadecapole (h) moments¹, 11.29 barns and 1.06 barns² to be compared with Coulomb excitation data [18] (11.58 ± 0.06 barns and 1.15 ± 0.28 barns²).

¹ Defined as $Q = \langle 2 r^2 P_2 \rangle$ and $h = \langle r^4 Y_{40} \rangle$.

TABLE II. VARIATION OF VARIOUS CALCULATED QUANTITIES WITH DEFORMATION

For a given mass quadrupole moment Q in barns, we have evaluated β_2 and β_4 parameters of a sharp-edged liquid drop for both mass and charge distributions. The Myers and Swiatecki value $r_0 = 1.2049$ fm of the radius parameter has been used. The quantity $V = \sqrt{\langle z^2 \rangle \langle \rho^2 \rangle}$, in arbitrary units, is also given. The expectation values of Coulomb energy (direct plus exchange in the Slater approximation) are given in MeV, and those of J^2 in units of \hbar^2 .

Q	β_2^C	β_2^M	β_4^C	β_4^M	V	$\langle E_{\text{coul}} \rangle$	$\langle J^2 \rangle$	
-0.08	0.001	0.001	0.015	0.015	152.9	979.42		Spherical point
19.54	0.173	0.174	0.044	0.044	151.6	980.09		
28.48	0.243	0.241	0.074	0.073	151.6	977.64	366.6	Ground state
37.53	0.319	0.313	0.069	0.068	152.3	972.87		
49.90	0.453	0.447	-0.032	-0.032	153.9	965.82		Near first barrier top
68.36	0.569	0.565	0.024	0.026	153.2	956.85		
81.84	0.660	0.650	0.050	0.052	153.7	948.62	959.4	Isomeric state
95.77	0.720	0.724	0.116	0.106	154.2	939.99		
125.84	0.782	0.767	0.307	0.307	154.8	921.52		
169.72	1.010	0.997	0.351	0.355	156.2	895.82		Near second barrier top
202.11	1.183	1.164	0.398	0.400	160.4	876.29		

Values of the β_2 and β_4 parameters of a sharp-edged liquid drop with the self-consistent quadrupole and hexadecapole moments are given in Table II. Inspection of this table shows that charge and mass distributions are very similar: $|\beta_2^C - \beta_2^M| \leq 0.03$ and $|\beta_4^C - \beta_4^M| \leq 0.01$.

A crude estimation of the volume is also given in this table, i.e. a quantity V proportional to $\sqrt{\langle z^2 \rangle \langle \rho^2 \rangle}$, which itself is proportional to the volume of a pure ellipsoidal shape. This quantity exhibits a minimum near the ground state deformation and local maxima for sphericity and at the top of the first barrier. Variations from the spherical value are less than 1% to a point beyond the isomeric state. Past this point, V increases rapidly. Bearing in mind the crudeness of the estimation, this is consistent with a rough volume conservation and seems to indicate, as expected, that in the vicinity of the second barrier the nuclear shape differs more and more from a pure ellipsoid. A more interesting point concerns the decrease of V from

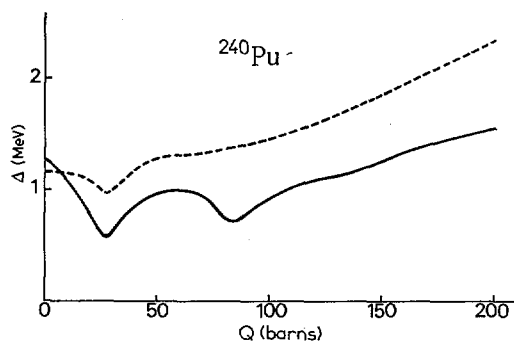


FIG. 3. Neutron and proton pairing gaps (in MeV) from the surface pairing calculations, as a function of mass quadrupole moment in barns. Solid and dashed curves correspond to neutron and proton curves respectively.

sphericity to the deformation defined by $Q \sim 20$ barns, which is correlated with an increase of the Coulomb energy. This effect, previously observed in a self-consistent calculation [9] of ^{150}Ce , seems to indicate a contraction of the nucleus which produces a bump of ~ 3 MeV in the Coulomb energy.

The secondary minimum is found to correspond to a deformation $\beta \sim 0.65$ or to a ratio of axes for an equivalent ellipsoid $q \sim 1.85$. This is roughly consistent with theoretical estimates based on the special degeneracy of the harmonic oscillator level scheme [19] around $q \sim 2$ (for a number of neutrons around 146). It is also in agreement with the deformation deduced from the measured rotational properties in the second well [20].

In Fig. 3 proton and neutron pairing gaps for surface pairing calculations are exhibited. Fluctuations in these curves imply shell effects. Apart from an increase of the gap versus deformation, one sees that the ground state shell effect is due to both proton and neutron single particle spectra, while neutrons alone are responsible for the shell effect at the isomeric state.

We turn now to the discussion of calculated energies. As expected, constant gap calculations give higher fission barriers than surface pairing calculations. For the second barrier the difference is found to be 7.5 MeV. As in previous phenomenological approaches [2] we consider energies calculated with surface pairing. Before comparison with experiment and in order to put the results in proper perspective we make the following points:

- (a) The static character of our calculations. One has to consider the possible distortion of the effective deformation energy curve when taking into account the effect of the inertial parameters evaluated e.g. by some generator coordinate or other method. In particular such a method will be necessary for the actual evaluation of fission properties, including life-times.
- (b) Self-consistent solutions are only intrinsic and, for even-even nuclei, the physical 0^+ ground state needs to be projected out. Assuming a

perfect rotational character of the projected spectra one can estimate [21, 22] the corresponding energy gain (using the usual notation) by

$$E_{\text{intrinsic}} - E_{0^+} = \frac{\hbar^2}{2J} \langle J^2 \rangle$$

From experimental moments of inertia for ground states [23] and isomeric states [20] one calculates a rotational zero point energy for these two deformations. Such an evaluation, in the case of self-consistent calculations, is free from the criticism of Ross and Warke [24] which applies only to Strutinsky-type calculations. In contrast with the results of Ref. [22], rather different corrections for ground and isomeric states are found (2.4 and 3.2 MeV, respectively).

- (c) Even though the fit of masses obtained in self-consistent calculations with our effective interaction is very satisfactory, it cannot be excluded that the liquid drop parameters deduced from it are not yet sufficiently good to allow a perfect reproduction of fission barrier heights. Work is in progress to determine e.g. the surface tension parameter by various approaches.
- (d) Convergence of our calculations have been tested by calculations with an enlarged basis ($N = 14$). Such tests indicated that the difference between $N = 12$ and $N = 14$ calculations is ~ 1 MeV for the second barrier height. This leads to an estimate < 2 MeV for the decrease of this quantity due to truncation effects.
- (e) It is expected that left-right asymmetry is needed to describe accurately the second saddle point [3, 16]. The decrease of the corresponding barrier has been evaluated in Refs [3] and [16] to be ~ 3 MeV. A similar discussion could have been made for the first barrier, where the inclusion of γ -asymmetry is expected to decrease the barrier height by ~ 1 MeV [15].

Bearing in mind the previous considerations (especially points (d) and (e)) one finds a reasonable agreement between calculated values and available experimental data, summarized in Table III.

Preliminary calculations of ^{238}Pu and ^{244}Pu have been performed for the height of the first fission barrier E_A and the isomeric excitation energy E_I . They indicate that E_A increases by 1.4 MeV, going from ^{238}Pu to ^{244}Pu .

TABLE III. EXPERIMENTAL ESTIMATIONS OF HEIGHTS OF FIRST (E_A) AND SECOND (E_B) BARRIERS AND OF ISOMERIC STATE EXCITATION ENERGIES (E_I)

Reference	E_A (MeV)	E_I (MeV)	E_B (MeV)
Björnholm and Lynn [25]	6.0 ± 0.2	2.0 ± 0.2	5.4 ± 0.2
Britt et al. [26]	6.0	2.0	5.35
Weigmann and Theobald [27]	6.05	2.35	

This trend seems in disagreement² with recent experimental analysis [26]. Within the accuracy of the estimation, the quantity E_1 seems constant for these 3 isotopes (4 MeV).

4. CONCLUSION

We conclude that the technical problems of self-consistent calculations are essentially solved, even for deformations over the fission saddle point in heavy nuclei. Bearing in mind the possibility that it may still be necessary to modify the effective force when all of the five points discussed above have been investigated, it appears that this type of calculation should be considered as quite reliable for purposes of extrapolation to new regions of the periodic table. It should also be said that proper dynamical calculations will probably require some form of self-consistent approach as a basis. Finally we point out that we have already quite remarkable agreement with single particle spectra, radii, shapes, masses and barriers with only 7 parameters in total.

ACKNOWLEDGEMENTS

We would like to express our appreciation to M. Veneroni and M. Beiner for interesting discussions. Two of us (P. Quentin and D. Vautherin) would like to thank Professor G.E. Brown for helpful comments and for his hospitality at the State University of New York at Stony Brook during the summer of 1972. The authors are also grateful to the Service de calcul de la Faculté des Sciences d'Orsay for the use of computing facilities.

REFERENCES

- [1] STRUTINSKY, V.M., Nucl. Phys. A95 (1967) 420; A122 (1968) 1.
- [2] NILSSON, S.G., TSANG, C.F., SOBICZEWSKI, A., SZYMANSKI, Z., WYCECH, S., GUSTAFSON, C., LAMM, I.L., MÖLLER, P., NILSSON, B., Nucl. Phys. A131 (1969) 1.
- [3] BOLSTERLI, M., FISET, E.O., NIX, J.R., NORTON, J.L., Phys. Rev. C5 (1972) 1050.
- [4] BRACK, M., DAMGAARD, J., JENSEN, A.S., PAULI, H.C., STRUTINSKY, V.M., WONG, C.Y., Rev. Mod. Phys. 44 (1972) 320.
- [5] ANDERSEN, B.L., DICKMANN, F., DIETRICH, K., Nucl. Phys. A159 (1970) 337.
- [6] MOSEL, U., SCHMITT, H.W., Nucl. Phys. A165 (1971) 73.
- [7] VAUTHERIN, D., BRINK, D.M., Phys. Rev. C5 (1972) 626.
- [8] VAUTHERIN, D., Phys. Rev. C7 (1973) 296.
- [9] FLOCARD, H., QUENTIN, P., KERMAN, A.K., VAUTHERIN, D., Nucl. Phys. A203 (1973) 433.
- [10] CAILLIAU, M., LETESSIER, J., FLOCARD, H., QUENTIN, P., to be published in Phys. Lett. (mercury isotopes).
- [11] BEINER, M., FLOCARD, H., GIALI, N.V., QUENTIN, P., to be published (SIII interaction and s-d region).
- [12] FLOCARD, H., QUENTIN, P., VAUTHERIN, D., to be submitted to Phys. Lett. (rare earth region).
- [13] MYERS, W.D., SWIATECKI, W.J., Nucl. Phys. 81 (1966) 1.
- [14] PAULI, H.C., LEDERGERBER, T., Nucl. Phys. A175 (1971) 545.
- [15] PASHKEVICH, V.V., Nucl. Phys. A133 (1969) 400; LARSSON, S.E., RAGNARSSON, I., NILSSON, S.G., Phys. Lett. 38B (1972) 269; GÖTZ, U., PAULI, H.C., JUNKER, K., Phys. Lett. 39B (1972) 436.

² Including proper axial asymmetry seems to improve the agreement with experimental data [28].

- [16] MÖLLER, P., NILSSON, S.G., Phys. Lett. 31B (1970) 283; PAULI, H.C., LEDERGERBER, T., BRACK, M., Phys. Lett. 34B (1971) 264; PASHKEVICH, V.V., Nucl. Phys. A169 (1971) 275; MUSTAFA, M.G., MOSEL, U., SCHMITT, H.W., Phys. Rev. Lett. 28 (1972) 1050.
- [17] TIERPE, D.R., BASSICHIS, W.H., KERMAN, A.K., Nucl. Phys. A142 (1970) 49.
- [18] BEMIS, C.E., et al., Oak Ridge preprint (1973) submitted for publication in Phys. Rev.
- [19] SHELIN, R.K., RAGNARSSON, I., NILSSON, S.G., Phys. Lett. 41B (1972) 15; RAGNARSSON, I., private communication.
- [20] SPECHT, H.J., et al., Phys. Lett. 41B (1972) 43.
- [21] BASSICHIS, W.H., KERMAN, A.K., SVENNE, J.P., Phys. Rev. 160 (1967) 746.
- [22] KELSON, I., SHOSHANI, Y., Phys. Lett. 40B (1972) 58.
- [23] LEDERER, C.M., HOLLANDER, J.M., PERLMAN, I., Table of Isotopes, Wiley, New York (1968).
- [24] ROSS, C.K., WARKE, C.S., Phys. Rev. Lett. 30 (1973) 55.
- [25] BJÖRNHOLM, S., LYNN, E., unpublished results quoted in Ref.[14].
- [26] BRITT, H.C., et al., Phys. Rev. C7 (1973) 801.
- [27] WEIGMANN, H., THEOBALD, J.P., Nucl. Phys. A187 (1972) 305.
- [28] LARSSON, S.E., LEANDER, G., Paper IAEA-SM-174/6, these Proceedings, Vol. 1.

DISCUSSION

C.F. TSANG: Have you calculated the volume and surface energy coefficients for your Hartree-Fock results using the Skyrme force with your newly determined parameters and how do they compare with empirical values? One way to extract these coefficients is to calculate the smooth energy part of the Hartree-Fock result by means of the method described by Brack³.

P. QUENTIN: There are many ways of extracting liquid drop parameters corresponding to a given effective interaction from Hartree-Fock results. One consists in playing the same game with calculated binding energies as liquid drop practitioners do with experimental ones. Another consists in calculating E/A and the symmetry-energy coefficient in nuclear matter. This gives -15.87 and 28.15 MeV respectively for the SIII Skyrme interaction, which is in good agreement with the usual liquid drop parameters. To obtain an estimate of the surface tension one could perform a semi-infinite nuclear matter calculation. Finally, I agree that liquid drop parameters could be extracted from the analysis of the behaviour of the smooth contribution \bar{E} to the energy using Brack's formalism. All these various possibilities are now being pursued.

³ See BRACK, M., QUENTIN, P., Paper IAEA-SM-174/98, these Proceedings, Vol. 1.

TEST OF STRUTINSKY'S METHOD USING HARTREE-FOCK RESULTS*

M. BRACK†

State University of New York at Stony Brook,
United States of America

P. QUENTIN**

Institut de Physique Nucléaire,
Division de Physique Théorique,
Orsay, France

Abstract

TEST OF STRUTINSKY'S METHOD USING HARTREE-FOCK RESULTS.

New results of Hartree-Fock (HF) calculations are used to estimate the validity of Strutinsky's shell-correction method in a way which is independent of the shell and liquid-drop models usually involved. Strutinsky writes the total binding energy E of a nucleus as sum of a classical liquid-drop (LD)-model energy E_{LD} and a shell correction energy δE , which is extracted from a sum of shell model energies ϵ_i . Here the HF energy is decomposed into three terms: $E_{HF} = \bar{E} + \delta E_1 + \delta E_2$, where \bar{E} is an average binding energy, δE_1 is a first order shell correction and δE_2 contains all higher order corrections, which usually are neglected in the Strutinsky method. By explicitly calculating E_{HF} , \bar{E} , and δE_1 , these higher order corrections are evaluated and the reliability of the shell-correction method from the HF point of view is estimated. The HF results were obtained using the effective δ -interaction of Skyrme in a new parametrization (SIII) which was recently demonstrated to give excellent fits to experimental ground-state energies, deformations and radii throughout the periodic table. A quadratic constraint of the quadrupole moment Q was used to obtain deformation energy curves. Pairing effects were included. Having calculated the self-consistent density matrix ρ , its average part $\bar{\rho}$ is determined by the usual energy averaging procedure. The HF energy can then be decomposed into the three terms stated above, of which \bar{E} is solely dependent on smooth quantities like $\bar{\rho}$. δE_1 contains the first-order and δE_2 all higher order terms in $\delta\rho = \rho - \bar{\rho}$. As a result of these computations, it is found that the quantity \bar{E} indeed behaves exactly like a LD model energy as a function of deformation. This, in itself, strongly confirms Strutinsky's renormalization method. The corrections δE_2 are found to have values of ~ 0.5 to ~ 3.0 MeV for nuclei with $A \geq 100$. Since only their oscillations contribute to the shell corrections, a reliability of the Strutinsky-calculated shell corrections to ground-state energies of $\sim 1-2$ MeV is concluded for medium and heavy nuclei. Similarly, the Strutinsky-calculated fission barriers are found to be affected by less than ~ 1 MeV. Fission lifetime estimates are expected to be lowered by inclusion of the second order correction.

INTRODUCTION

The present paper is devoted to an analysis of the shell-correction method introduced by Strutinsky [1,2], in terms of Hartree-Fock (HF) theory. Ever since the shell-correction method was used in calculations of nuclear deformation energies, the question has been asked to what extent this method is consistent with entirely microscopic descriptions of the nucleus using realistic effective nuclear interactions. Strutinsky pointed out [2] that the shell-correction expression for the total nuclear binding energy $E = E_{LD} + \delta E$

* Work supported in part by the US Atomic Energy Commission.

† Present address: Niels Bohr Institute, University of Copenhagen, Copenhagen, Denmark.

** Guest scientist from the Department of Theoretical Physics, CEA, Saclay.

can be obtained from a HF solution by defining an average part $\bar{\mathcal{G}}$ of the self-consistent density matrix \mathcal{G} and expanding the HF energy around $\bar{\mathcal{G}}$. In this way, one finds

$$E_{\text{HF}} = \bar{E} + \delta E_1 + \delta E_2 + \dots, \quad (1)$$

where \bar{E} depends only on smooth quantities like $\bar{\mathcal{G}}$, and the corrections δE_1 , δE_2 , etc. are of increasing order in the difference $\delta\mathcal{G} = \mathcal{G} - \bar{\mathcal{G}}$:

$$\delta E_n \propto O[(\delta\mathcal{G})^n]. \quad (2)$$

The fluctuations $\delta\mathcal{G}$ of the density matrix are expected to be relatively small [3] and the shell-correction expansion (1) should therefore converge rapidly.

So far, in all practical applications of the method, the second and higher order terms have been neglected. Usually, the smooth part \bar{E} is replaced by a liquid-drop (LD) energy E_{LD} , and the first order shell correction δE_1 (often also written as δU) is extracted from the eigenenergies \mathcal{E}_i of an average shell model potential [2-5]. An explicit expression for the second order shell correction δE_2 has been given in terms of shell model quantities only [3,5]. Bunatyan et al. [5] calculated δE_2 using Migdal's theory for a series of nuclei in the lead region and found δE_2 to be of the order of 0.5 to 3 MeV. Compared to the first order shell correction δE_1 which varies in that region from +5 to -13 MeV, these numbers are indeed quite small. Knowing that the shell effects are largest in spherical nuclei and extrapolating the quoted results to deformed nuclei, one would not expect the higher order terms to affect the usually calculated fission barriers by more than ± 0.5 to 1 MeV.

No consistent test of the shell-correction expansion (1) has so far been performed using HF results only. Bassichis et al. [6] proposed a method which differs slightly from the one outlined by Strutinsky and which will be discussed in this paper; but no results have been published yet. The same authors [7] recently compared HF results to a shell-correction calculation in which the parameters of a Nilsson potential and the liquid-drop model were fitted to give the least deviations from the HF results. However, they did not include the pairing interaction which is known to smooth out the shell effects in deformed nuclei. Furthermore, their test is dependent on the choice of a LD and a shell model, and therefore their conclusions, quoting a 30% unreliability of the first-order shell correction, cannot be considered to be very significant.

Within the last few years, the effective δ -interaction of Skyrme [8] has been successfully applied in HF calculations of both spherical [9] and deformed nuclei [10-14]. Encouraged by their success, we have used these results to perform the decomposition of the HF energy into the shell-correction

series (1). By explicitly calculating its first two terms \bar{E} and δE_1 , we can determine the sum of all higher order terms and check the convergence of the series (1) numerically. In addition, we can see whether the smooth part \bar{E} really behaves like a LD model quantity. This test is thus entirely independent of any LD or shell model parameters; on the other hand, it only tests the Strutinsky method within the HF framework. The only quantity which has to be defined ad hoc and exceeds the HF theory is the smooth part \bar{E} of the density matrix. We define it here consistently by applying Strutinsky's energy-averaging method [1-5].

In the first part of this paper we will present the detailed formalism of our calculations and in the second part present some numerical results and discuss their consequences.

THE METHOD

We first repeat here the main equations of the constraint Hartree-Fock (CHF) method using Skyrme's effective interaction, as described in detail in earlier publications [9-11].

The total binding energy of a nucleus with neutron and proton numbers N, Z and the total (mass-) quadrupole moment Q is found by minimizing the following functional:

$$\delta \{ \langle T + V_{\text{Sky}} \rangle + f(\mu, \langle Q \rangle) + E_{\text{pair}}(\lambda_q, n_i^q) \} = 0, \quad (3)$$

In eq.(3), V_{Sky} is the Skyrme interaction including spin-orbit term and Coulomb interaction [9,10]; $f(\mu, \langle Q \rangle)$ is a constraint of the quadrupole moment [11] and $E_{\text{pair}}(\lambda_q, n_i^q)$ is a pairing energy functional [10] depending on the single-particle occupation numbers n_i^q . The index q labels the isospin state of the nucleons, i.e. neutrons or protons. The Lagrange parameters μ and λ_q in (3) are used for the constraints

$$\langle Q \rangle = Q, \quad (4)$$

$$\sum_i n_i^p = Z, \quad \sum_i n_i^n = N. \quad (5)$$

The expectation values are taken between Slater determinants of orthonormalized single-particle wavefunctions $\Phi_i^q(\mathbf{r})$ which are expanded in a deformed harmonic oscillator basis $\{\varphi_\alpha(\mathbf{r})\}$:

$$\Phi_i^q(\mathbf{r}) = \sum_{\alpha=1}^{\infty} c_{\alpha}^{iq} \varphi_{\alpha}(\mathbf{r}) \quad (q = n, p) \quad (6)$$

The expansion coefficients c_{α}^{qi} and the occupation numbers n_i^q define the density matrices $\rho_{\alpha\beta}^q$:

$$\rho_{\alpha\beta}^q = \sum_i n_i^q (c_{\alpha}^{qi})^* c_{\beta}^{qi}, \quad (q = n, p) \quad (7)$$

$$\rho_{\alpha\beta} = \rho_{\alpha\beta}^n + \rho_{\alpha\beta}^p.$$

One of the advantages of the Skyrme interaction is that the expectation value of the total Hamiltonian $H = T + V_{\text{Sky}}$ for an even-even nucleus can be written as integral over an energy density $\mathcal{E}(\underline{r})$ [9]:

$$\langle H \rangle = \int d^3r \mathcal{E}(\underline{r}). \quad (8)$$

Here $\mathcal{E}(\underline{r})$ is a relatively simple algebraic function of the spatial densities $\rho_q(\underline{r})$, the kinetic energy densities $\tau_q(\underline{r})$ and the spin-orbit densities $\underline{J}_q(\underline{r})$ defined by

$$\rho_q(\underline{r}) = \sum_i n_i^q |\Phi_i^q(\underline{r})|^2 = \sum_{\alpha\beta} \rho_{\alpha\beta}^q \varphi_{\alpha}^*(\underline{r}) \varphi_{\beta}(\underline{r}),$$

$$\tau_q(\underline{r}) = \sum_i n_i^q |\underline{\nabla} \Phi_i^q(\underline{r})|^2 = \sum_{\alpha\beta} \rho_{\alpha\beta}^q \underline{\nabla} \varphi_{\alpha}^*(\underline{r}) \cdot \underline{\nabla} \varphi_{\beta}(\underline{r}),$$

$$\underline{J}_q(\underline{r}) = (-i) \sum_i n_i^q \Phi_i^q(\underline{r})^* (\underline{\nabla} \times \underline{\sigma}) \Phi_i^q(\underline{r}) = (-i) \sum_{\alpha\beta} \rho_{\alpha\beta}^q \varphi_{\alpha}^*(\underline{r}) (\underline{\nabla} \times \underline{\sigma}) \varphi_{\beta}(\underline{r}),$$

and

$$\rho(\underline{r}) = \rho_n(\underline{r}) + \rho_p(\underline{r}), \quad \tau(\underline{r}) = \tau_n(\underline{r}) + \tau_p(\underline{r}), \quad \underline{J}(\underline{r}) = \underline{J}_n(\underline{r}) + \underline{J}_p(\underline{r}).$$

The explicit expression for $\mathcal{E}(\underline{r})$ is [9,10]

$$\begin{aligned} \mathcal{E}(\underline{r}) = & \frac{\hbar^2}{2m} \tau(\underline{r}) + t_3 \frac{1}{4} \rho_n(\underline{r}) \rho_p(\underline{r}) \rho(\underline{r}) \\ & + \frac{1}{2} t_0 \left[\left(1 + \frac{1}{2} \chi_0\right) \rho^2(\underline{r}) - \left(\chi_0 + \frac{1}{2}\right) (\rho_n^2(\underline{r}) + \rho_p^2(\underline{r})) \right] \\ & + \frac{1}{4} (t_1 + t_2) \rho(\underline{r}) \tau(\underline{r}) + \frac{1}{8} (t_2 - t_1) (\rho_n \tau_n + \rho_p \tau_p) \\ & + \frac{1}{16} (t_2 - 3t_1) \rho(\underline{r}) \nabla^2 \rho(\underline{r}) + \frac{1}{32} (3t_1 + t_2) (\rho_n \nabla^2 \rho_n + \rho_p \nabla^2 \rho_p) \\ & - \frac{1}{2} W_0 (\rho(\underline{r}) \underline{\nabla} \cdot \underline{J}(\underline{r}) + \rho_n \underline{\nabla} \cdot \underline{J}_n + \rho_p \underline{\nabla} \cdot \underline{J}_p) \\ & + V_{\text{CD}}(\underline{r}) \rho_p(\underline{r}) + \frac{3}{4} V_{\text{CE}}(\underline{r}) \rho_p(\underline{r}), \end{aligned} \quad (10)$$

with the Skyrme parameters t_0, t_1, t_2, t_3, x_0 and W_0 . $V_{CD}(\underline{r})$ and $V_{CE}(\underline{r})$ are the direct and the exchange part of the Coulomb potential; the former is given by

$$V_{CD}(\underline{r}) = \int d^3\underline{r}' \rho_p(\underline{r}') \frac{e^2}{|\underline{r} - \underline{r}'|} \quad (11a)$$

and the latter by

$$V_{CE}(\underline{r}) = -\left(\frac{3}{\pi}\right)^{1/3} e^2 \rho_p^{1/3}(\underline{r}), \quad (11b)$$

where the Slater approximation has been used [15].

The quadrupole moment Q of the nucleus can be written in terms of the densities $\rho_q(\underline{r})$ and the quadrupole operator \hat{q}_q as

$$Q = \langle Q_p \rangle + \langle Q_n \rangle, \quad (12)$$

$$\langle Q_q \rangle = \int d^3\underline{r} \hat{q}_q \rho_q(\underline{r}).$$

A variation of the wavefunctions $\Phi_i^q(\underline{r})$ in (3) leads to the following Schrödinger equation which defines the single-particle energies ϵ_i^q :

$$\left[-\nabla^2 \frac{\hbar^2}{m_q^*(\underline{r})} + U_q(\underline{r}) + \underline{W}_q(\underline{r}) \cdot (-i)(\nabla \times \underline{\sigma}) + \hat{q}_q \cdot \frac{\partial f(\mu, \nu)}{\partial \nu} \Big|_{\nu=0} \right] \Phi_i^q(\underline{r}) = H_q \Phi_i^q(\underline{r}) = \epsilon_i^q \Phi_i^q(\underline{r}). \quad (13)$$

The effective masses $m_q^*(\underline{r})$, the local HF potentials $U_q(\underline{r})$ and the spin-orbit form factors $\underline{W}_q(\underline{r})$ are given by

$$\frac{\hbar^2}{2m_q^*(\underline{r})} = \frac{\hbar^2}{2m} + \frac{1}{4}(t_1 + t_2)\rho(\underline{r}) + \frac{1}{8}(t_2 - t_1)\rho_q(\underline{r}), \quad (14)$$

$$\begin{aligned} U_q(\underline{r}) = & t_0 \left[\left(1 + x_0 \frac{1}{2}\right) \rho(\underline{r}) - \left(x_0 + \frac{1}{2}\right) \rho_q(\underline{r}) \right] + \frac{1}{4} t_3 (\rho^2 - \rho_q^2) \\ & + \frac{1}{4} (t_1 + t_2) \tau(\underline{r}) + \frac{1}{8} (t_2 - t_1) \tau_q(\underline{r}) \\ & + \frac{1}{8} (t_2 - 3t_1) \nabla^2 \rho(\underline{r}) + \frac{1}{16} (3t_1 + t_2) \nabla^2 \rho_q(\underline{r}) \\ & + \delta_{q,p} (V_{CD}(\underline{r}) + V_{CE}(\underline{r})) - \frac{1}{2} W_0 (\nabla \cdot \underline{J}(\underline{r}) + \nabla \cdot \underline{J}_q(\underline{r})), \end{aligned} \quad (15)$$

$$\underline{W}_q(\underline{r}) = \frac{1}{2} W_0 (\nabla \rho(\underline{r}) + \nabla \rho_q(\underline{r})). \quad (16)$$

Variation of the occupation numbers n_i^q in (3) under the constraints (5) leads to a set of "generalized BCS equations" whose explicit form depends on the pairing functional chosen [10]. For the functional

$$E_{\text{pair}} = - \sum_q G_q \left\{ \sum_i \sqrt{n_i^q (1-n_i^q)} \right\}^2 \quad (17)$$

with constant pairing strengths G_n and G_p , one obtains the familiar BCS equations [16]

$$\frac{2}{G_q} = \sum_i \frac{1}{\sqrt{(\varepsilon_i^q - \lambda_q)^2 + \Delta_q^2}}, \quad (18)$$

$$n_i^q = \frac{1}{2} \left[1 - \frac{\varepsilon_i^q - \lambda_q}{\sqrt{(\varepsilon_i^q - \lambda_q)^2 + \Delta_q^2}} \right] \quad (19)$$

Vautherin [10] and Flocard et al. [11-14] chose in some calculations a different pairing functional

$$E'_{\text{pair}} = -2 \sum_q \Delta_q \left(\sum_i \sqrt{n_i^q (1-n_i^q)} \right), \quad (20)$$

in which the gaps Δ_q are kept constant and the n_i^q are again given by eq.(19).

As discussed in ref. [11], a quadratic constraint

$$f(\mu, \langle Q \rangle) = \frac{1}{2} c (\mu - \langle Q \rangle)^2 \quad (21)$$

is suitable to describe the deformation energy curve $E_{\text{HF}}(Q)$ in a monotonic way with the Lagrange parameter μ . In eq.(21), c is a constant which can be chosen once and for all in a certain region of nuclei [11].

Once a selfconsistent solution of the HF equations (13) is found, the total binding energy of the nucleus under consideration is given by (8) and (10):

$$E_{\text{HF}} = E_{\text{kin}} + E_{\text{pot}} + E_{\text{pair}}, \quad (22)$$

where the kinetic energy E_{kin} is the integral over the first term in eq.(10) and the potential energy E_{pot} is the integral over the sum of all other terms in (10). The HF energy can also be expressed in terms of the single-particle energies ε_i^q , by means of eq.(13):

$$E_{\text{HF}} = \sum_{q,i} \varepsilon_i^q n_i^q - E_{\text{pot}} + E_R - E_{\text{const}} + E_{\text{pair}}. \quad (23)$$

In eq.(23) E_R is a rearrangement energy term coming from the density-dependent part of the Skyrme interaction and the Coulomb exchange part; E_{const} is a constraint energy. In detail

$$E_R = -\frac{1}{4} t_3 \int d^3r \rho_n(r) \rho_p(r) \rho(r) - \frac{1}{2} \int d^3r V_{CE}(r) \rho_p(r), \quad (24)$$

$$E_{const} = Q \cdot \left. \frac{\partial f(\mu, \nu)}{\partial \nu} \right|_{\nu=Q}. \quad (25)$$

It is the expression (23) from which one has to start [2,3,5] in order to obtain the shell-correction expansion (1). For this purpose we must introduce a smooth part of the density matrix $\bar{\rho}$. "Smooth" here means slowly varying with deformation Q and nucleon numbers N and Z . Strutinsky's energy-averaging procedure [1,2] here immediately suggests itself. With this, the average density matrices are given by

$$\bar{\rho}_{\alpha\beta}^q = \sum_i \bar{n}_i^q (c_{\alpha}^i)^* c_{\beta}^i, \quad (26)$$

$$\bar{\rho}_{\alpha\beta} = \bar{\rho}_{\alpha\beta}^n + \bar{\rho}_{\alpha\beta}^p,$$

where the HF occupations numbers n_i^q in eq.(7) are replaced by some averaged occupation numbers \bar{n}_i^q . These are defined using an averaging function $f_M(x)$ (which includes curvature-corrections of order M) [3-5]:

$$\bar{n}_i^q = \frac{1}{\gamma} \int_{-\infty}^{\bar{\lambda}_q} dE f_M\left(\frac{E - \epsilon_i^q}{\gamma}\right). \quad (27)$$

The Fermi energies $\bar{\lambda}_q$ are determined by equations analogous to (5).

Using eqs. (9),(12),(14)-(16), we now define analogous averaged quantities $\bar{\rho}_q(r)$, $\bar{\tau}_q(r)$, $\bar{j}_q(r)$, and in turn \bar{Q} , $\bar{m}_q^*(r)$, $\bar{U}_q(r)$, and $\bar{W}_q(r)$ by replacing $\rho_{\alpha\beta}^q$ everywhere by $\bar{\rho}_{\alpha\beta}^q$. Inserting the average quantities in the single-particle Hamiltonian H_q defined by eq. (13), we find a smoothed Hamiltonian \bar{H}_q :

$$\bar{H}_q = -\nabla \cdot \frac{\hbar^2}{2\bar{m}_q^*(r)} \nabla + \bar{U}_q(r) + \bar{W}_q(r) \cdot (-i)(\nabla \times \underline{\sigma}) + \hat{q}_{rr} \cdot \frac{\partial f}{\partial \nu}(\nu, \bar{Q}), \quad (28)$$

which may be considered as a "shell model" Hamiltonian [2,3,5]. We shall denote here its eigenvalues by $\hat{\epsilon}_i^q$ and its eigenfunctions by $\hat{\Phi}_i^q(r)$

$$\bar{H}_q \hat{\Phi}_i^q(r) = \hat{\epsilon}_i^q \hat{\Phi}_i^q(r). \quad (29)$$

Now, if the density oscillations $\delta \rho_{\alpha\beta}^q = \rho_{\alpha\beta}^q - \bar{\rho}_{\alpha\beta}^q$ are sufficiently small - which will be checked numerically below - one can treat the difference $\delta H_q = H_q - \bar{H}_q$ as a small perturbation of H_q . Then the energies ϵ_i^q and $\hat{\epsilon}_i^q$ can be related in first order perturbation theory by

$$\epsilon_i^q \approx \hat{\epsilon}_i^q + \int d^3r \hat{\Phi}_i^q(r)^* \delta H_q \hat{\Phi}_i^q(r). \quad (30)$$

Multiplying eq.(30) by n_i^q and summing over i gives

$$\sum_{q_i} \epsilon_i^q n_i^q = \sum_{q_i} \hat{\epsilon}_i^q n_i^q + \int d^3r \delta H_1 \rho_1(r) + O[(\delta \rho)^2]. \quad (31)$$

Expanding the terms E_{pot} and E_R in eq.(23) around $\bar{\rho}_{\alpha\beta}^q$ and using eq.(31), the first order terms in $\delta \rho_{\alpha\beta}^q$ cancel each other so that

$$E_{\text{HF}} = \sum_{q_i} \hat{\epsilon}_i^q n_i^q - \bar{E}_{\text{pot}} + \bar{E}_R - E_{\text{const}} + E_{\text{pair}} + O[(\delta \rho)^2], \quad (32)$$

where \bar{E}_{pot} and \bar{E}_R are defined again in terms of the averaged densities.

Note in eq.(32), E_{const} , E_{pair} and the n_i^q are still the HF quantities. We now introduce the occupation numbers \hat{n}_i^q which are defined by eqs.(5) and (19), but in terms of the "shell model" energies $\hat{\epsilon}_i^q$, and define the corresponding pairing energy \hat{E}_{pair} :

$$\hat{E}_{\text{pair}} = E_{\text{pair}}(\hat{\lambda}_q, \hat{n}_i^q) \quad (33)$$

With these we can rewrite eq. (32) as

$$E_{\text{HF}} = \sum_{q_i} \hat{\epsilon}_i^q \hat{n}_i^q - \bar{E}_{\text{pot}} + \bar{E}_R - \bar{E}_{\text{const}} + \hat{E}_{\text{pair}} + \delta E_{\text{pair}} - \delta E_{\text{const}} + O[(\delta \rho)^2] \quad (34)$$

where

$$\delta E_{\text{pair}} = \sum_{q_i} \hat{\epsilon}_i^q (n_i^q - \hat{n}_i^q) + (E_{\text{pair}} - \hat{E}_{\text{pair}}), \quad (35)$$

and the constraint energy E_{const} has been split into a smooth part and a small correction term:

$$\bar{E}_{\text{const}} = \bar{Q} \cdot \frac{\partial f}{\partial \nu}(\mu, \nu) \Big|_{\nu=\bar{Q}}, \quad (36)$$

$$\delta E_{\text{const}} = E_{\text{const}} - \bar{E}_{\text{const}} \approx \delta Q \cdot \frac{\partial f}{\partial \nu}(\nu, \mu) \Big|_{\nu=\bar{Q}}. \quad (37)$$

Since the occupation numbers n_i^q and \hat{n}_i^q are expected to differ only slightly (only in the energy region $\sim \lambda_q \pm \Delta_q$ do they differ at all), the quantity δE_{pair} should be very small. Similarly, δE_{const} (37) is expected to be small, being the product of $\delta Q = Q - \bar{Q}$ ($\sim 1-2$ barns, see ref. [3]) times the slope of a LD-like deformation energy curve [11] (< 1 MeV/barn). Indeed, we will see numerically below that both quantities δE_{pair} and δE_{const} do not exceed ~ 0.5 MeV in magnitude in a medium-heavy nucleus, and therefore we treat them as quantities of second order.

Collecting all terms of second and higher order in δE_2 - note the slight change of notation from eq.(1) - we define

$$\delta E_2 = \delta E_{\text{pair}} - \delta E_{\text{const}} + O[(\delta \rho)^2] \quad (38)$$

and obtain from (34)

$$E_{\text{HF}} = \sum_{qi} \hat{\epsilon}_i^q \hat{n}_i^q + \hat{E}_{\text{pair}} - \bar{E}_{\text{pot}} + \bar{E}_{\text{R}} - \bar{E}_{\text{const}} + \delta E_2. \quad (39)$$

The first two terms in (39) correspond exactly to the usual shell model energy sum plus pairing, and contain all first order contributions from $\delta \rho$. These are now extracted as the first order shell correction δE_1 :

$$\delta E_1 = \sum_{qi} \hat{\epsilon}_i^q \hat{n}_i^q - \bar{U} + \hat{E}_{\text{pair}} - \bar{E}_{\text{pair}}. \quad (40)$$

The uniform quantities \bar{U} and \bar{E}_{pair} are defined as in the usual shell-correction theory [2,3,4] by

$$\bar{U} = \sum_{qi} \hat{\epsilon}_i^q \bar{n}_i^q, \quad (41)$$

$$\bar{E}_{\text{pair}} = -\frac{1}{2} \sum_q \bar{g}_q(\bar{\lambda}_q) \bar{\Delta}_q^2, \quad (42)$$

where the \bar{n}_i^q are defined by eq.(27) in terms of the $\hat{\epsilon}_i^q$, $\bar{\Delta}_q$ are the average pairing gaps and $\bar{g}_q(E)$ are the uniform level densities defined by

$$\bar{g}_q(E) = \frac{1}{\gamma} \sum_i f_m\left(\frac{E - \hat{\epsilon}_i^q}{\gamma}\right) \quad (43)$$

Collecting all smooth terms occurring in eqs.(39) and (40), we define the LD part of the HF energy by

$$\bar{E} = \bar{U} + \bar{E}_{\text{pair}} - \bar{E}_{\text{pot}} + \bar{E}_{\text{R}} - \bar{E}_{\text{const}}. \quad (44)$$

With the definitions (40) and (44) we thus have explicit expressions for the first two terms of the shell-correction expansion (1). Writing

$$\delta E_2 = E_{\text{HF}} - \bar{E} - \delta E_1, \quad (45)$$

we can calculate δE_2 and thereby check the convergence of the series (1). \bar{E} and δE_1 can separately be compared to the corresponding quantities found in the LD model and the usual shell-correction calculations.

A special point of interest is the argument that the smoothed constraint present in the definition of the "shell model" Hamiltonian \bar{H}_q (28) should be omitted, since we want to check the use of ordinary shell model potentials

in which no constraint is present. However, we expect this not to affect the results - at least not the smooth and the first order terms, \bar{E} and δE_1 . The reason can easily be seen using perturbation theory. Switching off the constraint in \bar{H}_q (28), which is a small disturbance, the i -th eigenvalue of \bar{H}_q is changed by

$$\Delta \hat{E}_i^q \approx - \int \hat{\Phi}_i^q(r)^* \frac{\partial f}{\partial \nu} (\mu, \nu = \bar{Q}) \hat{q}_{op} \hat{\Phi}_i^q(r), \quad (46)$$

and therefore

$$\Delta \sum_i \hat{E}_i^q \hat{n}_i^q \approx - \hat{Q} \cdot \frac{\partial f}{\partial \nu} (\mu, \nu = \bar{Q}), \quad (47)$$

where \hat{Q} is the "shell model" quadrupole moment which is close to the HF value Q . The change in \bar{U} (41) is then

$$\Delta \bar{U} = \sum_i \Delta \hat{E}_i^q \hat{n}_i^q \approx - \bar{Q} \cdot \frac{\partial f}{\partial \nu} (\mu, \nu = \bar{Q}), \quad (48)$$

so that the two contributions to δE_1 in (40) cancel up to a term comparable to δE_{const} (37). Similarly, the contribution of the constraint to \bar{U} is in eq.(46) cancelled in first order by the energy \bar{E}_{const} . Thus, all differences made by including or omitting the average constraint on \bar{H}_q are expected to be of second order only. This will be confirmed by our numerical results below.

Before presenting the results, we want to compare our method briefly to the one proposed by Bassichis et al. [6]. These authors define a smooth density $\bar{\rho}_{\alpha\beta}$ and a "shell model" Hamiltonian \bar{H}_q in a similar way to ours (not including the constraint in \bar{H}_q). The main difference in their approach lies in their explicit use of the "shell model" density matrix $\hat{\rho}_{\alpha\beta}^q$:

$$\hat{\rho}_{\alpha\beta}^q = \sum_i n_i^q (\hat{C}_{\alpha}^{q,i})^* \hat{C}_{\beta}^{q,i} \quad (49)$$

the $\hat{C}_{\alpha}^{q,i}$ being the expansion coefficients (cf. eq. (6)) of the eigenfunctions $\hat{\Phi}_i^q(r)$ of \bar{H}_q . Using the fact that the HF energy is stationary as a functional $E[\rho]$ of the density matrix ρ , they write

$$E_{\text{HF}}[\rho] = E[\hat{\rho}] + O[\delta c^2], \quad (50)$$

where $O[\delta c^2]$ is a term of second order in the changes of the wavefunctions, $\delta c = \hat{C}_{\alpha}^{q,i} - c_{\alpha}^{q,i}$. The right hand side of eq.(50) can then be transformed - without using perturbation theory - into a form which is similar to eq.(32), but in which one second order term is given explicitly. Thus the advantage of this method is that one part of the second order shell corrections can be

evaluated exactly. However, another part is still left in the term $\mathcal{O}[\delta c^4]$ in eq.(50) which can only be calculated indirectly. The advantage of our method is that one only needs to know the eigenvalues \hat{E}_q^0 of the average Hamiltonian \bar{H}_q , and therefore one does not have to compute the densities $\hat{\rho}_q(\underline{r})$, $\hat{t}_q(\underline{r})$, etc. The numerical evaluation of the second order terms given by Bassichis et al. [6] is planned for future calculations.

NUMERICAL RESULTS AND CONCLUSIONS

In our numerical calculations we used the set "SIII" of Skyrme parameters. These were recently shown to give excellent fits of the ground-state energies, radii and deformations throughout the periodic table [13]. For completeness we give the parameters in Table 1.

To check the shell-correction expansion in a medium-heavy nucleus, we performed a complete CHF-calculation for the rare-earth element ^{168}Yb . For the pairing effects we used the normal BCS treatment, thus choosing the pairing functional (17). As in ref. [3], a single parameter was used in the form of a uniform gap $\bar{\Delta}$, chosen here to be $\bar{\Delta} = 1.0$ MeV which corresponds to the pairing strengths $G_n = 0.15$ MeV and $G_p = 0.19$ MeV (at all deformations).

Figure 1 shows the deformation energy curve $E_{\text{HF}}(Q)$ of ^{168}Yb in a region containing the prolate ground-state, an oblate secondary minimum and the ascent towards the fission barrier. The curve $E_{\text{W.S.}}$ was obtained as a zeroth order approximation using the shell model wavefunctions found in a Strutinsky calculation with a deformed Woods-Saxon potential [3]. As recently described [17], these wavefunctions give an excellent approximation to the HF solutions. The total binding energy obtained in this approximation is at smaller deformations only $\sim 7 - 10$ MeV higher than the HF energy, as can be seen also in Fig. 1. The dashed line in Fig. 1 is the smooth energy \bar{E} obtained by eq.(44). This curve indeed behaves like a LD deformation energy. Within the numerical accuracy of our results, here $\sim \pm 0.5$ MeV in the total energies, the curve is smooth. This result strongly supports Strutinsky's theory of renormalization of the LD energy part.

TABLE 1. PARAMETERS OF THE SKYRME INTERACTION SIII USED IN OUR CALCULATIONS

t_0	t_1	t_2	t_3	x_0	W_0
- 1128.75	395.0	-95.0	14000.0	0.45	120.0

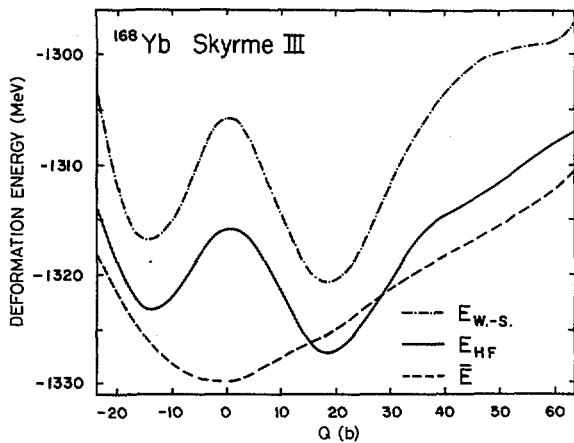


FIG. 1. Deformation energy curves $E(Q)$ for ^{168}Yb , obtained with Skyrme interaction SIII. Solid line: CHF result. Dashed-dotted line: approximation $E_{W.S.}$ with shell model wave functions. Dashed line: smooth part E of the HF energy.

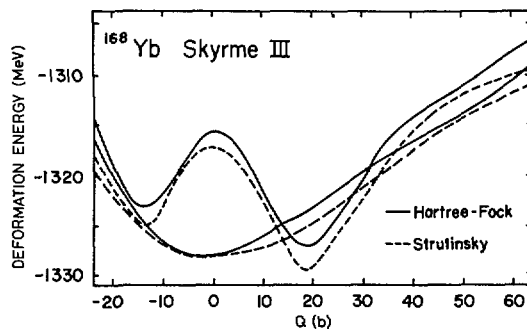


FIG. 2. Comparison of CHF and Strutinsky deformation energy curves for ^{168}Yb . Solid lines: E_{HF} and \bar{E} obtained with interaction SIII (see Fig. 1). Dashed lines: total energy $E_{\text{LD}} + \delta E_1$ and LD energy E_{LD} obtained in a shell-correction calculation with a deformed Woods-Saxon potential.

To check our arguments concerning the constraint in the smoothed Hamiltonian \bar{H}_q , we did the calculations twice, once with and once without the constraint. In both cases, the LD energy \bar{E} turned out to be exactly the same.

In Figure 2 we compare the HF energy curve and its LD part to the curves obtained in a Strutinsky-type calculation. In the latter, the shell-correction δE_1 was found from a deformed Woods-Saxon potential already mentioned above (see ref.[3]). The deformation energy $E_{\text{LD}} + \delta E_1$ was taken along a path going through the two minima and approximately following the LD valley at larger

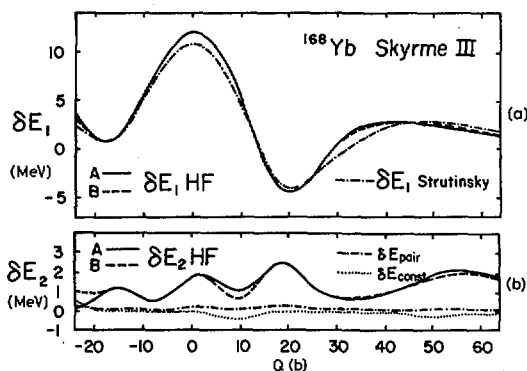


FIG. 3. (a) First order δE_1 and (b) higher order shell corrections δE_2 extracted from the HF energy. Solid lines (A): results obtained with constraint in the smooth Hamiltonian \bar{H}_Q . Dashed lines (B): results obtained without constraint in \bar{H}_Q . Figure 3b also shows the quantities δE_{pair} and δE_{const} contained in δE_2 . In Fig. 3a, the dashed-dotted curve is the first order shell correction found with the Woods-Saxon potential (see Fig. 2).

deformations. The quadrupole moment was calculated at each point from the shell model wavefunctions as in eq.(12). The position of the Strutinsky curves is adjusted so that the values of E_{LD} and \bar{E} at zero deformation are the same. In \bar{E} , we have included here a constant of +1.7 MeV in order to take the average contribution of the higher order terms δE_2 into account (see below). We can see in Fig. 2 that the two models predict the same equilibrium deformations within a few percent.

The first and higher order shell-corrections extracted from E_{HF} according to eqs.(40),(45) are displayed in Fig. 3. The solid lines show δE_1 and δE_2 obtained with the average constraint included in \bar{H}_Q , and the dashed lines show them without the constraint in \bar{H}_Q . As expected, the two cases give essentially the same results. In the upper part of the figure, the small corrections δE_{const} and δE_{pair} are shown.

For the definition of the average densities $\bar{\rho}_{\alpha\beta}^i$ by eqs.(25) and (26), a Gaussian averaging function with a fourth order curvature correction was chosen. The smearing range γ was chosen to be $\gamma \approx 1.1 - 1.4 \hbar\Omega$, with $\hbar\Omega$ being the average separation of the main shells in the spectra \mathcal{E}_i^{λ} . No significant change of the results shown in Figs. 1 - 3 was observed by varying γ within the range mentioned.

In the lower part of Fig. 3, the shell-correction δE_1 found from the Woods-Saxon potential [3] is shown with the dashed-dotted curve. Its agreement with the HF curve is remarkable, in view of the fact that no adjustment at all has been made of the Woods-Saxon potential parameters.

The sum of the higher order shell corrections δE_2 is quite small as compared to the first order correction δE_1 (note the enlarged scale in the upper part of the figure!). They oscillate by $\sim \pm 1$ MeV around an average value of $\sim +1.7$ MeV. Their relative smallness proves the rapid convergence of the shell-correction expansion (1). In looking closer at Fig. 3, we notice a clear correlation of the oscillations in δE_1 and δE_2 : The maxima of δE_2 coincide with the extrema of δE_1 . This can be understood by assuming that the terms of second order in $\delta \mathcal{Q}$ are predominant in δE_2 , as is made evident by the rapid convergence of the shell-correction expansion. Then it is clear that the "wavelength" of the oscillations in δE_2 must be one-half times that of the first order oscillations δE_1 . This has two consequences for the calculations of deformation energies with the traditional shell correction method: 1) The inclusion of a second order correction affects the relative position of the stationary points of the curve only very little, since the values at the maxima of δE_2 vary only little around their average ($\pm \sim 0.6$ MeV in the present case). 2) The regions between the extrema of the deformation energy curve are lowered with respect to the stationary points, which tends to make the barriers thinner. Both effects can be seen in Fig. 2.

If the pattern of these results is confirmed in calculations for actinide nuclei and with different effective interactions - which will be carried out in the future - we can therefore conclude that the static fission barriers and the equilibrium deformations are sufficiently well described in a Strutinsky calculation. For the calculations of fission lifetimes, however, the second order corrections might be important, as the lifetimes are well known to be crucially dependent on the thicknesses of the barriers [3,18]. The second order effects thus tend to lower the calculated halflives, which is in favour of the results of refs. [3,18].

One should of course check these conclusions by applying our test to a heavy fissioning nucleus. However, in this region the Skyrme-CHF calculations do not yet reproduce the experimentally known fission barriers, the outer barrier being more than twice as large as its experimental value [14]. Since our test of the Strutinsky method is meaningless when the CHF results are in clear disagreement with experiment, we cannot expect to get conclusive results in this region.

At ground-state deformations and especially for spherical nuclei, however, the Skyrme-III interaction is very successful, as mentioned above. We therefore used these results to calculate the higher order corrections δE_2 for a series of nuclei in their ground states. The results are shown in Figure 4. The crosses show the values of E_2 evaluated for the nuclei ^{108}Ru , ^{134}Ce , ^{140}Ce , ^{152}Sm , ^{158}Gd , ^{162}Dy , ^{166}Er , ^{168}Yb , ^{174}Yb , ^{178}Hf , ^{184}W , ^{190}Os , ^{208}Pb

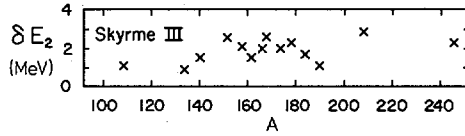


FIG. 4. Higher order shell corrections δE_2 for 14 nuclei in their ground state. Skyrme III interaction used; pairing effects included in all deformed nuclei.

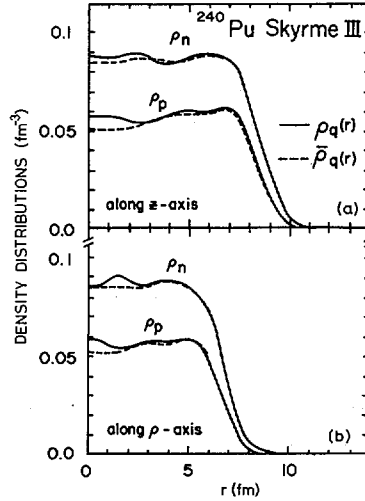


FIG. 5. Density distributions of ^{240}Pu in the ground state. (a) along the z -axis (symmetry axis); (b) along the ρ -axis (perpendicular to the z -axis). Solid lines: HF results (Skyrme III). Dashed lines: energy-averaged densities $\bar{\rho}_q(r)$.

and ^{240}Pu . In these calculations (except for ^{168}Yb , see above) the pairing functional (17) was used and the gaps Δ_q chosen to be approximately equal to their experimental values. All values of δE_2 lie within $\sim 2.0 \pm 1$ MeV, including the doubly magic ^{208}Pb . This result again demonstrates the smallness of the higher order effects, indicating that the first order shell corrections to the ground-state energies can be expected to be correct within $\sim \pm 1 - 2$ MeV.

We want to emphasize that the way in which we have defined the smooth part $\bar{S}_{\alpha\beta}^q$ of the density matrix is not the only possible one; other definitions may be tried. The Strutinsky averaging method is based on the belief that the most important shell effects come from the oscillations of the density of single-particle states in energy space, especially those in a region $\pm \hbar\Omega$ around the Fermi energy. This assumption might in our calculations be tested by the use of other averages for $\bar{S}_{\alpha\beta}^q$. The averaging in energy space does not imply that the spatial density distributions $\bar{\rho}_q(\mathbf{r})$ are completely smooth as functions of \mathbf{r} . This is illustrated in Figure 5, where the density distributions $\bar{\rho}_q(\mathbf{r})$ of

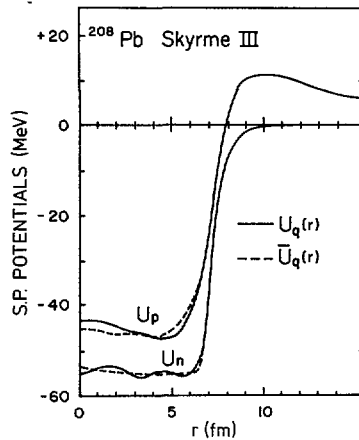


FIG. 6. Local parts $U_q(r)$ and $\bar{U}_q(r)$ of the HF and the averaged single-particle potentials, respectively, of ^{208}Pb in the ground state (Skyrme III).

^{240}Pu in the ground state are shown. Although the densities $\bar{\rho}_q(\underline{r})$ are much smoother than the selfconsistent ones, some oscillations still remain. These have been observed before [3,5] and are not believed to be responsible for shell effects. (For a detailed discussions of these remaining oscillations, see ref. [5].) Similarly, the smoothed single-particle potentials $\bar{U}_q(\underline{r})$ still oscillate slightly inside the nucleus, as can be seen in Figure 6 where they are compared to the HF potentials $U_q(\underline{r})$ for the case of ^{208}Pb . (The proton potentials include the Coulomb potential (11a,b).) Results similar to those displayed in Figs. 5 and 6 where obtained for the rare-earth nuclei. The smooth potentials $\bar{U}_q(\underline{r})$ look in general very similar to Woods-Saxon potentials, confirming the use of such potentials in Strutinsky calculations.

SUMMARY

We have found that the definition of $\bar{\rho}$ yields an average part of the total HF energy which - at least for a nucleus like ^{168}Yb - is perfectly smooth as a function of deformation. The shell-correction expansion (1) of E_{HF} , found by means of this smoothed density matrix $\bar{\rho}$, has been proved numerically to have rapid convergence. Our results for the higher order shell corrections are in good agreement with the results obtained previously by Bunatyan et al. [5] using a completely different method.

We conclude that first order shell corrections, calculated from a Woods-Saxon-type shell model potential, describe the stationary points of deformation energy curves sufficiently well: the higher order effects do not

affect them by more than $\sim \pm 0.5 - 1$ MeV. The second order effects might be important in calculating fission lifetimes, tending to make barriers narrower and thus the lifetimes shorter. In transition regions from spherical to deformed nuclei, or from oblate to prolate nuclei, where the first order corrections are small, the second order effects might also play a decisive role.

We have seen that the inclusion of a constraint in the average potential has only a negligible effect on the single terms obtained in the shell-correction expansion.

These conclusions are drawn from the HF point of view, and are only relevant for the Strutinsky method to the extent to which HF calculations can be considered more fundamental than the shell-correction approach. We therefore plan to repeat this type of calculations using different interactions.

The extraction of a LD-like average part from the HF energy allows us to determine LD parameters, such as surface and symmetry energy coefficients, for a given effective interaction. The determination of the average potentials $\bar{U}_q(\bar{r})$ should also help to improve the shell model potentials to be used in shell-correction calculations. Such investigations are in progress and will be published elsewhere.

ACKNOWLEDGEMENTS

The authors are very grateful to Prof. G.E.Brown for helpful discussions and for his hospitality at Stony Brook. We would like to thank D.Vautherin for letting us use his HF code. We acknowledge stimulating discussions with A.K.Kerman, K.Dietrich and H.Flocard.

REFERENCES

- [1] STRUTINSKY, V.M., Nucl. Phys. A95 (1967) 420.
- [2] STRUTINSKY, V.M., Nucl. Phys. A122 (1968) 1.
- [3] BRACK, M., DAMGAARD, J., JENSEN, A.S., PAULI, H.C., STRUTINSKY, V.M., WONG, C.Y., Rev. Mod. Phys. 44 2 (1972) 320.
- [4] BRACK, M., PAULI, H.C., Nucl. Phys. A207 (1973) 401.
- [5] BUNATYAN, G.G., KOLOMIETZ, V.M., STRUTINSKY, V.M., Nucl. Phys. A188 (1972) 225.
- [6] BASSICHIS, W.H., KERMAN, A.K., TSANG, C.F., TUERPE, D.R., WILETS, L., in "Magic Without Magic: John Archibald Wheeler", Freeman, San Francisco, 1972.
- [7] BASSICHIS, W.H., TUERPE, D.R., TSANG, C.F., WILETS, L., Phys. Rev. Lett. 30 (1973) 294.

- [8] SKYRME, T.H.R., Phil. Mag. 1 (1956) 1043; Nucl. Phys. 9 (1959) 615.
- [9] VAUTHERIN, D., BRINK, D.M., Phys. Rev. C5 (1972) 626.
- [10] VAUTHERIN, D., Phys. Rev. C7 (1973) 296.
- [11] FLOCARD, H., QUENTIN, P., KERMAN, A.K., VAUTHERIN, D., Nucl. Phys. A203 (1973) 433.
- [12] FLOCARD, H., QUENTIN, P., VAUTHERIN, D., Letter to be published.
- [13] BEINER, M., FLOCARD, H., GIAI, N.V., QUENTIN, P., to be published.
- [14] FLOCARD, H., QUENTIN, P., KERMAN, A.K., VAUTHERIN, D.,
Paper IAEA-SM-174/38, these Proceedings, Vol. 1.
- [15] NEGELE, J.W., VAUTHERIN, D., Phys. Rev. C5 (1972) 1472.
- [16] LANE, A.M., Nuclear Theory, Benjamin, New York (1964).
- [17] KO, C.M., PAULI, H.C., BRACK, M., BROWN, G.E., submitted to Phys. Lett.
- [18] LEDERGERBER, T., PAULI, H.C., Nucl. Phys. A207 (1973) 1.

DISCUSSION

K. DIETRICH: If the effective interaction depends on the density, a term linear in the fluctuation $\delta\rho$ arises which in general is not zero but would represent a correction to the Strutinsky term. You have told me that for the Skyrme interaction this term is zero. Is that fortuitous or is the Skyrme interaction so adjusted that this happens?

M. BRACK: One can easily verify that our method works for any density-dependent term of the form $\rho^\alpha(\mathbf{r}) \delta(\mathbf{r} - \mathbf{r}')$ in the interaction with α being a real number. Furthermore, it was shown by Bunatyan and co-workers (Ref. [5] of our paper) that, for any density-dependent effective interaction, if one makes the local density approximation and stays within the HF framework, no term linear in $\delta\rho$ will appear, as long as the rearrangement energy is taken properly into account.

K. DIETRICH: The first two terms of your expansion

$$\left(E[\bar{\rho}] + \left(\frac{\delta E}{\delta \rho} \right) \delta \rho \right)$$

are not very sensitive to the details of the decomposition $\rho = \bar{\rho} + \delta\rho$ as long as $\bar{\rho}$ is reasonably smooth. In the phenomenological Strutinsky method, the term $E[\bar{\rho}]$ is replaced by the phenomenological droplet energy. It is very important here how $\delta\rho$ is defined. In your method you cannot check this aspect of the Strutinsky method.

M. BRACK: You are right in that we have not checked the correctness of the commonly used liquid-drop and shell models. Our test was concerned with the basic principle of Strutinsky's method, namely the possibility of obtaining a shell-correction expansion at all. Examining which phenomenological models have to be used to obtain the single terms \bar{E} and δE_1 will be the next step.

FISSION ISOMERS
(Session III)

Chairman: S. Bjørnholm (Denmark)

Review Paper

FISSION ISOMER SYSTEMATICS*

R. VANDENBOSCH

University of Washington,
Seattle, Wash.,
United States of America

Abstract

FISSION ISOMER SYSTEMATICS.

The half-lives, decay properties, excitation energies and production cross-sections of spontaneously fissioning isomers are reviewed. Rotational, vibrational, and single-particle excitations of the shape-isomeric state are discussed.

1. INTRODUCTION

Spontaneous fission isomerism was discovered [1] prior to the first IAEA fission symposium in 1965. However it was not until shortly before the second symposium in 1969 that sufficient evidence was obtained to firmly support their interpretation as shape-isomeric states associated with a second minimum in the potential energy surface. This second minimum is a consequence of non-uniformities in the single particle spectrum for a deformation characterized by a nearly 2:1 ratio of the major to minor nuclear axes. For certain actinide nuclei the resulting shell correction is rather large in a region of deformation where the liquid drop potential energy surface is rather flat. The resulting potential energy function exhibits a second minimum lying several MeV above the first minimum. This review will concern itself with the properties of nuclear states associated with this second minimum.

The common characteristic of all presently known shape-isomeric states in the actinide region is their decay by spontaneous fission. Since the last fission symposium a number of new spontaneously fissioning isomers have been discovered. The boundaries in N and Z space of the "island" of observable isomerism has been fairly well mapped. More importantly, new kinds of information about the shape-isomeric states have been obtained. These include results on excitations of the shape-isomeric states as well as their decay properties. The moment of inertia and the pairing energy gap have been determined for several nuclei. Information about the spins of a few isomers has been obtained. The existence of another decay mode, gamma decay to the first minimum, has been demonstrated.

2. ISOMER HALF-LIVES

The most commonly measured property of a spontaneously fissioning isomer is its half-life. If an isomer is sufficiently long-lived to be observed, its half-life can usually be determined. The lightest known isomer is ^{236}U , and the heaviest is ^{245}Bk . These boundaries are undoubtedly

* Work supported in part by the US Atomic Energy Commission.

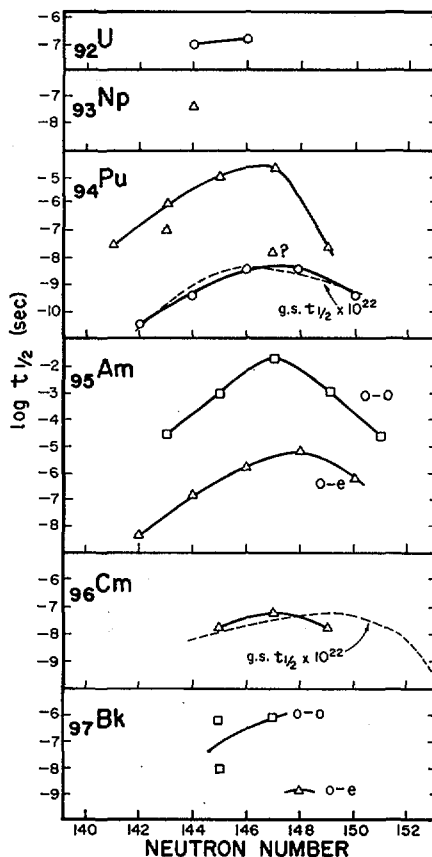


FIG. 1. Spontaneously fissioning isomer half-lives as a function of neutron number. Circles, triangles, and squares represent values for even-even, odd-A, and odd-odd nuclei, respectively. (This convention will be employed throughout this paper unless otherwise indicated.) The experimental data is taken from a summary in Ref. [6] except for more recent data (Refs [5, 7]).

determined in good part by limits imposed by experimental sensitivity, both with respect to yields and lifetimes. The isomeric half-lives are plotted as a function of neutron number in Fig. 1. This presentation is similar to that employed by Polikanov and Sletten [2]. We have omitted from this figure a few even-even isomers believed to correspond to two-quasiparticle excitations of the shape isomer. It was suggested at the last symposium [3] that there was a significant odd-even effect on the half-lives, and that the half-lives of the plutonium isomers exhibited a variation with mass number similar to that of the ground state half-lives. These trends have become clearer as more data has become available. The systematics of the plutonium isotopes has been extended considerably as a consequence of the very recent discovery [4,5] of new, very short-lived, plutonium isomers. These results, to be presented later in this session by Metag et al. [5], show that the even-even plutonium isomers exhibit a variation with neutron number quite similar to that of the even-odd isomers. The regularity of the odd-even effects and the dependence of half-life on neutron number exhibited by the americium isotopes is also quite striking.

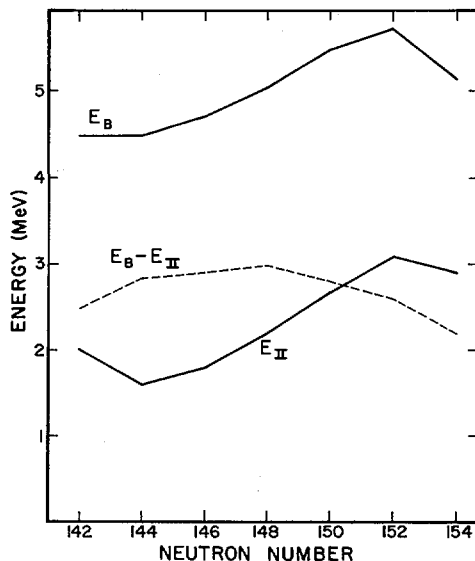


FIG. 2. Theoretical isomer excitation energies E_{II} , outer barrier heights E_B , and the differences $E_B - E_{II}$, as a function of neutron number for even-even plutonium isotopes. The values shown are an average of the calculation results of Möller [8], Pauli and Ledergerber [9], and Möller and Nix [10]. Reflection-asymmetric distortions at the outer barrier have been taken into account.

Some insight as to the origin of the maxima in the dependence of the half-life on neutron number can be obtained by examining the results of theoretical calculations [8-10]. The inner barrier for most isomers is higher than the outer barrier, so that the penetrability of the outer barrier should determine the lifetime of most isomers. The effective energy of the outer barrier which must be penetrated is given by $E_B - E_{II}$, where E_B and E_{II} are the outer barrier and isomer energies relative to that of the ground state. Theoretical outer barrier heights and isomer excitation energies are shown by the solid lines in Fig. 2. The difference $E_B - E_{II}$ is seen to exhibit a maximum at about the same neutron number as that corresponding to the longest half-lives. The detailed behavior of $E_B - E_{II}$ depends on the interplay between the dependence of E_B and E_{II} on neutron number, but is dominated by the neutron semi-magic number at the deformation corresponding to the isomer. The use of average values in Fig. 2 conceals some differences in the various theoretical calculations. The neutron number at which the gap in the single particle spectrum for the isomer deformation occurs is at $N = 142$ in the calculations of Pauli and Ledergerber [9,11], $N = 144$ in the calculations of Nilsson et al. [12], and $N = 148$ in the calculations of Mosel and Schmitt [13] and of Möller and Nix [10]. (It must also be remarked however that the experimental E_{II} values, discussed in a following section, do not clearly reflect the predicted trends. This may reflect errors in the ground state shell correction which cancel for the quantity $E_B - E_{II}$).

The variation in isomer half-lives with neutron number is surprisingly similar to that exhibited by the ground state half-lives, although there is an upward shift in the neutron number corresponding to the longest half-lives as one goes from the isomeric states to the ground states. The dependence of both the inner and outer theoretical barrier heights (relative

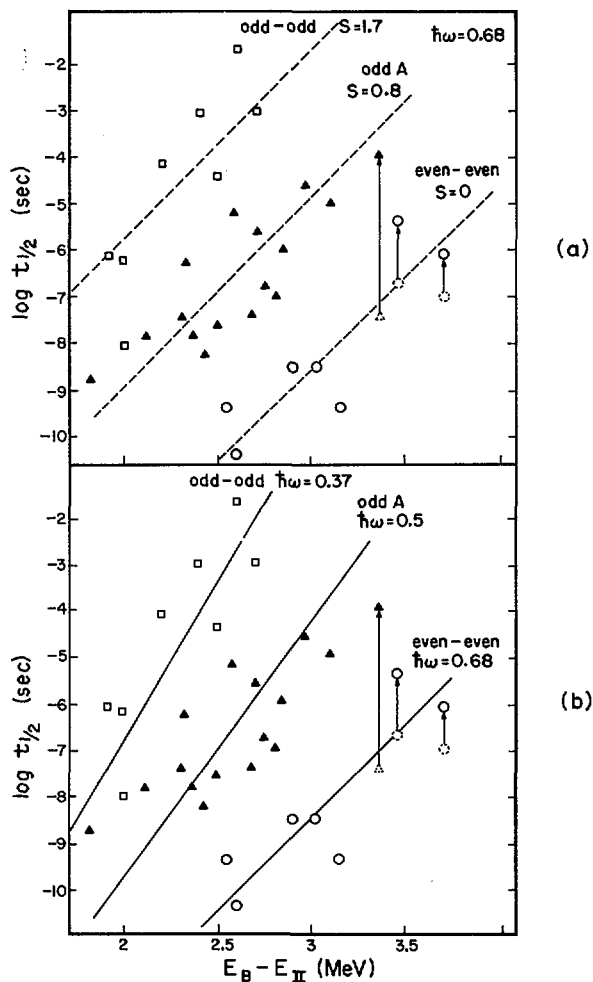


FIG. 3. Spontaneously fissioning isomer half-lives as a function of $E_B - E_{II}$. The circles, triangles, and squares refer to even-even, odd A, and odd-odd nuclei, respectively. The dashed triangle and circles at the base of the arrows represent the observed total half-lives of ^{237m}Np , ^{236m}U and ^{238m}U . The symbols at the top of the arrows are the partial fission half-lives after correction for gamma branching. The data points in (a) and (b) are identical; the straight lines in (a) and (b) differ as discussed in the text.

to the ground state) on neutron number exhibit a maximum at $N = 152$ due to a ground state shell effect. Apparently the maximum in the ground state half-lives is pulled toward a lower neutron number due to the neutron-number dependence of the depression of the potential in the region between the two barriers. Thus the similarity in the neutron number dependence of the ground and isomer half-lives can be traced to shell corrections in the region of the second minimum.

The success in understanding the origin of the neutron number variation of the half-lives in terms of the theoretical effective barrier height $E_B - E_{II}$

suggests that a universal correlation of all isomer half-lives might be possible. In Fig. 3 we plot the half-lives as a function of $E_B - E_{II}$. The $E_B - E_{II}$ values are an average of the Möller [8] and Pauli-Ledergerger [9] predictions. The values for odd-A and odd-odd nuclides were obtained by simple interpolation from the reported values for even-even nuclides. The observed half-lives tend to fall into distinct groups depending on their nuclear type. For a parabolic barrier the half-life is given by $t_{1/2} = \ln 2 / n p$ where n is the number of barrier assaults per unit time and the penetration factor p is given by $\exp[-2\pi(E_B - E_{II})/\hbar\omega_B]$. The quantity $\hbar\omega_B$, sometimes designated the barrier curvature energy, contains the barrier curvature and effective mass and is assumed to be the same for all nuclei. This is surely an oversimplification. We estimate n on the basis of a vibrational frequency corresponding to 1 MeV. In Fig. 3b we have drawn lines corresponding to the assumption that $p = 1$ at $E_B - E_{II} = 0$ for all nuclear types. The slope of the lines then gives the dependence of $\hbar\omega_B$ on nuclear type. Figure 3a corresponds to another limiting assumption, namely that $\hbar\omega_B$ is independent of nuclear type and that the odd-even effect can all be attributed to an energy shift S usually attributed to a "specialization" energy. (The S values obtained here will also include any difference between the gap parameter Δ at the isomeric state and outer barrier deformations.) The scatter in the data precludes determining a clear preference for one or the other of the limiting parameterizations on the basis of the comparisons in the two parts of Fig. 3. The unpaired nucleons undoubtedly affect both the effective mass (and hence $\hbar\omega_B$) and also the effective barrier height. The effect of an odd particle on the mass parameter has been estimated theoretically to be roughly 25% [14,15]. This would lead to a 12% change in $\hbar\omega$ in going from even-even to odd-A nuclei. The change in $\hbar\omega$ deduced from the correlations in Fig. 3b is much larger, suggesting that the specialization energy plays a significant and likely dominant role at the outer barrier.

The appropriateness of the parameterization employed in Fig. 3 depends on the outer barrier being determinative for the isomeric state half-life. For the lighter-mass nuclei the inner barrier decreases relative to the outer barrier and decay through the inner barrier is also expected. This decay mode has been recently established for ^{238}U , as has been reported by Russo, Pedersen and Vandenbosch [16]. There is also indirect evidence from yield data that ^{236}U and ^{237}Np decay predominantly by gamma emission [17,7]. The observed half-lives have been increased according to their measured or expected branching ratios so as to correspond to the partial fission half-lives. These corrections are indicated by the vertical arrows of Fig. 3. Of particular interest is the odd-even isomer of ^{237}Np recently discovered by Wolf and Unik [7]. This isomer has a spontaneous fission yield more than 10^3 times smaller than expected. It is therefore concluded that the gamma-to-fission decay ratio is of this order of magnitude. Perhaps more surprising is the relatively short half-life of this isomer. It appears to have a partial gamma-decay half-life (as indicated by the dashed triangle at the bottom of the arrow in Fig. 3) comparable to that of the partial gamma-decay half-life of the even-even nuclei ^{236}U and ^{238}U (indicated by dashed circles). This result may indicate that there is no specialization energy for the inner barrier. Such a result would be consistent with the recent theoretical findings [18-20] that the inner barrier is unstable with respect to deformation destroying the axial symmetry. In such a situation K is no longer a good quantum number. Since the specialization energy is largely a consequence of the energy cost associated with preserving K at single particle level crossings, the specialization energy may disappear for the inner barrier. The lack of axial symmetry would also be expected to have some effect on the mass parameter for a nucleus with an unpaired particle.

A weakening or absence of specialization energy effects at the inner barrier may play a role in determining the remarkably smooth dependence of the half-lives of odd-A and odd-odd isotopes on neutron number. An upper limit to the observed half-life may be imposed by the partial half-life for decay through the inner barrier via the gamma branch. The empirical barrier heights and isomer excitation energies [21] together with an $\hbar\omega$ value for the inner barrier deduced [16] from the gamma branch in ^{238}U are consistent with such an idea. If indeed the specialization energy was varying sufficiently from isomer to isomer that in some cases a gamma branch dominated, variations in the yield of delayed fission might be expected. At present there is not any definite evidence for such variations.

3. CROSS-SECTIONS FOR ISOMER FORMATION

There are two quantities relating to the yield of the isomer which are usually measured; the absolute cross-section for isomer production, and the ratio of isomer fission to prompt fission. The latter quantity can often be measured to better precision than the former. If both the isomer cross-section and the ground state cross-section are known, the isomer yield ratio σ_i/σ_g can be obtained. For reactions resulting from the decay of a compound nucleus this ratio for a nucleus with mass number A is determined by the branching ratio for decay of the nucleus with mass number $A + 1$. At the peak of the excitation function, where the population of the residual nucleus is concentrated near the top of the fission barriers, the "golden rule" leads us to expect a population ratio proportional to the ratio of the density of levels in the two wells. Since the level densities depend exponentially on energy, population of the ground state well is favored by a large factor. Let us consider a very simple model for this. A constant-temperature level density formula of the form $\exp E^*/T$ will be assumed, where E^* is the excitation energy and T is the nuclear temperature. For levels in the first well leading to ground state formation it is usually the height of the inner barrier E_A which determines the highest excitation energy at which trapping will occur. (The trapping in either well is not really effective until about 0.5 MeV below the top of the barrier where gamma decay becomes competitive with penetration through the barrier. For the first well neutron emission can also be important, but, for the cases considered, $E_n \gg E_A$.) For levels in the second well it is the height of the lower (outer) barrier E_B which determines the excitation energy $E_B - E_{II}$ at which trapping occurs. Therefore the ratio of level densities at the top of the respective wells, and hence the isomer ratio, is expected to be given by

$$\sigma_i/\sigma_g \approx \frac{\rho_{II}(E^* = E_B - E_{II})}{\rho_I(E^* = E_A)} \approx \exp \frac{-(E_A - (E_B - E_{II}))}{T}.$$

In Fig. 4 we compare experimental σ_i/σ_g values [6,21,22] with the behavior expected from this simple model. The E_A values are taken from (or extrapolated from) tabulations [6,21] of empirical barrier heights. The $E_B - E_{II}$ values are taken from the theoretical calculations of Pauli and Ledergerber [8] rather than empirical analyses [21] as the latter values would in turn have been deduced from isomer excitation function data. The nuclear temperature determining the slope of the line has been taken equal to the value suggested by the comparison in Fig. 5. The comparison suggests that the absolute value of σ_i/σ_g and maybe even some of the variations may be understood from this simple point of view.

The other quantity which is often measured is the isomer-to-prompt fission ratios, σ_i/σ_f . This value depends on the number of neutrons emitted and on the neutron-fission competition at each step of the evaporation. The

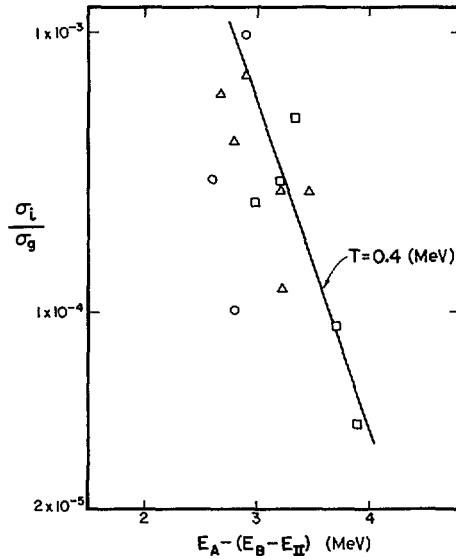


FIG. 4. The isomer yield ratio is plotted as a function of $E_A - (E_B - E_{II})$. The straight line represents the absolute magnitude and slope expected for the simple model described in the text. The symbols denote the same as in Fig. 3.

ratio of the isomer cross-section to the compound nucleus formation cross-section, σ_i/σ_c , for a reaction in which two neutrons are emitted can be written as

$$\sigma_i/\sigma_c = (\Gamma_n/\Gamma_T)_I^{A+2} \times (\Gamma_f/\Gamma_T)_I^{A+1} \times (\Gamma_n/\Gamma_T)_{II}^{A+1}$$

where $\Gamma_T = \Gamma_n + \Gamma_f$ and the subscripts indicate whether the values are appropriate to the first or second wells. The ratio σ_f/σ_c at energies close to the peak of the σ_i/σ_f excitation function is given by

$$\sigma_f/\sigma_c \approx (\Gamma_f/\Gamma_T)_I^{A+2} + (\Gamma_n/\Gamma_T)_I^{A+2} (\Gamma_f/\Gamma_T)_I^{A+1}.$$

This quantity is close to unity in the actinide region so $\sigma_f \approx \sigma_c$ and σ_i/σ_f becomes approximately equal to the above expression for σ_i/σ_c . Borggreen et al. [23] have deduced

$$(\Gamma_n/\Gamma_T)_{II}^{A+1} \approx (\Gamma_n/\Gamma_f)_{II}^{A+1}$$

values from the experimental σ_i/σ_f ratios [24] and literature [25] $(\Gamma_n/\Gamma_f)_I$ values. They have plotted these as a function of $E_B - E_{II} - \bar{S}_n$ as shown in the lower part of Fig. 5. \bar{S}_n is an effective neutron binding energy relevant to the $A + 1$ nucleus. Also shown are the empirical values for the first well, plotted as a function of $(\max\{E_A, E_B\} - \bar{S}_n)$. The extraction of the nuclear temperature is based on a simple expression for Γ_n/Γ_f , $\Gamma_n/\Gamma_f \propto \exp\{(E_{\text{barrier}} - \bar{S}_n)/T\}$. The success of the correlation indicates that the

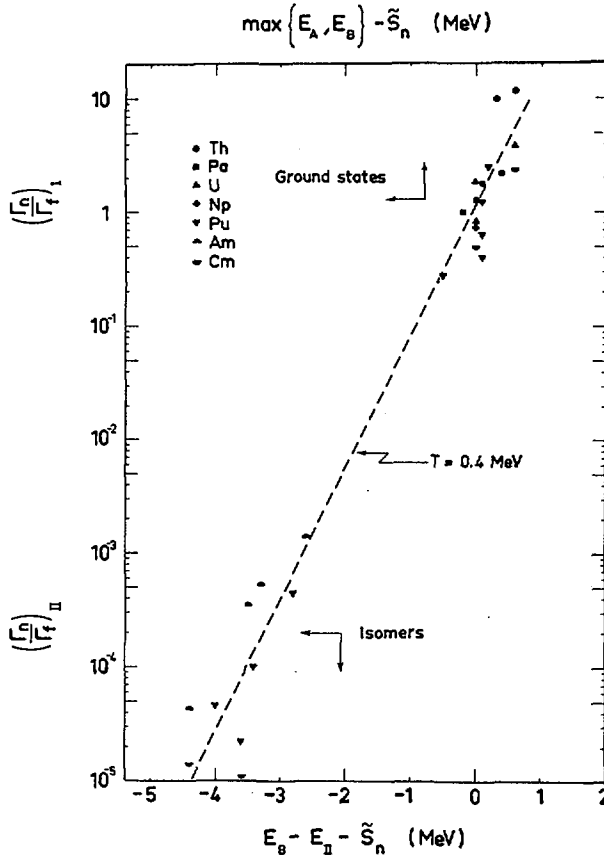


FIG. 5. Experimental Γ_n/Γ_f values for the first and second wells are plotted against the difference between the barrier height and effective neutron separation energy. Figure taken from Ref. [23].

qualitative features of σ_i/σ_f can be understood from rather simple considerations. Much more sophisticated analyses of isomer production excitation function data have been performed [24,21]. These analyses incorporate more realistic level densities from which the excitation energy dependence of Γ_n/Γ_f can be obtained. From these analyses information about E_{II} and E_B values can be extracted.

The isomer excitation energy E_{II} is obtained from the threshold behavior of the excitation function for isomer production [26]. Unfortunately considerable extrapolation from the lowest energy at which measurements are available to the threshold energy is required. This extrapolation is guided by theoretical considerations [27,28,24,22] which are model-dependent. The sensitivity to the model becomes apparent when comparing results from various analyses. Some indication of this sensitivity is apparent in Fig. 6 where we compare E_{II} values extracted from analyses of isomer production excitation functions with theoretical predictions. The empirical values exhibit significant variations. However there appears to be some real discrepancies between the empirical and theoretical E_{II} values. Specifically,

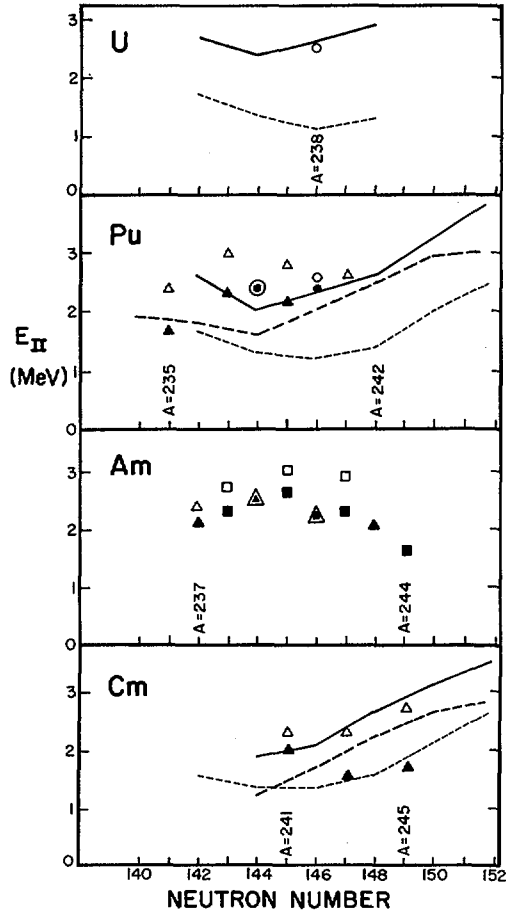


FIG. 6. Comparison of experimental and theoretical isomer excitation energies. The solid, long-dashed, and short-dashed lines are the theoretical results of Pauli and Ledergerber [9], Möller [8], and Möller and Nix [10], respectively. The experimental values indicated by open symbols are from the earlier analysis of Britt and co-workers [24] except for the ^{238}U [16], ^{237}Pu [29], and ^{238}Pu [4] values. The closed symbols are from the later analysis of Britt and co-workers [21]. The differences between the open and closed symbols are a measure of the uncertainties associated with the extraction of E_{II} values from the excitation function data. E_{II} values for isomers attributed to two-quasiparticle excitations have been excluded.

the average trend with neutron number for the heavier americium isotopes is opposite to that predicted. This may reflect inadequacies in the shell correction at the ground state as well as at the isomer deformation. There are indications in at least one theoretical calculation [10] that the deviations between the theoretical and experimental ground state shell corrections depend in a systematic way on neutron number.

4. EXCITATIONS OF THE SHAPE ISOMERS

4.1 Even-even Nuclei

The barriers stabilizing the shape isomers are several MeV high. This is sufficiently high that one can expect to form a variety of excited states which retain the purity of the deformation of the shape isomer. We shall start our discussion by considering even-even shape isomers.

Rotational excitations. The lowest excitations to be expected are rotational excitations. Last year Specht et al.[30] successfully identified a number of transitions between rotational states. Since the moment of inertia of the isomer was expected to be appreciably larger than that of the ground state, the energy levels were expected to be closer together and the low-energy transitions to be highly converted. Therefore they looked for the conversion electrons rather than the gamma rays involved in the rotational de-excitations. This is a very difficult experiment as the feeding of the isomer rotational band is 10^4 times smaller than that of the ground state band of a nucleus which does not fission. To select the electrons associated with population of the isomeric band a delayed coincidence with the fission fragments from the subsequent decay of the isomer was performed. The level scheme they deduced from the conversion electron spectrum is shown in Fig. 7. The value of $\hbar^2/2\mathcal{I}$ they obtained is 3.3 keV, less than half the

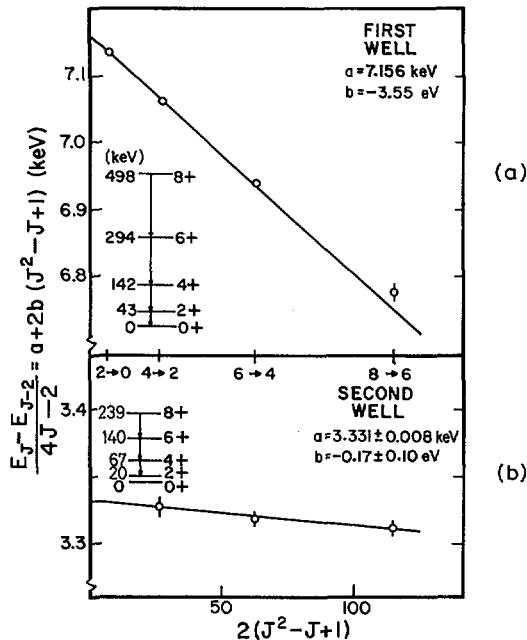


FIG. 7. Fit of the transition energies to the energy expression $E = aJ(J+1) + bJ^2(J+1)^2$ (a) for the ground state band of the first well ($a = 7.156 \text{ keV}$, $b = -3.55 \text{ eV}$) and (b) for the isomeric state band of the second well ($a = 3.33 \pm 0.008 \text{ keV}$, $b = -0.17 \pm 0.10 \text{ eV}$). The intercept gives the rotational constant a and the slope the non-adiabaticity parameter b . (After Specht and co-workers [30] as adapted by Vandenbosch and Huizenga [6]).

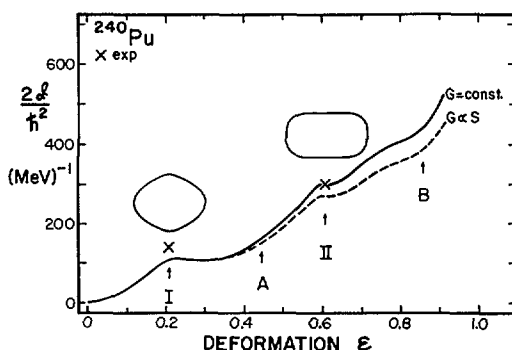


FIG. 8. Comparison of theoretical and experimental values of the moment of inertia as a function of deformation. Adapted from Ref. [33].

value of 7.1 keV exhibited by the ground state rotational band. This is the most direct evidence obtained thus far that the shape isomer has a distortion qualitatively different from that of the ground state. Several calculations of the dependence of the moment of inertia on deformation have been reported [31-33]. The results of Sobiczewski et al. [33] are compared with the experimental result in Fig. 8. Theoretically the dependence on deformation is rather complicated, largely because of pairing effects which depend on the single particle level density near the Fermi surface and hence fluctuate as a function of deformation with the same period but out of phase with the shell correction. There is also a small uncertainty depending on which variant of the pairing strength is chosen. For a pairing strength independent of surface areas, $G = \text{const.}$, the observed moment of inertia is in excellent agreement with the calculated deformation of the second minimum. Such good agreement may be somewhat fortuitous in view of the poorer agreement between the calculation and experiment at the ground state deformation. The theoretical nuclear shapes at the first and second minimum have also been sketched in the figure.

It can also be seen from the results presented in the previous figure (Fig. 7) that the shape isomer is a better rotator than the ground state, since the "correction" term in the expression

$$E(J) = aJ(J+1) + bJ^2(J+1)^2$$

is much smaller for the isomer than for the ground state. This result can be qualitatively understood from the point of view that the smaller rotational energies for isomers result in a better separation of this degree of freedom from other degrees of freedom such as vibrations and breaking of nucleon pairs. If one is willing to accept an identification of the second term as arising primarily from centrifugal stretching [34,35], further information about the properties of the shape isomer may be deduced. For such a model the total energy may be written in lowest order as

$$E(J) = (1/2)C(\beta - \beta_0)^2 + \frac{\hbar^2 J(J+1)}{2\mathcal{I}(\beta)} + \dots$$

where β_0 is the equilibrium deformation in the absence of rotation and C is a measure of the restoring force. [The quantity C may be evaluated in the present approximation from theoretical potential energy curves using

$C = d^2V(\beta)/d\beta^2$ evaluated at $\beta = \beta_0$. The minimum in the above expression for $E(J)$ for a given J determines the equilibrium deformation β for that J . If one assumes that the moment of inertia is proportional to β^2 , as expected for irrotational flow motion, and designates $\mathcal{I}_{\beta=\beta_0}$ as \mathcal{I}_0 , one obtains

$$E(J) = \frac{\hbar^2 J(J+1)}{2\mathcal{I}_0} - \frac{\hbar^4 J^2(J+1)^2}{2\beta_0^2 \mathcal{I}_0^2 C} + \dots$$

From this expression we see that the coefficient of the second term in the energy expansion is inversely proportional to the product of the square of the deformation times the square of the moment of inertia. The expression has been written with both β_0^2 and \mathcal{I}_0^2 appearing explicitly so as to eliminate the mass parameter B . The derivation assumes that B varies negligibly within a given well but we can expect a significant variation in going from the ground state well to the shape-isomeric well. If one assumes that the moment of inertia is proportional to β rather than β^2 , as indicated by the empirical data and predicted by the "governor" model [36], the second term in the expansion turns out to have the same dependence on β and \mathcal{I}_0 , but with a different coefficient. The quantity C is also expected to depend on deformation, and indeed precise measurements of the rotational state spacings may provide a means to deduce this interesting quantity. From the above relationship the ratio of the b coefficients for the isomeric and ground states is given by

$$\frac{b_{II}}{b_I} = \frac{C_I}{C_{II}} \left(\frac{\mathcal{I}_I}{\mathcal{I}_{II}} \right)^2 \left(\frac{\beta_I}{\beta_{II}} \right)^2.$$

Using the experimental \mathcal{I} values and the theoretical β values (assuming the present deformation parameter β to be dependent on the Nilsson deformation parameter as $\beta \approx \epsilon(1 + \epsilon/3)$) one obtains $C_I/C_{II} = 2.0 \pm 1.0$. This is in agreement with the theoretical results of Tsang and Nilsson [37] who present a potential energy function which is approximately twice as stiff at the first minimum as at the second minimum. More precise data as well as attention to the higher order terms in the theoretical expression would enable a more quantitative test to be performed.

Vibrational excitations. Our knowledge of vibrations about the equilibrium deformation of the shape isomer is unique in that the location of one or two of the higher vibrational states in uranium and plutonium nuclei is known whereas the first excited vibrational state has probably not ever been identified. These states show up as resonances in the fission cross-section excitation functions for neutron, photon, and direct reaction charged particle induced fission. One of the earliest examples of such a resonance was found in the $^{239}\text{Pu}(d, pf)$ reaction [38,39] where a prominent resonance occurs at 4.95 MeV above the ground state. The isomer excitation energy is about 2.4 MeV [21]. It is not clear whether the 4.95 MeV resonance is a 2, 3, or 4-phonon state. There appears to be another resonance at about 4.4 MeV, although the K value of this resonance is not known. If it is $K = 0$, then it is quite likely that the 4.95 MeV resonance is the $n = 3$ or $n = 4$ state. It would be very interesting to locate the lower states, as this would enable a direct determination of the $\hbar\omega$ value of the second well. This in turn contains information about the stiffness of the potential (C) and the inertial parameter (B) through the relation $\omega = (C/B)^{1/2}$.

Two-quasiparticle excitations. It has been thought for some time that a number of the observed even-even spontaneously fissioning isomers were not the lowest state in the second minimum. The conclusion was primarily based

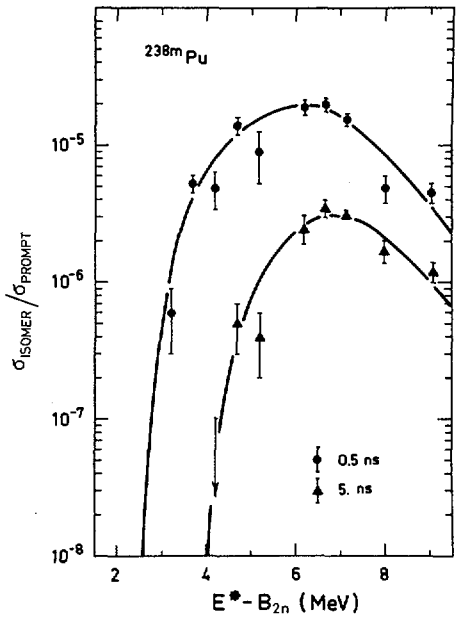


FIG. 9. Excitation functions for the two isomers of ^{238}Pu . From Ref. [4].

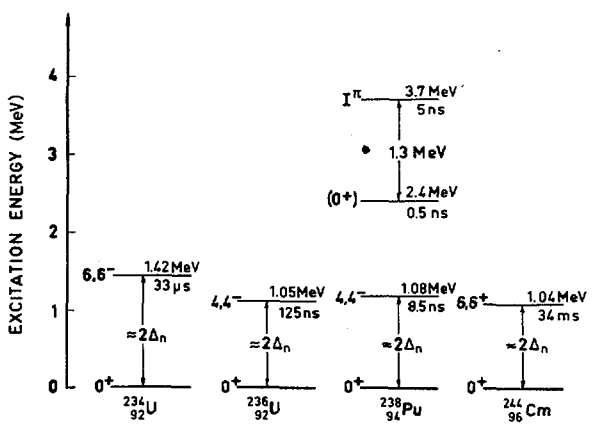


FIG. 10. Two-quasiparticle states in the first and second well. From Ref. [4].

on unusually high excitation energies, low yields, and long half-lives. This interpretation has received important experimental support by the recent discovery [4] of a second isomer in the even-even nucleus ^{238}Pu . The new shorter-lived 0.5-nsec isomer exhibited a lower threshold and higher yield than the 5-nsec isomer. The excitation function data is illustrated in Fig. 9. The level diagrams for this new two-quasiparticle state and of previously known two-quasiparticle states in the first well are shown in Fig. 10. The pairing gap at the two deformations appears to be fairly comparable. These results again do not allow us to distinguish whether the pairing strength G is independent of or more nearly proportional to the surface area. In the latter case one would expect the energy gap to be about 0.3 MeV greater at the second minimum than at the first minimum. It should also be remembered that the theoretically expected [40] dependence of the pairing strength on deformation is weaker than the often-assumed linear proportionality to the surface area.

The spin of the two-quasiparticle state in ^{238}Pu or in other suspected cases of two-quasiparticle isomerism is not known. If the orbitals involved in the ^{238}Pu isomer are the same as suggested (see later discussion) for the double isomers in even-odd ^{237}Pu , the spin is likely to be 3 or greater. One can hope to gain some qualitative information about the J and K values from new projectile-fragment angular correlations now being studied [41,42]. These results indicate that both 35-nsec ^{236}Pu and 5-nsec ^{238}Pu have non-zero spins and that $K \approx I$. Even with fairly precise anisotropies, I doubt that unique J and K values can be established. In addition to the smearing of the alignment by particle and gamma emission prior to fission and especially by re-orientation due to environmental interactions, it seems likely that some K -mixing will occur during passage through the barrier. An alternative method for characterizing the spin of the two quasiparticle isomers would be to study the conversion electrons associated with a possible gamma decay branch to the rotational band built on the lowest state of the second well.

4.2 Excitations of odd-A Isomers

The only known low-lying excitations of shape isomeric odd-A nuclei are those implied by the existence of two isomers in ^{237}Pu and possibly two isomers in ^{241}Pu . The former pair is more accessible for study by reason of the availability of appropriate targets for producing the isomers in $(\alpha, 2n)$ and $(d, 2n)$ reactions involving compound nucleus formation. The two isomers are thought to correspond to different single particle configurations for the odd nucleon. One of these configurations is presumably the lowest state in the second well, while the higher-lying state is a single particle or single-hole state. The two isomers presumably differ sufficiently in Ω values that the gamma decay of the upper isomer could be sufficiently long to support the observed half-life.

The relative yields of the two shape isomers in ^{237}Pu have been studied as a function of the angular momentum deposition in the compound nucleus [43]. The results illustrated in Fig. 11 show that the ratio of the production cross-sections for the short-lived (80 nsec) and long-lived (1100 nsec) isomers decreases with increasing angular momentum deposition. This result proves that the long-lived isomer has a higher spin than the short-lived isomer. Conventional isomer ratio statistical model calculations have been performed and more quantitative comparisons with the data indicate as possible spin combinations the values shown in Table I. This information by itself does not take us very far. If however we now examine the Nilsson diagram in the region of the second minimum some suggestive identifications are possible. Figure 12 shows the level diagram at the deformation of the

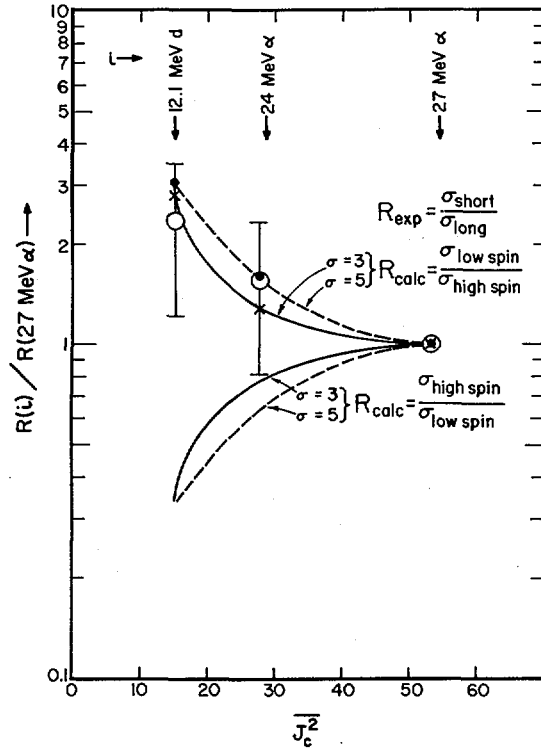


FIG. 11. Ratio of isomer ratios R as a function of the mean square initial compound nuclear angular momentum. Comparison of the experimental values (open circles) with the calculated values (solid and dashed curves) demonstrates that the short-lived ^{237}Pu isomer has the lower spin. From Ref. [43].

TABLE I. SPIN PAIRS CONSISTENT WITH STATISTICAL MODEL INTERPRETATION OF ^{237m}Pu ISOMER RATIOS

The pairs in parentheses are considered less likely on the basis of the isomer ratio calculations

Isomer	Spin Pairs					
82 nsec	$\frac{5}{2}$	$\frac{7}{2}$	$\frac{7}{2}$	$\frac{9}{2}$	$\left(\frac{3}{2}\right)$	$\left(\frac{5}{2}\right)$
1120 nsec	$\frac{11}{2}$	$\frac{9}{2}$	$\frac{11}{2}$	$\frac{11}{2}$	$\left(\frac{11}{2}\right)$	$\left(\frac{9}{2}\right)$

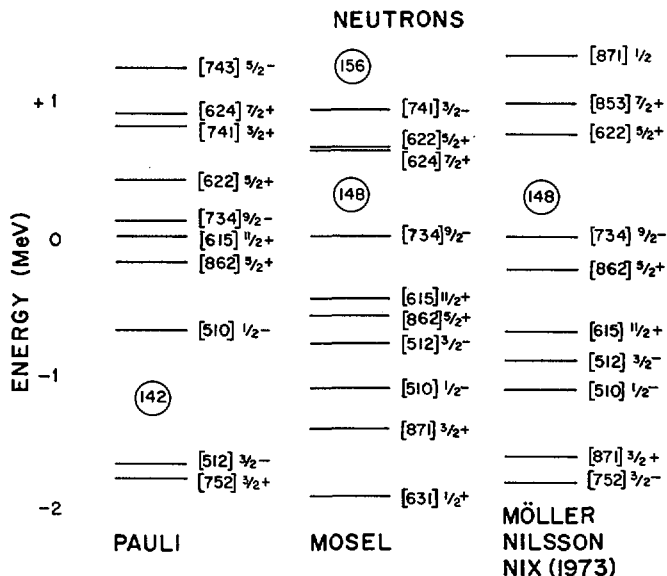


FIG. 12. The single-neutron level ordering at the second minimum. Most of the levels have been read from graphs and consequently their energies are only approximate. The asymptotic quantum number assignments are also ambiguous in a few situations where mixing occurs as levels of the same spin and parity approach each other. See text for references.

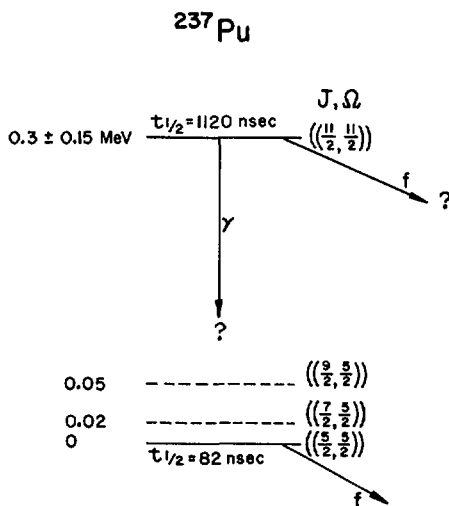


FIG. 13. Tentative decay scheme for the shape isomers of ^{237}Pu .

second minimum obtained in various theoretical calculations. The first column [11] is based on a deformed Woods-Saxon potential employed by the Copenhagen-Basel groups. The second column [13] is based on the two-center harmonic-oscillator potential employed by the Frankfurt-Oak Ridge groups. The last column [10] is based on the folded Yukawa potential of the Los Alamos group. ^{237}Pu has 143 neutrons. In all three level diagrams one observes a high spin $11/2^+$ level close to the Fermi surface. (An earlier diagram [12] based on a one-center harmonic oscillator had a $11/2^-$ level in this region.) The most likely orbitals to be occupied by the 143rd neutron in both the Mosel and Möller-Nilsson-Nix diagrams are the $5/2^+$ and $11/2^+$ orbitals, spin values consistent with the spin pairs given in Table I. It should be considered fortuitous if the theoretical calculations were to give the exactly correct ordering at the second minimum. In a subsequent experiment [29] it has been shown that the long-lived isomer lies 0.3 MeV above the shorter-lived isomer. We thus have the tentative decay scheme shown in Fig. 13. It is not clear from either the experimental observations or from theoretical expectations whether the excited state is a particle or a hole state. It is also not possible to conclude whether the apparent fission decay of the long-lived isomer is due to direct fission or from fission following gamma decay to the short-lived isomer. Thus the 1120-nsec half-life is a lower limit to the partial fission half-life of this state. The fact that the excited state has a partial fission half-life which is longer than that of the lower state should not be considered surprising. The ground state spontaneous fission half-lives of odd-A nuclei show large fluctuations from nucleus to nucleus, presumably due to the differing specialization energies depending on their spin and parity.

Although the fact that the long-lived state lies higher in energy makes the interpretation of its half-life ambiguous because of a possible gamma branch, this circumstance provides a unique opportunity to study the spectroscopy of an odd-A nucleus in its second well. If a gamma branch exists one expects a cascade through the rotational band based on the lower state. These transitions could be studied by conversion electron spectroscopy.

ACKNOWLEDGMENTS

It is a pleasure to acknowledge my colleagues here and elsewhere with whom I have had stimulating conversations. Among these are S. Björnholm, H.C. Britt, I. Halpern, R.H. Heffner, J.R. Huizenga, U. Mosel, J.R. Nix, J. Pedersen, P.A. Russo, G. Sletten, L. Willets, and K. Wolf.

REFERENCES

- [1] POLIKANOV, S.M., DRUIN, V.A., KARNAUKHOV, V.A., MIKHEEV, V.L., PLEVE, A.A., SKOBELEV, N.K., SUBBOTTIN, V.G., TER-AKOPYAN, G.M., FOMICHEV, V.A., Sov. Phys. JETP 15 (1962) 1016.
- [2] POLIKANOV, S.M., SLETTEN, G., Nucl. Phys. A151 (1970) 656.
- [3] VANDENBOSCH, R., WOLF, K.L., Second IAEA Symposium on Physics and Chemistry of Fission (IAEA, Vienna, 1969) p. 439.
- [4] LIMKILDE, P., SLETTEN, G., Nucl. Phys. A199 (1973) 504.
- [5] METAG, V., LIUKKONEN, E., GLOMSET, O., BERGMAN, A., Paper SM-174/26, these Proceedings, Vol. 1.
- [6] VANDENBOSCH, R., HUIZENGA, J.R., "Nuclear Fission", (Academic Press, New York, 1973).
- [7] WOLF, K.L., UNIK, J.P., Phys. Lett. 43B (1973) 25.

- [8] MÖLLER, P., Nucl. Phys. A192 (1972) 529.
- [9] PAULI, H.C., LEDERGERBER, T., Nucl. Phys. A175 (1971) 145.
- [10] MÖLLER, P., NIX, J.R., Paper SM-174/202, these Proceedings, Vol.1.
- [11] PAULI, H.C., Physics Reports 7C (1973) 35.
- [12] NILSSON, S.G., TSANG, C.F., SOBICZEWSKI, Z., WYCECH, S., GUSTAFSON, G., LAMM, I., MÖLLER, P., NILSSON, B., Nucl. Phys. A131 (1969) 1.
- [13] MOSEL, U., SCHMITT, H.W., Nucl. Phys. A165 (1971) 13.
- [14] URIN, M.G., ZARETSKY, D.F., Nucl. Phys. 75 (1966) 101.
- [15] SOBICZEWSKI, A., Proc. Robert A. Welch Found. Conf. Chem. Res.. (Houston, 1969) 13, Robert A. Welch Foundation, Houston (1970) 472.
- [16] RUSSO, P.S., PEDERSEN, J., VANDENBOSCH, R., Paper SM-174/96, these Proceedings, Vol.1.
- [17] PEDERSEN, J., RASMUSSEN, B., Nucl. Phys. A178 (1972) 449.
- [18] PASHKEVICH, V.V., Nucl. Phys. A133 (1969) 400.
- [19] LARSON, S.E., RAGNARSSON, I., NILSSON, S.G., Phys. Lett. 38B (1972) 269.
- [20] GÖTZ, U., PAULI, H.C., JUNKEN, K., Phys. Lett. 39B (1972) 436.
- [21] BRITT, H.C., BOLSTERLI, M., NIX, J.R., NORTON, J.L., Phys. Rev. C7 (1973) 801.
- [22] NAMBOODIRI, M.N., RUDDY, F.H., ALEXANDER, J.M., Phys. Rev. C7 (1973) 1222; FLEURY, A., RUDDY, F.H., NAMBOODIRI, M.N., ALEXANDER, J.M., Phys. Rev. C7 (1973) 1231.
- [23] BORGGREEN, J., KASHY, E., HATTULA, J., MAARBJERG, V., Nucl. Phys. (to be published).
- [24] BRITT, H.C., BURNETT, S.C., ERKKILÄ, B.H., LYNN, J.E., STEIN, W.E., Phys. Rev. C4 (1971) 1444.
- [25] HYDE, E.K., Nuclear Properties of the Heavy Elements, Vol. III: Fission Phenomena, (Prentice-Hall, Englewood Cliffs, New Jersey, 1964).
- [26] BJØRNHOLM, S., BORGGREEN, J., WESTGAARD, L., KARNAUKOV, V.A., Nucl. Phys. A95 (1967) 513.
- [27] JÄGARE, S., Phys. Lett. 32B (1970) 571.
- [28] VANDENBOSCH, R., Phys. Rev. C5 (1972) 1428.
- [29] VANDENBOSCH, R., RUSSO, P.A., SLETTEN, G., MEHTA, M., Phys. Rev. C (to be published).
- [30] SPECHT, H.J., WEBER, J., KONECNY, F., HEUNEMANN, D., Phys. Lett. 41B (1972) 43.
- [31] DAMGAARD, J., PAULI, H.C., STRUTINSKY, V.M., WONG, C.Y., BRACK, M., STENHOLM-JENSEN, A., Second IAEA Symposium on Physics and Chemistry of Fission, IAEA, Vienna (1969) 213.
- [32] KRUMLINDE, J., Nucl. Phys. A160 (1971) 471.
- [33] SOBICZEWSKI, A., BJØRNHOLM, S., POMORSKI, K., Nucl. Phys. A202 (1973) 274.
- [34] BOHR, A., MOTTELSON, B.R., Mat. Fys. Medd. Dan. Vid. Selsk. 30 (1955) No. 1.
- [35] DIAMOND, R.M., STEPHENS, F.J., SWIATECKI, W.J., Phys. Lett. 11 (1964) 315.
- [36] GUPTA, R.K., Phys. Rev. C6 (1972) 426.
- [37] TSANG, C.F., NILSSON, S.G., Nucl. Phys. A140 (1970) 275.
- [38] BRITT, H.C., BURNETT, S.C., CRAMER, J.D., Second IAEA Symposium on Physics and Chemistry of Fission (IAEA, Vienna, 1969) 375.
- [39] BACK, B.B., BONDORF, J.P., OTROSHENKO, G.A., PEDERSEN, J., RASMUSSEN, B., Second IAEA Symposium on Physics and Chemistry of Fission (IAEA, Vienna, 1969) 351.
- [40] KENNEDY, R.C., WILETS, L., HENLEY, E.M., Phys. Rev. Lett. 12 (1964) 36.
- [41] GANGRSKY, YU.P., KHANH, N.C., PULATOV, D.D., HIEN, P.Z., Dubna preprint P7-6466 (1972).

- [42] SPECHT, H.J., KONECNY, E., WEBER J., KOZHUHAROV, C., Paper SM-174/19, these Proceedings, Vol. 1.
 [43] RUSSO, P.A., VANDENBOSCH, R., MEHTA, M., TESMER, J.R., WOLF, K.L., Phys. Rev. C3 (1971) 1595.

DISCUSSION

L. WILETS: Could you say what dependence $\mathcal{J}(\beta)$ you assumed in deducing the C parameters?

R. VANDENBOSCH: Somewhat to our initial surprise, we found that it is possible to deduce the ratio C_I/C_{II} independently of whether the moment of inertia \mathcal{J} is proportional to β or to β^2 . This is a consequence of the fact that only the numerical coefficient and not the functional form of the second term in our final expression for $E(J)$ is determined by the dependence of \mathcal{J} on β . This coefficient cancels when one considers the ratio C_I/C_{II} . However, one needs to know both \mathcal{J} and β at both deformations, in order to deduce C_I/C_{II} .

H. C. PAULI: Does $C_I/C_{II} \sim 2$ imply that the spacing of vibrational states is smaller in the first than in the second well?

R. VANDENBOSCH: No, the vibrational energy depends on both the stiffness C and the mass parameter B. If we knew $\hbar\omega$ for the second well we could deduce information about the mass parameter B.

C. F. TSANG: You made a statement, which was also implied in one of the figures shown by Nix¹ in Session II, that the error in barrier heights is due to defects in ground-state mass calculations. While there is empirical support for this statement, it is difficult to imagine a defect in the ground-state calculation not propagating to the barriers. Also it is difficult to imagine that one can calculate the barrier energies more accurately than ground-state energies, when one knows much more about the ground-state properties. Could you comment on this?

R. VANDENBOSCH: I do not think that an inadequacy in calculating the ground-state mass defect necessarily propagates into the mass defect at the barrier. The point is that the shell correction is most sensitive to the location of the single particle states closest to the Fermi surface. A state which is misplaced close to the Fermi surface at the equilibrium deformation can have a great effect on the ground-state mass defect but be too far away from the Fermi surface at the saddle deformation to affect the barrier mass defect.

V. E. VIOLA: I should like to point out that the ground-state mass systematics show a distinct deviation at $N \approx 146$, which may be associated with the deviation in the isomer half-lives at this neutron number.

R. VANDENBOSCH: I do not think that the ground-state mass defect is directly related to the isomer half-life dependence on neutron number. I had thought that the second minimum shell correction might be influencing the ground-state spontaneous fission half-lives. Bjørnholm recently pointed out to me that the ground-state mass defects maximize at $N = 142$ for ($Z \sim 92$) and at $N = 152$ at $Z \sim 98$. These lead to maximum mass defects in the plutonium region at $N \approx 146$, as you have mentioned. Swiatecki

¹ MÖLLER, P., NIX, J.R., Paper IAEA-SM-174/202, these Proceedings, Vol. 1.

has shown that these ground-state mass defects account nicely for the deviations of the observed ground-state half-lives from the Z^2/A dependence expected from the simple liquid drop model.

N. VILCOV: I noticed that in your first slide there was an empty space for ^{243}Bk . We have produced this fission isomer in Bucharest and have measured its excitation energy in the $^{241}\text{Am}(\alpha, 2n)$ reaction. Its lifetime is of the order of a few nanoseconds and it was first observed by the Heidelberg group.

R. VANDENBOSCH: Thank you for the information.

C.D. BOWMAN: In your summary of the systematic properties of fission isomerism you omitted any discussion of the parameter $\hbar\omega_A$. Would you comment on this, please?

R. VANDENBOSCH: The only information on $\hbar\omega_A$ which is obtained from isomer studies comes from the gamma branch. This is discussed² in Paper IAEA-SM-174/96.

L.G. MORETTO: It may be worth pointing out that your quadratic form giving the energies in the 1st and 2nd well as a function of the deformation β also includes the dependence of the gap parameter on β . Thus the stiffness constant C in principle contains information about such a dependence, as well as information concerning the shell model energy.

R. VANDENBOSCH: I agree that in principle pairing effects may affect C . I would guess they are rather small at the second minimum because of the large energy difference between the rotational excitations and the pairing gap.

² RUSSO, P., PEDERSEN, J., VANDENBOSCH, R., Paper IAEA-SM-174/96, these Proceedings, Vol. 1.

GAMMA BRANCH OF THE ^{238}U SHAPE ISOMER*

P. A. RUSSO, J. PEDERSEN**, R. VANDENBOSCH

University of Washington,

Seattle, Wash.,

United States of America

Abstract

GAMMA BRANCH OF THE ^{238}U SHAPE ISOMER.

Systematics of the double-humped fission barrier predict a poorly developed inner barrier for the lower- Z actinide nuclei. Experimental evidence from delayed fission of even-even actinides suggests that the fission branch of the ^{238}U shape isomer decay represents only one-tenth of the total width for shape isomer de-excitation. These observations indicate an inner barrier for ^{238}U sufficiently penetrable that the greater strength for shape isomer de-excitation is in the gamma branch.

The 200-nsec ^{238}U shape isomer was produced by the (d, pn) reaction with 18-MeV deuterons incident on natural uranium targets. The deuteron beam from the FN Tandem is pulsed. A Ge(Li) detector was used to observe the delayed gamma rays. Time and energy information for each event was stored.

Most of the large number of delayed gamma lines have been attributed to normal isomers in fission fragments by comparison of the energy spectra with other gamma spectra obtained in the same experimental configuration using different reactions which are not capable of populating the ^{238}U shape isomer. Of the remaining lines, most can be excluded by their half-lives which are inconsistent with the 200-nsec half-life of $^{238}\text{U}^m$.

A line at 2.514 MeV has been observed which is attributed to the decay of the shape isomer to the 0.045-MeV 2^+ rotational state of ^{238}U . It has a half-life in agreement with that observed for the fission branch and is produced with a yield consistent with predictions of a more penetrable inner barrier. A second weaker line has been observed at 1.879 MeV corresponding in energy to the transition from the shape isomer to the first excited 1^- state at 0.680 MeV in ^{238}U . The decay of this line is also consistent with the measured half-life of $^{238}\text{U}^m$.

INTRODUCTION

The interpretation of spontaneously fissioning isomers as shape isomers has received considerable support from theoretical calculations [1] which apply deformation-dependent shell corrections to a smooth liquid drop potential. Three-MeV fluctuations in the shell correction energy at approximately twice the normal deformation give rise to a sufficiently deep second well from which isomeric fission can occur. The first direct experimental evidence connecting fission isomers with this larger deformation has been provided by the measurement of Specht et al. [2] who have found that the moment of inertia for rotations built upon the isomeric state is approximately twice as large as that measured for the normally deformed ground state.

Compound resonances from sub-barrier neutron-induced fission and vibrational resonances from near-barrier direct reaction fission give strong support to the hypothesis that the secondary minimum is a general phenomenon in actinide nuclei. These results and measurements of delayed fission with half-lives and yields consistent with fission from the calculated second minimum have contributed to a systematic understanding of single particle effects as a function of deformation.

* Work supported in part by the US Atomic Energy Commission.

** Permanent address: Niels Bohr Institute, University of Copenhagen, Copenhagen, Denmark.

The abundance of fission isomers among the isotopes of plutonium and americium leads to some speculation concerning shape isomer population and de-excitation processes. The delayed fission results show an abrupt decrease in the number of observed fission isomers for Z less than 94. Since shape isomerism is believed to be a general occurrence among the actinides, the systematics should also explain this abrupt change. An alternate mode of decay for the de-excitation of shape isomers could account for the absence of delayed fission in the low- Z actinides. Experimental and theoretical evidence suggests a sufficiently penetrable inner barrier for a competitive gamma branch in the low- Z actinide region. The shape isomer tunnels through the more penetrable inner barrier and de-excites by gamma ray emission to the ground state in the first minimum.

The fission barrier calculations of Tsang and Nilsson [3] show that the inner barrier is systematically higher than the outer barrier for the high- Z actinides. When asymmetric distortions are considered, the dominance of the inner barrier begins at about $Z = 94$. The dominance shifts to the outer barrier for actinide nuclei of lower Z .

Analysis [4] of data from near-barrier direct reaction fission and from delayed fission measurements indicates that the outer barrier height, E_B , exceeds the inner barrier height, E_A , for nuclei with Z less than 94. This is illustrated in Fig. 1 which shows barrier heights for even-even nuclei, obtained from such an analysis.

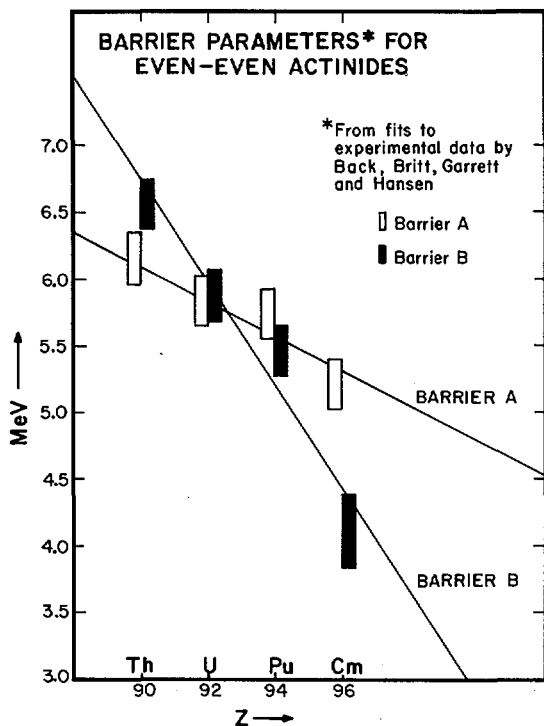


FIG. 1. Inner and outer barrier heights, E_A and E_B , as a function of Z . Bars indicate the limits of E_A and E_B averaged for each Z , obtained from fits to (t, pf) data. Error bars represent the range of values of E_A and E_B for each Z .

Björnholm and Strutinsky [5] have concluded from an interpretation of fission fragment angular distributions that the outer barrier is the higher one for Th and Pa isotopes. The anisotropy in fission fragment angular distributions is due to a non-uniformity in the distribution of the K-values at the fission barrier saddle point where K is the projection of the total angular momentum along the nuclear symmetry axis. The characteristic feature for the lighter elements ($Z \leq 92$) is a very strong energy dependence for $W(0^\circ)/W(90^\circ)$ whereas the heavier elements ($Z > 92$) all show a statistical type anisotropy. If the secondary minimum is deep, there will be large damping effects, and the nucleus might "forget" the K-value with which it penetrated the first barrier during the time it participates in the class II compound motion. If the second barrier is much lower than the first, several channels with different K-values will be open for fission and the angular distribution will consequently be of statistical nature. If the second barrier is larger than the first the nucleus will again obtain a certain K-value in penetrating the outer barrier. Thus, the conclusion of the authors is that a strongly energy-dependent anisotropy indicates that the second barrier is the highest one. The data shows that the transition region from statistical to strongly energy-dependent anisotropies occurs around uranium.

The systematics of photofission as interpreted by Vandenbosch [6] lead to the same conclusion regarding the systematics of the inner and outer barrier heights. The lowest barriers to dipole and quadrupole fission are the rotational $2+$ and octupole vibrational $1-$, $K = 0$ barriers. At the first barrier, these are separated by about 1 MeV with the $1-$ level lying higher. At the deformation of the second barrier, stabilization to asymmetric distortions creates a near-degeneracy in the two barriers. Since the ratio of quadrupole to dipole photoabsorption is very small, the presence of a sizable quadrupole component in the photofission fragment angular distributions indicates that the dipole barrier exceeds the quadrupole barrier. This is the case when the inner barrier is higher than the outer barrier. Fission fragment angular distributions for photofission near the barrier show a sizable quadrupole contribution for plutonium nuclei. The quadrupole component is small at all energies for lower-Z actinides. This suggests the dominance of the outer barrier over the inner barrier for Z less than 94.

Only one fission isomer has been observed in neptunium [7]. The ratio of the yield of delayed fission to the ground state yield (fission isomer ratio) is three orders of magnitude lower than fission isomer ratios of odd-A plutonium isotopes. The two shape isomers ^{236m}U and ^{238m}U [8] with half-lives 100 and 200 nsec respectively have isomer ratios that are an order of magnitude smaller than observed for the even-Pu isotopes. The lower yields of the even-even uranium fission isomers and the very low yield of the ^{237}Np fission isomer are consistent with the existence of a competitive branch in the decay of uranium and neptunium shape isomers.

An experimental investigation of the gamma branch of ^{238m}U has been motivated by the ideas in the preceding discussion. The ground state of the secondary minimum in ^{238}U has spin and parity $0+$ because of the even-even character of this nucleus. Thus a large fraction of its gamma decay is expected to populate the lowest lying $2+$ level in the first well. Population of the isomer by the (d,pn) reaction with 18 MeV deuterons results in a cross-section of $\sim 5 \mu\text{b}$ for delayed fission. The expected cross-section for a gamma decay is therefore 50 to 100 μb . From the general systematics of delayed fission thresholds the excitation energy is expected to lie between 2 and 3 MeV. The first excited $2+$ state in the primary minimum lies at 0.045 MeV. Therefore, a 2 to 3 MeV delayed gamma ray with a half-life of 195 ± 30 nsec is sought.

EXPERIMENTAL METHODS

$^{238}\text{m}\text{U}$ has been produced by the d,pn reaction with an 18 MeV pulsed deuteron beam incident on self-supporting natural uranium targets 3.67 mg/cm^2 thick. Delayed gamma rays were observed between beam bursts with a 25 cm^3 true coaxial Ge(Li) detector. The gamma rays were timed against a signal from the beam pulser oscillator.

Observation of the gamma branch is considerably more difficult than the delayed fission measurements because of the low Q-value for the gamma branch ($\sim 3\text{ MeV}$) compared to the fission branch ($\sim 150\text{ MeV}$). The very high fission fragment kinetic energies result in a delayed region which is essentially free of background for fission fragment detection. However, prompt fission cross-sections of 1b occur with 18 MeV deuterons on ^{238}U . For the delayed time region from 10 to 200 nsec after the beam burst, delayed gamma activity, primarily due to de-excitation of normal isomers in fission fragments, represents approximately 6.5% of the total gamma activity from prompt fission [9].

Reduction of delayed gamma-ray background has been accomplished by optimizing the beam-pulsing system. A 100 μsec interval between beam bursts was used to prevent buildup of shorter-lived activities.

Lead lining in the scattering chamber and a 20-foot-long Faraday cup, together with the use of lead collimators, beam stops and beam tube shields, reduced the background further. Since the major part of the background was due to decay from fission fragments, a relatively thin target was used, allowing approximately 85% of the fission fragments to leave the target (the range of fission fragments in uranium is $\sim 10\text{ mg/cm}^2$). About half of these travel in the direction of the detector and will be stopped near the detector surface. To diminish the solid angle for these fragments a rotating disc (speed 1000 rev/min) was placed in the vacuum chamber in front of the detector surface. The diameter of the disc was 25 cm corresponding to a velocity of $\sim 1\text{ cm/msec}$ for the portion of the disc in front of the detector.

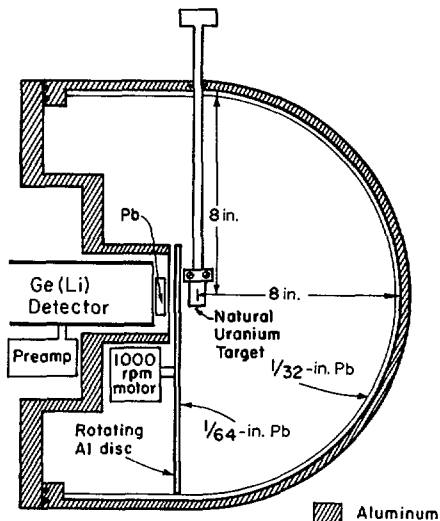


FIG. 2. Cross-sectional view of the 16-inch hemispherical scattering chamber.

For activities long-lived compared to the rotation period, the solid angle reduction factor for fragments flying in the direction of the detector is 8. Reduction of background from fission fragments escaping in the direction opposite the detector was accomplished with a chamber which was hemispherical with a radius of 20 cm. The velocity of an "average" fission fragment is ~ 1 cm/nsec which means that the solid angle for delayed gamma activity from the fragments flying in the direction opposite the detector is negligible. Figure 2 shows a cross-sectional view of the chamber. Since the interest is greatest for gamma rays above 1 MeV, lead was positioned between the target and the detector to absorb 75 percent of the 0.5 MeV gamma rays, permitting the use of higher beam currents.

Constant fraction timing with the true-coaxial Ge(Li) detector resulted in a resolution of 5 to 8 nsec, full width at one-half maximum, for timing against coincident gamma rays from ^{60}Co detected by a plastic scintillator. The use of pulse shape discrimination to gate the time spectrum improved the time resolution to 3 to 5 nsec.

The beam pulser oscillator signal was used to start a time-to-amplitude converter (T.A.C.) which was stopped by a signal from the Ge(Li) detector. The prompt coincidences were included in the 4 μs T.A.C. range so that pileup events between a prompt and delayed gamma ray were registered as prompt events leaving the delayed region free of pileup pulses. The two analog signals corresponding to the gamma-ray time and energy were digitized and stored in an on-line computer. Event-by-event data recording permitted correction of the energy spectra for fractional percent gain shifts and zero shifts which occurred during the typical 5-day data collection periods.

Several lines in the spectrum were outstanding after one hour of data collection. Two of these at 1.279 MeV and 1.313 MeV have been identified [10] as normal isomers in the fission fragments ^{134}Te and ^{136}Xe respectively. Several lines below 0.4 MeV come from a ^{133}Ba source which was positioned near the Ge(Li) detector during the experiment. A broad line at 0.693 MeV results from decay of the first 0+ state of ^{72}Ge excited by n,n' in the germanium crystal. These lines together with a pulser were used to monitor the gain and zero level of the energy spectrum on an hourly basis. Off-line correction of the data for gain and zero shifts restored the resolution to approximately 3 keV at 2.5 MeV.

The corrected data has been analyzed in separate time bins. The time spectrum corresponding to a given energy region was used to determine the optimum time region for a 200 nsec activity. Typically, the analysis of 2 to 3 MeV gamma rays began approximately 150 nsec from the beam burst edge.

For 200 nsec half-lives, the sensitivity of the experiment is 30 to 50 μb , based on two standard deviations. Subtraction of long-lived backgrounds from the early time periods improved this sensitivity by a factor of two.

Data was taken in four separate experiments. Two of these used 18 MeV deuteron beams and the natural uranium target. More than sixty delayed gamma lines between 0.9 and 3.7 MeV were common to the resulting energy spectra. Many of these were eliminated on the basis of half-lives which were incompatible with the 195 ± 30 nsec half-life on ^{238}mU . Others were known to be normal isomers in fission fragments based on data from ^{252}Cf spontaneous fission [10]. Others were observed in investigations similar to the present experiments using 11 MeV deuterons with a ^{235}U target [11]. Two additional experiments were performed with the same experimental setup to eliminate those remaining lines which result from processes other than de-excitation of the ^{238}U shape isomer. These used the same uranium target and

beams of 13 MeV deuterons and 13 MeV protons respectively. The duration of each experiment was sufficient to obtain approximately the same number of prompt fissions obtained in each of the runs with 18 MeV deuterons. This required approximately twice the number of beam particles at the lower energies. The 13 MeV proton experiment does not appreciably populate ^{238}U final states except by direct processes, and therefore will not lead to significant population of the ^{238}U shape isomer. The ^{238}U shape isomer cross section is at least a factor of 10 lower with 13 MeV deuterons than with 18 MeV deuterons on ^{238}U [8]. The experiment is insensitive to cross-sections of less than 25 μb for a 200 nsec decay. Since the measured cross-section for each gamma line is approximately 100 μb in the 18 MeV deuteron experiment, lines appearing in the spectra from the 13 MeV deuteron experiment cannot be the result of the gamma branch.

RESULTS

Table I summarizes the data from background-subtracted spectra for the indicated time intervals using the combined results of the two 18 MeV deuteron experiments. The lines included in the table are those with half-lives which are consistent with 195 ± 30 nsec, and which appear in each of the

Table I. Tabulation of gamma lines appearing in both 18-MeV deuteron experiments. Lines with half-lives incompatible with 195 ± 13 nsec have been excluded. Number of counts in peak corresponds to integration over the time interval from 150 to 750 nsec after the prompt peak, except where indicated by asterisk (*) in which cases the time interval was 150 to 450 nsec.

E (MeV) γ	No. of Counts in Peak after Background Subtraction	Observed In		
		13-MeV Proton Exp't.	13-MeV Deuteron Exp't.	$^{235}\text{U} +$ 11-MeV d Exp't. [14]
3.532	31 \pm 15			
2.833	47 \pm 16	x	x	
2.514	143 \pm 30			
2.247	45 \pm 21	x	x	
2.211	193 \pm 35	x		
2.034	106 \pm 35	x	x	
1.879	66 \pm 30*			
1.779	680 \pm 65	x	x	x
1.760	95 \pm 31	x		
1.719	74 \pm 33	x	x	
1.646	103 \pm 25	x		
1.592	60 \pm 30*		x	
1.492	80 \pm 45*			
1.408	156 \pm 45	x		
1.394	375 \pm 45	x	x	
1.362	156 \pm 60	x	x	
1.015	2360 \pm 100*	x	x	x
0.999	295 \pm 70*	x	x	x
0.976	5720 \pm 90*	x	x	x
0.956	340 \pm 45*	x	x	
0.899	785 \pm 100*	x	x	

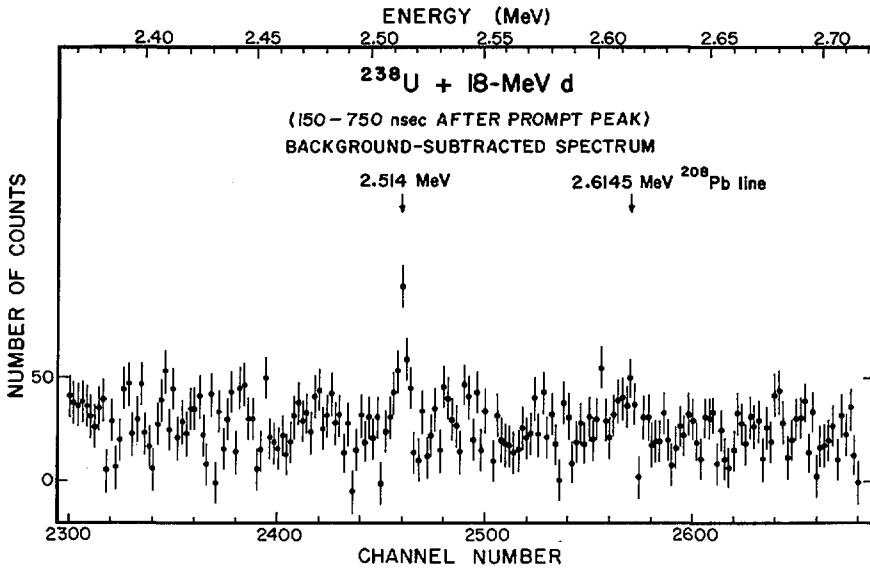


FIG. 3. Background-subtracted energy spectrum near 2.5 MeV for the 18-MeV deuteron bombardment. The data in adjacent channels were combined.

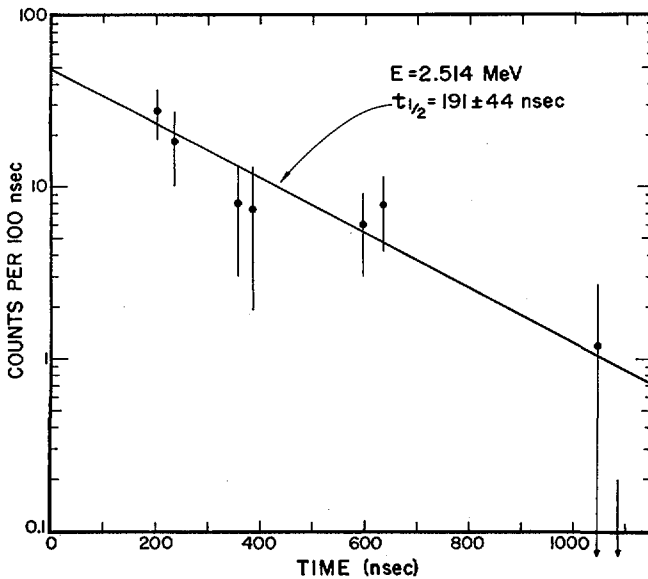


FIG. 4. Decay curve for the 2.514-MeV gamma ray observed in the 18-MeV deuteron experiments. The half-life of $191 \pm 44 \text{ nsec}$ is the result of a least squares fit to the data.

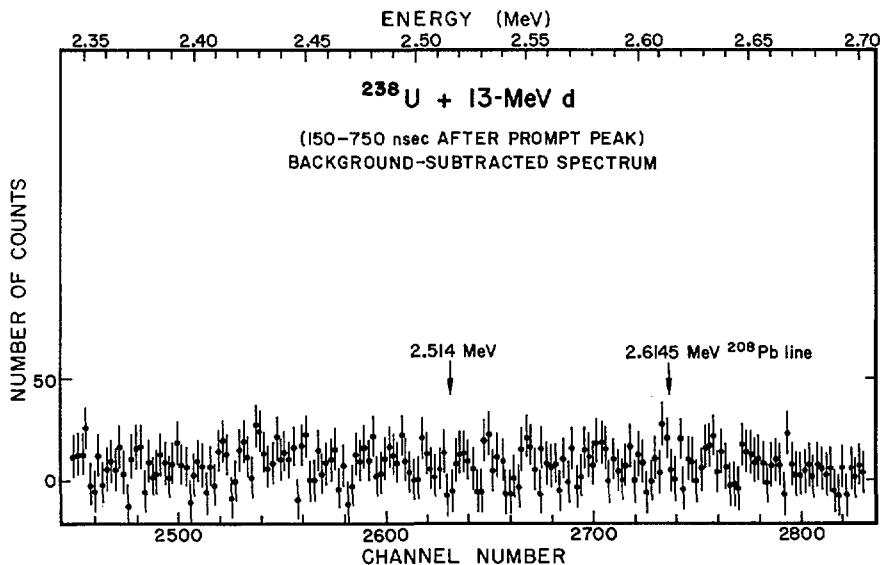


FIG. 5. Background-subtracted energy spectrum from 13-MeV deuteron data near 2.5 MeV for the time region from 150 to 750 nsec after the prompt peak. The data in adjacent channels were combined.

18-MeV deuteron spectra. The lines of interest should not appear in either the 13 MeV deuteron data or the 13 MeV proton data. The two high-energy lines that fulfill the requirements are at 3.532 MeV and 2.514 MeV. The line at 3.532 MeV is too high in energy to be consistent with the recent measurement of the 195 nsec ^{238}U shape isomer excitation energy of 2.2 ± 0.3 MeV [12]. However, the line at 2.514 MeV is consistent with this measurement. The spectrum for the summed 18 MeV deuteron data in the energy region near 2.5 MeV is shown in Fig. 3 with the long-lived background subtracted and pairs of channels combined to improve the statistics. The cross-section calculated for the line at 2.514 MeV based on a 195 nsec half-life is 90 ± 25 mb. Figure 4 shows the decay curve for the 2.514 MeV line. The half-life obtained from a least-squares fit to this data is 191 ± 44 nsec, in good agreement with the measured half-life of the ^{238}U shape isomer. Figure 5 shows the background-subtracted energy spectrum for the same time interval from the 13 MeV deuteron data. The 2.514 MeV line is absent in this spectrum as expected if this line is attributed to the ^{238}U shape isomer.

If the line at 2.514 MeV is assumed to result from decay of the isomeric state to the first excited $2+$ state at 0.045 MeV in the first well, then the isomer excitation energy is 2.559 MeV. Figure 6 shows a decay scheme corresponding to gamma decay from this $0+$ level at 2.559 MeV to the lowest $1-$ and $2+$ levels in ^{238}U . Figure 7 shows the background-subtracted energy spectrum for the energy region from 1.4 to 1.9 MeV. Peaks are observed at three energies, 1.454, 1.592 and 1.879 MeV, which might correspond to primary transitions from the $0+$ state at 2.559 MeV. Examination of the background spectrum used for subtraction [13] suggests that the structure at 1.454 MeV is an artifact of this subtraction since a strong, long-lived

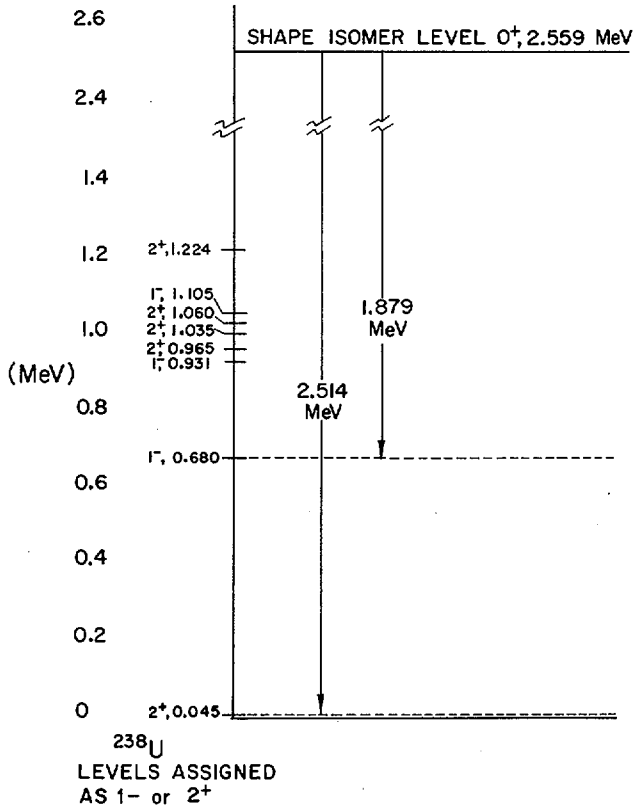


FIG. 6. Proposed decay scheme for the ^{238}U gamma branch based on the assumption that the 2.514-MeV transition is the decay from the shape isomer to the first excited 2^+ state at 0.045 MeV in normally deformed ^{238}U .

activity occurs just above 1.454 MeV. The line at 1.592 MeV is probably the double escape peak from the 2.6145 MeV line corresponding to decay of the first excited state of ^{208}Pb . The double escape peak for a gamma ray of this energy is approximately one-half the intensity of the full energy line. Within statistics, the results are consistent with this interpretation. The double escape peak for the 2.514 MeV line should be at 1.492 MeV. A peak of the right intensity appears at this energy. This peak is not present in the 13 MeV proton data but a weak line does appear at this energy in the 13 MeV deuteron spectrum. Thus there may exist an underlying low-intensity fission gamma ray at about this same energy which also contributes in the 18 MeV deuteron experiment.

The remaining line at 1.879 MeV does not appear in either the 13 MeV proton data or the 13 MeV deuteron data. The cross-section for this line, assuming a 195 nsec half-life is $40 \pm 20 \mu\text{b}$. The decay curve is shown in Fig. 8. The statistics are too poor to accurately determine the half-life, but the decay is consistent with a half-life of 195 nsec. The energy of this

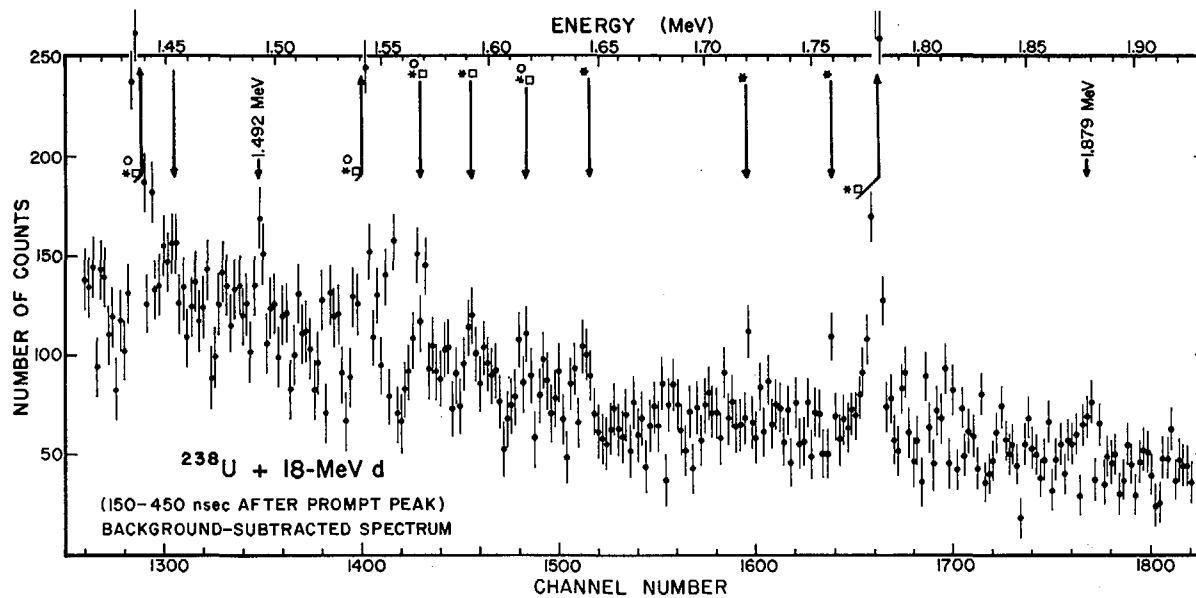


FIG. 7. Background-subtracted energy spectrum between 1.4 MeV and 1.9 MeV for the 18-MeV deuteron bombardment. The data in adjacent channels were combined. \square corresponds to lines observed in spectra for the 13-MeV deuteron bombardment, * corresponds to lines observed in spectra for the 13-MeV proton bombardment and \circ corresponds to lines which are long-lived compared to 200 nsec.

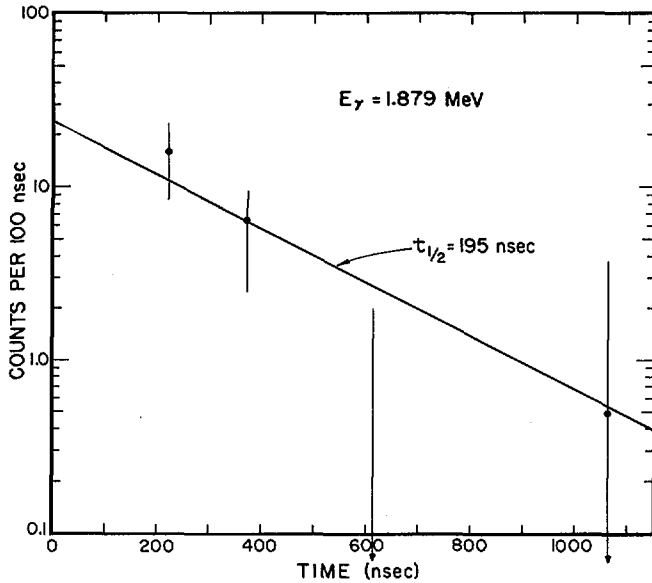


FIG. 8. Decay curve for the 1.879-MeV gamma ray observed in the 18-MeV deuteron experiments. The solid line represents an arbitrarily normalized decay with a half-life of 195 nsec.

Table II. Experimental cross-sections for gamma rays at 2.514 MeV and 1.879 MeV for the three reactions.

	^{238}U Target		
	18-MeV d	13-MeV d	13-MeV p
$\sigma_{2.514 \text{ MeV}} (\mu\text{b})$	90 ± 25	-22 ± 15	-10 ± 12
$\sigma_{1.879 \text{ MeV}} (\mu\text{b})$	40 ± 20	-12 ± 14	2 ± 15

line is consistent with a transition from the shape isomer to the lowest excited octupole state at 680 keV. A search for further gamma rays gave negative or inconclusive results.

Table II summarizes the results for the three experiments. A more complete presentation of the data appears elsewhere [13].

DISCUSSION

The half-life, energy and yield expectations for the $^{238\text{m}}\text{U}$ gamma branch are satisfied by the two gamma rays listed in Table II. The gamma rays do

not appear in two additional experiments with equivalent sensitivity to processes other than the ^{238}mU gamma branch. It is proposed from this evidence that the 2.514 MeV gamma ray is the primary transition from the 0+ ground state of the ^{238}mU shape isomer to the first excited 2+ state in the normally deformed nucleus.

The total measured cross-section for the ^{238}mU gamma branch based on the results in Table II is 130 ± 35 μb . This neglects contributions from decays to higher lying states and is, therefore, a lower limit. The delayed fission cross-section for the reaction $^{238}\text{U}(\text{d,pn})^{238}\text{mU}$ is 6 μb with 18 MeV deuterons [8]. The fission isomer yield ratio for ^{238}mU is 5×10^{-5} [8]. Therefore, the total isomer yield ratio for a gamma branch cross-section of 130 ± 35 μb is $(10 \pm 3) \times 10^{-4}$. This compares reasonably well with the fission isomer yield ratio for even-even ^{240}mPu , variously reported as $(8.6 \pm 2.4) \times 10^{-4}$ [14] and $(3.8 \pm 1) \times 10^{-4}$ [15]. The outer barrier of ^{238}U is higher than the outer barrier of ^{240}Pu while the inner barrier heights are approximately the same. Therefore, the isomer ratio for ^{238}mU is expected to be larger than for ^{240}mPu since the deeper well is a more effective "trap".

The observed ratio of radiation widths, $\Gamma_{\text{E2}}(2.514 \text{ MeV})/\Gamma_{\text{E1}}(1.879 \text{ MeV}) = 90 \pm 25/40 \pm 20$ or approximately 2.5 ± 2 is large compared to the single particle estimate of 0.01. However, the observed ratio is consistent with extrapolated data from neutron capture in the actinides at higher energies [16] and radioactive decay data at lower energies [17]. These results reflect the collective enhancement of E2 transitions and the retardation of low-energy E1 transitions.

Some of the gamma branch strength is also expected to go to the higher-lying 1- and 2+ levels in ^{238}U . Assuming a common reduced width for all primary E2 transitions and a different common value for the primary E1 transitions to the 2+ and 1- levels indicated in Fig. 6, the additional strength is estimated to be 70 ± 20 μb based on the energy dependence of the total gamma width and the cross-sections of the 2.514 MeV E2 and the 1.879 MeV E1 transitions. Thus, the ^{238}mU gamma isomer ratio increases by 50%. This is still not unreasonable compared to the measured ^{240}mPu fission isomer ratio. The analysis that follows will assume that the total ^{238}mU gamma branch cross-section is 250 μb , including 50 μb as an estimate of the decay to unknown 1- and 2+ levels. This leads to a partial fission half-life of 8300 nsec and a partial gamma half-life of 200 nsec.

It has been mentioned in the introduction that the observed predominance of gamma decay over fission decay was to be expected on the basis of the inner barrier becoming more penetrable than the outer barrier for the lighter actinides. In order to understand more quantitatively the results obtained for the partial gamma and fission half-lives, the theoretical expectations for the absolute half-lives for these two processes are reviewed. The simplest of these is that for fission,

$$t_{i,f} = \frac{\ln 2}{n P_B} = \frac{4 \times 10^{-21}}{P_B}$$

where n is the number of barrier assaults per sec, P_B is the penetrability of the outer barrier and $t_{i,f}$ is the partial half-life (in sec) for fission decay of the isomer. The numerical value of n is based on a vibrational frequency for $\hbar\omega_{\text{II}} = 1 \text{ MeV}$. Implicit in this expression is the expectation that once the outer barrier is penetrated the nucleus always fissions.

The situation for gamma decay is more complicated. Nix and Walker [18] have obtained the expression (valid if there is not an accidental near-degeneracy of the first and second well levels)

$$t_{i,\gamma} = t_{\gamma}/P_A = 10^{-14}/P_A$$

where t_{γ} is the half-life expected for a normal excited state in the first minimum with the isomer excitation energy, P_A is the penetrability of the inner barrier and $t_{i,\gamma}$ is the partial half-life (in sec) for the gamma branch. Thus, according to this estimate, if the inner and outer barriers have equal penetrabilities, fission decay will predominate over gamma decay by a factor of approximately $10^{6.5}$. This enhancement factor may be thought of as arising from the difference between the characteristic times for fission (of the order of a nuclear vibrational period) and for gamma decay (characterized by the longer lifetimes for the slower electromagnetic decay process). Lynn [19] has approached this problem somewhat differently, emphasizing the mixing of the first-minimum states into the second-minimum states. In the limit of complete damping (which Lynn does not necessarily expect to be valid) he obtains an expression

$$t_{i,\gamma} = \frac{t_{\gamma}}{P_A} \frac{4 D_I}{\hbar \omega_{II}}$$

differing from the previous estimate by the factor $4 D_I/\hbar \omega_{II}$. This factor is approximately 1/5 for an even-even nucleus with an isomer excitation energy of 2.5 MeV. Thus the difference between the two estimates for an even-even nucleus is less than the expected fluctuations from nucleus to nucleus which arise because of fluctuating matrix elements coupling the class I and class II states and because of possible accidental near-degeneracies of the class I and class II states. For our present purposes we take

$$t_{i,\gamma} = \frac{10^{-14}}{2.5 P_A} = \frac{4 \times 10^{-15}}{P_A},$$

assuming some but not complete damping.

A simple expression for the barrier penetrability is obtained for a parabolic barrier,

$$P = 1/[1 + e^{2\pi(\Delta E)/\hbar \omega}]$$

where ΔE is the height of the barrier to be penetrated and $\hbar \omega$ is the barrier curvature energy. Thus for penetration through the inner and outer barrier from the isomeric state at excitation energy E_{II} ,

$$P_A = e^{-2\pi(E_A - E_{II})/\hbar \omega_A}$$

and

$$P_B = e^{-2\pi(E_B - E_{II})/\hbar \omega_B}.$$

The value of E_{II} for ^{238}U has been determined in the present experiment to be 2.56 MeV. Back et al. [4] have obtained E_A and E_B values of 6.12 and 5.90 MeV, respectively in an analysis of (t,pf) reaction data. From our measured partial half-lives and the above theoretical expressions we can obtain values for the barrier curvature energies of $\hbar\omega_A = 1.18$ MeV and $\hbar\omega_B = 0.63$ MeV. These values are in reasonable agreement with values obtained in other analyses [15,4]. Since E_A is slightly larger than E_B , the predominance of gamma decay over fission decay is attributed in the case of ^{238}mU to the "thinner" inner barrier, reflected by $\hbar\omega_A > \hbar\omega_B$. Analysis of direct reaction data for ^{238}U [4] yields values of $\hbar\omega_A = 1.00$ MeV and $\hbar\omega_B = 0.62$ MeV. These values, while confirming the relatively greater penetrability of the inner barrier, are somewhat smaller than the above values. This is not surprising, since the direct reaction analysis is only sensitive to the curvature of the barrier for energies within 1 MeV of the top of the barrier, whereas the gamma and fission half-lives are very sensitive to the penetrability of the barrier 3-4 MeV below the top of the barrier.

ACKNOWLEDGMENTS

The participation of the following people is gratefully acknowledged: W. Jacobs for numerous contributions to many aspects of the project, J. Calarco for interest and assistance in the preliminary experiments, and R. Heffner for assistance in taking data.

REFERENCES

- [1] STRUTINSKY, V.M., Nucl. Phys. A95 (1967) 420.
- [2] SPECHT, H.J., KONECNY, E., HEUNEMANN, D., WEBER, J., Phys. Lett. 41B (1972) 43.
- [3] TSANG, C.F., NILSSON, S.G., Nucl. Phys. A140 (1970) 275.
- [4] BACK, B.B., HANSEN, O., BRITT, H.C., GARRETT, J.D., Paper IAEA-SM-174/27, these Proceedings, Vol.1.
- [5] BJØRNHOLM, S., STRUTINSKY, V.M., Nucl. Phys. A136 (1969) 1.
- [6] VANDENBOSCH, R., Phys. Lett. B (in press).
- [7] WOLF, K.L., UNIK, J.P., Phys. Lett. 43B (1973) 25.
- [8] WOLF, K.L., VANDENBOSCH, R., RUSSO, P.A., MEHTA, M.K., RUDY, C.R., Phys. Rev. C1 (1970) 2096.
- [9] JOHANSSON, S.A.E., Nucl. Phys. 64 (1965) 147.
- [10] JOHN, W., GUY, F.W., WESOŁOWSKI, J.J., Phys. Rev. C2 (1970) 1451.
- [11] BORGGREEN, J., KASHY, E., HATTULA, J., MAARBJERG, V., Nucl. Phys. (to be published).
- [12] WOLF, K.L., MEADOWS, J.W., private communication (1973).
- [13] RUSSO, P.A., Ph.D. Thesis, University of Washington (1973) unpublished.
- [14] VANDENBOSCH, R., WOLF, K.L., Second IAEA Symposium on the Physics and Chemistry of Fission, Vienna (1969) 439.
- [15] BRITT, H.C., BURNETT, S.C., ERKKILÄ, B.H., LYNN, J.E., STEIN, W.E., Phys. Rev. C4 (1971) 1444.
- [16] BOLLINGER, L.M., THOMAS, G.E., Phys. Rev. C6 (1972) 1322.
- [17] Nucl. Data Sheets 4 6 (1970) 635.
- [18] NIX, J.R., WALKER, G.E., Nucl. Phys. A132 (1969) 60.
- [19] LYNN, J.E., AERE M2505 (1971).

FRAGMENT ANISOTROPY IN ISOMERIC FISSION

H.J. SPECHT, E. KONECNY, J. WEBER, C. KOZHUHAROV

Beschleunigerlaboratorium der

Universität und Technischen Universität München,

Munich, Federal Republic of Germany

Abstract

FRAGMENT ANISOTROPY IN ISOMERIC FISSION.

Measurements of fragment angular distributions in fission from isomeric states — aligned by preceding nuclear reactions — can in principle provide information about the quantum numbers of the isomeric state, if independent information is known about the magnetic substate distribution and the perturbations due to extranuclear fields. Using $(\alpha, 2n)$ reactions on targets of ^{235}U , ^{236}U and ^{239}Pu with metallic Pb stoppers for the recoiling atoms (to preserve the alignment), fragment angular distributions at 90° , 125° and 167° were measured. The delayed fragments were detected with Si detectors in coincidence with the pulsed α -beam from the Munich Tandem Accelerator.

Anisotropies $W(167^\circ)/W(90^\circ)$ of 0.58 ± 0.16 , 1.41 ± 0.14 , 0.69 ± 0.09 and 2.0 ± 0.4 have been obtained for the 45-ns and 1.1- μs isomeric states of ^{237}Pu and the 6-ns ^{238}Pu and 10-ns ^{241}Cm isomers, respectively. Spin assignments for the four states are suggested on the basis of a simple Gaussian distribution for the magnetic substates, assuming that any perturbations are negligible.

1. INTRODUCTION

Our knowledge about fission isomeric states is, in most cases, still restricted to half-lives and excitation energies. More detailed spectroscopic information characterising these states like quantum numbers, magnetic dipole or electric quadrupole moments would be of great interest. The direct measurements of spins in odd A nuclei, for example, would allow one to identify specific Nilsson single particle states at the deformation associated with the second minimum of the potential energy surface, providing a crucial test of the parameters underlying the potential energy calculations. Such information in even nuclei would, moreover, help to clarify the nature and the decay mode of the "excited" states in the second well, apparently connected with K-isomerism.

The study of electromagnetic transitions in fission isomers from which, in principle, spins can be deduced, is extremely tedious. We have instead investigated fragment angular distributions in fission from isomeric states, aligned by a preceding $(\alpha, 2n)$ reaction. As is well-known from the study of gamma angular distributions [1,2], anisotropies occur because the projectile ions bring in large angular momenta (6-8 units of \hbar on the average at 25 MeV), producing compound nuclei with strong spatial alignment of their angular momenta in the plane perpendicular to the beam direction. Although the subsequent decay via neutron and gamma emission towards the isomeric state causes a certain spread in the magnetic substate distribution as discussed below, some alignment will be left. The fragment angular distribution in spontaneous fission from this state is

uniquely determined by its spin I and the quantum number K of the relevant band at the second barrier associated with this decay.

A principle difficulty (but possibly also a virtue) in investigations of this kind is the influence of extranuclear fields, i.e. the hyperfine interaction between the magnetic or electric moment of the isomeric state and some external field like the magnetic field of the highly ionized atom recoiling into vacuum or the magnetic field or electric field gradient at a lattice site. This interaction causes a perturbation of the angular correlation in times as short as 10^{-11} sec (depending on size), reducing (for static interactions) the time-integrated anisotropy to the very small "hard core" value [3] or (for time-dependent interactions) completely destroying it. If, on the other hand, the external fields can be controlled, a detailed investigation of the perturbation could, at least in principle, provide information about the moments of the isomeric state, as is, in fact, widely done for spin isomers.

To circumvent these difficulties in a first step, we have used the implantation technique of recoiling the compound nuclei into metallic Pb. The cubic lattice of Pb is known to preserve any alignment of, for example, high spin states in Po or At up into the μ s region [4], although it is not at all clear whether this should be expected for Actinide nuclei (with their unfilled 5 f electronic shell) in Pb as well. So far we have investigated the decay of four isomeric states (in ^{238}Pu , ^{241}Cm and two in ^{237}Pu), and have, in fact, found fragment anisotropies in each case. A similar study with the recoiling nuclei decaying in vacuum has been done independently by the Bucharest-Dubna group [5].

2. EXPERIMENTAL METHOD

A pulsed α -beam of 25 MeV from the Munich MP tandem accelerator was used on targets of ^{235}U , ^{236}U and ^{239}Pu to populate well-known isomeric states via the $(\alpha, 2n)$ reaction. Each target consisted of a multilayer sandwich, every layer containing 30 $\mu\text{g}/\text{cm}^2$ fissile material alternating with 50 $\mu\text{g}/\text{cm}^2$ Pb (both vacuum-evaporated as a metal on a carbon backing). The ^{235}U material was enriched to 90% (with 9% ^{238}U), the ^{236}U material also to 90% (with 9% ^{235}U and 1% ^{238}U).

The Munich pulsing system (chopper and buncher at the low-energy end of the machine, high-frequency sweeping system beyond the analyzing magnet) provides a beam with a FWHM of < 1 ns, a pulse separation of 400 ns and an unusual cleanliness between pulses (see below). Delayed fragments were detected with a Si annular detector at 180° and two further Si detectors at 90° and $\sim 125^\circ$ with respect to the beam direction (fig.1). Extreme care was taken to minimize any tails on the prompt fission time distribution. The effects of slit scattering of the beam were carefully investigated. All detectors were covered with appropriate apertures. Constant fraction discriminators, high-lying slow levels and fast pile-up inspection was used throughout. The experiments were performed in an "open" hall with the well-shielded beam stop several meters away from the target to keep the fission background due to scattered neutrons and γ -rays to a minimum. During all the runs, a ^{232}Th target (showing no isomeric fission) was frequently interchanged with the target under investigation to monitor the overall quality of the system. During some of the

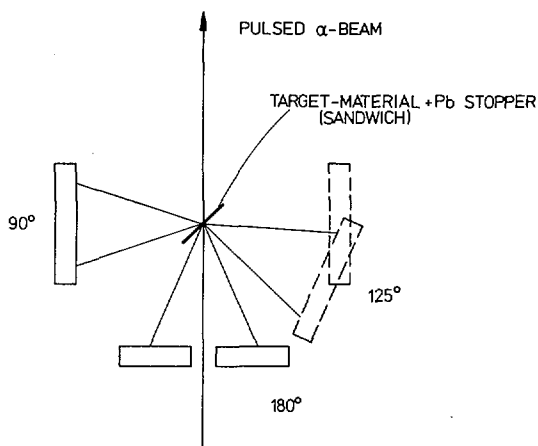


FIG.1. Diagram of the detector arrangement. During some of the runs, the 125° detector was used at 90° in coincidence with the other 90° detector.

runs, the 125° detector was used at 90° in coincidence with the other 90° detector to check any remaining deficiencies; this precaution turned out to be completely unnecessary.

3. RESULTS

We will first discuss the decay curves for the three reactions separately, and then turn to the anisotropies.

a) $^{232}\text{Th}(\alpha, f)$ and $^{236}\text{U}(\alpha, 2n)^{238}\text{Pu}$

The overall quality of our system is best demonstrated by the prompt fission time distribution of ^{232}Th shown in fig.2 (for the 180° detector). At 10^8 prompt events, there is no background at all beyond 15 ns, making the system especially suitable for investigation of fission isomers with low yields. The data from the ^{236}U target also shown in fig.2 (for the same number of prompt events) exhibit the well-known 6-ns decay of the ^{238}Pu isomer [6,7] with the low isomer/prompt ratio of $(3.7 \pm 0.3) \cdot 10^{-6}$ appearing far above background. The slower decay beyond 30 ns is due to contributions from the $^{236}\text{U}(\alpha, n)^{239\text{m}}\text{Pu}$ reaction [6] and the $^{235}\text{U}(\alpha, 2n)^{237\text{m}}\text{Pu}$ reaction from the ^{235}U target impurity which, of course, have been corrected for in the data analysis.

b) $^{239}\text{Pu}(\alpha, 2n)^{241\text{m}}\text{Cm}$

Consistently for the two independent detectors, a least squares fit to the decay of the ^{241}Cm isomer (fig.3) yields a half-life of 10 ± 1 ns, somewhat lower than the value 15.3 ± 1 reported previously [6]. Since the isomer/prompt ratio at 90° (table I) also appears to be lower, this discrepancy might possibly be caused by some background contribution to the older data [6]. Fig.3 also demonstrates the complete absence of any background due to neutrons on a thermal fissionable target.

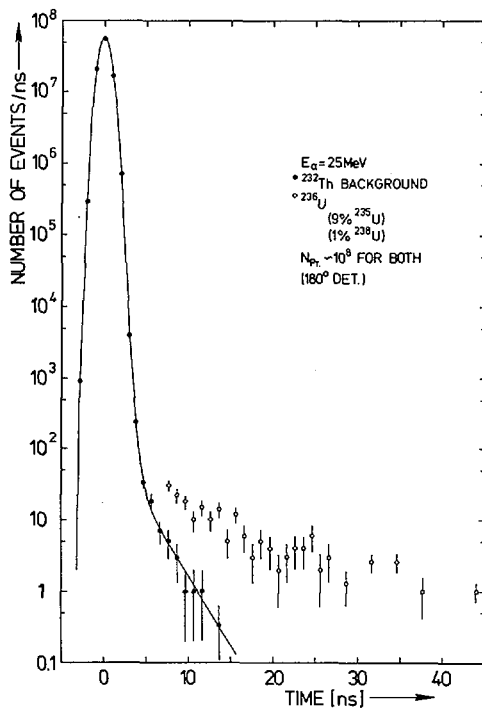


FIG. 2. Time distribution of prompt fission in ^{232}Th (α, f) and of delayed fission from the $^{238\text{m}}\text{Pu}$ fission isomer produced in the $^{236}\text{U}(\alpha, 2n)$ reaction. N_{Pr} = number of prompt events.

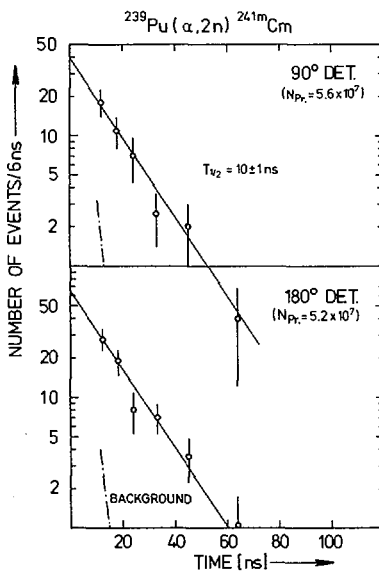


FIG. 3. Decay curve for the $^{241\text{m}}\text{Cm}$ fission isomer from the 90° and 180° detectors. The number of measured prompt events is given in brackets.

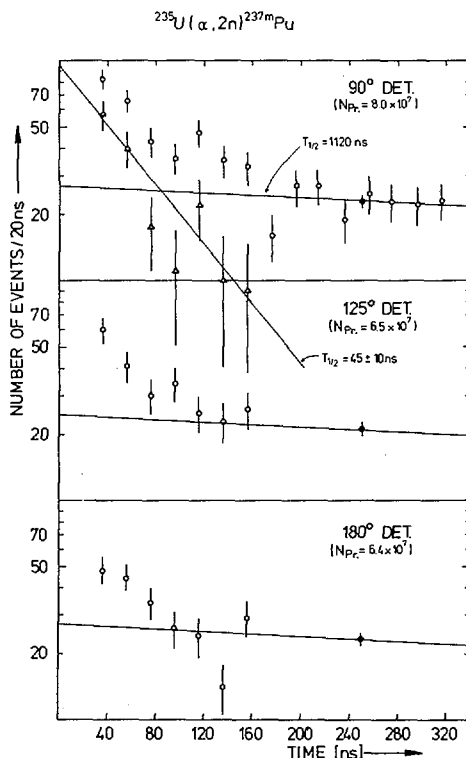


FIG. 4. Decay curves for the $^{237\text{m}}\text{Pu}$ fission isomer from the 90° , 125° and 180° detectors. The single solid point in each of the graphs gives the average intensity over the region 166-326 ns associated with the 1120-ns component. The measured data points are open circles. The triangles refer to the measured data points after subtraction of the 1120-ns component. The number of measured prompt events is given in brackets.

c) $^{235}\text{U}(\alpha, 2n)^{237\text{m}}\text{Pu}$

All three detectors show the composite decay of the two isomeric states in ^{237}Pu (fig. 4), investigated in detail previously [8-10]. The single full point in each of the graphs gives the average intensity (over the region 166-326 ns) associated with the long-lived component of $T_{1/2} = 1120 \pm 80$ ns [8] (drawn as a line). As a very interesting point, the intensity ratio of the short-lived and long-lived component gradually decreases in going from 90° to 180° . A least-squares fit to the decay of the short-lived component for the 90° data yields a value of 45 ± 10 ns, definitely lower than the 82 ± 8 ns quoted previously [8]. Our intensity ratio $\sigma_{\text{short}}/\sigma_{\text{long}}$ at 90° (0.59 ± 0.08) fully agrees with newer data (0.58 ± 0.09) for 25 MeV [9].

Isomer/prompt ratios and fragment anisotropies for the four isomeric states are summarized in table I. The entry " 13° " corresponds to the average angle 167° of the annular detector.

TABLE I. ISOMER/PROMPT FISSION RATIOS AND FRAGMENT ANISOTROPIES FOR ISOMERIC FISSION FOLLOWING ($\alpha, 2n$) REACTIONS AT $E_\alpha = 25$ MeV

Isomer	Half-life	$(\sigma_{\text{Isomer}}/\sigma_{\text{Prompt}}) \times 10^6$			$W(\theta) / W(90^\circ)$	
		(this work)		(other)		
		13°	90°	$\sim 90^\circ$	13°	55°
^{237}Pu	45 ns	2.25 ± 0.6	3.9 ± 0.5	4.1 ± 0.4^a	0.58 ± 0.16	0.67 ± 0.16
	1.1 μs	9.3 ± 0.7	6.6 ± 0.5	7.1 ± 0.8^a	1.41 ± 0.14	1.17 ± 0.12
^{238}Pu	6 ns	3.7 ± 0.3	5.3 ± 0.4	4.3 ± 0.5^b	0.69 ± 0.09	0.78 ± 0.20
^{241}Cm	10 ns	3.1 ± 0.3	1.6 ± 0.2	1.9 ± 0.2^b	2.0 ± 0.4	---

^a VANDENBOSCH, R., et al. [9]

^b BRITT, H.C., et al. [6]

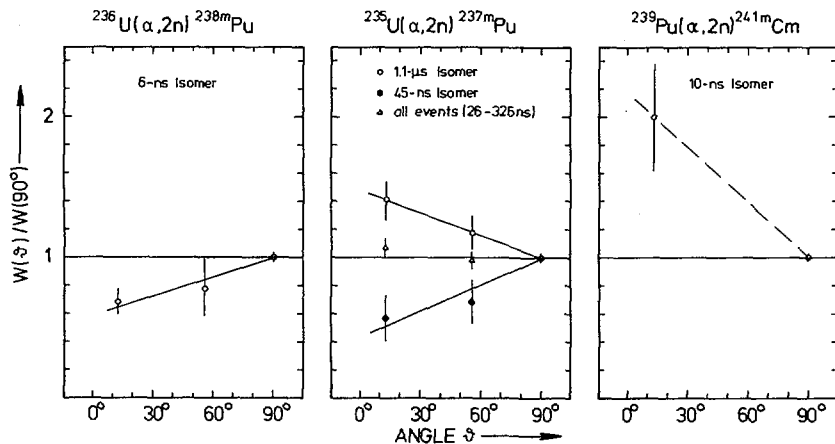


FIG. 5. Fragment anisotropies (relative to 90°) for ^{238}Pu -, ^{237}Pu - and ^{241}mCm -isomeric fission.

The σ_I/σ_P ratios for ^{237}Pu and ^{238}Pu have been multiplied by a factor of 1.1 to correct for the target impurities; all ratios at 13° have, in addition, been multiplied by a factor of 1.11 to account for the anisotropy of prompt fission [11] and the effects of center-of-mass motion at 167° . Only the data at 90° should, of course, be compared to other published values, which have always been obtained at approx. 90° . In general, the agreement is satisfactory.

The anisotropies (relative to 90°) at 13° and 55° ($\approx 125^\circ$) are, in addition, plotted in fig. 5. Evidently, all four isomers exhibit definite deviations from isotropy. This remarkable result even for the long-lived 1.1- μs component in ^{237}Pu is hardly influenced by any uncertainties in the subtraction procedure. Only if, somewhat artificially, all data for ^{237}Pu between 26-326 ns are summed up, is isotropy obtained.

Before drawing any detailed conclusions about the size and the sign of the effects observed, however, we should definitely point out that in none of the four cases does the deviation from complete isotropy exceed more than three standard deviations.

4. THEORETICAL ANALYSIS

The time-integrated fragment angular distribution for fission from an isomeric state with spin I and projection of the spin on the nuclear symmetry axis at the second barrier K (the lowest band allowed by angular momentum and parity conservation) can be quite generally written as

$$W_K^I(\theta) = \sum_{\lambda} A_{\lambda} G_{\lambda} P_{\lambda}(\cos\theta) \quad \lambda = 0, 2 \dots 2I$$

with [12]

$$A_{\lambda} = \frac{2I+1}{2} \sum_M (-1)^{K-M} f(M) C_{-MM0}^{II\lambda} C_{-KK0}^{II\lambda}$$

In the formulae, the P_λ are the Legendre polynomials, the $C_{\alpha\beta\gamma}$ Clebsch-Gordan coefficients, the $f(M)$ the occupation number distribution of the magnetic substates M of the spin I relative to the quantisation (i.e. beam) axis, and the G_λ the time-integrated attenuation factors[3] due to any perturbation of the correlation by extranuclear fields.

All the difficulties of this approach are hidden in the functions G_λ and $f(M)$. If they would be exactly known, a measurement of the complete angular distribution $W(\theta)$ would uniquely and independently determine I and K . In practice, of course, rough approximations have to be made about G_λ and $f(M)$, and the angular distribution has only been measured at three angles. We can therefore at most hope to make suggestions, but no definite spin assignments.

For static magnetic interactions in strong axially symmetric fields, the time-integrated attenuation factors ("hard core" values) are given by[3]

$$G_\lambda = \frac{1}{2\lambda+1}$$

The corresponding factors for a static quadrupole interaction can also be found in ref.[3]. Evidently, these factors reduce the angular correlation to a very great extent, in fact, to values (for any reasonable spin I) much smaller than the experimental ones. In view of the Pb stopper, we will in the following assume

$$G_\lambda \equiv 1$$

The occupation number distribution $f(M)$ of the magnetic substates M for the compound nucleus following α -capture on an even target nucleus is given by

$$\begin{aligned} f(M) &= 1 & \text{for } M &= 0 \\ f(M) &= 0 & \text{for } M &\neq 0 \end{aligned}$$

As pointed out already in the introduction, the subsequent emission of two neutrons and gamma rays introduces a spread in the distribution function. However, since the angular momentum taken away in anyone of these steps is small, of the order of 2 [1,13], and since the angular momentum vectors of the individual events are distributed in nearly random directions, the final alignment of the isomeric state may still be appreciable. If one knew the whole "spin history" from the completely aligned compound nucleus down to the final state, the distribution function $f(M)$ could be calculated. Although attempts in this direction have been reported[13,14], the uncertainties involved are appreciable. Specifically, the usual assumption of a final stretched E2 cascade along the Yrast line is not well-justified for the $(\alpha, 2n)$ reaction at these low energies because of considerable side-feeding, so that the spectroscopic details of the final decay will enter.

We have therefore taken a more phenomenological approach. A simple Gaussian distribution function

$$f(M) = \frac{1}{\sqrt{2\pi} \sigma_M} e^{-\frac{M^2}{2\sigma_M^2}}$$

has been found[1,2,15] to fit experimentally observed gamma angular distributions following (α, xn) reactions reasonably well. It has also been theoretically justified[13] for the neutron cascade, considered as a one-dimensional random walk in the projection M with the width

$$\sigma_M = \mu n^{1/2}$$

where n is the number of steps (2 in our case) and μ the average step length (1 for $\bar{l} = 2$), yielding $\sigma_M = 1.4$ for the neutron contribution in $(\alpha, 2n)$ alone. Experimental values of σ_M (containing the gamma contribution as well) have been found for (α, n) reactions on a whole range of nuclei[2,15] to be reasonably constant around 1.6, rather independent of I for $I \geq 5/2$. We therefore estimate the most plausible range of σ_M in our case to lie somewhere around 2 and not larger than 3.

Using these approximations, we have calculated the anisotropies $W(0^\circ)/W(90^\circ)$ as a function of the Gaussian width σ_M for all combinations of I and K (up to 11/2) which yield values in the region of the measured anisotropies. These dependences are plotted in fig.6, for even nuclei in the upper part, for odd in the lower. For clarity, full lines are used in the cases $K = 1/2$ and $I = K$, dashed lines for all other combinations. The shaded areas signify the experimental anisotropies of the four isomers with their statistical errors and the uncertainty in the width σ_M .

5. DISCUSSION

As pointed out above, any conclusions and tentative suggestions for spin assignments rely on the assumptions of negligible perturbations and values for σ_M within the shaded areas.

a) ^{237}Pu

The simple fact of a difference in the anisotropy (even in sign) for the two isomeric states allows the conclusion, that the higher-lying[9] 1.1- μs state decays predominantly by fission rather than by electromagnetic transitions down to the 45-ns state, as has been speculated before[9]. If the two states would have the same parity, they would presumably fission through the same band K at the second barrier, the longer half-life of the higher state being due to specialization energy effects because of a larger spin[8,9]. For the two shaded areas in fig. 6 connected with ^{237}Pu , only one common value for K (namely 5/2) is possible, leading to an assignment of $I = 11/2$ for the 1.1- μs isomer and $I = 5/2$ for the 45-ns isomer. It is most remarkable that this conclusion exactly coincides with the suggestions made

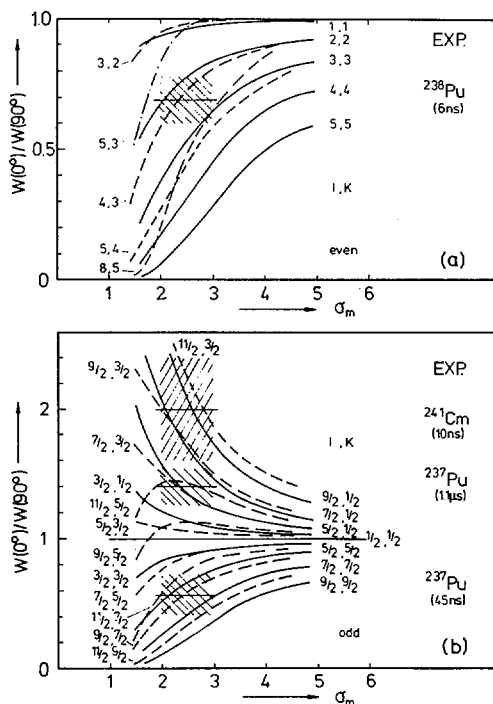


FIG. 6. Calculated anisotropies $W(0^\circ)/W(90^\circ)$ as a function of the Gaussian width σ_M of the substrate occupation number distribution $f(M)$ for all combinations of I and K (up to $11/2$), for even (a) and odd (b) nuclei. Solid lines are used in the cases $K = 1/2$ and $I = K$, dashed lines for all other combinations. The shaded areas represent the experimental anisotropies of the four isomers with their experimental errors and the uncertainty in the width σ_M .

earlier from isomer ratio investigations[8,9]. The corresponding Nilsson orbitals recently proposed by Vandenbosch[9] on the basis of three different calculations[16-18] are $[615] 11/2^+$ and $[862] 5/2^+$, which lie close to the Fermi surface and do, in fact, have the same parity. Independent information[19] from induced fission of ^{235}U (same neutron number) about the K quantum number of the lowest barrier suggests $5/2$ or $7/2$.

b) ^{241}Cm

The strong forward peaking observed would be consistent with $I, K = 7/2, 1/2$; $9/2, 1/2$ or $3/2$ and $11/2, 3/2$, although the errors are large and other combinations might also be possible. Since there are only two neutrons added as compared to ^{237}Pu , one might speculate that fission occurs from the same $11/2^+$ $[615]$ orbital mentioned above (with $[734] 9/2^-$ as an alternative). It is not clear whether this state is really the isomeric ground state.

c) ^{238}Pu

The bare existence of an anisotropy in this case directly supports the hypothesis[7] of the 6-ns isomeric state not being the ground state in the second well, but some excited (K -isomeric)

state above the pairing gap. We can furthermore conclude that, again, the isomeric state decays by fission rather than by electromagnetic transitions down to the 0^+ level. With the extreme assumption of the "true" anisotropy of this state being 0, the upper limit for the branching ratio between the "downward" and the "outward" decay is ≤ 2 .

Assuming now this ratio to be 0, we can again try to estimate the spin. Combinations I, K of 2, 2; 3, 3 and 4, 3 appear to be possible. However, the choice 4, 3 would correspond to a ratio $W(55^\circ)/W(90^\circ) > 1$ which is outside the error bars (fig.5), but definitely not ruled out. The most plausible spin 3 can be created by the coupling of the $5/2^+$ and $11/2^+$ orbitals of ^{237}Pu , leading to an unnatural parity state I, K = $3^+, 3^+$. It is not easy to see, however, why the fission half-life of this state should then be as long as observed.

REFERENCES

- [1] NEWTON, J.O., STEPHENS, F.S., DIAMOND, R.M., KOTAJIMA, K., MATTHIAS, E., Nucl. Phys. A95(1967)357.
- [2] SAWA, Z.P., Physica Scripta 7(1973)5.
- [3] FRAUENFELDER, H., STEFFEN, R.M., in Siegbahn, K., "Alpha-, Beta- and Gamma-Ray Spectroscopy", North-Holland, Amsterdam(1965)p.997.
- [4] BABA, C.V.K., FOSSAN, D.B., FAESTERMANN, T. FEILITZSCH, F., KIENLE, P., SIGNORINI, C., Phys. Letters 43B(1973)483 and Annual Report 1972 of the Beschleunigerlaboratorium der Universität und Technischen Universität München, p.96 and 98.
- [5] GANGRSKY, Yu. P., NGUYEN Cong Khanh, PULATOV, D.D., PHAM Zuy Hien, Dubna Rep. P7-6466(1972) and GALERIU, D., Paper IAEA-SM-174/15, these Proceedings, Vol.1.
- [6] BRITT, H.C., BURNETT, S.C., ERKKILA, B.H., LYNN, J.E., STEIN, W.E., Phys. Rev. C4(1971)1444.
- [7] LIMKILDE, P. SLETTEN, G., Nucl. Phys. A199(1973)504.
- [8] RUSSO, P.A., VANDENBOSCH, R., MEHTA, M., TESMER, J.R., WOLF, K.L., Phys. Rev. C3(1971)1595.
- [9] VANDENBOSCH, R., RUSSO, P.A., SLETTEN, G., MEHTA, M., Preprint(1973).
- [10] TEMPERLEY, J.K., MORRISSEY, J.A., BACHARACH, S.L., Nucl. Phys. A175(1971)433.
- [11] LEACHMANN, R.B., BLUMBERG, L., Phys. Rev. 137(1965)B814.
- [12] FRASER, J.S., MILTON, J.C.D., Ann. Rev. Nucl. Sci. 16(1966) 379.
- [13] RASMUSSEN, J.O., SUGIHARA, T.T., Phys. Rev. 151(1966)992.
- [14] PHAM Zuy Hien, Dubna Rep. P4-6625(1972).
- [15] SAWA, Z.P., BLOMQUIST, J., GULLHOLMER, W., Nucl. Phys. A205(1973)257.
- [16] NILSSON, S.G., TSANG, C.F., SOBICZEWSKI, A., SYMANSKI, Z., WYCECH, S., GUSTAFSON, G., LAMM, J., MÜLLER, P., NILSSON, B., Nucl. Phys. A131(1969)1.
- [17] BOLSTERLI, M., FISET, E.O., NIX, J.R., NORTON, J.L., Phys. Rev. C5(1972)1050.
- [18] MOSEL, U., SCHMITT, H.W., Nucl. Phys. A165(1971)13.
- [19] BRITT, H.C., CRAMER, J.D., Phys. Rev. C2(1970)1758.

DISCUSSION

V. METAG: I wonder whether you have checked your set-up by measuring the angular distribution from an isomeric state with $(I, K) = (0, 0)$. That should give you complete isotropy. The case to try would be the 3.8-ns isomer of ^{240}Pu which also has a half-life similar to that of the isomers you have studied.

H.J. SPECHT: We have already been asked this question several times and the answer is that we did not. We are quite confident about our simple procedure for normalizing the delayed intensity relative to the prompt, which is performed separately at each angle. I fully agree, however, that this check on the $^{240\text{m}}\text{Pu}$ isomer should be done.

G.C. SLETTEN: Did you try to use thicker lead absorbers? It appears to me that $50\text{ }\mu\text{g}/\text{cm}^2$ of lead is about the recoil range and, as a result, a fair proportion of the recoils would escape. This would tend to smear the distributions.

H.J. SPECHT: The target was positioned at an angle of 45° relative to the beam direction; the effective thickness of the Pb layers was therefore $70\text{ }\mu\text{g}/\text{cm}^2$, which should be sufficient.

R. VANDENBOSCH: I would like to propose a simple explanation as to why the long-lived ^{237}Pu isomer exhibits an anisotropy characterized by $K < I$, whereas the short-lived ^{237}Pu isomer exhibits an anisotropy with $K \approx I$. It has been suggested that the odd neutron of the long-lived isomer occupies the $[615] (11/2, +)$ orbital which is at, or very near to, the Fermi surface at the deformation of the second minimum. We now want to discuss the location of single particle states with $(K, \pi) = (11/2, +)$ at the deformation of the outer barrier. Mr. Möller has shown me his level diagram for the outer barrier including reflection-asymmetric distortions. The $[615] (11/2, +)$ level, which is an upward-sloping level, has moved up to about 6 MeV above the Fermi surface. There is no other $(K, \pi) = (11/2, +)$ orbital from lower shells, and the next higher $(11/2, +)$ orbital comes from the $N = 8$ shell and is expected to be $\sim 2\text{ }\hbar\omega$ or ~ 12 MeV higher. Thus, if K were to be preserved from the second minimum to the outer barrier, we would have a specialization energy of about 6 MeV and an extremely long isomer fission half-life, in contradiction to experiment. S.A.E. Johansson, however, pointed out many years ago that, even if K is a fairly good quantum number, so that at a level crossing there is only a small (say 10%) probability of jumping to a lower energy level with different K , the specialization energy may be lowered to the extent that the dominant contribution to fission may come from exploiting level crossings which change K . The half-life, however, will be increased owing to the small jump probability at such crossings. These effects could account for both the relatively long half-life (compared to the low-spin isomer) and the lowering of K for the fission of an $(11/2, +)$ isomer state.

DELAYED FISSION FRAGMENT ANGULAR DISTRIBUTIONS IN SOME ALPHA-PARTICLE-INDUCED REACTIONS

D. GALERIU, M. MARINESCU, D. POENARU, I. VÎLCOV,
N. VÎLCOV

Institute for Atomic Physics,
Bucharest, Romania

Yu.P. GANGRSKY, P.Z. HIEN, N.C. KHAN
Joint Institute for Nuclear Research,
Dubna, USSR

Abstract

DELAYED FISSION FRAGMENT ANGULAR DISTRIBUTIONS IN SOME ALPHA-PARTICLE-INDUCED REACTIONS.

This paper describes the measurement of the angular distribution of the fission fragments emitted by fission isomers, populated in alpha-particle-induced reactions. Such experimental data gives valuable information concerning the fission isomer spin values (there has been little data on the spin values of the fissioning isomeric states up to now). Owing to the very small yield of the fission fragments, only the "integral" anisotropy factor ($a = W(180^\circ)/W(90^\circ)$) could be measured, the angular resolution being dependent on the solid angle subtended by the detectors, as well as on the fission isomer lifetime. Solid state track detectors have been used to register the fission fragments emitted by recoiled nuclei in flight. The experimental arrangement consists of three systems of detectors: a mica annular detector looking downstream with respect to the ingoing alpha-particle beam (the 180° detector), several lead glass (to lower the overall background) plain detectors oriented parallel to the beam (the 90° detectors) and a mica detector facing the target, used for monitoring purposes (the prompt fission detector). Delayed fission fragment anisotropy factors for fission isomers, populated in $(\alpha, 2n)$ reactions on ^{235}U , ^{238}U , ^{239}Pu and ^{241}Am targets as well as in $(\alpha, 3n)$ reactions on ^{235}U and ^{242}Pu targets, have been measured. Anisotropy factors essentially differing from unity were obtained in some of the measured fission isomers, particularly in the case of ^{236}mPu ($T_{1/2}^{\text{mf}} = 30 \text{ ns}$), assumed to represent an excited state in the second potential well. An estimate of the spin values of the fission isomers has been made using a statistical model approach. The limitations of the above method, including the precision of measuring the experimental anisotropy factors as well as the possible perturbation of the angular distributions due to the extranuclear fields, are analysed.

1. INTRODUCTION

The problem of measuring the spin value of the fissioning isomeric states in transuranic nuclei arose in an earlier stage of fission isomer development. The first attempts to explain the unusual stability of such states against any transitions (including the gamma decay to the ground state of the nucleus) were based on a high spin value of the fissioning isomeric states. On the other hand, the experimental evidence of the constancy of the isomeric yield ratio in different nuclear reactions, characterized by input channel angular momenta from 1 to $15\hbar$ and leading to the 14-ms fissioning isomer of ^{242}Am [1], has been interpreted as a consequence of the relatively low value of the fission isomer angular momentum. The population of the same fission isomer in a low spin reaction such as neutron capture [2] confirmed this conclusion.

Because of these data, arguments other than the high spin value had to be found to explain the strange behaviour of the fissioning isomeric states.

And these arguments were found in the framework of the well-known Strutinsky two-humped potential barrier hypothesis [3]. The appearance of some metastable states at large deformations separated from the ground state by a potential barrier could explain almost everything, at least qualitatively, concerning the fission isomer properties. As has been pointed out [4] the constancy of the isomeric yield ratio, for instance, may be explained by taking into account the probabilities of populating the two (ground state and isomeric) potential wells rather than by using spin arguments. The spin values of the fissioning isomeric states must be deduced from other kinds of experiments.

There are some nuclei for which two fission lifetimes were observed. If both fission isomers belong to the same (second) potential well, only one of them (the lower) may be considered a true shape isomer. The other could be explained by the large difference in the spin values of the two isomeric states. By using the experimental dependence of the ratio of the cross-sections for populating the two fission isomers on the energy of the compound nucleus, spin values for the two isomeric states were assigned [5]. It would certainly be useful to get more information concerning the spin values of such double fission isomers from other experiments.

One possible way to obtain the spin value of a fission isomer is based on the measurement of the angular distribution of the fission fragments emitted by the fission isomer. It is known that the fission fragments are emitted along the symmetry axis of the deformed fissioning nucleus. The angular distribution (i. e. the angular distribution of the fission fragments) of the deformed nucleus is given by the following relationship:

$$W(\theta) = \sum_M f_M |\mathcal{D}_{MK}^I(\theta, \varphi, \chi)|^2$$

where $\mathcal{D}_{MK}^I(\theta, \varphi, \chi)$ represents the eigenfunction of the symmetrical rotator of total spin I with projection M and K on the z -axis and on the symmetry axis respectively, (θ, φ, χ) represent the angular coordinates and f_M are the relative amplitudes of the spin projection M . The amplitudes f_M depend on the nuclear reaction used to populate the fission isomer. A proper choice of the nuclear reaction is thus very important. The angular distribution of the fission fragments is sensitive to the spin value of the fissioning state in the case when a few amplitudes f_M are significantly different from zero otherwise one obtains isotropy. Such "good" reactions are those induced by alpha particles on low spin targets because the large orbital angular momentum carried by the spinless alpha particles leads to an orientation of the angular momentum of the fissioning nucleus almost perpendicularly to the beam direction (z -axis).

The purpose of the work described in this paper is to measure the delayed fission fragment angular distribution in some $(\alpha, 2n)$ and $(\alpha, 3n)$ reactions to obtain the possible spin values of the fission isomers involved. Analogous research has also been recently done [15].

2. EXPERIMENTAL ARRANGEMENT

The schematic diagram of the experimental arrangement used in this work is shown in the Fig.1. A recoil technique based on mica annular

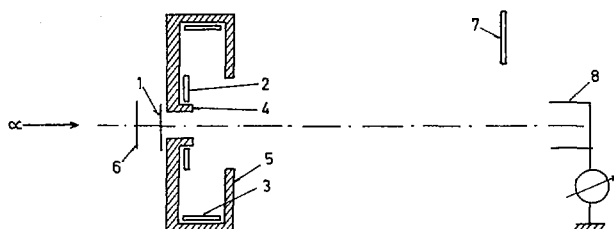


FIG.1. Schematic diagram of the experimental arrangement. See text for description of items 1-8.

detectors has been used, the arrangement looking similar to that described in Ref. [6] except that the 90° detector 3 and the collimators 4 and 5 have been introduced.

The delayed fission fragments emitted in flight by the recoil nuclei knocked out of target 1 by the bombarding alpha particles are registered by two mica detectors: the 180° ring detector 2 and the 90° circular detector 3. The collimators 4 and 5 prevent the registration of fission fragments incident at small angles on the detector surface. The small-step energy variation of the incident beam is achieved by using an aluminium absorber 6. There are two ways to monitor the incident beam: (1) the measurement of the prompt fission yield by using the mica detector 7 facing the target and (2) the integration of the beam current on the Faraday cup 8.

In the above experimental arrangement only the anisotropy factor a defined as:

$$a = \frac{W(180^\circ)}{W(90^\circ)}$$

can be measured. Owing to the very small yield of the delayed fission fragments the detectors have to work in a rather poor geometry. To obtain the anisotropy factor from the measured ratio of the fission fragments registered by detectors 2 and 3, the efficiencies of the detectors have to be known. Figure 2 shows the computed probabilities of registering, on the 180° counter, the delayed fission fragments as a function of the angle of emission $\langle \theta \rangle$ and FWHM $\Delta \theta$ of the distribution as well as the overall efficiencies are given in Table I. The overall efficiencies for the 90° mica detector are presented in Table II.

3. RESULTS

Targets of ^{235}U , ^{238}U , ^{239}Pu , ^{242}Pu and ^{241}Am with thicknesses 0.15-0.20 mg/cm² have been used. The energy of the incident alpha-particle beam was chosen in the 26-33 MeV range in such a way as to correspond to the maximum of the excitation function for the given reaction (Refs [6, 7]).

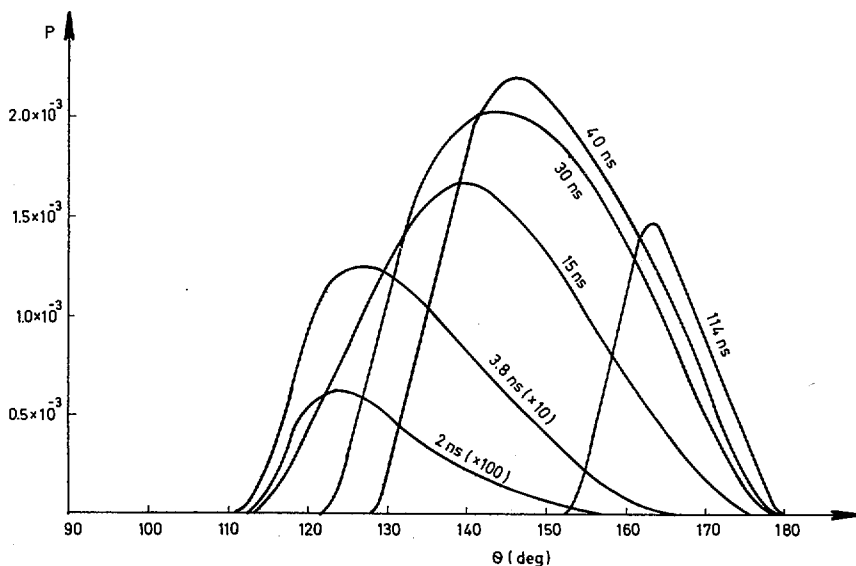


FIG. 2. Calculated probability of registering the delayed fission fragments on the 180° ring counter as a function of the angle of emission.

TABLE I. COMPUTED EFFICIENCIES FOR THE 180° RING DETECTOR

$T_{1/2}^{mf}$ (ns)	ϵ_{180°	$\langle \theta \rangle$ (deg)	$\Delta\theta(\text{FWHM})$ (deg)
2.0	0.006×10^{-2}	129	18
3.8	0.160×10^{-2}	133	27
15.0	2.250×10^{-2}	142	32
30.0	3.100×10^{-2}	147	35
40.0	3.070×10^{-2}	150	30
114.0	1.900×10^{-2}	165	13

The experimental data obtained are listed in Table III. The first two columns indicate the reaction used to populate the fission isomer and the energy of the incident alpha particles. By using the ratio of computed efficiencies (Tables I and II), the anisotropy factors listed in the third column were obtained from the experimental data.

4. DISCUSSION

Most of the measured fission fragment angular distributions are isotropic. This is the case for the $^{237mf}\text{Pu}$, $^{240mf}\text{Pu}$, $^{243mf}\text{Cm}$ and, possibly,

TABLE II. COMPUTED EFFICIENCIES
FOR THE 90° DETECTOR

$T_{1/2}^{mf}$ (ns)	ϵ_{90°
2.0	0.23×10^{-2}
3.8	2.09×10^{-2}
15.0	10.60×10^{-2}
30.0	10.20×10^{-2}
40.0	9.11×10^{-2}
114.0	4.56×10^{-2}

TABLE III. EXPERIMENTAL DATA

Reaction	E_α (MeV)	a
$^{235}\text{U}(\alpha, 2n)^{237}\text{mfPu}$ ($T_{1/2}^{mf} = 114$ ns)	26.7	0.90 ± 0.15
$^{235}\text{U}(\alpha, 3n)^{236}\text{mfPu}$ ($T_{1/2}^{mf} = 30$ ns)	33.0	0.70 ± 0.15
$^{238}\text{U}(\alpha, 2n)^{240}\text{mfPu}$ ($T_{1/2}^{mf} = 3.8$ ns)	26.7	1.50 ± 0.80
$^{239}\text{Pu}(\alpha, 2n)^{241}\text{mfCm}$ ($T_{1/2}^{mf} = 15$ ns)	26.7	1.87 ± 0.40
$^{242}\text{Pu}(\alpha, 3n)^{243}\text{mfCm}$ ($T_{1/2}^{mf} = 40$ ns)	33.0	1.20 ± 0.20

for the $^{243}\text{mfBk}$ fission isomer (the last one could not be measured owing to its very short lifetime). Marked anisotropies have been found for the 30-ns $^{236}\text{mfPu}$ as well as for the 15-ns $^{241}\text{mfCm}$ fission isomers.

Before proceeding to analyse the above data, we wish to emphasize the possible ambiguity in obtaining fission isomer spin values from the experimental delayed fission fragment angular distributions.

Basically, there are only two spin values, namely $I = 0$ and $I = 1/2$, for which an isotropic angular distribution has to be expected. Any other spin value should lead to a more or less marked anisotropy in the angular distribution of the fission fragments.

On the other hand, as we have pointed out before, the angular distribution depends not only on the spin value of the fission isomer but also on the nuclear reaction used to populate the fission isomer, through the amplitudes f_M . As a result of neutron and gamma-ray emission, the initial orientation of the compound nucleus angular momentum is partially lost. Consequently, the angular distribution becomes more uniform, approaching the isotropic one.

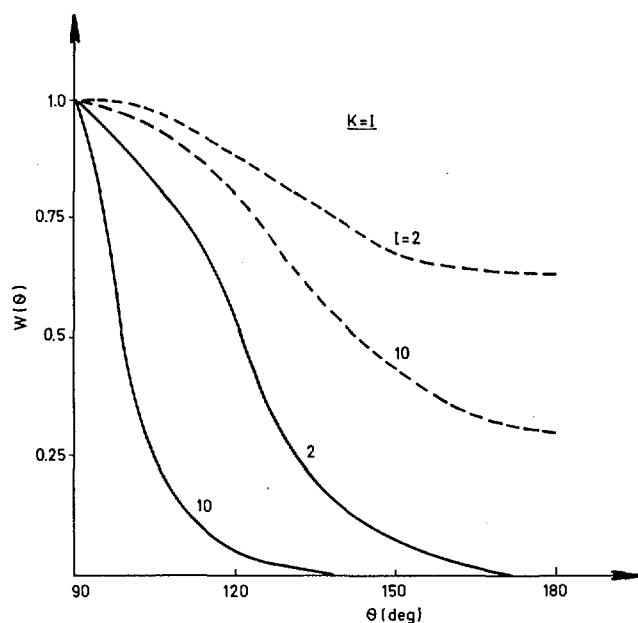


FIG.3. Calculated fission fragment angular distribution for the $^{235}\text{U}(\alpha, 3n)^{236}\text{Pu}$ reaction.

Figure 3 shows the above effect in the case of the $^{235}\text{U}(\alpha, 3n)^{236}\text{Pu}$ reaction. The angular distributions were calculated for the compound (solid line) and the residual (dashed line) nuclei by using the statistical model of the nuclear reactions (Ref. [9]).

Another factor disturbing the anisotropy is represented by the hyperfine interaction between the magnetic (or electric) moment of the recoiled nucleus and the extra-nuclear fields. As these fields are usually randomly distributed with respect to a given direction (z-axis), the initial orientation of the spin may be changed owing to the hyperfine transitions between different sub-states $|M\rangle$. The larger the ratio between the lifetime of the fission isomer and the precession period is, the more strongly perturbed is the fission fragment angular distribution. A rough estimate based on formulas developed in the theory of the γ - γ perturbed angular correlations [10] in the case of a very strong extranuclear field leads to the following result: the anisotropy factor calculated for the $^{235}\text{U}(\alpha, 3n)^{236}\text{Pu}$ reaction, by supposing a spin value of the fission isomer equal to $I=K=10$, is changed from 0.3 (see Fig. 3) to about 0.8. This could seriously affect the determination of the spin value. Although there are some possible ways to avoid this effect [11] we did not take any precautions on this matter in the present experiment.

$^{240\text{mf}}\text{Pu}$.

The obtained isotropy should be expected for the even-even $^{240\text{mf}}\text{Pu}$ ($T_{1/2}^{\text{mf}} = 3.8$ ns), assumed to be on the bottom of the second potential well, in an $(I, K) = (0, 0)$ state.

$^{237\text{mf}}\text{Pu}$, $^{243\text{mf}}\text{Cm}$.

The 114-ns $^{237\text{mf}}\text{Pu}$, as well as the 40-ns $^{243\text{mf}}\text{Cm}$, led to isotropic angular distributions of the delayed fission fragments. In both cases one has to deal with even-odd isotopes. A $5/2$ spin value has been deduced for the 114-ns $^{237\text{mf}}\text{Pu}$ from the relative population of the double fission isomer in ^{237}Pu [5]. Nothing is known as yet concerning the spin value of $^{243\text{mf}}\text{Cm}$. The calculated neutron single particle states in the second potential well for the 147th unpaired neutron ranges from $1/2^+$ [8] to $9/2^-$ [14]. In addition to the above-mentioned effects, some non-conservation of the K-value, which is very possible in such odd-A nuclei, could contribute to the obtained isotropy.

 $^{236\text{mf}}\text{Pu}$.

The marked anisotropy found for the even-even 30-ns $^{236\text{mf}}\text{Pu}$ could be explained by assuming the fission isomer to correspond to an excited state in the second potential well (because the ground state in the second potential well would correspond to $I=K=0$, thus leading to isotropy). The above statement seems to be in good agreement with the recent observation of a second fission isomer ($T_{1/2}^{\text{mf}} = 0.05$ ns) in ^{236}Pu [12], whose existence had been predicted by the lifetime systematics [13]. From the measured anisotropy factor

$$a = 0.70 \pm 0.16$$

a spin value $I=K=4$ has been obtained. This has to be considered however as the lowest limit of the spin value, if a possible hyperfine interaction effect is taken into account.

 $^{241\text{mf}}\text{Cm}$.

This case looks very strange, especially if compared with the analogous $^{243\text{mf}}\text{Cm}$. To explain the obtained anisotropy factor

$$a = 1.87 \pm 0.40$$

the total angular momentum of the fission isomer has to include a large collective motion component.

REFERENCES

- [1] VÎLCOV, N., Rev.Roum.Phys. 12 (1967) 487;
FLEROV, G.N., GANGRSKY, Yu.P., MARKOV, B.N., PLEVE, A.A., POLIKANOV, S.M., JUNGKLAUSSEN, H., Yad.Fiz. 6 (1967) 17.
- [2] BOCA, I., FLEROV, G.N., PLEVE, A.A., POLIKANOV, S.M., SEZON, M., TRETYAKOVA, S.P., VÎLCOV, I., VÎLCOV, N., Nucl.Phys. A102 (1967) 443.
- [3] STRUTINSKY, V.M., Nucl.Phys. 95A (1967) 420.
- [4] JUNGKLAUSSEN, H., Yad.Fiz. 7 (1968) 83.
- [5] VANDENBOSCH, R., RUSSO, P.A., SLETTEN, G., MEHTA, M., to be published.
- [6] VÎLCOV, I., VÎLCOV, N., GANGRSKY, Yu.P., MARINESCU, M., PLEVE, A.A., POENARU, D., HARISOV, I.F., Yad.Fiz. 16 (1972) 454.

- [7] GANGRSKY, Yu.P., KHAN, N.C., PULATOV, D.D., JINR Preprint P7-6286, Dubna (1972).
- [8] GUSTAFSSON, C., MÖLLER, P., NILSSON, S.G., Phys.Lett. 34B (1971) 349.
- [9] HIEN, P.Z., Yad.Fiz. 17 (1973) 489.
- [10] STEFFEN, R.M., FRAUENFELDER, H., Perturbed Angular Correlations, North-Holland, Amsterdam (1964).
- [11] SPROUSE, G.D., Proc.Conf.Hyperf.Interact.Exc.Nucl.St., p.931, Rehovot, (1971).
- [12] METAG, V., LIUKKONEN, E., GLOMSET, O., BERGMAN, A., Paper IAEA-SM-174/26, these Proceedings, Vol.1.
- [13] METAG, V., REPNOW, R., von BRENTANO, P., Nucl.Phys. A165 (1971) 289.
- [14] MOSEL, U., unpublished results.
- [15] SPECHT, H.J., KONECNY, E., WEBER, J., KOZHUHAROV, C., Paper IAEA-SM-174/19, these Proceedings, Vol.1.

DISCUSSION

S. BJØRNHOLM (Chairman): Does Mr. Specht agree with Mr. Vilcov's suggestion of a strong gamma branch in the decay of the 5-ns shape isomer in ^{238}Pu ?

H. J. SPECHT: Mr. Vilcov's suggestion was apparently based on the use of a rather small effective value for the width σ_M of the magnetic substate distribution, of the order of 1, as compared with our range of 2-3. Although I would consider such a small value to be very unlikely, one cannot rule it out completely. In fact, one can go to the other extreme and assume the "true" anisotropy for fission from this isomeric state to be 0, just to obtain an upper limit for the branching ratio between the gamma decay down to the ground state and fission. As indicated in our paper, we then obtain a value of 2 for this ratio.

SPONTANEOUS-FISSION DECAY CONSTANT OF ^{235}U

A. GRÜTTER, H.R. von GUNTEN*, V. HERRNBERGER
Eidg. Institut für Reaktorforschung, Würenlingen

B. HAHN, U. MOSER, H.W. REIST
Physikalisches Institut, Universität Bern, Bern,
Switzerland

G. SLETTEN
Niels Bohr Institute,
Tandem Accelerator Laboratory,
Risø, Roskilde, Denmark

Abstract

SPONTANEOUS-FISSION DECAY CONSTANT OF ^{235}U .

The partial spontaneous fission half-lives of odd-A and odd-odd actinides are observed to be orders of magnitude longer than for even-even nuclides with the same fissility parameter. For ^{233}U and ^{235}U , however, this difference in half-life is reported to be much smaller than for other even-odd actinides. This deviation from systematics could be due to inaccuracies in the measurements or to special features of the fissioning systems.

An attempt was made to remeasure the spontaneous fission decay constant for ^{235}U using the spinner detector technique. The principle of this detector is based upon producing negative pressure by centrifugal forces in a liquid containing the fissionable material. The metastable state created in this way in the solution can be destroyed as in normal bubble chambers. Very low background and a 100% efficiency even for gram quantities of fissionable material are the main features of this fission counter.

About 7 g of uranium with an isotopic composition of 99.7% ^{235}U were dissolved in ethyl alcohol. Since (α, n)-reactions in the alcohol influence the fission rate, spinner vessels with different diameters were used to enhance the escape probability for neutrons. In chambers of 8-cm and 4-cm diameter, count rates of $(2.43 \pm 0.05)/\text{h}$ and $(0.98 \pm 0.03)/\text{h}$, respectively, were obtained. These count rates are compared with those predicted by neutron transport calculations for the contribution of the (α, n, f)-reaction. Since the spinner was operated 15 m below rock, the contribution by cosmic interactions is estimated to be negligible.

After correction for the contribution of the spontaneous fission of ^{238}U , a conservative upper limit for the decay constant of ^{235}U of $3.9 \times 10^{-19} \text{ yr}^{-1}$ was obtained. This limit is at least five times lower than the values published by others. Therefore, it is concluded that the deviation in fission hindrance of ^{235}U compared with other even-odd actinides was at least partly due to an inaccuracy in the measurements.

1. INTRODUCTION

The available data on spontaneous fission decay constants (or half-lives) can be systematized by a method developed by Swiatecki [1]. According to these systematics a straight line is obtained for even-even nuclides if $[\log T_{1/2} + 5 \delta m]$ is plotted against the fissility parameter. The fissility parameter x used in the following has been defined by Myers and Swiatecki [2]. The factor 5 is an empirical number and δm is the difference between the experimental ground state mass and a smooth reference surface [2].

* and Anorganisch-chemisches Institut, Universität Bern, Bern, Switzerland.

TABLE I. FISSIONITY PARAMETERS AND HINDRANCE FACTORS FOR EVEN-ODD, ODD-EVEN AND ODD-ODD ACTINIDES WITH $Z \leq 100$

Nucleus	Fissionity parameter x	Hindrance factor H.F.
^{233}U	0.775	1.0
^{235}U	0.773	1.6
^{239}Pu	0.791	3.1
^{249}Cf	0.825	4.0
^{255}Fm	0.840	5.7
^{257}Fm	0.838	5.6
^{237}Np	0.782	> 4.2
^{241}Am	0.800	4.2
^{243}Am	0.798	5.0
^{249}Bk	0.813	3.2
^{253}Es	0.831	5.6
^{255}Es	0.829	6.6
^{242}Am	0.799	1.4
^{254}Es	0.830	7.7

The source material for spontaneous fission half-lives is taken from a recent compilation by Vandenbosch and Huizenga [3]. The hindrance factors have been extracted from a graph of $[T_{1/2}(\text{even-even}) + 5 \delta m]$ versus the fissionity parameter [2] drawn on the basis of these data.

Odd-A and odd-odd actinides show partial spontaneous fission half-lives which are orders of magnitude larger than the even-even nuclides with similar fissionity parameters. A measure of the increased half-life for odd nuclei can be obtained by a hindrance factor H. F. for spontaneous fission, which can be defined as

$$\text{H. F.} = [\log T_{1/2}(\text{exp.}) + 5 \delta m] - [\log T_{1/2}(\text{syst.}) + 5 \delta m]$$

where $T_{1/2}(\text{exp.})$ and $T_{1/2}(\text{syst.})$ represent the experimentally observed half-life for spontaneous fission, and the half-life according to the even-even systematics for a nucleus with the same fissionity parameter x , respectively. Hindrance factors for the odd-A, odd-Z and odd-odd actinides with $Z \leq 100$ are listed in Table I.

There seems to be no straightforward linear relationship between x and H. F. according to these data, but it is however remarkable that apart from the odd-odd ^{242}Am , both the odd-A uranium nuclei have low hindrance factors for spontaneous fission, if the published values for the half-lives are correct [4, 5]. The origin of the reduced spontaneous fission decay constant of odd-A and odd-odd nuclei is at present not fully understood. Only qualitative arguments in terms of specialization energy [6], change

of the pairing interaction with deformation [7] and variation in the inertial parameter [8,9] have been advanced. It is therefore not trivial to predict any general trend of the hindrance factors. To express the theory in more quantitative terms, however, it is of great importance to supply the most reliable and extensive experimental data on the spontaneous fission half-lives of odd-A and odd-odd nuclei.

These circumstances and the present availability of high-purity samples of ^{235}U , together with a suitable method, motivated a remeasurement of the spontaneous fission half-life for this nucleus.

2. EXPERIMENTAL

2.1. The spinner technique

The spinner technique which has been described in detail elsewhere [10-12] was used to measure the fission events. This method has proven to be successful in the determination of half-lives of spontaneously fissioning nuclides [13].

The spinner consists of a glass cylinder with glass arms on its top (Fig.1). This arrangement is filled with a solution containing the sample

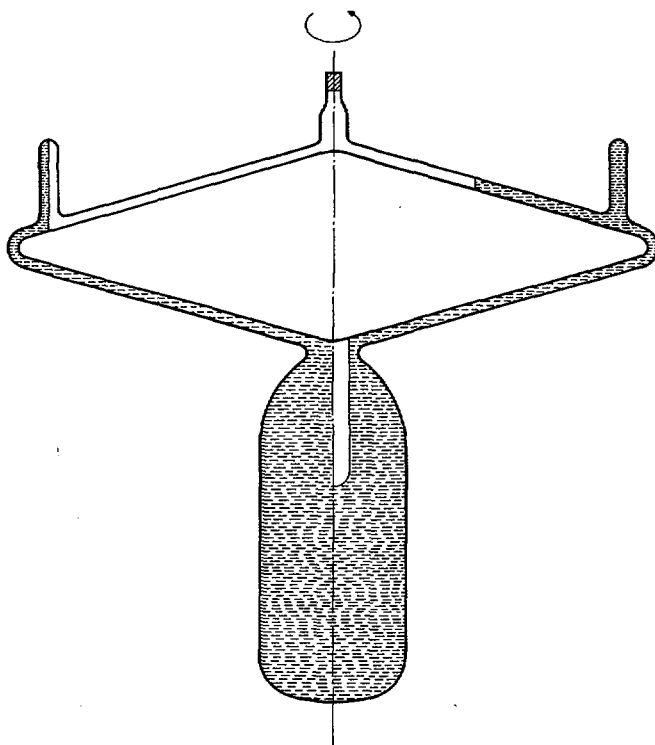


FIG.1. Spinner-detector. The glass container is filled with a liquid containing the fissionable material (shaded area). The assembly is rotated around the indicated axis, thus developing negative pressure through centrifugal forces. Left side: metastable state; right side: broken state.

of interest. The principle of the detector is based upon producing negative pressure in this liquid by centrifugal forces. The metastable state of the solution created in this way can be destroyed as in normal bubble chambers.

The main characteristics of the spinner are:

- (a) 4π geometry, if the radiation source is dissolved inside the spinner chamber.
- (b) No absorption corrections, since the liquid itself works as detector. 100% counting efficiency, even for several hundred grams of dissolved substance.
- (c) Very low background.
- (d) No pile-up effects for α - or β -particles.

The spinner is a low-level counter which is especially suitable for measuring rare events of spontaneous or induced fission. The operating characteristic rises sharply from a threshold to a plateau. This is shown in Fig. 2 for the measurement of spontaneous fission of ^{235}U .

To minimize the interference by cosmic-ray-induced reactions, the spinners were operated 15 m below rock.

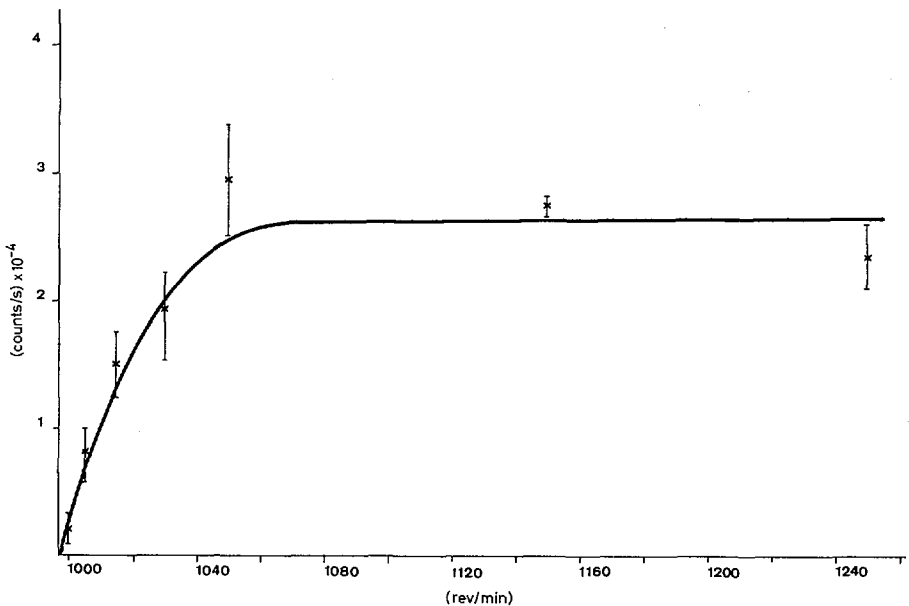


FIG. 2. Operating characteristics of a spinner containing about 7 g of 99.7% ^{235}U . Spontaneous fission events are counted. The operating point for the determination of the decay constant for spontaneous fission was at 1150 rev/min.

2.2. Measurements and materials

The measurement of highly enriched uranium samples with the spinner technique is difficult, owing to the fact that alpha particles from the decay of the uranium may interact with the solvent and produce neutrons of various energies by (α, n) -reactions. Part of these neutrons are moderated in the ethyl alcohol solvent. Hence, the observed fission rate will be the sum of spontaneous and induced fission events.

To enhance the escape probability for neutrons, the measurements were performed in spinner chambers with decreasing dimensions. The dimensions, the active volumes and the uranium concentrations used are shown in Table II.

More than a thousand fission events were registered in each of the two spinners. Operating characteristics were measured for spontaneous fission as well as for fission events induced with a neutron source. The working point for the measurements was always well in the plateau region of the operating curve (see Fig. 2).

Highly enriched ^{235}U was obtained from the USAEC. Its isotopic composition was determined independently by two different analyses which are shown in Table III. The mean value of the two determinations was used.

About 7 g of this material were converted to $\text{UO}_2(\text{NO}_3)_2$ and dissolved in ethyl alcohol (95 vol. %, p.A. Merck). This solution was measured in the two spinners. The concentration of the uranium, which was assayed by gravimetry of U_3O_8 and by spectrophotometry of the 8-hydroxyquinoline complex, is shown in Table II.

TABLE II. SUMMARY OF THE SPINNER CHAMBERS AND SOLUTIONS

Spinner No.	Diameter (mm)	Height of cylinder (mm)	Active volume (cm^3)	Concentrations (mgU/cm^3)
1	80	80	432	16.64
2	40	160	237	28.80

TABLE III. ISOTOPIC COMPOSITION OF URANIUM

Isotope	Analyses		Mean wt%
	(wt%)	(wt%)	
^{234}U	0.057	0.059	0.058
^{235}U	99.76	99.755	99.76
^{236}U	0.063	0.064	0.064
^{238}U	0.117	0.122	0.119

2.3. Calculations of (α , n, f)-contributions

Since it is impossible to distinguish experimentally between spontaneous and induced (α , n)-fission (see Section 2.2.) the latter contribution was estimated using a mathematical method. The calculation of the production rate of the neutrons in ethyl alcohol was difficult, owing to the fact that no data for this solvent and for α -particles from ^{234}U and ^{235}U were available. Therefore, the production rate had to be deduced from a neutron spectrum produced by α -particles of ^{244}Cm in Cm_2O_3 [14] and from values for carbon and oxygen [15]. The values had to be extrapolated for the lower α -particle energy of the uranium isotopes and for the carbon and oxygen ratios in the ethyl alcohol.

For neutron energies above 0.41 eV, cross-sections from the compilation of Adir and co-workers [16] consisting of 16 energy groups were used. This compilation was completed with data from Bondarenko [17] for one thermal energy group below 0.41 eV.

Neutron transport calculations were used to determine the neutron distribution and the induced fission rate. Since the neutron production rate was not accurately known, only approximate values were obtained for the two spinners. One-dimensional calculations were performed for the small spinner (40-mm diameter) using the fast integral transport theory [18] in a cylindrical geometry. This geometry was justified, since the diameter of this spinner chamber was small compared with its height. For the large chamber, however, it was necessary to apply a two-dimensional discrete ordinate transport calculation in 96 directions [19], since the diameter and height were roughly the same.

3. RESULTS AND DISCUSSION

The results of the measurements on the spontaneous fission of ^{235}U are shown in Table IV. The observed counting rate is the overall rate which includes contributions from spontaneous fission of the other uranium isotopes in the sample (see Table III) and from (α , n, f)-reactions. If these contributions are known, the measured overall rate can be corrected.

The error given for the counting rate is one standard deviation. No correction for the background of the apparatus was applied, since it is negligible compared with the observed counting rate. Estimates for the magnitude of contributions by cosmic-ray-induced reactions indicate that

TABLE IV. RESULTS OF MEASUREMENTS ON THE SPONTANEOUS FISSION OF 99.7% ENRICHED ^{235}U

Spinner No.	Amount of U measured (g)	Number of events observed	Counting rate (events/h)
1	7.19	2230	2.43 ± 0.05
2	6.83	1006	0.98 ± 0.03

TABLE V. DECAY CONSTANTS FOR SPONTANEOUS FISSION OF ^{234}U , ^{236}U AND ^{238}U

Isotope	Decay constant λ (yr^{-1})	Reference
^{234}U	$(4.3 \pm 2.2) \times 10^{-17}$	[20]
^{236}U	3.5×10^{-17}	[21]
^{238}U	$(8.46 \pm 0.06) \times 10^{-17}$	[13]

this influence is also quite small, since the measurements were performed in a shielded cave. Therefore, no correction was made for cosmic interactions.

To correct for the spontaneous fission of ^{234}U , ^{236}U and ^{238}U the constants for this decay mode must be known. The published values for these constants are shown in Table V.

The determinations of the decay constants for spontaneous fission of ^{234}U [20] and ^{236}U [21] date back to the 1940s and are probably not very reliable. For the ^{234}U measurement an error is given, whereas in the measurement of ^{236}U even the indication of the error is missing. The decay constant of ^{238}U , however, was measured recently by several authors [13, 22, 23]. From among the values of the different measurements, we have chosen our own result which was also determined with the spinner technique [13].

For a first correction of the measured counting rate we therefore use only the decay constant of ^{238}U [13] and do not apply any correction for either the other uranium isotopes or the (α, n, f) -reaction. Thus, with the isotopic composition of Table III, conservative limits for the counting rates and for the decay constants for ^{235}U are obtained. These limits are shown in Table VI. The errors in the decay constant in the table include errors for the chemical determination of the uranium content, the isotopic composition of the sample and the decay constant of ^{238}U .

The decrease in the counting rate between spinners No. 1 and No. 2 (Table VI) is due to a much lower contribution of the (α, n, f) -reaction in the smaller counter. The value of this measurement ($3.9 \times 10^{-19} \text{ yr}^{-1}$) is therefore taken as the upper limit for the decay constant of ^{235}U .

Using the calculated values for the (α, n, f) -reaction, a further correction may now be applied. Since the calculation of the production rate for the (α, n) -reaction is quite complicated (see Section 2.3) and therefore not very reliable, only the ratio for this reaction in the two spinners was taken for this correction. However, if one uses the measured counting rates in the two spinner vessels in combination with the calculated values for the (α, n, f) -reaction, the source strength can be estimated.

With this estimate, counting rates of 2.0 and 0.56 dis/h were obtained for the contribution of the (α, n, f) -reaction in the large and small spinner, respectively. A correction for ^{234}U and ^{236}U is rather uncertain, owing to the facts already pointed out. Nevertheless this correction was performed using the isotopic composition taken from Table III and the

TABLE VI. LIMITS FOR COUNTING RATES AND DECAY CONSTANTS OF ^{235}U

Spinner No.	Overall counting rate (events/h)	Overall decay constant (yr^{-1})	Counting rate of ^{238}U (events/h)	Corrected counting rate of ^{235}U (events/h)	Upper limit for decay constant (yr^{-1})
1	2.43 ± 0.05	$(1.16 \pm 0.05) \times 10^{-18}$	0.21	2.22 ± 0.05	$(1.05 \pm 0.06) \times 10^{-18}$
2	0.98 ± 0.03	$(4.92 \pm 0.25) \times 10^{-19}$	0.20	0.78 ± 0.03	$(3.9 \pm 0.2) \times 10^{-19}$

TABLE VII. COMPARISON OF DECAY CONSTANTS FOR SPONTANEOUS FISSION OF ^{235}U

Author	Decay constant λ (yr^{-1})	Remarks
Segrè (~1946) [4]	3.8×10^{-18}	Measurements with natural U and ~66% enriched U. Fission counting.
Aleksandrov and co-workers (1966) [5]	2.0×10^{-18}	Enrichment of sample: ~2% ^{235}U . Fission tracks in glass, 22 events observed.
This paper	$< 3.9 \times 10^{-19}$	99.7% ^{235}U , upper limit for decay constant. No correction for (α, n, f) and $^{234}, ^{236}\text{U}$.
This paper	$\sim 10^{-19}$	99.7% ^{235}U . Corrected for (α, n, f) and $^{234}, ^{236}, ^{238}\text{U}$. Estimate with large error.

decay constants of Table V. The corrections for the sum of ^{234}U and ^{236}U amount to 0.1 dis/h. Applying these two corrections, net counting rates for ^{235}U spontaneous fission of 0.12 dis/h result for the large and the small spinner.

Taking into account the large corrections and the errors of experiments and corrections, the resulting decay constant is rather unreliable. Therefore, we can only indicate that it is probably of the order of 10^{-19} yr^{-1} .

We plan to improve the measurements with a spinner of 20-mm diameter and also, we hope, with a sample of even more highly enriched uranium. However, until these improved data are available we suggest that, for the decay constant of ^{235}U , the upper limit

$$\lambda < 3.9 \times 10^{-19} \text{ yr}^{-1}$$

should be used. The only correction made to obtain this limit was a deduction for the well-known contribution of ^{238}U .

Table VII compares our new decay constants for spontaneous fission of ^{235}U with the older values of Segrè [4] and Aleksandrov [5]. It can be seen that our limit is at least a factor of 5 lower than the older determinations, whereas the corrected value ($\sim 10^{-19}$) is about 20 times lower than the published values.

Since highly enriched ^{235}U was used in our measurements, we believe that our values are more reliable than the older ones. Furthermore, better counting statistics were realized in our experiments because of the larger quantities of uranium involved.

The hindrance factors for spontaneous fission for a number of odd-A and odd-odd nuclides are plotted in Fig. 3 as a function of the fissility parameter. For ^{235}U the older values of Segrè [4] and Aleksandrov and co-workers [5] are shown as points in brackets, whereas our new value is indicated as a filled circle.

It has been observed that the hindrance factors for fission isomers (here defined as the ratio of half-lives at a given fissility parameter) are fairly constant. Experimental data for five even-even and four odd-A

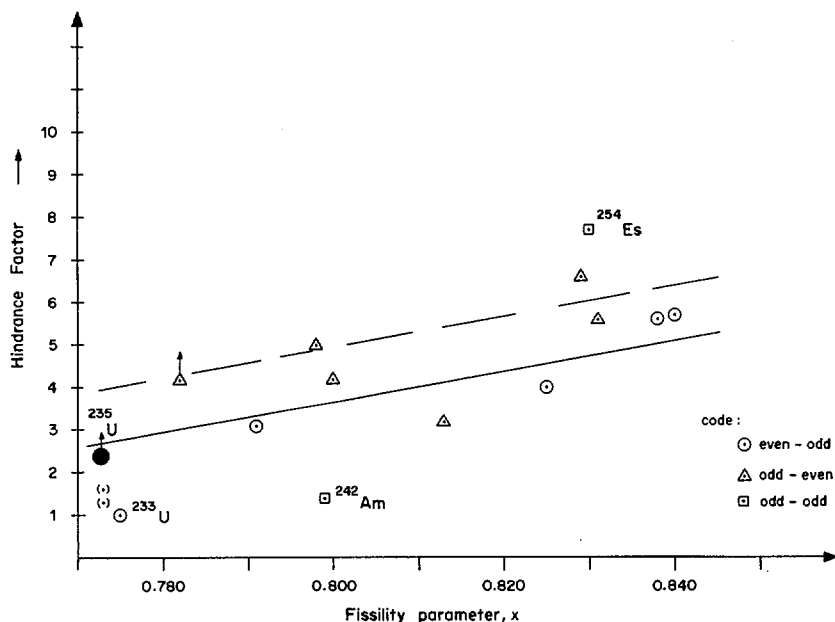


FIG. 3. Plot of the fissility parameter x versus hindrance factors H.F. for the nuclides indicated in Table I. The hindrance factor and the fissility parameter are defined as $H.F. = [\log T_{1/2}(\text{exp.}) + 5.6\text{m}] - [\log T_{1/2}(\text{syst.}) + 5.6\text{m}]$ and $x = (c_3 Z^2/A^{1/3})/(2 c_2 A^{2/3})$ (Ref. [2]). For more details see the introduction of this paper. The older values for ^{235}U are shown as (*), our new limit for ^{235}U as ●.

plutonium isomers vary from 5×10^3 to 8×10^3 . For five odd-A and five odd-odd Am isomers, the hindrance factors range from 8×10^2 to about 4×10^3 [24].

A similar constancy of hindrance factors is not observed in the case of ground state decays, but there seems to be a trend towards increasing factors with increasing x . We have therefore tentatively drawn two straight lines to fit the even-odd and the odd-even data. At present, however, nuclear theory does not provide arguments in favour of the linear relationship.

On the basis of the present remeasurement of ^{235}U it can be concluded that typical hindrance factors for ground state spontaneous fission decay are about 3 or larger, and that the few exceptions, i.e. ^{233}U and ^{242}Am , are probably low due to experimental inaccuracy.

It would therefore be interesting to remeasure these nuclides also. However, in the case of ^{233}U , the expected contribution from (α, n, f) -reactions would be too large to allow a meaningful measurement with our method. The other nuclides of interest ^{242}Am and ^{254}Es are not available in our laboratory in large enough quantities.

ACKNOWLEDGEMENT

The authors are indebted to Mr. B.G. Ganapol and Mr. J. Ligou for helpful discussions, and thank Mr. F. Rudin for the measurement of the isotopic composition of the uranium sample. They acknowledge the help of Mr. A. Schmid and the chemical analyses performed by Mr. R. Keil and Miss E. Roessler. Part of the work was supported by the Swiss National Science Foundation.

REFERENCES

- [1] SWIATECKI, W.J., Phys. Rev. 100 (1955) 937.
- [2] MYERS, W.D., SWIATECKI, W.J., Ark. Fys. 36 (1967) 343.
- [3] VANDENBOSCH, R., HUIZENGA, J.R., Nuclear Fission, Academic Press, New York, (1973).
- [4] SEGRE, E., Phys. Rev. 86 (1952) 21.
- [5] ALEKSANDROV, B.M., KRIVOKHATSKII, L.S., MALKIN, L.Z., PETRZHAK, K.A., Sov. J. At. Energy 20 (1966) 352; Atomnaya Energiya 20 (1966) 315.
- [6] WHEELER, J.A., Niels Bohr and the Development of Physics, (PAULI, W., Ed.), Pergamon Press, Oxford (1955) 163.
- [7] GRIFFIN, J.J., Phys. Rev. 132 (1963) 2204.
- [8] URIN, M.G., ZARETSKY, D.F., Nucl. Phys. 75 (1966) 101.
- [9] SOBICZEWSKI, A., in The Transuranium Elements - the Mendeleev Centennial, (Proc. Robert A. Welch Foundation Conf. on Chemical Research XIII, Houston, 1970), The Robert A. Welch Foundation, Houston (1970) 472.
- [10] HAHN, B., Nuovo Cim. 22 (1961) 650.
- [11] SPADAVECCHIA, A., HAHN, B., Helv. Phys. Acta 40 (1967) 1063.
- [12] HAHN, B., SPADAVECCHIA, A., Nuovo Cim. 54B (1968) 101.
- [13] GALLIKER, D., HUGENTOBLE, E., HAHN, B., Helv. Phys. Acta 43 (1970) 593.
- [14] RIMSHAW, S.J., KETCHEN, E.E., Curium-Data Sheets, USAEC-Rep. ORNL-4357 (1969).
- [15] ARNOLD, E.D., "Neutron sources", Engineering Compendium on Radiation Shielding, 1 (JAEGER, R.G., Ed.), Springer, Berlin (1968).
- [16] ADIR, J., CLARK, S.S., FROELICH, R., TODT, L.J., USAEC-Rep. GA-7157 (1967).
- [17] BONDARENKO, I.I., Ed., Group Constants for Nuclear Reactor Calculations, Consultants Bureau, New York, (1964).
- [18] LIGOU, J., THOMI, P.A., Swiss-Rep. EIR-188 and 189 (1970).
- [19] MYNATT, F.R., USAEC-Rep. K-1684 (1969).
- [20] GHIORSO, A., HIGGINS, G.H., LARSH, A.E., SEABORG, G.T., THOMPSON, S.G., Phys. Rev. 87 (1952) 163.
- [21] JAFFEY, A.H., HIRSCH, A., unpublished data (1949), quoted in HYDE, E.K., The Nuclear Properties of the Heavy Elements, III, Prentice-Hall, Englewood Cliffs, N.J. (1964) 75.
- [22] ROBERTS, J.H., GOLD, R., ARMANI, R.J., Phys. Rev. 174 (1968) 1482.
- [23] KLEEMAN, J.D., LOVERING, J.F., Geochim. Cosmochim. Acta 35 (1971) 637.
- [24] BRITT, H.C., preprint for Nuclear Data (1973), and METAG, V., private communication (1973).

DISCUSSION

R.C. BLOCK: It seems to me that there might be a contribution from photofission. If I remember correctly, you cover your equipment with cadmium, and this can be a source of photons from neutron capture. Did you make corrections for photofission?

H.R. von GUNTEN: No, we did not make corrections for photofission.

J.W.T. DABBS: Your detector obviously has a rather long dead time; I assume the rotation is stopped and restarted automatically. What is the dead time?

H.R. von GUNTEN: About 1 minute.

D.G. PERRY: Is your set-up sensitive to events occurring in the arms of the spinner and, if not, do you correct for these events?

H.R. von GUNTEN: The solution in the arms of the spinner is sensitive to events up to a certain distance from the axis of rotation. This distance is dependent on the speed of rotation. We apply a correction for the volume in the arms.

HALF-LIFE SYSTEMATICS OF FISSION ISOMERS IN EVEN-EVEN Pu ISOTOPES

V. METAG*, E. LIUKKONEN**, O. GLOMSET, A. BERGMAN†

Niels Bohr Institute,
University of Copenhagen,
Copenhagen, Denmark

Abstract

HALF-LIFE SYSTEMATICS OF FISSION ISOMERS IN EVEN-EVEN Pu ISOTOPES.

The recoil-distance method has been improved, allowing for the detection of fission isomers with half-lives in the psec to nsec region. This improvement is achieved by shortening the distance which the recoil nucleus is required to fly before its delayed fission can be distinguished from prompt fission. The recoil length of a short-lived isomer is magnified by geometrical projection and appears as a much longer distance on the detector. With special targets which are plane within $\pm 1\mu$, the shortest measurable half-life becomes 5 psec if the isomers are produced in α -particle-induced reactions.

With this technique the even-even isotopes of Pu have been studied in (d, pn) and also in (p, 2n) and (α , 2n) reactions. The assignment of the isomers is based on excitation functions and cross-bombardments. The measured half-lives are ^{236}Pu : 40 ± 15 ps, ^{238}Pu : 0.7 ± 0.2 ns, ^{242}Pu : 3.5 ± 0.6 ns, ^{244}Pu : 400 ± 100 ps. The isomers of ^{236}Pu , ^{242}Pu and ^{244}Pu have not been observed before.

It is believed that these isomers represent the lowest state in the second minimum whereas longer-lived isomers in the same nuclei should be considered as two-quasi-particle excitations in the second minimum. With these data a dependence of fission isomer half-lives on neutron number could be established for even-even isotopes which is similar to the known behaviour of fission isomers in odd-even and odd-odd nuclei. The results are included in a general discussion of systematic trends in fission isomer lifetimes. Special attention is paid to the effect the addition of an odd particle has on the half-life of a fission isomer.

INTRODUCTION

Previous attempts^{1,2,3)} to establish a systematics of fission isomer halflives suffered from the fact that only little was known about isomers in even-even nuclei. Until recently the only known even-even isomer which was considered the lowest state of the second minimum was ^{240}Pu . Despite the many isomers known in odd-even and odd-odd nuclei no reliable conclusions could be drawn for the isomeric halflives of the paired systems because of uncertainties in the nature and magnitude of the odd-even effect, although some rough predictions had been made.

In this paper the detection of 3 new isomers in even Pu isotopes is reported with halflives in the ps to ns region. This time region has become accessible to observation by a modification of the standard recoil distance technique.

The observed halflives show a pronounced dependence on neutron number suggesting the existence of a magic neutron number associated with the shape of the fission isomer.

* On leave from Max-Planck-Institut für Kernphysik, Heidelberg, Fed. Rep. of Germany.

** On leave from the University of Jyväskylä, Jyväskylä, Finland.

† On leave from Moscow Institute for Nuclear Research, Academy of Science, Moscow, USSR.

The clearer understanding of the behaviour of the even-even isomers suggests new intensive efforts to clarify the phenomenon of the odd-even effect.

EXPERIMENTAL METHOD

The observation of ps isomers with the recoil distance method requires measurements of recoil lengths of only a few μm since a halflife of 10 ps corresponds to a recoil length of 6 μm for typical recoil velocities of approximately $6 \cdot 10^7$ cm/s. A geometrical magnification of the decay length onto the detector is needed which views the decay of the recoiling isomers at backward angles. This detection technique has been introduced by Limkilde and Sletten⁴⁾ who identified an 0.5 ns isomer in ^{238}Pu . The principle of the method is illustrated in fig.1. The magnification can be varied stepwise by inserting shadow rings of different diameters in the target plane.

Fission fragments from short-lived isomers can only be distinguished from prompt fission events in the target if the unevenness of the target is considerably smaller than the decay length of the isomer. Targets have been used which are plane within ± 1 μm to guarantee a sufficient geometrical separation between prompt and delayed fission events. The shortest measurable halflife becomes 5 ps. Glassplates or Makrofol plastic foils have been used as detectors. Details of the experimental technique are published elsewhere⁵⁾.

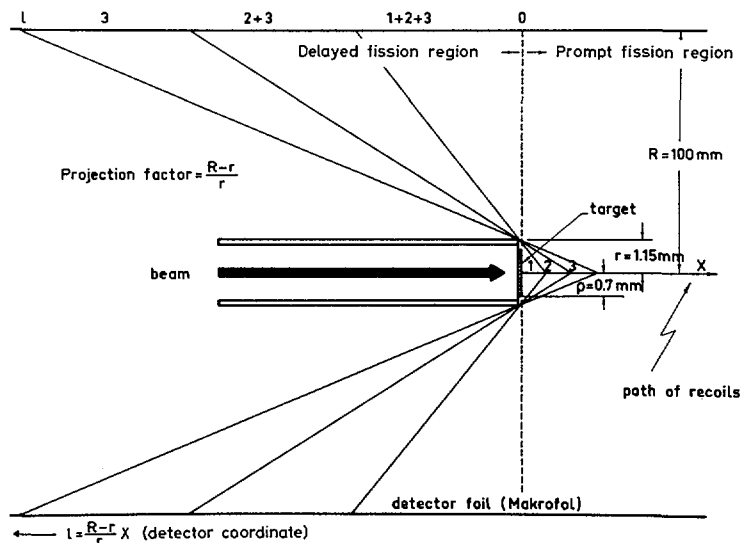


FIG.1. Experimental method: Fission isomers recoil out of the target and decay in flight. Straight lines indicate how the edge of the target holder defines a projection of the recoil axis on the detector. Close-lying points along the recoil axis correspond to wider-spaced points on the detector. The magnification is determined by the ratio of the radius R of the cylindrical detector to the radius r of the target holder. Fission fragments from short-lived isomers which decay within a short distance from the target are spread over a relatively large area on the detector (from Ref. [5]; see also Ref. [4]).

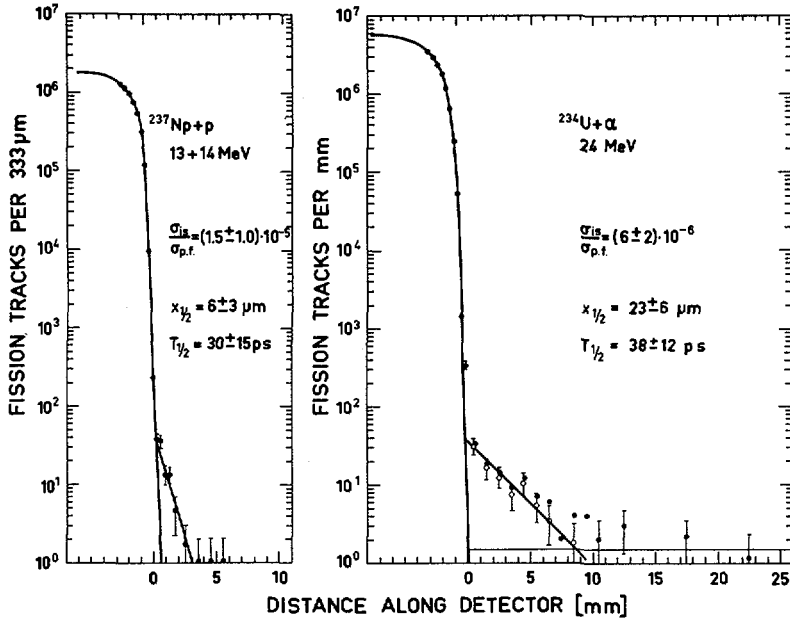


FIG. 2. Decay curves of the 40 ± 15 -ps isomer measured in two reactions with a projection factor 86 and assigned to ^{236}Pu . The density of fission tracks is plotted as a function of the distance along the detector. The track density decreases by more than 5 orders of magnitude over a 2-mm length when the fragments from prompt fission events in the target become shaded off by the cylindrical projection edge. The measured points of the 40-ps activity are corrected for the long-lived background from the 34-ns isomer in ^{236}Pu produced in the same irradiation. $x_{1/2}$ is the half-length along the recoil axis.

Proton-, deuteron-, and α -beams from the Super King Tandem accelerator of the Niels Bohr Institute have been used for the present studies. One α -irradiation was performed at the Max-Planck-Institut für Kernphysik in Heidelberg.

RESULTS

The results obtained for the various isotopes will be discussed separately.

^{236}Pu

A new fission isomer with a halflife of 40 ± 15 ps is assigned to ^{236}Pu . As shown in fig. 2, the decay of this isomer has been observed in the p-bombardment of ^{237}Np and the α -bombardment of ^{234}U . At proton energies of 13 and 14 MeV and an α -energy of 24 MeV the 2 neutron evaporation reactions are known to dominate. This cross bombardment suggests the assignment of this isomer to ^{236}Pu . The assignment is further supported by preliminary data for the excitation function of this activity in the $^{234}\text{U} + \alpha$ -irradiation. For the α -induced reaction the decay

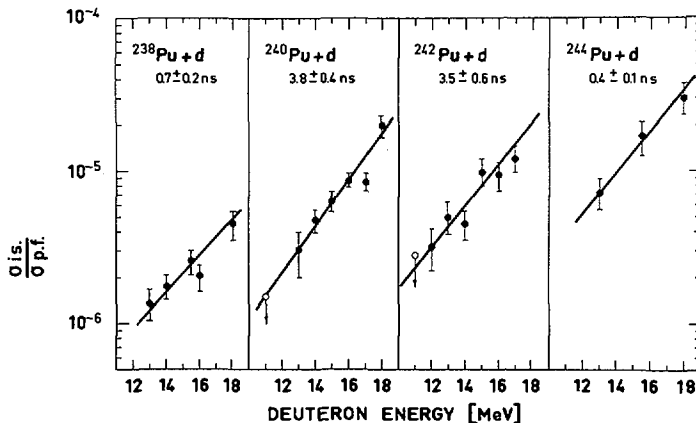


FIG. 3. Excitation functions for the fission isomers produced in the deuteron bombardment of ^{238}Pu , ^{240}Pu , ^{242}Pu , ^{244}Pu . The ratio of isomeric to prompt fission is plotted as a function of the bombarding energy. The observed half-lives are given in the figure.

of the isomer extends to a longer distance from the prompt fission edge than in the proton run since the recoil velocity is 3 times higher. This allows a more reliable determination of the halflife and cross-section. The ratio of delayed to prompt fission is directly given by the intersection of the decay curve with the prompt fission edge. A value of $(6 \pm 2) \cdot 10^{-6}$ is found.

An isomer with a halflife of $34 \text{ ns}^{(6)}$ and an exceptionally high excitation energy of $3.5 \pm 0.4 \text{ MeV}$ is already assigned to ^{238}Pu . The preliminary excitation function data indicate that the newly found fission activity represents the decay of the lowest state in the second minimum whereas the previously known isomer probably is an excited state in the second minimum.

^{238}Pu

Two isomers with halflives of 0.5 ns and 6.5 ns are known in $^{238}\text{Pu}^{(4)}$. The 0.5 ns isomer has been studied in the $^{238}\text{Pu}(d, pn)$ reaction. Its excitation function is shown in fig. 3. A halflife of $0.7 \pm 0.2 \text{ ns}$ is found in fair agreement with the value of $0.5 \pm 0.2 \text{ ns}$ quoted by Limkilde and Sletten⁽⁴⁾.

^{240}Pu

The decay of the known $3.8 \pm 0.3 \text{ ns}$ isomer in $^{240}\text{Pu}^{(7)}$ has been used for a calibration of the time-distance conversion. The yield of this isomer in the d-bombardment of ^{240}Pu exhibits the energy dependence typical for a (d, pn) reaction as shown in fig. 3.

^{242}Pu

A new fission isomer with a halflife of $3.5 \pm 0.6 \text{ ns}$ is observed in the deuteron bombardment of ^{242}Pu . The decay curve of this isomer is shown in fig. 4. The assignment to ^{242}Pu is based on the excitation function shown in fig. 3 which is typical for a (d, pn) reaction. The only other reaction which could

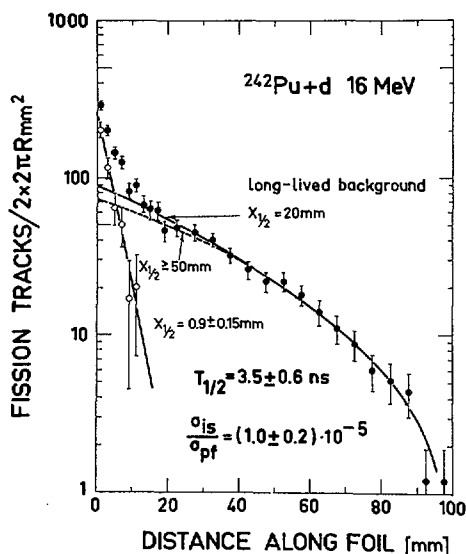


FIG. 4. The full (●) points represent the distribution of delayed fission tracks from the deuteron bombardment of ^{242}Pu using a projection factor 3. The open circles (○) show the decay of the 3.5-ns activity corrected for the background which contains several unresolved components of well-known isomers [2, 6-7].

show a similar energy dependence is (d,3n). This reaction can, however, be excluded since an attempt to produce the same activity by the $^{242}\text{Pu}(p,2n)$ reaction was unsuccessful. An upper limit of $2 \cdot 10^{-6}$ can be set on the isomer to prompt fission ratio.

Another fission isomer with a half-life of 30 ns is reported for ^{242}Pu (ref.2,6).

^{244}Pu

The irradiation of ^{244}Pu with deuterons yields a new fission isomer with a half-life of 400 ± 100 ps. The decay of this isomer is shown in fig.5. The long-lived background is presumably from an 85 ns isomer in ^{245}Pu and the 5.5 μs isomer in ^{243}Am . The activity is assigned to ^{244}Pu since the excitation function suggests a (d,pn) reaction (fig.3). A (d,3n) reaction can again be ruled out since the yield of this activity in the $^{244}\text{Pu}(p,2n)$ reaction is less than $4 \cdot 10^{-6}$ of the prompt fission cross-section.

It is interesting to note that for a given bombarding energy the cross-section of the (d,pn) reaction decreases from ^{244}Pu to ^{238}Pu . This can be understood on the basis of the reaction mechanism. A direct (d,p) process leading to the continuum is followed by neutron evaporation which occurs in competition with fission^{2,10,11}). The Γ_n/Γ_f ratio which governs this competition is known to decrease with decreasing neutron number.

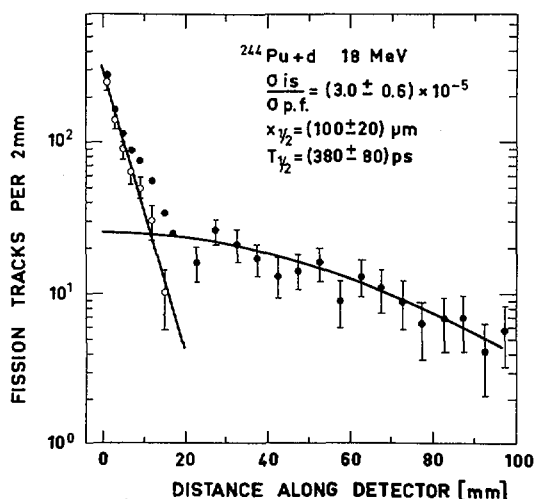


FIG. 5. The decay curves of fission activities observed in the irradiation of ^{244}Pu with deuterons of 18 MeV. The points for the 400 ± 150 -ps activity are corrected for the long-lived background presumably from an 85-ns isomer in ^{245}Pu (open and full points as in Fig. 4).

DISCUSSION

A: The magic neutron number

The experimental data known to date show the existence of fission isomers in the even-even isotopes $^{236}_{94}\text{Pu}$, $^{238}_{94}\text{Pu}$, $^{240}_{94}\text{Pu}$, $^{242}_{94}\text{Pu}$, $^{244}_{94}\text{Pu}$. The half-lives of the newly observed isomers are rather close to the predictions made earlier in attempts to establish a systematics of fission isomer half-lives^{1,2,3}.

The nuclei $^{236}_{94}\text{Pu}$, $^{238}_{94}\text{Pu}$ and possibly $^{242}_{94}\text{Pu}$ exhibit double isomerism. The 2 isomers in $^{238}_{94}\text{Pu}$ have been studied by Limkilde and Sletten⁴). The longer-lived 6.5 ns isomer has been interpreted as a K-isomer in the second minimum, the shorter 0.5 ns isomer as the ground state of the second minimum. A similar explanation may hold for the other double isomers in $^{236}_{94}\text{Pu}$ (and $^{242}_{94}\text{Pu}$). The interpretation of the 34-ns isomer in $^{236}_{94}\text{Pu}$ as a two-quasi-particle state in the second well was first proposed by Vandenbosch and Wolf¹²).

The shorter-lived isomers follow a smooth trend with neutron number as shown in the lower part of fig. 6. The longest half-lives are found for $N=146$ and $N=148$. The half-lives become shorter for the neighbouring isotopes suggesting that one of these numbers should be regarded as the magic neutron number associated with the deformation of the fission isomer. In the framework of the Strutinsky-type calculations¹³) one expects for the magic number the strongest negative shell correction at the deformation of the shape isomer, the most pronounced second minimum and consequently the longest half-life. A magic neutron number $N=148$ would agree with the predictions of Strutinsky and Pauli¹⁴) and with recent single particle energy calculations^{15,16}).

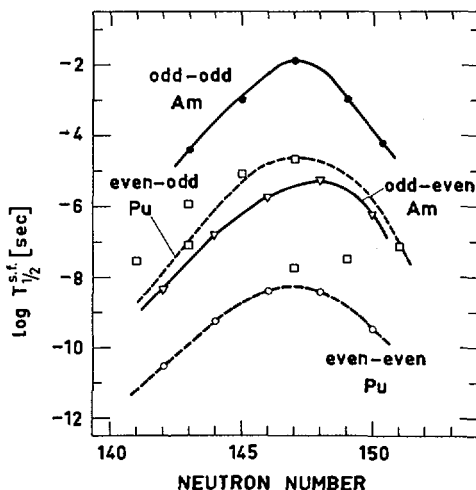


FIG. 6. Logarithm of the measured half-lives of fission isomers as a function of neutron number for even-even and even-odd Pu and odd-even and odd-odd Am isotopes. Lines are drawn to connect corresponding points and to guide the eye.

B: The odd-even effect

The smooth curve in the lower part of fig.6 is believed to reflect the variation of halflife with neutron number in the paired system. Now that this dependence is known it is possible to ask how the halflife is changed by the addition of one or two unpaired nucleons relative to this "zero line".

It is known from the systematics of halflives for the spontaneous fission from the groundstate of the actinide nuclei that odd mass and odd-odd isotopes exhibit longer halflives than their even neighbours. According to the presently known data¹⁷⁾, the variation of this retardation is, however, not readily understood. It appears to be of the order of 10 for the U isotopes but it is 10^7 for the Es isotopes.

In the case of fission isomers, the odd mass and odd-odd Am isotopes show an amazingly regular dependence of the halflives on neutron number with a retardation of about 10^3 per added odd particle relative to the "zero line" suggesting a systematic odd-even effect.

In contrast, the observed fission isomers in odd-mass Pu isotopes exhibit an irregular pattern although some of them seem to follow a smooth trend as indicated by the dashed curve in fig.6. This line, however, is arbitrary.

The two isomers in ^{237}Pu have been studied in detail¹⁸⁾. The 1.1 μs isomer is found to be an excited single particle state¹⁹⁾ lying above the ground state of the second minimum which decays with a halflife of 82 ns by spontaneous fission.

It is an open question whether the observed halflife of 1.1 μ s is determined by the fission or γ -decay of the excited state. A similar situation may apply to other isomers observed so far in the odd mass Pu isotopes. Further experiments are needed to find out which of the measured halflives are halflives for spontaneous fission in order to decide whether the odd-even retardation of halflives really is a systematic effect, as is suggested by the presently known data for the Am isotopes.

An answer to this question may shed some light on the nature of the odd-even effect. A retardation by a nearly constant factor would strongly suggest that the odd-even effect is mainly related to the difference in mass parameter and (or) pairing gap. If the effect is due to the specialization energy connected to the conservation of spin and parity of the odd particle under deformation, a stronger dependence on the actual spin values involved and consequently a more irregular pattern might be expected.

The measurements of the halflives for spontaneous fission from the groundstate of the first minimum of odd mass and odd-odd isotopes are difficult because of the possibility that rather small even-even impurities in the sample may lead to erroneous halflives. A confirmation of the presently available experimental data may also be helpful in clarifying the features of the odd-even effect.*

ACKNOWLEDGEMENT

The authors would like to thank Dr. S. Bjørnholm for his continuous interest in this work and his many helpful suggestions and comments throughout the whole series of measurements. We are indebted to Dr. R. Repnow from the Max-Planck-Institut für Kernphysik, Heidelberg, for his accurate and careful preparation of the run done in Heidelberg and his help in the experiment. We acknowledge the laborious work of Mrs. E. Bengtsson and Mrs. I. Bærentsen who scanned the glassplates and foils.

REFERENCES

- 1) V. Metag, R. Repnow and P. von Brentano, Nucl. Phys. A165 (1971) 289.
- 2) S.M. Polikanov and G. Sletten, Nucl. Phys. A151 (1970) 656.
- 3) H. Weigmann and J.P. Theobald, Nucl. Phys. A187 (1972) 305.
- 4) P. Limkilde and G. Sletten, Nucl. Phys. A199 (1973) 504.
- 5) V. Metag, E. Liukkonen, G. Sletten, O. Glomset, and S. Bjørnholm, Nucl. Instr. Methods, to appear.
- 6) N.L. Lark, G. Sletten, J. Pedersen, and S. Bjørnholm, Nucl. Phys. A139 (1969) 481.

* See GRÜTTER, A., et al., Paper IAEA-SM-174/05, these Proceedings, Vol. 1.

- 7) H.C. Britt, S.C. Burnett, B.H. Erkkila, J.E. Lynn, and W.E. Stein, Phys.Rev. C4 (1971) 1444.
- 8) E. Liukkonen and V. Metag, unpublished (1973).
- 9) K.L. Wolf and I.P. Unik, Phys.Lett. 38B (1972) 405.
- 10) K.L. Wolf, R. Vandenbosch, P.A. Russo, M.K. Mehta, and C.R. Rudy, Phys.Rev. C1 (1970) 2096.
- 11) R. Repnow, V. Metag, J.D. Fox, and P. von Brentano, Nucl.Phys. A147 (1970) 183.
- 12) R. Vandenbosch and K.L. Wolf, 2nd Symposium on Physics and Chemistry of Fission (IAEA, Vienna, Austria, 1969) p.439.
- 13) M. Brack, J. Damgaard, A.S. Jensen, H.C. Pauli, V.M. Strutinsky, and C.Y. Wong, Rev.Mod.Phys. 44 (1972) 320.
- 14) V.M. Strutinsky and H.C. Pauli, 2nd Symposium on Physics and Chemistry of Fission (IAEA, Vienna, Austria 1969) 155.
- 15) U. Mosel, private communication to the authors of ref.19).
- 16) P. Möller, S.G. Nilsson, and J.R. Nix, private communication to the authors of ref.19).
- 17) R. Vandenbosch and J.R. Huizenga, Nuclear Fission, Academic Press, New York (1973).
- 18) P.A. Russo, R. Vandenbosch, M. Mehta, J.R. Tesmer, and K.L. Wolff, Phys.Rev. C3 (1971) 1595.
- 19) R. Vandenbosch, P.A. Russo, G. Sletten, and M. Mehta, to be published.

DISCUSSION

R. VANDENBOSCH: I am very intrigued by your suggestion as to how we might possibly distinguish between the specialization energy and the effective mass parameter and I should like to refer you to my speculations on the subject which are contained in my paper (IAEA-SM-174/203) and which lack of time prevented me from discussing in my oral presentation.

L.G. MORETTO: Even though a system does not possess axial symmetry, it still may have an average K quantum number. At the onset of axial distribution the wave function does not have a good K quantum number. However, it can be expanded on a set of wave functions characterized by good K quantum numbers. One of these wave functions must be predominant even at small distortions, thus defining a most probable K value.

H.C. BRITT: I would like to point out that the specialization energy S referred to by Mr. Vandenbosch may also include some contributions from the difference between the pairing gaps at the second saddle point and the second minimum. Since the questions of surface-dependent pairing and the differences in Δ 's due to shell correction differences are not yet completely understood, it is not possible to establish firmly what fraction of the quantity S might be due to pairing effects.

FISSION BARRIERS: THEORY
(THERMODYNAMICS)

(Session IV)

Chairman: Z. Fraenkel (Israel)

Review Paper

FISSION PROBABILITIES IN LIGHTER NUCLEI A theoretical and experimental investigation of the shell and pairing effects in fissioning nuclei*

L. G. MORETTO

Department of Chemistry and Lawrence Berkeley Laboratory,
University of California,
Berkeley, Calif., United States of America

Abstract

FISSION PROBABILITIES IN LIGHTER NUCLEI: A THEORETICAL AND EXPERIMENTAL INVESTIGATION OF THE SHELL AND PAIRING EFFECTS IN FISSIONING NUCLEI.

The general features of the fission probabilities are reviewed in the light of modern developments on the statistical properties of nuclei. The general thermodynamical aspects of the fission probabilities are first discussed without relying on any specific nuclear model. The effects of the shell structure and of the collective degrees of freedom on the saddle-point and ground-state phase space volumes are then considered. A general method to include the effect of shells and pairing in the fission probability calculation is illustrated. The disappearance of the shell and pairing effects with increasing excitation energy and its influence on the fission probabilities is exemplified by means of a calculation performed on superheavy elements. The experimental data available in nuclei in the Pb region and in lighter nuclei are discussed in detail and an analysis based upon the present knowledge of shell and pairing effects is performed. It is found that the experimental evidence on shell effects in these data are accounted for satisfactorily by including the Nilsson model and the BCS Hamiltonian in the calculation. A reliable set of fission barriers is obtained and the liquid drop model predictions are tested. The saddle point single particle level densities which are also obtained in the analysis show the expected A dependence, and their magnitude, about 8% larger than the corresponding ground state quantity, seems to be due to an increase in the nuclear surface at the saddle point.

INTRODUCTION

Already in 1939, immediately after the discovery of fission, it became apparent that the fission decay rate is controlled by a rather impenetrable potential energy barrier [1]. The existence of this barrier found its natural explanation in the liquid drop model [2], which was to become the leading model in the fission process.

At the same time the theory of the chemical reaction rates, based upon the existence of an activated complex (or transition state), was employed to estimate the fission decay rate [1].

An equally good theoretical knowledge of the neutron and radiation decay widths [3], associated with the expected exponential rise of the level density with excitation energy, led to a very early theoretical understanding of the fission probabilities [1, 4].

The first data on fission probabilities to become available were in the actinide region [5]. In these elements the fission barrier height and the neutron binding energy are very close and the resulting fission probability at energies above the barrier varies very slowly with energy.

* Work performed under the auspices of the US Atomic Energy Commission.

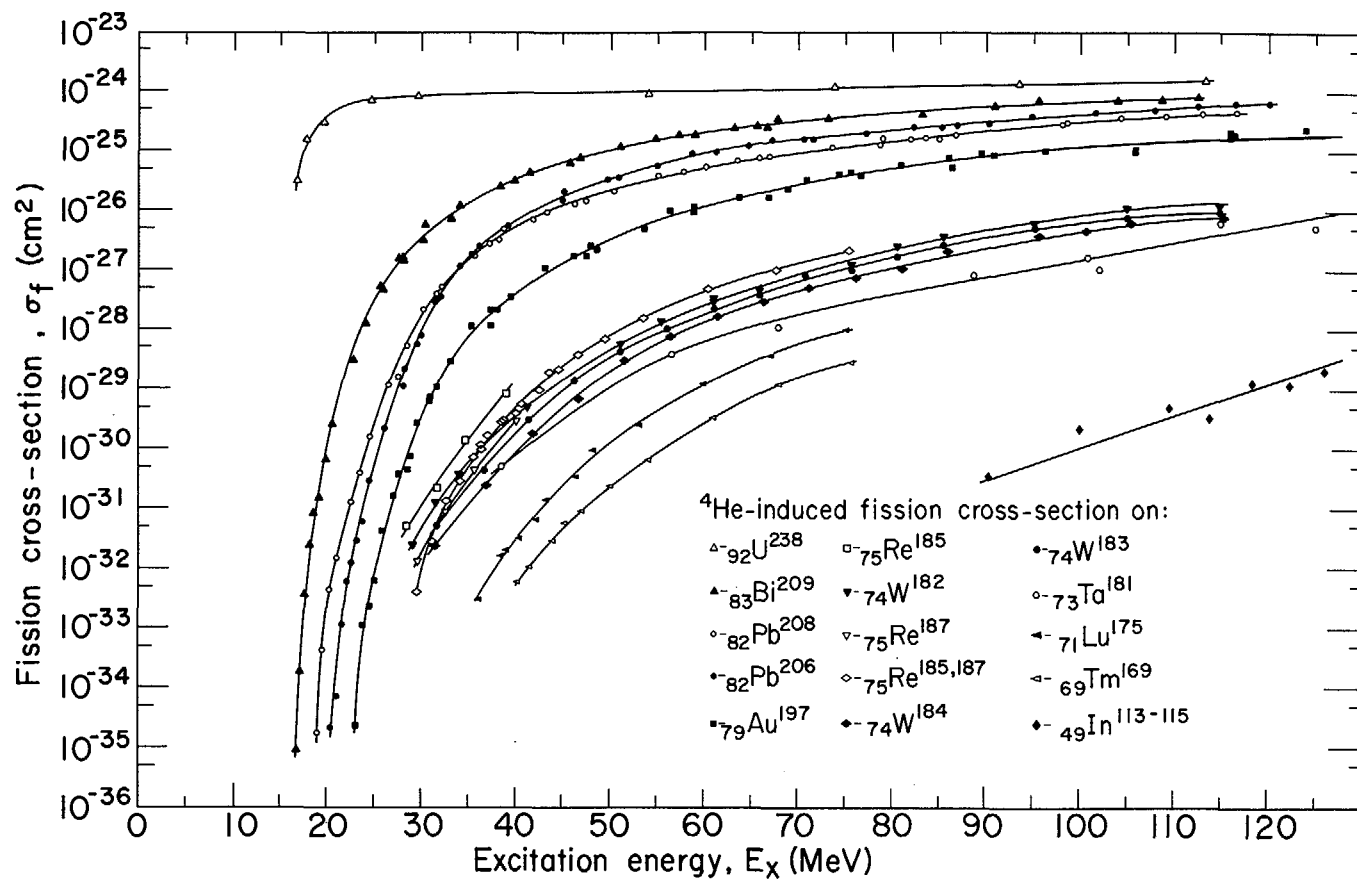


FIG. 1. Examples of ${}^4\text{He}$ -induced fission cross-sections of lighter elements. The data are taken from Refs [13, 14, 16-18].

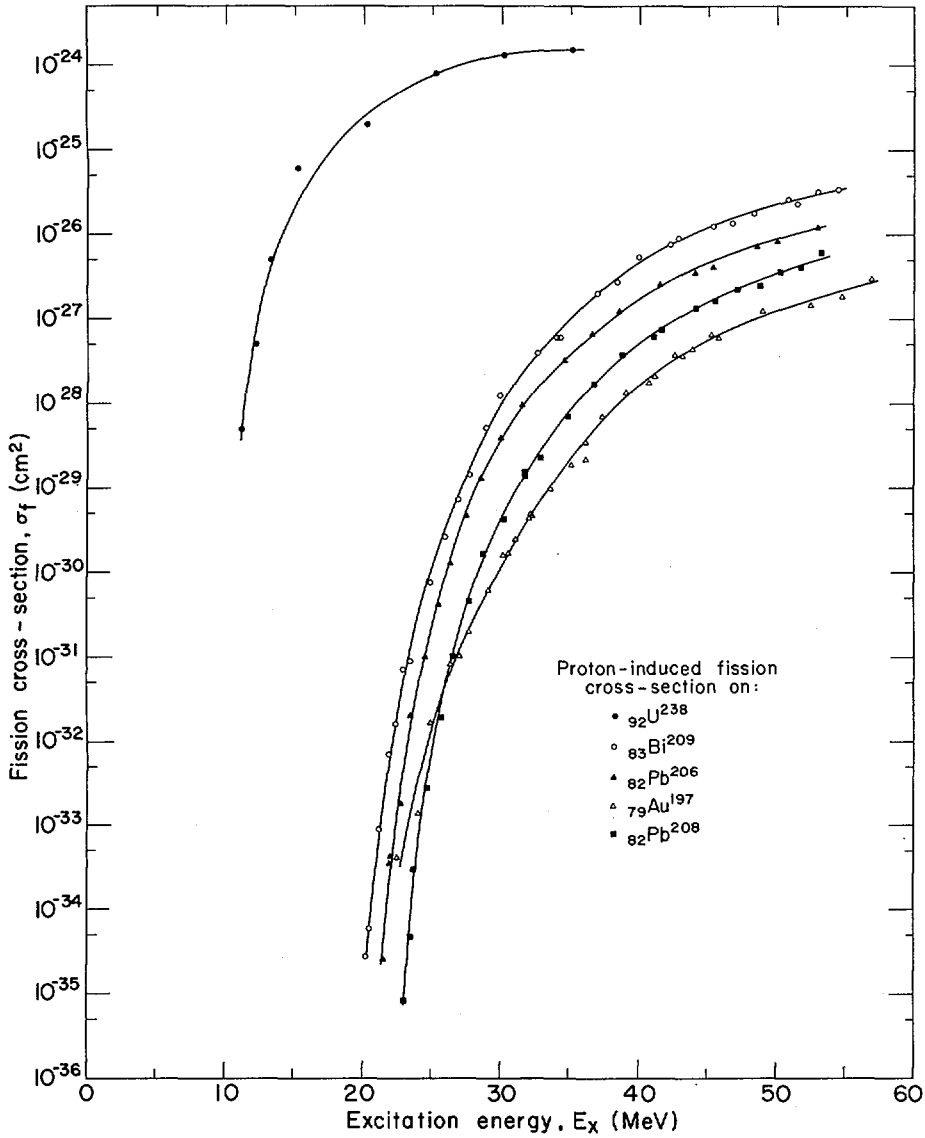


FIG. 2. Examples of ^1H -induced fission cross-sections of lighter elements. The data are taken from Ref. [16].

The observations of fission cross-sections rapidly rising with energy in lighter elements, for which the fission barrier is much larger than the neutron binding energy, prompted a new theoretical and experimental effort which on the one hand led to more accurate theoretical expressions for the fission probabilities on the basis of the uniform model [5, 6] and on the other produced an increasing wealth of experimental data on lighter elements [7-18] and at energies very close to the fission barrier [13, 14, 16-18]. One should explicitly mention the pioneering work by Huizenga and co-workers [13], the determination of the fission barrier of ^{201}Tl by Burnett and co-workers [14] and the work by the Berkeley group [16-18]. The greatest part of the available cross-section data which could be included in two figures is shown in Figs 1 and 2.

The analysis of the data on the basis of the early theories successfully accounted for the rapidly rising fission cross-sections and produced reliable fission barriers. To a large extent the barrier determinations have been and still are the most relevant results obtained in the analysis of fission probabilities, because of their contribution to the understanding of the potential energy surfaces and of the liquid drop model parameters. Clear indications of the shortcomings of the uniform model, and of the necessity for more accurate models to be used in the evaluation of the level densities, were also apparent [16]. The data, for nuclei close to the lead region, could be fitted only over a short energy range, and the level density parameters extracted from the data fitting showed marked fluctuations attributable to the shell structure.

More recently, refined level densities, generated on the basis of the shell model [19-22] and of the pairing Hamiltonian [23-30], have become available and have made it possible to account for the shell structure effects in a nearly quantitative way. These new level densities have proven to be remarkably successful in the analysis of the fission cross-sections of the lighter elements [31, 32] as well as in the analysis of the fission and isomer formation cross-sections in the actinides [33, 34]. A similar study has also been extended to the superheavy nuclei in order to investigate their stability towards fission at the compound nucleus stage [35-37].

In the present paper all of the above developments are presented to various extents. In Section 1 the general features of the fission probability theory are outlined, and the limiting behavior of the fission probability at high energies is derived. Furthermore, the insensitivity of this quantity to the fine details of the Hamiltonian is pointed out. In Section 2 the results obtained by using the uniform model in the analysis of the lighter element data are presented and the shortcomings of such a model are discussed. In Section 3 some recent and new aspects of the problem are treated, like the relevance of the collective degrees of freedom to the fission decay width, and the way in which shell and pairing effects can be included in the calculation of the fission probabilities. The latter point is illustrated with the calculation of the fission probabilities in superheavy elements. In Section 4 the available experimental data for lighter elements are critically analyzed and the results of the fitting procedure are discussed.

As a last comment, the data available for lighter elements and at small angular momenta have been given special attention in this paper. Very important work has been and is being performed in the actinide region and will appear in other contributions to this symposium.

1. FISSION AND NEUTRON WIDTHS: STANDARD FORMULAE AND LIMITING BEHAVIOR

In this section an effort is made to derive various limiting forms of the fission probability without resorting to any detailed nuclear model. It can be shown that the physical features of the system can be summarized in terms of simple thermodynamical quantities, like the temperature, which are rather independent of the nuclear structure details and vary slowly with energy.

A nucleus, whose excitation energy is equal to or larger than the fission barrier, is expected to move randomly in a restricted region of configuration space (the compound nucleus region) until, by chance, it finds access to the potential energy saddle which leads to a new, almost unrestricted region of configuration space (the region of the forming fission fragments). The decay probability is equal to the number of systems per unit time overcoming the barrier divided by the number of systems remaining in the compound nucleus region. If the access to the barrier is random, the population of the compound nucleus region and that of the saddle region can be taken to be proportional to the respective phase space volumes. The randomness assumption should be met if the total decay width of the compound nucleus is small, namely, if its lifetime is long.

Under these conditions the fission decay width can be written as:

$$\Gamma_F = \frac{1}{2\pi\rho(E)} \int_0^E \rho_S(x) P(E - B_F - x) dx \quad (1)$$

where $\rho(E)$ is the level density of the compound nucleus at the excitation energy E , B_F is the fission barrier height, $\rho_S(x)$ is the saddle point level density at the excitation energy x and $P(E - B_F - x)$ is the quantum mechanical probability of penetrating the barrier. This last quantity, for a parabolic barrier takes the form [38]:

$$P = \frac{1}{1 + \exp - \frac{2\pi(E - B_F - x)}{\hbar\omega}}$$

where $\hbar\omega$ is the phonon energy associated with the parabolic potential, called barrier penetrability coefficient. An important feature of the level density $\rho_S(x)$ is that it refers to all the collective and intrinsic modes of the system with the exclusion of the fission mode.

The neutron decay width can be evaluated along similar lines and takes the form:

$$\Gamma_N = \frac{1}{2\pi\rho(E)} \frac{4m_N}{\pi\hbar^2} \int_0^{E-B_N} \sigma_{inv} \rho_R(x) (E - B_N - x) dx \quad (2)$$

where m_N is the neutron mass, B_N is the neutron binding energy, σ_{inv} is the cross-section associated with the inverse process and $\rho_R(x)$ is the level density of the residual nucleus.

One can take advantage of the strong energy dependence of the level densities and evaluate both expressions by suitably expanding the integrand about the upper limit of integration. The following expression is obtained for the fission width:

$$\Gamma_F = \frac{1}{2\pi\rho(E)} \frac{1}{D_S} \rho_S(E - B_F) \quad (3)$$

where the penetrability P has been taken equal to one above, and zero below, the barrier and

$$D_S = \left. \frac{d \ln \rho_S(x)}{dx} \right|_{x=E-B_F}$$

For the neutron width one obtains:

$$\Gamma_N = \frac{1}{2\pi\rho(E)} \sigma_{inv} \frac{4m_N}{\pi\hbar^2} \frac{1}{D_R^2} \rho_R(E - B_N) \quad (4)$$

where the inverse cross-section has been assumed to be independent of energy and

$$D_R = \left. \frac{d \ln \rho_R(x)}{dx} \right|_{x=E-B_N}$$

Recalling that in statistical mechanics

$$\frac{d \ln \rho}{dx} = \frac{dS}{dE} = \frac{1}{T}$$

the quantities $1/D_S$ and $1/D_R$ assume the meaning of the saddle point and residual nucleus temperatures T_S and T_N , respectively.

The ratio Γ_F/Γ_N can then be expressed in the following simple form:

$$\frac{\Gamma_F}{\Gamma_N} = \frac{\pi\hbar^2}{4\sigma_{inv} m_N} \frac{T_S}{T_R^2} \frac{\rho_S(E - B_F)}{\rho_R(E - B_N)} \quad (5)$$

This approximation is accurate even at rather low excitation energies. The above equation can be further simplified by expanding both level densities about the energy $E - \bar{B}$ where \bar{B} is intermediate between B_F and B_N :

$$\frac{\Gamma_F}{\Gamma_N} = \frac{\pi\hbar^2}{4\sigma_{inv} m_N} \frac{T_S}{T_R^2} \frac{\rho_S(E - \bar{B})}{\rho_R(E - \bar{B})} \exp \left(\frac{B_N}{T_R} - \frac{B_F}{T_S} \right) \quad (6)$$

where T_R' and T_S' are the effective temperatures in the residual nucleus and at the saddle at an excitation energy $E - \bar{B}$. Such an approximation becomes

better the closer B_F is to B_N and the larger the excitation energy E is. In fact, as the excitation energy increases, the temperatures T_S , T_R , T'_S , T'_R tend to become closer and closer. One can also assume that the two level densities $\rho_S(E - \bar{E})$ and $\rho_R(E - \bar{E})$ are equal, which may be a good approximation in the absence of shell and pairing effects. Assigning to the inverse cross-section its geometric value one obtains:

$$\frac{\Gamma_F}{\Gamma_N} = 5.25 A^{-2/3} T^{-1} \exp \left(\frac{B_N - B_F}{T} \right) \quad (7)$$

Equation (7) and to a large extent Eqs (5) and (6) are remarkable for their almost total lack of physical details aside from the neutron binding energy and the fission barrier height. One does not even need to assume any special form for the level densities. This is an aspect of statistical theories which has both good and bad features and which, while easily and simply interpreting experimental data, yield information very reluctantly on the detailed Hamiltonian of the system. By means of Eq. (7) the asymptotic behavior of Γ_F/Γ_N can be estimated. For $(B_N - B_R) \geq 0$ the function is monotonically decreasing and eventually tends to zero as $1/T$. For $(B_N - B_F) < 0$ the function has a maximum at $T = B_F - B_N$ and then it decreases again, tending to zero at large temperatures like $1/T$. The dominance of the neutron decay over the fission decay at high energies is a consequence of the phase space volumes available to the two modes of decay when energy restrictions become irrelevant as in the case of large temperatures. Everything being equal, three unbound modes are available for the emission of neutrons (the three cartesian coordinates of the free neutron) while only one unbound mode is available for fission (the saddle-point fission mode). It is also quite interesting to notice that Γ_F/Γ_N tends to zero as the mass number of the system tends to infinity. The $A^{-2/3}$ dependence of Γ_F/Γ_N signifies the increasing "surface area" from which neutrons can evaporate.

The formalism described so far can be generalized to include the effect of angular momentum. The presence of angular momentum implies that a certain amount of energy is present in the form of rotational energy, and it is not available to excite the internal degrees of freedom. Therefore, Eq. (5) can be modified as follows:

$$\frac{\Gamma_F}{\Gamma_N} = \frac{\pi \hbar^2}{4\sigma_{\text{inv}} m_N} \frac{T_S}{T_R^2} \frac{\rho_S(E - B_F - E_S^I)}{\rho_R(E - B_N - E_R^{I'})} \quad (8)$$

where $E_S^I = \frac{\hbar^2 I^2}{2 \mathcal{I}_S}$ is the rotational energy at the saddle point; $E_R^{I'} = \frac{\hbar^2 I'^2}{2 \mathcal{I}_R}$

is the rotational energy in the residual nucleus after neutron emission; I is the total angular momentum; $I'^2 = I^2 - \bar{l}^2$ and \bar{l}^2 is the average angular momentum associated with the emitted neutrons. (The approximate way in which the angular momentum is handled in Γ_N is well-justified at moderate excitation energies [39]). The two moments of inertia \mathcal{I}_R and \mathcal{I}_S depend in general upon both the excitation energy and the angular momentum. A very complete study of the equilibrium shapes of liquid drop nuclei in the ground state and at the saddle point has been performed by Cohen, Plasil and Swiatecki [40, 42] and by Cohen and Swiatecki [41]. For relatively small

angular momenta one can assume the zero angular momentum shapes for the evaluation of the rotational energies. Rewriting Eq. (7) on this basis one obtains:

$$\frac{\Gamma_F}{\Gamma_N} = 5.25 A^{-2/3} T^{-1} \exp \frac{\{B_N - B_F - (E_R^{I'} - E_S^I)\}}{T} \quad (9)$$

This expression indicates that the presence of angular momentum decreases the effective fission barrier by an amount $(E_R^{I'} - E_S^I)$ which is always positive since $\mathcal{I}_S > \mathcal{I}_R$. At larger angular momenta the fission barrier itself is decreasing due to a change in the saddle point deformation, thus increasing even more the fissionability of the nucleus.

2. PRELIMINARY DATA ANALYSIS WITH SIMPLE LEVEL-DENSITY EXPRESSIONS

The formalism presented in the previous section requires the use of specific level density expressions both in Γ_F and in Γ_N . It is mainly in these quantities that all the physical information concerning the nucleus at the saddle point and the residual nucleus after neutron emission is contained [43].

Until very recently, the statistical properties of nuclei have been described on the basis of the uniform model [44, 45]. In this model the nucleus is represented as a system of non-interacting fermions occupying equidistant non-degenerate single particle levels. Although this picture contains little physics beyond the Pauli principle, still its application to problems like the present one has had a reasonable success.

The expression for the uniform model level density is:

$$\rho(E) = \frac{\sqrt{\pi}}{12} \frac{e^{2\sqrt{aE}}}{a^{1/4} E^{5/4}} \quad (10)$$

where E is the excitation energy of the system and a is the level density parameter, which is related to the single particle level density g by the expression

$$a = \frac{\pi^2}{6} g$$

The level density parameter a is expected to vary in proportion to the mass number of the nucleus: $a = A/K$, where K is a constant whose value is estimated to be around 8 or 9 [46]. Explicit expressions for the quantity Γ_F/Γ_N have been given by Huizenga and Vandenbosch [6] on the basis of the uniform model. In these calculations only the exponential factor of Eq. (10) has been used, namely:

$$\rho(E) \propto e^{2\sqrt{aE}} \quad (11)$$

Almost all of the experimental data available at present have been analyzed in terms of the uniform model level density [13, 14, 16, 17]. Here we shall report the overall conclusions of such an analysis applied to lighter nuclei,

without any critical comment on the data themselves, which will be delayed until Section 4.

The free parameters typically employed in this data-fitting procedure are: the fission barrier B_F ; the penetrability coefficient $k\omega$, and the Γ_F and Γ_N level density parameters a_F and a_N . The quantities which the fitting procedure can most solidly establish are the fission barrier B_F and the ratio a_F/a_N .

The experimental Γ_F/Γ_N quantities have been readily fitted up to 20 MeV above the fission barrier. In this energy range some of the experimental data cover more than six orders of magnitude. The fission barriers have proven to be rather insensitive to small variations in the other parameters. The individual values of a_F and a_N turn out to be quite uncertain, while their ratio tends to remain constant. Two difficulties immediately arise. The first is related to the a_F/a_N ratio which appears to be close to unity in nuclei far away from the shell region and as high as 1.5 for nuclei close to ^{208}Pb . The second difficulty is the inability to fit the data in a larger energy interval for the latter kind of nuclei. Because of the large ratio of a_F/a_N necessary to fit the low-energy data, the fission probability increases much too rapidly with energy to fit the higher-energy data. In other words, it appears that for these kinds of nuclei the effective a_F/a_N ratio varies smoothly from a rather large value close to the fission barrier to a value close to unity at higher energies. At the same time it is found that the experimental fission barriers can be decomposed in two parts: a smooth liquid drop quantity and a ground state shell effect which measures the deviation between the experimental ground state mass and its liquid drop prediction. This shell correction is at a maximum in the Pb region and has the effect of producing a strong local increase in the fission barriers. The mounting evidence indicates that the anomalously high fission barriers in the Pb region and the corresponding large ratio of a_F/a_N are two facets of the same physical fact, namely the small single particle level density at the Fermi surface of the spherical nuclei due to the double shell closure in ^{208}Pb . At the same time the data strongly suggest that the effect of the shells disappears rather rapidly with increasing excitation energy.

An overall view of the studies illustrated above allows one to reach the following conclusions.

- (a) The statistical formalism is potentially able to fit the experimental fission probabilities over many orders of magnitude.
- (b) Fission barrier heights can be extracted rather safely from the analysis of low-energy cross-sections.
- (c) The fission barriers so obtained can be decomposed into a smooth liquid drop component and the ground state shell correction.
- (d) The uniform model is inadequate in justifying the widely varying ratio of a_F/a_N and in reproducing the fission probabilities over a large energy range for nuclei close to the ^{208}Pb shell.

3. MODERN PROBLEMS IN THE EVALUATION OF THE PHASE SPACE VOLUMES RELEVANT TO FISSION PROBABILITIES

The use of the uniform model in the evaluation of the fission probabilities does not allow one to interpret the experimental data satisfactorily. Rather

serious problems are met in the attempt to evaluate the detailed form of the phase space volume associated with the fission and neutron decay. Some of these problems can be solved, others have not yet been considered in depth. In the present section some of these problems will be considered. In the first part, the coupling between the collective and the internal degrees of freedom will be studied, especially insofar as the fission width is concerned. In the second part the simpler and better-understood problem of the inclusion of shell and pairing effects in the formalism will be discussed. In the third part some examples of calculation of the fission probabilities of superheavy nuclei will be shown to illustrate the disappearance of the shell effects with excitation energy.

3.1. Relevance of the collective degrees of freedom in Γ_F

The peculiar collective nature of the fission process raises serious questions regarding the contribution of the collective degrees of freedom to the shape and volume of the phase space which controls the fission decay widths. This is particularly important when one needs to consider the fission width as a differential in the various saddle point collective coordinates and momenta. To explore to what extent such collective degrees of freedom affect the fission widths, let us express them explicitly in Eq. (1). The introduction of n bound normal modes, besides the fission mode, leads to the following expression:

$$\Gamma_F = \frac{1}{2\pi\rho(E)} \int d\epsilon \int \Pi \frac{dx_i dp_i}{h^n} \rho'_S(E - B_F - \epsilon - \sum \{\frac{1}{2} a_i x_i^2 + p_i^2/2m_i\}) \quad (12)$$

where ϵ is the kinetic energy along the fission coordinate; x_i and p_i are the saddle point normal coordinates and momenta; a_i and m_i are the stiffnesses and the inertias associated with the same normal modes; the quantity ρ'_S is the level density due to the intrinsic degrees of freedom; and the integration limits in the multiple integral are taken in such a way as to conserve energy. By profiting again from the strong energy dependence of ρ'_S and by setting

$$\frac{d \ln \rho'_S(x)}{dx} = \frac{1}{T}$$

we can rewrite Eq. (12) as follows:

$$\Gamma_F = \frac{1}{2\pi\rho(E)} \rho'_S(E - B_F) \frac{1}{h^n} \int_0^\infty e^{-\epsilon/T} d\epsilon \int_{-\infty}^{+\infty} e^{-\sum p_i^2/2m_i T} \Pi dp_i \int_{-\infty}^{+\infty} e^{-\sum \frac{1}{2} a_i x_i^2/T} \Pi dx_i \quad (13)$$

In this expression the energy is not rigorously conserved: in fact such an expression is well known in statistical mechanics as the canonical expansion where the temperature, instead of the energy, characterizes the system. In this case, the many internal degrees of freedom of the nucleus are acting as a thermostat with which the collective degrees of freedom are in equilibrium.

The integration of Eq.(13) can be easily performed:

$$\Gamma_F = \frac{1}{2\pi\rho(E)} \rho'_S(E - B_F) \prod \left(\frac{2\pi T}{h} \right)^n \prod \sqrt{\frac{m_i}{a_i}} \quad (14)$$

where the quantity in the box represents the contribution of the collective degrees of freedom to the phase space volume. This expression can be compared with Eq.(3). The two expressions are identical if one sets,

$$\rho_S(E - B_F) = \rho'_S(E - B_F) \left(\frac{2\pi T}{h} \right)^n \prod \sqrt{\frac{m_i}{a_i}} \quad (15)$$

The above discussion leads to interesting observations regarding the validity of Eq.(3). An obvious failure of this equation occurs if one or more normal modes besides the fission mode are unbound, namely if one or more of the a_i are negative. This is predicted to occur by the liquid drop model below the Businaro-Gallone point ($x = 0.396$) where the mass asymmetry mode becomes unbound [47]. Increasing displacements away from the saddle point along this coordinate lead to a rapidly diverging integrand in Eq.(12). Under these circumstances the canonical expansion about the saddle point cannot be justified. In fact, the main contribution to the integral along the mass asymmetry coordinate comes from around the extreme mass asymmetries and not from the symmetric region around the saddle point. In this region of the fissility parameter, fission loses its identity and merges into the evaporation (spallation) reaction; the decay width calculated by Eq.(12) refers to the statistical emission of particles as a whole. As a consequence, a naive analysis of "fission" cross-sections for elements below Ag ($x \approx 0.4$) may indicate fission barriers smaller than those predicted by the liquid drop model. In these kinds of experiments, "fission" and the resulting fission barrier are defined only by the arbitrariness of the experimenter, or by the mass cut-off of the detector.

Besides the above glaring inapplicability of Eqs (3) and (14), more delicate points can be raised by the peculiar factorization of the phase space in Eqs (14) and (15). It is possible that the collective degrees of freedom are sharply defined and nearly uncoupled from the intrinsic degrees of freedom, leading to such a simple factorization of the phase space. On the other hand, the single particle degrees of freedom may be very pure, leading to a much less collective description of the system.

It is not very clear which of the two alternatives is more realistic, the second one being further plagued by the extra complication of having to define the number of collective degrees of freedom. These two extreme possibilities bring forth the problem of the microscopic nature of collective degrees of freedom in a many-body system. The collective states, born out of very special combinations of intrinsic states, may be coupled to the remaining internal degrees of freedom to a varying extent. In the limit of complete uncoupling, the collective states have a physical existence and do play an explicit role in the form of the phase space volume at the saddle point. This phase space volume should have the form of Eq.(14) in the high-temperature limit, and a more complicated form accounting for the quantum mechanical effects at lower temperatures [48, 49]. The coupling

of the collective states to the intrinsic states has the effect of diluting the collective nature of the levels over the neighboring intrinsic levels. The collective aspects of the system now appear as strength functions. In classical terms, the motion along the collective coordinates becomes affected by viscosity, the largest momenta are strongly damped-out and the phase space associated with them is distorted and limited. As the collective motion becomes damped beyond criticality, the strength function loses its structure and the collective state is reabsorbed into the background of intrinsic levels. Therefore, depending on whether viscosity is large or small, the two extremes of the picture do apply. This uncertainty is not very important at high energies or when the integrated form of the decay width is considered. Instead, it is of extreme relevance when the differential form of the decay width in the coordinates and momenta of some collective coordinates is to be used to establish the distribution of the initial conditions for the dynamical descent from the saddle to the scission point. Unfortunately complication adds to complication since similar considerations apply for the neutron width Γ_N as well, although to a somewhat smaller degree. In fact, this very modern problem directly involves the overall theory of level densities.

3.2. Shell and pairing effects in level densities

While, because of its difficulty, the problem of the strength functions associated with the collective features of the system has not yet received the amount of attention it deserves, other detailed features of the level densities have been worked out to a satisfactory degree. The level densities at low excitation energies are expected to be greatly influenced by the detailed structure of the single particle levels close to the Fermi surface, as well as by the two-body residual interaction. Recently a substantial success has been achieved in the development of a theoretical formalism which allows one to calculate the level density of a nucleus on the basis of a given shell model and of the pairing interaction [19-30]. The simplest Hamiltonian containing both features is the following:

$$H = \sum_{\pm k} \epsilon_k a_k^\dagger a_k - G \sum a_k^\dagger a_{-k}^\dagger a_{-k} a_k \quad (16)$$

where ϵ_k are the shell model single particle energies, a_k^\dagger and a_k are the creation and annihilation operators respectively, and G is the strength of the pairing interaction. The diagonal form of this Hamiltonian can be used to evaluate the grand partition function e^Ω [27, 28, 30]:

$$\begin{aligned} \Omega = & \sum \beta(\epsilon_k - \lambda - E_k) + \sum \ln[1 + \exp - \beta(E_k - \gamma m_k)] \\ & + \sum \ln[1 + \exp - \beta(E_k + \gamma m_k)] - \frac{\beta \Delta^2}{G} \end{aligned} \quad (17)$$

where m_k are the single particle spin projections, λ is the chemical potential, γ is the angular velocity, β is the reciprocal of the temperature, Δ is the gap parameter which indicates the extent of the pairing correlation, and $E_k = \sqrt{(\epsilon_k - \lambda)^2 + \Delta^2}$ represent the energies of the intrinsic modes of excitation of the system (quasi-particles).

The boundary conditions are introduced in the formalism by means of the following equations:

$$\frac{\partial \Omega}{\partial \Delta} = 0 \text{ or } \sum \frac{1}{2E_k} [\tanh \frac{1}{2} \beta(E_k - \gamma m_k) + \tanh \frac{1}{2} \beta(E_k + \gamma m_k)] = \frac{2}{G}$$

gap equation (18)

$$\frac{\partial \Omega}{\partial \alpha} = N = \sum \left[1 - \frac{\epsilon_k - \lambda}{2E_k} \left\{ \tanh \frac{1}{2} \beta(E_k - \gamma m_k) + \tanh \frac{1}{2} \beta(E_k + \gamma m_k) \right\} \right]$$

particle equation (19)

$$\frac{\partial \Omega}{\partial \mu} = M = \sum m_k \left[\frac{1}{1 + \exp \beta(E_k - \gamma m_k)} - \frac{1}{1 + \exp \beta(E_k + \gamma m_k)} \right]$$

angular momentum equation (20)

$$-\frac{\partial \Omega}{\partial \beta} = E = \sum \epsilon_k \left[1 - \frac{\epsilon_k - \lambda}{2E_k} \left\{ \tanh \frac{1}{2} \beta(E_k - \gamma m_k) + \tanh \frac{1}{2} \beta(E_k + \gamma m_k) \right\} \right] - \frac{\Delta^2}{G}$$

energy equation (21)

where $\alpha = \beta\lambda$ and $\mu = \beta\gamma$. This set of four equations defines the quantities β , γ , λ , Δ in terms of E , M , N , G . This set of values is used to evaluate the entropy:

$$S = \Omega + \beta E - \alpha N - \mu M \quad (22)$$

The level density of the system is then obtained by means of the expression:

$$\rho = \frac{e^S}{(2\pi)^{n/2} D^{1/2}} \quad (23)$$

where n is the number of first integrals of motion which are explicitly considered in the problem, and

$$D = \det \left| \frac{\partial^2 \Omega}{\partial \alpha_i \partial \alpha_j} \right|$$

where α_i is the set of Lagrange multipliers associated with the first integrals of motion. Although very simple, the present formalism accounts rather well for the pairing effects, the shell effects, their mutual interaction and their dependence upon the excitation energy.

The pairing correlation, in the ground state, depends upon the single particle level density at the Fermi surface. When the nucleus is in a shell region, the single particle level density at the Fermi surface is small and the pairing effects are also small. The opposite occurs in an antishell region

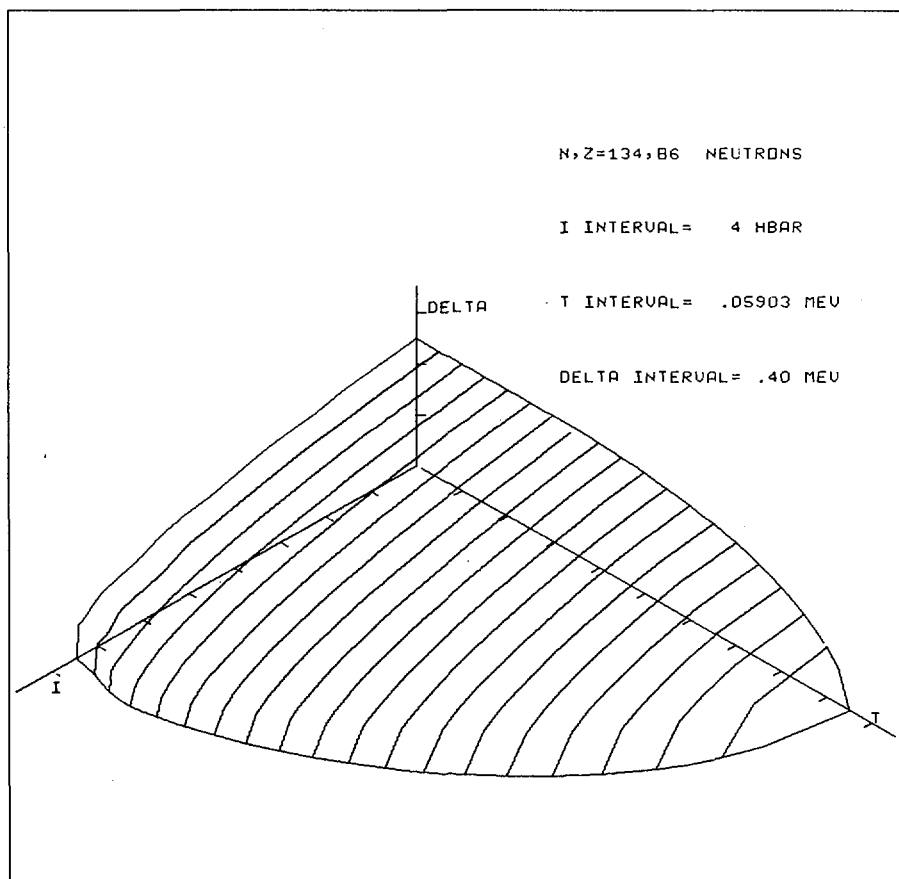


FIG. 3. Isometric projection of the neutron gap parameter as a function of temperature and angular momentum for the neutron component of $^{220}_{86}\text{Rn}$ [30]. The angular momentum refers to the neutron component only.

where the single particle level density is large and so is the pairing correlation. In other words, the pairing effects tend to counteract the shell effects: when the latter is large the former is small and vice versa.

As the excitation energy increases, the gap parameter Δ and the pairing correlation steadily decrease and eventually vanish because of the blocking effect of the quasi-particles. The shell effects also are washed away by the increasing excitation energy. This is due to the fact that the fluctuations in the single particle level density are averaged out by the Fermi distribution. The statistical averaging function is in fact the negative derivative of the Fermi function, which becomes broader as the temperature and the excitation energy increase.

The angular momentum of the system is generated by breaking pairs and by aligning the spins of the resulting quasi-particle excitations. Each quasi-particle blocks a single particle level, making it unavailable for the

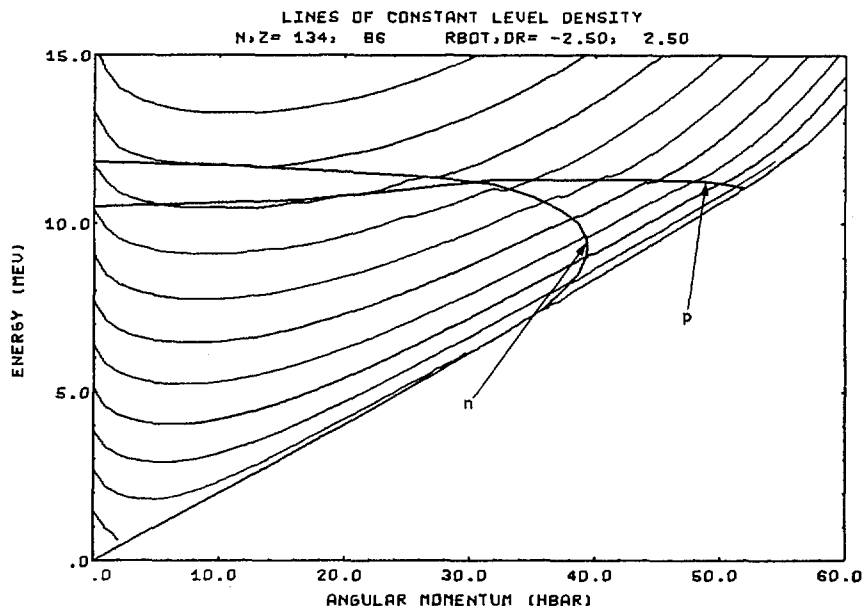
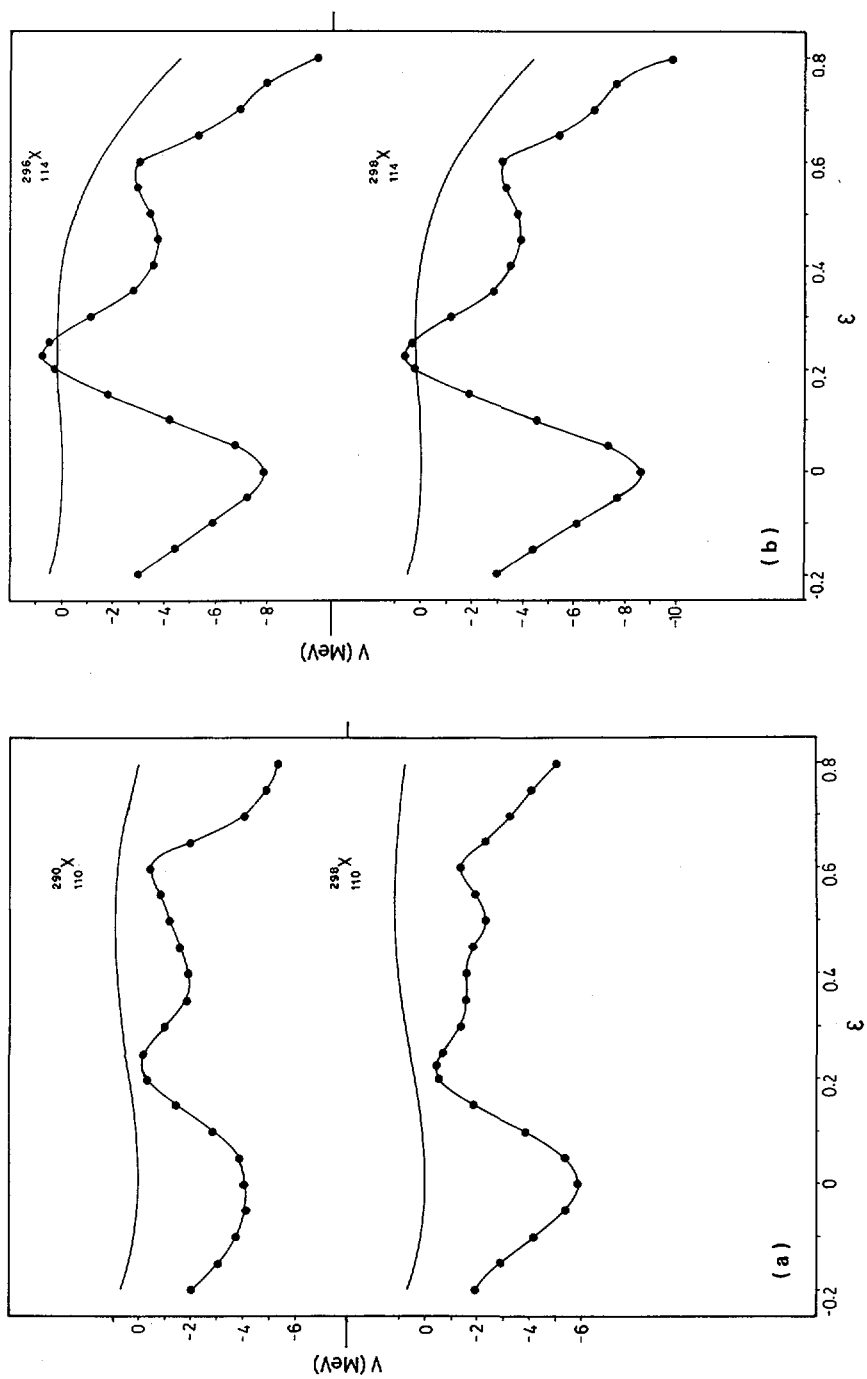


FIG. 4. Lines of constant natural logarithm of the level density in the (energy, angular momentum)-plane for the nucleus ^{220}Rn [30]. The lowest line going diagonally from lower left to upper right is the yrast line. The boundaries of the neutron and proton superfluid phases are also shown.

pairing interaction. Therefore, the pairing correlation and the gap parameter decrease and eventually vanish as the angular momentum increases. Some of the features discussed above can be observed in Figs 3 and 4 where the results of a calculation based on the Nilsson model and on the pairing Hamiltonian are shown for the nucleus ^{220}Rn [30]. In Fig. 3 the dependence of the neutron gap parameter upon the temperature T and the angular momentum I is presented in the form of an isometric projection. The surface $\Delta(T, I)$ intersects the (T, I) -plane along a curve which defines the boundary between the paired and the unpaired region. In Fig. 4 the level density surface is projected on the (energy, angular momentum)-plane. The lower near-diagonal line in the figure represents the yrast line, or the locus of the states with lowest energy at fixed angular momentum. The boundaries between paired and unpaired phases for neutrons and protons are also shown. Their peculiar crossing is due to the way in which the angular momentum is shared between the neutron and proton components.

3.3. Application of the level density formalism to the calculation of the fission probabilities

To illustrate the effect of shells and pairing on the fission probabilities, the above formalism will be applied to superheavy nuclei [35, 36]. For such nuclei the relevance of shell and pairing effects is overwhelming and a calculation applied to them clearly displays the features discussed above.



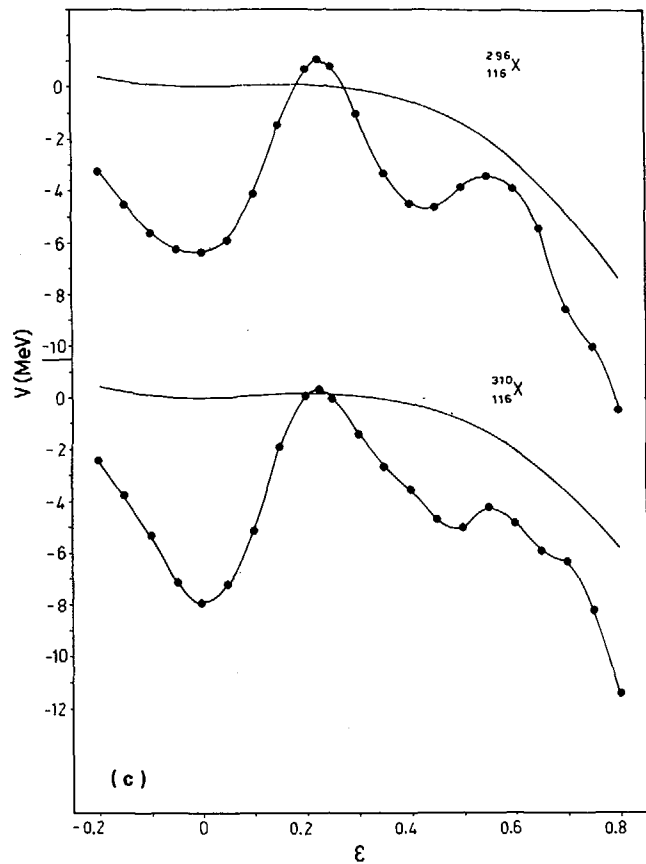


FIG. 5. Potential energy profiles [36] of some superheavy nuclei calculated on the basis of the liquid drop model (solid line) and of the Strutinsky method (solid line with dots). Potential energy is shown as a function of the deformation parameter ϵ for (a) $^{290}_{110}\text{X}$ and $^{298}_{110}\text{X}$; (b) $^{296}_{114}\text{X}$ and $^{298}_{114}\text{X}$; (c) $^{296}_{116}\text{X}$ and $^{310}_{116}\text{X}$.

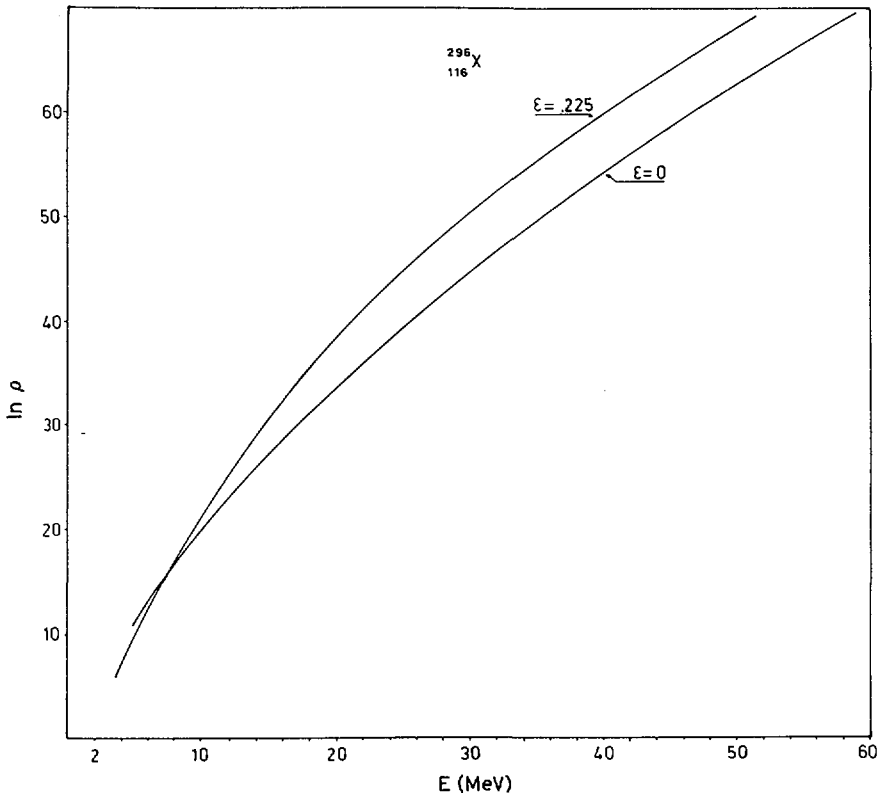


FIG. 6. Level densities as a function of local excitation energy [36] calculated for the ground state and saddle point deformation of $^{296}_{116}\text{X}$.

First the shell structure in the potential energy surface will be discussed. In Fig. 5c the potential energy of $^{296}_{116}\text{X}$ is shown as a function of the deformation parameter ϵ . This calculation has been performed using the Nilsson model and the Strutinski normalization procedure. In the same figure the liquid drop potential energy is also shown as a function of ϵ . The latter curve shows that for this nucleus, whose fissility parameter is close to unity, the liquid drop fission barrier is vanishingly small. The former curve shows that the shell structure generates a rather deep minimum at sphericity and, because of it, the nucleus is stabilized against fission by a barrier of about 7.5 MeV. Similar plots for other nuclei are shown in Figs 5a-c.

To observe how the shell effects disappear with excitation energy, the level density at the ground state deformation and at the saddle point deformation can be calculated. This calculation is shown in Fig. 6. It can be observed that the saddle point level density rises faster than the ground state level density. In fact, the level density value reached at 60 MeV excitation energy by the nucleus in the ground state deformation is reached at about 7.5 MeV lower local excitation energy by the nucleus at the saddle point. Since the potential energy difference between the ground state and

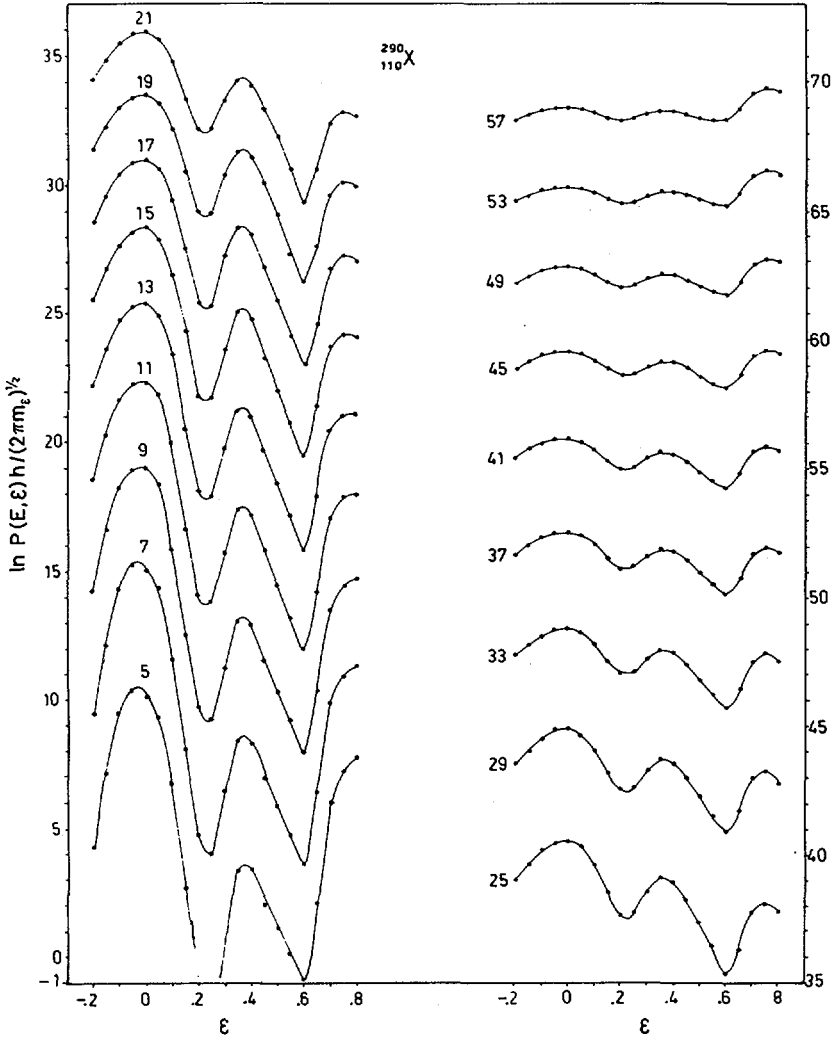
the saddle point is in fact 7.5 MeV; and since such a difference is exclusively due to the shell effects, it is possible to conclude that, at 60 MeV, the nucleus does not retain any relevant trace of shell effects. To better appreciate the evolution of the system as the excitation energy increases, it is possible to calculate, for each excitation energy, the probability of finding the nucleus at the various deformations. Assuming statistical coupling between the intrinsic modes and the collective fission mode, one obtains [25, 26]:

$$P(E, \epsilon) d\epsilon = \frac{\sqrt{2\pi m}}{h} D^{-1/2} \rho(E_T) d\epsilon \quad (24)$$

where E is the compound nucleus excitation energy, $E_T = E - V(\epsilon)$ is the local excitation energy at the deformation ϵ , m is the inertia along the coordinate ϵ and $D = \left. \frac{d \ln \rho(x)}{dx} \right|_{x=E_T}$.

The natural logarithm of the deformation probability of $^{296}_{116}\text{X}$ is shown in Fig. 7b for various excitation energies. At low excitation energy, the deformation probability shows a marked peak at $\epsilon = 0$ and a deep minimum at $\epsilon = 0.225$. If the nucleus were stable against fission, the deformation probability would be bounded along any deformation coordinate. Since the system can undergo fission, the probability goes through a minimum and eventually increases indefinitely as the deformation increases. This minimum actually controls the flow of probability from the compound nucleus region to the region of forming fragments [35, 36]. As the excitation energy increases, the structure of the deformation probability becomes less pronounced, the compound nucleus peak becomes broader and the rate-controlling minimum fills in. At the highest excitation energy, the deformation probability becomes almost flat from sphericity to the location of the fission barrier, indicating that the oscillations of the potential energy are completely irrelevant to the behavior of the excited system. In other words, the system behaves as if the fission barrier had vanished. Similar comments can be made about the nucleus $^{290}_{110}\text{X}$ whose deformation probability is shown in Fig. 7a. Another important point can be made in this discussion. The critical stage, or transition state, controlling the fission decay probability has been assumed, so far, to be located at the saddle point. The saddle point is an extremum in the potential energy surface and does not have any direct connection with the phase space region which controls the decay. The deformation probability surface includes the overall phase space and determines the position of the transition state which is located on a saddle point which is unstable in $n-1$ degrees of freedom and stable along the fission mode. The locations of the deformation probability saddle point and of the potential energy saddle point in general do not coincide. In particular, the disappearance of the shell effects discussed above may be responsible for a shift in the location of the transition state [35, 36]. Some evidence that this is occurring is available from the fission fragment angular distributions in the actinide region. The moment of inertia for the saddle point configuration appears in fact to shift from the expected value corresponding to the actual potential energy saddle point to the value consistent with the liquid drop saddle point [21, 29, 50].

(a.)



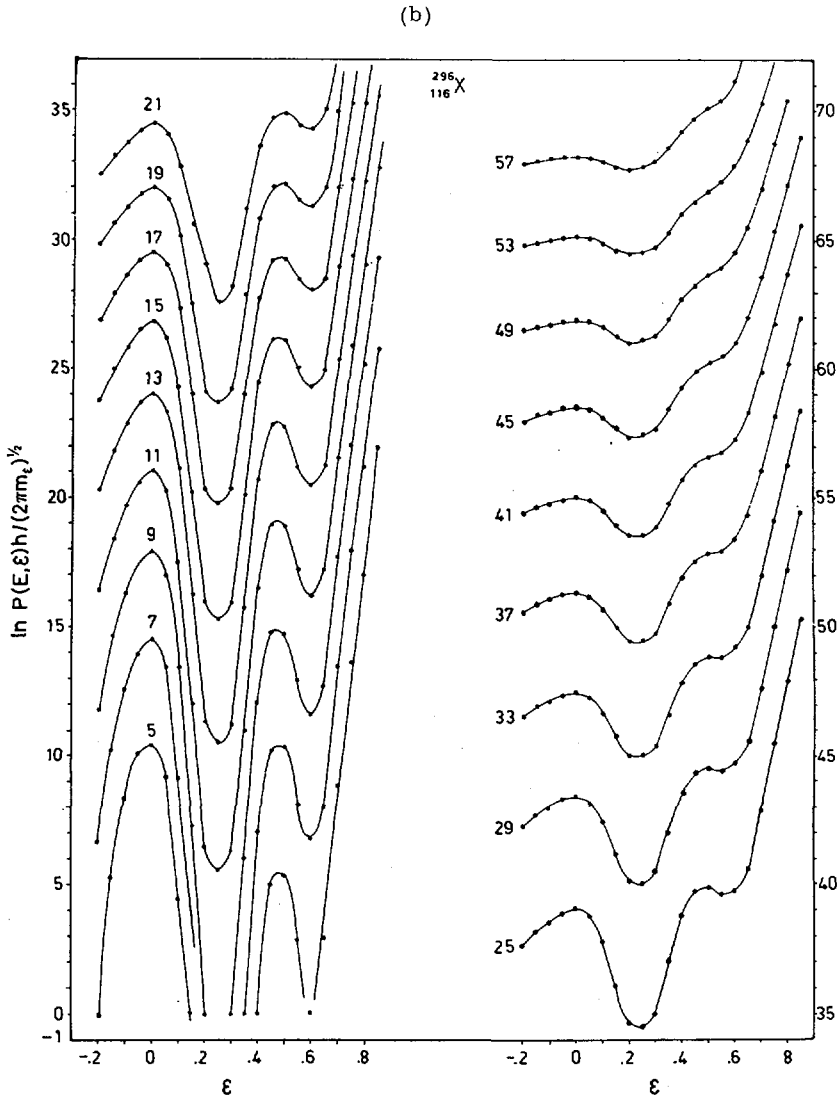
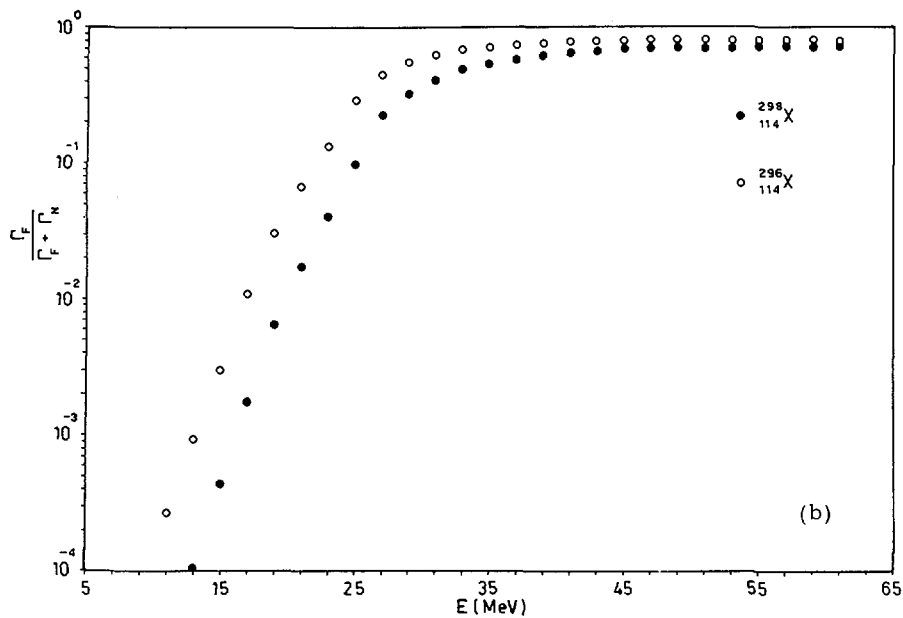
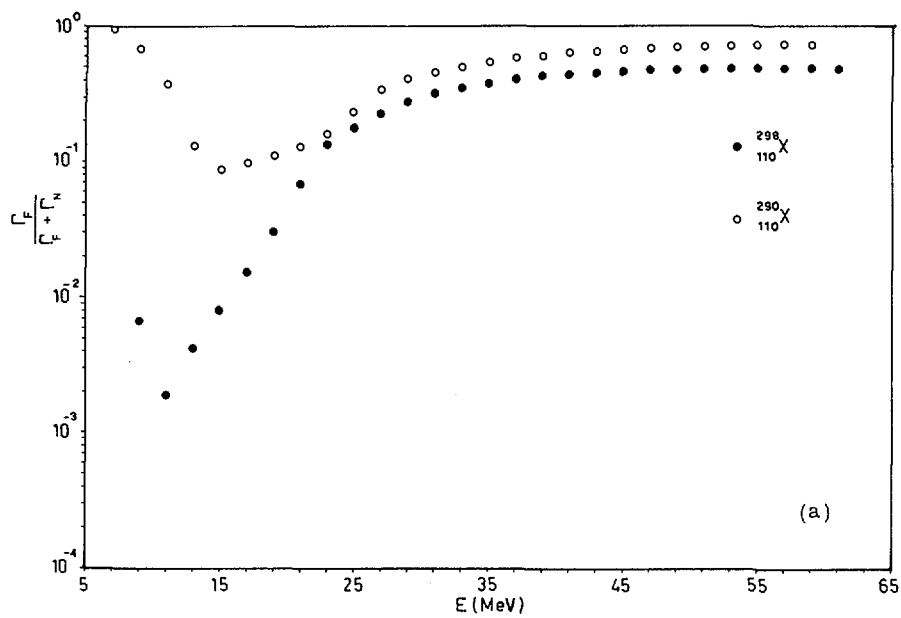


FIG. 7. Logarithms of the deformation probabilities at various excitation energies (in MeV) [36] for the nuclei $^{290}_{110}\text{X}$ (a) and $^{296}_{116}\text{X}$ (b).



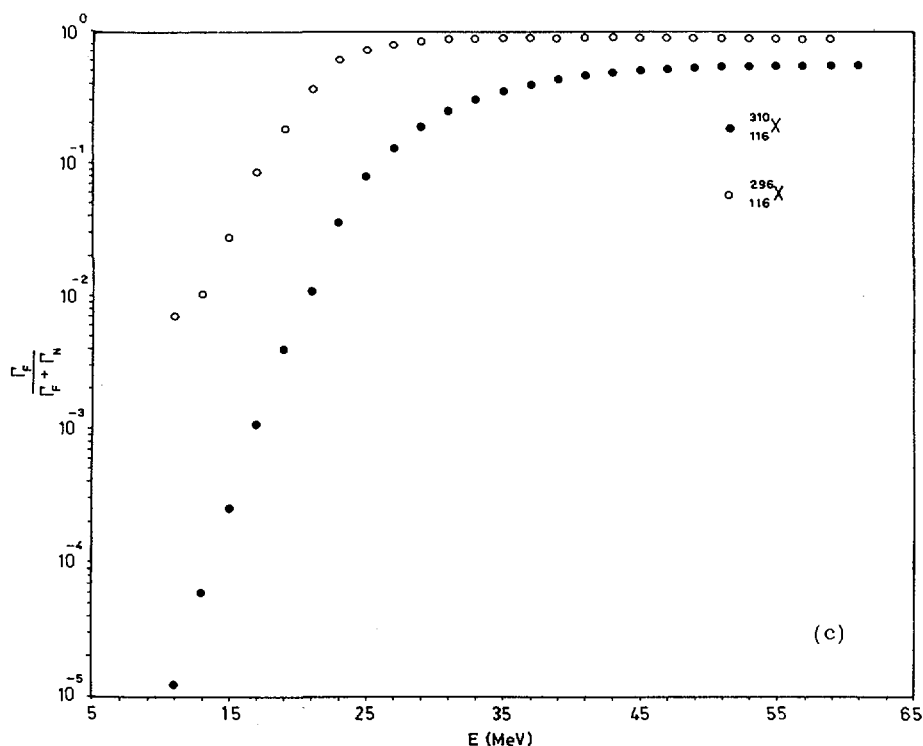


FIG. 8. First-chance fission probabilities for various superheavy nuclei [36]: (a) ^{290}X and ^{298}X ; (b) ^{296}X and ^{298}X ; (c) ^{296}X and ^{310}X .

The final product of this formalism is the first-chance fission probability shown for various isotopes in Figs 8a-c. To obtain a reference point in the interpretation of these quantities one can use Eq.(7) as an approximation to the Γ_F/Γ_N expression. For a nucleus with $A \sim 300$, the temperature $T = 1$ MeV corresponds to an excitation energy between 30 and 40 MeV. When $B_F = B_N$ the fission probability at that temperature is $P_F \sim 0.1$. Similarly, in order to obtain $P_F = 0.5$, $B_N - B_F = 2.15$ MeV; for $P_F = 0.7$, $B_N - B_F = 2.88$ MeV; for $P_F = 0.8$, $B_N - B_F = 3.5$ MeV; for $P_F = 0.9$, $B_N - B_F = 6.35$ MeV. In all of these cases, the fission probability should decrease slowly with energy. An inspection of the fission probabilities calculated for the superheavy nuclei shows that for excitation energies larger than 35 MeV they assume very high values, as high as 0.95. Such high values are predicted by the Eq.(7) for neutron binding energies 4 to 6 MeV larger than the fission barriers. Since the neutron binding energies are about 4 to 6 MeV, the effective barrier felt by these superheavy nuclei is practically zero. On the other hand, at lower excitation energies the effective barriers are very close to the true barriers. In particular, the fission probabilities are indeed very small for the isotopes of elements 114 and 116, where the shell effects are responsible for very large fission barriers. Furthermore,

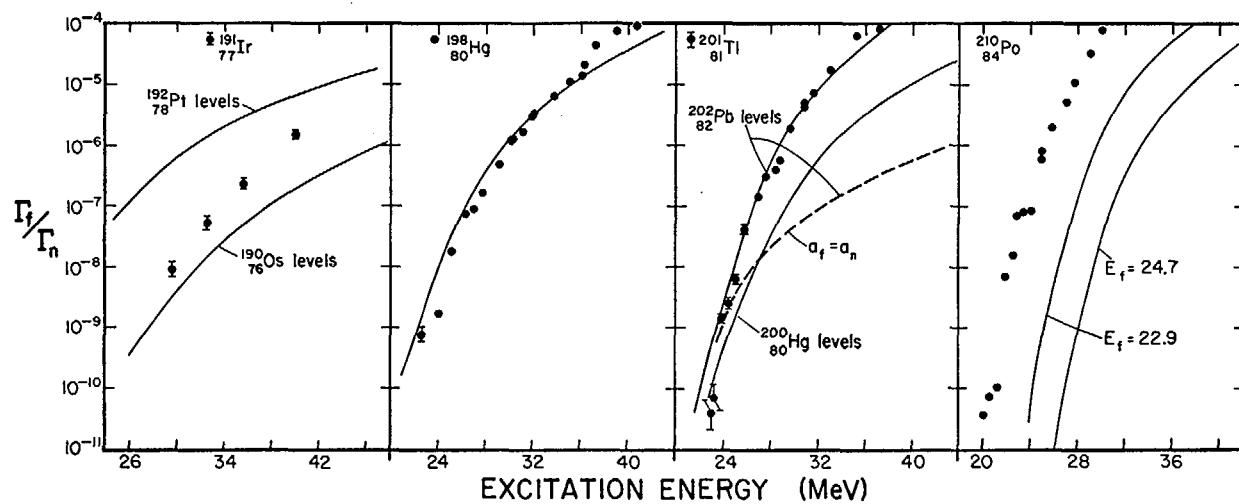


FIG. 9. Comparison between some experimental fission probabilities (\square and \bullet) and some shell model calculations (\longrightarrow) [32].

for nuclei where $B_F \sim B_N$, the fission probabilities are subjected to peculiar fluctuations at low energies mainly related to the different energy dependence of the pairing correlation at the saddle point and in the ground state (Fig. 8a).

4. EXPERIMENTAL FISSION PROBABILITIES IN LIGHTER ELEMENTS

4.1. Extraction of the total fission probabilities

The experimental data available for lighter elements at energies reasonably close to the barrier are proton- and alpha-induced fission cross-sections as a function of energy for various targets ranging from the heavy rare earths to bismuth. The cross-sections which are going to be analyzed here [16-18] are characterized by errors between 10% and 30%, due to various causes, such as uncertainties in the beam current reading, in the solid angle, in the detection efficiency, in the angular distributions and in the beam energy.

The observed fission events arise from two sources. The first and hopefully the main source is from the compound nucleus formed by the complete fusion of target and projectile with a subsequent thermalization of the kinetic energy. The second source is the compound nucleus formed after a direct reaction or a pre-equilibrium decay has taken place. The latter source is expected to be of minor importance in the first 20 MeV above the barrier, because of the strong energy dependence of the fission probability, but it is expected to be substantial in the high bombarding energy region. Even if one can disregard the contribution to fission due to direct reactions, one should estimate the fraction of the total reaction cross-section associated with direct reactions. This is important in the calculation of the total fission probability, $P_{F,T} = \sigma_F / \sigma_C$, where σ_F and σ_C are the fission cross-section and the compound nucleus cross-section, respectively. Recent work in ^4He -induced reactions in the Pb region [51] shows that the compound nucleus cross-section is very close to the reaction cross-section up to 55-MeV bombarding energy, it decreases by perhaps 30% with respect to the total cross-section at 70 MeV, and may be a factor of 2 to 5 lower at 120 MeV. One of the greatest uncertainties is related to the precompound emission of neutrons. For these reasons it is very hard to analyze the data above 70 MeV. The total fission probabilities up to this energy were determined by dividing the total fission cross-section by the reaction cross-section obtained by an optical model. The use of the optical model may produce systematic errors as large as 25%.

4.2. The first-chance fission probabilities

The quantity predicted by the theory is the first-chance fission probability $P_{F,1} = \Gamma_F / (\Gamma_F + \Gamma_N)$. The experimental total fission probability $P_{F,T}$ includes also the probability that the nucleus undergoes fission after one or more neutrons have been emitted. The problem then arises of estimating the higher order fission probability in order to transform $P_{F,T}$ into $P_{F,1}$. In principle, if the total fission probability $P_{F,T}$ is available for two nuclei with the same Z and differing only by one neutron, it should be possible to extract $P_{F,1}$ for the heavier nucleus. Unfortunately, the various uncertainties associated with the experimental data, but especially the uncertainty in the

compound nucleus cross-section, make this procedure very dubious. The only safe conclusion which can be usually drawn is the establishment of an upper energy limit below which the contribution of higher order fission becomes unimportant.

One might also consider the possibility of obtaining a theoretical estimate of the higher order fission probability. Unfortunately, here the problem is even more serious. With a saddle temperature of about 2 MeV, a variation of 10% in the saddle single particle level density g_F produces a variation in Γ_F/Γ_N of a factor of about 150! Even a small variation of 1% in g_F produces a variation of $\sim 70\%$ in Γ_F/Γ_N ! This means that any attempt to correct for higher order fission is likely to fail. Fortunately, the counterpart is more pleasant; large variations in the fission probabilities at high energies involve only minute changes in the single particle level density parameters. We shall make use of this conclusion later on. In practice, the fission cross-section is divided by the total reaction cross-section and the resulting quantity is assumed to be equal to the total fission probability $P_{F,T}$ up to 25-30 MeV above the barrier, where the contribution of higher order fission is small. In the next 10-15 MeV the effect of higher order fission is expected to be approximately counterbalanced by the decreasing compound nucleus cross-section. For these reasons, it has been assumed that the above-defined $P_{F,T}$ is also equal to $P_{F,1}$ or to Γ_F/Γ_T up to 70-MeV excitation energy in ^4He -induced fission.

4.3. Analysis of the data

At this point one might be tempted to consider the possibility of comparing the experimental data directly with the theoretical fission probabilities calculated on the basis of the shell model. This attempt has been made by Vandenbosch and Mosel [32]. The results of such an investigation are shown in Fig. 9. The agreement between experiment and theory mainly depends on the ability of the model to reproduce the fission barrier height. The fission probabilities are very sensitive to the height of the fission barrier and to the ratio of the single particle level densities to be used in Γ_F and Γ_N . The present models do not predict both quantities accurately enough to reproduce in detail the experimental data. Calculations of this kind, which do not contain any free parameter, are very useful for testing the adequacy of the models to be applied to an experimentally unexplored region such as the island of superheavy nuclei.

An approach which leads to a better result is a hybrid formalism. In this formalism the neutron binding energy is taken from the experimental masses and the level density to be used in Γ_N is calculated from the Nilsson model and from the pairing Hamiltonian. Insofar as the evaluation of Γ_F is concerned, the fission barrier height as well as the barrier penetrability are taken to be free parameters; the level density is evaluated on the basis of the uniform model and of the pairing Hamiltonian. The single particle level density at the saddle and the saddle gap parameter are also free parameters. The angular momentum is accounted for both in Γ_F and in Γ_N .

As discussed before, the use of the shell model in the evaluation of Γ_N does account for the ground state shell effects. One might then consider the possibility of accounting for the shell effects at the saddle point in the same way. This has been done by Britt and co-workers [33] in the analysis of the fission and isomer formation probabilities in the actinide region. In

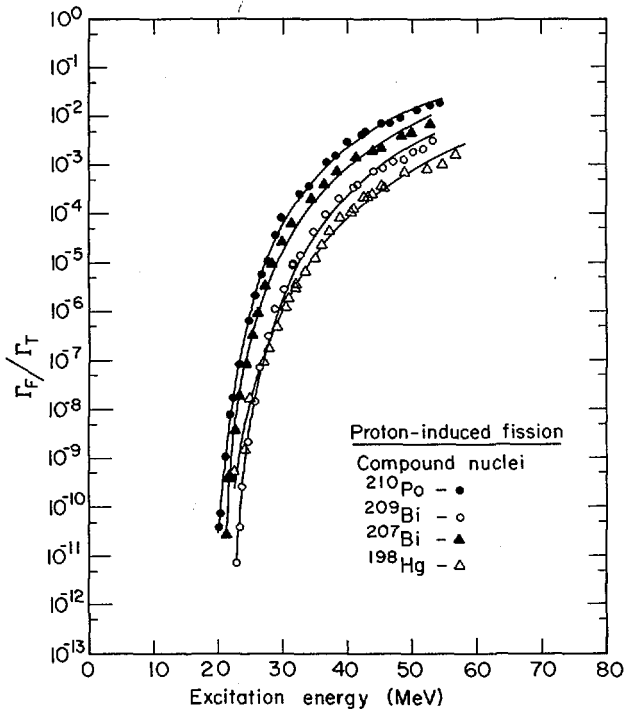


FIG. 10. Least-squares fits to the fission probabilities of some compound nuclei produced with proton bombardment [31].

this work, however, it has been decided not to follow that approach for the following reasons. First, in the lead region and below, the shell effects in the neighborhood of the saddle point are expected to be small because of the large deformation. Furthermore, the saddle point cannot be located in a shell region, because it would be a minimum, nor can it be in an antishell region because it would be a maximum. It must be somewhere between a shell and an antishell region which means close to the liquid drop surface. This situation is quite different from that of the ground state which always is in a shell region, namely in a minimum. In other words, the saddle masses are expected to be far smoother than the ground state masses. This argument does not apply if the shell corrections are strongly correlated with deformation and appear in the form of ridges and valleys. A superficial glance at some shell model calculations may give the impression that the shell fluctuations at the saddle are quite large. This impression is somewhat misleading and stems from an inadequate parametrization of the nuclear shape. In fact, a shell model calculation with a truncated deformation space has a tendency to locate the saddle point in an antishell region. When more collective degrees of freedom are introduced, the saddle moves toward the liquid drop surface in between a shell and an antishell region. Therefore, one may feel justified in using the uniform model for the evaluation of Γ_F because of the small shell effects to be

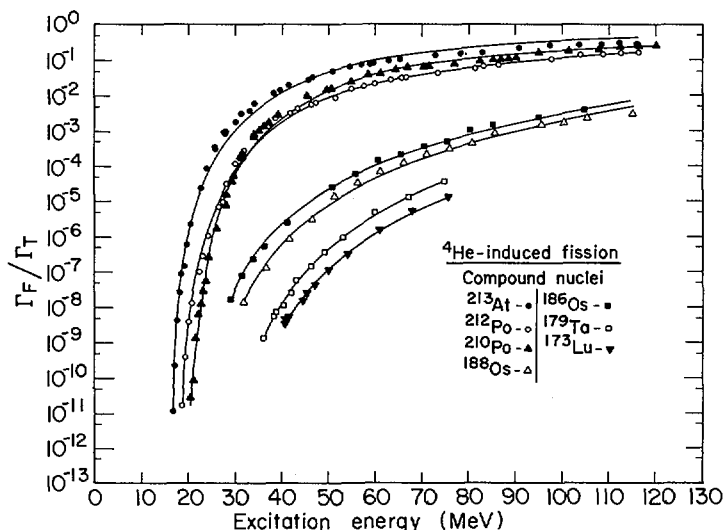


FIG. 11. Least-squares fits to the fission probabilities of some compound nuclei produced with ^4He bombardment [31].

expected at the saddle point, and furthermore because of a major lack of information about whatever shell structure does exist in the saddle region.

The formalism used in fitting the data contains five parameters which in principle can be considered to be free: in Γ_N one has the oscillator quantum $\hbar\omega_0$ which specifies the level spacing of the Nilsson model; in Γ_F , the barrier penetrability coefficient $\hbar\omega$; the fission barrier B_F ; the density of the doubly degenerate single particle levels g_F ; and the gap parameter Δ assumed to be the same for neutrons and protons. Two different energy ranges have been studied. The first includes the data up to 70 MeV excitation energy and the second up to 120 MeV.

In a preliminary attempt to fit the data, all of the five parameters have been considered free. The most interesting result has been the large uncertainty with which both $\hbar\omega_0$ and g_F are determined. Equivalently good fits could be obtained by keeping the product of these two quantities constant and by adjusting the fission barrier in a minor way. This effect can be predicted on the basis of Eq. (7).

Because of the above conclusion, $\hbar\omega_0$ was assigned the value $41/A^{1/3}$ which contains the proper A dependence and should be reasonably accurate. The data were then fitted with the remaining four parameters. The resulting fits appear to be quite good and the parameters are essentially identical in both energy ranges. Some of the fits are shown in Figs 10 and 11.

The barrier penetrabilities for those cases where data are available very close to the barrier have an average value of 1 MeV. The rather large dispersion observed in these quantities depends mainly upon the way in which the corrections for U or Th contaminants were performed close to the barrier.

TABLE 1. PARAMETERS OBTAINED FROM THE ANALYSIS OF FISSION PROBABILITIES^a [31]

Reaction	Ref.	B_f (MeV)	g_f (MeV ⁻¹)	Δ (MeV)
${}^{209}_{83}\text{Bi} + {}^4_2\text{He} \rightarrow {}^{213}_{85}\text{At}$	[16]	17.0	7.67	0.38
${}^{208}_{82}\text{Pb} + {}^4_2\text{He} \rightarrow {}^{212}_{84}\text{Po}$	[16]	19.5	7.36	0.06
${}^{207}_{82}\text{Pb} + {}^4_2\text{He} \rightarrow {}^{211}_{84}\text{Po}$	[16]	19.7	7.08	0.84
${}^{206}_{82}\text{Pb} + {}^4_2\text{He} \rightarrow {}^{210}_{84}\text{Po}$	[16]	20.5	7.42	0.60
${}^{209}_{83}\text{Bi} + {}^1_1\text{H} \rightarrow {}^{210}_{84}\text{Po}$	[16]	21.4	7.33	0.17
${}^{208}_{82}\text{Pb} + {}^1_1\text{H} \rightarrow {}^{209}_{83}\text{Bi}$	[16]	23.3	7.55	0.22
${}^{206}_{82}\text{Pb} + {}^1_1\text{H} \rightarrow {}^{207}_{83}\text{Bi}$	[16]	21.9	7.63	0.11
${}^{197}_{79}\text{Au} + {}^4_2\text{He} \rightarrow {}^{201}_{81}\text{Tl}$	[16]	22.3	7.57	0.39
${}^{197}_{79}\text{Au} + {}^1_1\text{H} \rightarrow {}^{198}_{80}\text{Hg}$	[16]	20.4	7.43	0.68
${}^{187}_{75}\text{Re} + {}^4_2\text{He} \rightarrow {}^{191}_{77}\text{Ir}$	[17]	23.7	7.16	0.05
${}^{185}_{75}\text{Re} + {}^4_2\text{He} \rightarrow {}^{189}_{77}\text{Ir}$	[17]	22.6	6.84	0.10
${}^{184}_{74}\text{W} + {}^4_2\text{He} \rightarrow {}^{188}_{76}\text{Os}$	[18]	24.2	6.89	0.54
${}^{183}_{74}\text{W} + {}^4_2\text{He} \rightarrow {}^{187}_{76}\text{Os}$	[18]	22.7	6.84	0.83
${}^{182}_{74}\text{W} + {}^4_2\text{He} \rightarrow {}^{186}_{76}\text{Os}$	[18]	23.4	6.66	0.43
${}^{181}_{83}\text{Ta} + {}^4_2\text{He} \rightarrow {}^{185}_{75}\text{Re}$	[16]	24.0	6.51	0.60
${}^{175}_{71}\text{Lu} + {}^4_2\text{He} \rightarrow {}^{179}_{73}\text{Ta}$	[17]	26.1	6.53	0.99
${}^{169}_{69}\text{Tm} + {}^4_2\text{He} \rightarrow {}^{173}_{71}\text{Lu}$	[17]	28.0	6.17	0.87

^a The barrier penetrations have been set equal to 1.0 MeV.

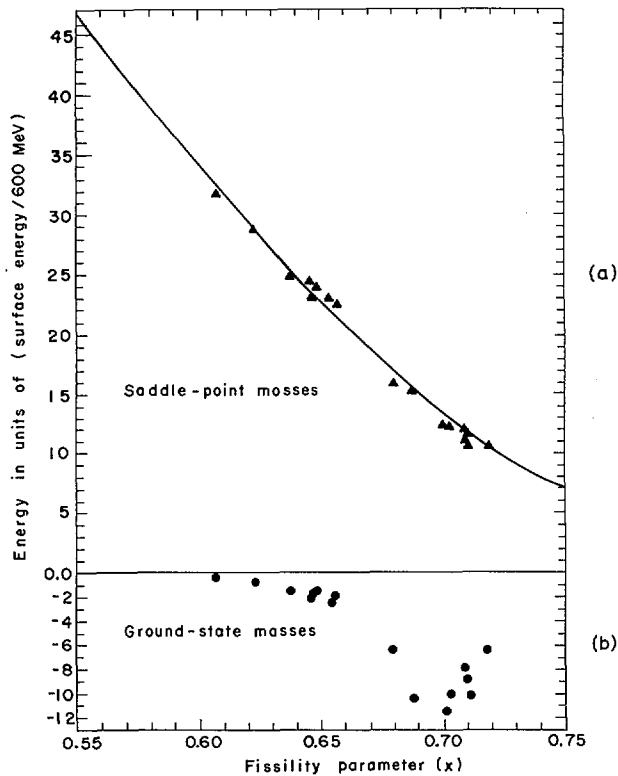


FIG. 12. (a) Experimental fission barriers corrected for the ground state shell effects as a function of the fissility parameter x . The solid line represents the smooth liquid drop prediction [31]. Figure 12b gives the ground state shell effects as a function of x .

In order to obtain a more consistent set of fission barriers, the barrier penetrability coefficients were fixed at 1 MeV. The fits obtained in this way are as good as the previous ones and the resulting parameters are shown in Table I. The fission barriers quoted in the table should be considered to be accurate within 1 MeV. Assuming that no shell effects are present at the saddle point, the experimental barriers from which the ground state shell effects are subtracted should follow closely the smooth liquid drop prediction. In Fig. 12a the experimental barriers corrected for the ground state shell effects, and expressed in units of $1/600$ of the surface energy of the corresponding spherical nucleus, are plotted as a function of the fissility parameter x . In Fig. 12b the ground state shell effects are shown. The solid line represents the smooth liquid drop prediction. The experimental fluctuations about the liquid drop value are at most 1 MeV, well within the experimental uncertainties. Therefore, one is led to the conclusion that the experimental shell effects at the saddle point are, for this region of elements, rather small.

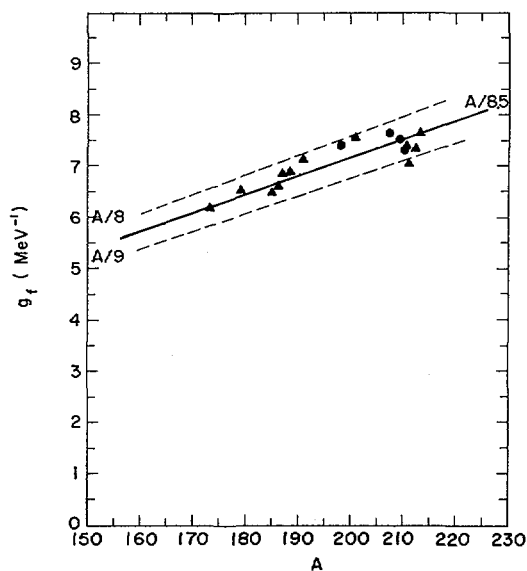


FIG. 13. Experimental saddle point single particle level densities g_f as a function of mass number. The two dashed lines correspond to a level density parameter a_F equal to $A/8$ and $A/9$, respectively [13].

The saddle single particle level densities are shown as a function of mass number in Fig. 13. The two lines bracketing the data correspond to the level density parameters $a_F = A/9$ and $a_F = A/8$ where $a_F = (\pi^2/3) g_F$. A reasonable average line passing through the data corresponds to $a_F = A/8.5$. The fluctuations about the average are smaller than 5%. When the fits are performed with Fermi gas level densities, the ratio a_F/a_N varies from about 1.0 in the upper rare earths to 1.5 in the ^{208}Pb shell region. Thus, it appears that the level densities based upon the Nilsson diagram have accounted for the major part of the shell effects and for their disappearance with energy. A closer examination shows that the deviations are not statistical in nature, but correlate quite well with the residual shell effects [52] not accounted for, or overaccounted for, by the Nilsson model. It is interesting to notice the average value of a_F , equal to $A/8.5$, as compared with the corresponding average quantity in Γ_N obtained by smoothing the shell model spectrum. This last quantity is $a_N = A/9.2$, giving a ratio $a_F/a_N = 1.08$. Although it is not possible at this stage to reach any definite conclusion regarding this experimental point, an increase in the saddle point single particle level density should be expected on the basis of a very simple argument. In a Fermi gas the single particle level density at the Fermi surface depends upon the particle density. The higher the particle density, the lower the single particle level density. The nuclear matter is less dense on the surface of the nucleus and the surface is larger in a deformed nucleus. Bishop and co-workers [53] have shown that the ratio of the single

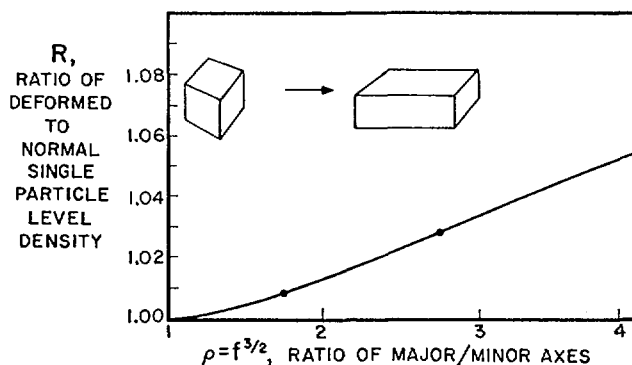


FIG. 14. Ratio of the single particle level densities for a deformed and a non-deformed Fermi gas nucleus as a function of the major to minor axis ratio [53].

particle level densities at the Fermi surface for the deformed to the undeformed nucleus is given by

$$R = \frac{11}{15} + \frac{4}{45} (f^{-1} + 2f^{1/2})$$

where $f^{3/2}$ is the ratio of the major to minor axis (Fig. 14). This ratio varies from 1.05 at $x = 0.7$ to 1.1 at $x = 0.65$, in surprising agreement with the experimental ratio of 1.08 obtained in the same fissility range.

The saddle gap parameters Δ shown in Table I are characterized by rather large uncertainties. The only safe experimental indication is that the gap parameters are rather small. The average value is in fact somewhat smaller than the ground state value in the same region. While the large uncertainties associated with this quantity do not justify any serious speculation, it may be possible that the smallness of the gap parameters may be due to some extent to the rather large angular momentum with which the compound nuclei are prepared at excitation energies close to the barrier. The gap parameter and the pairing correlation are in fact diminished by the presence of angular momentum, as can be seen in Figs 3 and 4. It is also possible that this parameter is actually compensating for other quantities not included in the formalism, like the saddle point shell effects. In fact, pairing effects and shell effects behave much in the same way with excitation energy. However, if one assumes the decrease in pairing to be fully due to shell effects at the saddle point, such shell corrections would amount to 1 MeV at most.

Indications of a rather large gap parameter at the saddle point of ^{210}Po were obtained from the fission fragment angular distributions of the ^4He -induced fission of ^{206}Pb and ^{207}Pb [54]. These very low-energy angular distributions suggested a gap parameter as large as 1.5 MeV. The experiment has been recently duplicated by Itkis and co-workers [55] with complete agreement on the data. While the high-energy data seem to be consistent with $\Delta \sim 1$ MeV the lowest-energy data remain unexplained with such a value.

Shell model calculations are in progress to estimate the value of Δ necessary to fit the experimental data. While the fission probabilities are not the most sensitive quantities to use in the exploration of the superfluid properties of the system, the present analysis seems to indicate a saddle gap parameter definitely lower than 1.5 MeV.

CONCLUSION

It appears that the most relevant features associated with the fission probabilities are now understood in fair to good detail. The shell model, in conjunction with the liquid drop model, can provide a nearly quantitative description of the potential energies relevant to the problem. At the same time the statistical-thermodynamical behavior of the system can be predicted in equivalently good detail. In fact, a new picture is emerging where the ground state and the saddle point properties are discussed on the same basis as the statistical properties of the compound nucleus and of the transition state. The same physical structure responsible for the anomalously small masses of nuclei in the ^{208}Pb region is seen to be responsible for the unusually high fission barriers of the same nuclei and for the very rapid increase in their fission probabilities.

It is to be recognized that the present status of the theory still falls short of a completely quantitative understanding. The fission barriers cannot be predicted with accuracies better than a few MeV and similar difficulties are encountered in reliably predicting the details of the potential energies. The same uncertainties in the shell structure affect the evaluation of the level densities and of other related statistical quantities. Furthermore, in the actinide region where the fission probabilities can be observed at extremely low energies above the barrier, delicate problems arise associated with the inapplicability of statistical mechanics and to the onset of fluctuations requiring more of a spectroscopical than a statistical interpretation.

ACKNOWLEDGMENTS

It is a pleasure to thank Dr. S.G. Thompson for his valuable comments on the paper; Mr. R.C. Gatti and Mrs. D. Valentine are thanked for their help with some of the figures.

REFERENCES

1. N. Bohr and J. A. Wheeler, Phys. Rev. 56, 426 (1939).
2. L. Meitner and O. R. Frish, Nature 143, 239 (1939).
3. V. F. Weisskopf, Phys. Rev. 52, 295 (1937).
4. J. A. Wheeler, "Channel Analysis of Fission," Fast Neutron Physics, ed. by J. B. Marion and J. L. Fowler (Interscience Publishers, New York - London, 1963), Part II, 2051.

5. R. Vandenbosch and J. R. Huizenga, Proceeding of the Second United Nations International Conference on the Peaceful Uses of Atomic Energy, 15 (United Nations, Geneva, 1958) 285.
6. H. R. Huizenga and R. Vandenbosch, "Nuclear Fission," in Nuclear Reactions, ed. by P. M. Endt and P.B. Smith (North-Holland Publishing Co., Amsterdam, 1962), Vol. II.
7. G. N. Flerov, Proceedings of the Second United Nations International Conference on the Peaceful Uses of Atomic Energy, 14, (United Nations, Geneva, 1958) 151.
8. S.A. Baraboshkin, A.S. Karamyan, and G.N. Flerov, J. Exptl. Theoret. Phys. (USSR), 32 1294 (1957).
9. A.S. Karamyan, Yu.B. Gerlit, and B.F. Myasoedov, J. Exptl. Theoret. Phys. (USSR), 36, 621 (1959).
10. V.A. Druin, S.M. Polikanov, and G.N. Flerov, J. Exptl. Theoret. Phys. (USSR), 32, 1298 (1957).
11. S. M. Polikanov and V. A. Druin, J. Exptl. Theoret. Phys. (USSR), 36, 744 (1959).
12. V. A. Karnankhov, J. Exptl. Theoret. Phys. (USSR), 36, 1933 (1959).
13. J. R. Huizenga, R. Chaudhry, and R. Vandenbosch, Phys. Rev. 126, 210 (1962).
14. D. S. Burnett, R. C. Gatti, F. Plasil, B. P. Price, W. J. Swiatecki, and S. G. Thompson, Phys. Rev. 134, 952 (1964).
15. T. Sikkeland, Phys. Rev. 135, 669 (1964).
16. A. Kodai-Joopari, Ph.D. Thesis, University of California, Lawrence Radiation Laboratory Report UCRL-16489 (1966).
17. G. M. Raispeck and J. W. Cobble, Phys. Rev. 153, 1270 (1967).
18. L. G. Moretto, R. C. Gatti, and S. G. Thompson, Lawrence Radiation Laboratory Report UCRL-17989, Nuclear Chemistry Division Annual Report, January 1968, p. 141.
19. F. C. Williams, Nucl. Phys. A133, 33 (1968).
20. L. G. Moretto, R. Stella, and V. Caremella-Crespi, Energia Nucleare 17, 436 (1970).

21. V. S. Ramamurthy, S. S. Kapoor, and S. K. Kataria, Phys. Rev. Letters 25, 386 (1970).
22. F. C. Williams, G. Chan, and J. R. Huizenga, Nucl. Phys. A187, 225 (1972).
23. M. Hillman and J. R. Grover, Phys. Rev. 185, 1303 (1969).
24. P. Decowski, W. Grochulski, A. Marcinkowski, K. Siwek, and Z. Wilhelmi, Nucl. Phys. A110, 129 (1968).
25. L. G. Moretto and R. Stella, Phys. Letters 32B, 558 (1970).
26. L. G. Moretto, Nucl. Phys. A182, 641 (1972).
27. L. G. Moretto, Phys. Letters 35B, 379 (1971).
28. L. G. Moretto, Nucl. Phys. A185, 145 (1972).
29. M. Sano and M. Wakai, Prog. Theor. Phys. 48, 160 (1972).
30. L. G. Moretto, Lawrence Berkeley Laboratory Report LBL-1298 (1972).
31. L. G. Moretto, S. G. Thompson, J. Routti, and R. C. Gatti, Phys. Letters 38B, 471 (1972).
32. R. Vandenbosch and V. Mosel, Phys. Rev. Letters 28, 1726 (1972).
33. H. C. Britt, M. Bolsterli, J. R. Nix, and J. L. Norton, Los Alamos Laboratory Report LA-DC-72-1307, November 1972.
34. V. Metag, S. M. Lee, E. Liukkonen, G. Sletten, S. Bjørnholm, and A. S. Jensen, preprint.
35. L. G. Moretto, Phys. Letters 34B, 191 (1971).
36. L. G. Moretto, Nucl. Phys. A180, 337 (1972).
37. V.S. Ramamurthy and S.S. Kapoor, Proceedings of the Nuclear Physics and Solid State Physics Symposium, Madurai-India (1972) 2, Bhabha Atomic Research Centre, Dept. of Atomic Energy, Bombay (1972) 279.
38. D. L. Hill and J. A. Wheeler, Phys. Rev. 89, 1102 (1953).
39. T. Ericson, Advan. Phys. 9, 425 (1960).
40. S. Cohen, F. Plasil, and W. J. Swiatecki, Proceedings of the Third Conference on Reactions Between Complex Nuclei, ed. by A. Ghiorso, R. M. Diamond, and H. A. Conzett, University of California Press (1963), p. 325.

41. S. Cohen, F. Plasil, and W. J. Swiatecki, Lawrence Berkeley Laboratory Report LBL-1502 (1972).
42. S. Cohen and W. J. Swiatecki, Ann. Phys. (New York) 19, 67 (1962); ibid. 22, 406 (1963).
43. For a recent review on Nuclear Level Densities, see: J. R. Huizenga and L. G. Moretto, Ann. Rev. Nucl. Sci. 22, 427 (1972).
44. H. Bethe, Phys. Rev. 50, 332 (1936).
45. D. W. Lang, Nucl. Phys. 77, 545 (1965).
46. H. Baba, Nucl. Phys. A159, 625 (1970).
47. U. L. Businaro and S. Gallone, Nuovo Cimento 1, 629 (1955).
48. J. R. Nix, Ph.D. Thesis, University of California, Lawrence Radiation Laboratory Report UCRL-11338 (1964).
49. L. D. Landau and E. M. Lifshitz, Statistical Physics (Addison-Wesley Publishing Company, Inc., Reading, Mass., 1958), p. 86.
50. R. Vandenbosch, preprint.
51. R. Bimbot et Y. Le Beyec, J. Physique 32, 243 (1971).
52. S. G. Nilsson, C. F. Tsang, A. Sobiczewski, Z. Szymanski, S. Wychech, G. Gustafson, J. L. Lamm, P. Moeller, and B. Nilsson, Nucl. Phys. A131, 1 (1969).
53. C. J. Bishop, I. Halpern, R. W. Shaw, Jr., and R. Vandenbosch, Nucl. Phys. A198, 161 (1972).
54. L. G. Moretto, R. C. Gatti, S. G. Thompson, J. R. Huizenga, and J. O. Rasmussen, Phys. Rev. 178, 1845 (1969).
55. M. G. Itkis, K. G. Kuvatov, V. N. Okolovich, G. Ya. Ruskina, G. N. Smirenkin, and A. S. Tishin, Yad. Fiz. 16, 958 (1972); Translation Sov. J. Nucl. Phys. 16, 144 (1973).

DISCUSSION

F. PLASIL: It is comforting to learn from your work that if we wish to extract fission barriers from excitation functions, it is possible to do so in the simple unified model, and that if we wish to understand the excitation functions at high bombarding energies, it is possible to do so with the help of the effects on level densities which you describe. This situation is true for the ^4He -induced results which you presented. In view of the title of your paper, I would like, for the sake of completeness, to comment on fission probabilities obtained from heavy-ion-induced fission. Most of the fission barriers from heavy-ion reactions have been determined by Sikkeland and co-workers. Recently, we have attempted to re-analyse Sikkeland's data and to interpret our own recent measurements with a calculation that includes angular-momentum-dependent fission barriers. We find that it is not possible to extract unambiguous values for fission barriers because of the uncertainty in the fraction of the total reaction cross-section that results in compound nucleus formation. We feel at this time that there may be problems with previously extracted fission barriers from heavy-ion-induced fission and that the published values may not be reliable.

L.G. MORETTO: The heavy-ion fission cross-sections have not been considered here because the Coulomb barrier prevents us from measuring the fission probabilities close to the barrier.

U. MOSEL: With regard to your theory that one would not expect shell corrections at the saddle except in the presence of shells that exhibit a canal-like correlation with deformation, I would like to point out that such structures can be expected at the fission barriers in lighter nuclei. And in fact my calculations for these nuclei¹ show that the fragment shells do reach into the potential energy surface from scission to the saddle which is rather constricted in these lighter nuclei and thus closer to the final fragments. Care must also be taken in concluding from agreement between experimental and theoretical Γ_f/Γ_N values that no shells are present at the barrier. In the case of ^{198}Hg , as calculated by R. Vandenbosch and myself and mentioned in your paper, very good agreement is reached in spite of a shell correction at the saddle of ≈ -2 MeV.

L.G. MORETTO: I agree with what you say. Our fission barriers are uncertain by about 1 MeV. This can accommodate your saddle point shell effects.

¹ MOSEL, U., Phys. Rev. C6(1972) 971.

Review Paper

ROLE OF SYMMETRY OF THE NUCLEAR SHAPE IN ROTATIONAL CONTRIBUTIONS TO NUCLEAR LEVEL DENSITIES

S. BJØRNHOLM, A. BOHR
Niels Bohr Institute,
University of Copenhagen

B.R. MOTTELSON
Nordita,
Copenhagen, Denmark

Abstract

ROLE OF SYMMETRY OF THE NUCLEAR SHAPE IN ROTATIONAL CONTRIBUTIONS TO NUCLEAR LEVEL DENSITIES.

In nuclei that have static deformations, the level density is appreciably greater than for spherical nuclei because of the contribution of the low-energy rotational levels. The magnitude of this effect depends on the symmetry of the nuclear shape, which determines the collective rotational degrees of freedom. A number of symmetry types are considered that may be relevant for the shape of nuclei in the ground states as well as at the saddle point for fission. The transition between systems with different symmetries can be studied in terms of the effect of the collective shape oscillations on the level densities.

INTRODUCTION

The exciting developments in the understanding of the fission process that have followed the discovery of the fission isomers have brought into focus the crucial role of the symmetry of the nuclear shape. The dependence of the shell structure on the symmetry is reflected in the potential energy surface as well as in the statistical properties connected with the level densities for intrinsic excitations.¹ The symmetry of the nuclear shape is also the decisive element in defining the rotational degrees of freedom, and in the present paper we shall consider the contribution of these degrees of freedom to the level densities.^{2,3}

1. SPHERICAL SHAPE

We begin by summarizing the conventional analysis of the level densities of a spherical nucleus, considered as a function of the angular

¹ For a discussion of the effect of shell structure on level densities, see Ref.[1].

² For a discussion of the role of symmetry in defining the rotational degrees of freedom, and a derivation of the resulting rotational band structure, see Ref.[2].

³ The present considerations were stimulated by discussions with E. Lynn and H.C. Britt concerning the analysis of experimental data on the competition between fission and neutron emission.

momentum, I . The total level density, for a given excitation energy E , can be decomposed in the form

$$\rho(E) = \sum_{M=-\infty}^{\infty} \rho(E, M) = \sum_I (2I+1) \rho(E, I) \quad (1)$$

$$\rho(E, I) = \rho(E, M=I) - \rho(E, M=I+1)$$

where M is the projection of I on a fixed axis. When many independent degrees of freedom contribute to M , one expects a normal distribution,

$$\rho(E, M) = (2\pi)^{-\frac{1}{2}} \sigma^{-1} \exp \left\{ -\frac{M^2}{2\sigma^2} \right\} \rho(E) \quad (2)$$

where σ is referred to as the spin cut-off factor and can also be thought of in terms of a statistical moment of inertia

$$\sigma = \left(\frac{\hbar^2}{\mathcal{J}_{\text{stat}}} \frac{1}{T} \right)^{-\frac{1}{2}} \quad (3)$$

where T is the nuclear temperature. From Eqs (1) and (2), one obtains

$$\rho(E, I) = (2I+1) (8\pi)^{-\frac{1}{2}} \sigma^{-3} \exp \left\{ -\frac{I(I+1)}{2\sigma^2} \right\} \rho(E) \quad (4)$$

2. SHAPES WITH NO ROTATIONAL SYMMETRY

In a deformed nucleus, each intrinsic state gives rise to a rotational band and the total level spectrum, for a given angular momentum, is therefore obtained by summing over a set of intrinsic states rather than by a decomposition of the level spectrum, as for a spherical system [3].

We first consider a system that possesses the full rotational degrees of freedom of a three-dimensional body. Such systems are characterized by an equilibrium shape that completely violates rotational symmetry, in the sense that it is not invariant with respect to any rotation of the coordinate axes. In this case, the rotational band, for a given intrinsic state, involves $(2I+1)$ levels, for each value of the total angular momentum I , as for the asymmetric rotor. (Each of these levels is itself $(2I+1)$ -fold degenerate, corresponding to the different components M .)

If the level density of the intrinsic states is denoted by $\rho_{\text{intr}}(E)$, the total level density, as a function of I , can be expressed in the form

$$\rho(E, I) = \sum_{\tau=1}^{2I+1} \rho_{\text{intr}}(E - E_{\text{rot}}(\tau, I))$$

$$\approx \rho_{\text{intr}}(E) \sum_{\tau} \exp \left\{ -\frac{1}{T} E_{\text{rot}}(\tau, I) \right\} \quad (5)$$

where τ labels the different rotational levels in a given band having the same value of I . The last expression in Eq. (5) assumes that E_{rot} is small compared with the total excitation energy and follows from the definition of the temperature as the inverse of the logarithmic derivative of $\rho_{\text{intr}}(E)$. For sufficiently small values of I , the dependence on E_{rot} in Eq. (5) can be neglected, and one obtains

$$\rho(E, I) \approx (2I+1) \rho_{\text{intr}}(E) \quad (6)$$

$$(E_{\text{rot}} \ll T)$$

It is seen that the level density (4), for the spherical nucleus in the limit of $I \rightarrow 0$, involves an extra factor $(8\pi)^{-1/2} \sigma^{-3}$ in comparison with expression (6). This factor, depending on the statistical moment of inertia, represents the fraction of the total number of levels in the spherical nucleus that have $I=0$; in the deformed nucleus, each intrinsic state gives rise to a level with $I=0$.

While the density $\rho(E, I)$ for small values of I is proportional to $(2I+1)$, as a very general feature of the statistical distribution, the expression (5), for larger values of I , contains a cut-off resulting from the rotational energy. Thus, the total level density of the deformed nucleus depends on the moments of inertia for the collective rotation. By summing the expression (5) over I , with the weight factor $(2I+1)$ as in Eq. (1), we obtain

$$\begin{aligned} \rho(E) &\approx \rho_{\text{intr}}(E) \sum_{I, \tau} (2I+1) \exp \left\{ -\frac{1}{T} E_{\text{rot}}(\tau, I) \right\} \\ &\approx \rho_{\text{intr}}(E) \frac{1}{\pi} \iiint dI_1 dI_2 dI_3 \exp \left\{ -\frac{1}{T} \sum_{\kappa=1}^3 \frac{\hbar^2}{2\mathcal{J}_{\kappa}} I_{\kappa}^2 \right\} \quad (7) \\ &= \rho_{\text{intr}}(E) (8\pi)^{\frac{1}{2}} \left(\frac{\hbar^2}{\mathcal{J}_1} \frac{\hbar^2}{\mathcal{J}_2} \frac{\hbar^2}{\mathcal{J}_3} \frac{1}{T^3} \right)^{-\frac{1}{2}} \end{aligned}$$

where \mathcal{J}_{κ} denote the moments of inertia with respect to the three principal intrinsic axes. The approximation of the sum by an integral assumes large values of $\hbar^{-2} \mathcal{J}_{\kappa} T$; the volume element $\pi^{-1} dI_1 dI_2 dI_3$ (which represents the element of phase space, in units of $(2\pi\hbar)^3$, integrated over the total solid angle, $8\pi^2$) ensures that the number of quantum states per unit of I is $4I^2 \approx (2I+1)^2$. In Eq. (7), the factor multiplying $\rho_{\text{intr}}(E)$ is of the order of the total number of states in the rotational spectrum with $E_{\text{rot}} \lesssim T$. Indeed, quite generally, the occurrence of a low-frequency collective mode leads to an increase in the total level density, by a factor of the order of the total number of states in the collective spectrum with energies less than the temperature.

In the nuclear many-body system, the occurrence of rotational motion implies a corresponding reduction in the number of the intrinsic degrees of freedom, and the question arises concerning the effect of this constraint on the intrinsic level density. The collective rotational motion can be expressed as a coherent superposition of single particle excitations, and the energies of these excitations are, in a heavy nucleus, typically of the order several MeV.

For temperatures small compared with these energies, the removal of the "spurious" degrees of freedom is therefore not expected to have a significant effect on $\rho_{\text{intr}}(E)$. If the nuclear temperature becomes comparable with these particle excitation energies, the fluctuations in the orientation of the nucleus associated with the particle motion become so large that one can no longer speak of a well-defined deformation or of a separation between rotational and intrinsic motion. (The particle excitations involved in the rotational motion are those generated by the Coriolis coupling, and the main contribution is associated with energies of order $\hbar(\omega_2 - \omega_3)$, where ω_2 and ω_3 are the characteristic frequencies for particle motion in the two directions perpendicular to the axis of rotation. This difference can also be expressed in the form $\hbar(\omega_2 - \omega_3) \approx \hbar\omega_0 \delta \approx 40 \text{ MeV A}^{-1/3} \delta$, in terms of the mean oscillator frequency ω_0 and the deformation δ . For the ground state equilibrium shapes in the actinide region, $\delta \approx 0.25$; for the saddle-point shape, $\delta \approx 0.6$.)

3. AXIALLY SYMMETRIC SHAPES

If the equilibrium shape, though non-spherical, is invariant under a subgroup of rotations, the collective rotational degrees of freedom are correspondingly reduced. An example of particular importance for nuclei is a shape with axial symmetry and invariance with respect to a rotation \mathcal{R} of 180° about an axis perpendicular to the symmetry axis.

Axial symmetry implies that the intrinsic states can be specified by the quantum number K , representing the component of I along the symmetry axis, and that there is no collective rotation about this axis. The intrinsic states are degenerate with respect to the sign of K , as a result of \mathcal{R} invariance, which also requires that the conjugate intrinsic states be combined in a definite manner in the total wave function. For $K \neq 0$, the rotational band based on the pair of intrinsic states $\pm K$ contains the levels

$$I = |K|, |K| + 1, |K| + 2, \dots \quad (8)$$

while, for $K = 0$, the intrinsic states are eigenfunctions of the rotation \mathcal{R} with eigenvalue $r = \pm 1$, and the states in the rotational band are

$$\left. \begin{array}{ll} I = 0, 2, 4 \dots & r = +1 \\ I = 1, 3, 5 \dots & r = -1 \end{array} \right\} K = 0 \quad (9)$$

The total level density of intrinsic states can be decomposed into partial densities with specified K

$$\rho_{\text{intr}}(E) = \sum_{K=-\infty}^{\infty} \rho_{\text{intr}}(E, K) \quad (10)$$

and the assumption of many independent degrees of freedom leads to a normal distribution, as in Eq. (2),

$$\rho_{\text{intr}}(E, K) = (2\pi)^{-1/2} \sigma_K^{-1} \exp \left\{ -\frac{K^2}{2\sigma_K^2} \right\} \rho_{\text{intr}}(E) \quad (11)$$

The level density for specified I is obtained by summing over intrinsic states with $|K| \leq I$

$$\rho(E, I) = \frac{1}{2} \sum_{K=-I}^I \rho_{\text{intr}}(E - E_{\text{rot}}(K, I), K) \quad (12)$$

where $E_{\text{rot}}(K, I)$ is the rotational energy. (For convenience, we have expressed the densities in Eqs (10) and (12) in terms of sums extending over negative as well as positive values of K , despite the fact that the rotational bands are labelled by $|K|$ and involve only a single level I , associated with the conjugate pair of intrinsic states $\pm K$. The relative weights of $|K| \neq 0$ and $K=0$ bands is correctly given by such sums, since, for a given I , only half the $K=0$ bands contribute (see Eq. (9)). This can also be seen from the fact that an isotropic (statistical) distribution of the direction of the symmetry axis, for a given I and M , requires, for each value of $|K| \neq 0$ ($|K| \leq I$), twice as many bands as for $K=0$.

For values of I such that $E_{\text{rot}}(K, I)$ is small compared with the temperature, T , and $I \ll \sigma_K$, one can neglect the dependence on E_{rot} in Eq. (12) as well as the exponential factor in Eq. (11) to obtain

$$\rho(E, I) = (2I+1) (8\pi)^{-1/2} \sigma_K^{-1} \rho_{\text{intr}}(E) \quad (13)$$

It is seen that the level density (13) exceeds the expression (4) by a factor of order σ^2 , but is smaller than Eq. (6) by a factor of order σ^{-1} , corresponding to the fact that the axially symmetric nucleus can rotate about two axes (perpendicular to the symmetry axis), while the general rotor has three rotational axes.

4. EFFECTS OF DISCRETE SYMMETRY ELEMENTS

If the equilibrium shape is invariant with respect to a group of finite rotations, the number of states in the rotational bands are reduced by a factor representing the number of elements in the corresponding point group. Thus, for example, the most general quadrupole deformation is invariant with respect to rotations \mathcal{R}_κ by 180° about each of the three principal axes. This invariance group, referred to as D_2 , has four elements, and the resulting level density is one-quarter of that given by Eqs (5), (6), or (7).

Additional collective degrees of freedom result from deformations that violate space reflection, \mathcal{P} , or time reversal \mathcal{T} . A deformation violating either of these symmetries leads to a doubling of the energy levels, and hence to an increase of the level density by a factor of 2.

5. TRANSITION FROM SYMMETRIC TO NON-SYMMETRIC SHAPE. VIBRATIONAL CONTRIBUTIONS TO LEVEL DENSITY

The treatment of rotational contributions to the level density assumes that the symmetry-violating deformation is large compared with the zero-point fluctuations in the shape. The gradual transition from the symmetric to the non-symmetric case can be studied in terms of the vibrational modes of shape oscillation.

The occurrence of a collective vibrational mode superposed on intrinsic excitations leads to a level density of the form

$$\begin{aligned}\rho(E) &= \sum_{\nu} \rho_{\text{intr}}(E - E_{\text{vib}}(\nu)) \\ &\approx \rho_{\text{intr}}(E) \sum_{\nu} \exp\left\{-\frac{1}{T} E_{\text{vib}}(\nu)\right\}\end{aligned}\quad (14)$$

where the set of quantum numbers ν labels the different states in the vibrational spectrum. For a one-dimensional harmonic mode of vibration, with frequency ω , the sum over ν yields

$$\begin{aligned}\rho(E) &= \rho_{\text{intr}}(E) \sum_{n=0}^{\infty} \exp\left\{-\frac{n\hbar\omega}{T}\right\} \\ &= \rho_{\text{intr}}(E) \left(1 - \exp\left\{-\frac{\hbar\omega}{T}\right\}\right)^{-1} \\ &\approx \left(\frac{T}{\hbar\omega}\right) \rho_{\text{intr}}(E) \quad \text{for } \hbar\omega \ll T\end{aligned}\quad (15)$$

corresponding to the well-known expression for the partition function for a boson excitation. For a vibrational mode with g -fold degeneracy, the factor multiplying $\rho_{\text{intr}}(E)$ in Eq. (15) becomes $(1 - \exp\{-\hbar\omega/T\})^{-g}$, where $g = 2\lambda + 1$ for a shape vibration of multipole order λ in a spherical nucleus and $g = 2$ for γ -vibrations in a deformed axially symmetric nucleus.

The transition from spherical to deformed shape is associated with a vibrational mode with low frequency, which becomes anharmonic in such a manner that a subset of the vibrational excitations with especially low energy separates from the rest and forms a rotational sequence. This set, in Eq. (14), gives the rotational contribution to the level density, as discussed above.

DISCUSSION

The dependence of the absolute level density on the symmetry of the nucleus can be quite appreciable, since the spin cut-off factors, σ , are about 5 for a heavy nucleus with excitation energies in the region from a few to 10 MeV. (For independent particle motion, the statistical moment of

inertia in Eq. (3) is equal to the moment for rigid rotation, which for $A \approx 240$ is $\hbar^2/I \approx 7$ keV; for a review of empirical evidence on spin cut-off factors, see Ref. [4].) In the comparison between the level densities of spherical and deformed nuclei, one must, however, include the appreciable effects of shell structure and variations in the pair correlation. In addition, one must take into account the occurrence of low-frequency quadrupole vibrations in a large class of spherical nuclei. (For an analysis of absolute level densities with the inclusion of rotational contributions, see Ref. [5].)

The analysis of the fission widths involves an enumeration of the number of open channels at the saddle point and is thus sensitive to the symmetry of the saddle point shape. Tentative evidence on this symmetry has come from recent analyses of the competition between fission and neutron emission. The empirical values of Γ_f/Γ_n for a number of nuclei at excitations of a few MeV above the fission threshold are found to be significantly larger than the theoretical estimates [6]. Such an enhancement could result from the collective contributions if the saddle point shape has a lower symmetry than that of the ground state. In particular, a departure from axial symmetry, with preservation of D_2 symmetry, implies an increase in the number of channels with small values of I by a factor of $(\pi/2)^{1/2} \sigma_K$; an additional factor 2 would result from a departure from reflection symmetry.

REFERENCES

- [1] MORETTO, L.G., Paper IAEA-SM-174/204, these Proceedings, Vol. 1.
- [2] BOHR, A., MOTTELSON, B.R., Nuclear Structure, II, W.A. Benjamin, New York, (to be published).
- [3] ERICSON, T., Nucl. Phys. 6 (1958) 62.
- [4] HUIZENGA, J.R., in Statistical Properties of Nuclei, (GARG, J.B., Ed.), Plenum-Press, New York (1972).
- [5] DØSSING, T., JENSEN, A.S., (to be published).
- [6] LYNN, E., private communication (1973); BRITT, H.C., private communication (1973).

DISCUSSION

J. R. HUIZENGA: Although I shocked Bjørnholm on his arrival in Rochester by pointing out to him that T. Ericson had considered the question of the enhancement in the level density for nuclei with static deformation as early as 1958 [3], I now wish to come to his defence. In collaboration with Behkami, Britt and Freiesleben, we have obtained evidence (and I understand that a group in Copenhagen has also done so) that one needs to add collective rotations to the level density in order to fit the neutron resonance data of deformed lanthanide and actinide nuclei. If one attempts to fit the neutron resonance data with the standard level density formula, one needs an energy shift of about 1.5 MeV, a quantity which is approximately equal to the total condensation energy for an even-even nucleus. Hence, I feel that at an excitation energy of about 6 MeV (neutron binding energy) one does need to use the level density formula presented by Bjørnholm which gives an enhancement in the level density due to collective rotations.

K. DIETRICH: Mr. Bjørnholm, is it possible that your considerations imply a larger density of states at the "symmetric saddle" compared to the "asymmetric saddle". In their recent experiments Konecny and Specht observed a very rapid increase of the ratio between symmetric and asymmetric fission at energies above the symmetric barrier. This increase would

imply that the level density parameter a in a uniform model would have to be 30% larger for symmetric fission than for asymmetric fission. This is quite a lot.

S. BJØRNHOLM: Yes, it is a lot. However, the existence of the highly asymmetric mass peaks in radium fission together with the symmetric peak will require an exceptionally strong shell effect for asymmetric fission, compared to symmetric fission. Therefore, in this case a difference of 30% in the parameter " a " (and hence in the single particle level densities g_s) is plausible.

L.G. MORETTO: I should like to make two comments on the paper. Firstly, I agree with the enhancement at low energies appearing in Britt's data. I am not convinced about the Γ_n/Γ_f at ~ 10 MeV being close to unity because of collective enhancement. In actinides the barriers have substantial shell effects which may be partially washed out at 10 MeV, thus increasing the fission probability.

Secondly, the collective enhancement of the level densities due to collective states cannot be preserved at high energies. At low energies the collective features are concentrated in a single quantum mechanical level; at high energies one should expect stronger and stronger coupling of the collective levels into the intrinsic background, which leads to an absorption of the collective phase space into the intrinsic level density. Knowledge of the strength functions should provide a smooth connection between the limit of uncoupled collective states (sharp quantum states) and the limit of strong coupling when all the intrinsic levels contain an approximately equal share of the collective strength.

S. BJØRNHOLM: Here is a point where there is a real difference of opinion. I should like to refer to Mr. Huizenga's comment and to Figs 7a and b in your own paper [5] as a basis for assessing the fading away of the enhancement factor due to collective rotations.

SINGLE PARTICLE EFFECTS ON FISSION BARRIERS AND STATISTICAL INTERPRETATION OF FRAGMENT ANISOTROPIES AND MASS DIVISION IN FISSION

S.S. KAPOOR, V.S. RAMAMURTHY

Bhabha Atomic Research Centre,
Trombay, Bombay, India

Abstract

SINGLE PARTICLE EFFECTS ON FISSION BARRIERS AND STATISTICAL INTERPRETATION OF FRAGMENT ANISOTROPIES AND MASS DIVISION IN FISSION.

For nuclei having significant shell effects around fission barrier deformations, the transition state shape becomes excitation energy dependent and should be determined by locating minima in the locus of conditional maxima of entropy for different nuclear elongations, as has been pointed out earlier. In this paper, implications of this feature on the interpretation of fragment anisotropies and mass division are discussed on the basis of entropy maps calculated with single particle level schemes of Nix and co-workers and using the Pauli-Ledergerber (PL) liquid drop model (LDM) parameters for the smooth part. For a typical case of ^{242}Pu , it is found that, at compound nucleus excitation energies $E_x \geq 25$ MeV, the nucleus goes through a mass symmetric shape at the outer barrier, as this shape has maximum entropy with respect to the mass asymmetry coordinate. The entropy calculations with the asymmetric level schemes for the outer barrier deformation were used to study the excitation energy dependence of fragment mass distributions and the correlation between fragment mass asymmetry and anisotropy on the assumptions that (1) these are decided by the characteristics of the outer barrier, and (2) the probability that the nucleus will go through a specified mass asymmetric shape is proportional to the appropriate level density. These calculations, which do not involve any free parameters, are shown to bring out the essential features of the fragment mass distributions. It is also shown that at $E_x \geq 25$ MeV, where only mass symmetric shapes are relevant, there is a gradual shift of the transition state towards the LDM saddle point, and at $E_x \sim 40$ MeV the transition state essentially coincides with the LDM saddle point. The "experimental" values of the shape parameter $\beta_0/\beta_{\text{eff}}$ derived from fragment anisotropy data at $E_x \sim 37$ MeV are shown to be consistent with the above conclusions and with the LDM parameters of Pauli and Ledergerber. It is also shown that a microscopic calculation of K_0^2 should incorporate a normalization procedure, since this quantity is dependent on the radius parameter of the level scheme used.

1. INTRODUCTION

The last few years have seen intensive theoretical studies of the single particle effects on the potential energy of deformation of nuclei, based on the now well-known macroscopic-microscopic method [1, 2]. Much of our current thinking about the fission process has resulted from these theoretical calculations which show a double-humped fission barrier for nuclei in the actinide region. It is now well known that these theoretical developments have provided a simple explanation for many near-threshold fission features such as isomeric fission and intermediate structure in fission cross-sections. In addition, these calculations for axially symmetric reflection-asymmetric nuclear shapes also show that for actinide nuclei the second barrier has a lower total energy for mass-asymmetric shapes, suggesting that the observed mass-asymmetry in fission might be a result of this feature of the deformation potential energy surface [1-6]. However,

with the realization of the existence of single particle effects at the fission barrier, it has also become necessary to re-examine earlier interpretations [7, 8] of the fragment angular distributions and fission excitation functions which were based on the identity of fission transition state shape with the liquid drop model (LDM) saddle shape. This identity, however, is justified only in the absence of shell effects, since then the level density can be calculated on the basis of the usual Fermi gas expression $S = 2(aE_x)^{1/2}$ for the entropy S , where E_x is the excitation energy and a is the level density parameter assumed to be shape-independent; consequently the transition state shape, which by definition is the point of minimum number of open channels encountered along the fission path, coincides with the LDM saddle shape. If, however, the shell effects are included, the above expression is no longer valid and the transition state shape needs to be determined directly from the level density considerations as has been pointed out earlier [9]. Just as the LDM saddle point is located by finding out the maximum in the locus of conditional minima in the deformation energy surface, the transition state shapes of excited nuclei should be determined by locating minima in the locus of conditional maxima of entropy for different nuclear elongations. Interpretation of super-barrier fission data is, therefore, closely linked to the calculation of level density as a function of nuclear shapes taking into account shell effects. Such calculations have been made possible in recent years with the availability of single particle levels for different nuclear shapes and the application of numerical methods of calculation of nuclear level densities [9, 10].

In this paper, numerical calculations of the entropy of fissioning nuclei have been carried out for various nuclear shapes starting with the appropriate single particle level schemes. The results of these calculations are used to discuss the excitation energy dependence of the probability of the fissioning nucleus going through different mass-asymmetric shapes at the second barrier in order to correlate these results with the observed fragment mass distributions in fission. The entropy calculations have also been used to study the excitation energy dependence of the fission transition state shape relevant for the interpretation of fission fragment angular distributions.

2. METHOD OF CALCULATION

Most of the discussion which follows is based on the present calculations of entropy S , nuclear level density ρ and the moment of inertia \mathcal{J}_{\parallel} parallel to the nuclear symmetry axis for different excitation energies and nuclear shapes encountered in fission. These quantities have been calculated on the basis of a microscopic model starting with the appropriate single particle level schemes of Nix and co-workers [5] for the folded Yukawa potential. An outline of the present calculations is given below.

The single particle states are characterized by their energies ϵ_{ν} and by their component K_{ν} of angular momentum along the nuclear symmetry axis. Considering the excited nucleus as a system of non-interacting fermions, the occupation probability of these states at a temperature T is given by

$$n_{\nu} = \frac{1}{1 + e^{(\epsilon_{\nu} - \mu)/T}} \quad (1)$$

where the chemical potential μ is determined by the particle conservation condition.

At a given temperature T , the excitation energy E_x , entropy S and the quantity $\mathcal{J}_{||}$ are then obtained by a numerical calculation from the following set of equations [9, 10].

$$E_x = \sum n_\nu \epsilon_\nu - \sum_{\nu=1}^{Z, N} \epsilon_\nu \quad (2)$$

$$S = - \sum n_\nu \ln n_\nu + (1 - n_\nu) \ln (1 - n_\nu) \quad (3)$$

$$\mathcal{J}_{||} = \frac{1}{T} \sum n_\nu (1 - n_\nu) K_\nu^2 \quad (4)$$

where the sums are taken over both neutrons and protons.

3. EXCITATION ENERGY DEPENDENCE OF THE FRAGMENT MASS DISTRIBUTIONS

Most of the explanations proposed in the past for the observed asymmetry in the fragment mass distributions at low excitation energies were based on the assumption that the mass distribution is determined by statistical considerations near the scission point. The mass asymmetry has therefore been generally attributed to the shell structure of fragment nuclei. However, in a stochastic model proposed earlier [11] the basic idea was that if the time of descent from saddle to scission is long enough for nucleon transfers between the two sides of the fissioning nucleus, a mass-asymmetric shape would develop due to nuclear shell structure. The recent calculations [1-5] of deformation potential energy surfaces with the inclusion of nuclear shell effects clearly bring out that already at the second barrier deformation a mass-asymmetric shape is energetically favoured. It was first pointed out by Möller and Nilsson [3] that for actinide nuclei the second fission barrier has a lower deformation potential energy for mass-asymmetric shapes as compared to mass-symmetric shapes. Calculations with more general shape parameters [4, 5] for the fissioning nucleus carried out by other groups have confirmed this result. Recently, Tsang and Wilhelmy [6] have carried out an analysis to interpret quantitatively the observed results on the mass asymmetry in fission in terms of the probabilities of the fissioning nucleus going through different mass-asymmetric shapes at the second barrier. Their calculations made use of the simple Fermi gas expression for nuclear level density which involved free level density parameters and the role of dynamics from the second barrier to scission was not considered. In the present work, we have calculated the probabilities for the fissioning nucleus to go through different mass-asymmetric shapes at the second barrier with the use of level densities calculated numerically for the appropriate shapes starting from the relevant single particle levels. The present calculations thus do not involve any free parameters and therefore a comparison of the calculated mass

yields with those observed can bring out the importance of the role of dynamics in mass division.

The present calculations were carried out with the single particle level scheme of Nix and co-workers [5] for the folded Yukawa potential, whose shape is specified by suitable parameters including a mass-asymmetry coordinate α_2 . The starting point of the present calculations is the assumption that the probability $P(\alpha_2)$ of the fissioning nucleus going through a mass-asymmetric shape α_2 at the second barrier deformation is proportional to the total number of open channels for that configuration. Restricting oneself to the study of super-barrier fission, where excitation energy of the compound nucleus is above both the symmetric and asymmetric barriers, one can write

$$P(\alpha_2) \propto \int_0^{E_x - E(\alpha_2)} \rho(x) dx \quad (5)$$

where $E(\alpha_2)$ is the deformation potential energy of the asymmetric shape α_2 relative to ground state and E_x is the compound nucleus excitation energy.

Qualitatively, it follows from Eq. (5) that in this case $P(\alpha_2)$ is proportional to $\rho(E_x - E(\alpha_2))$ owing to the fact that most of the contribution to the integral comes from the upper limit. Also, since the predominant energy dependence of the level density is governed by the entropy, one can write

$$P(\alpha_2) \propto e^{S(\alpha_2)}$$

where $S(\alpha_2)$ is the entropy of the configuration α_2 for a given compound nucleus excitation energy E_x . It then follows that

$$\frac{P(\alpha_2)}{P(\alpha_2 = 0)} \approx e^{S(\alpha_2) - S(\alpha_2 = 0)}$$

Therefore, a plot of $S(\alpha_2) - S(\alpha_2 = 0)$ versus E_x can bring out the main features of the excitation energy dependence of the probability for the nucleus to pass through different mass-asymmetric shapes. Results of present calculations of $S(\alpha_2)$ for a typical case of a ^{242}Pu fissioning nucleus are shown in Fig. 1. In these calculations the potential deformation energy $E(\alpha_2)$ was taken from the microscopic-macroscopic calculations of Nix and co-workers [5]. The following conclusions can be directly drawn from the figure:

- (1) At low excitation energies corresponding to near-threshold fission, the entropy is maximum for $\alpha_2 = 0.8$, implying that the nucleus predominantly passes through a mass-asymmetric shape at the second barrier.
- (2) At excitation energies exceeding 25 MeV, the entropy is maximum for $\alpha_2 = 0$, again implying that at those energies the nucleus predominantly passes through a mass-symmetric shape at the second barrier. This result is a direct consequence of the rapid washing-out, with increasing excitation energy, of shell effects associated with entropy [9].

Figure 2 shows the results of calculations of the probabilities $P(\alpha_2)$ for the same nucleus ^{242}Pu and it can be seen that the points of the above

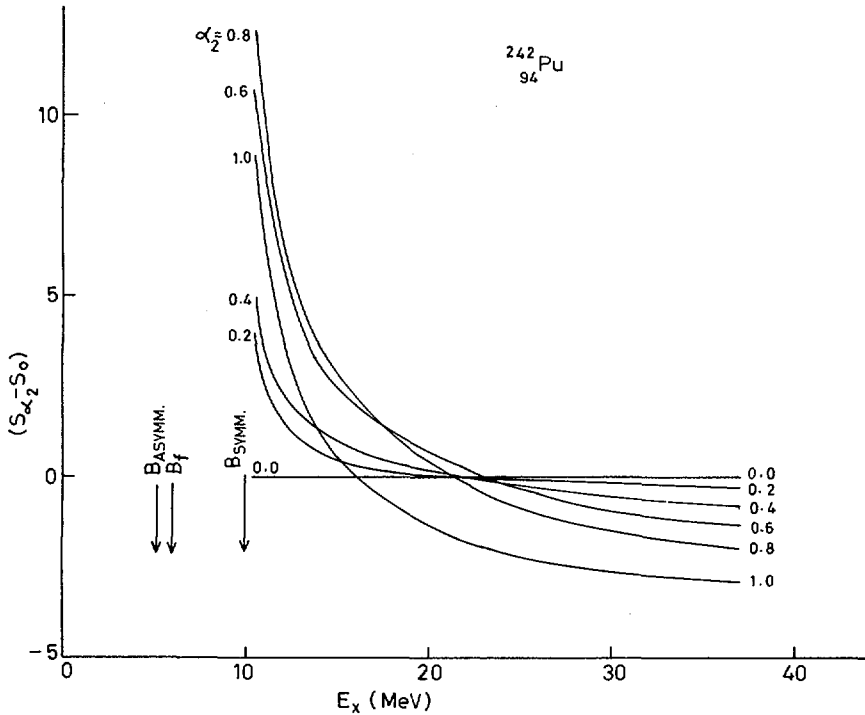


FIG. 1. Plots of the calculated entropy difference ($S_{\alpha_2} - S_0$) of the fissioning nucleus $^{242}_{94}\text{Pu}$ as a function of the compound nucleus excitation energy E_x , where S_{α_2} and S_0 are the entropies for the mass-asymmetric shape specified by the parameter α_2 and for the mass-symmetric shape, respectively, corresponding to the outer barrier deformation.

qualitative discussion are also brought out in this figure. Also shown in Fig. 2 is a plot of the calculated variation of the ratio of the probabilities for the nucleus to go through asymmetric and symmetric shapes as a function of the compound nucleus excitation energy. This plot clearly brings out the rapid filling up of the valley in the mass distribution with excitation energy, resulting in a symmetric mass division at excitation energies exceeding about 30 MeV. It may be pointed out here that the present calculations of $P(\alpha_2)$ versus excitation energy are based on a set of single particle levels corresponding to the second barrier deformation. However, as is pointed out in the next section, the fission transition state itself shifts from the second barrier towards the LDM saddle point with increasing excitation energy. Inclusion of this effect in the present calculations should lead to a more rapid filling up of the valley than indicated in Fig. 2. For lower values of E_x the plots in Fig. 2 are expected to be quantitatively correct since at these values of E_x the transition state coincides with the second barrier. The relation between expected fragment mass ratio and the asymmetry parameter α_2 on the assumption of a "knife-cut" at the middle

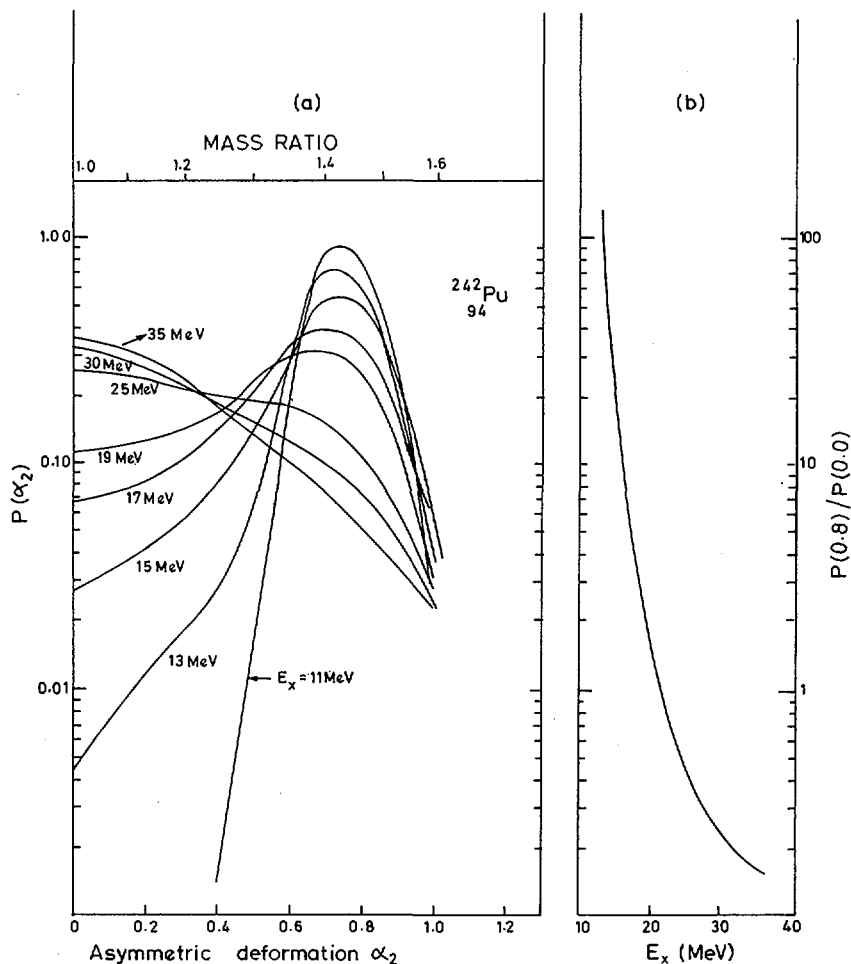


FIG. 2(a). Plots of the probability $P(\alpha_2)$ of the nucleus going through a mass-asymmetric shape α_2 at the outer barrier deformation versus the parameter α_2 for different excitation energies. FIG. 2(b) shows the ratio $P(\alpha_2 = 0.8)/P(\alpha_2 = 0)$ as a function of the excitation energy, showing the variation of the peak-to-valley ratio with excitation energy.

of the nuclear shape at the outer barrier is also indicated in Fig. 2. It is seen that in the range of excitation energies where the mass distributions are asymmetric, the calculated most probable mass ratio is surprisingly close to the experimental value. However, at the lowest excitation energy of 11 MeV for which the present calculations were carried out, the width of the calculated mass distribution is only about 5 mass units, which is considerably smaller than the experimental value. This comparison therefore shows that considerable broadening of the fragment mass distributions

takes place during its descent from the second barrier to scission. It therefore appears that the experimental fragment mass distributions can not be quantitatively understood on the basis of the properties of the transition state of the fissioning nucleus alone, without including the dynamics during the descent from the transition state to scission.

4. STATISTICAL INTERPRETATION OF THE FRAGMENT ANGULAR DISTRIBUTIONS

The presence of shell effects in the deformation potential energy of nuclei introduces a new feature which needs to be taken into account in the statistical interpretation [7] of the fission fragment angular distributions at moderate excitation energies. For nuclei in the actinide region where the shell effects result in a pronounced double-humped fission barrier, the question arises: to which nuclear shape does the effective moment of inertia $\mathcal{I}_{\text{eff}} (= \mathcal{I}_{\parallel} \mathcal{I}_{\perp} / (\mathcal{I}_{\perp} - \mathcal{I}_{\parallel}))$ derived from the analysis of the fragment anisotropies correspond. In near-threshold fission, the anisotropy data show that the angular distributions are characteristic of the states on the top of the second barrier [12]. It has been pointed out earlier [9] that, owing to the washing-out of shell effects with increasing excitation energy, the transition state shape of the nucleus will shift from the second barrier shape towards the LDM saddle shape, and will finally coincide with the

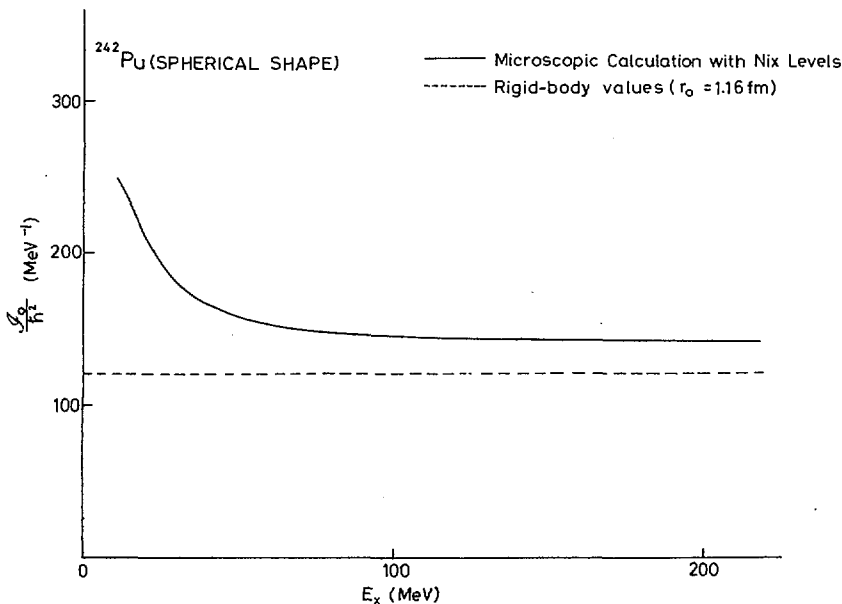


FIG. 3. Results of the numerical calculations of the moment of inertia \mathcal{I}_0 / \hbar^2 versus the excitation energy for a typical case of spherical shape of ^{242}Pu . The dotted line represents the corresponding rigid body value with $r_0 = 1.16$ fm for the radius parameter.

LDM saddle at an excitation energy at which shell effects have completely disappeared. This would imply that \mathcal{J}_{eff} becomes excitation energy dependent not only because of the shell and pairing effects on the moments of inertia for a given shape but also because the shape itself changes with excitation energy. This feature then needs to be included in the interpretation of the parameter $K_0^2 (= \mathcal{J}_{\text{eff}} T / \hbar^2)$ versus excitation energy, derived from the statistical analysis [7] of the fragment anisotropy data.

A calculation of \mathcal{J}_{eff} at a specified excitation energy consequently involves (1) determination of the transition state shape relevant for fragment angular distributions and (2) calculation of \mathcal{J}_{eff} for that nuclear shape. The transition state shapes of the nucleus at a specified excitation energy can

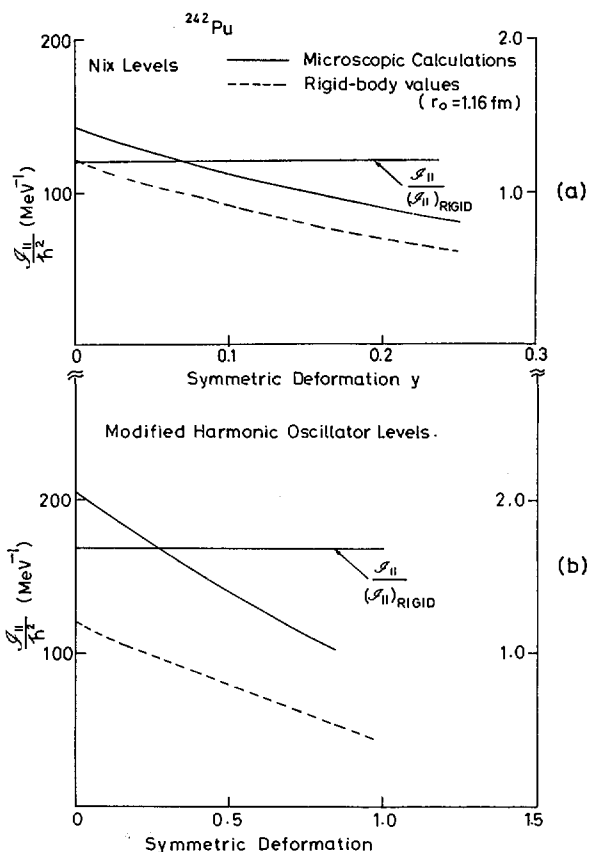


FIG.4. Results of calculations of $\mathcal{J}_{\parallel} / \hbar^2$ as a function of deformation for the nucleus ^{242}Pu . The calculations have been carried out for (a) the single particle levels of Nix and co-workers [5] and (b) the modified harmonic oscillator levels of Seeger and Perisho [14]. The dotted lines represent the corresponding rigid body values with $r_0 = 1.16$ fm. Also shown in the figure is the ratio $\mathcal{J}_{\parallel} / (\mathcal{J}_{\parallel})_{\text{RIGID}}$ as a function of the deformation for both the level schemes.

be located from the map of entropy calculated for different mass-asymmetric shapes α_2 for each elongation parameter y , from the criterion of minima in the locus of conditional maxima with respect to the coordinate α_2 for different elongation parameters y . Such calculations are now possible with the availability of single particle levels for different nuclear shapes, which are required as inputs for the calculation of entropy. Having located the transition state shape, microscopic calculation of \mathcal{S}_{eff} can then be carried out starting with the single particle levels for the appropriate nuclear shape. It is also pointed out in the following discussions that these calculations should incorporate a normalization procedure for the calculations of the moments of inertia from single particle levels.

Figure 3 shows the results of numerical calculations of the moment of inertia \mathcal{J}_0/\hbar^2 versus excitation energy on the basis of Eqs (1-4) for a typical case of a spherical shape of ^{242}Pu . It is seen that, after the disappearance of shell effects, \mathcal{J}_0/\hbar^2 asymptotically reaches a constant value which should be identified with the rigid body value. It is found that this asymptotic value in the present calculation corresponds to a radius parameter $r_0 = 1.27$ fm which is also nearly equal to the sharp surface radius parameter of the potential used to generate the input single particle levels. This value of r_0 , however, differs from the value 1.16 fm which is known to represent better the spatial properties of nuclei [13]. The above discrepancy arising from the non-self-consistent nature of the shell model calculations of single particle levels shows that reliable calculations of moments of inertia based on shell model level schemes should incorporate a normalization procedure to ensure that the asymptotic values of \mathcal{J}_0/\hbar^2 correspond to the rigid body values corresponding to the radius parameter $r_0 = 1.16$ fm. However, such a normalization procedure is useful only if the normalization constant is independent of nuclear deformation. Figure 4 shows the results of calculations of $\mathcal{J}_{\parallel}/\hbar^2$ as a function of deformation for the same nucleus ^{242}Pu for the single particle levels of Nix and co-workers [5] and also for the modified harmonic oscillator levels of Seeger and Perisho [14] along with the rigid body values for $r_0 = 1.16$ fm. It can be seen that, for both the level schemes, the quantity $\mathcal{J}_{\parallel}/\hbar^2$ exceeds the rigid body estimates and these differences can be directly traced to the different $\langle r^2 \rangle$ of the single particle potentials in the two cases. However, it is seen that the normalization factor $C = (\mathcal{J}_{\parallel})/(\mathcal{J}_{\parallel})_{\text{rigid}}$ is almost independent of the deformation, although the magnitude of C is itself different in the two cases. The calculated values of $\mathcal{J}_{\parallel}/\hbar^2$ versus the excitation energy E_x for any deformation should therefore be divided by the factor C to ensure the correct asymptotic value of the quantity $\mathcal{J}_{\parallel}/\hbar^2$. Similar renormalization will also be required in the calculations of moments of inertia, $\mathcal{J}_{\perp}/\hbar^2$, perpendicular to the nuclear symmetry axis.

For the same reasons as mentioned above, the level density parameter a derived from the asymptotic values of the calculated thermodynamic quantities needs to be normalized to a value corresponding to the radius parameter $r_0 = 1.16$ fm, which can be done on the basis that a is proportional to r_0^2 . Since the parameter K_0^2 characterizing fragment anisotropies is given by

$$K_0^2 = \frac{\mathcal{J}_{\text{eff}}}{\hbar^2} T \approx \frac{\mathcal{J}_{\text{eff}}}{2} \left(\frac{E_x}{a} \right)^{1/2}$$

it follows that a microscopic calculation of K_0^2 will be nearly proportional to the input radius parameter $\langle r^2 \rangle^{1/2}$ of the potential used to generate the single particle levels, and therefore needs to be normalized to the radius parameter r_0 of the actual nucleon density distribution. Without incorporating the above normalization procedure, the microscopic calculations could lead to a significant overestimate of K_0^2 , which when compared with "experimental" values of K_0^2 might result in misleading conclusions regarding the transition state shape. In some earlier work [15, 16] the microscopically calculated values of K_0^2 versus the excitation energy for the shape corresponding to the second barrier have been found to fit the experimental values of K_0^2 up to about 30 MeV barrier excitation energy, but this agreement appears to be due to a larger value of $\langle r^2 \rangle$ of the input level schemes. It is shown below that at $E_x \sim 37$ MeV, the transition state shape is expected to be quite different from the second barrier shape and coincides very nearly with the LDM saddle shape.

It has been shown in an earlier section that at $E_x \gtrsim 25$ MeV the fissioning nucleus predominantly goes through mass-symmetric shapes at the second barrier. Therefore, at these excitation energies, the transition state can be located from the calculated entropy S versus excitation energy E_x considering only the symmetric deformation parameter y . The results of these calculations for the typical case of the fissioning nucleus ^{242}Pu are shown in Fig. 5. For these calculations the deformation potential energy as a function of symmetric deformation was obtained with the use of the LDM parameters of Pauli and Ledergerber [17] for the smooth part and the shell corrections calculated by Nix and co-workers [5]. For this nucleus the fissility parameter $x = 0.805$ and therefore the LDM saddle point is at the deformation $y = 1 - x = 0.195$. It can be seen from the figure and the insert that with increasing excitation energy the transition state point (minimum entropy point) gradually shifts from the second barrier to the LDM saddle point and, at $E_x \sim 40$ MeV, the transition state point coincides with the LDM saddle point.

It should be pointed out here that the excitation energy at which the transition state shape coincides with the LDM saddle shape depends on the shape of the LDM potential energy surface and thereby on the LDM parameters used. Some recent calculations for the same nucleus by Vandenbosch [16] show that the LDM saddle point is reached only at $E_x \sim 65$ MeV, but this appears to be due to the use of LDM parameters which are different from the more reliable Pauli-Ledergerber parameters since these latter parameters were extracted from fission barrier systematics. It is further shown below that the experimental results of fragment anisotropies for a wide variety of nuclei in the actinide region at excitation energies $E_x \sim 37$ MeV present convincing evidence that, for these fissioning nuclei, the transition state shape coincides very nearly with the LDM saddle point shape at these energies.

The first-chance anisotropy values for a number of actinide nuclei have been obtained by Reising and co-workers [18] for the case of 42.8-MeV alpha-induced fission. These anisotropy values were used to determine the parameter K_0^2 on the basis of the statistical theory [7, 19], neglecting the effect of target spin. From the values of K_0^2 thus obtained for each case, the values of \mathcal{J}_{eff} were determined. The values of the temperature T used were those corresponding to the excitation energy at the LDM saddle point deformation and were obtained from the numerical thermodynamic

calculations with single particle level schemes of Nix and co-workers [5] after normalization to correspond to $r_0 = 1.16$ fm. The pairing effects were approximately taken into account by subtracting a condensation energy equal to $\frac{1}{2}g\Delta_0^2 - k\Delta_0$ from the excitation energy, where $k=0$ for even nuclei and 1 for odd-mass nuclei, $\Delta_0 = 11/\sqrt{A}$ MeV, and the single particle level density g is that corresponding to the level scheme used. The moment of inertia \mathcal{J}_0 for the spherical shape was also calculated with $r_0 = 1.16$ fm.

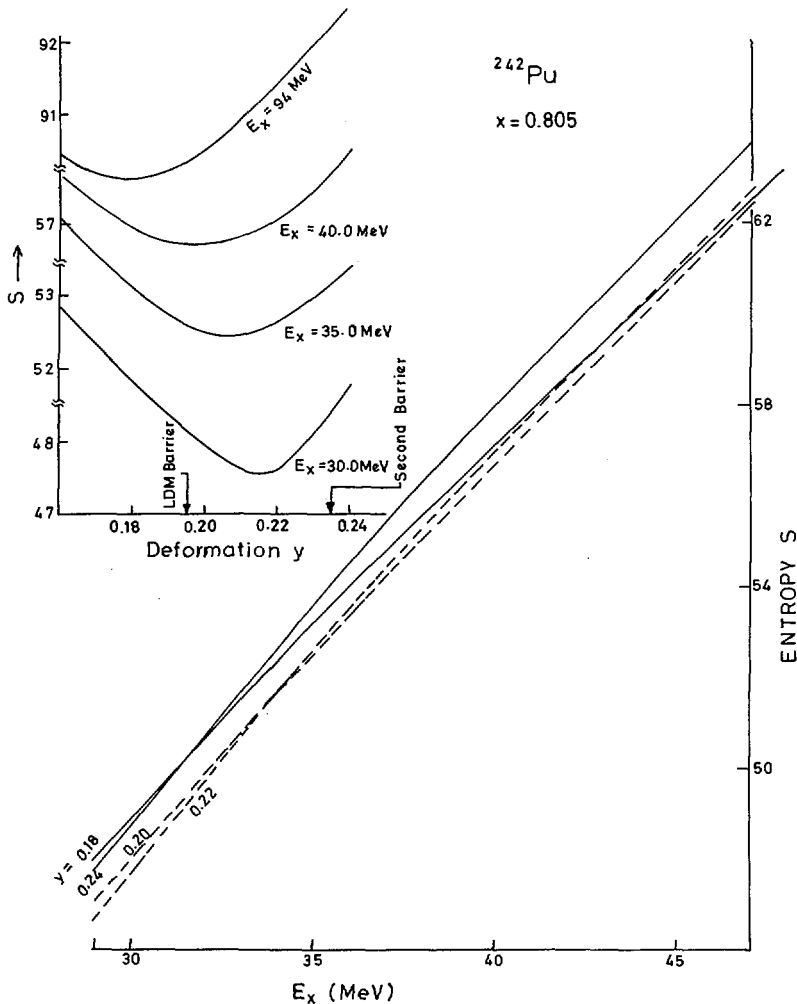


FIG. 5. Plots of calculated entropy S for the nucleus ^{242}Pu as a function of the compound nucleus excitation energy E_x for different values of the symmetric deformation parameter γ . The insert shows entropy S versus deformation parameter γ , for specified values of E_x .

Assuming that the transition state shape corresponds to the LDM saddle point, each value of $\mathcal{S}_0/\mathcal{S}_{\text{eff}}$ was converted to give the fissility parameter x of the nucleus on the basis of the liquid drop model without curvature correction. Figure 6 shows the values of the parameter $\xi = (Z^2/A)/x$ derived in this manner versus the isospin parameter $I^2 = (N - Z/A)^2$. It can be seen from Fig. 6 that the values of ξ derived in this manner from anisotropy data even bring out the expected isospin dependence of the surface energy. It should be pointed out that part of the scatter in the data points can be ascribed to the effect of target spin which was not included in the above analysis. In fact, the points showing maximum deviation from the average trend do correspond to targets with spins of 5/2 and 7/2. The curves based on the Pauli and Ledergerber [17] and Myers and Swiatecki [20] LDM parameters are also shown in the figure for the sake of comparison. In spite of appreciable errors on the "experimental" points, it is seen that the anisotropy data are in good agreement with the Pauli-Ledergerber LDM parameters. It should be pointed out that if in fact, at excitation energies of about 37 MeV encountered in these experiments, the transition state was either at the second barrier or between the second barrier and the LDM saddle point, the above analysis should lead to values of ξ significantly higher than the LDM predictions, whereas it in fact leads to values of ξ even smaller than those shown in Fig. 6 if the temperature T is

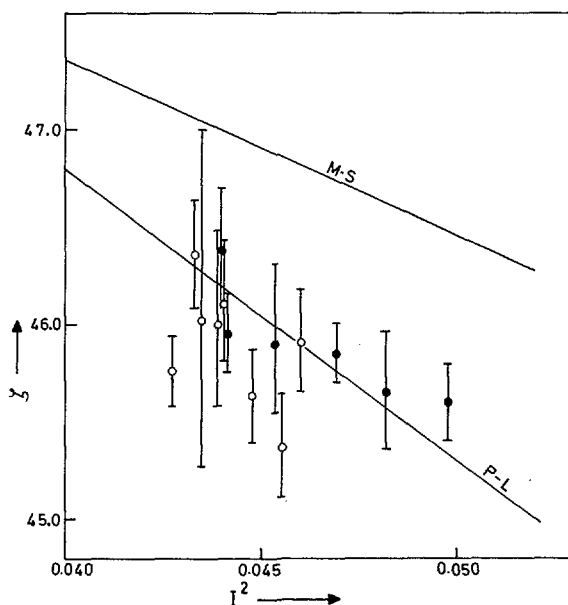


FIG. 6. The values of $\xi = (Z^2/A)/x$ versus $I^2 = ((N - Z/A)^2)$ for a number of nuclei in the actinide region derived from the first-chance anisotropy values given by Reising and co-workers [18]. The open points refer to nuclei with non-zero target spin. The expected isospin dependence of ξ based on the Pauli and Ledergerber (P-L) [17] and Myers and Swiatecki (M-S) [20] liquid drop parameters are also shown in the figure.

evaluated at the second barrier deformation. Considering that the experimental points are well below the Myers-Swiiatecki curve and lie almost on the Pauli-Ledergerber curve, it can be concluded that, even at compound nucleus excitation energies of about 37 MeV, the fission transition state relevant for fragment angular distributions indeed almost coincides with the LDM saddle point shape. The same conclusions were reached on the basis of results of Fig. 5 where, at $E_x \sim 40$ MeV, the transition state point (minimum entropy point) is found to coincide with the LDM saddle point. There is, however, one feature of the results shown in Fig. 5 which is somewhat puzzling. It is seen that as the excitation energy is further increased, the minimum entropy point further shifts at excitation energy of about 90 MeV to a deformation $y = 0.18$ which remains the minimum entropy point even at higher excitation energies. The reason for this small further shift of the minimum entropy point towards a lower deformation ($y = 0.18$) at these excitation energies are at present under investigation. One possibility is that this further shift inside the LDM saddle is spurious since this can arise due to small errors of about 0.5 MeV in the relative values of the shell corrections for the deformations $y = 0.18$ and 0.20 and uncertainties of this order are known to be present in the shell correction values given by the Strutinsky smearing procedure.

5. CONCLUSIONS

In general, the transition state of an excited fissioning nucleus is to be located by finding the minima in the locus of conditional maxima of entropy for different nuclear elongations. For nuclei with significant shell corrections at the fission barrier, this introduces an excitation energy dependence of the transition state shape. One of the consequences of this feature is that fissioning nuclei in the actinide region go predominantly through a mass-asymmetric shape at low excitation energies and through a mass-symmetric shape at excitation energies exceeding about 25 MeV. On the assumption that the probabilities of the nucleus fissioning through different mass-asymmetric shapes at the second barrier are proportional to the respective level densities, it is shown that the observed systematics in the excitation energy dependence of fragment mass distributions can be understood on the basis of the present numerical calculations of level densities without involving any free parameters. These calculations also bring out that considerable broadening of the fragment mass distributions take place during the descent from the second barrier to scission, pointing out the need for the inclusion of dynamics for a quantitative understanding of the mass distributions. The present investigations have also shown that with increasing excitation energy the transition state shape of a typical nucleus ^{242}Pu gradually shifts from the second barrier towards the LDM barrier and, at excitation energies of about 40 MeV, it almost coincides with the LDM saddle point. It is also shown that the fragment anisotropy data for nuclei in the actinide region contain strong evidence to this effect.

ACKNOWLEDGEMENTS

We are grateful to Dr. R. Ramanna for his keen interest in this work and for several useful discussions. We thank Dr. J. R. Nix for providing

us with the single particle level schemes used in this work. We also gratefully acknowledge fruitful correspondence with Dr. R. Vandenbosch pertaining to some points discussed in this work.

REFERENCES

- [1] NIX, J.R., *Annu. Rev. Nucl. Sci.* **22** (1972) 65, and references therein.
- [2] BRACK, M., DAMGAARD, J., JENSEN, A.S., PAULI, H.C., STRUTINSKY, V.M., WONG, C.Y., *Rev. Mod. Phys.* **44** (1972) 320, and references therein.
- [3] MÖLLER, P., NILSSON, S.G., *Phys. Letters* **31B** (1970) 283.
- [4] PAULI, H.C., LEDERGERBER, T., BRACK, M., *Phys. Lett.* **34B** (1971) 264.
- [5] BOLSTERLI, M., Fiset, E.O., NIX, J.R., NORTON, J.L., *Phys. Rev.* **C5** (1972) 1050; and Nix, J.R., private communication.
- [6] TSANG, C.F., WILHELMY, J.B., *Nucl. Phys.* **A184** (1972) 417.
- [7] HALPERN, I., STRUTINSKY, V.M., *Int. Conf. peaceful Uses atom. Energy* (Proc. Conf. Geneva, 1958) **15**, UN, New York (1958) 408.
- [8] BOHR, N., WHEELER, J.A., *Phys. Rev.* **56** (1939) 426.
- [9] RAMAMURTHY, V.S., KAPOOR, S.S., KATARIA, S.K., *Phys. Rev. Lett.* **25** (1970) 386.
- [10] HUIZENGA, J.R., MORETTO, L.G., *Annu. Rev. Nucl. Sci.* **22** (1972) 427, and references therein.
- [11] RAMAMURTHY, V.S., RAMANNA, R., "Mass and charge distributions", *Physics and Chemistry of Fission* (Proc. Symp. Vienna, 1969), IAEA, Vienna (1969) 41.
- [12] STRUTINSKY, V.M., PAULI, H.C., "Shell-structure effects in the fissioning nucleus", *Ibid.*, p. 155.
- [13] MYERS, W.D., *Nucl. Phys.* **A145** (1970) 387.
- [14] SEEGER, P.A., PERISHO, R.C., Los Alamos Scientific Laboratory Rep. LA-3751, (1967).
- [15] SANO, M., WAKAI, M., *Prog. Theor. Phys.* **48** (1972) 160.
- [16] VANDENBOSCH, R., *Phys. Rev.* **C7** (1973) 2092.
- [17] PAULI, H.C., LEDERGERBER, T., *Nucl. Phys.* **A175** (1971) 545.
- [18] REISING, R.F., BATE, G.L., HUIZENGA, J.R., *Phys. Rev.* **141** (1966) 1161.
- [19] HUIZENGA, J.R., BEHKAMI, A.N., MORETTO, L.G., *Phys. Rev.* **177** (1969) 1826.
- [20] MYERS, W.D., SWIATECKI, W.J., *Ark. Fys.* **36** (1967) 343.

DISCUSSION

R. W. HASSE: I think the discrepancies mentioned in your paper may arise from the fact that your calculations are inconsistent insofar as you only take into account the smearing out of shell effects with increasing compound nuclear temperature but not the equally important dependence of the liquid-drop potential on temperature. Recently, we performed calculations on this subject with a modified Thomas-Fermi model,¹ and naturally obtained the result that the surface tension and the nuclear equilibrium density decreases with increasing temperature (the latter due to the nucleus being more easily compressed). Thus, for example, the fission barrier of ²³⁶U at a temperature of 2 MeV is decreased by about 2 MeV and its corresponding saddle point shape is less necked-in, giving rise to larger $\mathcal{I}_{\text{eff}}/\mathcal{I}_0$ values.

S. S. KAPOOR: Let me first point out that there is no discrepancy between the results of our analysis of anisotropy data and the LDM predictions, if Pauli-Ledergerber LDM coefficients are used. The temperature involved here is only about 1 MeV, and probably the effects you pointed out become significant only at higher temperatures. In fact, your results showing that

¹ HASSE, R.W., STOCKER, W., *Phys. Lett.* **44B** (1973) 26.

LDM \mathcal{J}_{eff} values increase with temperature appear to explain some of our earlier Berkeley results on fragment anisotropy, where an increase of \mathcal{J}_{eff} with temperature in the region of 1 to 2 MeV was indicated.

M.G. MUSTAFA: I think Mr. Kapoor and Mr. Hasse are going in two different directions. I believe the problem could be resolved by including temperature effects in the liquid-drop model, if it is important, and then by a thorough investigation of the shell correction energy in the statistical model and also in the Strutinsky method.

FISSION OF ^{238}U , ^{209}Bi AND ^{197}Au WITH INTERMEDIATE-ENERGY ^4He IONS*

V.E. VIOLA, Jr., M.M. MINOR**, C.T. ROCHE, R.G. CLARK
Department of Chemistry,
University of Maryland,
College Park, Md.,
United States of America

Abstract

FISSION OF ^{238}U , ^{209}Bi AND ^{197}Au WITH INTERMEDIATE-ENERGY ^4He IONS.

The fission of ^{238}U , ^{209}Bi and ^{197}Au induced by 140- and 150-MeV ^4He ions has been studied in order to investigate the dependence of the effective moment of inertia at the fission saddle point on excitation energy. Particular emphasis has been placed on the investigation of the reaction mechanism which produces the fissioning species in these systems. From fission fragment angular correlation measurements it is found that $49.3 \pm 4.4\%$ of the fission in ^{238}U results from the formation of a compound nucleus. The non-compound nucleus component of the fission cross-section includes a large fraction of high linear momentum transfer events, presumably produced in reactions where pre-equilibrium decay is highly probable. The fission of ^{197}Au and ^{209}Bi with 140-MeV ^4He ions is found to proceed almost completely via a compound nucleus mechanism. Examination of the forward-backward symmetry of the angular distributions measured in this work substantiates the angular correlation results. From the anisotropy in the angular distributions, values for $\mathcal{J}_{\text{eff}}/\hbar^2 a_f^2$ have been determined. These calculations have included corrections for the effects of non-compound nucleus mechanisms on the orbital angular momentum distribution of the fissioning nuclei and for neutron evaporation prior to fission. Contrary to earlier work, we find that $\mathcal{J}_{\text{eff}}/\hbar^2 a_f^2$ is constant within the uncertainties of the calculation.

1. INTRODUCTION

The measurement of fission fragment angular distributions at moderate excitation energies provides an important means of deducing information concerning the nuclear shape which characterizes the fission transition state. By selection of appropriate projectile-target combinations and projectile energies it is possible to study the dependence of saddle point shapes upon the fissility parameter Z^2/A and on excitation energy and to compare these results with the predictions of fission theory [1-4]. The theoretical treatment of fission fragment angular distribution data at moderate excitation energies, where statistical considerations should be valid, was originally proposed by Halpern and Strutinski [5] and by Griffin [6]. Recently, Huizenga, Behkami and Moretto [7] have modified the expressions of Refs. [5,6] and show that the fission angular

* Work supported by US Atomic Energy Commission Contract AT-(40-1)-4028.

** Present address: Los Alamos Scientific Laboratory, Los Alamos, N. Mex., USA.

distribution $W(\theta)$ for the case of spinless projectile and target nuclides can be expressed as

$$W(\theta) \propto \sum_{I=0}^{\infty} \frac{(2I+1)^2 T_I \exp[-(I+\frac{1}{2})^2 \sin^2 \theta / 4K_O^2] J_0[i(I+\frac{1}{2})^2 \sin^2 \theta / 4K_O^2]}{\text{erf}[(I+\frac{1}{2}) / (2K_O^2)^{1/2}]} \quad (1)$$

where θ is the center-of-mass angle of the fragments.

Here J_0 is the zero-order Bessel function of imaginary argument and erf is the standard error function. The total angular momentum of the fissioning nucleus I is equal to the reaction orbital angular momentum $l = \ell$ and T_I represents the transmission coefficient for each ℓ -state. The projection of I on the symmetry axis of the fissioning nucleus is given by the quantum number K and K_O^2 represents the variance of the distribution in K -states, which is assumed to be Gaussian. The quantity K_O^2 is given by

$$K_O^2 = \mathcal{I}_{\text{eff}} T / \hbar^2 \quad (2)$$

where T is the nuclear temperature and \mathcal{I}_{eff} is the effective moment of inertia defined by

$$\mathcal{I}_{\text{eff}} = \mathcal{I}_{\parallel} \mathcal{I}_{\perp} / (\mathcal{I}_{\perp} - \mathcal{I}_{\parallel}) \quad (3)$$

Here \mathcal{I}_{\parallel} and \mathcal{I}_{\perp} are the respective moments of inertia about axes parallel and perpendicular to the fission axis.

Reising et al. [3] have shown that the agreement between experimental and theoretical \mathcal{I}_{eff} values as a function of Z^2/A is generally good, except at high Z^2/A values where the experimental values are larger than predicted by liquid drop model calculations. Vandenbosch [8] has recently attributed this effect to the influence of the outer fission barrier on fission fragment anisotropies. Although the dependence of \mathcal{I}_{eff} on Z^2/A seems consistent with theory, the behavior of \mathcal{I}_{eff} as a function of excitation energy remains poorly understood. From Eq. (2) a simple Fermi gas model predicts that the measureable quantities, K_O^2 and the excitation energy above the fission saddle point, E_f^* , can be expressed as the following ratio

$$\frac{K_O^2}{(E_f^*)^{1/2}} = \frac{\mathcal{I}_{\text{eff}}}{\hbar^2 a_f^{1/2}} \quad (4)$$

where a_f is the level density parameter appropriate to states which undergo fission. The fission excitation energy is defined by $E_f^* = (E^* - E_f^B - E_{\text{ROT}})$ where E^* is the total excitation energy, E_f^B is the fission barrier and E_{ROT} is the rotational energy. Theoretical calculations [9,10] indicate that \mathcal{I}_{eff} should be approximately independent of excitation energy and hence the ratio $K_O^2/(E_f^*)^{1/2}$ should be constant for a given fissioning system. However, the results of Kapoor et al [10] have shown that $K_O^2/(E_f^*)^{1/2}$ increases by a factor of two

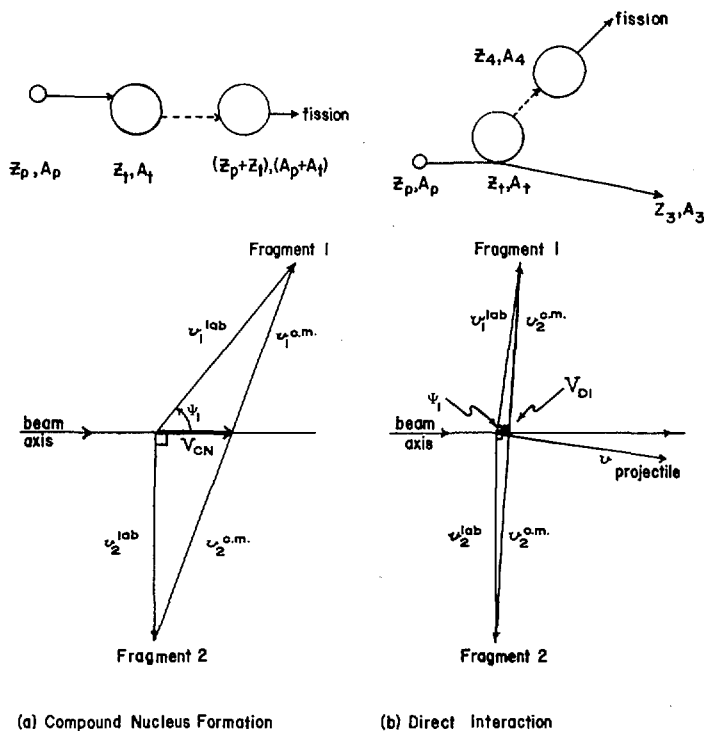


FIG. 1. Schematic and vector diagrams representing binary fission reactions preceded by (a) compound nucleus formation and (b) direct interaction (NCN). In the vector diagram, V is the velocity of the fissioning nucleus and v^{lab} and $v^{\text{c.m.}}$ are the laboratory and center-of-mass velocities of the fission fragments respectively. The laboratory angle ψ_2 for fragment 2 is fixed in these experiments at 270° and ψ_1 represents the correlation angle of the complementary fragment 1. The center-of-mass transformation parameter is $X^2 = (V/v^{\text{c.m.}})^2$.

for ^{238}U fission with ^4He ions between the energies of 23 and 115 MeV. Kapoor concluded from his data that either the theoretical calculations of \mathcal{I}_{eff} must be in error or that the results implied a breakdown in the statistical assumptions used in the angular distribution theory. Vandenbosch [8] has suggested that this behavior may represent a possible transition from the second barrier to the liquid drop barrier in higher excitation energy fission.

The purpose of the present research has been to investigate the behavior of \mathcal{I}_{eff} on excitation energy by performing studies of fission induced in ^{238}U , ^{209}Bi and ^{197}Au by 140-MeV ^4He ions. Particular emphasis has been placed on understanding the nuclear reaction mechanism which generates the fissioning species in order that the best possible values for the transmission coefficients, T_1 , can be derived for use in Eq. (1). The fission fragment angular correlation technique [11,12], illustrated in Figure 1, has been used for the reaction mechanism studies. This technique takes advantage of the dependence of the angle between coincident fragments on the linear momentum

imparted to the fissioning nucleus by the incident bombarding particle. From the angular correlation studies on ^{238}U a linear momentum transfer distribution is obtained for the fissioning nuclei, which can then be utilized to interpret the measured angular distributions for ^{238}U , ^{209}Bi and ^{197}Au fission at these energies. The results are then compared with those obtained at lower excitation energies.

2. EXPERIMENTAL TECHNIQUES

Three types of experiments were performed in this work: (1) fission-fragment angular correlation measurements, which provided information concerning the target-projectile reaction mechanism, (2) fission fragment angular distribution measurements which were analyzed to obtain K_0^2 values, and (3) the total fission cross-section for the ^{238}U plus 140-MeV ^4He ion system, which was needed to predict the λ -wave distribution in the reaction from an optical model fit to the data. All measurements were carried out in a 75 cm diameter scattering chamber using a magnetically analyzed and focused beam of 140-MeV or 150-MeV ^4He ions from the University of Maryland Cyclotron. Isotopically enriched ^{238}U and monoisotopic ^{209}Bi and ^{197}Au targets having thicknesses in most cases of 80 to 140 $\mu\text{g}/\text{cm}^2$ were prepared by vacuum evaporation onto carbon films of 20 to 100 $\mu\text{g}/\text{cm}^2$ thickness.

The angular correlation experiments were performed using a heavy-ion surface-barrier semiconductor detector in coincidence with a 50 mm long position-sensitive semiconductor detector, placed at the appropriate correlation angles for binary fission from these systems [11]. The heavy-ion detector was placed at -90° deg with respect to the beam axis in all cases and had an angular acceptance of $\pm 0.7^\circ$ deg. The position detector intercepted approximately $\pm 10^\circ$ deg of the reaction plane and was covered by a 15-slit collimator, each slit having an angular acceptance of $\pm 0.2^\circ$ deg. Appropriate corrections (less than 4.3 percent in all cases) for angular geometry were applied to the data derived from this arrangement.

A schematic diagram of the detector arrangement and the associated electronics for this three-parameter experiment is shown in Fig. 2. In Fig. 3 a two-dimensional position versus energy spectrum and the one-dimensional projection of each parameter is shown for a ^{252}Cf calibration source incident upon a surface-barrier position detector, covered by an eleven-slit collimator. Angular correlation measurements were performed with the longitudinal axis of the position detector in the reaction plane formed by the beam and the heavy-ion detector placed at -90° deg (planar events) and with the position detector rotated perpendicular to this reaction plane (non-planar events). The non-planar measurements were necessary to insure that reactions which did not involve formation of a compound nucleus (NCN, or non-compound nucleus reactions) and which possess linear momentum components out of the reaction plane, were properly accounted for. In performing the planar measurements, care was taken to insure the systematic accuracy of the angular correlation obtained for each target nuclide by keeping both detector angles fixed during the measurement of each series of targets. Targets were alternated by means of a remote-controlled target ladder, which kept the target angle fixed at 45° to the beam

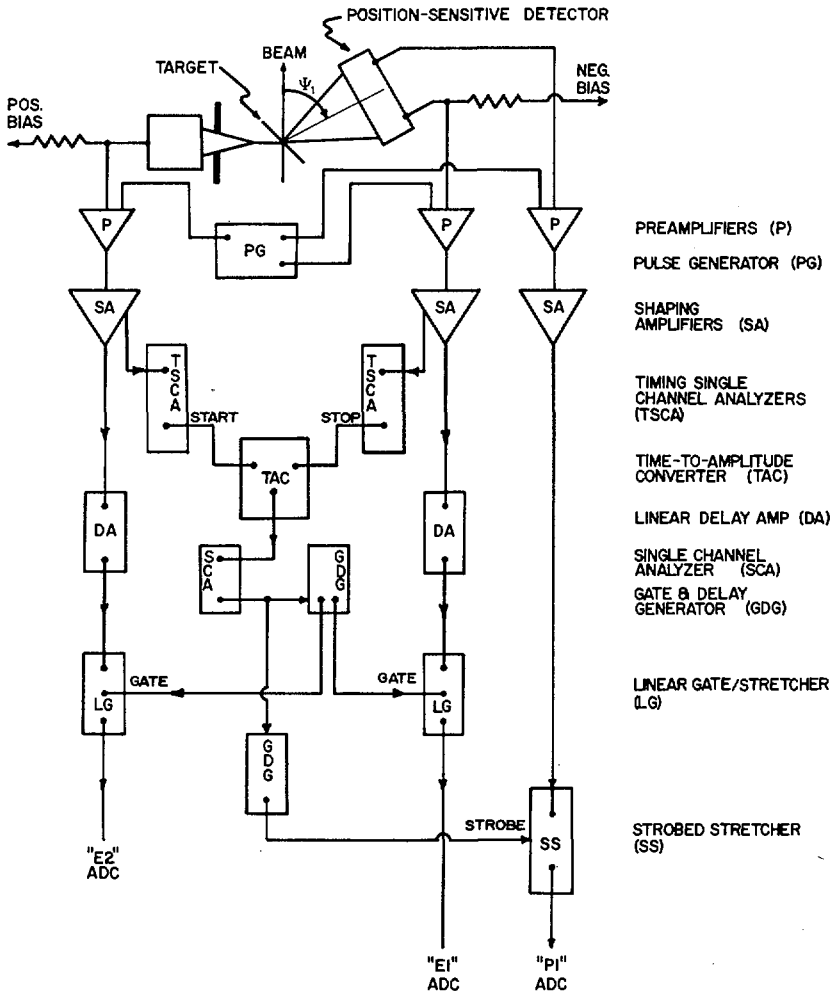


FIG. 2. Schematic diagram of electronics used in fission fragment correlation experiments.

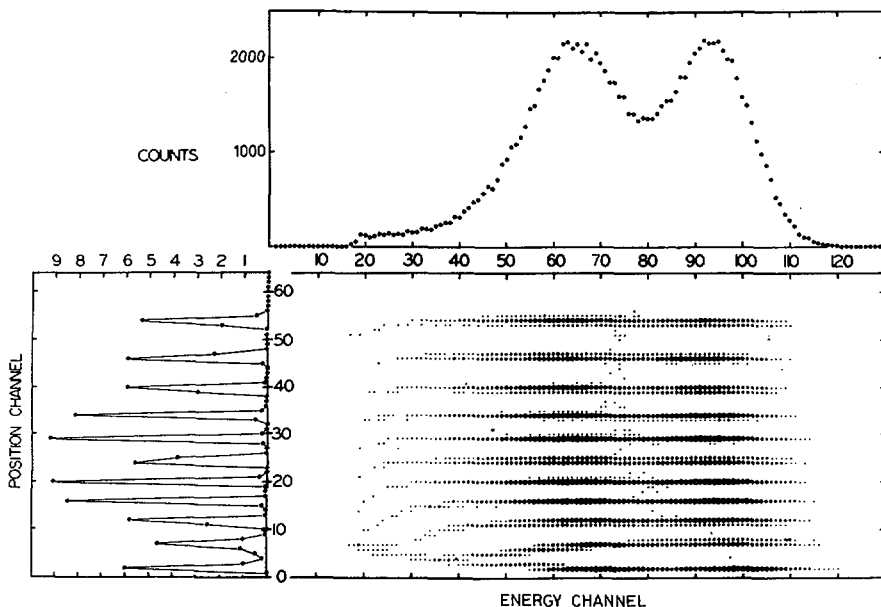


FIG. 3. Display of ^{252}Cf calibration data with an eleven-slit collimator. In the lower right-hand drawing a two-dimensional display of the position versus energy spectrum is shown. At the lower left, the projection of this spectrum on the position axis is given, i.e. the position singles spectrum. The upper drawing represents the projection of the two-dimensional spectrum on the energy axis, i.e. the gross fission kinetic energy spectrum.

axis. At least two separate angular correlation measurements were performed for each target system to eliminate the possibility of electronic effects on the data. The results agreed to within ± 0.1 deg for the most probable fragment correlation angle and ± 0.2 deg for the full-width-at-half-maximum (FWHM) of the correlation. For the broader correlation observed with the uranium target, measurements were carried out at several position detector angles between 75 deg and 90 deg. Non-planar measurements were made only at the most probable correlation angle for gold and bismuth targets, but for the more complex uranium correlation, data were taken at 2-deg intervals from 68 deg to 92 deg. Most of the non-planar measurements on ^{238}U were performed with 150-MeV ^4He ions, but comparison of results from the two energies showed them to be identical within the experimental limits of error.

The three coincident signals from each event—position detector energy E_1 and position P_1 and fixed detector energy E_2 —were fed into three 4096-channel analogue-to-digital converters and the data were processed using the IBM 360/44 on-line computer at the Maryland Cyclotron. Data were also stored sequentially on magnetic tape, providing all possible correlations of the three parameters. The results presented here are restricted to

the position-energy portion of the data. Data were recorded similarly in the single parameter experiments described below.

Fragment angular distributions for ^{238}U , ^{209}Bi and ^{197}Au bombarded by 140-MeV ^4He ions were determined using two independent heavy-ion detectors with an angular acceptance of ± 0.7 deg. Targets were oriented at a 45° angle to the beam direction. One detector recorded fission fragment spectra at several angles in the laboratory system, Ψ and $(\Psi + 180 \text{ deg})$, where Ψ ranged from zero to 90 deg with respect to the beam axis. This provided angular distribution data from both forward and backward hemispheres, in order to test for symmetry about 90 deg in the center of mass system, discussed in Section 4. A second detector measured spectra at a constant angle of 90° and served as a monitor, along with the beam current integrator, for use in normalization of data taken with the movable detector. The total fission cross-section for ^{238}U bombarded by 140-MeV ^4He ions was measured using targets of 165, 162 and $498 \mu\text{g}/\text{cm}^2$ respectively. Two separate detectors with accurately determined geometries were used to record spectra at two different angles for each target. From a knowledge of the integrated beam current, counting rates, detector geometries, target thicknesses and the measured angular distributions, a total fission cross-section of

$$\sigma_f = 2760 \pm 244 \text{ mb}$$

was determined.

3. REACTION MECHANISM RESULTS

The comparative results of the fission-fragment angular correlation measurements for the three systems studied in this work are shown in Fig. 4, which presents the planar angular correlation data, and Fig. 5, which is a contour diagram showing both the planar and non-planar components of the angular correlations. The correlation parameters derived from the data are summarized in Table I. The calculated most probable correlation angle, Ψ_{mp} , for reactions in which a compound nucleus is formed are indicated by arrows in Fig. 4 and dots in Fig. 5 for each target. The relative error in the correlation angles for the three targets is $\pm 0.1 \text{ deg}$ and the absolute angles are known to $\pm 0.3 \text{ deg}$. For reactions induced in heavy elements by 140-MeV ^4He ions, the linear momentum transferred to the fissioning nucleus from the incident projectile, p_{fN} , can be expressed in terms of the correlation angle Ψ (as defined in Sect. 2) by the approximate function

$$p_{\text{fN}} \propto \left(\frac{\pi}{2} - \Psi\right),$$

where $\Psi = \Psi_{\text{mp}}$ represents complete momentum transfer and $\Psi = \pi/2$ represents zero momentum transfer. An inherent symmetric dispersion in the correlation functions for a given value of p_{fN} arises from the kinematic effects of two factors: (1) mass asymmetry of the fragments and (2) neutron evaporation from the fragments or the fissioning nucleus.

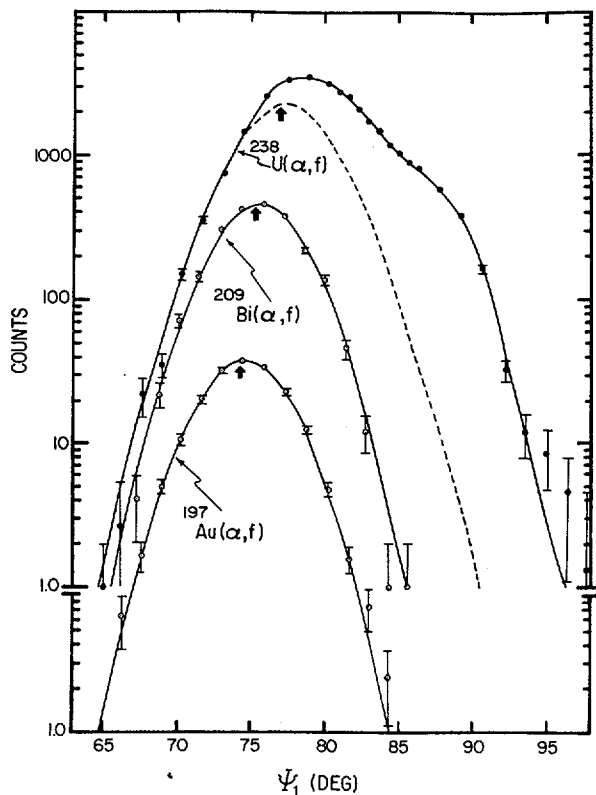


FIG. 4. Angular correlations for the fission of ^{238}U , ^{209}Bi and ^{197}Au with 140-MeV ^4He ions. Data were taken in the reaction plane and represent the coincidence counting rate as a function of correlation angle, ψ_1 , defined in Fig. 1. Arrows indicate the position of the most probable correlation angle calculated from kinematics for each system. The solid curves for the ^{209}Bi and ^{197}Au targets (data: open circles) are empirically fitted functions described in text. The dashed curve for ^{238}U fission is that predicted from systematics for fission following compound nucleus formation. The solid curve for ^{238}U is calculated from the linear momentum distribution shown in Fig. 7.

From examination of the ^{209}Bi and ^{197}Au data it is concluded that the fission of these nuclides with 140-MeV ^4He ions proceeds almost completely via a compound nucleus reaction mechanism. The most probable correlation angles for these two systems coincide with the value calculated under the assumption of compound nucleus formation, within the limits of experimental error. Further, the correlation functions $y(x)$ are symmetric about the most probable correlation angle, whereas if any appreciable amount of fission resulted following incomplete momentum transfer, these functions would be skewed toward 90 deg. This conclusion does not agree with the conclusions of Bimbot and LeBeyec [13] from studies of intermediate energy reactions in lead isotopes. The ^{197}Au and ^{209}Bi results are described well

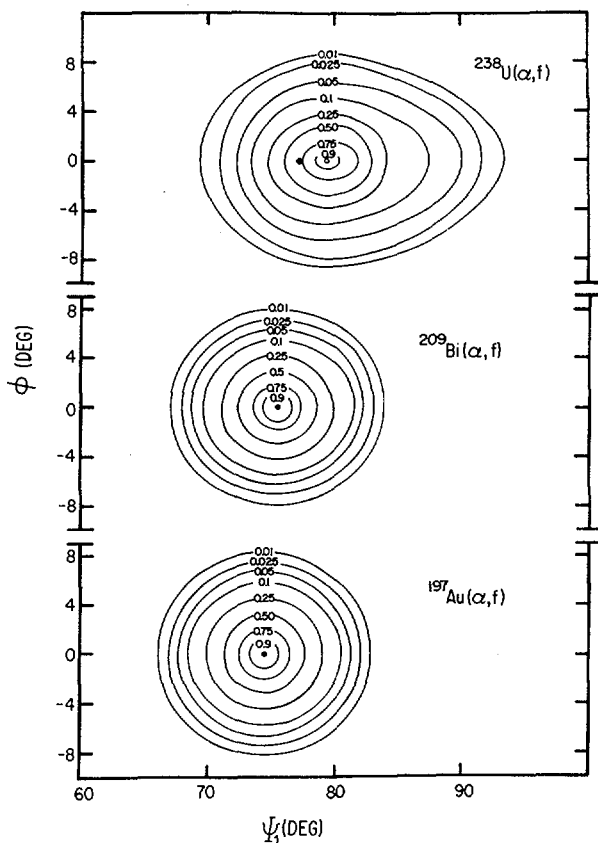


FIG. 5. Contour diagram of angular correlations for ^{238}U , ^{209}Bi and ^{197}Au systems. The planar angle is represented by Ψ and the non-planar angle is given by ϕ . Contours are labelled in terms of the fraction of events at a given angle pair with respect to the most probable correlation angle. The most probable correlation angle predicted by kinematics is shown as a black dot on each diagram.

by an empirical function of the form $y = Ae^{-bx^n}$ (solid lines in Fig. 4). Here y is the correlation coincidence rate and x is the absolute value of the deviation in angle from the most probable value, $x = |\Psi - \Psi_{mp}|$. These functions have been normalized to the data using $n = 1.94$ and 1.87 for gold and bismuth, respectively. The shape of the non-planar angular correlations (for constant Ψ) for bismuth and gold follow the same functional behavior as the planar data within the limits of error, although there is some indication that the planar correlation is slightly broader.

From comparison of the angular correlation for uranium fission with the gold and bismuth results in Figs. 4 and 5, it is evident that reaction mechanisms other than compound nucleus

TABLE I. Summary of fission-fragment angular correlation parameters derived from data shown in Figs. 4 and 5. The relative angular accuracy between the three target systems is ± 0.1 deg and the absolute error in the knowledge of the detector angles Ψ is ± 0.3 deg. Full-width-at-half-maximum (FWHM) values for the correlations have an error of ± 0.2 deg in each case.

	^{197}Au	^{209}Bi	^{238}U
Most probable correlation angle, Ψ_{mp}			
Experimental (deg)	74.5	75.5	78.5
Calculated (deg)	74.2	75.2	76.9
FWHM			
Planar (deg)	6.4	6.2	7.9
Non-planar (deg)	6.2	6.1	6.9

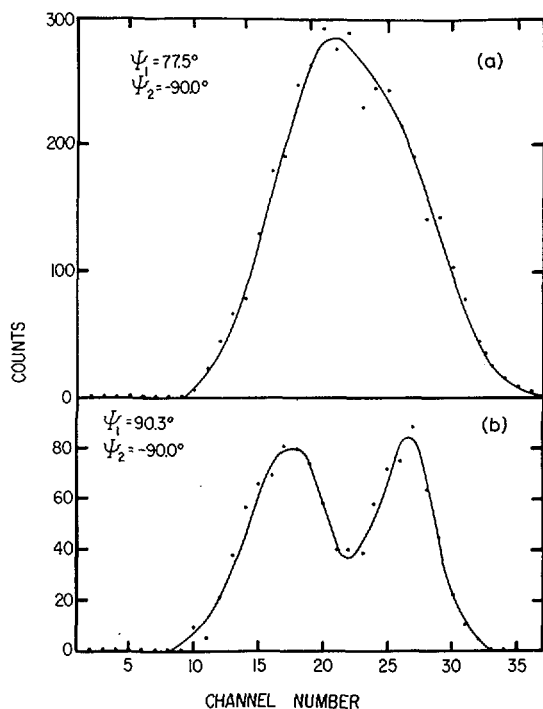


FIG. 6. Kinetic energy distribution for fission fragments produced in bombardment of ^{238}U with 140-MeV ^4He ions. (a) $\Psi_1 = 77.5^\circ$ and $\Psi_2 = -90.0^\circ$ represents high-energy fission; (b) $\Psi_1 = 90.3^\circ$ and $\Psi_2 = -90.0^\circ$, is characteristic of low-energy fission.

formation contribute significantly to the total fission cross-section for ^{238}U . This fact is demonstrated more directly in the fragment kinetic energy distributions shown in Fig. 6. For a correlation angle of $\Psi_1 = 77.5$ deg a broad single peak is observed in the fragment energy spectrum, indicative of high-energy fission, whereas for $\Psi_1 = 90.3$ deg an asymmetric fragment distribution is observed, characteristic of low-energy fission. In order to estimate the relative contributions of CN versus NCN reactions, we have utilized the systematic behavior of the angular correlation functions for fission reactions in which compound nucleus formation can be clearly distinguished. The gold and bismuth data from the present studies have been used to predict a most probable correlation angle of $\Psi_{\text{mp}} = 77.2$ deg for the data in Figs. 4 and 5 and a FWHM = 6.5 deg for fission following compound nucleus formation. These parameters are consistent with the results of heavy-ion-induced fission studies [11], which show (1) excellent agreement between the calculated and experimental values of Ψ_{mp} and (2) for a given projectile and bombarding energy, the FWHM of the angular correlation is nearly independent of target nuclide for ^{197}Au , ^{209}Bi and ^{238}U fission. Using these assumptions, a correlation function $y = Ae^{-0.0858 \times 1.77}$ is derived to account for fission following compound nucleus formation in reactions of 140-MeV ^4He ions with ^{238}U . The normalization constant A is determined using the kinematic restriction that the lowest angles Ψ_1 of the correlation function in Fig. 4 must correspond to complete momentum transfer reactions. This function is plotted as the dashed curve in Fig. 4.

By integrating over the entire reaction surface in Fig. 5 for both total experimental events and predicted compound nucleus events, we determine the cross-section for compound nucleus formation in ^{238}U , σ_{CN} , to be

$$\sigma_{\text{CN}} = (0.493 \pm 0.044)\sigma_{\text{R}} = 1361 \pm 121 \text{ mb.}$$

Here we assume that because of the high fissionability of ^{238}U , the total reaction cross-section, σ_{R} , is equal to the total fission cross-section, σ_{f} . Error limits are based on a possible error of ± 0.1 deg in Ψ_{mp} and ± 0.5 deg in the FWHM for the compound nucleus correlation function. Our result is in major disagreement with the value of $\sigma_{\text{CN}} = 0.91 \sigma_{\text{R}}$ determined by Kapoor et al. [10] at 110 MeV. However, reexamination of the data in Ref. [10] indicates that their value of σ_{CN} should have been much lower. The implications of this result will be discussed in more detail in Sections 4 and 5.

Comparison of the experimental angular correlation for ^{238}U with that determined assuming compound nucleus formation (Fig. 4) reveals that a considerable fraction of the NCN events involve large transfers of linear momentum from the projectile to the fissioning nucleus. We interpret this result as evidence of a high probability for pre-equilibrium decay in the nuclear reaction mechanism. This result is consistent with previous workers who have studied spallation product yields in reactions of intermediate energy ^4He ions with heavy elements [13,14] and with the (α, α') studies of Halpern et al [15].

By further utilizing the angular correlation systematics for ^4He -ion-induced fission reactions [10-12], the distribution of linear momenta which characterize the fissioning nuclei in

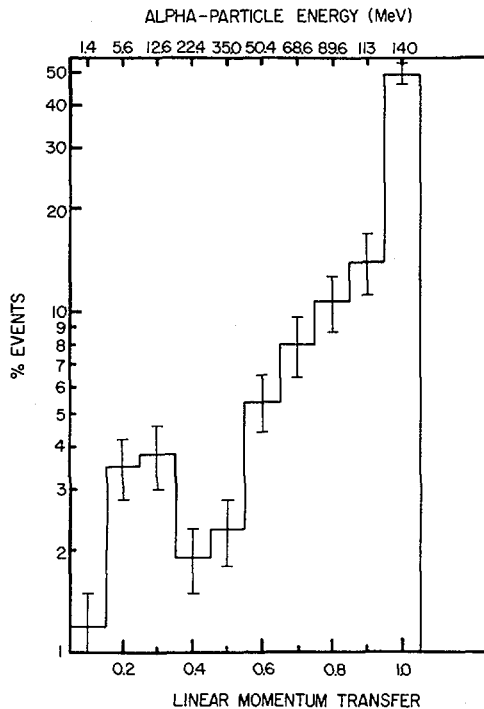


FIG. 7. Linear momentum distribution for fissioning nuclei produced in bombardment of ^{238}U with 140-MeV ^4He ions. The percentage of events is plotted as a function of the ratio of the observed linear momentum transfer to that for complete momentum transfer. Histogram was derived from angular correlation data for ^{238}U and the systematic behavior of angular correlations from other systems.

^{238}U reactions can be derived. This is shown in Fig. 7. This analysis reinforces the conclusion that high momentum transfer, pre-equilibrium decay events play an important role in these reactions. In addition, the bump in the histogram corresponding to low momentum transfers presumably reflects the extent to which direct surface reactions contribute to the total cross-section. Thus, it is apparent from our data that any attempt to derive information about fission from studies using intermediate-energy ^4He ions as projectiles must pay careful attention to the details of the nuclear reaction mechanism. Otherwise, one cannot possibly understand the distribution of fissioning species, excitation energies and angular momenta that characterize these reactions.

4. ANGULAR DISTRIBUTION RESULTS

The importance of understanding the projectile-target reaction mechanism in the interpretation of intermediate energy fission data is well-illustrated by the results of fission fragment angular distribution studies. The center-of-mass

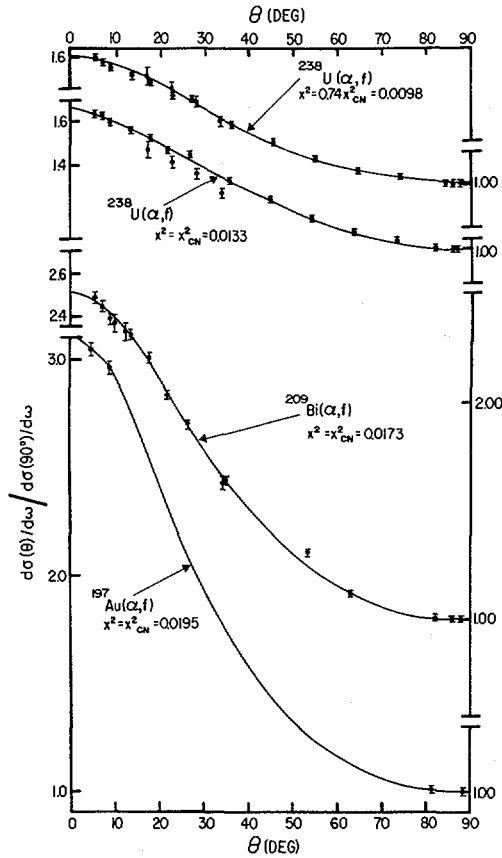


FIG. 8. Angular distributions in the center-of-mass for fission of ^{238}U , ^{209}Bi and ^{197}Au by 140-MeV ^4He ions. The relative differential cross-section, $[d\sigma(\theta)/d\omega]/[d\sigma(90^\circ)/d\omega]$, is plotted as a function of center-of-mass angle θ . The transformation parameter, X^2 , is shown for each set of data. For ^{238}U the transformation is performed using a value of X^2 corresponding to (1) compound nucleus formation ($X^2 = 0.0133$) and (2) the best forward-backward symmetry about 90° ($X^2 = 0.0098$).

angular distributions for 140-MeV ^4He ion-induced fission of ^{197}Au , ^{209}Bi and ^{238}U are shown in Fig. 8. The ^{209}Bi data were taken in both forward and backward reaction planes and transformation from the laboratory to the center-of-mass systems was accomplished using a value for the transformation parameter, X^2 , equal to the value calculated for compound nucleus formation, X_{CN}^2 . For ^{209}Bi the forward-backward symmetry required for binary processes is met with this assumption, thus confirming the conclusion based on the angular correlation data that ^{209}Bi fission proceeds almost entirely via a compound nucleus mechanism at these energies. Consequently, the angular distribution for the less fissionable gold target was transformed

TABLE II. Results of fission-fragment angular distribution measurements.

	^{197}Au	^{209}Bi	^{238}U	
Transformation parameter, X^2	0.0195	0.0173	0.0133	0.0098
Anisotropy, $W(175)/W(90)$	3.04 ± 0.03	2.48 ± 0.03	1.64 ± 0.02	1.59 ± 0.02

assuming $X^2 = X_{\text{CN}}^2$. The ^{238}U data were transformed into the center-of-mass system under two assumptions. First, X_{CN}^2 was used—which does not yield an angular distribution that is symmetric about 90 deg, as shown in Fig. 8. However, the value for the anisotropy, $W(175)/W(90)$, obtained from this procedure does serve as a lower limit for the anisotropy that would be observed in the absence of any NCN fission and has been treated as such in subsequent calculations. Second, a search was made to determine the transformation parameter that would yield the best forward-backward symmetry for the angular distribution. A value of $X^2 = 0.0098 = 0.74 X_{\text{CN}}^2$ was obtained in this way, in excellent agreement with the value of $X^2 = 0.743 X_{\text{CN}}^2$ determined from the linear momentum distribution shown in Fig. 7. This again substantiates our conclusions of Sect. 3 concerning the reaction mechanism for ^{238}U . In Table II the values for the anisotropy are listed along with the corresponding transformation parameters.

To derive K_0^2 values appropriate to fission reactions which follow compound nucleus formation from these systems, it was necessary to make appropriate assumptions concerning the distribution of orbital angular momenta, l , among the fissioning nuclides and also the effects of neutron evaporation prior to fission. The problem of calculating the transmission coefficients, T_0 , is complicated greatly by the high probability for pre-equilibrium decay in these reactions. In the absence of a detailed theoretical calculation which predicts the orbital angular momentum distribution in a system where direct, pre-equilibrium and compound nucleus reactions occur simultaneously, we have made the following assumptions, illustrated in Fig. 9, which should bracket the true situation. Under assumption I the orbital angular momentum distribution for the compound nuclei formed in these reactions is restricted to the lowest possible l -waves. Thus, all partial cross-sections, σ_l , up to the point where $\sigma_{\text{CN}} = 0.493 \sigma_R$ are considered to make up the compound nucleus cross-section. All higher l -waves are considered to produce NCN reactions. This model minimizes the average angular momentum of the fissioning nuclei and is consistent with the expectation that complete absorption should be most probable for projectiles with the smallest impact parameters. The upper limit on the average angular momentum (assumption II) is then obtained by assuming that the transmission coefficients for compound nucleus reaction products are the same as those calculated for the total reaction cross-section, but that only 49.3 percent of each partial cross-section results in compound nucleus formation. Transmission coefficients were calculated using the deformed optical model potential of Rasmussen and Sugawara-Tanabe [16] with parameters derived from fitting the

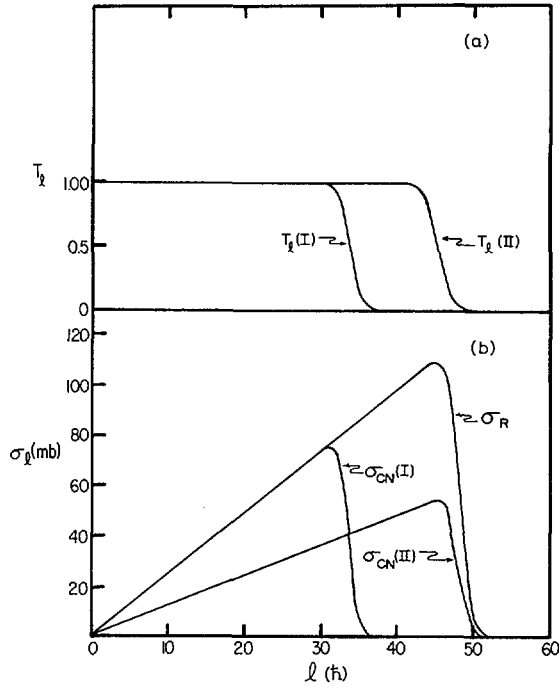


FIG. 9. Plot gives (a) transmission coefficients, T_l , and (b) partial cross-sections, σ_l , as a function of orbital angular momentum, which were used to derive K_O^2 values. The curve labelled σ_R represents an optical model fit to the total fission cross-section for 140-MeV ^4He ion-induced fission of ^{238}U . The quantities $\sigma_{CN(I)}$ and $T_l(I)$ represent the low orbital angular momentum extreme for K_O^2 , whereas $\sigma_{CN(II)}$ and $T_l(II)$ give the upper limit for this quantity.

TABLE III. Comparison of $K_O^2/(E_f^*)^{1/2} = \mathcal{J}_{eff}/a_f^{1/2}\hbar^2$ values obtained in this work compared with the low-energy results from [3]. The results in [3] have been corrected to be consistent with Eq. 1, based on [7].

	$K_O^2/(E_f^*)^{1/2} = \mathcal{J}_{eff}/a_f^{1/2}\hbar^2$		
	^{197}Au	^{209}Bi	^{238}U
This work (assumption I)	7.7	10.5	20.3
This work (assumption II)	16.0	21.9	42.2
Reference [3]	9.0	13.6	25.0

experimental excitation function for ^{238}U fission. The parameters were: well-depth, $V_0 = 130$ MeV; radius parameter, $r_0 = 1.194$ fm, and diffuseness, $d = 0.35$ fm. Deformation parameters were $\beta_2 = 0.261$ and $\beta_4 = 0.106$ for ^{238}U and zero for gold and bismuth. The compound nucleus radius parameter for calculations under assumption I above was $r_0 = 0.843$ fm.

The K_0^2 values were corrected for pre-fission neutron evaporation as follows. For ^{238}U the Γ_n/Γ_f values of Vandenbosch and Huizenga [17] were used, whereas average values of Γ_n/Γ_f were determined for ^{197}Au and ^{209}Bi from the work of Jodai-Koopari [18]. In the latter two cases values of $(\Gamma_n/\Gamma_f) = 9$ and 55 were used for 140-MeV ^4He -ion-induced reactions in ^{209}Bi and ^{197}Au respectively. In order to determine the appropriate excitation energy above the fission barrier, the barrier heights of Ref. [18] were used for gold and bismuth and that for ^{238}U was taken from Ref. [19]. Corrections were also made to the fission excitation energy for energy tied up in rotation.

In Table III the values of $K_0^2/(E_f^*)^{1/2}$ —which should be a constant, independent of excitation energy for each nuclide—are compared with the low-energy values determined by Reising et al [3]. It is observed that our values bracket the low energy value and consequently, there is no experimental basis for concluding that the effective moment of inertia is a function of excitation energy or that the assumptions of the angular distribution theory are inadequate to describe fission at intermediate excitation energies. Thus, the results of Ref. [10], which led Vandenbosch to suggest the possibility of a transition from the second maximum to the liquid drop value for the saddle point deformation in ^{238}U fission, is more an artifact of the reaction mechanism than of the fission process.

5. CONCLUSIONS

In summary, the present research demonstrates the importance of reaction mechanism studies to the interpretation of intermediate energy fission data. We find that less than one-half of the total reaction cross-section involves formation of a compound nucleus at a bombarding energy of 140-MeV and that a large fraction of the non-compound nucleus events involve linear momentum transfers with 50-90 percent of this value expected for compound nucleus formation. Based on these results, it is probable that similar effects occur at lower energies to an extent much larger than previously thought. The large fraction of NCN events complicates the analysis of fission data obtained at intermediate energies due to the broad spectrum of fissioning nuclei and excitation energies that result, as well as the difficulty in calculating the orbital angular momentum distribution of the products. Thus, previous conclusions drawn from intermediate energy fission data need to be re-evaluated if a knowledge of these quantities is involved. Our results do show that the fission of nuclides lighter than bismuth occurs only via compound nucleus formation reactions, which is an important consideration in the study of less fissile systems. However, assuming the reaction mechanism differs little between uranium and gold nuclei, the compound nucleus cross-section should be a factor of two lower than has been assumed for these reactions.

The results of the angular distribution studies carried out in this work show no evidence for previous conclusions that the quantity $\mathcal{J}_{\text{eff}}/k^2 a_f^2$ increases with increasing excitation energy. Values of $\mathcal{J}_{\text{eff}}/k^2 a_f^2$ have been determined for reaction models which maximize and minimize the angular momentum distribution of the fissioning nuclides. The low-energy value falls between these two extremes, although nearer the low angular momentum model. This result implies that most of the NCN reactions occur at the expense of the highest ℓ -waves in the angular momentum distribution. Furthermore, the failure to observe fission associated with NCN mechanisms in gold and bismuth targets may be evidence that the NCN reactions produce less fissile low angular momentum states in the residual reaction products. In order to understand these reactions fully, a comprehensive calculation which accounts for all features of the reaction mechanism needs to be undertaken. Only then can one interpret intermediate-energy ^4He ion-induced fission data with confidence.

ACKNOWLEDGEMENT

We are grateful to W. G. Meyer for his assistance with several aspects of this work.

REFERENCES

- [1] VANDENBOSCH, R., WARHANEK, H., HUIZENGA, J. R., Phys. Rev. 124, 846 (1961).
- [2] CHAUDHRY, R., VANDENBOSCH R., HUIZENGA, J. R., Phys. Rev. 126, 220 (1962).
- [3] REISING, R. F., BATE, G. L., HUIZENGA, J. R., Phys. Rev. 141, 1161 (1966).
- [4] VIOLA, V. E. JR., THOMAS, T. D., SEABORG, G. T., Phys. Rev. 129, 2710 (1963).
- [5] HALPERN, I., STRUTINSKI, V., in Int. Conf. peaceful Uses atom. Energy (Proc. Conf. Geneva, 1958) 15, UN, New York (1958) 408.
- [6] GRIFFIN, J. J., Phys. Rev. 116, 107 (1959).
- [7] HUIZENGA, J. R., BEHKAMI, A.N., MORETTO, L. G., Phys. Rev. 177, 1826 (1969).
- [8] VANDENBOSCH, R., Phys. Rev. C, 7, 2092 (1973).
- [9] NIX, J. R., SWIATECKI, W. J., Nucl. Phys. 71, 1 (1965).
- [10] KAPOOR, S. S., BABA, H., THOMPSON, S. G., Phys. Rev. 149, 965 (1966).
- [11] SIKKELAND, T., HAINES, E. L., VIOLA, V. E. JR., Phys. Rev. 125, 1350 (1962); VIOLA, V. E. JR., MINOR, M. M., SALWIN, A. E., et al., Nucl. Phys. A 174, 321 (1971).
- [12] NICHOLSON, W. J., HALPERN, I., Phys. Rev. 116, 175 (1959).
- [13] BIMBOT, R., LEBEYEC, Y., J. de Physique 32, No. 4, 18 (1971).
- [14] BLANN, M., LANZAFAME, F. M., Nucl. Phys. A 142, 559 (1970); LANZAFAME, F. M., BLANN, M., Nucl. Phys. A 142, 545 (1970).
- [15] HALPERN, I., private communication; CHENEVERT, G., CHANT, N. S., HALPERN, I. et al., Phys. Rev. Lett. 27, 434 (1971).
- [16] RASMUSSEN, J. O., SUGAWARA-TANABE, K., Nucl. Phys. A 171, 497 (1971).
- [17] HUIZENGA, J. R., VANDENBOSCH, R., in Int. Conf. peaceful Uses atom. Energy (Proc. Conf. Geneva, 1958) 15, UN, New York (1958) 284.

- [18] KHODAI-JOOPARI, A., University of California Radiation Laboratory Report, UCRL-16489, 1966.
- [19] HYDE, E. K., Nuclear Properties of the Heavy Elements III: Fission Phenomena, (Prentice-Hall, New Jersey, 1964).

DISCUSSION

L. G. MORETTO: Your excitation energy is very large and one would therefore expect the correction for multiple-chance fission to be substantial. These kinds of corrections are very difficult to perform. At high energy a variation of 10% in θ_f/θ_n produces a change of a factor >100 in Γ_f/Γ_n . Therefore I do not understand how you could determine a reliable value of K_0^2 .

V. E. VIOLA: In order to make a consistent comparison of our K_0^2 values for ^{238}U with those obtained by others at lower excitation energies, we have used the low-energy Γ_f/Γ_n values tabulated by Huizenga and Vandebosch. For gold and bismuth we have extrapolated the fission cross-section results of Khodai-Joopari (Ref. [18] of the paper) to 140 MeV and then derived average Γ_f/Γ_n values which matched the results. One could go through a more sophisticated treatment of Γ_f/Γ_n and probably obtain somewhat better limits of K_0^2 . However, given the status of our knowledge of the target-projectile interaction mechanism, this hardly seems worthwhile. This is the main point we are trying to make — if K_0^2 is in error by a factor of two owing to uncertainties in the knowledge of the transmission coefficients, then we cannot expect to learn much about the fission transition state however sophisticated our treatment of Γ_f/Γ_n .

J. MILLER: What did you do about the angular-momentum dependence of the fission probability when you calculated the angular distribution? This dependence would be particularly important for gold, where the fission probability is considerably less than unity and thus much of the fission could come disproportionately from the high-spin states.

V. E. VIOLA: We did not attempt to use an angular-momentum-dependent value of Γ_f — largely for the same reasons mentioned in the previous question. I agree that this could have an effect on results — especially for gold fission, as you mention. If the fission is angular-momentum-dependent, then K_0^2 will indeed be increased. On the other hand, an angular-momentum-dependent Γ_f value would serve to increase Γ_f/Γ_n , which would also increase our value for the average excitation energy of the fissioning nuclei. Thus, the value for $K_0^2/(E_f^*)^{1/2}$ might remain approximately constant to the first order approximation. However, this is not necessarily the case and it is possible to conceive of an angular momentum distribution for the fissioning gold nuclei that would give \mathcal{L}_{eff} results which did not bracket the low-energy result for this nucleus. However, for bismuth and uranium fission, I do not believe that an angular momentum Γ_f value could change the results appreciably.

STATISTICAL CALCULATION OF THE MASS DISTRIBUTION IN FISSION

A. S. JENSEN

Nordita, Copenhagen

T. DØSSING

Niels Bohr Institute,
University of Copenhagen,
Copenhagen, Denmark

Abstract

STATISTICAL CALCULATION OF THE MASS DISTRIBUTION IN FISSION.

The mass distribution of the fission fragments is calculated as a function of excitation energy from the saddle point properties of the fissioning nucleus. The nuclei investigated are ^{226}Ra , ^{228}Th , ^{240}Pu and ^{258}Fm .

The essential quantities involved are the potential energy surface and the level density as a function of deformation, angular momentum and excitation energy. The potential energy surface is obtained by addition of the liquid drop energy and the shell correction energy. The single particle spectrum needed is calculated in a deformed axially symmetric Woods-Saxon potential. Two symmetric deformation parameters and one left-right asymmetry parameter span the deformation space.

The level density is also calculated directly from the single particle spectrum. For a given nucleus, the number of levels as a function of the excitation energy and of the projection of the total angular momentum on the intrinsic symmetry axis are first evaluated. This is consistently done with the effects of pairing included in the BCS-approximation. The total level density as a function of energy E and angular momentum I is then obtained as a sum of the rotational bands built on top of each of these intrinsic level densities.

The probability for finding the nucleus with given E and I at a given deformation is an integral of the level density for the deformation considered.

The mass distribution of the fission fragments is assumed to be determined around the second saddle point and given by statistical arguments. It is shown for ^{240}Pu that, as one goes away from the saddle point, the correlation between observed and calculated distributions disappears. The results for ^{258}Fm are similar to observations for ^{256}Fm . Both ^{226}Ra and ^{228}Th give in the calculation predominantly symmetric fission. A shoulder around a fragment mass of 138 is obtained for low energies.

1. INTRODUCTION

We investigate as function of excitation energy the qualitative agreement between the observed mass distribution in fission and the instability around the second saddle point against left-right asymmetric distortions. This has been tried before when angular momentum effects are ignored [1], [2].

The philosophy behind the approach is that the system develops adiabatically with statistical equilibrium between collective and internal degrees of freedom, until it reaches the exit region. This deformation region [3] is situated outside the second barrier. At this point the adiabaticity is broken—very quickly the neck of the nucleus develops and scission occurs. Thus the mass distribution of the fission fragments is determined in the exit region.

The existence of a well-defined exit was pointed out in ref. [3]. It is a very crucial assumption in this work.

We try to localize the exit by comparison of the observed mass distributions with calculations done at different deformations on the outer side of the second saddle point.

No penetration through barriers is taken into account and we are therefore limited to excitation energies well above the second barrier. The uncertainties in the energy surface do not come in with their full strength because we only need relative energies in the deformation region of interest. The absolute heights of the barriers are therefore unimportant.

In order to cover a reasonable region of nuclei we study firstly ^{240}Pu , (in the middle of the asymmetrically fissioning nuclei) then ^{258}Fm , which presumably fissions symmetrically and lastly ^{226}Ra and ^{228}Th in the interesting region where three peaks in the mass distribution have been observed.

2. MODEL

2.1 Probability surface

The parametrization of the shape of the potential is described by the deformation parameters (c, h, α) [3], [4]. Left-right symmetry is preserved for $\alpha = 0$ while non-zero α -values describe asymmetric shapes. The radial form is of the Woods-Saxon type.

A crucial quantity in this approach is the level density. It is like the collective potential energy surface $V(c, h, \alpha)$ calculated directly from the single particle spectrum.

The total level density ρ as a function of energy E and angular momentum I is obtained as a sum of the rotational bands built on top of each of the intrinsic levels [5], i.e.

$$\rho(E, I) = \sum_{K=-I}^I \rho_i \left(E - \frac{(I + \frac{1}{2})^2 - K^2}{2j_L}, K \right) \quad (1)$$

where $\rho_i(X, K)$ is the intrinsic level density as a function of the intrinsic excitation energy X and the projection K of I on the intrinsic symmetry axis. It is obtained with the effects of pairing included in the BCS-approximation [6]. The moment of inertia j_L around an axis perpendicular to the symmetry axis is in principle a function of energy and deformation.

The relative probability for finding the nucleus at the deformation (c, h, α) with given E and I is approximately given by (see e.g. refs. [7] and [1])

$$S(E, I, c, h, \alpha) = T_{av}^{3/2} \rho(E_T, I) \quad (2)$$

where T_{av} is an average of the local temperature corresponding to the different arguments of ρ_i in eq. (1), and E_T is the local excitation energy above the collective potential energy

$$E_T = E - V(c, h, \alpha) \quad (3)$$

2.2 Mass distribution

The assumption is now that the mass distribution can be determined by the probability distribution at exit. This is the region in deformation space where the motion towards fission changes from adiabatic (i.e. slow enough that statistical equilibrium is maintained at each step) to sudden (i.e. so fast that scission occurs before any adjustment can take place). Thus we assume that up to a certain point statistical arguments are applicable and then suddenly the nucleus disappears out of our static model. At this point the mass distribution is frozen.

If the exit region is sufficiently narrow, the mass distribution M is determined by a one-dimensional cut in the probability surface. Otherwise an extended region is needed to determine M . In this simple case we have

$$M(E, I, \alpha) = S(E, I, c(\alpha), h(\alpha), \alpha) \quad (4)$$

where c and h are the functions of α describing where the cut is made.

When M is obtained from eq. (4) we take a distribution $a(E, I)$ of angular momenta similar to the one in the actual experimental situation. After normalization of $M(E, I, \alpha)$ we have for the observable mass distribution

$$M(E, \alpha) = \sum_I a(E, I) M(E, I, \alpha) \quad (5)$$

where now

$$\int M(E, I, \alpha) d\alpha = 1 \quad (6)$$

The cut in deformation space needed in eq. (4) is still arbitrary. Several possibilities were tried: (i) (c, h) -values fixed at the saddle point value or along the path to fission [1]. (ii) A cut through both the symmetric and asymmetric probability saddle point in the direction where the surface is steepest or curves parallel with this at larger deformations. (iii) Cuts with constant c and the h -value with the highest probability for the c and α considered.

One could also make cuts with fixed distance between the centers of mass of the future fragments [8]. Although it is difficult to define what we mean by fragments for deformations around the saddle point, this is to first order in c the same as (iii). This can be seen by simple estimates [4]. Roughly speaking the distance between the centers of mass of the fragments is proportional to c .

In order to compare calculations with observations we must find a connection between α and e.g. the mass A^+ of the heavy fragment. If the nucleus is divided in two by a plane in the middle of and perpendicular to the symmetry axis, the

ratio between the volume of the heavy fragment and the total volume can be interpreted as the ratio between the corresponding masses. This leads to (see ref. [4])

$$A^* = \frac{1}{2} A \left(1 + \frac{3}{8} \alpha c^3 \right) \quad (7)$$

Of course this relation is somewhat arbitrary. It does, however, suggest a linear dependence, which instead could be found phenomenologically [1] .

3. RESULTS

The parameters used in the Woods-Saxon potential [9] are given in table I for ^{240}Pu . The single particle levels for ^{240}Pu are, after an $A^{1/3}$ -scaling [3], applied to the other nuclei investigated. The liquid drop part of the collective potential energy is calculated with parameters from ref. [10]. The rigid body value with a radius parameter $r_0 = 1.2$ fm is taken for the moment of inertia. This is justified for large deformations and high temperatures [3] and applies therefore to our case.

The energies are all measured from the energy of the spherical liquid drop. They are therefore not excitation energies but 2-3 MeV smaller.

The distribution $a(E, I)$ of angular momenta depends on the experimental conditions. Simple classical estimates give a maximum spin value of around 20 \hbar for the energies considered here. Calculations of the probability surface according to eq. (2) show that the spin dependence for our purpose is completely negligible. The difference in $\ln(S)$ between two I -values fluctuates with deformation by less than 0.1 around the average value. Since a statistical treatment like the present one is only applicable for $\ln(S) \gg 1$ this fluctuation is well below errors introduced by other approximations. For convenience we consider therefore in the following only spin zero states.

TABLE I. PARAMETERS FOR THE SINGLE PARTICLE POTENTIAL FOR ^{240}Pu

V_0 is the depth of the potential; R and a are respectively the radius and diffuseness of the central (v) and spin orbit (so) potentials. The strength of the spin orbit potential is κV_0 [3]

	$-V_0$ (MeV)	R_v (fm)	a_v (fm)	R_{so} (fm)	a_{so} (fm)	κV_0 (MeV)
Neutrons	47.46	7.73	0.66	7.22	0.55	12.0
Protons	62.54	7.79	0.66	6.90	0.55	12.0

3.1 ^{240}Pu

The nucleus ^{240}Pu is in the middle of the actinide region and it is quite well known how the mass distribution depends on excitation energy [11].

Although we have restricted ourselves to spin zero states the probability surfaces are very similar to those of ref. [1]. The saddle point c -value is 1.60 and it is practically constant for energies below 30 MeV.

The mass distributions are obtained as described in section 2.2. First we consider case (iii), cuts for constant c -values corresponding to an approximately fixed distance between the centers of mass of the fragments. Two of the characteristic quantities describing the mass distribution are shown in fig. 1 for different energies.

As we go away from the saddle point the peak position moves towards smaller asymmetry, the peak-to-valley ratio increases first and then decreases rapidly. Each energy has a characteristic c -value beyond which symmetric ($\alpha = 0.0$) fission is most probable. For $c \geq 1.70$ we get symmetric fission at much too small energies. Thus in this case the exit must, for small energies, occur for $c \leq 1.65$.

The results with this restriction ($c \leq 1.65$) for different cuts (see section 2.2) all come out fairly similar. Case (ii), a cut through both symmetric and asymmetric saddle point, is typical. With the translation in eq. (7) this leads to the mass distributions in fig. 2. The resemblance to the measured distributions [11] is striking.

The characteristics of the distributions in fig. 2 are plotted in fig. 3 as functions of energy. In the same figure is also shown the experimental numbers for ^{240}Pu [11] together with results extracted from the work of Baba et al. [12] which are from proton-induced fission of ^{238}U .

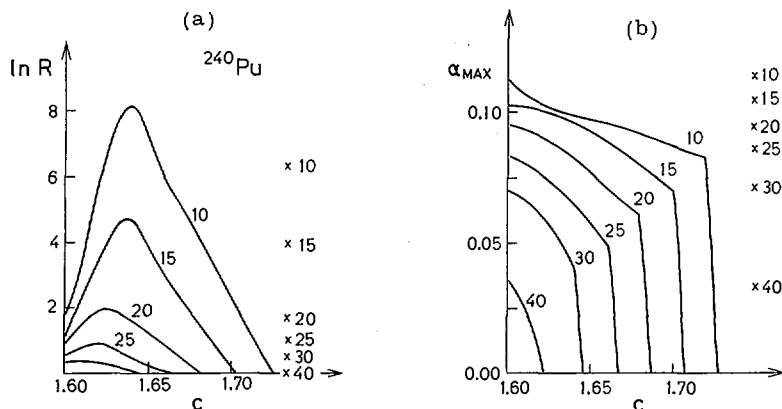


FIG. 1. (a) The natural logarithm of the peak-to-valley ratio R and (b) the value of the asymmetry parameter α_{\max} of the peak position as function of the elongation c of the ^{240}Pu nucleus. For $\alpha_{\max} = 0$, symmetric fission dominates. The lowest c -value on the figure is the saddle point value. The crosses at the right-hand side are the results of case (ii) calculations described in Section 2.2.

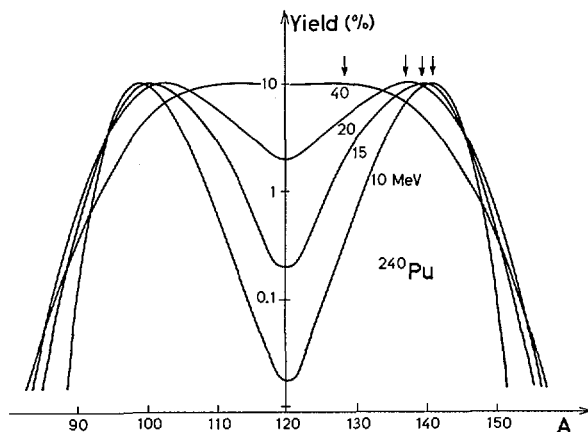


FIG. 2. Calculated mass distributions for ^{240}Pu fission fragments for the energies in MeV given on the curves in the figure. All the peaks are normalized to 10. The arrows indicate the peak position.

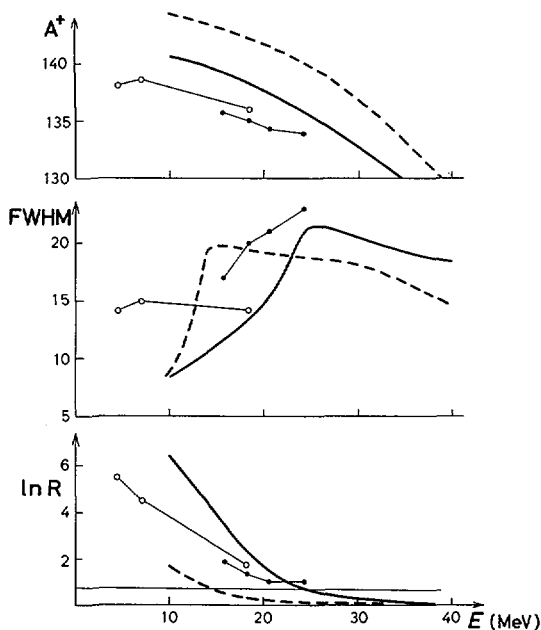


FIG. 3. The characteristics of the mass distributions in Figs 2 and 5 as a function of the energy E . The quantity A^+ is the most probable mass of the heavy fragment. The full width at half maximum is denoted by FWHM and $\ln R$ is the natural logarithm of the peak-to-valley ratio. The full curves are for ^{240}Pu and the dashed are for ^{258}Fm . The open circles are experimental numbers for ^{240}Pu from Ref. [11] and the closed circles are for ^{239}Np from Ref. [12]. A ground state energy for ^{240}Pu of 2.5 MeV below the spherical liquid drop energy was used. The thin line in the $\ln R$ figure corresponds to $R = 2$.

The position of the heavy fragment is about two mass units larger than the experimental values. This difference would be reduced by 1 unit if the neutron yield was taken into account, i.e. symmetric fission corresponding to $A^+ \approx 119$. The decrease with energy is reproduced.

The full width at half maximum (FWHM) for one peak increases first, reaches a maximum and then decreases slowly. It continues although it ceases to exist for one peak. The continuation is the half width of the full (symmetric peak). The behavior for small energies is not consistent with observations while the ^{239}Np -data indicates that the trend is correct for the intermediate energies.

The peak-to-valley ratio is too big for small energies but becomes very close to the experimental value for energies ≥ 20 MeV. The deviations at small energies would disappear if 2.5% of the asymmetric fission was converted into symmetric. The important point is that, when symmetric fission begins to dominate, the energy comes out about right.

These conclusions for ^{240}Pu are very similar to those from ref. [1] .

3.2 ^{258}Fm

Experimentally, little is known about the energy dependence of the mass distribution for the nuclei around ^{258}Fm . Spontaneous fission of ^{256}Fm is believed to be asymmetric [13] with a fairly small peak-to-valley ratio ≈ 12 . Also spontaneous fission of ^{257}Fm is predominantly asymmetric [13] whereas neutron-induced fission of ^{257}Fm (i.e. ^{258}Fm) is symmetric [14] .

The properties of the probability surface are seen in fig. 4. It is the analog of fig. 1, showing results from cuts of constant c . The saddle point c -value is 1.53 and it is practically constant for energies below 30 MeV. Clearly asymmetry is favored for low energies for all values of $c \lesssim 1.70$. The figure is not at all like that for ^{240}Pu (see fig. 1). At

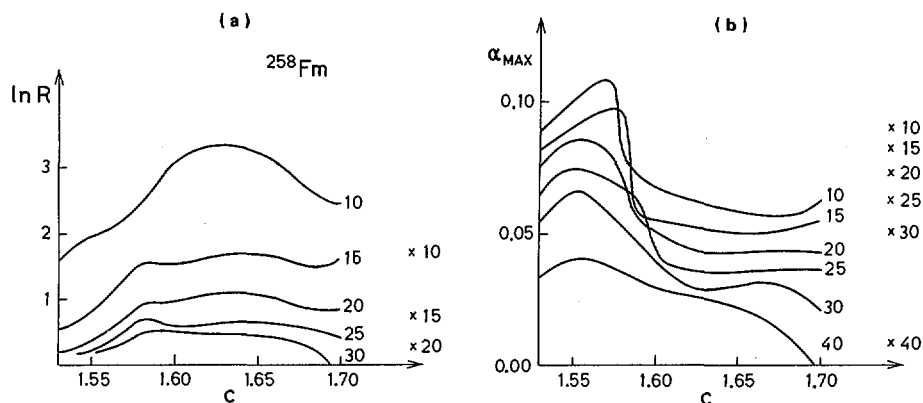
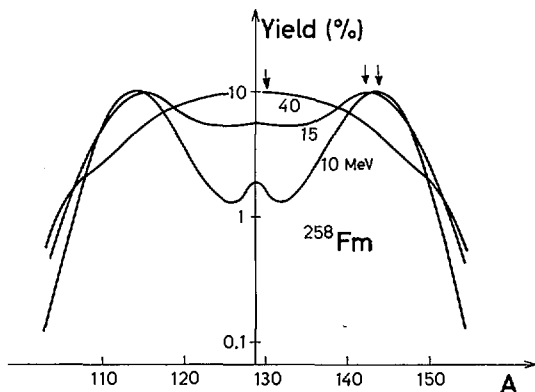


FIG. 4. The same as Fig. 1 for ^{258}Fm . The lowest c -value on the figure is the saddle point value.

FIG. 5. The same as Fig. 2 for ^{258}Fm .

$c = 1.70$, which is the largest elongation considered in this case, there is only a very small inclination (if any) towards a dominance of symmetric fission.

Of course it would be possible to continue even farther out in the hope that at some point one would find symmetric fission. Between $c = 1.60$ and $c = 1.70$ the energy has, however, decreased ≈ 5 MeV. This drop in energy is larger than the corresponding drop for ^{240}Pu when the latter gives completely unreasonable results (see fig. 1). To be consistent the exit should therefore lie for $c \approx 1.60$.

As in the case of ^{240}Pu , the mass distributions are not very different when they are determined in the region around the saddle point. Thus we prefer again case (ii) in section 2.2. With the use of eq. (7) we obtain the mass distributions shown in fig. 5.

Characteristic quantities of these distributions are shown with the ^{240}Pu results in fig. 3. The absolute value of the peak position is larger by about 3 units but decreases in the same way as for ^{240}Pu . Also the FWHM behavior is the same for the two nuclei. The slow decrease is only reached for ^{258}Fm at a lower energy, reflecting the faster transition from asymmetric to symmetric fission. This can be seen more clearly in the peak-to-valley ratio which drops below 2 (thin line in the figure) already at $E = 13$ MeV.

These results are clearly not compatible with the observations of ^{258}Fm [14]. They look much more like they belong to a nucleus on the asymmetric side of a region, where transition from asymmetric to symmetric fission occurs. Taking this point of view, the discrepancy between experiments and calculations is not very big.

In other words, the single particle model used does not give this transition at exactly the correct place in the periodic table. Indications [15] are that the transition will take place when a few more nucleons are added. The calculation here should therefore rather look like the experimental

findings of ^{256}Fm . Of course this explanation can be checked by investigating more nuclei in this region. Unfortunately we have not done that yet.

3.3 ^{226}Ra and ^{228}Th

The radium region is interesting in this connection because of the observed three peaks in the mass distribution of the Ac-isotopes [16], [17]. We study here the adjacent even-even nuclei ^{228}Th and ^{226}Ra . Little is known about the mass distributions of these. It has been measured [18] for thermally induced fission of ^{227}Th (i.e. fission of ^{228}Th). It is clearly asymmetric with only two peaks, the heavy fragment at $A^+ = 137$, a peak-to-valley ratio of 230 and FWHM of 11.5.

For both ^{226}Ra and ^{228}Th the energy saddle point comes out with a small but non-zero value of the asymmetry parameter ($\alpha \approx 0.05$). The surfaces are very similar and there is certainly no jump in saddle point from asymmetry ($\alpha \neq 0$) to symmetry ($\alpha = 0$). In the α -direction we see only the two peaks symmetric around $\alpha = 0$.

The surfaces differ from those of ^{240}Pu and ^{258}Fm in the very fast shift from asymmetry to symmetry being favored, when we move away from the saddle point towards fission. Only a change of 0.02 in c is needed. Thus consistency with the point of view taken in the discussion of ^{240}Pu and ^{258}Fm requires an exit region leading to symmetric fission.

In this case the peak position and the peak-to-valley ratio are of no interest. Thus we are left with only the FWHM. It is shown in fig. 6 for ^{226}Ra as a function of energy. Each point is obtained from cuts of constant c and each curve represents a constant difference δc in c from the energy-dependent c -value of the probability saddle point. As we go away

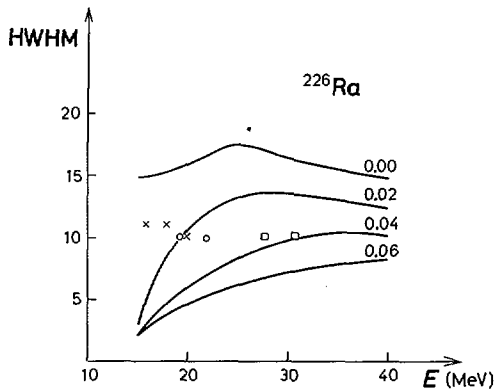


FIG. 6. The half width at half maximum of the symmetric peak of ^{226}Ra as a function of energy. The numbers give the distance in c from the energy-dependent c -value of the probability saddle point. The crosses (^{221}Ac) from Ref. [16], circles (^{221}Ac) from Ref. [17] and squares (^{228}Ac) from Ref. [17] are experimental numbers. A ground state energy 2 MeV below the spherical liquid drop energy was used.

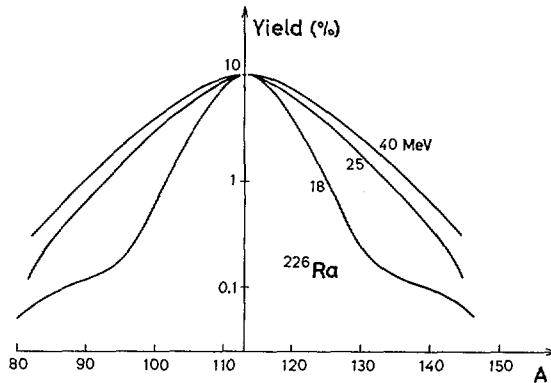


FIG. 7. The same as Fig. 2 for ^{226}Ra . The cut used has a c -value differing from the saddle point value by 0.04.

from the saddle (going from curve to curve with fixed E) the FWHM decreases. For small energies the calculated values are smaller than the experimental values of the symmetric part of the mass distribution of the Ac-isotopes. Higher energies seem to favor cuts with $\delta c \approx 0.03 - 0.04$. We take this for another indication that the saddle point region is important for the mass distributions.

Using eq. (7) we obtain the distributions shown in fig. 7. The cut was made for $\delta c = 0.04$. For the energy 18 MeV there is a shoulder around $A = 138$ showing a tendency towards an asymmetric peak at this place. For higher energies the shoulder is washed out.

The origin of it is a large negative shell correction for $\alpha \approx 0.15$. The steep increase of liquid drop energy with α does however not allow this tendency to develop into a real peak.

The results for ^{228}Th are very similar to those of ^{226}Ra and far from the observations [18]. Again only symmetric fission is found together with an asymmetric shoulder for small energies.

4. SUMMARY

The single particle energy spectra are obtained in the three-dimensional space of the deformation parameters of an axially symmetric Woods-Saxon-type average potential. From these the collective potential energy and the level density as a function of energy and angular momentum are evaluated. Then the mass distribution is extracted from the properties of the saddle point region. This is done without introducing any new parameters and without changing any of the old parameters. We have shown that for ^{240}Pu the correlation between observed and calculated distributions is strongest close to the saddle point. As we go away this correlation disappears. For ^{258}Fm the calculations are more similar to the observations for ^{256}Fm . It is argued that this is because the Woods-Saxon parameters do not give the

transition from asymmetric to symmetric fission at exactly the correct place in the periodic table. Also for ^{226}Ra and ^{228}Th we are, in our present model, in one of these transition regions. For both nuclei we find symmetric fission and a shoulder in the distribution for a fragment mass of around 138. No abrupt switch from asymmetric to symmetric fission between the two nuclei is obtained.

ACKNOWLEDGEMENTS

We wish to thank Dr. S. Bjørnholm for suggestions and discussions. We are also indebted to Professor B. Mottelson for his advice concerning level densities.

REFERENCES

- [1] Jensen, A.S., Damgaard, J., Nucl.Phys. to be published, 1973.
- [2] Tsang, C.F., Wilhelmy, J.B., Nucl.Phys. A184 (1972) 417
- [3] Brack, M., et al., Rev.Mod.Phys. 44 (1972) 320
- [4] Pauli, H.C., Phys.Reports 7C (1973) No. 2
- [5] Mottelson, B., private communication
- [6] Moretto, L.G., Nucl.Phys. A185 (1972) 145
- [7] Moretto, L.G., Nucl.Phys. A182 (1972) 641
- [8] Swiatecki, W.J., private communication
- [9] Damgaard, J., et al., Nucl.Phys. A135 (1969) 432
- [10] Pauli, H.C., Ledergerber, T., Nucl.Phys. A175 (1971) 545
- [11] Günthen, H.R. von, Actinides Rev. 1 (1969) 275
- [12] Baba, S., et al., Nucl.Phys. A175 (1971) 177
- [13] Flynn, K.F., et al., Phys.Rev. C5 (1972) 1725
- [14] John, W., et al., Phys.Rev.Lett. 27 (1971) 45
- [15] Pauli, H.C., et al., Phys.Lett. 34B (1971) 264
- [16] Konecny, E., et al., Nucl.Phys. A139 (1969) 513
- [17] Perry, D.G., Fairhall, A.W., Phys.Rev. C4 (1971) 977
- [18] Flynn, K.F., Günthen, H.R. von, Proc. IAEA Symp., Vienna 1969, p. 731

DISCUSSION

H. J. KRAPPE: For calculating mass distributions in the dynamical model one has to know something about the inertia and viscosity parameters besides the potential energy surface. As you do not specify these quantities, you have to make certain model assumptions instead. Would you please explain the physical content of these assumptions in terms of the liquid drop model?

A. S. JENSEN: In principle, the mass tensor enters into this formalism, as can be seen from Ref. [7], but it is here assumed to be independent of energy and deformation. Furthermore, we use the following assumptions: up to the exit region the viscosity is large, because we assume statistical equilibrium between collective and intrinsic degrees of freedom; then on the other side of the exit region the viscosity is small, because all the energy is assumed to go into the collective degrees of freedom.

S. S. KAPOOR: How does the width of your calculated mass distributions compare with the experimental values? As you may know, our work reported at this symposium¹ shows that the static model gives mass distributions which are too narrow.

A. S. JENSEN: For the lowest energies that we considered, the width is around a factor of two too small but, as the excitation energy increases, the width approaches the experimental value.

U. MOSEL: Since we have heard in previous papers that the potential energy surfaces are accurate only to within $\approx 1-2$ MeV, I wonder how strongly the width of the mass distributions would be affected by a change of this magnitude in the dependence of the potential on the asymmetry coordinate.

A. S. JENSEN: Since we only need relative energies around the second saddle point, the uncertainties in the energy surface do not enter fully into the calculations.

¹ KAPOOR, S. S., RAMAMURTHY, V. S., Paper IAEA-SM-174/10, these Proceedings, Vol. 1.

POTENTIAL ENERGY SURFACES AND DEPENDENCE OF FISSION MASS ASYMMETRY ON THE INTERNAL EXCITATION ENERGY OF THE FISSIONING NUCLEUS*

H. W. SCHMITT

Oak Ridge National Laboratory,
Oak Ridge, Tennessee

M. G. MUSTAFA[†]

Department of Physics and Astronomy,
Vanderbilt University,
Nashville, Tennessee and

Oak Ridge National Laboratory,
Oak Ridge, Tennessee,
United States of America

Abstract

POTENTIAL ENERGY SURFACES AND DEPENDENCE OF FISSION MASS ASYMMETRY ON THE INTERNAL EXCITATION ENERGY OF THE FISSIONING NUCLEUS.

A theoretical treatment of medium- and high-excitation fission has been developed within the context of the shell-correction method of Strutinsky. The effective potential energy surfaces for ^{236}U at various excitation energies have been calculated by extending our earlier two-centre-model calculations to include a distribution of occupation probabilities of the single particle states obtained in the model. It is assumed that excitation of a compound fissioning nucleus of any given shape gives rise to a distribution of occupation probabilities that may be represented by a Fermi function

$$F = \left[1 + e^{(\epsilon_i - \epsilon_{FT})/T} \right]^{-1}$$
, where ϵ_i , ϵ_{FT} , and T are the energy of a single particle level, the Fermi energy, and the nuclear temperature, respectively.

For all shapes from the second saddle point to scission, the results of calculations to date show a decrease in deformation energy with increasing T for mass ratios near symmetry, and an increase in deformation energy with increasing T for asymmetric mass ratios. For ^{236}U , the absolute potential energy minimum shifts from asymmetry (140/96) to symmetry (118/118) at a nuclear temperature in the range 1.5 to 2 MeV, corresponding to an excitation energy of 60 to 100 MeV. The shell-correction energy is found to approach zero asymptotically with increasing temperature; the specific form of this function depends on the nuclear shape.

As a by-product of these potential-energy calculations, the relationship between excitation energy E_X and nuclear temperature T can be obtained, for any of the deformed shapes encountered. It appears that the relationship is not very sensitive to shape, and may be represented approximately by $E_X \approx (A/9) T^2$.

INTRODUCTION

It has long been known that the relative yield of fission fragment masses in the valley of the mass-yield distribution increases as the excitation energy of the compound fissioning nucleus increases. This phenomenon

* Research sponsored by the US Atomic Energy Commission under contract with the Union Carbide Corp.

[†] On leave from the Atomic Energy Centre, Dacca, Bangladesh, and recently supported in part by NSF Contract No. GP-34634.

has been shown in various compilations of mass yield data, e.g., by Hyde¹ and in other more recent papers. Recently, our experimental group at Oak Ridge has published the results of a series of measurements of the systematics of this effect for proton-induced fission of the uranium isotopes.² Fragment energy correlation methods were used, and the systematics of mass distributions, fragment kinetic distributions, and energy-vs-mass correlations were obtained.

An outstanding problem in the field of fission physics has been the lack of a theoretical description of fragment mass and energy distributions with increasing compound-nucleus excitation energy. It is this problem that we discuss in this paper.

The formulation which we present here, we believe, provides a sound basis for the study of this subject. It introduces the concept of "effective potential energy surfaces" for internally excited nuclei. The dynamics of the motion within such surfaces is not treated here, nor is the transfer of motion from one surface to another. In this sense the formulation to follow is analogous to the calculation of potential surfaces with the Strutinsky prescription, in which the lowest-energy surface, corresponding to zero excitation energy, is obtained.

THE MODEL

We assume that internal excitation in a nucleus gives rise to a probability distribution for the occupation of the single-particle levels and that this distribution may be represented by a Fermi distribution function:

$$1/[1 + e^{(\epsilon_n - \epsilon_{FT})/T}],$$

where ϵ_n is the energy of a given single-particle level, ϵ_{FT} is the Fermi energy, and T is the nuclear temperature.³ Such a function would exist for both protons and neutrons. We may then write the sum of single-particle energies of the excited nucleus as the sum of two terms, one for protons and one for neutrons, of the form

$$E_T = 2 \sum_{n=1}^{\infty} \frac{\epsilon_n}{1 + e^{(\epsilon_n - \epsilon_{FT})/T}}, \quad (1)$$

where ϵ_n is the energy of a single-particle level for a given nuclear shape; these values are obtained from our two-center model calculations⁴ which, in turn, make use of the Strutinsky prescription⁵. The Fermi energy ϵ_{FT} is different for protons and neutrons and is determined for each type of particle and for each temperature by the conservation of particle number N , that is,

$$\frac{N}{2} = \sum_{n=1}^{\infty} \frac{1}{1 + e^{(\epsilon_n - \epsilon_{FT})/T}}. \quad (2)$$

The smoothly varying part of the total energy (protons or neutrons) is given by a formula analogous to that of the usual Strutinsky prescription⁵ but incorporating the Fermi function as follows:

$$\tilde{E}_T = 2 \int_{-\infty}^{\infty} \sum_{n=1}^{\infty} \frac{\epsilon \tilde{g}(\epsilon, \epsilon_n)}{1 + e^{(\epsilon - \tilde{\epsilon}_{FT})/T}} d\epsilon, \quad (3)$$

where $\tilde{\epsilon}_{FT}$ is the Fermi energy of the smooth distribution of levels and is determined by proton or neutron conservation:

$$\frac{N}{2} = \int_{-\infty}^{\infty} \sum_{n=1}^{\infty} \frac{\tilde{g}(\epsilon, \epsilon_n)}{(e^{(\epsilon - \tilde{\epsilon}_{FT})/T} + 1)} d\epsilon. \quad (4)$$

The function $\tilde{g}(\epsilon, \epsilon_n)$ is the usual Gaussian smoothing function used in the Strutinsky prescription, given by

$$\tilde{g}(\epsilon, \epsilon_n) = \frac{1}{\gamma\sqrt{\pi}} e^{-(\epsilon - \epsilon_n)^2/\gamma^2} \cdot \sum_{m=0}^p c_m H_m \left(\frac{\epsilon - \epsilon_n}{\gamma} \right),$$

where

$$c_m = \frac{(-1)^{m/2}}{2^m (m/2)!}, \quad m \text{ even},$$

$$= 0, \quad m \text{ odd}.$$

$H_m(x)$ are Hermite polynomials; these differ from the usual Hermite function in that each H_m is normalized to unity with a suitable Gaussian weighting factor γ . The summation over m extends only to p , which defines the order of the shell correction. The quantities γ and p are not physical quantities and must be chosen so that over some range the smooth energy, \tilde{E}_T , is independent of them. For $T = 0$, the values of $\gamma = 1.2 \times 41 \text{ MeV/A}^{1/3}$ and $p = 6$ are nearly optimum choices,⁴ and we have used these values in the calculations to date.

We may now define the shell correction δU_T at temperature T as

$$\delta U_T = (E_T - \tilde{E}_T)_{\text{protons}} + (E_T - \tilde{E}_T)_{\text{neutrons}}. \quad (5)$$

For $T = 0$, Eqs. (1-5) reduce to those of the standard Strutinsky prescription.⁵

The deformation energy at a given temperature is given by

$$E_{\text{DEF}} = E_{\text{LDM}} + \delta U_T, \quad (6)$$

where E_{LDM} is the liquid-drop-model energy whose dependence on temperature is neglected.

The internal excitation energy E_x for a given nuclear shape may be obtained from the relation

$$E_x(T) = (E_T - E_{T0})_{\text{protons}} + (E_T - E_{T0})_{\text{neutrons}}, \quad (7)$$

where E_{T0} for protons or neutrons is the sum of single-particle energies up to the usual ($T = 0$) Fermi surface.

In our calculations to date we have neglected the effects of pairing. Although these effects are expected to influence the results at excitation energies up to several MeV, we do not expect the results presented below to be changed significantly for $T \gtrsim 0.5 \text{ MeV}$.

RESULTS AND DISCUSSION

Calculations based on the above model have been carried out for the compound fissioning nucleus ^{236}U , for a variety of shapes from saddle to scission. We have used the same computer program as was used in our earlier two-center-model calculations⁴ to generate the single-particle energies for each shape considered. Shapes are characterized by four independent shape variables; however, we minimize the potential energy with respect to two of these and will discuss results, as before, in terms of the quantity D , the neck radius, and λ , the volume ratio of the two portions of the nucleus on either side of the neck plane. (The reader is referred to the longer paper of Ref. 4 for an explanation of the shape parameterization and other details of the calculations.)

Let us first consider the shell correction energy δU_T . It is expected that, for a given shape, the magnitude of this term will decrease with increasing temperature and will approach zero asymptotically, corresponding to the washing out of shell effects as T becomes larger. Figure 1 shows δU_T as a function of temperature for several values of the neck radius D , and for several values of the asymmetry λ at each D . (The reader may wish to refer to Figure 2 of Reference 4; it is seen there that, in the region from the saddle point to scission, the direction of decreasing D closely approximates the fission direction along the minimum potential energy path.)

In the lower portion of Fig. 1 we see that, at $D = 5.0$ fm (saddle point), the lowest energies occur for $\lambda = 1.8$ and that the energies generally increase with decreasing λ . All of the curves asymptotically approach $\delta U_T = 0$ as T becomes large, as expected.

In the upper portion of Fig. 1 we see that, at $D = 2.5$ fm (near scission), the lowest energies occur for $\lambda = 1.45$ for temperatures up to ~ 2 MeV, when the curves for $\lambda = 1.45$ and 1.7 begin to overlap. Again, all curves approach $\delta U_T = 0$ as T becomes large. The center portion of this figure shows an intermediate point between saddle and scission, at $D = 3.5$ fm, where the curves for $\lambda = 1.45$ and $\lambda = 1.8$ almost overlap, and again the same washing-out of shell effects with increasing temperature is observed.

Figure 2 shows the total effective potential energy (here labeled E_{DEF} ---it is also the effective deformation energy of the nucleus) as a function of the asymmetry λ , for the same three values of D as above and for several temperatures for each D .

Let us first examine the uppermost portion of Fig. 2, for which $D = 2.5$ fm. The curve for $T = 0.5$ MeV has a minimum at $\lambda \approx 1.45$; this corresponds to a mass ratio of $\sim 140/96$ and is in agreement with the most probable mass ratio observed at low compound-nucleus excitation energies. As the temperature is increased two interesting phenomena occur:

First, the energy corresponding to the minimum in $E_{\text{DEF}}(\lambda)$ increases, while that corresponding to $\lambda = 1$ decreases. The implication of this occurrence is that the peak-to-valley ratio of the fragment mass distribution or, more precisely, the ratio of asymmetric to symmetric yields, decreases with increasing temperature.

Second, the asymmetry at which the minimum in $E_{\text{DEF}}(\lambda)$ occurs decreases somewhat with increasing T up to $T \approx 1.7$ MeV. The implication here is that the peak of the mass distribution shifts toward symmetry with increasing temperature in this range. The behavior of these curves is such that the mass distribution should become peaked at symmetry for $T \approx 1.8$ MeV, where the minimum in $E_{\text{DEF}}(\lambda)$ shifts to $\lambda = 1$.

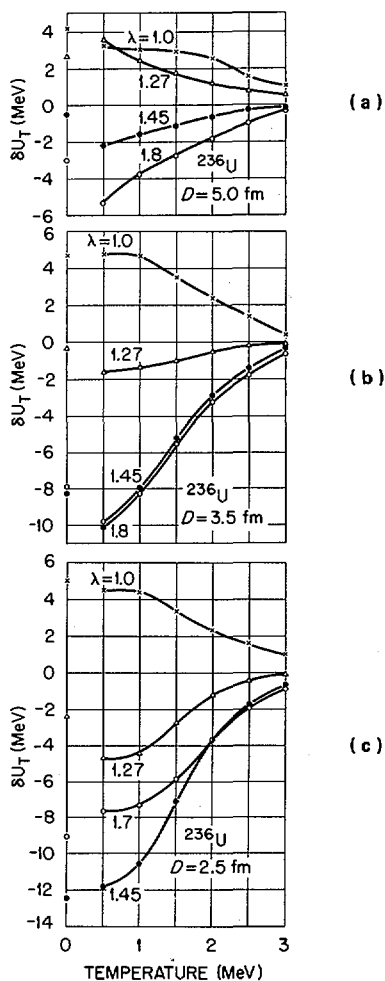


FIG. 1. Shell correction energy δU_T as a function of nuclear temperature T for selected symmetric and asymmetric shapes of the fissioning nucleus ^{236}U . (a) shows the results for the shapes at the second saddle point, i.e., neck radius $D = 5.0$ fm. λ , the volume ratio of the portions of the nucleus on either side of the neck plane, identifies different curves. (b) and (c) show the results for $D = 3.5$ fm and 2.5 fm, respectively. These shapes are beyond the second saddle point and are close to scission. The shapes included in the calculation are the minimum energy shapes taken from our earlier calculations at $T = 0$ (Ref. [4]).

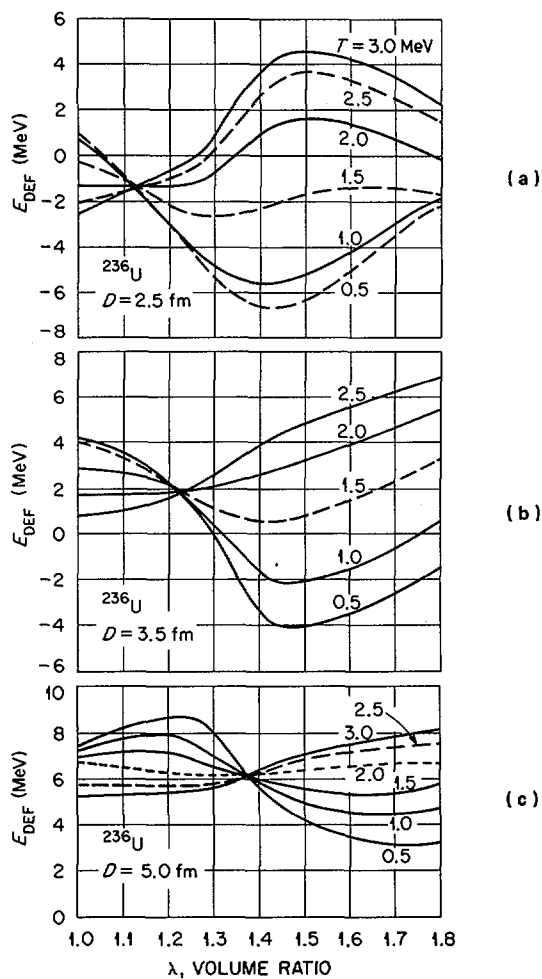


FIG. 2. The deformation energy E_{DEF} as a function of volume ratio λ for various temperatures T of the nucleus $^{236}_{92}\text{U}$. (a) (b) and (c) are for the shapes at $D = 2.5$ fm, 3.5 fm, and 5.0 fm, respectively. These are the minimum energy shapes taken from our earlier calculations at $T = 0$ (Ref.[4]). The figure shows a transition from symmetry to asymmetry at $T \approx 1.8$ MeV corresponding to an excitation energy of about 90 MeV.

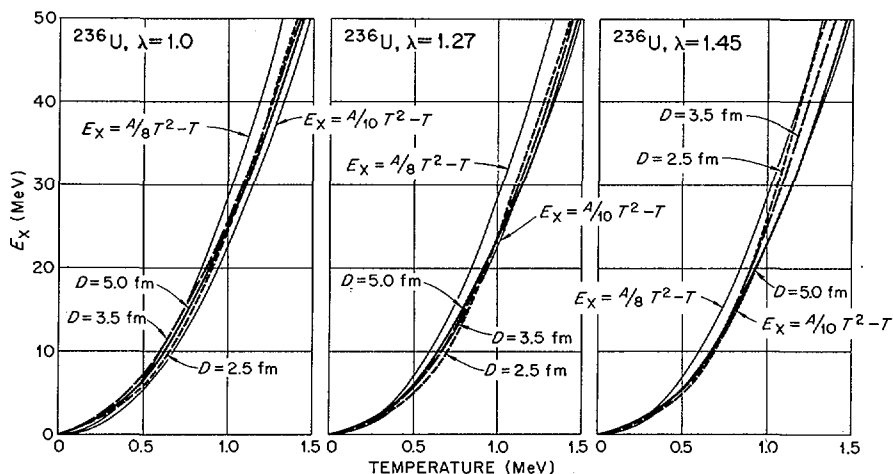


FIG. 3. Excitation energy E_X of the fissioning nucleus $^{236}_{92}\text{U}$ as a function of nuclear temperature T for various shapes identified by D and λ . The excitation energies calculated from the empirical relations,

$$E_X = \frac{A}{8} T^2 - T \text{ and } E_X = \frac{A}{10} T^2 - T, \text{ are also shown for comparison.}$$

All of the implications drawn from the observations described depend, of course, on the assumption that the characteristics of the mass distributions are controlled primarily by the potential surface and that dynamical considerations do not appreciably alter these characteristics. Implicit also is the assumption that the potential energy surface near scission is more important in this respect than that at or near the saddle point.

In the lowest portion of Fig. 2, which corresponds to the saddle region, we see a generally similar behavior of $E_{\text{DEF}}(\lambda; T)$, except that the minima occur at large values of the asymmetry λ . In the center portion of the figure, at an intermediate value of D , namely 3.5 fm, the curves already resemble those for $D = 2.5$ fm, near scission.

Figure 3 shows the internal excitation energy E_X of the ^{236}U nucleus as a function of temperature for three values of λ and for three values of D ; all combinations are shown. The excitation energy E_X is obtained from Eq. (7), for each shape and temperature. The upper thin curves in the figure show the Lang-LeCouteur⁶ formula, $E_X = (A/8)T^2 - T$, where A is the nuclear mass. Since these curves lie generally higher than our calculated curves, we also show the equation $E_X = (A/10)T^2 - T$ for comparison.

The conclusions to be drawn from Fig. 3 are, then, that the internal excitation energy $E_X(T)$ is relatively insensitive to λ and D , and that the statistical-model formula of Lang and LeCouteur⁶ is confirmed, within some reasonable uncertainty in the coefficient of T^2 .

Finally, we wish to point out that the conclusions and implications discussed above in connection with Fig. 2 are qualitatively consistent with known experimental observations to date. In particular, the relative symmetric yield in the mass distribution increases with increasing compound-nucleus excitation energy.^{1,2} Further, the careful measurements of Ferguson et al.² showed a slight shift in peak position towards symmetry,

as the compound-nucleus excitation energy was increased from about 13 to 18 MeV. These consistencies, coupled with earlier observations, would seem to enhance the credibility of the assumption that the potential surface dominates in determinations of the mass distributions and kinetic energies, and that the potential surface near scission is particularly important. Dynamic effects, however, must be determined in detail; also, viscosity effects, which are to be discussed later in this symposium, must be treated and may be important even for very low-excitation fission. It is interesting to note that if viscosity effects are such that, in the saddle-to-scission descent, the system is heated to the same temperature T independent of mass, then the effective potential energy near scission will be given by results such as those shown in Fig. 2 at $D = 2.5$ fm, for temperature T .

An especially interesting and germane experiment in the future will be the measurement of mass distributions at excitation energies corresponding to temperatures of 1.5 to 2 MeV, to observe the transition to distributions peaked at symmetry. The analysis of such experiments will not be simple because of the competition from neutron emission, but as greater sophistication in this kind of analysis is achieved the necessary information will perhaps become attainable.

REFERENCES

- [1] HYDE, E. K., "The nuclear properties of heavy elements", Prentice-Hall, Englewood Cliffs, N.J., 1964, Vol. III.
- [2] FERGUSON, R. L., PLASIL, F., PLEASANTON, F., BURNETT, S. C., and SCHMITT, H. W., Phys. Rev. C 7 (1973) 2510.
- [3] ADEEV, G. D. and CHERDANTSEV, P. A., Phys. Lett. 39B (1972) 485.
- [4] MUSTAFA, M. G., MOSEL, U., and SCHMITT, H. W., Phys. Rev. Lett. 28 (1972) 1536; Phys. Rev. C 7 (1973) 1519.
- [5] STRUTINSKY, V. M., Nucl. Phys. A95 (1967) 420; A122 (1968) 1.
- [6] LANG, J. M. B. and LeCOUTEUR, K. J., Proc. Phys. Soc. (London) A67 (1954) 586; also Nucl. Phys. 13 (1959) 32.

DISCUSSION

S. BJØRNHOLM: Do I take it that your calculation assumes statistical equilibrium (i. e. viscosity) all the way from the barrier down to a point near scission, where the neck is quite thin?

M. G. MUSTAFA: Nothing is assumed about the path from saddle to scission. We have carried out an investigation of the effect of internal excitation energy, or temperature, on the total "effective potential energy" surface within the Strutinsky framework. Just how the fission process proceeds from saddle to scission, the sequence of shapes and temperatures through which the nucleus passes, etc. must be determined from other considerations, preferably from the solution of the complete Hamiltonian including dynamics.

S. S. KAPOOR: I feel that one cannot say much about the agreement of the calculations with the experiment, unless one also calculates the distributions of the fragment masses and compares their widths with the experimental values.

M. G. MUSTAFA: I agree with you. The comparison between the results of potential energy calculations and experimental mass distributions should be considered qualitative.

H. C. PAULI: This comment applies both to your work and to Jensen's. You have merely calculated the mass distribution whereas, in order to have a firmer basis for your theory, you should also calculate the kinetic energy distribution and the excitation energy distribution. Only when the same model describes all these factors can the model be regarded as conclusive.

M. G. MUSTAFA: I would agree. As I have already indicated, this is a parametric study of the effect of internal excitation energy on the total "effective potential energy" surface. To some extent we can check the kinetic and excitation energy distributions of the fragments from our results near scission, but this will be simple and straightforward only if the path from saddle to scission turns out (from other considerations) to be almost completely viscous.

Z. FRAENKEL (Chairman): One may add that such calculations must also reproduce the experimental prompt neutron emission as a function of the fragment masses.

J. J. GRIFFIN: This question is addressed to all the speakers. But let me say first of all that I have no objection to studying mass asymmetry via phenomenological analyses. However, I am disturbed that no one has underlined the fact that insufficient information is put into these analyses to ever achieve a complete solution. I refer to the fact that any deformation space is in general a curved space whose properties are well defined only when the metric tensor (inertia) is specified. Without the metric tensor, one who sets a certain deformation co-ordinate equal to a constant may believe that he has selected a plane perpendicular to the scission path - but someone else may view his plane as a paraboloid from his alternative co-ordinate system. Only the metric tensor can resolve this difference. Without it the description is not co-ordinate invariant. It follows that, if one is doing phenomenology like this, one should be aware of the fact that any bad fit might be considerably improved merely by judiciously redefining the co-ordinates.

L. G. MORETTO: I agree completely with Mr. Griffin. However, at high viscosity the system cannot acquire large velocities and thus the inertia tensor becomes of secondary importance with respect to the viscosity tensor. The dynamics of the system is thus controlled by inertia at small viscosity and by the potential energy and viscosity tensor at large viscosity. In other words the metric at high viscosity is determined by the potential energy and by the viscosity tensor, while at low or zero viscosity the metric is determined by the potential energy and by the inertia tensor.

J. J. GRIFFIN: I find it hard to believe that viscosity renders the curvature of the space irrelevant. It may be so, but I wish there had been a paper presented here to prove that claim.

M. G. MUSTAFA: It is clear, as I indicated before, that a complete dynamical calculation is required.

H. C. PAULI: If you have a completely phenomenological approach (as practised by Metag and von Brentano for the lifetime systematics of isomers), there is nothing much wrong with choosing some effective mass. But, if you choose a well-defined deformation, you are bound to a particular metric, which you cannot simply ignore. I strongly disagree with the statement that it is a point of view; it is a matter of principle.

M. G. MUSTAFA: As I indicated, we need a complete dynamical calculation of the path to scission. In those cases where this problem is to be approached phenomenologically, the model assumptions should be made as realistic as possible and should be made clear and explicit; then such kinds of calculations may have something to contribute to our understanding of fission.

PROMPT AND DELAYED NEUTRON YIELDS FROM LOW-ENERGY PHOTOFISSION OF ^{232}Th , ^{235}U , ^{238}U AND ^{239}Pu

J. T. CALDWELL, E. J. DOWDY, G. M. WORTH
Los Alamos Scientific Laboratory,
University of California,
Los Alamos, N. Mex.,
United States of America

Abstract

PROMPT AND DELAYED NEUTRON YIELDS FROM LOW-ENERGY PHOTOFISSION OF ^{232}Th , ^{235}U , ^{238}U AND ^{239}Pu .

Enriched or mono-isotopic samples of ^{232}Th , ^{235}U , ^{238}U and ^{239}Pu were irradiated with bremsstrahlung from electrons of 8-, 10-, and 12-MeV energy. Neutrons produced as a result of the bremsstrahlung pulses were detected in a large 4π neutron detector with a neutron dieaway time of $\sim 30 \mu\text{s}$ and an efficiency for ^{252}Cf spontaneous fission neutrons of 50%. Multiplicity sorting was done on the prompt neutrons with a Los Alamos Scientific Laboratory (LASL) designed sorter and, after correction for background and overlap, events of order ≥ 2 were fitted with an analytic, two-parameter Gaussian expression to determine $\bar{\nu}_p$, the mean number of prompt neutrons per photofission. Since, at the energies measured, negligible $(\gamma, 2n)$ reactions occur for any of the four isotopes, events of order ≥ 2 were used to determine the photofission reaction rate and, after correction for the photofission component, the events of order 1 were then used to determine the (γ, n) reaction rate and thus Γ_n/Γ_d ratios weighted over the bremsstrahlung photon spectrum for each electron energy. Absolute β (delayed neutron per photofission) fractions were determined from counts obtained between beam bursts (but after prompt dieaway) and the photofission reaction rate.

Thus, $\bar{\nu}_p$, Γ_n/Γ_f and β values were determined for low-energy photofission using a single detector and in the course of a single experiment. These values are thus free of systematic errors that often arise when the results of two or more detectors and/or experiments must be combined. The $\bar{\nu}_p$ values obtained are the first measured photofission values reported for three of the four isotopes.

1. INTRODUCTION

There have been only a few previous measurements [1-3] of $\bar{\nu}_p$, the mean number of prompt neutrons emitted per fission event, for photofission of the major fissionable isotopes at low energies, and no previous measurement of the dependence of $\bar{\nu}_p$ on photoexcitation energy. We find only one report [4] of measurements of the absolute delayed neutron fractions, β , for photofission. A somewhat larger body of information [5-7] is available on the determination of the competition between neutron emission and fission for photoexcitation, made possible through measurements of $\langle \Gamma_n/\Gamma_f \rangle$, the average ratio of the neutron emission width to the fission width. There have been no previous simultaneous measurements of these quantities.

Values of these parameters are useful in establishing or confirming fission systematics for expanding the understanding of the fission process and in interpreting the results of measurements of dependent quantities such as the partial cross-sections.

TABLE I. FISSIONABLE MATERIAL SAMPLE DESCRIPTION

Sample	Physical Description	Isotopic Analysis
^{232}Th	Disk, 5-cm diameter, 76 grams	100% Th-232
^{235}U	Disk, 5-cm diameter, 20 grams	1.0% U-234 93.23% U-235 0.36% U-236 5.41% U-238
^{238}U	Disk, 5-cm diameter, 58.6 grams	0.02% U-235 99.98% U-238
^{239}Pu	Disk, 2.29-cm diameter, 4.98 grams canned with Ni	$\leq 0.004\%$ Pu-238 97.67% Pu-239 2.28% Pu-240 0.048% Pu-241 0.002% Pu-242

In this paper, we report on the simultaneous measurement, using a single detector of γ_p , β , and $\langle \Gamma_n/\Gamma_f \rangle$ for photo-excitation of ^{232}Th , ^{238}U , ^{235}U , ^{239}Pu using electron bremsstrahlung from 8-, 10-, 10.2-, and 12-MeV electrons.

2. EXPERIMENTAL METHOD

2.1. Irradiation

Electrons were accelerated to the appropriate energy in 10-nsec pulses with a repetition rate of 360 pps in the USAEC Electron Linear Accelerator in Santa Barbara, Ca., operated by EG&G, Inc. Conversion to bremsstrahlung took place in a 10-cm

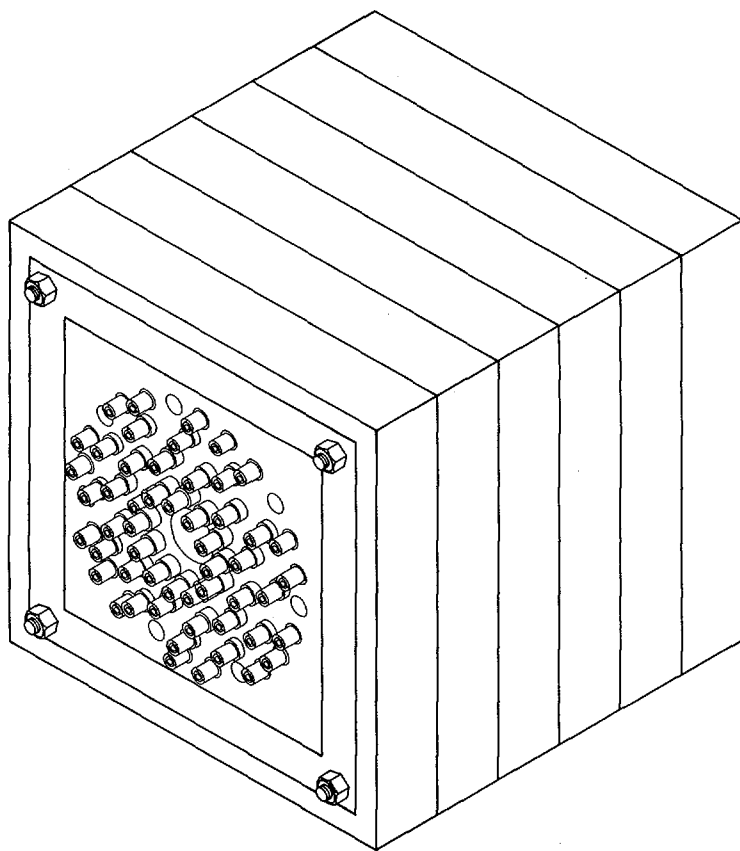


FIG. 1. The neutron detector. A 61-cm cube of polythene with four rings of 2.54-cm diameter, 61-cm-long ^3He proportional counter tubes, and a central sample hole. The hole is 3.8 cm in radius, and the tubes are in rings with radii of 6, 4, 10, 8, 14, 6, and 17.8 cm. Fifty-three ^3He tubes were used in the work described in this paper.

cube of aluminum. The bremsstrahlung in the forward direction was collimated to a 2.5 cm diameter beam using a 20 cm thick iron collimator. Samples of fissionable material, described in Table I, were placed at the center of the detector shown in Fig. 1, with the detector axis aligned with the beam. The sample-to-converter distance was approximately 1 meter. The electron beam currents were monitored using the converter as a Faraday cup. The detector was shielded on all sides with borated polythene blocks, and materials with low (γ, n) reaction thresholds were excluded from the vicinity of the converter. Machine-generated backgrounds were determined by irradiating an aluminum disk in the sample position.

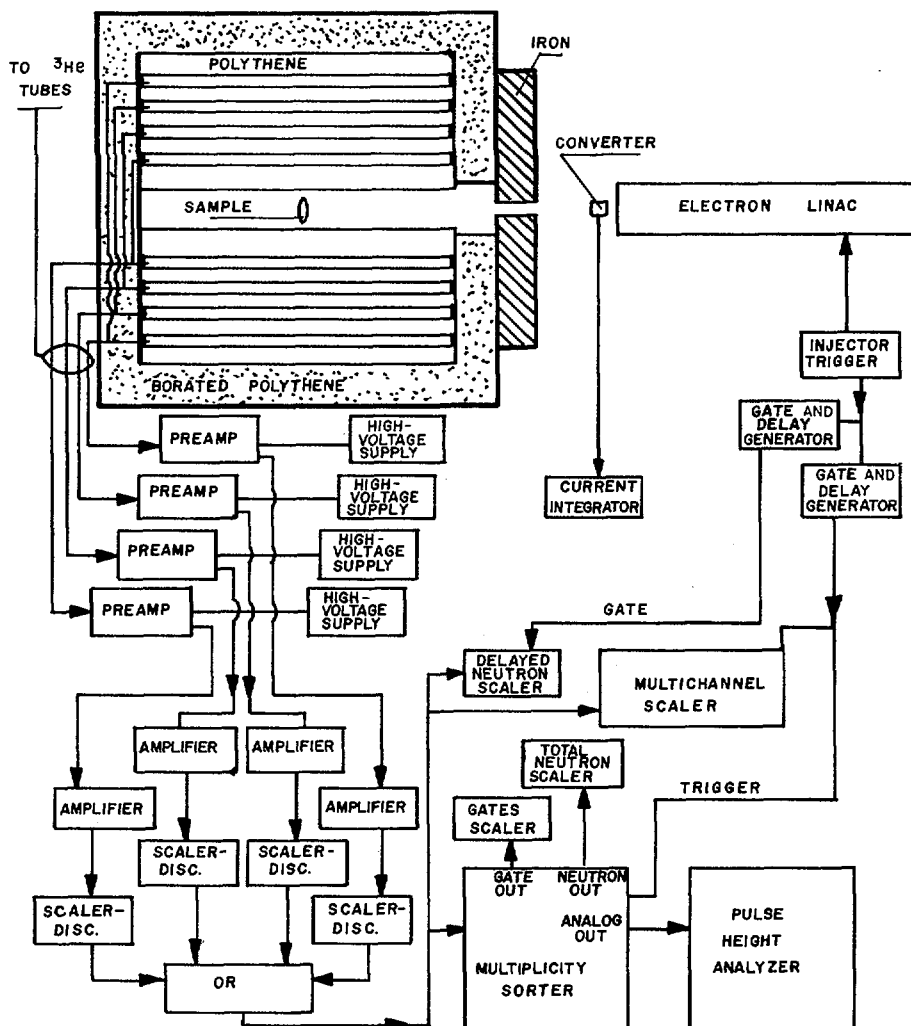


FIG. 2. Block diagram of the neutron detection system.

2.2. Neutron Detection System

The detection system has been described in detail elsewhere [8]. The neutron detector was a polythene cube, 61 cm on a side, containing fifty-three ^3He proportional counter tubes (in four concentric rings), each 2.54 cm diameter and 61 cm long, with filling pressures of 6, 4, 4, and 3 atmospheres for the innermost-to-outermost ring of tubes, respectively. Neutrons generated in photoreactions in the samples were moderated in the polythene and captured with high probability in the ^3He tubes. The efficiency for detecting the prompt neutrons from the spontaneous fission of ^{252}Cf was measured to be 52%, assuming $V_p = 3.784$, and the efficiency as a function of neutron energy has been calculated using Monte Carlo techniques.

The neutron slowing-down process and the increased probability of capture at lower energies produced a broad capture-time distribution with a distinct "dieaway" time for each ring of ^3He tubes. This distribution in time permitted the detection of prompt neutrons with high efficiency even though the detection system was paralyzed during the gamma flash, and for a few μsec thereafter.

The pulses from the ^3He tubes were processed as indicated in Fig. 2. Each ring of tubes had common high voltage and amplification modules, and the amplified pulses were presented to discriminators, set to fire at voltages just above the noise level. The standard slow logic pulses from the discriminators were routed to a logic OR module, and the OR output line served as the data path. The pulses from the OR module were routed to a LASL-designed unit identified as a multiplicity sorter, and also to a multichannel scaler and a delayed neutron scaler. The multichannel scaler was used to record the time dependence of pulses from the neutron detector following a trigger derived

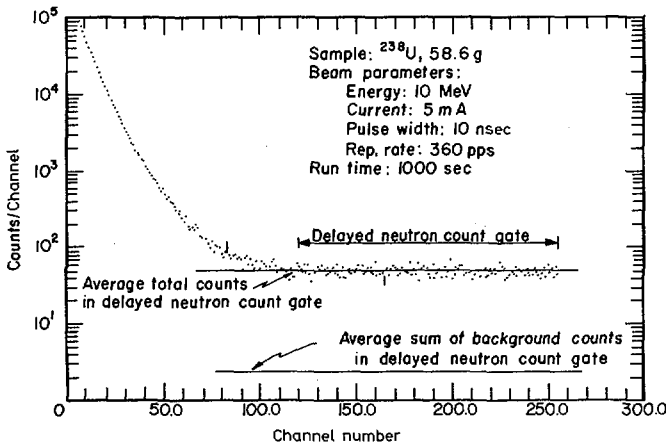


FIG. 3. Time variation of pulses from the neutron detector during a typical run.

from the linac. The delayed neutron scaler was used to scale the pulses from the detector following the dieaway of the prompt neutrons. The multiplicity sorter, described in detail elsewhere [9], is basically a digital-to-analog converter with a variable count gate width. Pulses appearing at the input following the linac-derived count gate trigger are scaled and the output pulse height is uniquely determined by the number (up to 9) of pulses arriving during the count gate. The pulse height analyzed output of the multiplicity sorter provided the measured multiplicity distribution.

With the linac pulse repetition rate of 360 pps, the time between pulses was 2778 μsec , and the prompt neutron population was negligible beyond 1200 μsec . So, the prompt neutrons were detected in a count gate opening a few microseconds after the gamma flash and closing at a variable time (usually 500 μsec) after that. The delayed neutrons were detected in a time window opening at 1200 μsec and closing before the next linac pulse. The time history of pulses from the neutron detector obtained from a typical run is shown in Fig. 3.

3. DATA REDUCTION

3.1. $\bar{\nu}_p$ Determination

Terrell [10] first demonstrated with an analytical derivation and a comparison with a large body of experimental data that the emitted prompt fission neutron multiplicity distribution $\{\rho_\nu\}$ can be described with the expression

$$\sum_0^{\nu} \rho_\nu = \frac{1}{2} + \frac{1}{2} f \left(\frac{\nu - \bar{\nu}_p + \frac{1}{2} + b}{\sigma} \right) \quad (1)$$

where

$$f(x) = \frac{1}{\sqrt{2\pi}} \int_{-x}^x e^{-\frac{t^2}{2}} dt \quad (2)$$

Here $\bar{\nu}_p$ is the average number of prompt neutrons emitted per fission, σ is a distribution width parameter, and

$$b \approx 0.01 \approx \frac{1}{2} - \frac{1}{2} f \left(\frac{\bar{\nu}_p + \frac{1}{2}}{\sigma} \right) \quad (3)$$

Thus the $\{\rho_\nu\}$ distribution is a function only of the two parameters $\bar{\nu}_p$ and σ .

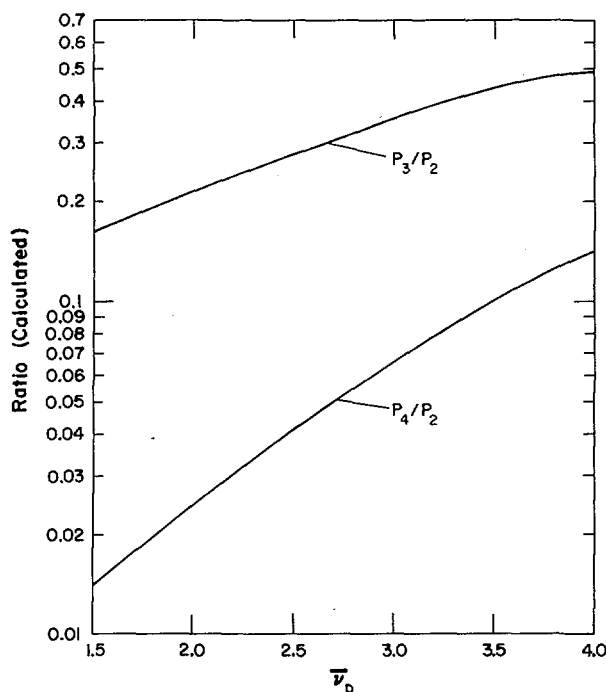


FIG.4. Typical variation of the ratios of observed multiplicities with $\bar{\nu}_p$, with $\sigma = 1.15$ and a typical efficiency.

Consideration of the effects of non-unity detector efficiency leads to the following expression for the observed multiplicity distribution $\{P_v\}$:

$$P_v = \epsilon^v \sum_{n=v}^N \left(\frac{n! (1-\epsilon)^{n-v}}{v! (n-v)!} \right) \rho_n \quad (4)$$

This expression is valid after the observed data has been corrected for background, pulse pileup, and deadtime effects. Here ρ_n is the emitted multiplicity of order n as determined from Eq. (1), ϵ is the detector efficiency and N is the maximum order emitted multiplicity, usually taken to be 9. Since ϵ varies slightly with neutron energy, a small correction is made by using Terrell's approximate expression

$$\langle \epsilon \rangle \approx 0.74 + 0.653 (\bar{\nu}_p + 1)^{\frac{1}{2}} \quad (5)$$

The magnitude of the efficiency correction is about 2% between $\bar{\nu}_p = 3.784$ and $\bar{\nu}_p = 2.50$.

As can be seen from Eq. (4) the shape of the observed multiplicity distribution $\{P_\nu\}$ is a fairly sensitive function of $\bar{\nu}_p$ and σ . This is demonstrated in Fig. 4 which shows the ratios P_3/P_2 and P_4/P_2 as a function of $\bar{\nu}_p$ for $\sigma = 1.15$ and for a typical value of ϵ . For a given isotope and excitation energy, $\bar{\nu}_p$ was actually determined by performing a weighted least squares fit of the observed multiplicity data of all orders ≥ 2 to Eq. (4) as a function of $\bar{\nu}_p$, σ . Since only bremsstrahlung energies of 12 MeV or less were used, $(\gamma, 2n)$ reactions in all isotopes were negligible and thus all observed net \geq order 2 events were uniquely associated with a fission event.

Since a fairly narrow range of excitation energies was covered it was felt that the width parameter σ for a given isotope should be essentially constant. This was found to be the case within the statistical accuracy of the data. Thus, an average value of σ for each isotope (different for each of the four isotopes) was determined and $\bar{\nu}_p$ at each excitation energy found from a one parameter least squares fit. The overall statistical error in $\bar{\nu}_p$ as determined in this fashion ranged between 0.07 and 0.14.

3.2. $\langle \Gamma_n / \Gamma_f \rangle$ Determination

Once $\bar{\nu}_p$ and σ were determined from the multiplicity shape distribution, Eq. (4) was used to determine a fission detection efficiency for the experimental quantity

$$\sum_{\nu=2}^N P_\nu$$

This served to determine the number of fission events occurring in a given run. Equation (4) was then also used to calculate the number of singles events due to photofission. This enabled us to determine, from the total observed singles events and the singles background, the number of singles due to (γ, n) reactions only and thus to determine the quantity $\langle \Gamma_n / \Gamma_f \rangle$. The overall experimental error in $\langle \Gamma_n / \Gamma_f \rangle$ was generally in the range of 5 to 10 percent.

3.3. Delayed Neutron Fraction

The delayed neutron fraction β was obtained by counting between beam bursts but after prompt dieaway. A typical time history of this data is shown in Fig. 4. This measurement was generally done simultaneously with the neutron multiplicity measurements. To improve statistical accuracy some high beam intensity delayed neutron runs were also made, notably for the

Pu samples. For these runs the number of fission events was determined by scaling the prompt part of the dieaway between high and low intensity runs. Some data utilizing the "ring ratio spectrometer" [11] technique were also taken to determine the average energy of photofission delayed neutrons and thus a suitable ϵ . The overall experimental error in β ranged between 5 and 10 percent.

3.4. Further Corrections and Errors

Where warranted, corrections for the presence of minor isotopes have been made. This correction was most notable for the case of β for the ^{235}U sample and amounted to about 10 percent. Generally speaking the largest source of error in all quantities is the uncertainty generated by the error in $\langle \sigma \rangle$. This error was approximately ± 0.05 for ^{235}U , ^{238}U , and ^{232}Th and ± 0.10 for ^{239}Pu and derives from the quality of the multiplicity shape distribution fit to the data.

4. RESULTS

4.1. $\bar{\nu}_p$

The values of $\bar{\nu}_p$ determined from this experiment are given in Table II. Included in Table II are the expected values of $\bar{\nu}_p$ as calculated from the expressions contained in the evaluations of Davey [12] for neutron induced fission of ^{234}U , ^{237}U , and ^{238}Pu and from the equation provided by Tu and Prince [13] for neutron-induced fission of ^{231}Th . These expressions are:

$$\begin{aligned}\bar{\nu}_p(E) &= 2.352 + 0.1349E && \text{for } ^{234}\text{U} + n \\ \bar{\nu}_p(E) &= 2.386 + 0.1412E && \text{for } ^{237}\text{U} + n \\ \bar{\nu}_p(E) &= 2.914 + 0.1436E && \text{for } ^{238}\text{Pu} + n\end{aligned}$$

$$\text{and } \bar{\nu}_p = 2.13 \quad \text{for } ^{231}\text{Th} + n_{\text{th}}$$

To calculate the $\bar{\nu}_p$ values to compare with our measured values, the excitation energies in these expressions were taken as the difference between the average photoexcitation energies and the neutron separation energies for the compound nuclei. The average photoexcitation energies were calculated as

$$\langle E_\gamma \rangle = \frac{\int_0^\infty E \sigma_{\gamma,f}(E) \times (E) dE}{\int_0^\infty \sigma_{\gamma,f}(E) \times (E) dE}$$

TABLE II. $\bar{\nu}_p$ VALUES

Electron Energy (MeV)	^{232}Th		^{235}U		^{238}U		^{239}Pu	
	Meas.	Calc. [13]	Meas.	Calc. [12]	Meas.	Calc. [12]	Meas.	Calc. [12]
8	1.963 ± 0.108	2.13	2.456 ± 0.086	2.55	2.457 ± 0.088	2.48	-----	3.09
10	1.891 ± 0.111	-----	2.697 ± 0.081	2.71	2.628 ± 0.083	2.65	3.32 ± 0.08	3.25
10.2	1.891 ± 0.111	-----	2.612 ± 0.079	-----	2.585 ± 0.082	-----	3.17 ± 0.14	-----
12	2.084 ± 0.107	-----	2.963 ± 0.072	2.91	2.802 ± 0.078	2.85	3.43 ± 0.10	3.46
Av. Gaussian width $\langle \sigma \rangle$	1.15 ± 0.05		1.20 ± 0.05		1.22 ± 0.05		1.18 ± 0.10	

where $x(E)$ is the bremsstrahlung spectrum as given by Sandifer [14] and $\sigma_{\gamma,f}(E)$ are the differential photofission cross-sections for the appropriate target nuclei [6,15-18]. These average photoexcitation energies were very nearly the same for all the nuclei studied, being 6.80-, 7.99-, and 9.44-MeV for electron energies of 8, 10, and 12 MeV respectively.

The agreement among the measured values and those calculated from the evaluations is exceptionally good. Assuming linear dependence of \bar{v}_p on photoexcitation energy for our data results in the following expressions obtained from least squares analyses:

$$\bar{v}_p(\langle E_\gamma \rangle) = 1.595 + 0.0449 \langle E_\gamma \rangle \text{ for } {}^{232}\text{Th with a correlation coefficient of 0.557}$$

$$\bar{v}_p(\langle E_\gamma \rangle) = 1.215 + 0.1819 \langle E_\gamma \rangle \text{ for } {}^{235}\text{U with a correlation coefficient of 0.967}$$

$$\bar{v}_p(\langle E_\gamma \rangle) = 1.619 + 0.1240 \langle E_\gamma \rangle \text{ for } {}^{238}\text{U with a correlation coefficient of 0.981}$$

$$\bar{v}_p(\langle E_\gamma \rangle) = 2.248 + 0.1244 \langle E_\gamma \rangle \text{ for } {}^{239}\text{Pu with a correlation coefficient of 0.826.}$$

It appears that a linear dependence is consistent with our data except for the ${}^{232}\text{Th}$ values. Previous evaluations [12,19] have noted a deviation from a single straight line fit for neutron induced fission of ${}^{232}\text{Th}$ and ${}^{233}\text{U}$ at low energies, and it is plausible that similar behavior might be found for the ${}^{232}\text{Th}$ compound nucleus.

4.2. β

The β values determined from this experiment are given in Table III, along with the data of Nikotin and Petrzhak [4] and the calculated values of Keepin [20]. The agreement between the values obtained by Nikotin and Petrzhak for 15-MeV electron bremsstrahlung and our weighted average is quite good. Keepin's correlation, however, requires higher values than the measured ones for all the nuclei except ${}^{235}\text{U}$.

4.3. $\langle \Gamma_n / \Gamma_f \rangle$

The values of $\langle \Gamma_n / \Gamma_f \rangle$ obtained in the analysis of our experimental data are given in Table IV. We find strong

TABLE III. $\bar{\nu}\beta$ VALUES

Electron Energy (MeV):	^{232}Th	^{235}U	^{238}U	^{239}Pu
8	0.0310 ± 0.0027	0.0090 ± 0.0008	0.0306 ± 0.0024	-----
10	0.0306 ± 0.0030	0.0088 ± 0.0008	0.0276 ± 0.0017	-----
10.2	0.0267 ± 0.0016	0.0113 ± 0.0007	0.0306 ± 0.0014	0.00371 ± 0.00017
12	0.0259 ± 0.0031	0.0112 ± 0.0008	0.0275 ± 0.0019	0.00375 ± 0.00022
Average ($1/\sigma^2$ weighted)	0.0280 ± 0.0012	0.0102 ± 0.0004	0.0291 ± 0.0009	0.00372 ± 0.00013
Previous Measurement [4]	0.038 ± 0.006	0.0096 ± 0.0013	0.031 ± 0.004	0.0036 ± 0.0006
Correlation Value [20]	0.0309	0.0101	0.0309	0.0048

TABLE IV. $\langle \Gamma_n / \Gamma_f \rangle$ VALUES

Electron Energy (MeV):	^{232}Th	^{235}U	^{238}U	^{239}Pu
8	1.05 ± 0.12	0.98 ± 0.10	1.65 ± 0.12	-----
10	3.77 ± 0.32	1.06 ± 0.09	2.59 ± 0.14	-----
10.2	3.56 ± 0.32	1.09 ± 0.09	2.608 ± 0.147	0.29 ± 0.08
12	6.28 ± 0.48	1.18 ± 0.08	2.89 ± 0.14	1.02 ± 0.08
Correlation Value [21]	3.16	1.22	3.22	0.65

dependence on excitation energy as have other recent investigations [6]. Their value for the ratio at the highest excitation energy for ^{238}U is consistent with ours, but their reported value of $\langle \Gamma_n / \Gamma_f \rangle = 18.5$ for ^{232}Th is considerably different from ours. They assumed values for $\bar{\nu}_p$ and their assumed value for ^{232}Th was higher than our measured value, but a re-analysis of their data with our measured $\bar{\nu}_p$ value reduces the value for the ratio to ≈ 12 , still much larger than our measured value. Our ^{232}Th value gives a qualitatively better fit to the Z^2/A correlation of Huizenga and Vandenbosch [5]. Mafra, et al. [7] also reported some evidence of an energy dependence for the ratio $\langle \Gamma_n / \Gamma_f \rangle$ for ^{232}Th and ^{238}U . Their data were analyzed on the assumption of a constant $\bar{\nu}_p = 2.5$ for both nuclei, and we have made no re-analysis of their data with our measured $\bar{\nu}_p$ values.

Included in Table IV are the values for the ratio calculated using the empirical fit of Sikkeland, et al. [21]. Again, the value for ^{232}Th at the highest excitation energy represents a large deviation from the evaluation.

REFERENCES

- [1] LAZAREVA, L. E., GAVRILOV, B. I., VALUEV, B. N., ZATSEPINA, G. N., STAVINSKY, V. S., Proc. Conf. of the Academy of Sciences of the USSR on the Peaceful Uses of Atomic Energy, Physical Sciences Section in English translation, Consultants Bureau, New York (1955) 217.
- [2] PROKHOROVA, L. I., SMIRENKIN, G. N., At. Ehnerg. 8 (1960) 457.
- [3] CONDE, H., HOLMBERG, M., in Physics and Chemistry of Fission (Proc. Symp. Salzburg, 1965) 2, IAEA, Vienna (1965) 57.
- [4] NIKOTIN, O. P., PETRZHAK, K. A., At. Ehnerg. 20 (1966) 268.
- [5] HUIZENGA, J. R., VANDENBOSCH, R., in Nuclear Reactions, (ENDT, P. M., SMITH, P. B., Eds) II, North-Holland Publishing Co., Amsterdam (1962) 42.
- [6] VEYSSIERE, A., BEIL, H., BERGERE, R., CARLOS, P., LEPRETRE, A., Nucl. Phys. A199 (1973) 45.
- [7] MAFRA, O. Y., KUNIYOSHI, S., GOLDEMBERG, J., Nucl. Phys. A186 (1972) 110.
- [8] DOWDY, E. J., CALDWELL, J. T., WORTH, G. M., to be published, Nucl. Instrum. Methods.
- [9] WORTH, G. M., CALDWELL, J. T., DOWDY, E. J., to be published, Nucl. Instrum. Methods.
- [10] TERRELL, J., Phys. Rev. 108 (1957) 783.
- [11] CALDWELL, J. T., UCRL-50287 (1967).
- [12] DAVEY, W. G., Nucl. Sci. Eng. 44 (1971) 345.
- [13] TU, PING-SHIU, PRINCE, A., J. Nucl. Energy 25 (1971) 599.
- [14] SANDIFER, C. W., Edgerton, Germeshausen & Grier Inc., Santa Barbara, Cal., private communication.
- [15] BOWMAN, C. D., AUCHAMPAUGH, G. F., FULTZ, S. C., Phys. Rev. 133 (1964) B676.
- [16] KHAN, A. M., KNOWLES, J. W., Nucl. Phys. A179 (1972) 333.
- [17] SHAPIRO, A., STUBBINS, W. F., Nucl. Sci. Eng. 45 (1971) 47.
- [18] KATZ, L., BAERG, A. P., BROWN, F., in Peaceful Uses of Atomic Energy (Proc. Conf. Geneva, 1958) 15, UN, New York (1958) 188.
- [19] FILLMORE, F. L., J. Nucl. Energy 22 (1968) 79.
- [20] KEEPIN, G. R., Physics of Nuclear Kinetics, Addison Wesley Publ. Co., Reading, Mass. (1965) 101.
- [21] SIKKELAND, T., GHIORSO, A., NURMIA, M. J., Phys. Rev. 172 (1968) 1232.

DISCUSSION

T. GOZANI: Since 1968, we at Intelcom (formerly Gulf) Rad Tech have been measuring some basic integral quantities related to low-energy photofission phenomena. The interest in this domain stems from the

application of photoinduced reactions to the non-destructive assay of nuclear materials. The most sensitive energy region for the identification of the various isotopes is around and below the photofission barrier. The systematics of prompt and delayed neutron production was studied in this region for ^{232}Th , ^{235}U , ^{238}U and ^{239}Pu , by simultaneous measurement of the fission yield and the prompt and delayed neutron yields. The results for ^{232}Th and ^{238}U are very interesting, especially below their relatively high (γ, n) thresholds (6.4 MeV and 6.1 MeV respectively). In this energy range one can investigate the photofission process with no competition from neutron channels. The measured delayed and prompt neutron yields, as well as the previously measured fission yield in the sub-threshold region of ^{232}Th , show clearly the existence of structure in the photofission cross-section around 5.7 to 5.8 MeV. Measurements on the other isotopes, namely ^{235}U , ^{238}U and ^{239}Pu , made under exactly the same conditions, did not indicate such an obvious structure in the energy region above 5.4 MeV. The ratio Y_n/Y_f (which is related to the number of prompt neutrons emitted per photofission, ν_n , and to much lesser extent to their energy spectrum) did not show, as expected, any significant dependence on E_e around the threshold energy. However, it did show, unexpectedly, an increase below the threshold energy for both ^{232}Th and ^{238}U , which, in the case of ^{232}Th , is rather dramatic. Significant increases in the effective delayed neutron fraction (Y_d/Y_n) in the sub-threshold regions were also observed.

P. L. REEDER: In this connection, I should like to mention that E. Chulick at Washington University measured delayed neutrons from ^4He bombardment of ^{232}Th and at an energy just above the fission threshold and found an unusually high yield of delayed neutrons.

E. J. DOWDY: Our absolute values of $\bar{\nu}_p$ for ^{232}Th (which should not be directly compared to the relative cumulative neutron yields of Gozani and co-workers) show only a deviation from the reasonably expected increase with excitation energy, i. e. there is no statistically significant increase of $\bar{\nu}_p$ over an energy range of more than 2.5 MeV. Similarly, for β , our absolute fractions should not be compared with relative yields: our measured values are statistically invariant over the same energy range. The contention that there are variations and structure at these lower energies is not substantiated by our measurements. But an increase of $\bar{\nu}_p$ with decreasing excitation energy (sub-barrier) is, as I have said, consistent with the behaviour found for neutron-induced fission of ^{232}Th and ^{233}U .

ENERGY DEPENDENCE OF Γ_f/Γ_n FOR THE NUCLEUS $^{216}\text{Rn}^*$

H. FREIESLEBEN⁺, H. C. BRITT⁺⁺, J. R. HUIZENGA

Nuclear Structure Research Laboratory,
University of Rochester, Rochester, N. Y.,
United States of America

Abstract

ENERGY DEPENDENCE OF Γ_f/Γ_n FOR THE NUCLEUS ^{216}Rn .

The $^{209}\text{Bi} + ^7\text{Li}$ reaction has been used to determine experimentally Γ_f/Γ_n for the initial compound nucleus ^{216}Rn . Cross-sections for the $(^7\text{Li}, f)$ reaction were measured at bombarding energies between 24 and 34 MeV by detecting coincident fission fragments. All the other components of the total reaction cross-section are due to $(^7\text{Li}, xn)$, $(^7\text{Li}, txn)$ and $(^7\text{Li}, \alpha xn)$ reactions. They were determined by observing known-energy alpha particles from the short lifetime decays of various Rn, At and Po isotopes. The background due to prompt reaction particles was eliminated by using a pulsed ^7Li -beam and detecting the decay particles between beam pulses. Correction for the effects of second-chance fission were obtained from measurements of cross-sections for the $(^6\text{Li}, f)$ and $(^6\text{Li}, xn)$ reactions at appropriate energies. The results give a direct measurement of Γ_f/Γ_n since both fission and neutron evaporation cross-sections were determined. The experimental values of Γ_f/Γ_n for ^{216}Rn and earlier data for ^{210}Po are analysed with a J-dependent statistical model and the effect of incorporating an enhancement of the level density at the saddle point due to coupling to collective rotations is investigated. Fission barriers extracted with a variety of assumptions about the level densities are compared with theoretical predictions.

1. INTRODUCTION

Previous measurements [1-4] of fission excitation functions for nuclei in the rare earth and lead region have been used to determine fission barrier heights for a range of nuclei from ^{147}Lu through ^{213}At . These results, which were obtained from reactions with alpha particle and proton beams, have shown [5] that the fission barrier decreases rapidly from 23.3 MeV for ^{209}Bi to 17.0 MeV for ^{213}At . This change in threshold is due primarily to the decreasing influence of the strong spherical shell at $Z=82$, $N=126$ on the ground state mass. Due to a lack of target isotopes with reasonable lifetimes, there are no fission barrier measurements between ^{213}At , which has a spherical equilibrium shape with a barrier of 17.0 MeV and ^{227}Ra , which has a deformed equilibrium shape with a barrier of 8.1 MeV [6].

With the availability of high-energy heavy ion beams, it is possible to study the fission barrier of nuclei with $Z>85$ making use of stable Pb and Bi targets. One particularly

* Work supported in part by the US Atomic Energy Commission and the National Science Foundation.

⁺ On leave of absence from Fachbereich Physik, Universität Marburg, Fed. Rep. of Germany.

⁺⁺ Permanent address: Los Alamos Scientific Laboratory, Los Alamos, N. Mex., United States of America.

advantageous reaction is $^{209}\text{Bi} + ^7\text{Li} \rightarrow ^{216}\text{Rn}$. In this case, the residual nuclei formed by multiple neutron evaporation are easily observed short-lived alpha particle emitters. By measuring both the fission cross-section and the cross-sections for forming the residual products $^{216-x}\text{Rn}$ from xn reactions, it is possible to obtain a direct measure of Γ_f/Γ_n . This method can be contrasted with earlier measurements [1-4] where Γ_f/Γ_n was determined from a measured fission cross-section and a calculated total reaction cross-section.

From the experimental Γ_f/Γ_n measurements, the extraction of the height of the fission barrier requires a statistical model to calculate Γ_f and Γ_n . Recent calculations [5,7] have shown that it is essential to include shell effects in the Γ_n calculation in order to account for the influence of the double shell closure. In this connection, Moretto et al. [5] have shown that it is possible to reproduce the shapes of the experimental excitation functions without specifically considering the effects of shells at the saddle point. Vandenbosch and Mosel [7] attempted an absolute calculation of Γ_f/Γ_n incorporating shell effects in both Γ_f and Γ_n and using theoretically calculated heights for the fission barriers. However, both these calculations neglected a fundamental difference between the level densities for the deformed saddle point used in Γ_f and the spherical ground state appropriate for Γ_n . In particular, for a deformed nucleus the level densities can be enhanced by coupling to collective degrees of freedom.

In this paper, we report direct experimental measurements of Γ_f/Γ_n for ^{216}Rn . The results are analyzed with a statistical model that includes an improved microscopic calculation of Γ_f which explicitly contains the effects of collective rotations on the level density at the saddle point. In addition, Γ_f/Γ_n is calculated as a function of J and then weighted over the distribution of angular momenta in the entrance channel. Calculations from this statistical model are compared to the experimental ^{216}Rn data and also to the more extensive data [3] reported previously for the compound nucleus ^{210}Po produced by the $^{206}\text{Pb} + \alpha$ reaction. The data are first compared to an absolute prediction, which includes both (1) theoretical level densities incorporating realistic shell corrections and (2) the corresponding theoretical value for the fission barrier height [8]. In an alternate approach the height of the fission barrier and a normalization factor are deduced empirically from a fit to the experimental data.

2. EXPERIMENTAL PROCEDURE

Bismuth targets were bombarded with $^6,^7\text{Li}$ -projectiles from the Emperor tandem Van de Graaff with energies of 25 to 34 MeV. The fission cross-section was measured using a d.c. Li-beam. Fission fragments were detected in coincidence in high geometry surface barrier detectors. It was necessary to detect fission fragment pairs in order to measure this small cross-section in presence of the intense elastic scattering.

If the compound nucleus does not fission, multiple neutron emission leads to the residual Rn-nuclei, which are shown in fig. 1. Since all of these nuclei are α -emitters,

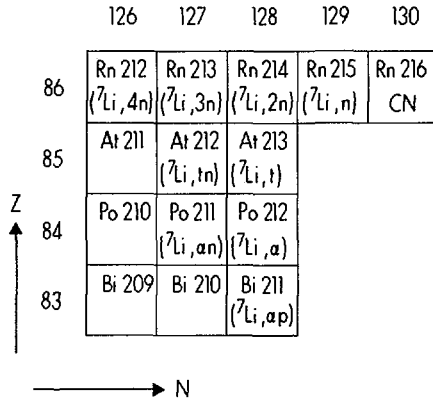


FIG. 1. Portion of the nuclide chart in the region $A = 209$ to 216 . Listed are the ${}^7\text{Li}$ -induced reactions on ${}^{209}\text{Bi}$ populating the residual nuclei which were observed by their α -decay properties.

their formation cross-sections are easily determined by measuring their α -activities. The identification of the α -groups is unique, based on the known α -energies and half-lives, which range from about a hundred nanoseconds to minutes. Using a pulsed Li-beam to produce the Rn-isotopes, we could measure the α -activities between beam pulses with standard surface barrier detectors essentially free of background due to prompt α -groups. All expected α -groups were found, including those following the (${}^7\text{Li}, xn$) reactions and a variety of transfer reactions leading to Po, At and Bi isotopes as shown in fig. 1. All reaction channels together give a complete measurement of the total reaction cross-section, which will be discussed elsewhere^[9].

3. RESULTS

The excitation function for the compound nucleus formation is shown in fig. 2, together with the fission and multiple neutron evaporation decay channels. To obtain values for Γ_f/Γ_n as close to the fission barrier as possible, the measurements were done mainly below the Coulomb barrier of about 33 MeV. Hence the compound nucleus formation cross-section and the resulting cross-sections of the various exit channels are mainly controlled by the Coulomb barrier, and it is very difficult to extend the measurements to lower incident energies.

The total fission cross-sections are calculated from the differential cross-section at 90° . A measurement of the anisotropy at 33 MeV gave $W(165^\circ)/W(90^\circ) = 1.19 \pm 0.15$. Hence, isotropy was assumed over the whole energy range. The fission excitation function obtained for ${}^6\text{Li}$ yields a larger cross-section at a fixed incident energy than ${}^7\text{Li}$. This is mainly due to the Q-value of the ${}^{209}\text{Bi} + {}^6\text{Li}$ reaction, which is 660 keV larger than that for the ${}^{209}\text{Bi} + {}^7\text{Li}$ reaction, and partially due to the change of the fissility parameter in going from ${}^{216}\text{Rn}$ to ${}^{215}\text{Rn}$.

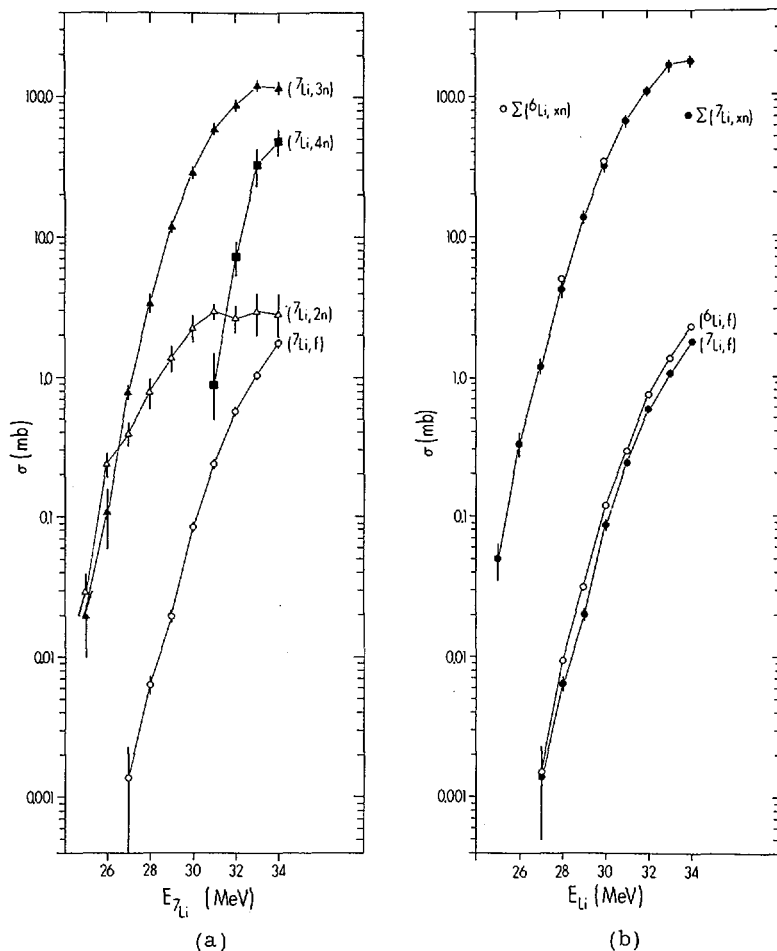


FIG. 2. (a) Cross-sections for the dominant decay channels of the compound nucleus ^{216}Rn as a function of projectile energy. (b) Comparison of the decay of ^{215}Rn and ^{216}Rn by fission and multiple neutron evaporation as a function of the Li-ion energy incident on ^{209}Bi .

The ^6Li induced fission cross-sections were used to correct the ^7Li induced fission data for the contribution of second-chance fission. An effect of less than 6% was obtained at our highest incident ^7Li energy of 34 MeV.

The results for the $(^7\text{Li}, xn)$ cross-sections show the dominance of evaporation of three neutrons in the measured range of incident energies, with the 4n threshold at approximately 30 MeV ^7Li energy. The cross-section for one neutron emission is below our detection system efficiency of $\sim 1\mu\text{b}$ and hence not measured.

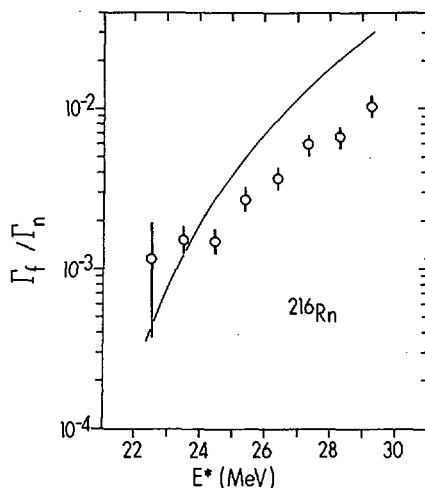


FIG. 3. The ratio Γ_f/Γ_n for ^{216}Rn as a function of excitation energy. The curve is calculated using Eq. (4) and a fission barrier [8] of 14.8 MeV without additional free parameters. Single particle levels at a symmetric saddle point deformation have been used.

The experimental ratio Γ_f/Γ_n as a function of the compound nucleus excitation energy is displayed in fig. 3. This ratio varies only slowly with excitation energy since one is still well above the fission barrier, but nevertheless deep in the Coulomb barrier. The theoretical curves included in the figure will be discussed later.

4. THEORY

The calculation of the fission width has been performed using the formula of Bohr and Wheeler [10] which has been generalized to include a J dependence,

$$\Gamma_f(J) = \frac{D(J)}{2\pi} \int_0^{E-E_f} \rho_f(E-E_f-\epsilon, J) d\epsilon \quad (1)$$

where E_f is the effective fission barrier, ρ_f the level density at the saddle point deformation for a total angular momentum J and $D(J)$ the level spacing in the compound nucleus at excitation energy E and angular momentum J.

On the neutron side, the J-dependent neutron width $\Gamma_n(J)$ is given by

$$\Gamma_n(J) = \frac{D(J)}{2\pi} \int_0^{E-B_n} \sum_{L=0}^{L_{\max}} T_L \sum_{S=|J-L|}^{J+L} \sum_{I=|S-1/2|}^{S+1/2} \rho_n(E-B_n-\epsilon, I) d\epsilon \quad (2)$$

where B_n is the neutron binding energy in the compound nucleus and ρ_n the level density for total angular momentum I in the residual nucleus. The neutron transmission coefficients^[11] T_n are those describing the formation of the compound nucleus at excitation energy E via neutron capture by the residual nucleus. These calculations are straightforward, if the J -dependent level densities are provided, a problem which shall be discussed in greater detail.

Given a set of single particle spectra, a realistic state density calculation with the inclusion of nuclear pairing can be performed using the partition function method^[12]. Details on the calculations may be found in ref. 13. Single particle levels of Möller and Nix^[8] were used to obtain state densities $\omega(E)$ for the spherical nuclei ^{209}Po and ^{215}Rn . The level densities $\rho(E, J)$, which later are used to calculate $\Gamma_n(J)$ following eq. (2), are obtained from the relation

$$\rho(E, J) = \frac{J+1/2}{\sqrt{2\pi} \sigma^3(E)} \omega(E) \cdot \exp\left(-\frac{J(J+1)}{2\sigma^2(E)}\right) \quad (3)$$

where the spin cut-off factor $\sigma^2(E)$ is also calculated microscopically.

For the fissioning nuclei ^{210}Po and ^{216}Rn , the state densities $\omega(E)$ were calculated using Möller and Nix's^[8] single particle levels at the saddle point deformation. In the case of ^{210}Po , single particle levels for both a symmetric and an asymmetric saddle point deformation were used. For the deformed saddle point the level density is enhanced by coupling to low-lying collective excitations as described by Ericson and by Bjørnholm and co-workers^[14]. For an axially symmetric shape where only the coupling to collective rotations is considered the level density can be written as:

$$\rho_c(E, J) = \frac{\omega_K(E) \hbar}{\sqrt{8\pi} \mathcal{J}_\parallel T} \sum_{K=-J}^{+J} \exp\left\{-\frac{\hbar^2 K^2}{2 \mathcal{J}_\parallel T} - \frac{\hbar^2}{2 \mathcal{J}_\perp T} [J(J+1) - K^2]\right\} \quad (4)$$

where $\omega_K(E)$ is the state density calculated microscopically in the K formalism appropriate for a deformed nucleus and the analogous cutoff factor $\sigma_K^2(E) = \mathcal{J}_\parallel T / \hbar^2$ is also calculated microscopically. In the actual calculations, a rigid-body estimate for the perpendicular moment of inertia, $\hbar^2 / 2 \mathcal{J}_\perp = 2.5$ keV, was used. If it is assumed that $\omega_K(E)$ contains all the available states (i.e. no enhancement due to rotations) then Sano and Kawai^[15] have shown that the level density becomes:

$$\rho_D = \frac{\hbar^2}{\mathcal{J}_\perp T} \cdot \rho_c \quad (5)$$

Previous calculations^[5,7] have essentially used eq.(5) with the further approximation that $\sigma^2 \sim \sigma_K^2 \sim \hbar^2 / \mathcal{J}_\perp T$, where σ^2 is the spin cutoff factor for the spherical nucleus formed in neutron emission. In this limit the spin cutoff factors cancel and the final Γ_f / Γ_n expressions are J independent.

Since the experimentally determined Γ_f/Γ_n is a weighted sum over the distribution of angular momenta in the entrance channel, a final summation is needed.

$$\left\langle \frac{\Gamma_f}{\Gamma_n} \right\rangle = \frac{\sum_{J=0}^{J_{\max}} P_J \cdot (\Gamma_f/\Gamma_n)_J}{\sum_{J=0}^{J_{\max}} P_J}$$

where P_J is the probability for forming the compound nucleus with angular momentum J . These probability coefficients are calculated with transmission coefficients from a parabolic approximation of the potential barrier as introduced by Thomas [16]. The ratio of $(\Gamma_f/\Gamma_n)_J/(\Gamma_f/\Gamma_n)_{J=0}$ as a function of J for three different excitation energies in the compound nucleus ^{210}Po are shown in Fig. 4. One interesting feature of these curves is that at the lower excitation energies the higher angular momentum values favor neutron emission. This is a result of the large difference in the fission barrier and neutron threshold and the corresponding difference in the appropriate spin cutoff factors.

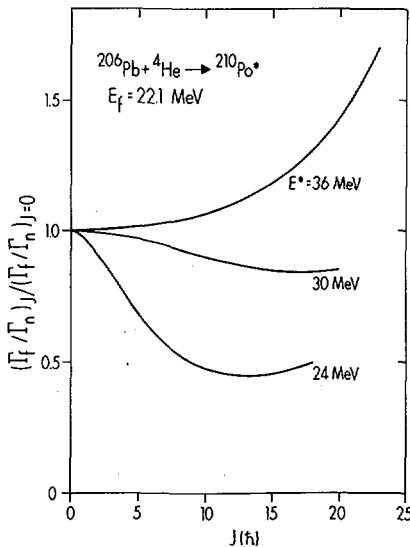


FIG. 4. The dependence of Γ_f/Γ_n on angular momentum J for the compound nucleus ^{210}Po at three excitation energies. These results are based on Eq. (4) and an asymmetric saddle with a fission barrier of 22.1 MeV.

5. DISCUSSION

The statistical model was first used for an absolute prediction of Γ_f/Γ_n for ^{210}Po and ^{216}Rn using the single particle levels and theoretical barriers from Möller and Nix[8]. These calculations, therefore, contain no adjustable parameters. The results are compared to experimental data in Figs. 3 and 5. The absolute calculations tend to reproduce experimental results near threshold but rise too steeply and give too large values for Γ_f/Γ_n at high excitation energies. This comparison may indicate that the present

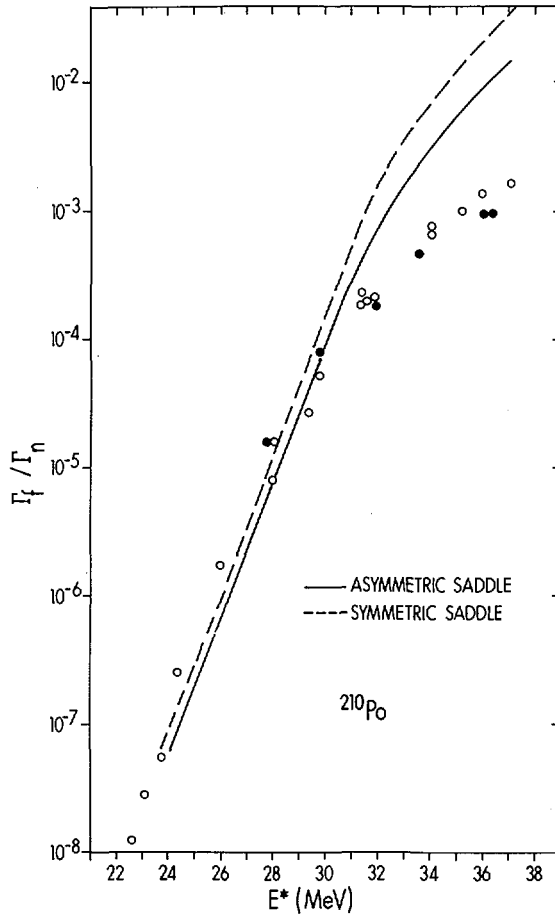


FIG. 5. The ratio Γ_f/Γ_n for ^{210}Po as a function of excitation energy. The curves with level densities based on the single particle spectra for an asymmetric and a symmetric saddle point deformation are calculated using Eq. (4) and a fission barrier of 22.1 MeV in both cases without additional free parameters. Open circles are taken from Ref. [3] and filled circles from Ref. [1].

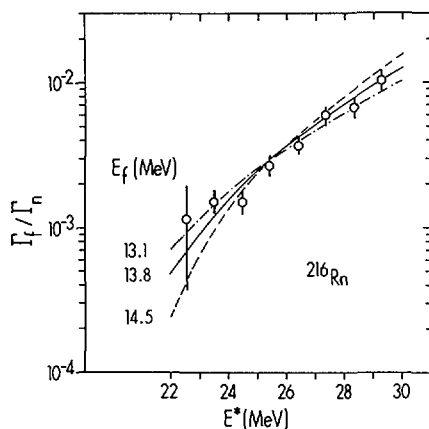


FIG. 6. The ratio Γ_f/Γ_n for ^{216}Rn as a function of excitation energy. The curves for the different barriers are calculated with Eq.(5). The normalization constants used to reproduce the experimental magnitude of Γ_f/Γ_n are given in Table I. Single particle levels at a symmetric saddle point deformation have been used.

statistical model yields an incorrect energy dependence for Γ_f/Γ_n . Alternately, the theoretically calculated barriers and level densities may be incorrect.

Since comparisons for actinide nuclei have shown deviations of up to 2 or 3 MeV in some cases between experimental fission barriers and those calculated theoretically by Möller and Nix^[8], it is also interesting to investigate an alternative approach where the height of the fission barrier, E_f , and a normalization factor, N_f , are extracted from a fit to the experimental data. The results of these fits are shown in Figs. 6 and 7 and the parameters obtained are listed in Table I. In these fits, level densities from both eqs.(4) and (5) were used. For ^{210}Po , single particle levels for both symmetric and asymmetric saddle points were used.

In Figs. 6 and 7 it is shown that the shapes of the experimental Γ_f/Γ_n functions are well described in all cases. However, the parameters E_f and N_f depend both on the single particle spectrum and the type of level density formula which is used. For ^{210}Po the use of symmetric or asymmetric saddle point single particle levels results in only a small difference in the fitted parameters. In contrast the two different forms for the level density give N_f values which change by a factor of about 400 and fitted values of E_f which change by ~ 0.8 MeV. Using the level density including collective rotations, N_f values in the range 10^{-2} to 10^{-3} are obtained rather than the expected values of ~ 1 . Conversely, the approach (eq. 5) which neglects these new levels gives a normalization factor of ~ 1 . For the ^{216}Rn case the collective level density gives $N_f \sim 1/20$, whereas, the other approach gives $N_f \sim 20$ so that $N_f \sim 1$ is between the two extremes.

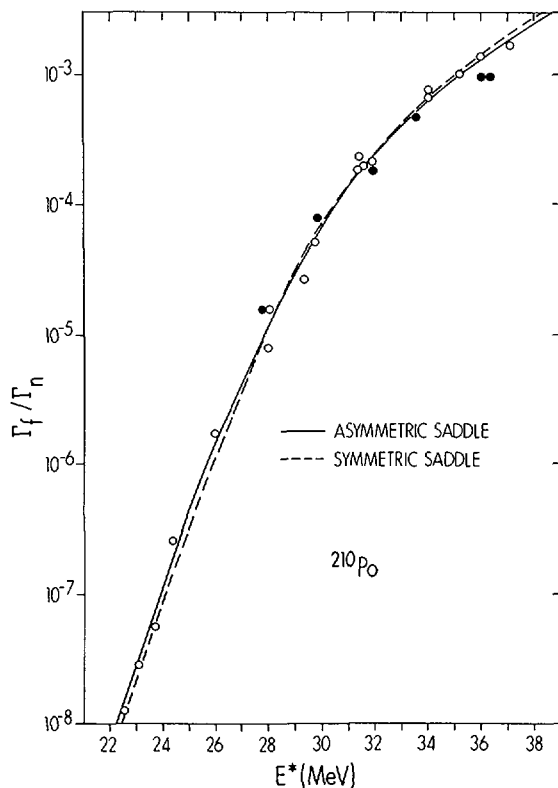


FIG. 7. The ratio Γ_f/Γ_n for ^{210}Po as a function of excitation energy. The curves are calculated with Eq. (5), using level densities based on the single particle spectra for an asymmetric and a symmetric saddle point deformation. Fission barrier heights of 20.2 MeV and 20.0 MeV, respectively, were used. The normalization constants used to reproduce the experimental magnitude of Γ_f/Γ_n are given in Table I.

Operationally the theoretical energy-dependent values of Γ_f/Γ_n are compared with the experimental ratios of this quantity at several energies. Since the theoretical values of Γ_f/Γ_n depend on three different variables, namely the fission barrier and the level densities of both the deformed saddle nucleus and the spherical nucleus following neutron emission, it is not possible to unambiguously determine both N_f and E_f . Hence, it is not possible to verify the necessity of introducing the deformed nucleus level density given by eq. 4 for estimating Γ_f/Γ_n at our excitation energies. If, however, the level density incorporating the enhancement due to collective rotations at the saddle point is correct then these results suggest that Γ_n is significantly underestimated at high excitation energies [17]. Whether this underestimate is a function of excitation energy depends on the value chosen for E_f . An underestimate of Γ_n could arise in two ways 1) through a neglect of possible couplings to collective

TABLE I. FISSION BARRIERS AND NORMALIZATION FACTORS BASED ON FITS OF THE SHAPE OF Γ_f/Γ_n WITH TWO DIFFERENT FORMS OF THE LEVEL DENSITY FOR THE DEFORMED SADDLE NUCLEUS
Theoretical barriers in the last column are based on experimental ground state masses

NUCLEUS	Values obtained with eq. 4		Values obtained with eq. 5		Theoretical ^a barrier
	E_f (MeV)	N_f	E_f (MeV)	N_f	
^{210}Po (asym. saddle)	+0.8	1.9×10^{-2}	+0.8	6.6	22.1
	19.5	6.0×10^{-3}	20.2	2.2	
	-0.8	2.0×10^{-3}	-0.8	0.67	
^{210}Po (sym. saddle)	+0.8	4.5×10^{-3}	+0.8	2.5	22.1
	19.1	1.5×10^{-3}	20.0	0.75	
	-0.8	0.5×10^{-3}	-0.8	0.23	
^{216}Rn (asym. saddle)	+1.0	20×10^{-2}	+1.0	64	14.8
	13.1	4.8×10^{-2}	13.8	16	
	-1.0	1.1×10^{-2}	-1.0	4.6	

^a Ref. 8. In Figs 3 and 5 the theoretical values of Γ_f/Γ_n were calculated with these theoretical fission barriers and no other adjustable parameters.

vibrations at higher E^* (although this effect is also neglected in Γ_f) or 2) because of an overestimate of the shell effect on the level density in this region. This second possibility is consistent with the trend that the theoretical calculations^[8] underestimate the ground state mass of ^{210}Po by 1.6 MeV and by 0.3 MeV for ^{216}Rn and the resulting N_f values are ~ 10 times smaller for ^{210}Po than for ^{216}Rn .

ACKNOWLEDGEMENTS

We would like to thank J.R. Nix and P. Möller for supplying the single particle spectra used in our calculations, and A.N. Behkami for assisting in the microscopic state density calculations.

REFERENCES

- [1] J.R. HUIZENGA, R. CHAUDHRY, and R. VANDENBOSCH, Phys. Rev. 126(1962)210.
- [2] D.S. BURNETT, R.C. GATTI, F. PLASIL, P.B. PRICE, W.J. SWIATECKI, and S.G. THOMPSON, Phys. Rev. 134B (1964) 952.
- [3] A. KHODAI-JOOPARI, University of California, Lawrence Radiation Laboratory Report UCRL-16489(1966).
- [4] G.M. RAISBECK and J.W. COBBLE, Phys. Rev. 153(1967)1270.
- [5] L.G. MORETTO, S.G. THOMPSON, J. ROUTTI, and R.C. GATTI, Phys. Letts. 38B(1972)471.
- [6] N. GROENING and W. LOVELAND, Paper IAEA-SM-174/81, these Proceedings, Vol.I.
- [7] R. VANDENBOSCH and U. MOSEL, Phys. Rev. Letts. 28(1972) 1726.
- [8] P. MÖLLER and J.R. NIX, Paper IAEA-SM-174/202, these Proceedings, Vol.I, and private communication.
- [9] H. FREIESLEBEN, H.C. BRITT, and J.R. HUIZENGA, to be published.
- [10] N. BOHR and J.A. WHEELER, Phys. Rev. 56(1939)426.
- [11] E.H. AUERBACH and F.G.J. PEREY, Brookhaven National Laboratory Report BNL 765(T-286).
- [12] J.R. HUIZENGA and L.G. MORETTO, Am. Rev. Nucl. Sci. Vol.22, 1972, p.427 and refs. given therein.
- [13] A.N. BEHKAMI and J.R. HUIZENGA, University of Rochester, Nuclear Structure Research Laboratory Report, UR-NSRL-72 (1973).
- [14] T. ERICSON, Nucl. Phys. 6 (1958) 62;
S. BJØRNHOLM, A. BOHR, B.R. MOTTELSON,
Paper IAEA-SM-174/205, these Proceedings, Vol.I.
- [15] M. SANO and M. WAKAI, Prog. Theor. Phys. 48(1972)160.
- [16] D.T. THOMAS, Phys. Rev. 116(1959)703.
- [17] The evidence in support of the level density given by eq. 4 for reproducing the experimental level densities of deformed nuclei at the neutron binding energy is discussed in a separate paper by J.R. HUIZENGA, A.N. BEHKAMI, H.C. BRITT and H. FREIESLEBEN, submitted for publication.

DISCUSSION

W. LOVELAND: In one of your slides you showed calculations of Γ_f/Γ_n for asymmetric and symmetric saddle point deformations in which the calculated values of Γ_f/Γ_n were higher for symmetric than for asymmetric deformations. Why does this occur, if there is a doubling of rotational levels in the transition nucleus for the asymmetric deformation compared to the symmetric deformation?

H. FREIESLEBEN: The difference in Γ_f/Γ_n is due to the fact that the single particle levels change, going from a symmetric to an asymmetric saddle deformation. The negative shell correction at the symmetric saddle gives rise to a smaller level spacing and hence to an increased level density compared with the asymmetric saddle, which has a large positive shell correction.

S. BJØRNHOLM: I am in some disagreement with Moretto as to the energy at which the collective enhancement disappears. I would say that it is at a very low energy. Huizenga remarked that you have studied it at 6 MeV – the neutron binding energy – and you seem to imply that the enhancement is still there. That is one piece of evidence. I would say you would have to go to temperatures of 2 or 3 MeV to see it disappear; I would simply point to Moretto's entropy diagram that shows how the intrinsic shape probability, which is narrow around equilibrium, broadens out to also include all spherical shapes at about 50 MeV. I think that is how one can tell when the rotation of the shape disappears as a separate degree of freedom, when the shape becomes washed out.

L.G. MORETTO: I suspect that Mr. Bjørnholm's reference to my probability distribution as a means of determining the energy region where the collective phase space is absorbed back into the intrinsic states, may not be so relevant. We need another factor, like the coupling matrix elements, in order to be able to estimate the width of the strength function at the various energies.

J.R. HUIZENGA: The discussion between Moretto and Bjørnholm about the temperature or energy at which the extra levels due to the collective rotations disappear is of a highly speculative nature; and what I am about to say is of a similar quality. It is an attempt to overcome the present lack of experimental information on the energy at which these extra levels disappear. It is based on the Γ_f/Γ_n analysis in our paper. Prior to giving the result, I remind you of the hazards in drawing final conclusions on this subject from Γ_f/Γ_n analyses, owing to uncertainties in the single particle levels, the fission barrier, etc. With this warning, I wish to state that we found a good absolute fit to the Γ_f/Γ_n data for ^{210}Po near the barrier with a saddle point level density which includes the collective rotations. However, some 8 to 10 MeV above the barrier the theoretical values of Γ_f/Γ_n become too large. This might be interpreted to mean that the enhancement in the level density due to collective rotations begins to disappear at energies of the order of 8 to 10 MeV.

S. BJØRNHOLM: Is your analysis really sufficiently unique to allow such considerations?

J.R. HUIZENGA: If we allow the fission barrier to vary and then fit the Γ_f/Γ_n data, we obtain a smaller fission barrier and the enhancement in the level density due to collective rotations at the barrier is no longer required. In addition, there is another argument for favouring the larger barrier for ^{210}Po , which is based on a comparison of experimental and theoretical values of K_0^2 .

U. MOSEL: I should like to point out another possible uncertainty that enters into the calculation of Γ_f , namely the effect of volume conservation in the single particle model. While this effect, which is deformation-dependent, does not affect the Strutinsky-type shell corrections, it does enter rather directly into the single particle levels and thus into the level densities at the saddle point.

R. VANDENBOSCH: I believe there are two criteria that must be satisfied, in order to expect an enhancement of the fission width relative to the neutron width discussed by Bjørnholm. One is that the saddle shape should have a lower symmetry than the equilibrium shape, and Bjørnholm has pointed out that Moretto's calculation would indicate that 50 or 60 MeV is required to dissolve the shell effects causing such differences in

shape. I would like to call attention to the second of the two criteria, namely that the energies of the rotational states should be lowered by coherent residual interaction effects by an amount that is larger than the nuclear temperature. Otherwise these states should be considered as being included in the statistical calculation of the level density. I would guess that this lowering is of the order of an MeV, which would suggest that these effects would dissolve out at a temperature of about 1 MeV, or perhaps an excitation energy of about 25 MeV.

FISSION PROCESS: THEORY (DYNAMIC)
(Session V)

Chairman: H. J. Specht (Federal Republic of Germany)

Review Paper

THE DYNAMICS OF FISSION IN THE
SUBBARRIER REGION OF DEFORMATION

H.C. PAULI*, T. LEDERGERBER**

Institut für theoretische Physik der
Universität Basel,
Basel, Switzerland

Abstract

THE DYNAMICS OF FISSION IN THE SUBBARRIER REGION OF DEFORMATION.

A solvable model for the dynamics of fission is formulated. It is argued in which phase the process is likely to be adiabatic and in which not. This model is checked by calculating the lifetime for spontaneous fission from the ground state and from the shape-isomeric state. Reasonable agreement with experiments is found. The discrepancies are understood and can be improved in future calculations, presumably to give predictive power to these methods. It is claimed that fission barriers are dynamic (not static) quantities and the pre-formation of the nascent fragments arises in the parent nucleus around the outer barrier.

1. INTRODUCTION

It is an astonishing fact that 30 years after the strange reports of Hahn and Strassmann [1] and their interpretation by Frisch and Meitner [2] virtually none of the observables of the fission process are understood. What one has is a vast collection of empirical rules to order the data, and a variety of specific models which "work" for particular aspects but fail badly for others. In addition, quite a number of concepts have been developed in the past, as for example that of "deformation" or that of a "fission barrier" which were so successful that one has forgotten how model-dependent they in fact are.

We agree — of course — that the utter complexity of the nuclear many-body problem has not left much choice for doing better and that rules are desperately needed not to get lost in the flood of data. But because of the rapid and sudden progress in the past few years, it might now be worth the effort to collect things and put them in their proper places. This means a lot of work, but we hope that one day life may be simpler again.

This presentation is meant to be a modest contribution to an eventual unified theory. Although — by reason of simplicity and survey — we shall give a rather superficial presentation, we shall try to remain as close as possible to a more basic approach. We shall be careful that things remain solvable but that the mathematical assumptions do not spoil the physics and that the main conclusions are based on actual calculations.

* Present address: Max-Planck-Institut für Kernphysik, Heidelberg, Federal Republic of Germany.

** Work supported in part by "Schweizerischer Nationalfonds zur Förderung der wissenschaftlichen Forschung".

We proceed by presenting first the concept of collectivity of nuclei — in particular of fissioning nuclei — and show that it offers room enough to include refinements of the theory step by step (Section 2). Thereafter, we discuss in Section 3 the corner-stone of the collective model, the potential and the "kinetic" energies and compare them — as far as possible — to the experiments. Without prejudice to further experiments, we restrict ourselves in Section 4 to the lifetimes for spontaneous fission. Finally, (Section 5) we tackle seriously the least action trajectory and arrive at conclusions on the nature of the fission barriers and the preformation of fragments.

Without even mentioning it, we restrict ourselves to the even-even nuclei and omit with pleasure the complications of an odd nucleus due to the conservation of axial symmetry.

None of the methods presented is really original and new and the presentation may even be (too) simple-minded. But this may help younger people among us to enter this field and to participate in the certainly possible and exciting future developments, to mention only a few of these: viscosity, odd nuclei and inverse fission.

2. THE CONCEPT OF COLLECTIVITY

A rigorous dynamic model of the fission process is identical to its complete quantum mechanical description, of course. We shall have solved this problem, if we know the state vector of the total nucleus and its development in time, that is, if we have found the solution of the time-dependent Schrödinger equation

$$i\hbar \frac{\partial \psi(t)}{\partial t} = \mathcal{H} \psi(t) \quad (1)$$

The state vector is to be normalized so that

$$(\psi(t), \psi(t)) = 1 \quad (2)$$

Apart from the difficulty in finding a rigorous solution of the nuclear many-body problem — we refer to the recent review of Bethe [3] — the complication due to the large number of degrees of freedom in a heavy nucleus has been a serious problem and will continue to be one. Phenomenological models, however, are usually solvable, but their application is bound to the field for which they have been developed. Nevertheless, they are useful to explore a field and, eventually, pave a way for handy solutions of the full problem.

In the following we shall outline a sequence of approximation and interpretation, which relates the more fundamental approach to those phenomenological concepts we finally work with.

2.1. The formulation of the collective model¹

Assume the many-body Hamiltonian \mathcal{H} is known. Rather than being interested in the full range of information provided by knowing the state vector $\psi(t)$, let us be interested in some particular feature which we label by a c-number q . We assume that q may be a function of time

$$q = q(t) \quad (3)$$

and that we can label the state vector by q , too, in such a way that

$$\psi(q(t)) \quad (4)$$

is still a solution of the time-dependent Schrödinger equation (1). In addition, we assume the existence of a complete set of orthonormal states

$$(\phi_m(q), \phi_n(q)) = \delta_{mn} \quad (5)$$

They are to be characterized by the same number q , and shall be eigenstates of the stationary Schrödinger equation

$$\mathcal{H}(q) \phi_m(q) = \epsilon_m(q) \phi_m(q) \quad (6)$$

for all values of q . The indices m are to order the eigenvalues ϵ_m , i. e.

$$\epsilon_0 \leq \epsilon_1 \leq \epsilon_2 \leq \dots \quad (7)$$

By virtue of the completeness and by putting $q = q(t)$ we can expand the time-dependent state vector into a series of the stationary solutions

$$\psi(t) = \sum_{m=0} c_m(q) \phi_m(q) \exp \left\{ -\frac{i}{\hbar} \int_0^t \epsilon_m(q(t')) dt' \right\} \quad (8)$$

at any time. By means of Eqs (8) and (2) the coefficients must obey the relation

$$\sum_{m=0} |c_m(q)|^2 = 1 \quad (9)$$

Inserting the expansion, Eq. (8), into the time-dependent Schrödinger equation (1) and making use of Eq. (5), one obtains a "coupled channel" differential equation for the coefficients c_m

$$\dot{c} = -i \sum_{n=0} c_n \left(\phi_m(q), \frac{\partial \phi_n(q)}{\partial q} \right) \exp \left\{ -\frac{i}{\hbar} \int_0^t [\epsilon_n(t') - \epsilon_m(t')] dt' \right\} \quad (10)$$

¹ We follow to some extent the formulation of Wilets [4].

which is of course equivalent to the time-dependent Schrödinger equation but sometimes easier to solve. Once the c_m are known the total energy is calculated according to

$$E = (\psi(t), \mathcal{H}\psi(t)) = \sum_{m \geq 0} |c_m|^2 \epsilon_m(q) \quad (11)$$

which by means of Eq. (9) can be rewritten as

$$E = \epsilon_0(q) + \sum_{m \geq 1} |c_m(q, \dot{q})|^2 (\epsilon_m(q) - \epsilon_0(q)) \quad (12)$$

The second term in this equation

$$K(q, \dot{q}) = \sum_{m \geq 1} |c_m(q, \dot{q})|^2 (\epsilon_m(q) - \epsilon_0(q)) \quad (13)$$

depends on the "collective velocities" \dot{q} and could be called a "collective kinetic energy", whereas the first term,

$$W(q) = \epsilon_0(q) \quad (14)$$

depends only on the "collective coordinate" q and, consequently, could be called a "collective potential energy". It is thus possible to formulate a Hamilton function for the collective energy

$$H_{\text{coll}} = K(q, \dot{q}) + W(q) = E \quad (15)$$

which forms the basis for the collective model. Under these circumstances we can interpret the collective variables q and \dot{q} as operators, which can be quantized according to the prescriptions of Schrödinger and Pauli [5]. We should note here that we did not have to assume adiabatic motion to derive Eq. (10).

We have introduced the collective variable q to replace the many degrees of freedom of the original many-body problem. This additional parameter does not present unsolvable difficulties and can be understood as a kind of generator coordinate. A rigorous formulation in terms of the generator coordinate [6] will not be gone into here — the more so as the essential conclusions are the same — and reference is made to the available literature [7, 8] for its treatment. In fission the nucleons are initially concentrated in a rather well-defined area of space and separate into two or more slabs of nuclear matter which are highly correlated in space. If we describe this collective process par excellence by the time development of the spatial density distribution, we can restrict it to the description of the surface area, as the saturating nature of the nuclear forces prevents a large change of the central density. Consequently, we are almost forced to identify the collective coordinate with the shape of the density distribution. Therefore, the

potential energy $W(q)$ is often called the nuclear deformation energy. In the following we shall refer to q as the fission mode and shall specify it later.

2.2. The adiabatic limit

Let us concentrate now on the adiabatic limit. By adiabaticity we mean that the state of the system is constant in time, i. e. that

$$\dot{c}_m(t) = 0 \quad (16)$$

If at some time t the system was in its ground state expressed in terms of the stationary solution for the time t , it will remain in this state, i. e.

$$\psi(t) \sim \phi_0(q(t)) \exp \left\{ -\frac{i}{\hbar} \int^t \epsilon_0(t') dt' \right\} \quad (17)$$

and the total energy E , which is conserved, has no contribution from the intrinsic excitations. All the excess energy which is provided by the motion $q = q(t)$ will transform into kinetic energy of the system as a whole, i. e.

$$E = W(q(t)) + \frac{1}{2} B_q(q) \dot{q}^2 \quad (18)$$

In the adiabatic limit we can derive an expression for this so-called effective mass B_q in terms of the stationary eigenfunctions ϕ_m . This approach is known as the "cranking model" [9].

The cranking model is based on two assumptions, i. e. (1) that at some time t_0 the system is essentially in its ground state:

$$t = t_0: \quad c_0 \approx 1, c_m \approx 0 \quad \text{for } m \geq 1 \quad (19)$$

and (2) that all the quantities in the coupled channel Eq. (10) vary sufficiently slowly in the small time interval $\delta t = t - t_0$ that we can restrict ourselves to lowest order in δt . This gives

$$c_m(t) = i\hbar \dot{q}(t_0) c_0(t_0) \left(\phi_m, \frac{\partial \phi_0}{\partial q} \right)_{q_0} \frac{\exp \left\{ -\frac{i}{\hbar} \delta t (\epsilon_m(q_0) - \epsilon_0(q_0)) \right\}}{\epsilon_m(q_0) - \epsilon_0(q_0)} + \text{const} \quad (20)$$

Assuming no real excitations, i. e. choosing the equality sign in Eq. (19), the integration constant is zero. Inserting Eq. (20) into Eqs. (12) and (18) one arrives at

$$B_q(q) = 2\hbar^2 \sum_{m \geq 1} \left(\phi_0(q), \frac{\partial \phi_m(q)}{\partial q} \right) \left(\phi_m(q), \frac{\partial \phi_0(q)}{\partial q} \right) (\epsilon_m - \epsilon_0)^{-1} \quad (21)$$

The notation should underline the fact that the effective mass B_q corresponds to virtual excitation. In fact, Eq. (20) is no contradiction to Eq. (16), since

we express the wave function at time $t = t_0 + \delta t$ by the wave function at time t_0 : the mass is a measure of the overlap of those two.

Thus, in this adiabatic limit, one can formulate the collective model with considerable ease, provided one can find decent approximations to the stationary many-body functions ϕ_m .

2.3. The three-phase model of fission

The assumption of adiabaticity simplifies considerably our approach to fission. Where is this assumption justified?

It is meaningful to use the deformation energy $W(q)$ as a guide for the qualitative discussion. Since the total energy E is a constant of the motion, the quantity W tells us immediately the upper limit of the energy which might be shared with the other degrees of freedom of the fissioning nucleus: according to Eq. (15) we have

$$K(q, \dot{q}) = E - W(q) \quad (22)$$

$K(q, \dot{q})$ is just the kinetic energy of the fission mode if the excitations are virtual. If some of them are real, the corresponding amount of energy is transferred to degrees of freedom other than fission, possibly to other collective modes. In this sense, real excitations can be called friction or viscosity, even if those terms seem to have a meaning only in classical physics.

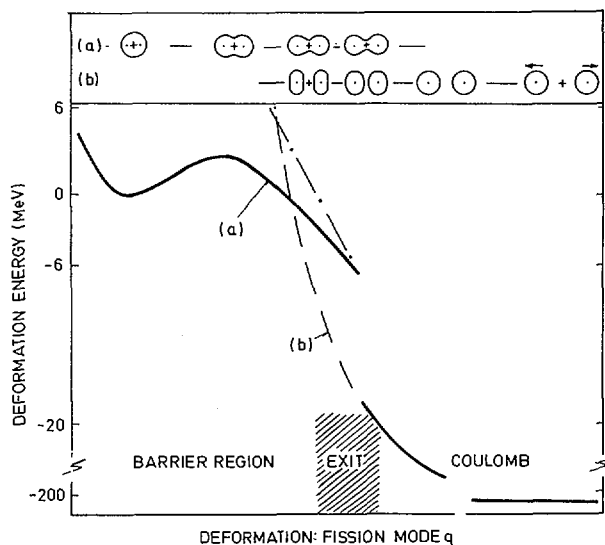


FIG. 1. Qualitative behaviour of the deformation energy in the liquid drop model. At the top of the figure, the two families of shapes in the fission mode are shown. The family of connected shapes (a) has the deformation energy (a), shown on the lower part; the family of separated shapes (b) has the deformation energy (b), which is essentially the energy of the mutual Coulomb repulsion. In a multidimensional plot, both families are separated by a ridge (— · —), which disappears at larger deformations.

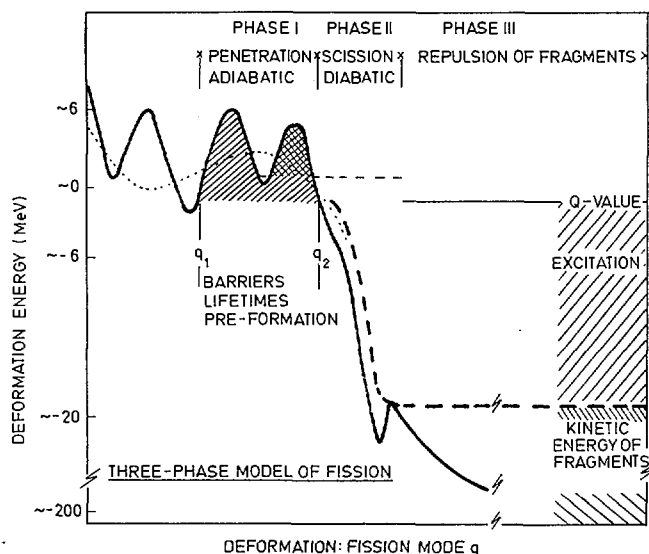


FIG.2. Qualitative behaviour of the deformation energy in fissioning nuclei. Total deformation energy is shown by the thick solid line. In phase I — the subbarrier region — the total energy in the fission mode is given by the Q-value. Areas relevant for the lifetimes are hatched. In phase II the energy in the fission mode decreases by non-adiabatic processes (shown by the dashed line). In phase III the completely disconnected fragments move apart by their mutual Coulomb repulsion. In the barrier region the liquid drop model energy is shown separately by the dotted line. The (hypothetical) scission barrier is inserted as well.

In the past, only exploratory work was done on this problem [4,10]. Some promising attempts are presented in later papers in this session. Hopefully, this field will be in the centre of future activity.

Thus, the stages of the fissioning nucleus can be classified according to Eq. (22), i.e. according to the deformation energy. We shall now discuss this cornerstone of the collective model qualitatively and postpone the quantitative discussion to Section 3.2.

The classical approach to the deformation energy is the liquid drop (LD) model [11-13]. But even in this simple model the description of the deformation energy is by no means trivial: two families of shapes exist [13] which are comparable in energy. This is schematically shown in Fig. 1. For larger deformations at and behind the liquid drop barrier, the total LD energy of two separated fragments and of the parent nucleus become comparable. In a multidimensional plot, the two families correspond to valleys in the deformation energy which are separated by a ridge. This ridge disappears gradually for the larger deformations, which fact may enable an unambiguous definition of the scission point which is called the exit [14]. The Coulomb energy at exit correlates extremely well with the average kinetic energy of the fragments [14].

If we add the shell energy [15] to the liquid drop energy (see Section 3.3), we may arrive at the situation as shown in Fig. 2, where the above-mentioned ridge has been omitted in order not to overload the sketch. We insert in this

figure the total energy E (called Q -value) and identify it with the ground state energy of the fissioning system.

At the ground state the collective kinetic energy is zero by definition, (Eqs (22) and (14)). In other words there is no "zero-point vibrational motion", contrary to many statements in the literature.

In the subbarrier region of deformation, or according to Fig. 2 in phase I of the fission process, the term kinetic energy becomes classically meaningless, since

$$K(q, \dot{q}) < 0 \quad (23)$$

No kinetic energy can be distributed and consequently all excitations have to be virtual. Thus, the adiabatic assumption is justified in this region, if anywhere at all.

In phase II, the region behind the barriers and before scission (see Fig. 2), the kinetic energy becomes increasingly large

$$K(q, \dot{q}) > 0 \quad (24)$$

Real excitation or viscous effects are possible and may even be dominant; the fissioning nucleus is heated up. This process comes to rest if all the kinetic energy is consumed or if the interaction between the translational fission mode and the intrinsic modes is no longer possible.

The latter takes place in phase III (see Fig. 2). There, the two (or more) fragments move apart by their mutual Coulomb repulsion. This presentation differs only minutely from that of Swiatecki and Björnholm [16].

Careful experimental investigations [17] reveal a strong correlation between the distribution of mass, kinetic and excitational energy of the fragments. From this we must conclude that those distributions are formed in phase II of the fission process, i. e. shortly before or at scission. As indicated in the figure, diabatic effects are important in this region. To describe these effects microscopically one should solve the coupled channel equation (Eq. (10)) explicitly. In a macroscopic approach one may calculate a viscosity coefficient and then solve the corresponding hydro-mechanical equations.

A last word about the scission act which is probably even more complicated than outlined here. The approximation to replace the leptodermous nuclei by equivalent drops eventually breaks down for the fission fragments if their density tails overlap a little. The interaction of those tails may eventually overcome the repulsive Coulomb energy of the well-separated equivalent drops. Such a scission minimum — obtained in the calculations of Nörenberg [8] — has thus a different origin than the by now familiar two or more shell minima [14, 15].

2.4. The lifetime for spontaneous fission and the fission mode

The calculations of Nix [18] may tell us that the fissioning nucleus stays in phase II in the very short time of about 10^{-22} s. Thus, even if we restrict our following considerations to phase I, the lifetimes can be calculated rigorously. Future inclusion of phase II (and III) will have predictive power

only for the distributions (of mass and kinetic energy); but these we have to disregard completely in the present work.

The lifetime τ of any state is connected to the width in energy by the uncertainty relation

$$\tau \approx \frac{\hbar}{\Gamma} \quad (25)$$

The width Γ is proportional to the square of some overlap integral of the wave function in the initial and final state

$$\Gamma \propto |(\psi_f, \psi_i)|^2 \quad (26)$$

For the case of spontaneous fission, the overlap integral can be given in WKB approximation [11], i. e.

$$\Gamma \approx \hbar \omega_f \exp \left\{ -2 \frac{S}{\hbar} \right\}, \quad \text{if } S \gg \hbar \quad (27)$$

In the case of adiabatic motion, the action integral S can be expressed by the potential energy $W(q)$ and the effective mass $B_q(q)$

$$S = \int_{q_1}^{q_2} \sqrt{|E - W(q)| 2 B_q(q)} dq \quad (28)$$

This equation can also be derived by the generator coordinate method [6-8]. The integral extends only over the region

$$W(q) \leq E$$

As will become clear later, the width Γ or the lifetime τ is mostly sensitive to the action integral S . Therefore, we confine ourselves to the rather crude estimate

$$\hbar \omega_f \sim 1 \text{ MeV} \quad (29)$$

for the characteristic energy or frequency and keep in mind that this factor is correct at most within a factor of two.

So far, we have not yet given a prescription for the "fission mode q ". The choice of $q(t)$ is essentially free and each choice, within the framework presented above, would lead to another lifetime. One way of reducing the ambiguity is given in the following.

Instead of a single coordinate q , we introduce a whole set of coordinates or deformation parameters, i. e.

$$\{\beta\} = \{\beta_1, \beta_2, \dots, \beta_n\} \quad (30)$$

For each combination, the deformation energy

$$W(\beta) = W(\beta_1, \beta_2, \dots, \beta_n) \quad (31)$$

and the kinetic energy shall be evaluable

$$T = \frac{1}{2} \sum_{i,j=1}^n B_{\beta_i \beta_j}(\beta) \dot{\beta}_i \dot{\beta}_j \quad (32)$$

Thus, instead of a simple effective mass, one has now to evaluate all the components of a mass tensor. They have the symmetry property

$$B_{\beta_i \beta_j} = B_{\beta_j \beta_i} \quad (33)$$

In this complicated space one defines now a trajectory,

$$q: (\beta_1(q), \beta_2(q), \dots, \beta_n(q))$$

i. e. a new coordinate q , embedded in the larger space for which the potential energy and the effective mass can easily be given in terms of the old ones,

$$W(q) = W(\beta_1(q), \beta_2(q), \dots, \beta_n(q)) \quad (34)$$

$$B_q(q) = \sum_{i,j} B_{\beta_i \beta_j}(\beta_1(q), \dots, \beta_n(q)) \frac{\partial \beta_i}{\partial q} \frac{\partial \beta_j}{\partial q} \quad (35)$$

Finally, one determines the trajectory by the requirement of shortest lifetime, i. e. by the requirement of least action

$$\delta S = 0 \quad (36)$$

By this procedure, one removes by definition a good deal of arbitrariness. The latter is reduced now to the choice of a large enough space $\{\beta_1, \dots, \beta_n\}$. What one has found is, so to speak, the best one-dimensional sequence of shapes — i. e. the fission mode.

3. THE COLLECTIVE POTENTIAL ENERGY AND THE COLLECTIVE INERTIA

The procedure outlined in Section 2 can be carried through if one knows the solutions of the stationary many-body Hamiltonian for each "deformation". The rigorous solution of the many-body problem is not yet known but, as shown below, one can find reasonable approximations to it.

3.1. A trial wave function for the many-body problem

According to Eq. (14) the deformation energy is defined by

$$W(q) = \frac{(\phi_0(q), \mathcal{H} \phi_0(q))}{(\phi_0(q), \phi_0(q))} \equiv \epsilon_0(q) \quad (37)$$

Its minimum is, of course, identical to the binding energy

$$\mathcal{B} = - \min W(q) \equiv - W(q_0) \quad (38)$$

An upper limit to this quantity is obtained with any trial wave function ϕ , i. e.

$$\frac{(\phi(q), \mathcal{H} \phi(q))}{(\phi(q), \phi(q))} = W_t(q) \geq W(q) \quad (39)$$

following the variational principle of Ritz. This trial function is largely arbitrary and therefore we may confine ourselves to the ground state wave function of the BCS approach (we use indices again) [19]

$$\phi_0(q) \equiv |0\rangle = \prod_{\nu} (U_{\nu} + V_{\nu} C_{\nu}^{\dagger} - C_{\nu}^{\dagger}) |\tilde{0}\rangle \quad (40)$$

where U and V are the particle and hole amplitudes, respectively. In analogy, the excited states are quasiparticle-quasihole states, i. e.

$$\phi_m(q) \equiv |\bar{\mu}\nu\rangle = \alpha_{\mu}^{\dagger} \beta_{\nu}^{\dagger} |0\rangle \quad (41)$$

and have an energy

$$\epsilon_m(q) = E_{\mu}(q) + E_{\nu}(q) + \epsilon_0(q) \quad (42)$$

The operators C_{ν}^{\dagger} and C_{ν}^{\dagger} create a "particle" in the time conjugate state $|\nu^{-}\rangle$ and $|\nu^{+}\rangle$, the operators α_{ν}^{\dagger} and β_{ν}^{\dagger} create the quasiparticles. Both are connected by the famous unitary transformation

$$\begin{aligned} \alpha_{\nu}^{\dagger} &= U_{\nu} C_{\nu}^{\dagger} - V_{\nu} C_{\nu}^{-} \\ \beta_{\nu} &= U_{\nu} C_{\nu}^{-} - V_{\nu} C_{\nu}^{+} \end{aligned}$$

In r -space the states $\phi_{\nu}(\vec{r}) = |\nu\rangle$ shall be eigenfunctions of a (so far) arbitrary "single particle Hamiltonian",

$$H_{sp} \varphi_{\nu}(\vec{r}) = e_{\nu} \varphi_{\nu}(\vec{r}) \quad (43)$$

with eigenvalues e_{ν} . Any of these may depend on "deformation". They are members of an orthonormal set

$$(\varphi_{\nu}, \varphi_{\mu}) = \delta_{\nu\mu} \quad (44)$$

The particle and the hole amplitudes, V_{ν} and U_{ν} , are, as usual, defined by

$$U_{\nu}^2 + V_{\nu}^2 = 1 \quad (45)$$

and

$$V_{\nu} = \left[\frac{1}{2} \left(1 - \frac{e_{\nu} - \lambda}{E_{\nu}} \right) \right]^{1/2}$$

with the quasiparticle energy

$$E_{\nu} = \left[(e_{\nu} - \lambda)^2 + \Delta^2 \right]^{1/2} \quad (46)$$

The pairing gap Δ and Fermi energy λ are solutions of the familiar BCS equations:

$$\frac{2}{G} = \sum'_{\nu} \frac{1}{E_{\nu}} \quad \text{and} \quad N = \sum''_{\nu} V_{\nu}^2 \quad (47)$$

For the choice of the coupling constant G and the handling of the cut-off — marked by the primes in the summation symbols — we refer to the literature [14, 20].

For a varying deformation, the single particle energies e_{ν} change, to lowest order, by

$$\delta e_{\nu} = \frac{\partial e_{\nu}}{\partial q} \delta q \quad (48)$$

The BCS equations (Eqs (47)) hold for all deformations; their solutions depend exclusively on the single particle spectrum around the Fermi energy. Consequently, the changes of the occupation amplitude V_{ν} and of the quasiparticle energy E_{ν} , which have to obey the relation

$$\sum'_{\nu} E_{\nu}^{-2} \delta E_{\nu} = 0 \quad \text{and} \quad \sum'_{\nu} V_{\nu} \delta V_{\nu} = 0 \quad (49)$$

can be calculated from the matrix elements

$$\frac{\partial e_\nu}{\partial q} = \left\langle \nu \left| \frac{\partial H_{sp}}{\partial q} \right| \nu \right\rangle \quad (50)$$

and one can derive expressions for the change of the pairing gap and Fermi energy [14, 20, 21]

$$\frac{\partial \Delta}{\partial q} \quad \text{and} \quad \frac{\partial \lambda}{\partial q}$$

Using them, all matrix elements which occur in the coupled channel equation (Eq. (10) can be evaluated, provided we know the single particle matrix elements

$$\left\langle \mu \left| \frac{\partial H_{sp}}{\partial q} \right| \nu \right\rangle$$

In particular, one obtains for the matrix elements between the ground state and an excited state [14, 20, 21]

$$\left\langle \bar{\nu} \nu \left| \frac{\partial}{\partial q} \right| 0 \right\rangle = -\frac{1}{V_\nu} \frac{\partial U_\nu}{\partial q} = -\frac{\Delta}{2E_\nu^2} \left[\left\langle \nu \left| \frac{\partial H_{sp}}{\partial q} \right| \nu \right\rangle - \frac{\partial \lambda}{\partial q} - \frac{\partial \Delta}{\partial q} \frac{(e_\nu - \lambda)}{\Delta} \right] \quad (51)$$

or for $\bar{\mu} \neq \nu$

$$\left\langle \bar{\mu} \nu \left| \frac{\partial}{\partial q} \right| 0 \right\rangle = -\frac{U_\mu V_\nu + U_\nu V_\mu}{E_\mu + E_\nu} \left\langle \mu \left| \frac{\partial H_{sp}}{\partial q} \right| \nu \right\rangle \quad (52)$$

The matrix elements between excited states differ from zero only if the quasiparticles are the same, i. e.

$$\begin{aligned} \left\langle \bar{\kappa} \lambda \left| \frac{\partial}{\partial q} \right| \bar{\mu} \nu \right\rangle &= \delta_{\lambda \nu} [1 - \delta_{\kappa \mu}] \frac{U_\kappa U_\mu + V_\kappa V_\mu}{e_\kappa - e_\mu} \left\langle \mu \left| \frac{\partial H_{sp}}{\partial q} \right| \kappa \right\rangle \\ &+ \delta_{\kappa \mu} [1 - \delta_{\nu \lambda}] \frac{U_\nu U_\lambda + V_\nu V_\lambda}{e_\lambda - e_\nu} \left\langle \lambda \left| \frac{\partial H_{sp}}{\partial q} \right| \nu \right\rangle \quad (53) \end{aligned}$$

3.2. The deformation energy

In none of the last equations does the energy of the ground state occur explicitly. The calculations of the latter can thus be decoupled, even using different methods.

As a matter of fact, one can obtain a decent description of nuclear bulk properties by means of a trial function (see Eqs (37) and (39)) if only one finds a proper choice of the average fields occurring in the trial single particle Hamiltonian

$$H_{sp} = H_{sp}(q) = \frac{p^2}{2m} + V(\vec{r}) - \frac{\kappa}{\hbar} \left[\vec{\nabla} S(\vec{r}) \times \vec{p} \right] \cdot \vec{\sigma}$$

i. e. by a proper choice of the average nuclear potential $V(\vec{r})$ — including the Coulomb potential — and of the spin-orbit field $S(\vec{r})$.

Indeed, using a Skyrme force [22] for the many-body Hamiltonian \mathcal{H} and constructing a trial function with the single particle functions ϕ_p [23], the outcome of Eq. (39) differs from the available self-consistent calculations [22] almost negligibly [24]. It seems that self-consistency in itself is not very important. Details of work on this will be published soon.

In spite of the conceptual simplicity, both approaches [22, 24] are cumbersome and time-consuming. It is therefore important to have simple approximations which, however, still are correct. They may even be phenomenological. Such is the shell correction approach of Strutinsky [14, 15], presumably.

It is certainly correct to separate the total energy, Eq. (39), into an average energy and a remaining shell energy

$$W(q) = [W(q)]_{\text{average}} + [W(q)]_{\text{shell}} \quad (54)$$

The problem starts when we interpret these quantities. According to Strutinsky one does it by

$$[W(q)]_{\text{average}} \approx E_{LD}(q) \quad (55)$$

$$[W(q)]_{\text{shell}} \approx (\delta U + \delta P)_{\text{neut.}} + (\delta U + \delta P)_{\text{prot.}}$$

The deformation energy in the liquid drop model, E_{LD} , is sensitive essentially to the reduced fissility ξ [26]

$$\xi = \frac{2a_2}{c_3} (1 - \kappa I^2), \quad I = \frac{N - Z}{N + Z} \quad (56)$$

which replaces the once universal critical value of Z^2/A for the case where the Weizsäcker formula contains a surface symmetry term [25].

The most important contribution to the shell energy comes from the shell correction proper

$$\frac{1}{2} \delta U = \sum_{\nu} n_{\nu} e_{\nu} - \langle \sum_{\nu} n_{\nu} e_{\nu} \rangle_{\text{average}} \quad (57)$$

while corrections due to residual interactions, δP , are usually small [14].

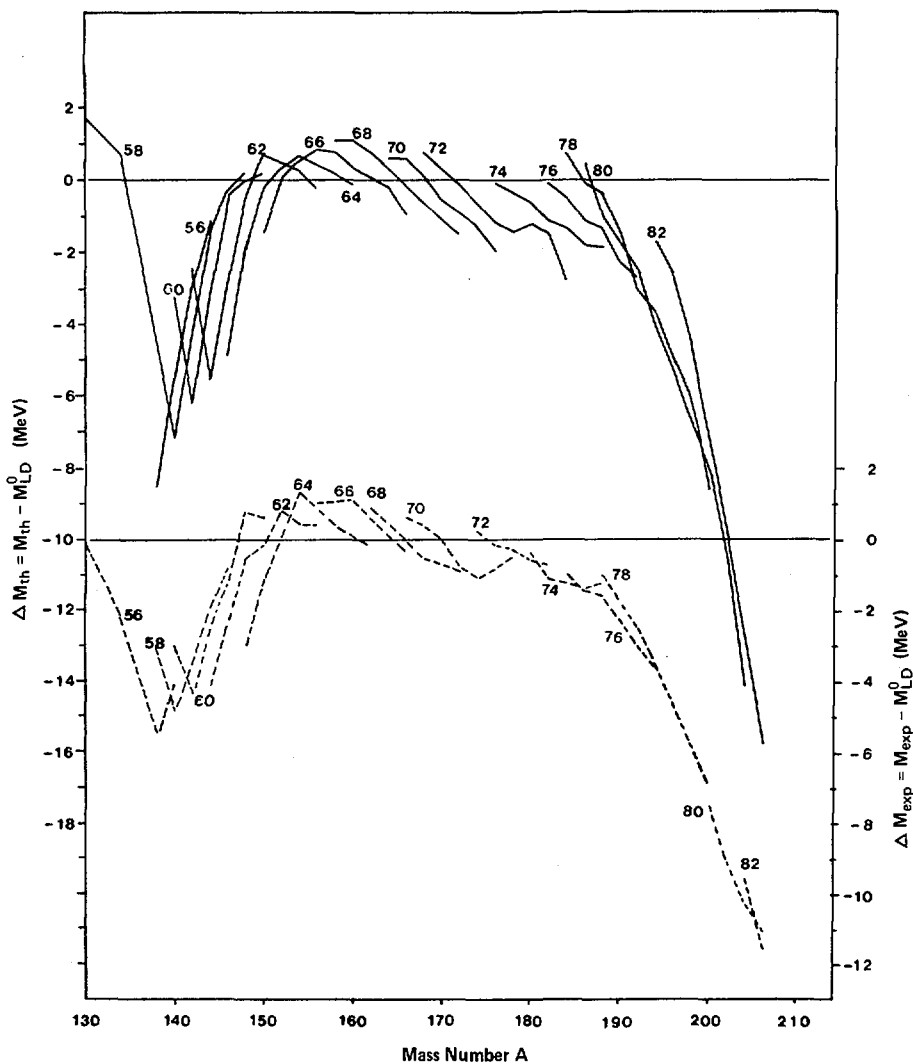


FIG.3. Theoretical and experimental masses of even-even nuclei, relative to the values of the liquid drop model (spherical), versus the mass number A (taken from Ref.[29]).

It may be a disturbing fact that the deformation energy — being such a basic quantity — can be evaluated without knowledge of the nuclear interaction; obviously the nuclear interaction is reduced to the knowledge of one single parameter, the fissility $x = (Z^2/A)/\zeta$, and to the shell energy δU which depends only on the single particle energies ϵ_ν . They can be taken from any shell model, as long as it approximately reproduces the correct magic numbers for spherical and deformed shapes.

The shell effects, however, arise from the phase space distributions of the nucleons [14], which depend more on the symmetry of the mass density distribution and on the size of the mass density distribution compared with the de Broglie wavelength, rather than on particular aspects of a nuclear force. The qualitative arguments for the validity of the shell correction approach have been discussed and reviewed thoroughly [14]. The contributions of Brack and Quentin to this Symposium [26] give quantitative support as well.

Agreement between theory and experiment can never prove the validity of a theorem, but one is impressed by the bulk of experience which is covered by the Strutinsky approach. These comparisons are the subject of reviews [23, 27, 28]. Therefore, we shall restrict ourselves to only a few selected results. They shall demonstrate the power of the method while indicating the limitations of the present approximations and the possible improvements in the future.

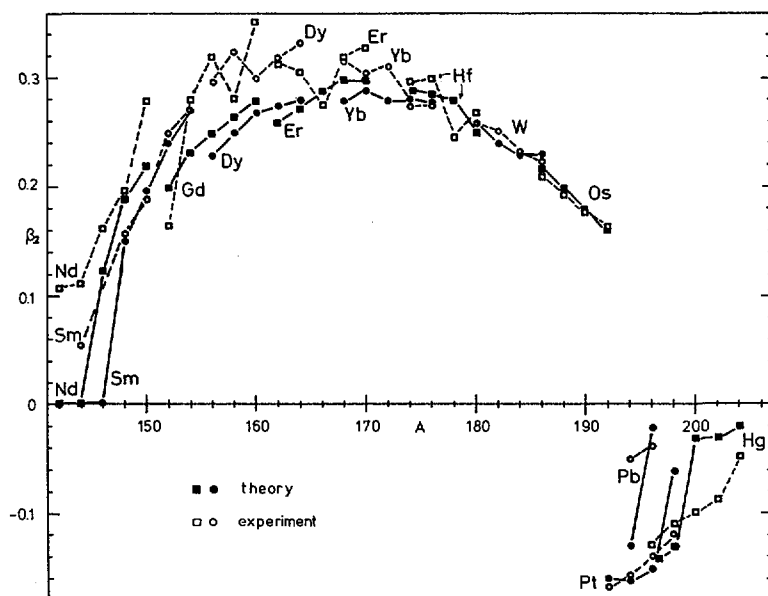


FIG.4. Theoretical and experimental ground state deformations β_2 versus mass number A . The data are taken from Ref.[29].

In Fig. 3 we present the deformation energies for the ground states of the rare earth nuclei and compare them to their "experimental" values, i.e. the differences between a fit of the spherical liquid drop binding energies [29] and the experimental masses. For the well-deformed nuclei we do not observe a serious discrepancy in magnitude or trend, but the shell corrections for all spherical nuclei are off considerably. This so-called "lead anomaly" has already been discussed in some detail [14]. At present we interpret it as being due to the mistake of fitting the parameters of the average potential to the spectroscopic single particle states in the lead region [14, 23], rather than to the binding energies directly.

This obviously does not affect the ground state deformations which are shown in Fig. 4. Possibly, this supports the suspicion that ground state deformations are not sensitive at all to the particular assumptions made. Nevertheless, it is remarkable that the transition from spherical to deformed, and from prolate to oblate shapes seems to be given accurately [29].

Finally, we present in Fig. 5 the results of calculations in several dimensions, left-right asymmetry included, for the static fission barriers [30]. The latter are defined as the energy of the stationary point of the deformation energy and calculated to have a value of

$$\zeta = 52.8 (1 - 2.84 I^2) \quad (58)$$

Whereas the energy of the outer barrier E_B seems to be reproduced quite well, we note a serious discrepancy for the inner barrier E_A — the curium-thorium anomaly [30]. A possible explanation for the latter fact is given in Section 5.1.

3.3. The collective inertia

The collective potential energy has central importance, but it is not the only piece of information which we need for a dynamic description of the fissioning nucleus. According to the action integral, Eq. (28), the mass

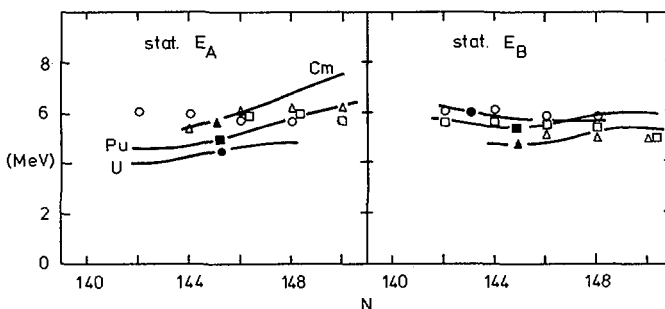


FIG. 5. Static fission barriers for U isotopes (●), Pu isotopes (■) and Cm isotopes (▲) versus the neutron number N. The inner barrier is denoted by E_A and the outer by E_B . Experimental values are shown by the corresponding open symbols. The data are taken from Refs [30, 31]. For the Cm isotopes the experimental value of the next heaviest odd isotope is used.

parameters are equally important. In the framework of the approximations developed in Section 2.1, we have found those matrix elements which we need for the collective mass, according to Eq. (21). If we make use of Eqs (51) and (52), we arrive at the expressions

$$B_{ij}(\beta) = [B_{ij}(\beta)]_1 + [B_{ij}(\beta)]_2 + [B_{ij}(\beta)]_3$$

where the components

$$[B_{ij}(\beta)]_1 = \hbar^2 \frac{\Delta^2}{4} \sum_{\nu} \left\langle \nu \left| \frac{\partial H_{sp}}{\partial \beta_i} \right| \nu \right\rangle \left\langle \nu \left| \frac{\partial H_{sp}}{\partial \beta_j} \right| \nu \right\rangle E_{\nu}^{-5} \quad (59)$$

$$[B_{ij}(\beta)]_2 = 2\hbar^2 \sum_{\mu \neq \nu} \left\langle \nu \left| \frac{\partial H_{sp}}{\partial \beta_i} \right| \mu \right\rangle \left\langle \mu \left| \frac{\partial H_{sp}}{\partial \beta_j} \right| \nu \right\rangle \frac{(U_{\mu} V_{\nu} + U_{\nu} V_{\mu})^2}{(E_{\mu} + E_{\nu})^3} \quad (60)$$

$$\begin{aligned} [B_{ij}(\beta)]_3 = & \hbar^2 \frac{\Delta^2}{4} \sum_{\nu} \left\{ \left\langle \nu \left| \frac{\partial H_{sp}}{\partial \beta_i} \right| \nu \right\rangle - \frac{\partial \lambda}{\partial \beta_i} - \frac{(\epsilon_{\nu} - \lambda)}{\Delta} \frac{\partial \Delta}{\partial \beta_i} \right\} \\ & \times \left\{ \left\langle \nu \left| \frac{\partial H_{sp}}{\partial \beta_j} \right| \nu \right\rangle - \frac{\partial \lambda}{\partial \beta_j} - \frac{(\epsilon_{\nu} - \lambda)}{\Delta} \frac{\partial \Delta}{\partial \beta_j} \right\} \\ & - \left\langle \nu \left| \frac{\partial H_{sp}}{\partial \beta_i} \right| \nu \right\rangle \left\langle \nu \left| \frac{\partial H_{sp}}{\partial \beta_j} \right| \nu \right\rangle \right] \frac{1}{E_{\nu}^5} \end{aligned} \quad (61)$$

are ordered according to their magnitude under normal conditions, i. e.

$$[B_{ij}]_1 \gg [B_{ij}]_2 > [B_{ij}]_3 \quad (62)$$

The leading term is connected to the "diagonal" matrix element

$$\left\langle \nu \left| \frac{\partial H_{sp}}{\partial \beta} \right| \nu \right\rangle$$

but it should be noted that just this term disappears for a vanishing pairing gap Δ . Therefore, residual interactions are especially important for the collective inertia.

The mass parameters depend strongly on the deformation. This may be seen in the example of Fig. 6. The correlation with the undulating shell correction energy is extremely strong, and therefore it may be justified to

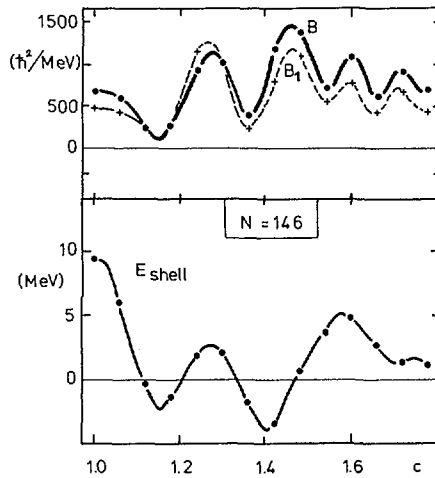


FIG.6. Mass parameter B_{cc} ($=B$) and the shell correction energy E_{shell} for the neutrons of ^{240}Pu versus the elongation c . The leading diagonal part of the mass parameter, B_1 , is shown separately by the dashed line (c.f. Eq.(59)).

speak of the shell structure in the mass parameters. This can be understood by a simple approximation [14] that is, by considering only the first component, $[B_{ij}]_1$, and replacing the summation by an integration

$$\sum_{\nu} \rightarrow \int g_{\text{eff}}(E) dE$$

Thus

$$B = \frac{\hbar^2 \Delta^2}{4} \int_{\lambda}^{\infty} |\langle \nu | \frac{\partial H}{\partial \beta} | \nu \rangle|^2 \frac{g(E)}{E^5} dE \sim \frac{\hbar^2 \Delta^2}{4} \left| \langle \frac{\partial H}{\partial \beta} \rangle \right|_{\text{av}}^2 g_{\text{eff}}(\lambda) \int_{\Delta}^{\infty} \frac{dE}{E^5}$$

which leads to

$$B \sim \left| \langle \frac{\partial H}{\partial \beta} \rangle \right|_{\text{av}}^2 \frac{g_{\text{eff}}(\lambda)}{\Delta^2} \quad (63)$$

From this it becomes evident that the shell structure is contained in the quantity $g_{\text{eff}}(\lambda)$, the effective level density at the Fermi energy. According to Eq. (63) the mass parameter is proportional to the square of the inverse pairing gap, and this proportionality has been checked in actual calculations. The mass parameter also has the correct asymptotic behaviour, (see Fig. 7). For details, we refer to a more extensive presentation [21]. The strong energy cut-off, E^{-5} , in the leading term $[B_{ij}]_1$

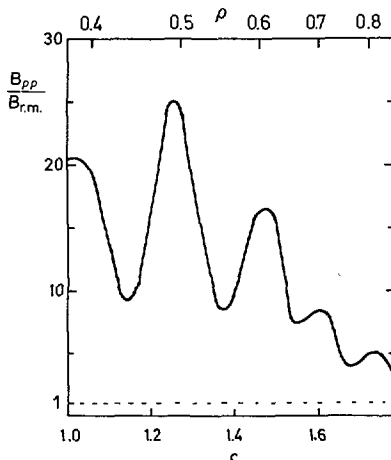


FIG. 7. Effective mass $B_{\rho\rho}$ of ^{240}Pu versus the elongation c . The distance between the centres of mass of the two forming fragments, 2ρ , is given in the upper scale. Note that $B_{\rho\rho}$ converges towards its asymptotic value $B_{r.m.}$, the reduced mass of the separated fragments.

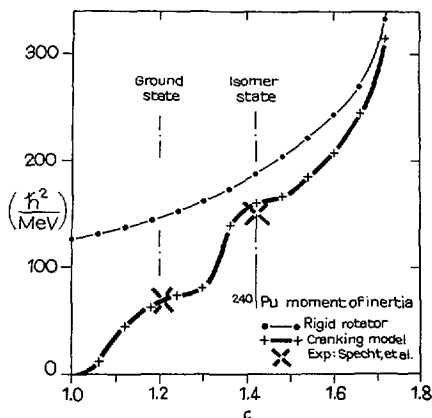


FIG. 8. Moment of inertia of ^{240}Pu versus the elongation c . The thicker line represents the moment of inertia calculated with the cranking model, the thin line gives the value for a corresponding rigid body. The experimental value of the isomeric state is taken from Ref.[32].

ensures that only levels close to the Fermi energy contribute at all. It can be assumed that this region is described sufficiently well by the phenomenological shell models. Consequently, unlike the case of the deformation energy, no renormalization seems necessary.

Unfortunately, no direct and independent comparison of this piece of information with experimental data seems possible at the moment, except

that from our results on the lifetimes one may conclude that the approach has at least some validity.

However, based on the very same approximation, the effective moments of inertia can be calculated [14], i. e.

$$\mathcal{J} = \sum_{\mu, \nu} |\langle \mu | j_x | \nu \rangle|^2 \frac{(U_\mu V_\nu - U_\nu V_\mu)^2}{(E_\mu + E_\nu)}$$

If one compares this quantity, taken at the theoretical deformations of the ground state and the isomer state, with the respective quantities extracted from the important experiments of the Munich group [32], one arrives at an agreement which is almost too good, as seen by Fig. 8.

4. LIFETIMES FOR SPONTANEOUS FISSION

We restrict ourselves now exclusively to phase I, the sub-barrier region of deformation, and calculate the lifetimes for spontaneous fission according to the procedure outlined in Section 2.

4.1. The least action trajectory for ^{240}Pu

The most important problem is the determination of the least action trajectory. The central equation (Eq. (36)) can be solved rigorously by the variational calculus of Euler. But within a reasonable accuracy the same goal can be achieved more economically and with greater numerical stability by searching the trajectory using the following method [21]. One chooses a Spline function of degree two or three to pass through a given number of points in the space of the deformation coordinates. Along the trajectory one calculates the action integral according to Eq. (28). One varies the points — the integration limits included — until one has found a trajectory of least action. This procedure converges reasonably well to the final value. We estimate the final accuracy to one or two units of \hbar corresponding roughly to one or two orders of magnitude in the lifetimes.

The variation of the least action trajectory has been carried out for all the nuclei referred to in the following parts of Section 4 for the full space of three deformation coordinates (c, h, α) . The latter include an elongation (c) , a neck formation (h) , and a left-right asymmetry (α) of the shape; their detailed definition may be found elsewhere [23].

As an example we select the least action trajectory for the ground state fission of ^{240}Pu . In Fig. 9a its projection into the "symmetric" space, i. e. $c(q)$ and $h(q)$, is drawn into the contour plot of the deformation energy $W(c, h, \alpha = 0)$. In Fig. 9b, its projection into the asymmetric space is shown, i. e. $c(q)$ and $\alpha(q)$. The contours in this figure refer to the deformation energy $W(c, h(q), \alpha)$.

It is obvious that the least action trajectory does not pass through the saddle points of the deformation energy, but bypasses them at a somewhat higher energy. This is not peculiar to this special case and has been observed in virtually all of the cases. To some extent it is a consequence of the large effective mass at the barriers, noted in Section 3.4.

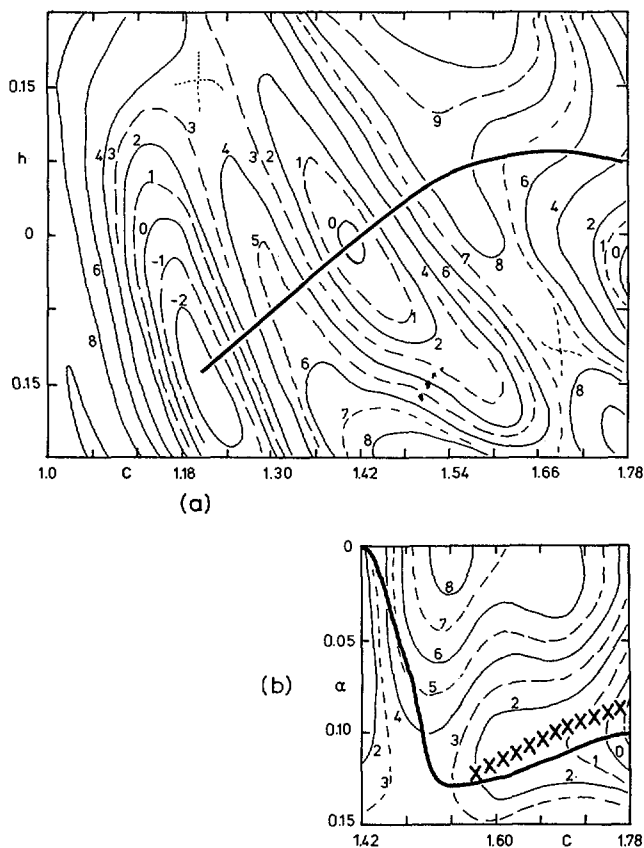


FIG. 9. (a) Deformation energy of ^{240}Pu versus the two symmetric deformations c (elongation) and h (constriction) is shown as a contour plot. Equidistance is 1 MeV. The projection of the least action trajectory into the symmetric subspace (c, h) is shown by the thick solid line. Note the discrepancy between the static and dynamic barriers. (b) Deformation energy $W(c, h(q), \alpha)$ of ^{240}Pu versus the asymmetry α and the elongation c . The least action trajectory is shown by the thick line. Note that the projection of the trajectory, i.e. $\alpha = 0$, coincides with the trajectory shown in Fig. 9a. Crosses (x) indicate the line of constant mass estimate, $\chi = 1.43$ (cf. Eq. (68)).

The same calculations can be performed for the spontaneous fission from the isomer state and for the penetration from the second into the first well. As it turns out, both these calculations yield virtually the same least action trajectory as for fission from the ground state. This may be taken as a hint for the physical relevance of the trajectory proper.

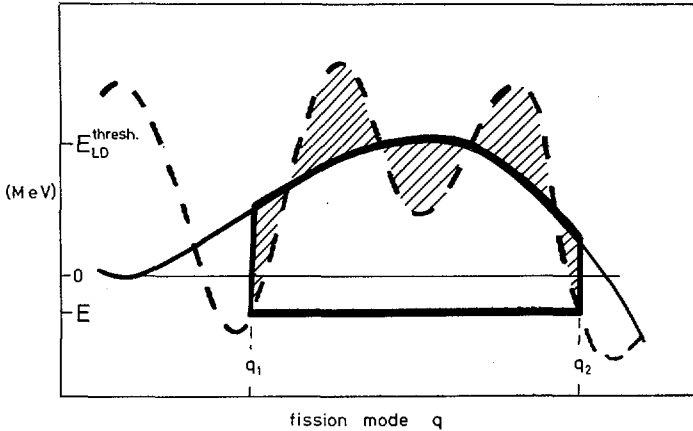


FIG.10. Qualitative behaviour of the total deformation energy (dashed line) and the liquid drop model energy (solid line) versus the fission mode q . The lifetime for ground state spontaneous fission is essentially determined by the area below the liquid drop model energy and above the ground state shell correction. In the action integral, the shaded areas (almost) cancel.

4.2. The role of pairing and of the liquid drop

According to Section 3.4, the mass parameters depend strongly on the pairing gap. Inserting Eq. (63) into Eq. (28), we realize that the action integral is roughly proportional to the inverse pairing gap. Changing the latter by only 10%, which is a conservative choice of the uncertainty, the lifetime changes by roughly five orders of magnitude. Thus, the correct choice of the pairing gap is very important. Nevertheless, we have chosen the usual parameters [21, 14] corresponding to a pairing coupling constant proportional to the surface area.

Obviously, the action integral is proportional to the area of the deformation energy. As shown in Fig. 10 this area is essentially given by the liquid drop energy and the shell correction energy of the ground state. It is evident that the other fluctuations, i.e. the areas hatched in the figure, average out almost completely. This has been confirmed by an actual check calculation [21], and agrees very well with the early observations of Swiatecki [33] that the logarithm of the fission lifetime is proportional to the liquid drop barrier plus the ground state shell correction, i.e.

$$\log \tau \sim E_{LD}(\text{barrier}) + [W(g.s.)]_{\text{shell}} \quad (64)$$

Consequently, the lifetime for fission is linked to the true fission barrier, i.e. the one which includes shell corrections and determines the threshold behaviour, only indirectly. This is contrary to many statements in the literature.

The lifetime for spontaneous fission is an observable, i.e. model independent, while the fission barriers are not (see discussion in Section 5).

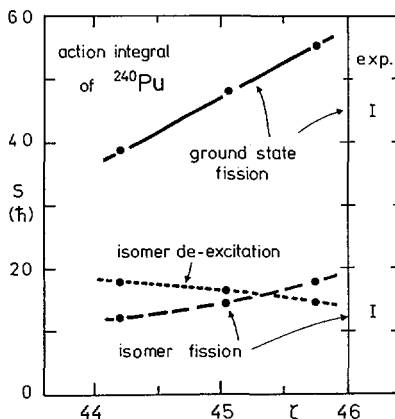


FIG.11. Action integral S along the least action trajectory for ^{240}Pu as a function of the reduced fissility ζ . S is calculated for the three possible processes: (1) spontaneous fission from the ground state, (2) spontaneous fission from the isomer state, and (3) spontaneous decay of the isomer state by penetration through the first barrier. "Experimental" values are given on the right side.

Therefore, one should fit the one relevant liquid drop model parameter, the reduced fissility, directly to the lifetime, rather than to the barriers, as done before [30]. In doing so, one assumes tacitly that (a) the calculated mass parameters are correct and (b) the shell corrections at the ground state are correct. Especially on the latter point some doubt has to be cast: There is the ^{208}Pb anomaly [14], which must have consequences on the deformed nuclei as well, especially on the behaviour of the shell corrections with N and Z . (This anomaly, as observed also in other spherical nuclei [23, 28, 29], has prevented us from calculating lifetimes for super-heavy nuclei.) In such an approach all these eventual shortcomings will show up in the liquid drop parameters and, as we see later, they behave rather strangely.

In Fig. 11 we show how strongly the action integrals for the three processes considered depend on the value of ζ . We take it as a strong argument in favour of the present approach to the dynamics that the lifetimes of the ground state and of the isomer state both agree with the calculated lifetimes for a single value of ζ .

4.3. Results of the calculations in the actinide region

First, we determine for each isotope that particular value of ζ which brings the theoretical and the experimental lifetime for the ground state into full agreement. If we plot the obtained values versus I^2 , all "experimental" values of ζ should lie only on a straight line if the present interpretations and calculations are correct. As can be seen from Figs. 12 and 13, this holds only within some limits. There is definitely some correlation, but a closer look shows that the correlation within one element is by far stronger than within one isotope chain. To compensate for the various shortcomings of the present calculation (see also Section 5), we choose

preliminarily different values of the reduced fissility for the different elements. In particular, these values are

$$\text{U and Pu:} \quad \zeta = 49.0 (1 - 1.87I^2) \quad (65a)$$

$$\text{Cm:} \quad \zeta = 49.41 (1 - 2.12I^2) \quad (65b)$$

$$\text{elements above Cf:} \quad \zeta = 50.47 (1 - 2.84I^2) \quad (65c)$$

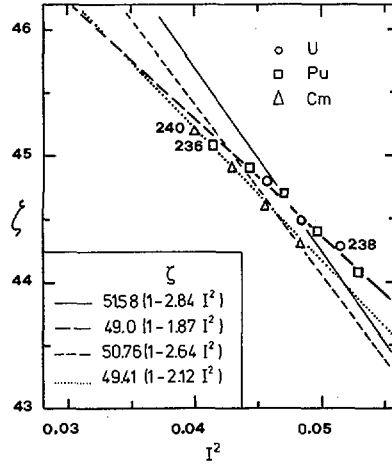


FIG.12. Reduced fissility ζ versus $I^2 = ((N-Z)/A)^2$. The values of ζ are obtained by a fit of the lifetimes for ground state spontaneous fission to the experimental values. Different parametrizations of the reduced fissility $\zeta = \zeta_0 (1 - \kappa I^2)$ are shown by straight lines. Experimental values are taken from Hyde [34].

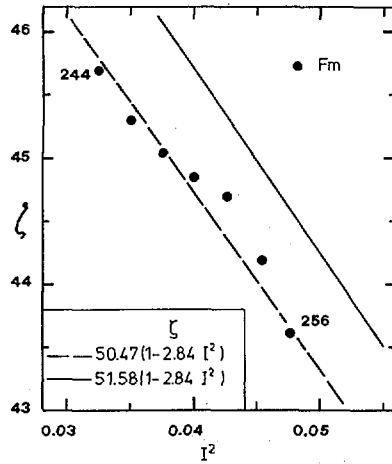


FIG.13. Reduced fissility ζ versus $I^2 = ((N-Z)/A)^2$ for the fermium isotopes (same as Fig.12). Experimental values are taken from Ref.[35].

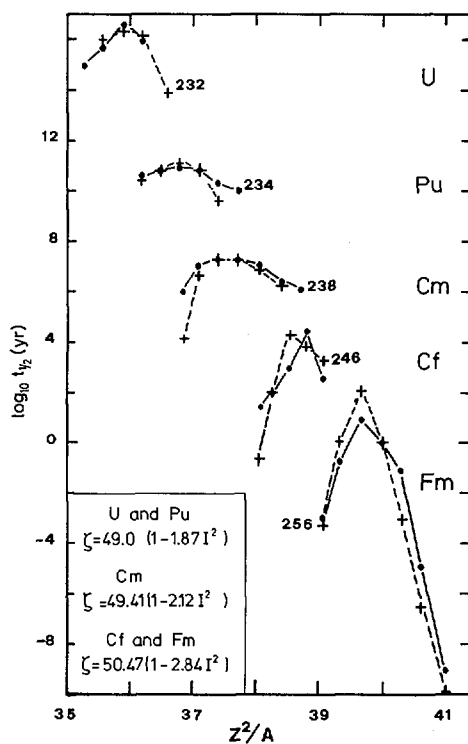


FIG. 14a. Theoretical (•) and experimental (+) half-lives (in years) for ground state spontaneous fission, plotted versus Z^2/A . The parametrization of ζ for the different elements is given in the inset. The experimental data are taken from Refs [34, 35].

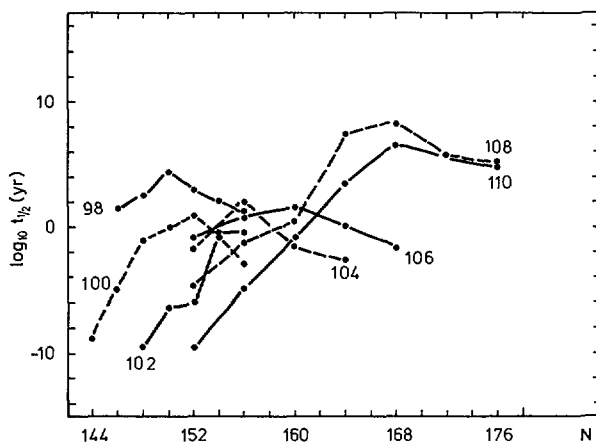


FIG. 14b. Predicted fission half-lives (in years) for the heavier actinides up to element 110 are plotted versus the neutron number N . The parametrization of ζ is given by Eq. (65c). Each element has an isotope which is most stable with respect to spontaneous fission. Among these, the species with the shortest lifetime is the nucleus $^{258}_{102}\text{No}$.

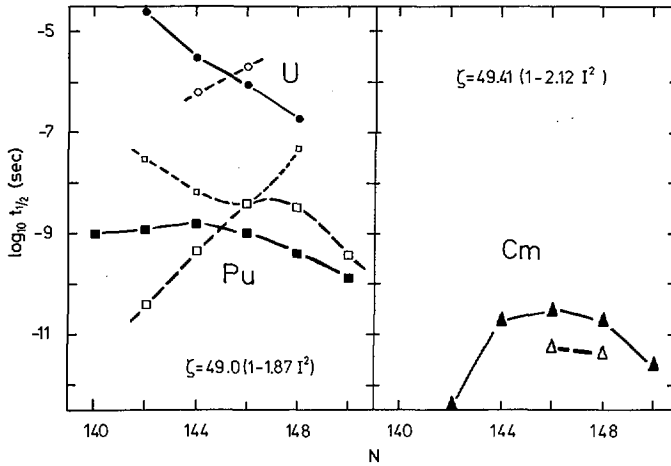


FIG. 15. Theoretical (filled symbols) and experimental (open symbols) half-lives (in seconds) for isomeric fission of U-, Pu- and Cm-isotopes plotted versus the neutron number N . The reduced fissility is the same as for ground state fission half-lives. The experimental half-lives are compiled in Table I. For Cm, refer to Eq.(66). Note the discrepancy between the most recent (larger squares) and the former (smaller squares) experimental half-lives of the Pu isotopes.

The resulting lifetimes are plotted in Figs 14a,b. For elements up to Fm the experimental lifetimes — to the extent they were available — have been inserted in Fig. 14a. The agreement between the two sets of data is surprising, but one should not forget that it was achieved by introducing several liquid drop parameters. (Using a single set, one arrives at the results shown later in Fig.17.) Nevertheless, we have used the present parameters, given by Eq.(65c), to attempt to make predictions for the heavier actinides up to element 110, as shown in Fig.14b. In this figure we have chosen the neutron number as ordinate to show that, while the magic neutron number 152 is exceedingly strong for the usual actinides [38], it is not a "universal constant" but ceases to be magic for just those elements and isotopes above and around element 102. (cf. also discussion in Ref.[26] on this point.) As for the quality of the prediction, we refer to the discussion in Section 4.2.

With the parameters set we have calculated the lifetimes for the spontaneous fission from the isomer states. They are plotted in Fig. 15 and compared with the experimental values which are given in Table I. We should like to point out that the order of magnitude is reproduced. On the other hand, the systematic behaviour shows some discrepancy. It is remarkable that the most recent experimental values [38], which are corrected for the de-excitation into the first well, agree much better with the present results than the earlier values. Of course, in Cm no isomers have so far been observed for the even-even isotopes. To get an order of magnitude estimate, we have extrapolated the available even-odd values by making use of the systematic odd-even effects in the Pu isotopes, according to

$$\tau(\text{Cm}, N) = \tau(\text{Cm}, N-1) \cdot \frac{\tau(\text{Pu}, N)}{\tau(\text{Pu}, N-1)} \quad (66)$$

TABLE I. EXPERIMENTAL HALF-LIVES FOR ISOMERIC SPONTANEOUS FISSION

Nucleus Z A		Half-life (nsec)		Nucleus Z A		Half-life (nsec)	
92	236	110	c)	94	241	27080	b)
		2000	e)				
	238	200	b)		242	50	c)
		6300	e)			3.5	d)
	235	30	a)		243	60	c)
94	236	34	c)	96	240	< 2	b)
		0.04	d)				
	237	100	a)		241	15.3	a)
		100	c)			19	b)
		900	b)				
	238	6.5	a)		242	< 2	b)
		0.7	d)				
	239	8000	b)		243	38	b)
	240	3.8	a)		245	23	a)
		3.8	d)				

Note: The experimental values are taken from the following references:

- a Ref.[31].
- b Ref.[36].
- c Ref.[37].
- d Ref.[38].
- e Ref.[39].

The data of Liukkonen and Metag [39] are corrected for γ -branching, estimated from the "missing cross-section".

With regard to the discrepancy observed in the U isotopes one may wonder whether some correction of the experimental numbers may occur in the future as well.

In Fig. 16 we present our results for the de-excitation into the first well. We do not show the absolute lifetimes but rather the branching ratio of penetration factors. No experimental values are available here, so far. Whereas the chance of falling back into the first well is very small for the Cm isotopes and nearly independent of the neutron number, we predict this branching ratio to be about 1 for the U isotopes, depending somewhat on the neutron number. We predict the same order of magnitude for ^{236}Pu .

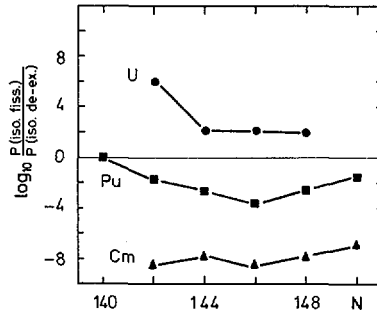


FIG.16. Ratios of penetration for isomer deexcitation and isomer fission for some U-, Pu-, and Cm-isotopes plotted versus neutron number N. The reduced fissility is the same as for ground state fission.

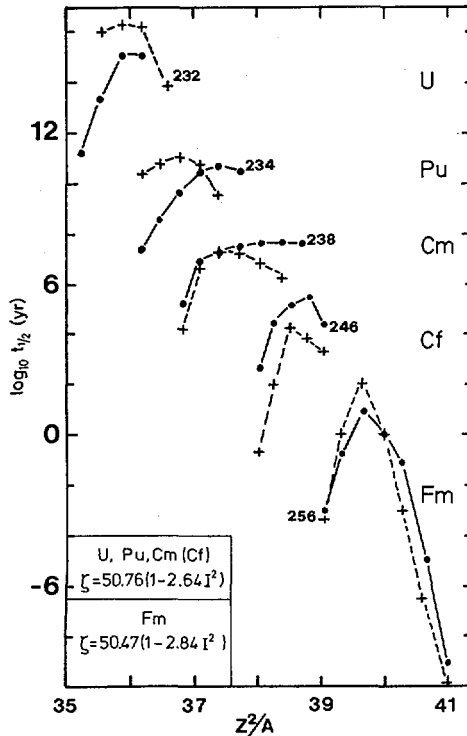


FIG.17. Theoretical (•) and experimental (+) half-lives (in years) for ground state spontaneous fission versus Z^2/A . Except for Fm and Cf, the same parametrization of ζ has been used. (Theoretical values for the Cf-isotopes are taken from Ref.[30].)

For increasing neutron number, the branching ratio decreases. The uncertainty of the absolute branching ratio is at least two orders of magnitude, and somewhat less for the systematic behaviour. It is remarkable that no effect of the neutron number $N=148$, magic for isomeric processes, can be observed. In other words, this neutron number should be magic both for decay and for isomer fission.

To conclude this section, and to stress the significance of the fissility parameter ξ for the lifetime, we present in Fig. 17 the fission half-lives for the ground state, calculated with

$$\xi = 50.76 (1 - 2.64I^2) \quad (67)$$

being the same for all the actinide nuclei, except Fm and Cf. The discrepancy with the experimental numbers is now of course much greater than in Fig. 14. Not only the order of magnitude changes, but also the peaks within one element are slightly shifted.

5. IMPLICATIONS OF THE LEAST ACTION TRAJECOTY

The least action trajectory is a construction which enters the above calculations in a decisive way. Does it have physical relevance to aspects of the fission process other than the lifetimes?

In all the work on the fission process the stationary points of the deformation energy have been related to the threshold behaviour of induced fission cross-sections. This identification deserves a closer inspection for two reasons. First of all, as shown in Section 2, the deformation energy is the ground state energy of the nucleus at the various deformations. A similar construction could be given for the excited states, at least in principle. We know that for high excitation the shell effects which are so important for low excitation damp out. But, for low excitation around the energies corresponding to the fission threshold, these damping effects are small and it might be not unreasonable to assume that the deformation energy looks the same as for the ground state. This is a working hypothesis subject to later correction. Secondly, we have observed in Section 4.1. that the least action trajectory for spontaneous fission does not necessarily go through the points of stationary deformation energy but bypasses the saddles at energies up to 2-3 MeV above them. Is it possible that the trajectory is different at higher excitations? Some years ago, the question was investigated concerning whether the mass parameters depend on the temperature, i. e. on the excitation energy. They do. But the change was insignificant for the low excitations of 6-10 MeV with which one deals at the threshold and which correspond roughly to a temperature of 0.1 MeV.

5.1. Dynamic fission barriers

If both the deformation energy and the mass parameters are the same for ground state and induced fission, their least action trajectory should be the same. We repeat: this is a working hypothesis. If so, then the threshold energy should be correlated to the local maxima of the deformation energy along the least action trajectory and not with the points of stationary

deformation energy. Henceforth we refer to these maxima as the dynamic barriers. In Fig. 18 we have plotted them for all those isotopes for which a dynamic calculation has been carried out. The liquid drop parameters are the same as those used to calculate the lifetimes, cf. Eq. (65). Compared with the static values they vary less from one isotope to the other and the inner saddle is remarkably constant over the whole region. Compared with the values extracted from the experiments, which are inserted into the figure as well, they do not have the thorium-curium anomaly as do the static ones [30]. Instead, they differ by an almost constant value over the whole region. The discrepancy has a different sign for the inner and the outer barrier.

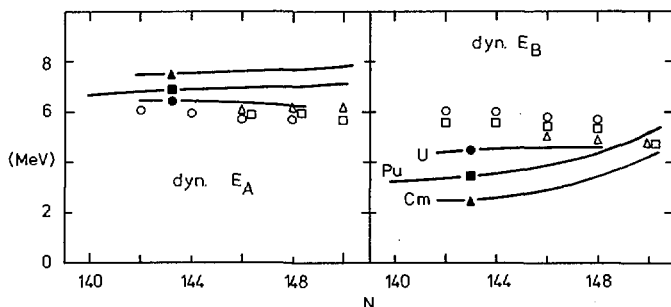


FIG. 18. Dynamic fission barriers for U isotopes (\bullet), Pu isotopes (\blacksquare) and Cm isotopes (\blacktriangle) plotted versus neutron number N . Experimental values are shown by the corresponding open symbols. The reduced fissility ζ is the same as for the lifetimes (see (Fig. 14)).

At the moment we do not mind this, rather we stress the point that the trend of the theoretical and experimental values is now the same which — as so often in physics — might be more important than the absolute value. We recall at this point that the shell corrections for the spherical nuclei are off as well. All these effects we relate to an inappropriate choice of the single particle model, rather than to the use of the Strutinsky method.

5.2. Dynamic relevance of the self-consistent calculation

A posteriori we claim that the stationary points of the deformation energy have no physical relevance. Most probably the threshold properties of induced fission are to be correlated with the deformation energy along the least action trajectory, which cannot be obtained without taking the mass parameters into account. Consequently, the lowering of the static fission barrier for the heavier actinides due to non-axial degrees of freedom [40] are not necessarily dynamically relevant. It must be investigated whether the fissioning nucleus proceeds through such shapes. The consequences drawn from the static features alone [40, 41] may be spurious.

The above statement implies also that self-consistent calculations may give spurious information, as long as they do not explore at least two or three dimensions in deformation. They are based on a variational concept and if only one shape degree of freedom is included, they drive us by definition through the minimal potential energy, i. e. over the static barrier.

Consequently, in a dynamical treatment, which of course could be done, such calculations should result in lifetimes which are orders of magnitude too large, even if the respective barriers look reasonable.

5.3. Pre-formation of fragments

A more careful inspection of the trajectories shows that the smallest among them is found only if, after having passed the asymmetric saddle, the trajectory bends back to the line of symmetric shapes (cf. Fig. 9b). Does this imply that at sufficiently large deformations the shape again becomes symmetric? It is a peculiar and unpleasant feature of our parametrization (c, h, α) that neither the necking h nor the asymmetry α has a physical meaning. The latter, α , is related to the mass asymmetry of the future fragments only indirectly. To avoid this, the drop was divided through its geometrical centre and the mass ratio of the two halves was taken as a new measure, which gives [14]

$$\chi = \frac{1 + \frac{3}{8}\alpha c^3}{1 - \frac{3}{8}\alpha c^3}$$

This definition is sufficiently simple and unambiguous and goes asymptotically over into the ratio of the fragment masses. For connected shapes, χ probably has no meaning, but in any case it is a better estimate for the mass ratio than anything else, just because it arises from a volume integral. As seen from Fig. 9b, the least action trajectory — found independently of these considerations — closely follows a line of constant mass ratio estimate χ . The bending-back of the least action trajectory may now be taken as a hint that the mass ratio of the future fragments is more or less conserved, after it was built up rather quickly around the second barrier. In other words, we observe a distinct pre-formation of the future fragments at shapes which by no means are strongly necked in. Such a pre-formation is observed even if the second barrier is the lower of the two. Therefore, the pre-formation is not really a threshold effect as was thought earlier. Rather the nucleons may "feel" the shell structure of the future fragments already at unconstricted but sufficiently stretched shapes. If nuclei are sensitive to those structures already at the second barrier, one should not be surprised if they conserve their composition all the way down to and at scission. Some support for such a speculation is given by the strong correlation between the experimental peak-to-peak ratio of the mass distribution and our estimate χ , which is displayed in Fig. 19. The correlation is linear: one may tend to say that χ is the peak-to-peak ratio.

The pre-formation certainly gives only a mean value of the mass distribution, but it should be difficult for the system to override such leading order terms, even at high excitation. As an example we present in Fig. 20 the mass distribution for the spontaneous fission of ^{257}Fm . The mass distribution looks rather symmetric, but it could be interpreted as being built up by two Gaussian-like distributions, centered at about the vertical bars inserted in the figure. The latter are given by our mass ratio estimate for ^{256}Fm .

A full description of the distribution of mass and kinetic energy is another problem which cannot be solved just by considering collective

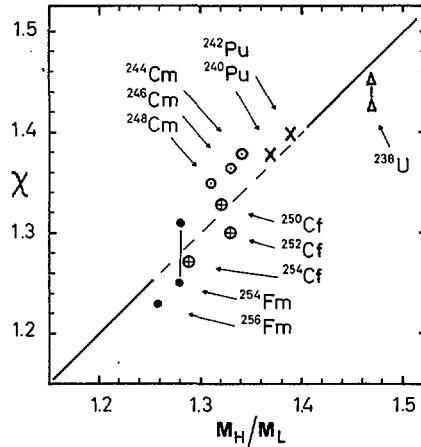


FIG.19. Mass asymmetry estimate χ at the dynamic outer saddle plotted versus the experimental mass ratio M_H/M_L of the fission fragments. For ^{238}U and ^{254}Fm two values of χ are shown, corresponding to two different fission trajectories with almost the same action integral. The figure is taken from Ref.[21].

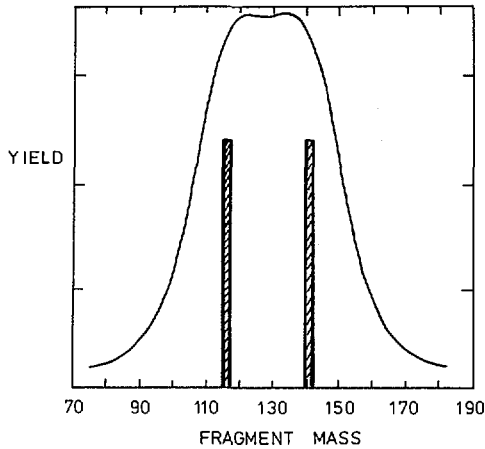


FIG.20. Fragment mass distribution of spontaneous fission of ^{257}Fm , taken from Ref.[42]. The two vertical bars represent the estimate $\chi = 1.23$, as obtained from the calculation for ^{256}Fm (cf also Fig.19).

kinetic and potential energies alone. The effects of viscosity, for example in phase II of the fission process, are not negligible, as the very existence of fragment excitation may show. We should like to stress the point that calculations done for phase II of the fission process must result in a simultaneous description of distributions for the masses and the kinetic energies. After 30 years of speculation it seems possible to do this in the framework of a unified model. We are looking forward to such developments, the more so as another field of activity seems to be so nicely complementary to fission, especially to phase II: the scattering of heavy ions.

6. SUMMARY AND CONCLUSIONS

In a series of not very stringent assumptions, a coupled channel equation for the state vector of a fissioning nucleus is derived. This approach — known as the cranking model — gives a framework for the discussion of those quantities which usually appear in the phenomenological collective models. In particular, we discuss the collective potential and the collective kinetic energy, and leave room for a future inclusion of viscous effects.

Assuming that the excited states of the system can be understood as quasiparticle-quasihole excitations, all terms appearing in the coupled channel equation can be calculated with the usual BCS-approach for the pairing theory and with the single particle wave functions and eigenvalues. For the latter we use the solutions of the Schrödinger equation for a deformed average field of Woods-Saxon shape.

The approach simplifies considerably for adiabatic motion of the quasiparticles. Formulating a three-phase model of fission, we discuss why the adiabatic assumption is reasonable in the subbarrier region of deformation. We also discuss why this region determines the lifetime for spontaneous fission.

To test this concept, we restrict ourselves to the subbarrier region and calculate the lifetime related to barrier penetration in the fission mode. The fission mode gives by definition the shortest possible lifetime for a given set of deformation parameters. Three types of deformations have been included: an elongation, a constriction in the middle and a left-right asymmetry.

After an adjustment of the relevant liquid drop parameters we obtain half-lives which agree with the available experimental material to a large extent, not only for spontaneous fission from the ground state, but also for fission from the isomer state.

Finally, we discuss whether the so-called static or the dynamic saddle should be identified and compared with the experimental threshold energies. Last but not least, we observe a pre-formation of the future fission fragments within the parent nucleus at and around the second barrier, which correlates extremely well with the empirical peak-to-peak ratio of the fragment mass distribution.

We conclude that the traditional Bohr-Wheeler picture of the fission process is valid, if only the proper collective potential and collective kinetic energies are used. Both quantities depend significantly on shell structure. The results give additional evidence that Strutinsky's shell correction method is essentially correct.

We also conclude that the assumption of adiabatic motion is justified for the subbarrier region. This conclusion is not affected by the observation of excitation energy in the fragments, as the distributions of mass, kinetic energy and excitation energy will develop at a later stage, behind the barrier region.

Essentially the same methods can be extended to the post-barrier region and the scission region. In the future, the latter deserves more investigation, both experimentally and theoretically.

REFERENCES

- [1] HAHN, O., STRASSMANN, F., *Naturwissenschaften* 27 (1939) 11.
- [2] MEITNER, L., FRISCH, O.R., *Nature* 143 (1939) 239.

- [3] BETHE, H.A., *Annu.Rev.Nucl.Sci.* 21 (1971) 93.
- [4] WILETS, L., *Theories of Nuclear Fission*, Clarendon Press, Oxford (1964).
- [5] PAULI, W., "Die allgemeinen Prinzipien der Wellenmechanik", *Handbuch der Physik V/1*, Springer-Verlag, Berlin (1958); SCHRÖDINGER, E., *Ann.Phys.(Leipzig)* 79 (1926) 489.
- [6] HILL, D.L., WHEELER, J.A., *Phys.Rev.* 89 (1953) 1102.
- [7] GRIFFIN, J.J., WHEELER, J.A., *Phys.Rev.* 108 (1957) 311.
- [8] NÖRENBERG, W., *Habilitationsschrift, Heidelberg* (1970); NÖRENBERG, W., *Phys.Rev.* C5 (1972) 2020.
- [9] INGLIS, D.R., *Phys.Rev.* 96 (1954) 1059, 103 (1956) 1786.
- [10] WILETS, L., *Phys.Rev.* 116 (1959) 372.
- [11] BOHR, N., WHEELER, J.A., *Phys.Rev.* 56 (1939) 426.
- [12] COHEN, S., SWIATECKI, W.J., *Ann.Phys.(N.Y.)* 19 (1962) 67.
- [13] STRUTINSKY, V.M., LYASHCHENKO, N.Ya., POPOV, N.A., *Nucl.Phys.* 46 (1963) 639.
- [14] BRACK, M., DAMGAARD, J., PAULI, H.C., JENSEN, A.S., STRUTINSKY, V.M., WONG, C.Y., *Rev.Mod.Phys.* 44 (1972) 320.
- [15] STRUTINSKY, V.M., *Nucl.Phys.* A95 (1967) 420; A122 (1968) 1.
- [16] SWIATECKI, W.J., BJØRNHOLM, S., *Phys.Reports* 4C (1972) 325.
- [17] SCHMITT, H.W., NEILER, J.H., WALTER, F.J., *Phys.Rev.* 141 (1966) 1146; NEILER, J.H., WALTER, F.J., SCHMITT, H.W., *Phys.Rev.* 149 (1966) 894.
- [18] NIX, J.R., *Nucl.Phys.* A130 (1969) 241.
- [19] BELYAEV, S.T., *K.Dan.Vidensk.Selsk., Mat.-Fys.Medd.* 31 11 (1959).
- [20] BËS, D., *K.Dan.Vidensk.Selsk.,Mat.-Fys.Medd* 33 2 (1961).
- [21] LEDERGERBER, T., PAULI, H.C., *Nucl.Phys.* A207 (1973) 1.
- [22] VAUTHERIN, D., BRINK, D.M., *Phys.Rev.* C5 (1972) 626.
- [23] PAULI, H.C., *Phys.Reports* 7C (1973) 35.
- [24] KO, C.M., PAULI, H.C., BRACK, M., BROWN, G.E., to be published (*Phys.Lett.*); a more complete communication is in preparation.
- [25] MYERS, W.D., SWIATECKI, W.J., *Nucl.Phys.* 81 (1966) 1.
- [26] BRACK, M., QUENTIN, P., Paper IAEA-SM-174/98, these Proceedings, Vol.1.
- [27] NIX, J.R., *Annu.Rev.Nucl.Sci.* 22 (1972), with a survey of literature up to Feb.1972.
- [28] NIX, J.R., MÖLLER, P., Paper IAEA-SM-174/202, these Proceedings, Vol.1.
- [29] GÖTZ, U., PAULI, H.C., ALDER, K., JUNKER, K., *Nucl.Phys.* A192 (1972) 1.
- [30] PAULI, H.C., LEDERGERBER, T., *Nucl.Phys.* A175 (1971) 545.
- [31] BRITT, H.C., BURNETT, S.C., ERKKILÄ, B.H., LYNN, J.E., STEIN, W.E., *Phys.Rev.* C4 (1971) 1444.
- [32] SPECHT, H.J., WEBER, J., KONECNY, E., HEUNEMANN, D., *Phys.Lett.* 41B (1972) 43.
- [33] SWIATECKI, W.J., *Phys.Rev.* 100 (1955) 937.
- [34] HYDE, E.K., *The Nuclear Properties of the Heavy Elements, III*, Prentice Hall, Inc., Englewood Cliffs, N.J. (1964).
- [35] HULET, E.K., WILD, J.F., LOUGHEED, R.W., EVANS, J.E., QUALHEIM, B.J., NURMIA, M., GHIORSO, A., *Phys.Rev.Lett.* 26 (1971) 523.
- [36] POLIKANOV, S.M., SLETTEN, G., *Nucl.Phys.* A151 (1970) 656.
- [37] LARK, N., SLETTEN, G., PEDERSEN, J., BJØRNHOLM, S., *Nucl.Phys.* A139 (1969) 481.
- [38] METAG, V., LIUKKONEN, E., GLOMSET, O., BERGMAN, A., Paper IAEA-SM-174/26, these Proceedings, Vol.1. We are grateful for communication of data prior to publication.
- [39] LIUKKONEN, E., METAG, V., private communication.
- [40] LARSSON, S.E., RAGNARSSON, I., NILSSON, S.G., *Phys.Lett.* 38B (1972) 269. GÖTZ, U., PAULI, H.C., JUNKER, K., *Phys.Lett.* 39B (1972) 436.
- [41] MÖLLER, P., NILSSON, S.G., SHELINE, R.K., *Phys.Lett.* 40B (1972) 329.
- [42] JOHN, W., HULET, E.K., LOUGHEED, R.W., WESOŁOWSKI, J.J., *Phys.Rev.Lett.* 27 (1971) 45.

DISCUSSION

J. R. NIX: First of all, I agree that in spontaneous fission the path of maximum penetrability will in general not lead over the static saddle point. But in induced fission, where the energy lies above the saddle point energy, standard statistical arguments tell us that most of the time the nucleus will proceed along a path close to the saddle point, where the penetrability is

close to unity, rather than along a path where it must penetrate a 2-MeV potential barrier! Secondly, I feel that at present we are able to calculate the potential energy more accurately than the kinetic energy. It therefore seems strange to accept the calculated inertias and adjust the potential energy. Do you know of any experimental confirmation of the large fluctuations in the inertias that you calculate with the cranking model?

H. C. PAULI: Any effective mass is meaningful only with respect to a particular choice of deformation. As we do not really know which deformations nature likes to use, it is a difficult problem to find experimental evidence of a fluctuating effective mass. In addition, let me remind you that — as Dietrich and Hofmann once pointed out — any oscillation in a mass can be transformed away in a one-dimensional space. The mass just tells us how "thick" a barrier is. This brings me to your question. If we do not calculate the masses and the potential with the same types of deformation, we lose track of the metric. Even if the cranking model were inaccurate, it does keep track of the metric. As mentioned in the paper, renormalization does not seem to be necessary, as only few levels around the Fermi energy contribute at all. With regard to your first point, in a multi-dimensional approach you must remember that "penetration" is actually an overlap of the total wave functions in deformation space. This overlap is probably smaller at the static than at the dynamic barrier. The dynamic barrier lies on the "classical" trajectory, where the wave function is large by definition.

L. WILETS: I would like to raise a word of caution in regard to using the adiabatic cranking (squeezing)-model mass parameter for barrier penetration. That method assumes a classical deformation parameter developing in time with a real velocity. This makes sense so long as the collective kinetic energy is positive. This is the case for rotations, translations, and over-the-barrier quadrupole deformation development. P.K. Haff and I have developed a modified generator co-ordinate method which is related to cranking above the barrier but is different below. We do not have quantitative results at present, but the indications are that the subbarrier mass parameter is less.

H. C. PAULI: I do not think it is a matter of real or imaginary velocity. It has been shown by Nörenberg (Ref. [8] of this paper) that the generator co-ordinate method gives the cranking model expression without very stringent assumptions. Unfortunately, I did not know about your work and therefore I am not sure at the moment how to resolve this contradiction.

J. J. GRIFFIN: The inclination of Nix and Wilets to dichotomize the subbarrier fission from the super-barrier fission prompts me to say that the empirical evidence on fission does not seem to support any qualitative difference between penetrative fission and fission with positive energy above the barrier.

With regard to your correlation between inertia and level density, it seemed to me that the correlation was not so strong and I would like to suggest that, if the comparison were made against the density of level crossings instead of the density of levels, the correlation might be much improved, since we know that level crossings dominate the inertial parameters in simple models.

H. C. PAULI: The simple formula of the mass parameter holds only on the average. As we have shown in detail in a recent paper², there are

² LEDERGERBER, T., PAULI, H.C., Nucl.Phys. A207 (1973) 1.

pathological situations where it does not hold at all. Otherwise, I agree with you.

U. MOSEL: I would like to support your reply to Nix that the mass parameter may be expected to be as accurate as the potential energy surfaces. However, we have learnt from the work of Wilets and co-workers and of Brack and Quentin that the latter are accurate only up to 1-2 MeV. Since the main point to emerge from your paper was the difference between the static and the dynamic path, it is interesting to note that the latter misses the saddle points by only 1-2 MeV, i.e. within the limits of uncertainty of the method. This inaccuracy is even increased here by the corresponding uncertainties in the mass parameter. It should, therefore, serve as a note of warning that the strong conclusions you have drawn are based on results which are within the range of uncertainty of the method used for their calculation. This would be more evident if we theorists were to adopt the experimentalists' method of drawing error bars on the potential energy surfaces and mass parameters.

H.C. PAULI: I am always grateful for warnings, and certainly we are not free from errors. However, it would be hard for me to agree that we should be out by 1-2 MeV at the dynamic but not at the static saddles. Brack's calculations rather indicate a systematic error. Actually I am glad that we have now got a discrepancy in the barrier heights (dynamic), as we should have agreement with experiments. I always found it difficult to understand why the Strutinsky method applied to the levels of a Woods-Saxon well produced good results for deformed shapes but not for spherical ones (the ^{208}Pb anomaly). Now we have the first hint that something might be wrong with both. Perhaps if we improve one of them, better results will also be obtained for the other.

J. RANDRUP: It might be of interest in this context to mention some results we have recently obtained at Berkeley on the calculation of spontaneous-fission half-lives in the actinide region. We used the modified oscillator model to establish potential energy surfaces, including the effects of axial asymmetry in the first-barrier region (by the method reported by Larsson³ and of reflection asymmetry in the second-barrier region (as described in Möller's work). We used the same method as Pauli to readjust the surface-energy coefficients in the liquid drop model. However, in contrast to Pauli, we made the readjustment so as to bring the second barriers into good agreement with the available experimental information. Then we calculated the fission half-lives by the simple WKB method, using a one-dimensional fission path passing through the minima and saddle points in the multi-dimensional distortion space. For the associated inertial-mass function we simply took a smooth function resembling the irrotational-flow mass but with one adjustable overall scaling parameter. This one and only free parameter in the approach was then fixed by a fit to known fission half-lives. The corresponding half-lives are shown in Fig. A.

It turns out that with this simple method it is actually possible to reproduce the experimental half-lives to within a factor of 25 on the average (i.e. 1.4 in the logarithm), which we consider most encouraging. It should also be noted that this method provides some semi-empirical information on the inertial-mass function.

³ LARSSON, S.E., LEANDER, G., Paper IAEA-SM-174/06, these Proceedings, Vol.1.

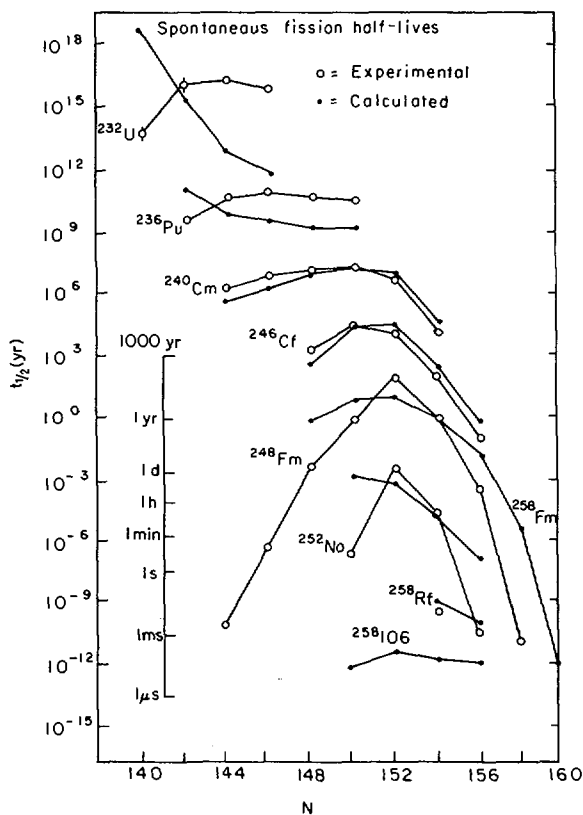


FIG. A. Spontaneous fission half-lives $t_{1/2}$ as a function of neutron number N for even-even nuclides in the actinide region $Z \geq 92$.

H. C. PAULI: You might have everything correct in your treatment but you have lost the metric and that is the essential thing. Even if the inertia is wrong here and there, I think the present approach gives us the correct metric for the deformation.

R. W. HASSE: I do not think that your statement about shuffling all the information about the masses into the collective co-ordinates is correct. To the best of my recollection, according to Hofmann and Dietrich's paper, you can only do this with one co-ordinate.

Secondly, I am strongly in favour of Nix's standpoint and opposed to J. J. Griffin's. We have just learnt from Pauli that the mass distributions probably only contain information on the potential energy surface between saddle and scission and no information about the barrier region. Thus there need not be a rapid change in the experimental data going from spontaneous to induced fission.

Finally a question about the least-action (minimum-time) method. I remember Michel Baranger talking about the tunnelling time always being zero. Has this discrepancy been resolved yet? In addition, I feel that finding the minimum-time path is only half the problem, as you also have to take the number of impacts into account. Thus it may be that the number of impacts needed to tunnel along your path is much higher than the number of impacts in the direction of the saddle, so that although the time required to tunnel through the saddle is longer, penetration may still be easier to achieve via this path.

H. C. PAULI: I do not see any contradiction between Baranger's point of view and ours. The time needed for penetration is zero — a jump such as an electron makes in an atom. To some extent we use the time as a generator co-ordinate, entering via $q(t)$, and we finally consider the overlap of wave functions to get a probability.

VISCOSITY IN THE FISSION PROCESS*

G. SCHÜTTE**, L. WILETS

Physics Department,
University of Washington,
Seattle, Wash.,
United States of America

Abstract

VISCOSITY IN THE FISSION PROCESS.

The fission process is often described in the adiabatic limit. The dynamical path is determined by an adiabatic potential energy surface and kinetic energy with mass parameters calculated by the cranking model. A model calculation for even-even nuclei is performed to study deviations from adiabaticity. The Hamiltonian consists of the sum of (1) a time-dependent Nilsson-type Hamiltonian, the deformation parameter of which is either a prescribed linear or oscillating function of time or is determined by energy conservation in the mean, (2) a pairing force of the BCS type between time-reversed Nilsson states, and (3) a small residual interaction between quasi-particle states, the matrix elements of which have random sign. There is no interaction between states of different isospin (n-p). In the calculations, the Hilbert space is limited to the BCS ground state and a limited number of two quasi-particle excitations corresponding to the lowest energies of excitation at each deformation. Within this space, the time-dependent Schrödinger equation is solved numerically. The difference between the expectation value of the Hamiltonian and the cranking model expression for the collective energy can be interpreted as viscous heat only as long as this difference is small. Calculations have been performed for calcium and uranium.

1. INTRODUCTION

A quantitative understanding of the nuclear energy-of-deformation surface has been made possible by the impressive efforts of Strutinsky and collaborators [1], by other groups using their methods [1], and by constrained Hartree-Fock calculations [2]. This represents only half of the problem of fission, namely, statics. The other part, the dynamical problem, has been studied mainly in the adiabatic limit of the Inglis cranking model [3]. To examine the validity of its adiabatic approximation, we have made calculations in the framework of this model.

We assume a Hamiltonian $H(\alpha(t))$ where α is a (quadrupole) deformation parameter. We either prescribe the time dependence of α or we introduce a phenomenological potential $V(\alpha)$ and use conservation of energy in the mean to determine the time dependence of α . The eigenstates ψ_n of the time-independent Schrödinger equation $H\psi_n(r, \alpha) = E_n(\alpha)\psi_n$ do not satisfy the time-dependent Schrödinger equation. The expectation value of H can be evaluated as $\langle H \rangle = E_0(\alpha) + 1/2 B(\alpha)\dot{\alpha}^2 +$ (higher order terms in the derivatives of α). We will not enter into a full discussion of the evaluation of the mass parameter B (in general a tensor B_{ij}) here. Although we believe that there are better ways of calculating B (especially by modified generator coordinate techniques [4]), we use in this paper the Inglis expression for B to determine the collective kinetic energy, $1/2 B\dot{\alpha}^2$.

The term $\dot{\alpha}^2$ is said to arise from "virtual" excitations. The distinction between "virtual" and "real" excitation in a cranking model is artificial

* Supported in part by the US Atomic Energy Commission.

** Supported by NATO funds.

because energy is not conserved anyway! Loosely speaking, the second order (mass parameter) effects arise from excitations from and to the ground state. Higher order processes can lead to excitations which do not lead directly back to the ground state. The simplest example is the two-level crossing model of Landau-Zener which leads to a "permanent" excitation. Level spectra in the fission region are too complex to be modelled in terms of pair-wise level crossings. This type of excitation has been described in terms of diffusion of probability [5]. The resulting master equation is based upon the incoherence of the excitations because of the large number of states available. This mechanism can be checked by the present calculation.

In any event, what is of interest are those higher order terms which are not time reversible. The magnitude of the resulting excitation (nuclear heating) plays an important role in fission and other collective phenomena.

We first describe our model, which is based on a Nilsson-type IPM plus pairing plus residual interaction. Three types of time dependence for $\alpha(t)$ are considered: linear, oscillatory and "self-consistent." Preliminary numerical results are presented for ^{40}Ca and ^{238}U . The model presented is highly schematic and further calculations are in progress.

For an internally consistent calculation, which avoids the problem of the infinite energy reservoir of the cranking model, we would propose solving the equation

$$\left[H(\vec{r}, \vec{p}; \alpha) - \frac{1}{2} \frac{\partial}{\partial \alpha} \frac{1}{B_0(\alpha)} \frac{\partial}{\partial \alpha} + V(\alpha) \right] \Psi(\vec{r}, \alpha) = E \Psi(\vec{r}, \alpha)$$

where $H \equiv H(\alpha)$ has the same meaning as elsewhere in this paper. This equation is second order in α rather than first order in time, and hence somewhat more difficult to solve than that described below.

2. MODEL

Our model is defined by the pairing-plus-residual Hamiltonian,

$$H = \sum \epsilon_\nu a_\nu^\dagger a_\nu - \frac{G}{2} \sum a_\nu^\dagger a_\nu^\dagger a_\nu a_\nu + V_r \quad (1)$$

The single particle energies ϵ_ν are eigenvalues of a Nilsson-type single particle operator with simplified forms for the spin-orbit and l^2 terms:

$$h = t + \frac{1}{2} M (\omega_z^2 z^2 + \omega_x^2 (x^2 + y^2)) + C m_s m + D m^2 \quad (2)$$

$$\epsilon_\nu \equiv \epsilon(n_z, n_\rho, m_s, m) = \omega_z (n_z + \frac{1}{2}) + \omega_x (2n_\rho + |m| + 1) + C m_s m + D m^2 \quad (3)$$

Volume conservation is asserted by

$$\omega_z \omega_x^2 = \bar{\omega}_0^3 \quad (4)$$

As a deformation parameter we define

$$\alpha = \bar{\omega}_0 / \omega_z$$

The residual interaction is defined below. We either prescribe a time dependence for α in analogy to the cranking model or add a phenomenological potential $V(\alpha)$ to the Hamiltonian and determine $\dot{\alpha}$ by energy conservation in the mean.

The BCS-ground state of the operator $H_0 = H - V_r$ is denoted by $|0\rangle$. Excitation energies are measured relative to this ground state energy. With the help of quasiparticle creation operators, α_{ν}^\dagger , excited states $|n\rangle$ of an even-even system described by H_0 can be written as two-quasiparticle excitations:

$$|n\rangle = \alpha_{\nu'}^\dagger \alpha_{\nu}^\dagger |0\rangle \quad (5)$$

With $\nu' = (n_z', n_p', m_s', m')$, then $\bar{\nu} = (n_z, n_p, -m_s, -m)$. We will here limit consideration to two-quasiparticle excitations. Because we are dealing with axial symmetric deformations, it follows that $m_s(\bar{\nu}) + m_s(\nu') = 0 = m(\bar{\nu}) + m(\nu')$. The excitation energy is $E_n = [(\epsilon_{\bar{\nu}} - \lambda)^2 + \Delta^2]^{1/2} + [(\epsilon_{\nu'} - \lambda)^2 + \Delta^2]^{1/2}$, with λ the chemical potential and Δ the gap parameter. In our calculations, we take a constant value of Δ for each nucleus and readjust λ at each deformation in order to keep the mean value of the particle number constant.

All calculations are performed in a Hilbert space spanned by a limited number of two-quasiparticle states corresponding to the lowest excitation energies. Within this space we solve the time-dependent Schrödinger equation

$$i\dot{\psi} = H\psi \quad (6)$$

In the expansion

$$\psi = \sum_n a_n(t) e^{-i \int E_n(t') dt'} |n\rangle \quad (7)$$

the coefficients a_n , the energies E_n and the states $|n\rangle$ depend on time. This expansion inserted into the Schrödinger equation yields a system of linear, first order differential equations (with $\partial_\alpha \equiv \partial/\partial\alpha$).

$$i\dot{a}_m = \sum_n \left[\langle m | V_r | n \rangle - i\dot{\alpha} \langle m | \partial_\alpha | n \rangle \right] e^{-i \int (E_n - E_m) dt'} \quad (8a)$$

or in matrix form

$$i\dot{\underline{a}} = \underline{G}\underline{a} \quad (8b)$$

Because of the property $\langle m | \partial_\alpha | n \rangle = - \langle n | \partial_\alpha | m \rangle^*$ no states of the form $2^{-1/2} |n - \bar{n}\rangle$ are excited by the operator ∂_α : the matrix of ∂_α is reducible. Therefore we restrict our Hilbert space to the symmetric combinations $2^{-1/2} |n + \bar{n}\rangle$ if n and \bar{n} are different. These combinations are now denoted by $|n\rangle$. In this space we represent the residual interaction V_r by non-diagonal matrix elements of constant absolute value and random sign; there are no matrix elements between the ground state and any excited state. The essential effect of a residual interaction is to prevent level-crossings.

3. FIRST ORDER PERTURBATION THEORY

The basic assumption of time-dependent perturbation theory is that there is a dominant state (here the ground state) with $a_0 \approx 1$; the amplitudes of other states are taken small compared with unity. The adiabatic limit is obtained by further assuming that the variation of the matrix elements and energy eigenvalues is slow; that is, that there is a scale of time which is taken long ($\dot{\alpha}$, $\ddot{\alpha}/\dot{\alpha}$, etc. go to zero). The following gives the amplitudes to order $\dot{\alpha}$, but is also exact (in first order) if the matrix elements and energies are constant in time:

$$a_n \approx i\dot{\alpha} \frac{\langle n | \partial_\alpha | 0 \rangle}{E_n - E_0} \left\{ \exp \left[i \int_0^t (E_n - E_0) dt' \right] + \text{const} \right\} \quad (9)$$

We here denote by $|n\rangle$ the adiabatic eigenstates of the complete Hamiltonian, including V_r . A minimum in $\langle H \rangle$ obtains in the mean when the constant is set equal to zero. The adiabatic cranking model mass parameter is given by the identification

$$\begin{aligned} \langle H \rangle &= E_0(\alpha) + \frac{1}{2} B \dot{\alpha}^2 \\ B &= 2 \sum_n \frac{|\langle n | \partial_\alpha | 0 \rangle|^2}{E_n - E_0} \end{aligned} \quad (10)$$

4. SOLUTION OF THE TIME-DEPENDENT SCHRÖDINGER EQUATION

Numerically, the system of differential equations (8) is solved by proceeding by time steps Δt according to

$$\underline{a}(t + \Delta t) = \left[1 + i \frac{\Delta t}{2} \underline{G}(t + \frac{\Delta t}{2}) \right]^{-1} \left[1 - i \frac{\Delta t}{2} \underline{G}(t + \frac{\Delta t}{2}) \right] \underline{a}(t) \quad (11)$$

which is correct through order $(\Delta t)^2$. Note that because the transformation going from $\underline{a}(t)$ to $\underline{a}(t + \Delta t)$ is unitary, it is unconditionally stable. The difference between the exact solution and the numerical solution after a time T is smaller than $\Delta t^2 \cdot T \cdot M$, where the constant M is given by upper bounds of the norms of the matrix G and its first and second order time derivatives.

In a cranking model the total energy is not conserved but the expectation value is a function of time:

$$\langle H \rangle = \sum_n E_n |a_n|^2 + \sum_n a_n^* a_m \langle n | V_r | m \rangle \quad (12)$$

Because of the small size and random sign of the matrix element of V_r , the last term in Eq. (12), is omitted. This energy contains both collective energy and single particle excitations.

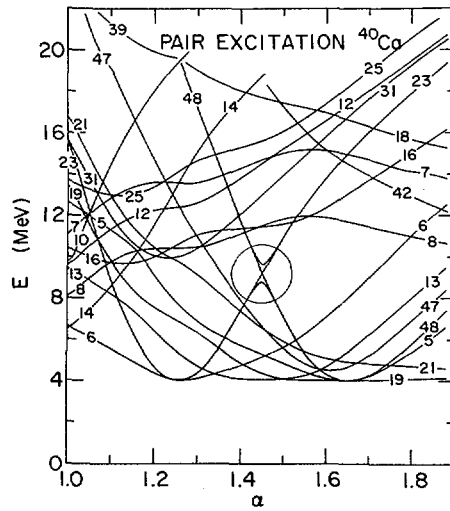


FIG. 1. Two-quasiparticle spectrum for ^{40}Ca as a function of deformation α . $\Delta = 2$ MeV. The numbers are an identification code used in the computer program. The residual interaction is not included in the spectrum; the encircled region shows its effect near a level crossing.

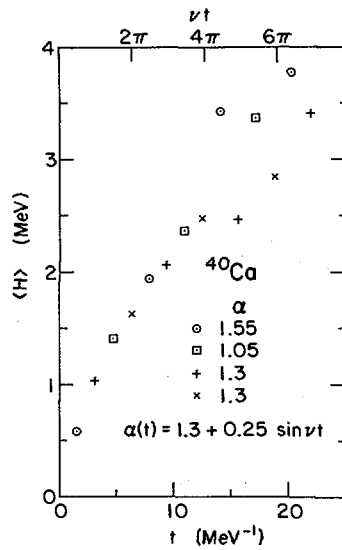


FIG. 2. Excitation energy $\langle H \rangle$ for an oscillating ^{40}Ca nucleus for the turning points and for points of maximum α . Parameters: $\nu = 1$, $V_t = 0.1$ MeV.

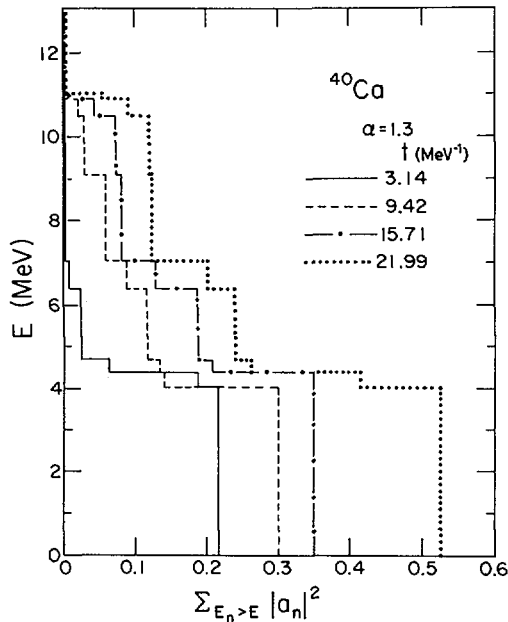


FIG. 3. Integrated occupation probability $\sum_{E_n > E} |a_n|^2$ for the oscillating Ca nucleus. (Parameters same as Fig. 2).

5. RESULTS AND DISCUSSION

Preliminary studies have been made in ^{40}Ca and ^{238}U .

The two-quasiparticle spectrum as a function of α for ^{40}Ca is shown in Fig. 1. The parameters are given in the caption. Although we studied excitation with $\dot{\alpha} = \text{constant}$, we found the form $\alpha = \alpha_0 + \epsilon \cos \nu t$ to be more useful. By varying ϵ and ν we can vary the amplitude and mean square velocity. Therefore, the excitation energy can be studied for fixed α as a function of time. Results of such studies are shown in Figs 2 and 3. Only neutrons or protons are considered. The excitation energy rises initially roughly linearly with time. At late times (when the ground state is depleted), one would expect a growth $\langle H \rangle \propto \sqrt{t}$ [5].

The viscosity effects which interest us here are necessarily of order higher than $\dot{\alpha}^2$. They involve features of the solution which are non-time-reversible. The Schrödinger equation is, to be sure, time reversible; the irreversibility has to do with the choice of initial conditions. If we begin with a state of low excitation, it will, in general, develop with time to a state of high excitation. We expect, therefore to find

$$\frac{d\langle H \rangle}{dt} = \text{a function which is even in the time derivatives of } \alpha$$

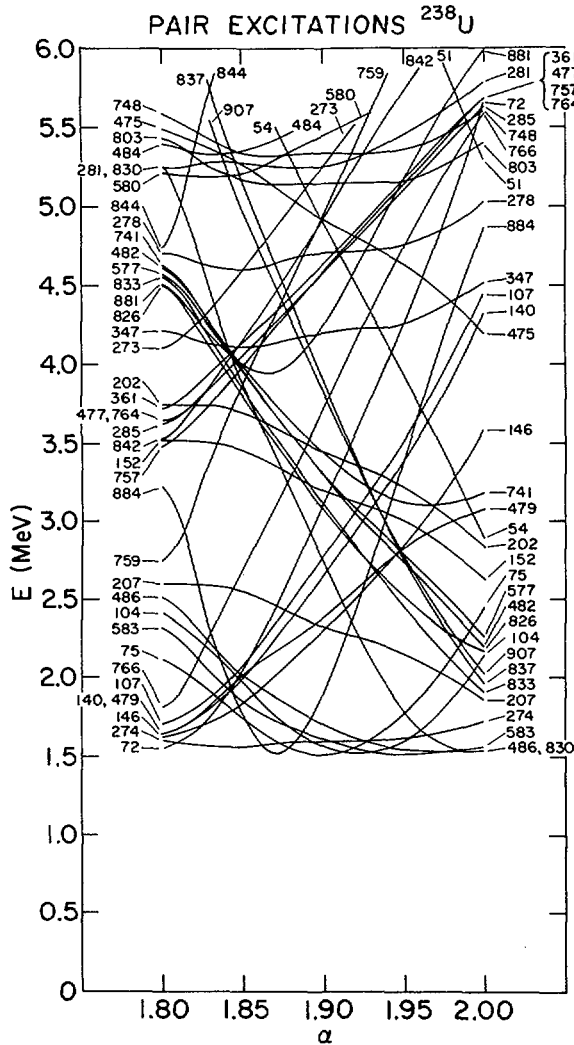


FIG. 4. Two-quasiparticle spectrum for ^{238}U . $\Delta = 0.76$ MeV. Numbers are identification code used in the computer program.

Since to order $\dot{\alpha}^2$ the system is adiabatic, the lowest order dependence would be $\dot{\alpha}^4$, $\dot{\alpha}^2 \ddot{\alpha}$, $\ddot{\alpha}$. In the case of oscillations all terms are proportional to ν^4 , which can be replaced by $\langle \dot{\alpha}^4 \rangle = \frac{3}{8} (\nu \epsilon)^4$. We find, for the ^{40}Ca case studied, $d\langle H \rangle / dt = D \langle \dot{\alpha}^4 \rangle$ with $D \sim 100$.

The spreading width can be extracted in the following manner. The occupation probability of the dominant (ground) state should decay with time, for early times, according to

$$|a_0|^2 \propto e^{-\Gamma t} \text{ or } \Gamma = -d \ln |a_0|^2 / dt$$

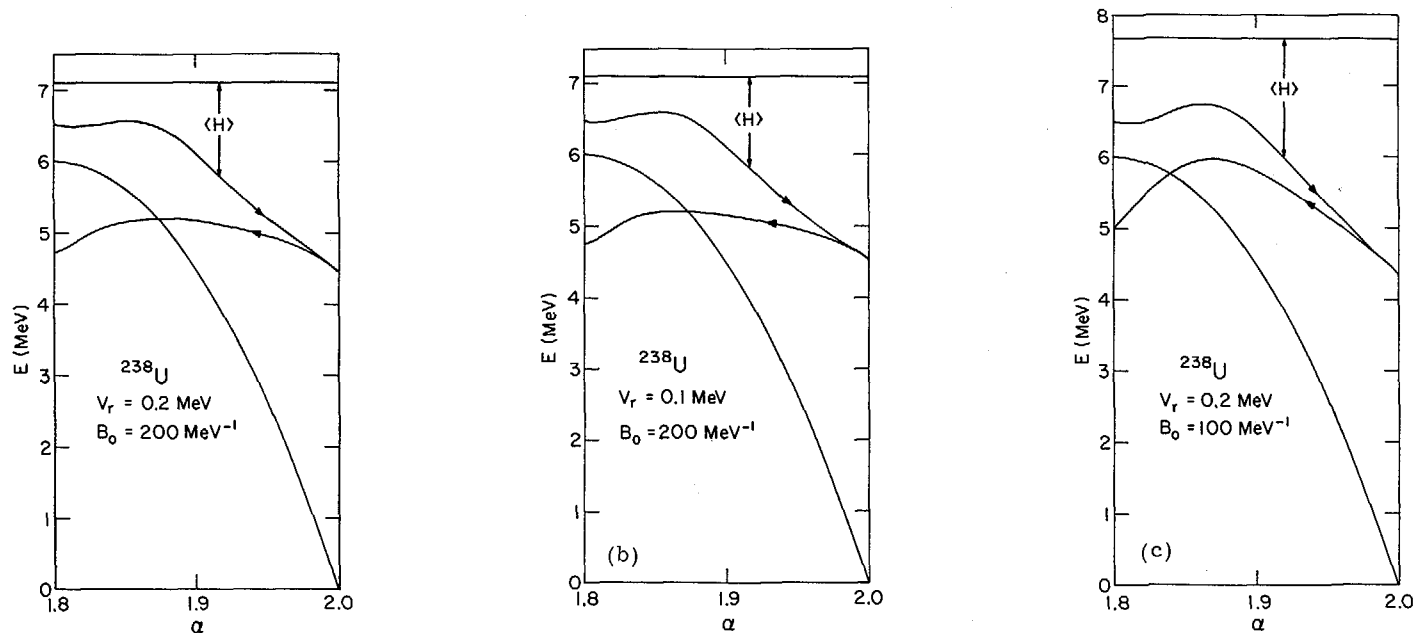


FIG. 5. (a) The excitation $\langle H \rangle$ for ^{238}U sliding down a parabolic barrier $V(\alpha) = \frac{1}{2} C (\alpha - \alpha_0)^2$, with $C = 300 \text{ MeV}$, $V_r = 0.2 \text{ MeV}$, $B_0 = 200 \text{ MeV}^{-1}$. $\alpha_0 = 1.8$ corresponds to the deformation of the second barrier. The horizontal line is the total energy available. The distance from the parabola to the arrowed path is $\frac{1}{2} B_0 \delta^2$. The distance from the path to the horizontal line is $\langle H \rangle$. The outgoing trajectory $\alpha(t)$ is determined by energy conservation in the mean. On the return path, $\alpha(t)$ is given by the time reversed history of the outgoing $\alpha(t)$ and there is then no energy conservation. The difference in $\langle H \rangle$ upon return is to be identified with irreversible viscous heat; (b) same as Fig. 5a, with $V_r = 0.1 \text{ MeV}$, $B_0 = 200 \text{ MeV}^{-1}$; (c) same as Fig. 5a, with $V_r = 0.2 \text{ MeV}$ and $B_0 = 100 \text{ MeV}^{-1}$.

In the ^{40}Ca example reported here, which is not realistic, we find $\Gamma \sim 0.02$ MeV. It would be of interest to study this width as a function of the vibrational amplitude ϵ , identifying ϵ with the vibrational quantum state n by

$$\epsilon = \left[(2n+1)/B\nu \right]^{\frac{1}{2}}$$

When $\Gamma > \nu$, the collective nature of a state begins to disappear.

For the study of a fissioning nucleus, we use a "self-consistent" prescription for determining $\dot{\alpha}(t)$. Instead of prescribing the function $\alpha(t)$ a priori, we add a phenomenological potential $V(\alpha)$ to the Hamiltonian and use the conservation of the total energy in the mean:

$$E = \langle H \rangle + V(\alpha) + \frac{1}{2} B_0 \dot{\alpha}^2 \quad (13)$$

where E is (say) the initial value of the right-hand side. In the calculations reported here, only neutrons contribute to $\langle H \rangle$. B_0 , here taken as a constant, is to be interpreted as the contribution to the mass parameter from the protons and the core of neutrons not included in our Hilbert space; it is called the partial mass parameter. $\langle H \rangle$ is the sum of both inertial kinetic energy and excitation energy contributions. A separation of these contributions is not required for the dynamical calculations. Note that double counting has been avoided in Eq.(13). By including protons and extending our Hilbert space, we could eliminate B_0 completely. It is mathematically convenient to utilize B_0 to advance the system in time by solving

$$\frac{1}{2} B_0 \dot{\alpha}^2 \Big|_{t+\frac{1}{2}\Delta t} = E - \langle H \rangle \Big|_t + V(\alpha) \Big|_{t+\frac{1}{2}\Delta t} \quad (14)$$

The two quasi-particle spectrum of ^{238}U for large deformations is shown in Fig.4. The excitation energy $\langle H \rangle$ as a function of α as the nucleus slides part way down the second fission barrier is shown in Fig.5 for various values of the residual interaction and partial mass parameters. The starting value of the partial kinetic energy $\frac{1}{2} B_0 \dot{\alpha}^2$ was chosen to be 0.5 MeV. Amplitudes were distributed over excited states according to the first order adiabatic solution of the cranking model. The initial decrease in $\langle H \rangle$ shows that even for the initial α , the first order adiabatic solution overestimates the excitation. In terms of occupation probabilities, this is also seen in Fig.6, where we find that the total excitation probability first decreases and later increases.

At the deformation $\alpha = 2$, the system is squeezed back along the same time path from which it came. Upon return to the starting point, we obtain a difference in $\langle H \rangle$ between 1.5 and 1.8 MeV. Half of this difference might be identified with the viscous heat of the nucleus at $\alpha = 2$. By allowing for necking-in and carrying the calculation to the point of scission or beyond, the separation of $\langle H \rangle$ into inertial kinetic energy and heat could be made uniquely, since then the kinetic energy is known exactly.

Our calculations indicate that, once the system is excited out of the BCS ground state, then it behaves more diabatically than adiabatically; namely, the jump probability is nearly unity at a level crossing. This can be seen by the insensitivity of the excitation energy to V_r (compare Figs 5a and 5b). We also find the surprising result that non-reversible effects are

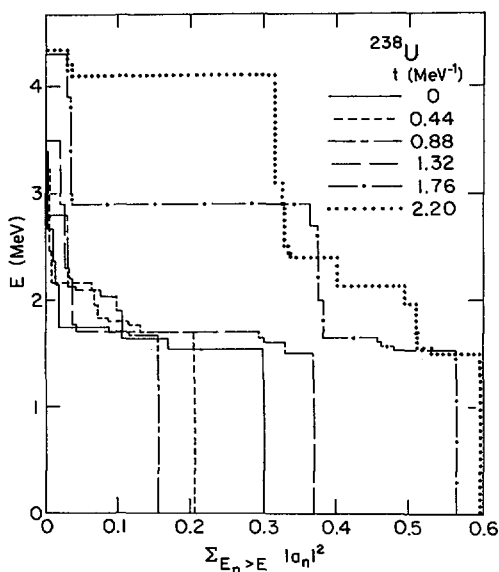


FIG. 6. Analogue to Fig. 3 for the fissioning nucleus ^{238}U ; parameters are the same as for Fig. 5a except $B_0 = 350 \text{ MeV}^{-1}$.

smaller for higher \dot{a} (Fig. 5c, $B_0 = 100 \text{ MeV}$) than for lower \dot{a} (Fig. 5a, $B_0 = 200 \text{ MeV}$). This further indicates that we are closer to a sudden, rather than adiabatic, limit.

It is seen in Fig. 6 that the ground state is depleted to a large extent during the process; thus one of the basic assumptions of the adiabatic solution of the cranking model is violated. Another reason why this solution is probably inadequate is the rise of \ddot{a}/\dot{a} from zero to 0.8 MeV while the nucleus slides down the barrier. We found in this case that the collective kinetic energy $1/2 B \dot{a}^2$ increases more rapidly with increasing \dot{a} than does $\langle H \rangle$.

6. CONCLUSIONS

From preliminary calculations performed with the simple model, we can already draw several conclusions.

Calculations on oscillatory deformations for ^{40}Ca show that nonadiabatic effects can play an important role. Such calculations permit the extraction of a viscosity coefficient and a spreading width.

The fission barrier calculations point up the failure of the first order adiabatic form for the collective kinetic energy, $\frac{1}{2} B \dot{a}^2$, where B is the INGLIS mass parameter. In particular, we found that this term is greater than the calculated $\langle H \rangle$ even for the moderate energies involved. Thus $\langle H \rangle$ increases more slowly with \dot{a} than the expected quadratic dependence, even

though about $1/3$ of $\langle H \rangle$ is time irreversible: For the limited barrier calculations performed, we find the remarkable result that higher order processes may speed up the fission dynamics even though viscous heating may be significant. Ultimately, of course, viscosity will reduce late-stage velocities.

Further calculations are planned to include the use of more realistic IPM potentials, with appropriate paths through the deformation space (especially necking-in of the potential towards scission), and the extraction of parameters for comparison with phenomenological models and experiment.

REFERENCES

- [1] For an excellent review and bibliography, see BROCK, M., DAMGAARD, J., JENSEN, A.S., PAULI, H.C., STRUTINSKY, V.M., WONG, C.Y., Rev. Modern Phys. 44 (1972) 320. For a critique of the method, see BASSICHIS, W.H., TIERPE, D.R., TSANG, C.F., WILETS, L., Phys. Rev. Letters 30 (1973) 294.
- [2] References can be traced in the paper of BASSICHIS, W.H., TIERPE, D.R., Phys. Rev. C8 (1973) 1146.
- [3] SOBICZEWSKI, A., SZYMAŃSKI, Z., WYCECH, S., NILSSON, S.G., NIX, J.R., TSANG, C.F., GUSTAFSON, C., MÖLLER, P., NILSSON, B., Nucl. Phys. A131 (1969) 67.
- [4] HAFF, P.K., WILETS, L., Phys. Rev. C7 (1973) 951.
- [5] WILETS, L., Theories of Nuclear Fission, Ch. 5, Clarendon Press, Oxford (1964).

DISCUSSION

K. DIETRICH: Your results are very interesting and I should like to know how much the production of viscous heat is increased when you switch off pairing. Have you done such a calculation within your model?

L. WILETS: We have not switched off pairing. A similar situation would be to have appreciable excitation above the superconducting ground state. In either of those cases it would probably change our conclusion that $d\langle H \rangle/dt \sim \dot{\alpha}^4$ (which is valid for short times, beginning in the BCS ground state) to $d\langle H \rangle/dt \sim \dot{\alpha}^2$.

H.C. PAULI: You mentioned that the cranking model might work especially well because of the level spacing of single-particle states. Let me recall that down the fission valley (conserved pre-formation, see also Mosel's results) the shells are conserved, which means that the level spacing is essentially a constant. Thus one might conclude that the cranking model would work especially well there.

L. WILETS: At very late stages, at scission and beyond, the cranking model should work well to yield the correct collective kinetic energy. Before scission, the first-order adiabatic cranking model, based on the deformed ground state, could become suspect — it fails in the vicinity of the barrier.

S. BJØRNHOLM: Pauli has raised a very interesting point because, as I understand it, in rotation there is no viscous loss and therefore in Mosel's valley there is no change of a single particle and no crossing, which means that you run down it without viscous loss.

L. WILETS: Well, eventually that is right.

S. BJØRNHOLM: Yes, but not from the beginning. The valley extends all the way from the barrier down to scission but at the end the neck becomes

thin; we can believe that things are moving without great viscous losses because the neck is thin – but not at the beginning.

L. WILETS: There are different regions and one has to be very careful. There will continue to be viscous heating until it eventually goes over to a translation, where the cranking model ought to give the right mass parameter

U. MOSEL: In the context of Dietrich's question I should like to mention that D. Glas and myself have performed calculations at Giessen for the "inverse" problem of heavy ion scattering. These calculations are very similar both in spirit and in method to those performed by Schütte and Wilets. Although no pairing is used, the jump probability to higher non-adiabatic channels is found to be very high. Even at fairly small relative energies just above the Coulomb barrier the probability that the two ions will emerge from the interaction region in their ground state, i.e. in the elastic channel, is found to be very small, of the order of $\approx 1\%$.

CONSERVATION OF SINGLE PARTICLE QUANTUM NUMBERS IN FISSION

Y. BONEH

Nuclear Research Centre, Negev, and
Weizmann Institute of Science, Rehovot

Z. FRAENKEL, Z. PALTIEL

Weizmann Institute of Science, Rehovot
Israel

Abstract

CONSERVATION OF SINGLE PARTICLE QUANTUM NUMBERS IN FISSION.

It is shown in a calculation of single particle energies for a finite potential well that the total energy of the nucleus at scission is smaller for an asymmetric scission configuration than for a symmetric one if the single particle quantum numbers are conserved between the saddle point and the scission point.

A dynamical model is used to investigate the problem of the conservation of these quantum numbers in the transition from the saddle point to the scission point as a function of the time scale of this transition. The initial shape of the potential is the saddle point shape of the nucleus (A, Z) as predicted by the liquid drop model. The shape of the potential is changed continuously as a function of time to that of the scission configuration. The time-dependent Schrödinger equation is solved for the transition and in this way the nuclear configuration at the scission point is arrived at.

Based on the present calculation we have indications that the single particle quantum numbers are partially conserved in the saddle-to-scission transition. Thus the mass asymmetry at scission may in part be the result of dynamical effects of the fission process.

Another consequence of the partial conservation of the single particle quantum numbers is that the saddle-to-scission transition excites single particle degrees of freedom in the nucleus or, in liquid-drop-model language, the transition causes viscous heating of the nucleus.

1. INTRODUCTION

It was pointed out by Griffin [1] that a rapid collective motion of the fissioning nucleus from the saddle point to the scission point may lead to potential energy surfaces which favour an asymmetric mass division. This conjecture is based on the fact that in such a motion the single particle energies do not follow the lowest static solutions of the Schrödinger equation for a nucleus with residual interactions (which would be the case for a very slow ("adiabatic") motion) but follow more closely the static solutions for a nucleus without residual interactions in which the single particle quantum numbers are conserved. This subject has also been discussed by Hill and Wheeler [2].

Let us denote by n the number of particles in the nucleus and by V_R the sum of the n lowest single particle energies for rapid motion (which conserves single particle quantum numbers) and V_S the sum of the n lowest single particle energies for slow motion (in which, due to the residual interaction, the single particle quantum numbers are not conserved) then $V_R \geq V_S$. The difference $V_R - V_S$ depends on the shape of the nucleus. According to the conjecture of Griffin, $(V_R - V_S)$ is quite large for symmetric scission shapes whereas there exists a family of nuclear shapes extending from the symmetric saddle point configuration to an asymmetric scission configuration for which $V_R = V_S$, i.e. V_R at each stage in the transition from

saddle point to scission follows the lowest potential energy surface. Thus rapid motion from saddle point to scission may favor asymmetric fission.

A similar conjecture has been made by Kelson [3] and Brandt and Kelson [4]. They also show that mass asymmetry in fission may be the result of conservation of single particle quantum numbers. However, contrary to Griffin's conclusion that mass asymmetry is the result of the rapid transition from the saddle point to scission, Brandt and Kelson consider the transition of the nucleus from the ground state to the saddle point to be responsible for the mass asymmetry.

In the present paper we shall be concerned with the transition between the saddle point and the scission point, i.e. with the mechanism proposed by Griffin. We shall try to answer, at least partially and within the context of a very simplified model, two questions:

(1) What is the dependence on mass asymmetry of the difference ($V_R - V_S$), which in the Griffin model determines to a large extent the predominance of asymmetric over symmetric fission.

(2) What must be the time scale of the transition from saddle point to scission for the assumption of approximate conservation of single particle quantum numbers to hold and how does this time scale compare with the transition time obtained by Nix [5] in his calculation which is based on a non-viscous liquid drop model.

Other questions of fundamental nature arise with respect to the Griffin conjecture. These will not be discussed here. It is clear, however, that the question whether the saddle-to-scission transition is rapid or adiabatic, or, in classical language viscous or non-viscous, is of fundamental importance to our understanding of the fission process and not restricted to the Griffin conjecture.

2. THE MODEL

2.1. The static model

In order to answer the first question, namely the dependence of ($V_R - V_S$) at scission on the mass asymmetry we must calculate the single particle energies of the nucleus. In our model the nucleus is described by a finite potential well which is filled with Z "protons" and $A-Z$ "neutrons" with no spin-orbit force and no residual interaction (pairing). The depth of the potential is equal to the Fermi energy plus the binding energy of the last proton (neutron). The boundary of the potential at the saddle and scission points is taken to be that of the nucleus as given by the liquid drop model [5]. Figure 1 shows this shape for the nucleus $^{237}_{93}\text{Np}$ at the saddle point and the scission point for symmetric and asymmetric scission configurations. The asymmetric scission shapes were obtained from the symmetric one by changing only the volume ratio of the two fragments. Since the liquid drop shapes are cylindrically symmetric they may be best described by cylindrical coordinates. Denote by $\rho_{\text{SAD}}(Z)$ the envelope of the saddle point shape and by $\rho_{\text{SCI}}(Z)$ this function for the scission shape, then the intermediate shapes between saddle and scission points are obtained by the relation

$$\rho^2(\beta, Z) = \rho_{\text{SAD}}^2(Z) + (\rho_{\text{SCI}}^2(Z) - \rho_{\text{SAD}}^2(Z)) \cdot \beta \quad (1)$$

where β changes continuously from $\beta = 0$ at the saddle point to $\beta = 1$ at scission. This family of shapes follows closely the liquid drop shapes and explicitly conserves the nuclear volume.

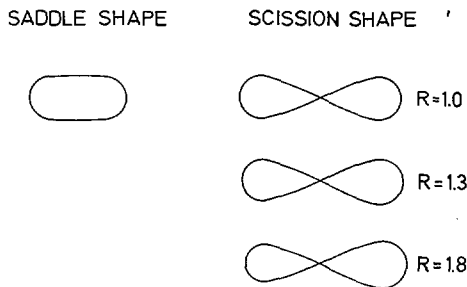


FIG. 1. The saddle-point and symmetric scission shapes of the ^{237}Np nucleus (as calculated in Ref. [5]) and two asymmetric scission shapes with the fragment volume ratio of $R = 1.3$ and $R = 1.8$.

Since our model does not include a residual interaction between the nucleons, the single particle quantum numbers are inherently conserved during the change from the saddle-point shape to the scission shape. $(V_R(\beta) - V_S(\beta))$ is therefore readily obtained from our model: $V_S(\beta)$ is equal to the sum of the Z lowest single-particle energies in the proton potential and the $(A-Z)$ lowest energies in the neutron potential for any given value of β . $V_R(\beta)$ is obtained by adding up the energies of the same orbitals which are the lowest ones at the saddle point configuration (but not necessarily the lowest ones for other values of β). In the present paper we are in particular interested in the dependence of $(V_R(\beta=1) - V_S(\beta=1))$ on the mass asymmetry.

2.2 The dynamic model

In order to determine to what extent the single-particle quantum numbers are conserved in the transition between saddle point and scission one must in principle solve the time-dependent Schrödinger equation for this transition. The nuclear potential part of the Hamiltonian is changed as a function of time from the saddle shape to the scission shape according to Eq. 1 except that now β is a function of time. It should be chosen so as to reproduce as accurately as possible the time sequence of the nuclear deformations in the fission process. Denote by $\phi_i(0)$ the i -th single-particle eigenfunction for the saddle point configuration and by ψ_j the j -th function for the scission configuration. Denote by $\phi_i(t)$ the time-dependent wave function which evolved from $\phi_i(0)$ and T the transition time from saddle point to scission. Then

$$P_{ij} = |\langle \phi_i(T) | \psi_j \rangle|^2 \quad (2)$$

is the transition probability from level i to level j during this process. Fuller [6] has shown that our total wave function is strictly antisymmetric or, in other words, the Pauli principle is strictly observed by the expressions P_{ij} , i.e. (because of spin degeneracy)

$$\sum_i P_{ij} \leq 2$$

For a nuclear model which incorporates a residual interaction, the values of the transition probabilities P_{ij} are a measure of the conservation of the

single particle quantum numbers. As already mentioned, our model does not include a residual interaction and hence the single particle quantum numbers are inherently conserved in the transition. Transitions are therefore only allowed between orbits with the same single particle quantum numbers, or more specifically, with the same parity (for symmetric shapes) and magnetic quantum number M . Our model therefore cannot give us directly information on the question of the conservation of single particle quantum numbers in fission. However as we shall show below, essential information on this problem can nevertheless be obtained, from the study of the transition probabilities and the single particle energies in our model.

A more detailed description of our calculation is given elsewhere [7].

3. RESULTS

Table I shows the energy difference ($V_R - V_S$) for the scission shape as a function of the mass ratio (more accurately the volume ratio) of the fragments. Our calculations were made for the nucleus $^{237}_{93}\text{Np}$ which is the heaviest nucleus for which liquid drop calculations are available [5]. Also shown in Table I is the potential energy of the scission configuration as predicted by the liquid drop model. The values have been normalized to zero for the symmetric scission configuration. The liquid-drop model parameters used in the calculation were those of Nix [5]. Finally we show in the last column of Table I the sum of the liquid drop model energy and ($V_R - V_S$). It is seen from the table that this sum reaches a maximum for the symmetric scission shape, and reaches a shallow minimum for the mass ratio $R \approx 1.3$ which is approximately the experimentally most probable value.

The study of the single-particle energies as a function of the deformation parameter β is crucial for the understanding of the dynamic behaviour of the nucleus during the transition from saddle point to scission [8]. The closer the energy levels approach each other and the steeper their slope as a function of β , the higher the probability of transitions between these levels. Fig. 2 shows the dependence of the lowest $M = 1^+$ levels on β for symmetric fission. Since the levels have the same quantum number they do not cross. It is however seen that while levels 1 to 3 are

TABLE I. LIQUID-DROP MODEL ENERGY V_{LD} , SINGLE-PARTICLE ENERGY DIFFERENCE ($V_R - V_S$) AND $\tilde{V}_R = V_{LD} + (V_R - V_S)$ AT THE SCISSION POINT AS A FUNCTION OF THE FRAGMENT VOLUME RATIO R

V_{LD} has arbitrarily been set to zero for the symmetric scission configuration. ($V_R - V_S$) includes a factor of 2 due to the spin degeneracy.

R	V_{LD} (MeV)	$(V_R - V_S)$ (MeV)	$\tilde{V}_R = V_{LD} + (V_R - V_S)$ (MeV)
1.0	0	70.1	70.1
1.2	4.7	30.1	34.8
1.3	9.9	26.9	36.8
1.4	14.4	32.6	47.0
1.8	22.0	42.1	64.1

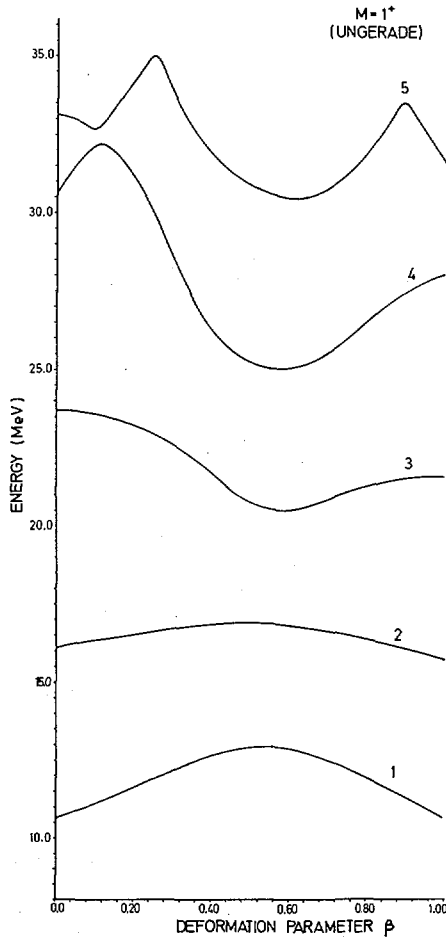


FIG. 2. The variation of the lowest five levels with the same quantum number $M = 1^+$ as a function of the deformation parameter β .

well-separated, the higher levels show a much stronger β -dependence and occasionally approach each other to a distance of a fraction of an MeV. It follows that for a given time interval T from the saddle point to scission, the transition probability between the higher levels will be much higher than for the lowest ones. This statement is of general validity and not restricted to our model. Fig. 3 shows the dependence on β of levels of different single particle quantum numbers. Since in our model these quantum numbers are conserved, the levels can cross as evident from Fig. 3. The inclusion of a weak residual interaction in the model will not change Fig. 3 substantially, except in the region where two levels cross. Instead of crossing, the two levels will approach each other up to a distance of the order of the strength of the (residual) interaction and then separate again.

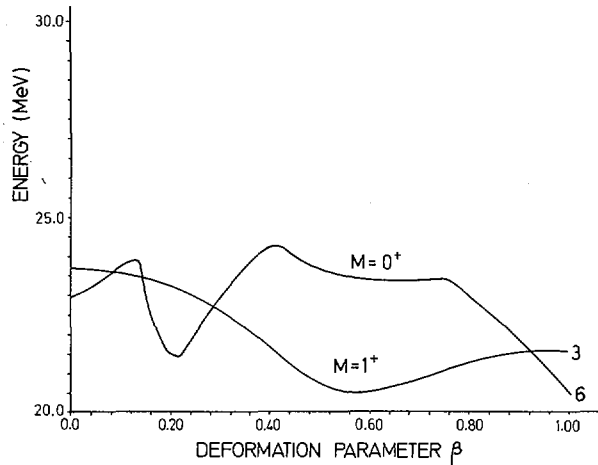


FIG. 3. The variation of levels with different quantum numbers ($M = 0^+$ and $M = 1^+$) as a function of the deformation parameter β .

For the dynamical calculations we have chosen the functional dependence $\beta(t)$ [6]

$$\beta(t) = \frac{1}{2} \left\{ 1 + \frac{1}{2} \left[3 \left(\frac{t}{\tau} - 1 \right) - \left(\frac{t}{\tau} - 1 \right)^3 \right] \right\} \quad (3)$$

This function satisfies the boundary condition $\beta(0) = 0$ and $\beta(2\tau) = 1$ (i.e. the total transition time from saddle point to scission is $T = 2\tau$). While this function is probably not a very realistic description of the dynamics of nuclear fission, it has the advantage of having a zero slope ($\dot{\beta} = 0$) not only at $t = 0$ (which is certainly physical) but also at $t = 2\tau$ (scission) and therefore it is unnecessary to correct for the center-of-mass motion of the two fragments at scission. The results obtained for the above functional form for $\beta(t)$ do not differ substantially from those obtained with a function $\beta(t)$ which approximately reproduces the dynamic behaviour of the liquid drop model [5].

Table II shows the transition probability P_{ij} between the single particle levels shown in Fig. 2 for three values of τ . In view of the peculiar time dependence of $\beta(t)$ (Eq. 3) it seems appropriate to denote τ as the effective transition time between saddle point and scission, to be compared to the value obtained from the liquid drop model [6]. For the nucleus ^{237}Np this time interval is $3 \cdot 10^{-21}$ sec (the intermediate value in Table II). It is seen that levels 1 to 3 exhibit an essentially adiabatic behaviour ($P_{ij} \approx \delta_{ij}$) for all three values of τ , while the transition probability to other levels is quite appreciable for the higher levels. This behaviour is typical for the whole level spectrum of the nucleus considered: The low-lying levels behave adiabatically for the time scale predicted by the liquid-drop calculations whereas a few levels near the Fermi surface approach each other to within a fraction of an MeV and hence give rise to large transition probabilities to other levels.

TABLE II. THE TRANSITION PROBABILITY FROM THE LOWEST FIVE $M = 1^+$ LEVELS FOR THREE VALUES OF THE EFFECTIVE TRANSITION TIME τ

The numbers shown are the transition probability from a given level in the first column to all the other levels with the same quantum numbers.

level number	$\tau=1.5 \cdot 10^{-21}(\text{sec})$	$\tau=3.0 \cdot 10^{-21}(\text{sec})$	$\tau=6.0 \cdot 10^{-21}(\text{sec})$
1	0.01	0.00	0.00
2	0.07	0.00	0.00
3	0.07	0.00	0.00
4	0.94	0.82	0.75
5	0.95	0.85	0.76

4. DISCUSSION

It is well known that the sum of single particle energies (e.g. V_R) is a very poor approximation of the total potential energy of the nucleus. A better estimate for the potential energy surface for rapid motion is obtained by adding the difference $(V_R - V_S)$ to the potential energy of the nucleus as obtained from the liquid drop model. The replacement of V_S by the liquid drop potential energy V_{LD} is based on the results of Brandt and Kelson [4]. These authors have shown that the lowest total potential energy surface of the single particle model of the nucleus is essential equivalent to the liquid drop model potential. Similar considerations underly the Strutinsky [9] renormalization procedure. We therefore show in Table I both $(V_R - V_S)$ as obtained by our single particle model and the liquid drop model value V_{LD} (normalized for convenience to $V_{LD} = 0$ for the symmetric scission configuration).

Two features are evident from Table I. (1) The total potential energy for rapid motion $V_R = (V_R - V_S) + V_{LD}$ has a minimum close to the mass ratio $R = 1.3$ which is approximately the most probable experimental value. (2) The value of V_R for symmetric fission is higher than the liquid-drop model value for the potential energy of the saddle point (~ 40 MeV higher than the liquid-drop model value for symmetric scission). It follows that rapid motion as defined in the present context (i.e. strict conservation of single particle quantum numbers) cannot lead from the symmetric saddle point to the symmetric scission point, since in this case the nucleus would have to gain potential energy in its transition from the saddle point to the scission point. Table I shows that similar considerations hold for very asymmetric fission.

The results of the dynamic calculation (Table II) show that the lowest energy levels, which are separated by approximately 5 MeV, behave almost adiabatically for the transition-time scale of the liquid drop model ($\sim 3 \cdot 10^{-21}$ sec) whereas some of the higher levels, which approach each other to within a fraction of an MeV, have a very high transition probability to other levels. Based on these results we may conclude that if the residual interaction between the nucleons has a strength less than ~ 1 MeV the picture obtained from our model (which does not include a residual interaction) is not substantially changed and the single particle quantum number will be

approximately conserved. On the other hand, if the residual interaction is much larger than 1 MeV the level structure will be substantially changed by it and the assumption of the conservation of the single particle quantum numbers is not justified for the time scale predicted by the liquid drop model.

REFERENCES

- [1] GRIFFIN, J.J., Phys. Rev. Letters 21 (1968) 826.
- [2] HILL, D.L. and WHEELER, J.A., Phys. Rev. 89 (1953) 1102.
- [3] KELSON, I., Phys. Rev. Letters 20 (1968) 867.
- [4] BRANDT, A. and KELSON, I., Phys. Rev. 183 (1969) 1025.
- [5] NIX, J.R., Nucl. Phys. A130 (1969) 241.
- [6] FULLER, R.W., Phys. Rev. 126 (1962) 684.
- [7] BONEH, Y. and FRAENKEL, Z., to be published.
- [8] WILETS, L., "Theories of nuclear fission", Clarendon Press, Oxford (1964).
- [9] STRUTINSKY, V.M., Nucl. Phys. A95 (1967) 420.

DISCUSSION

S. BJÖRNHOLM: The shapes you have chosen tend to miss the shell effects associated with $N = 82$, $Z = 50$, $A = 132$, as was emphasized in connection with Mr. Nix's talk. How then do you explain the preference for asymmetric fission that you find?

Y. BONEH: In the present work we did not explain asymmetry on the basis of shell effects at the saddle point. We were more interested here in the transition from saddle to scission and have shown by direct calculations that the assumption of the conservation of single particle quantum numbers on the way to scission leads to potential energy surfaces which prefer asymmetric fission.

Z. FRAENKEL: The reason why the asymmetric potential energy surface is lower than the symmetric one in this model has already been discussed by J.J. Griffin several years ago, namely the greater number of "ungerade" orbitals as compared to the "gerade" orbitals.

FIRST ESTIMATES OF THE NUCLEAR VISCOSITY CONSTANT FROM THE DAMPING OF THE FISSION DYNAMICS AND FROM THE WIDTHS OF β -VIBRATIONS AND GIANT DIPOLE RESONANCES

R. WIECZOREK, R.W. HASSE, G. SÜSSMANN*

Sektion Physik der Universität München,
Garching, Federal Republic of Germany

Abstract

FIRST ESTIMATES OF THE NUCLEAR VISCOSITY CONSTANT FROM THE DAMPING OF THE FISSION DYNAMICS AND FROM THE WIDTHS OF β -VIBRATIONS AND GIANT DIPOLE RESONANCES.

Using three different approaches the nuclear viscosity constant of heavy nuclei is estimated to be $\eta \approx 10^{-23} \text{ MeV} \cdot \text{s} \cdot \text{fm}^{-3} \approx 10^{10} \text{ poise}$: (i) The dissipation energy $-\dot{E}_{\text{diss}} = \sum Z_{ij} \dot{\alpha}_i \dot{\alpha}_j$ (Z_{ij} are the hydrodynamical viscosity coefficients depending on the deformation coordinates α_i) is integrated in a dynamic fission model for various paths from saddle to scission and equated to an assumed value of 10 MeV obtained from experimental data; (ii) the widths of the higher vibrational states in the first minimum are interpreted as damping resulting from coupling into the second minimum and the fission continuum; (iii) the widths of the giant dipole resonances are explained by damping of the hydrodynamical flow.

1. INTRODUCTION

During the past years the concept of viscosity has been introduced into nuclear physics, especially nuclear fission. For a general discussion about viscosity we therefore refer to the review articles of Swiatecki /1/ and Bjørnholm /2/, to Wilet's book /3/, and to textbooks on classical hydrodynamics /4/. Here we just list the major evidence for and objections against the necessity of introducing viscosity (or friction or damping) terms into existent models.

(i) During the descent from saddle to scission there is a variety of collective and noncollective levels available to the system. Slippages at level crossings or near-crossings are caused by the residual interaction and give rise to a loss of energy which appears as heat in the energy balance. (ii) Results of dynamic calculations, however, show that damping is negligible because the energies at scission calculated without viscosity fit the experiments reasonably well. (iii) The higher vibrational levels in the first minimum become broader through coupling into the second minimum and into the fission continuum. But this means strong damping. (iv) The same argument holds also for the broad giant resonances.

In this paper the experimental information is analysed with the help of hydrodynamic models. For this purpose existing models have been refined by inclusion of damping terms proportional to the relevant velocities and the nuclear viscosity constant is extracted.

* Presently at the Nuclear Chemistry Division, Lawrence Berkeley Laboratory, Berkeley, Calif., United States of America.

Unexpectedly, all estimates yield about the same value of the viscosity constant regardless of the process involved, thus indicating that the nuclear viscosity might be a fundamental constant characteristic to all nuclei.

2. DAMPING FROM SADDLE TO SCISSION

Liquid drop calculations on binary /5-7/ and ternary fission, i.e. fission accompanied by a long-range α -particle /8/, do not give evidence for damping between saddle and scission. That is to say, the balances at the scission point of kinetic and excitation energies of the fragments agree rather well with the experimental ones. Dissipation of energy would not fit into the liquid drop picture.

These dynamic models, however, for computational reasons are calculated with a rather limited number of only collective shape degrees of freedom, usually three to five. As Nörenberg /9/ points out, most of the energy may be associated with these coordinates but it is still unclear what fraction it is. The remaining energy can either be hidden in other collective coordinates or, more likely, in non-collective ones arising from non-collective transitions between collective states enhanced by the residual interaction. In ref. /9/ it is estimated that the coupling constant G^2 in the probability of level slippage $P = \exp(-\pi G^2)$ varies between 10^{-5} and 3 according to the nature of the levels in mind. This exactly means damping of the collective motion at least to some extent. In application to fission it was concluded that there is about 2 MeV in the fission degree of freedom rather than 20 MeV calculated with dynamic models.

Although still very uncertain, in this way one can estimate the dissipation energy from saddle to scission to be at least 10 MeV. In what follows we therefore use this number to establish the connection between dissipation energy and viscosity in the dynamic model of Hasse /6,7/.

This model, by inclusion of a semi-phenomenological shell energy, essentially is a modified version of Nix's studies in the liquid drop theory of nuclear fission /5/. Mass distributions, distributions of kinetic energies etc. are obtained by integrating the classical equations of motion of an ideal fluid from saddle to scission. The initial conditions near the saddle were determined randomly by the Monte Carlo method.

The classical Hamiltonian of the system consists of the potential energy, i.e. liquid drop and shell energies, and the kinetic energy of potential flow of an ideal fluid. For the family of shapes the following expression for the sharp nuclear surface in cylindrical coordinates ρ, z was chosen

$$\rho^2(z) = \lambda \{z_0^2 - z^2\} \{(z - z_1)^2 + z_2^2\} \quad (1)$$

In eq.(1) z_0 serves as elongation parameter, z_1 as asymmetry parameter and z_2 as constriction or necking-in parameter, and λ guarantees volume conservation. Thus a sphere is described by $z_0 = R_0$, $z_2 \rightarrow \infty$ and the scission point by $z_2 = 0$, where $R_0 = r_0 A^{1/3}$ is the radius of the equivalent sphere. Reflection asymmetric shapes are given by $z_1 \neq 0$.

By using this parameterization the kinetic energy can be written as

$$T = \frac{1}{2} \sum M_{ij} \dot{z}_i \dot{z}_j, \quad i, j=0, 1, 2, \quad (2)$$

where the inertias (or effective masses) $M_{ij}(z_0, z_1, z_2)$ are calculated according to refs. /6, 10/.

Damping by viscosity can be incorporated into the model by introducing the Rayleigh dissipation function /4/

$$F = \frac{1}{2} \sum Z_{ij} \dot{z}_i \dot{z}_j, \quad (3)$$

where the viscosity (or friction) coefficients $Z_{ij}(z_0, z_1, z_2)$ are calculated similarly to the inertias under the assumption of ideal flow. This was recently done by Schirmer et al. /11/. Twice the dissipation function then gives the change in time of the energy lost because of internal friction

$$-\dot{E}_{\text{Diss}} = \sum Z_{ij} \dot{z}_i \dot{z}_j. \quad (4)$$

Eq.(4) is derived from the general expression of the dissipation energy for incompressible fluids /4/

$$-\dot{E}_{\text{Diss}} = \frac{1}{2} \eta \int dV \left[\left(\frac{\partial v_i}{\partial x_j} + \frac{\partial v_j}{\partial x_i} \right)^2 \right], \quad (5)$$

where \vec{v} is the velocity of flow and \vec{x} the space vector. For potential flow, the volume integrals in eq.(5) can be converted into surface integrals. Thus the equations of motion are modified to

$$\sum_j (M_{ij} \ddot{z}_j + Z_{ij} \dot{z}_j) + \sum_{j,k} \left(\frac{\partial M_{ij}}{\partial z_k} - \frac{1}{2} \frac{\partial M_{jk}}{\partial z_i} \right) \dot{z}_j \dot{z}_k + \frac{\partial V}{\partial z_i} = 0, \quad i=0, 1, 2 \quad (6)$$

The Navier-Stokes hydrodynamic equations simplified by irrotational flow of an incompressible fluid and the coordinate- and time-independent viscosity constant η demand Z_{ij} to be proportional to η . Hence we introduce the dimensionless viscosity coefficients $\bar{Z}_{ij} = Z_{ij}/\pi R_0 \eta$ which now only depend upon the shape of the nucleus ij rather than on its size or its viscosity. As a result, the total dissipation energy from saddle to scission

$$-E_{\text{Diss}} = \pi R_0 \eta \int_{\text{saddle}}^{\text{scission}} \bar{Z}_{ij} \dot{z}_i \dot{z}_j \quad (7)$$

is directly proportional to η , and the relative dissipation energy

$$-\epsilon_{\text{Diss}} = -E_{\text{Diss}} \frac{t_0}{\pi R_0^3 \eta} \quad (8)$$

with $t_0 = R_0 \sqrt{M_0/E_0}$, $M_0 = m_0 A$, $E_0 = a_s A^{2/3}$ being the natural units of time, mass, and energy, respectively /7/ (a_s is the surface energy

coefficient: $a_s = 18 \text{ MeV}$), is independent of η and size and thus characteristic of the path in deformation space from saddle to scission.

In the present calculations $-\epsilon_{\text{Diss}}$ is obtained by first order perturbation method, i.e. eq.(7) is integrated along various path obtained previously without viscosity. The paths in turn are determined by the Lagrangian equations (6) with vanishing Z_{ij} and are taken from ref./7/ for thermal neutron fission of ^{235}U .

The resulting relative dissipation energies of four different paths are displayed in fig.1. All curves end at scission about at the same value of $-\epsilon_{\text{Diss}} = 0.5$ thus indicating that in all cases about the same amount of energy is dissipated en route from saddle to scission regardless of the details in between.

As discussed above there is good reason for about 10 MeV being dissipated from saddle to scission during fission of heavy nuclei. By inserting $R_0 = 6.94 \text{ fm}$, $t_0 = 4.374 \cdot 10^{-22} \text{ sec}$, $-\epsilon_{\text{Diss}} = 0.5$, and $-E_{\text{Diss}} = 10 \text{ MeV}$ into eq.(8), we obtain the result $\eta = 0.9 \cdot 10^{-23} \text{ MeV} \cdot \text{sec} / \text{fm}^3$.

The fact that 10 MeV out of a total of 40 MeV is assumed to be dissipated indicates the necessity of solving the unapproximated equations of motion (6) rather than using the first order perturbation method. Such calculations are now being carried out in Munich as well as in Los Alamos.

In looking at the viscosity coefficients along the paths, in fig.2, one observes that the one associated with elongation, Z_{00} , is smoothly decreasing, while Z_{11} and Z_{22} , the viscosity coefficients of asymmetry and necking-in, respectively, are increasing

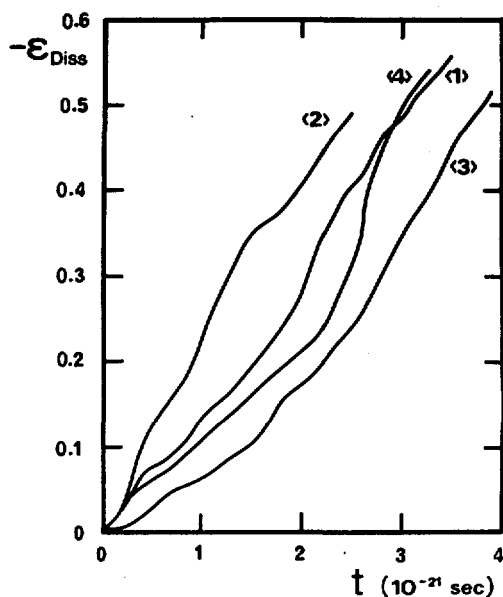


FIG. 1. The relative integrated dissipation energies of four paths from saddle to scission of thermal neutron fission of ^{235}U . Note that all curves at scission time end about at the same value of $-\epsilon_{\text{Diss}} = 0.5$.

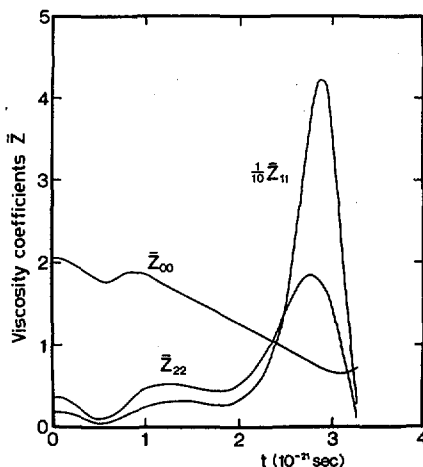


FIG.2. The relative diagonal viscosity coefficients along path (4) of Fig. 1. \bar{Z}_{00} , \bar{Z}_{11} , \bar{Z}_{22} are measures for the viscosity in the elongation, asymmetry, and constriction directions, respectively.

towards scission (the fact that Z_{11} and Z_{22} vanish at scission is due to a peculiarity of the parameterization, and the same holds for \bar{Z}_{11} , being so large). As is well known, fission in the early stages proceeds by a slow elongation and in the later stages by a rapid necking-in. In connection with the viscosity coefficients, this explains the overall constant dissipation energy per time interval. Hence damping seems to be approximately constant after the saddle although distributed in different ways among the different degrees of freedom.

3. DAMPING OF VIBRATIONAL STATES

The broad resonance structure in the fission cross-section can best be explained by the assumption of strongly damped vibrational levels in the first minimum, the damping arising from coupling into the vibrational levels of the second minimum as well into the fission continuum. This is schematically drawn in fig.3. Back et al. /12/, using this model, estimate damping widths of $\Gamma > 0.8$ MeV for the vibrational levels near the barrier.

In this section we use this result to estimate η by a simple hydrodynamical model calculation. Suppose the first minimum is spherical, then in the harmonic parameterization

$$R(\theta) = R_0 \left(1 + \sum_{l=1}^{\infty} \alpha_l P_l(\cos\theta) \right) \quad (9)$$

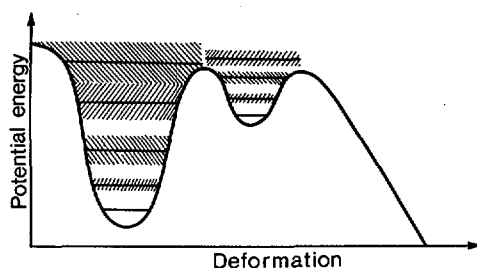


FIG. 3. Schematic drawing of damping in the first and second minimum (after Back et al. [12]). The states are vibrational states and hatching indicates their widths.

and quadratic approximation of the energy, the dissipation, kinetic and potential energies are diagonal, i.e.

$$-\dot{E}_{\text{Diss}} = 2F = \Sigma Z_{\ell\ell} \dot{\alpha}_{\ell}^2 = 8\pi\eta R_0^3 \int \frac{\ell-1}{\ell} \dot{\alpha}_{\ell}^2 \quad (10a)$$

$$T = \frac{1}{2} \Sigma M_{\ell\ell} \dot{\alpha}_{\ell}^2 = \frac{3}{2} M_0 R_0^2 \int \frac{1}{\ell(2\ell+1)} \dot{\alpha}_{\ell}^2 \quad (10b)$$

$$V = \frac{1}{2} \Sigma C_{\ell\ell} \alpha_{\ell}^2 = E_0 \int \left(\frac{(\ell-1)(\ell+2)}{2(2\ell+1)} - \frac{10x(\ell-1)}{(2\ell+1)^2} \right) \alpha_{\ell}^2 \quad (10c)$$

Here, the viscosity coefficients $Z_{\ell\ell}$ were calculated in Ref./11/ and the inertias $M_{\ell\ell}$ and stiffnesses $C_{\ell\ell}$ in refs./10,13/, and x is the Bohr-Wheeler fissility. The equations of motion of this system of uncoupled but damped harmonic oscillators follow from eq.(6),

$$M_{\ell\ell} \ddot{\alpha}_{\ell} + C_{\ell\ell} \alpha_{\ell} + Z_{\ell\ell} \dot{\alpha}_{\ell} = 0 \quad (11)$$

From the characteristic equation $M_{\ell\ell} \omega_{\ell}^2 - C_{\ell\ell} - i\omega_{\ell} Z_{\ell\ell} = 0$ follows the typical relaxation time $2M_{\ell\ell}/Z_{\ell\ell}$ for the state with multipolarity ℓ . The energy is quadratic in the coordinates or velocities but already is down to $1/e$ of its original value after the time $\tau = M_{\ell\ell}/Z_{\ell\ell}$. This decay time is to be compared with the lifetime of the higher β -vibrational states in the first minimum which in turn is approximately \hbar/Γ via the Heisenberg uncertainty relation. Inserting $\ell=2$ for quadrupole vibrations gives the viscosity constant

$$\eta = \frac{3\Gamma M_0}{40\pi\hbar R_0} \quad (12)$$

which, again, for the ^{236}U parameters $M_0 = 2.22 \cdot 10^5 \text{ MeV}/c^2$, $\Gamma = 0.8 \text{ MeV}/12$ yields about the same value $\eta = 0.96 \cdot 10^{-23} \text{ MeV} \cdot \text{sec}/\text{fm}^3$.

4. DAMPING OF GIANT DIPOLE RESONANCES

A similar analysis can be done for the broad giant dipole resonances. The width is approximately constant $\Gamma \approx 3\text{MeV}$ over the wide range of mass numbers $50 < A < 150$, cf. the collection of data in ref. /14/.

The giant resonance was first investigated theoretically by Goldhaber and Teller /15/ and Steinwedel and Jensen /16/ in a hydrodynamic model, later on by numerous authors in microscopic models. The widths in the latter models are due to fine structures. The connection between both models is not yet found although Wild /17/ investigated this question thoroughly.

Since in general up to now viscosity cannot be reduced to fine structures or other microscopic phenomena we follow the idea of Steinwedel and Jensen, use their model and carry out the suggested inclusion of a damping term.

In this model local deviations of the proton and neutron densities ρ_p, ρ_n from their static values ρ_p^0, ρ_n^0 are described by

$$\rho_{p,n} = \rho_{p,n}^0 \pm \gamma(\vec{r}, t) \quad (13)$$

The restoring force against the deviations is derived from a generalized volume symmetry energy density

$$\epsilon = E_{vs} \frac{(\rho_n - \rho_p)^2}{\rho_0} \quad (14)$$

with $E_{vs} \approx 20\text{MeV}$, and $\rho_0 = \rho_p + \rho_n$ the nuclear matter density. Using the relative velocity $\vec{v} = \vec{v}_p - \vec{v}_n$, where $\rho_p \vec{v}_p + \rho_n \vec{v}_n = 0$, the authors suggest a damping term $-M\chi \vec{v}$ in the Euler equations. After inserting the continuity equation $\vec{\nabla} \cdot \vec{v} = -\dot{\gamma}/\rho_{red}^0$ with $\rho_{red}^0 = \rho_p^0 \rho_n^0 / \rho_0$ into the Euler equations, the resulting wave equation reads

$$\ddot{\gamma} = u^2 \nabla^2 \gamma - \chi \dot{\gamma} \quad (15)$$

Herein, χ is related to η and the velocity of sound is given by $u^2 = 8E_{vs}\rho_{red}^0/M\rho_0$. The dipole solution of eq.(15) which satisfies the boundary condition $\partial\gamma/\partial r = 0$ at $r=R_0$ is

$$\gamma(\vec{r}, t) = e^{i\omega t + \alpha} j_1(r/\Lambda) Y_{10}(\theta, \phi) \quad (16)$$

where Λ is the lowest zero of $R_0 j_0(R_0/\Lambda) = 2\Lambda j_1(R_0/\Lambda)$, namely $\Lambda = R_0/2.08$ and ω is to be computed from $\omega^2 - u^2/\Lambda^2 - i\omega\chi = 0$.

Since $\text{Im}(\omega) = \chi/2$, the constant χ has the physical meaning of twice the reciprocal half-life of the giant dipole state, whose relation to viscosity is still to be established. One way of doing this is to compare the above-mentioned damping term $-M\chi \vec{v}$ with the one demanded by the Navier-Stokes equations, i.e. $M\nu \nabla^2 \vec{v}$, where ν is the so-called kinematic viscosity $\nu = \eta/\rho_0$. In this case one is led to the wave equation

$$\ddot{\gamma} = \nabla^2 (u^2 \gamma + \nu \dot{\gamma}) \quad (17)$$

By the very nature of eqs. (15) and (17) these are identical via the relation $-\chi\dot{\gamma} = \chi\Lambda^2\dot{\gamma}^2$ and, hence, $v = \chi\Lambda^2$. In this way one may write $1/\chi = \hbar/\Gamma$ where Γ is the experimental width of the giant dipole state. The resulting viscosity constant then is

$$\eta = \Lambda^2 \rho_0 \Gamma / \hbar = \frac{3\Gamma m_0 A^{2/3}}{2.08^2 4\pi \hbar r_0} \quad (18)$$

which, for $\Gamma = 3\text{MeV}$ and $A = 50 \dots 150$, has the numerical value $\eta = (2 \dots 5) \times 10^{-23} \text{ MeV} \cdot \text{sec}/\text{fm}^3$.

The viscosity constant obtained in this way depends strongly on the mass number. This is quite understandable because it results from the collective flow of the proton fluid against the neutron fluid. This kind of flow, however, is governed by the typical distance $\Lambda = r_0 A^{1/3} / 2.08$. On the other hand, the viscosity constants calculated in the previous sections resulted from collisions of nucleons with the typical distance r_0 . In following this philosophy and in order to have comparable viscosities one should replace Λ by r_0 which gives

$$\eta = r_0^2 \rho_0 \Gamma / \hbar = \frac{3\Gamma m_0}{4\pi \hbar r_0} \quad (19)$$

and its numerical value is $\eta = 0.95 \cdot 10^{-23} \text{ MeV} \cdot \text{sec}/\text{fm}^3$.

5. DISCUSSION AND OBJECTIONS

The three estimates of the viscosity constant are approximately equal, namely $\eta = 10^{-23} \text{ MeV} \cdot \text{sec}/\text{fm}^3$, or in more familiar units $\eta = 10^{10} \text{ poise}$ ($\text{poise} = \text{g}/(\text{cm} \cdot \text{sec})$) which is similar to the viscosity of pitch, 10^8 poise . A macroscopic concept like viscosity, however, can be applied to microscopic quantities like nuclei only in a qualified sense. Because of this one cannot expect nuclear matter to behave like a blob of pitch.

On the other hand, dimensionless parameters like the Reynolds number $Re = \rho_0 R_0 v / \eta$, where v is a characteristic velocity, e.g. $v = R_0 / \tau$ or Swiatecki's $1/\tau$ creep parameter $z = \eta / \sqrt{\sigma \rho_0 R_0}$ with the nuclear surface tension $\sigma = 18 \text{ MeV}/4\pi r_0^2$ take into account more attributes associated with nuclei and, hence, are more adequate to describe the nuclear situation. Using the constants given above one obtains $Re = 2.5$ and $z = 0.09$. A Reynolds number smaller than about 50 in macroscopic hydrodynamics does not allow for turbulences to be formed and thus the assumption of potential flow is sustained. The creep parameter is a constant relevant for describing the bulk properties of pieces of matter of finite size and therefore best suited to nuclei, and it is independent of the dynamics involved. Only recently it was invented for this purpose. Although it has not yet been investigated very well, one expects systems with $z < 1$ to be mobile and systems with $z \gg 1$ to be "creepy". The parameter z is only slowly varying with the nuclear mass number, in our case $z = 0.24 A^{-1/6}$. For this very reason the estimates given above hopefully are valid for a large portion of the nuclidic mass table and not only for the very heavy nuclei.

The analyses show that η seems to be independent of deformation. To the accuracy of our results (the error might be as large as a

factor of $10^{\pm 1}$), however, we are not able to draw a final conclusion. At least the result is in agreement with Bjørnholm's picture (cf. footnote of ref./2/) in which the damping is strong from the ground state to about half way down to scission and is weak in the very last stages before scission. The latter statement is thereby confirmed by the relatively small viscosity coefficient in the elongation direction close to the scission point.

One major objection to the calculations can be raised because of the use of the hydrodynamic model. The viscosity coefficients in this paper are calculated similar to the irrotational inertias which one knows can be ten times smaller than the inertias obtained with the cranking model. But, unfortunately, apart from the level slippage scheme, hitherto there is no microscopic foundation of the concept of viscosity. This problem is now being investigated by Immele /18/ on the basis of radiation theory.

The temperature dependence of the viscosity constant is another open question. In the first minimum the damping width increases with temperature, cf. fig.3. This means that η increases with temperature, just the opposite to the usual hydrodynamics of liquids. The nuclear temperature also increases en route from saddle to scission and, hence, one should not use a temperature independent viscosity. These effects, however, are refinements to the above calculations which may be treated similarly to the temperature dependence of the liquid-drop potential energy /19/.

REFERENCES

- /1/ W.J.Swiatecki, Proc. Int. Conf. on Reactions Induced by Heavy Ions, Heidelberg 1969, North Holland, Amsterdam (1970) p.729
- /2/ W.J.Swiatecki, S.Bjørnholm, Phys. Reports 4 (1972) 325
- /3/ L.Wilets, "Theories of Nuclear Fission", Clarendon, Oxford (1964) Ch.5
- /4/ H.Lamb, "Hydrodynamics", Dover, New York (1945); L.D.Landau, E.M.Lifshitz, "Fluid Dynamics", Addison-Wesley, Reading (1959); H.Goldstein, "Classical Mechanics", Dover, New York (1959)
- /5/ J.R.Nix, W.J.Swiatecki, Nucl. Phys. 71 (1965) 1; J.R.Nix, Nucl. Phys. A130 (1969) 241
- /6/ R.W.Hasse, R.Ebert, G.Süssmann, Nucl. Phys. A106 (1968) 117
- /7/ R.W.Hasse, Nucl. Phys. A118 (1968) 577; Nucl. Phys. A128 (1969) 609; Phys. Rev. C4 (1971) 572
- /8/ Y.Boneh, Z.Fraenkel, I.Nebenzahl, Phys. Rev. 156 (1967) 1305; A.Katase, J. Phys. Soc. Japan 25 (1968) 933
- /9/ W.Nörenberg, Habilitationsschrift Heidelberg 1970, unpublished; Paper IAEA-SM-174/24, these Proceedings, Vol.1.
- /10/ J.R.Nix, Ann. Physics 41 (1967) 52
- /11/ J.Schirmer, S.Knaak, G.Süssmann, Nucl. Phys. A199 (1973) 31
- /12/ B.B.Back et al., Proc. Second Int. Symp. on the Physics and Chemistry of Fission, Vienna 1969, IAEA, Vienna (1969) p.351; Nucl. Phys. A165 (1970) 449
- /13/ R.W.Hasse, Ann. Physics 68 (1971) 377
- /14/ H.Arenhövel, J.M.Maison, Nucl. Phys. A147 (1970) 305
- /15/ M.Goldhaber, G.Teller, Phys. Rev. 74 (1948) 1046

- /16/ H.Steinwedel, J.H.D.Jensen, Z. Naturf. 5a (1950) 413;
H.Steinwedel, J.H.D.Jensen, P.Jensen, Phys. Rev. 79 (1950) 1019
- /17/ W.Wild, Bayer. Akad. Wiss. 18 (1955) 371
- /18/ J.D.Immele, preprint, Univ. of Munich (1973).
- /19/ R.W.Hasse, W.Stocker, Phys. Lett. 44B (1973) 26

DISCUSSION

C.Y. WONG: I would like to comment on the treatment of the flow pattern assumed here. We have considered the problem independently on the basis of the vibration of a viscous charged liquid-drop. It is well known that the flow pattern becomes rotational when there is viscosity. Therefore, a treatment of vibration with irrotational mass parameters is incorrect. If one uses the correct treatment, in which the flow pattern is assumed to be rotational, one arrives at a limit of the viscosity coefficient above which complete damping of the vibrational motion occurs. This limit has the value of $\eta = 1.0 \times 10^{-23} \text{ MeV} \cdot \text{s}/\text{fm}^3$. The coefficient you have obtained is about the same as this limit and thus, if one takes your viscosity coefficient at its face value, one must conclude that there is almost complete damping of the hydrodynamical oscillation, a conclusion which I think is incorrect.

R.W. HASSE: We are well aware of the fact that the boundary conditions for the Navier-Stokes equations demand that the flow be rotational when one allows for viscosity. Our treatment of the problem, however, is not incorrect when we assume irrotational flow, but it is an approximate treatment. Lack of time prevented me from going into all the details in my paper and I should now therefore like to point out briefly the influence of rotational flow on the resulting viscosity constant. Since $\tau \propto M/Z \propto 1/\eta$ where τ is the damping time, M the inertial mass and Z the viscosity coefficient, $\tau_{\text{rot}} \cdot \eta_{\text{rot}} \approx \tau_{\text{irrot}} \cdot \eta_{\text{irrot}}$. In looking at your paper, one finds $\tau_{\text{rot}}/\tau_{\text{irrot}} > 1$ and, hence, $\eta_{\text{rot}} < \eta_{\text{irrot}}$, which results in a smaller viscosity constant and less damping, so that an oscillatory motion still remains.

C.Y. WONG: Your coefficients therefore have to be modified by multiplying by a small fraction.

R.W. HASSE: Yes. I think this fraction may be of the order of 0.7.

H. DIEHL: You mentioned the possibility of using heavy-ion collisions as a macroscopic approach to the study of nuclear friction. However, I should like to point out that one can also calculate nuclear friction by comparing the fission paths of binary and true-ternary fissions with the experimentally known ratio of the ternary to binary fission yield. Moreover, because these fissioning nuclei have high excitation energy, one obtains the friction constant at high temperature. Work on this subject is in progress.

Z. FRAENKEL: We have performed a calculation in which we try to relate the transition time between saddle point and scission to the emission of light particles in fission and have tried to obtain a measure of this transition time from the experimentally measured probability of light-particle emission in fission.

COMPRESSIBILITY IN NUCLEAR COLLECTIVE DYNAMICS*

J.J. GRIFFIN[†]

Lawrence Berkeley Laboratory,
University of California,
Berkeley, Calif.
and

University of Maryland,
College Park, Md.,

K.-K. KAN

University of Maryland,
College Park, Md.,
United States of America

Abstract

COMPRESSIBILITY IN NUCLEAR COLLECTIVE DYNAMICS.

Because the energy of nuclear matter increases very rapidly with changes in density, the nucleus as a fluid is generally assumed to be incompressible. This paper proposes that this assumption is valid only on the average. It is shown that to impose it as a microscopic identity is inconsistent with a realistic description of finite nuclei and precludes the consideration of certain phenomena which may play an essential role in collective dynamics.

THE NUCLEAR FLUID

The nucleus has been analogized to a liquid drop [1] from the earliest days [2] of its theoretical consideration. The nuclear liquid has usually been assumed to be incompressible because of both empirical [3] and theoretical evidence [4] that the energy of bulk nuclear matter increases rapidly when its average density deviates from that corresponding to the least energy.

The nuclear fluid has also long been treated as non-viscous, rather from the fact that nuclear theorists¹ have been, until recently [5], [6] unready to treat nuclear viscosity in a realistic detailed manner, than from any suspicion that most large scale distortions of the nuclear fluid would in fact prove to be uncoupled from the internal degrees of freedom analogous to thermal excitation.

* Research supported in part by the US Atomic Energy Commission. From a dissertation to be submitted to the Graduate School, University of Maryland, by K.-K. Kan, in partial fulfilment of the requirements for the Ph.D. degree in physics.

[†] Support of a John Simon Guggenheim Fellowship at the Lawrence Berkeley Laboratory of the University of California during 1972-73, is gratefully acknowledged.

¹ We shall soon be forced by the data from new experimental machines to confront questions which only recently would have been very speculative. This could easily lead to a rapid growth in interest in the viscous properties of nuclei.

The assumption of irrotationality in the flow of nuclear matter arrived early from the classical theory of fluids with the strong recommendation of simplicity. It was sidetracked by the phenomenological success of microscopic methods for calculating rotational and vibrational excitations, which methods had their most distinct success in producing inertial moments (especially rotational), which deviated from simple irrotational values in such a way as to agree with experiment. These microscopic descriptions made no reference to a classical velocity field, and so provided no place for such a characteristic as irrotationality. As a result classical analogies with fluids fell into disuse. We feel that this trend is due for reversal, and that a new attempt to understand collective motion in macroscopic terms is a timely and promising line of investigation. We hope that this paper can stir interest in this approach.

MICROSCOPIC INCOMPRESSIBILITY

In the present paper we wish, paradoxically, to omit discussion of that assumption (nonviscosity) which seems weakest and most certain to fall². Instead we wish to question the assumption of nuclear incompressibility and to re-introduce in the process a discussion of irrotational velocity fields. We shall of course not argue that this assumption is erroneous when applied overall to a nucleus, for it is, to a good approximation, an established fact. Instead, we suggest only that it is theoretically premature in dynamical analyses, and ought quite specifically and consciously to be listed among the characteristics to be demonstrated, and not assumed, for the nuclear fluid in collective motion.

A simplistic argument against the assumption of incompressibility can be suggested by exhibiting the matter density of a single particle in some state of a specific nuclear well. Such a density varies so strongly with position that it is almost absurd to think of imposing any constant density assumption upon it. But if we cannot impose the assumption on this basic component of the nuclear density, then how can we be comfortable with an assumption (as opposed to a proof) that it applies to the sum of many such single particle contributions?

This argument is, however, too simple a basis for any strong inference against incompressibility. It merely underlines the obvious fact that the single particle densities into which the theory of nuclear matter is constructed do not individually exhibit constant density. In collective motion, they might still however obey the law of incompressible flow which does not exclude a variable density but rather requires that any given microscopic volume element of the fluid as it moves according to the prescribed velocity field retains a constant density. Formally, the convective derivative of the density,

$$\frac{D\rho}{Dt} = \frac{\partial\rho}{\partial t} + \vec{v} \cdot \nabla\rho \quad (1)$$

must vanish in incompressible flow.

² Some promise of this on empirical grounds can be found in Ref. [6].

On the other hand the continuity condition between the matter current and the matter density requires

$$\nabla \cdot (\rho \vec{v}) + \frac{\partial \rho}{\partial t} = 0. \quad (2)$$

The combination of (2) and (1) implies

$$-\rho \nabla \cdot \vec{v} = \frac{D\rho}{Dt} = 0 \quad (3)$$

as a simpler form of the incompressibility requirement when continuity is satisfied.

TIME-DEPENDENT SCHROEDINGER THEORY

To advance the discussion further, we need a structure in which at least the collective motion of an independent single particle can be described. We assume therefore that a Hamiltonian is given in which an externally determined collective parameter, α , occurs, which may vary with time in a manner also determined externally. Thus the Hamiltonian is implicitly time dependent by means of the time dependence of the collective parameter, $\alpha(t)$. Then we seek a solution of the time-dependent Schroedinger equation defined by $H[\alpha(t)]$:

$$H\Psi = i\hbar \frac{\partial \Psi}{\partial t} \quad (4)$$

Also, we seek to construct a solution of (4) which reduces to a real eigenfunction of $H(\alpha_0)$ in the stationary limit, $0 = \dot{\alpha} = \ddot{\alpha} = \ddot{\alpha} = \dots$.

We first assume that the explicit dependence of Ψ upon t occurs via an exponential factor

$$\Psi = \psi \exp\left\{-\frac{i}{\hbar} \int^t \tilde{E}(\alpha(t'), \dot{\alpha}(t'), \dots) dt'\right\}. \quad (5)$$

Then (4) becomes

$$H\Psi = \tilde{E}(\alpha)\Psi + \exp\left\{-\frac{i}{\hbar} \int^t \tilde{E} dt'\right\} \sum_k \alpha^{(k)} \frac{\partial \Psi}{\partial \alpha^{(k-1)}} \quad (6)$$

where, for the deformation coordinate, we use the notation $\alpha^{(k)} = d^k \alpha / dt^k$, and where

$$\tilde{E}(\alpha) = \sum_i \tilde{E}_i \alpha^{(i)} = \tilde{E}_0 + \tilde{E}_1 \dot{\alpha} + \tilde{E}_2 \ddot{\alpha} + \dots \quad (7)$$

Then multiply (6) by $\exp\left\{+(i/\hbar) \int^t \tilde{E} dt'\right\}$ to get:

$$H\Psi = \tilde{E}\psi + i\hbar \sum_k \alpha^{(k)} \frac{\partial \psi}{\partial \alpha^{(k-1)}}. \quad (8)$$

We now assume that only $\dot{\alpha}$ is non-zero, i.e. $\ddot{\alpha} = \ddot{\alpha} = \dots = 0$. Then in (6) one needs to consider only the dependence of ψ upon α and not on $\dot{\alpha}$, $\ddot{\alpha}$, \dots . Then (8) becomes

$$H\Psi = \tilde{E}\psi + i\hbar \dot{\alpha} \frac{\partial \psi}{\partial \alpha}. \quad (9)$$

THE IRROTATIONAL FLUID FORM OF WAVE FUNCTION

Next we assume that ψ has the form³

$$\psi(\alpha) = \phi(\alpha) \exp\left\{-\frac{im}{\hbar} S(\alpha)\right\} \quad (10)$$

where ϕ and S are real.

When $\alpha(t)$ is an externally imposed function of time and ϕ and S are functions in the configuration space of the problem, which functions are parametrized by α , the Irrotational Fluid form is a rather flexible form for the wave function.

Its name is chosen to suggest the fact that the momentum operator for the i^{th} particle operates on Ψ to give a momentum density

$$\Psi^* \vec{p}_i \Psi = -i\hbar \phi \nabla \phi - m \phi^2 \vec{\nabla}_i S \quad (11)$$

Thus the momentum density corresponding to $S = 0$ is augmented locally by an addition $m \phi^2 \vec{\nabla}_i S$, where

$$\vec{\nabla}_i S = -\vec{v}_i \quad (12)$$

describes an irrotational velocity field completely prescribed by a knowledge of S . One thus arrives naturally at the interpretation that Ψ describes a quantum fluid constrained to move collectively in accordance with the classical field defined by the velocity potential, S .

THE QUANTUM EQUATIONS OF MOTION

The insertion of (10) into equation (4) reduces that equation to the following two simultaneous partial differential equations for the real functions ϕ and S :

(A) The "Continuity" equation

$$\frac{1}{2} \phi \nabla^2 S + \nabla S \cdot \nabla \phi = \frac{\partial \phi}{\partial t} \quad (13)$$

and (B), the "Modified Schroedinger" equation

$$\left\{ H(\alpha) - m \frac{\partial S}{\partial t} + \frac{1}{2} m \nabla S \cdot \nabla S \right\} \phi = \tilde{\epsilon} \phi. \quad (14)$$

The simplifying assumptions leading to (9) result in straightforward simplifications of the time-derivative terms. (In the special cases of rotational and Center-of-Mass motion the resulting equations have been considered by Gross, [8].)

The name given (A), equation (13), is meant to emphasize that it can be re-written in terms of the density $\rho = \phi^2$ as follows:

$$\rho \nabla^2 S + \nabla S \cdot \nabla \rho = \frac{\partial \rho}{\partial t}. \quad (15)$$

³ This form was proposed by D. Hill and J. H. Wheeler [7].

This form is identical with the familiar continuity equation (2) for a fluid of density ρ which moves with the classical irrotational velocity, v , of equation (12).

The corresponding label for (B), equation (14), underlines the presence of additional "stress potential" terms,

$$\chi = m \frac{\partial S}{\partial t} - \frac{1}{2} m (\nabla S)^2 \quad (16)$$

which arise from the collective motion described by non-constant values of velocity potential, S . This name is chosen because the negative gradient of the quantity, χ , describes in the classical fluid theory the force per unit density acting on the fluid element.

The collective kinetic energy in this formalism is identified with the term proportional to $\dot{\alpha}^2/2$ in the energy expectation value, and its coefficient is the collective inertia. In Appendix I we show that this calculation results in the expression

$$\langle E \rangle = \langle \Psi | H | \Psi \rangle = \tilde{\epsilon}^{(0)}(\alpha) + m \langle \phi | \frac{\partial \hat{S}}{\partial t} | \phi \rangle \quad (17)$$

where $\tilde{\epsilon}^{(0)}(\alpha)$ is defined so as to be independent of time derivatives of α , and \hat{S} is equal to $S + S_0$, as discussed in Appendix I. Then the $\dot{\alpha}^2$ term in the expectation value of $\partial \hat{S} / \partial t$ yields the collective kinetic energy and thence the collective inertial parameter.

We believe that a careful study of (A), equation (13), and (B), equation (14), will illuminate many qualitative features of collective motion. Here we wish to support this viewpoint first by discussing the relationship between continuity and compressibility. The results underline the qualitative difference between (A) and (B) and the formulation in which Hill and Wheeler utilized equation (10). Then we consider the special case of rotational motion and exhibit what seems to us the intriguing, if not paradoxical, result that the Irrotational Fluid form of wave function (10) can describe a system which rotates with a rigid moment of inertia.

CONTINUITY AND COMPRESSIBILITY

On the basis of the physical argument that in an approximate wave function of the form of Eq. (10), the nodes and values of ϕ ought to be carried along with the classical fluid velocity, Wheeler and Hill [7] assumed the relationship

$$\dot{\alpha} \frac{\partial \phi}{\partial \alpha} = \nabla S \cdot \nabla \phi. \quad (18)$$

Equations (3) and (15) show that this assumption is very closely related to the incompressibility of the fluid: If continuity is imposed on a wave function ψ of the form (5) via (13), then the Wheeler-Hill condition, equation (18), implies the incompressibility condition, equation (3), and vice versa. Alternatively, in the flow of an incompressible fluid, continuity is sufficient to guarantee the Wheeler-Hill assumption, (18). Conversely, continuity implies that if the flow is compressible then the Wheeler-Hill condition, must be violated.

Thus the Continuity Equation (A), (13), emerges as a natural generalization of the Wheeler-Hill assumption (18) which frees the description from an unstated restriction to incompressibility and allows the possibility of compressible flow for individual nucleons.

COMPRESSIBILITY AND COLLECTIVE INERTIAL PARAMETERS

Although one might expect from the results in simple cases [9] that each single particle density follows a nearly incompressible flow pattern so long as the nodal structure evolves without disruption of its topology, no such expectation applies in regions of deformation where the nodal topology is changing, as is the case, e.g., when the system follows adiabatically through a deformation where there occurs a crossing of a filled and an unfilled independent particle state, which crossing is split by some residual interaction.

Then one can show that from the general expression for the collective kinetic energy that a large, even dominant, contribution to the inertia arises from such level crossings, [10] and that a significant compressibility is inevitably associated with this situation. We do so in Appendix II.

One result is a natural intuitive basis for interpreting these large inertial parameters: If, as the nuclear shape changes, the density is compressing and decompressing in different regions of space (even if only to a slight fractional degree), then a given velocity of shape change, $\dot{\alpha}$, may be associated with an energy exhibiting a very large value for the coefficient of $\dot{\alpha}^2$, which describes the large increases in local particle velocity which are required for the density changes to conform to the continuity condition. Order of magnitude estimates indicate that the compressible flow of even a few particles in the last filled orbits can dominate the incompressible contributions of the nearly A other nucleons.

ROTATIONAL MOTION: A PHYSICAL PARADOX?

We turn now to our second illustration of the use of the Irrotational Fluid Form of wave function: its application to nuclear rotations. For this discussion we note that to leading order the present method gives the well-known "cranking model" formula [11] for the moment of inertia, and that the approximate velocity field, S , in this description is regular everywhere⁴. It therefore defines everywhere a momentum density of the form (11) and an associated irrotational velocity field of the form (12).

These results seem to us to present a paradox, as follows. It is well known [12] that in the case of independent particles moving in an oscillator potential deformed to the value which minimizes their independent particle model energy, the cranking model formula gives a value of the moment of inertia exactly equal to that of a rigid body with the same density as that of the nucleus.

Additionally, theoretical evidence suggests that the rigid body moment will be the result of applying the cranking model to any independent

⁴ In this respect our treatment differs from that of Ref. [8]. See discussion in Appendix II.

particle system [13]. Thus our result leads to the rigid body moment, which would seem most naturally associated with the collective velocity field of rigid body rotation

$$\vec{v}_R = \vec{\omega} \times \vec{r} \quad (19)$$

But our derivation is based upon the curl-free collective velocity field (12), which differs in that qualitative feature from (19), which has $\text{curl } \vec{v}_R = \vec{\omega}$.

One thus is impelled to consider the following question: Does there exist an ambiguity in the association of a classical velocity field with the collective motion of a particle in a specified quantum state, such that two (or more) distinct velocity fields might be associated with a single wave function, describing a unique physical motion?

We are not prepared at present to settle this question. We simply propose it as a worthwhile example of the kind of question which arises naturally in the context of the Irrotational Fluid Form of wave function, and the Continuity and Modified Schroedinger equations, (13) and (14), to which it leads.

SUMMARY

This paper proposes that a re-emphasis on the concepts of classical fluid dynamics is a timely shift in the study of nuclear collective dynamics. A formalism is presented which provides prominence for such concepts. It focuses attention upon the compressibility of the microscopic nuclear fluid in a natural way.

The example of the huge contribution of level crossings to adiabatic inertial parameters is cited as a result of such microscopic compressibility. In turn, compressibility offers a simple intuitive understanding of these huge inertia.

A second application, to the problem of collective nuclear rotation, suggests a still unresolved paradox concerning the classical velocity fields associated with collective motion of the microscopic quantum fluid; namely that a regular irrotational velocity field can be exhibited for a rotation characterized by the rigid body value of the moment of inertia.

APPENDIX I. THE COLLECTIVE KINETIC ENERGY

At any instant of time, the total energy of our system in collective motion is

$$\langle E \rangle = \langle \Psi | H | \Psi \rangle = \langle \Psi | i\hbar \partial / \partial t | \Psi \rangle \quad (\text{I-1})$$

$$= \tilde{\epsilon} + \langle \phi | i\hbar \partial / \partial t | \phi \rangle + \langle \phi | i\hbar \left(-\frac{im}{\hbar} \right) \frac{\partial S}{\partial t} | \phi \rangle. \quad (\text{I-2})$$

By normalization, $\langle \Psi | \Psi \rangle = \langle \phi | \phi \rangle = 1$, so that the second term of equation (I-2) vanishes.

To obtain equation (17) we note that, considered as a velocity potential or as a gauge function, S and \hat{S} describe the same physical situation if

$$S = \hat{S} - S_0 \quad (\text{I-3})$$

where S_0 is independent of position (so that $\nabla S_0 \equiv 0$). Then S_0 is an arbitrary function of collective coordinates which has no effect upon the physical content of ψ in equations (5) and (10). We utilize this freedom of choice of S_0 to arrange that the energy eigenvalue, $\tilde{\epsilon}$, shall be equal to $\tilde{\epsilon}^{(0)}$, and independent of all time derivatives of α . Thus S_0 is defined by the requirement

$$\tilde{\epsilon} = \tilde{\epsilon}^{(0)} + m \frac{\partial S_0}{\partial t} \quad (\text{I-4})$$

where $\tilde{\epsilon}$ is the correct eigenvalue if $S_0 \equiv 0$, and where $\tilde{\epsilon}^{(0)}$ is independent of all powers of $\dot{\alpha}$, $\ddot{\alpha}$, ... With this convention for S_0 , equation (I-2) reduces to

$$\langle E \rangle = \tilde{\epsilon}^{(0)}(\alpha) + m \langle \phi | \frac{\partial \hat{S}}{\partial t} | \phi \rangle \quad (\text{I-5})$$

which is identical to the result cited earlier (equation (17)). We note that the freedom to choose S_0 in this way is also evident by inspection of the modified Schroedinger equation, (14).

We next consider some time-dependent eigenfunction,

$$\psi = \chi + i\omega \quad (\text{I-6})$$

obtained by some approximation method, and the corresponding irrotational fluid form (10) of the same wave function. By evaluating

$$\langle E \rangle = \langle \psi | i\hbar \frac{\partial}{\partial t} | \psi \rangle = 2\hbar \langle \omega | \frac{\partial}{\partial t} | \chi \rangle \quad (\text{I-7})$$

also in terms of ϕ and S ,

$$\langle \psi | i\hbar \frac{\partial}{\partial t} | \psi \rangle = m \langle \phi | \frac{\partial S}{\partial t} | \phi \rangle \quad (\text{I-8})$$

we are able to utilize (I-7) in an alternative expression for the collective kinetic energy:

$$T_c = 2\hbar \langle \omega | \frac{\partial}{\partial t} | \chi \rangle + m \frac{\partial S_0}{\partial t} \quad (\text{I-9})$$

In case equation (9) is solved to leading order perturbation theory, one finds

$$\psi = \chi + i\omega \approx u_0 + i v_1 \quad (\text{I-10})$$

and

$$\tilde{\epsilon} = \epsilon^{(0)} + \epsilon^{(2)} + \dots \quad (\text{I-11})$$

where

$$\epsilon^{(2)} = -\hbar \left\langle v_i \left| \frac{\partial}{\partial t} \right| u_0 \right\rangle. \quad (\text{I-12})$$

Also, our conventional choice (specified by eq. (I-4)) of S_0 in this approximation is such that

$$m \frac{\partial S_0}{\partial t} = \epsilon^{(2)}. \quad (\text{I-13})$$

Thus, S_0 can be eliminated from (I-9) to yield

$$T_c = \hbar \left\langle v_i \left| \frac{\partial}{\partial t} \right| u_0 \right\rangle \quad (\text{I-14})$$

or, by equating (I-7) and (I-8),

$$T_c = \frac{1}{2} m \left\langle \phi \left| \frac{\partial S}{\partial t} \right| \phi \right\rangle. \quad (\text{I-15})$$

The result (I-14) reduces to the well-known "cranking model" formula when the perturbation approximation result

$$v_i = \hbar \sum_j \frac{\langle u_i | \partial / \partial t | u_0 \rangle}{\epsilon_i - \epsilon_0} u_j \quad (\text{I-16})$$

is inserted. Likewise the use of equation (II-4) to define S from ψ reduces (I-15) to the same formula.

APPENDIX II. COMPRESSIBILITY AT LEVEL CROSSINGS

We consider a Hamiltonian, $H = H_0 + V_{ab}$, which in the stationary limit of adiabatic motion, ($\dot{\alpha} \rightarrow 0$, $S \rightarrow 0$), exhibits a crossing of two single particle states, $|a\rangle$ and $|b\rangle$, when the weak coupling between them, V_{ab} , is neglected. We assume that, if V_{ab} were identically zero, then for slow collective motion the collective velocity field for both the uncoupled states would be incompressible and irrotational. i.e., we assume

$$\nabla^2 S_a = \nabla^2 S_b = 0 \quad (\text{II-1})$$

and

$$m \left\langle \phi_a \left| \frac{\partial S_a}{\partial t} \right| \phi_a \right\rangle = m \int \phi_a^2 (\nabla S_a)^2 d\tau \quad (\text{II-2})$$

Finally, for simplicity, we assume that the states $|a\rangle$ and $|b\rangle$ are coupled only by V_{ab} and not at all by the generator $\dot{\alpha} (d/d\alpha)$ of the collective motion.

Then one can analyze the problem of the slow collective motion of the system through deformations near the level crossing for two distinct cases. In one case V_{ab} is neglected and the states $|a\rangle$ and $|b\rangle$ are the natural bases for treating the collective motion. In the second case $H_0 + V_{ab}$ is diagonalized to provide a mixed eigenbasis in which to treat the collective motion.

The result for the uncoupled problem has been predetermined by the assumptions we have made to give incompressible flow with an irrotational inertia.

We then wish to show only that the coupling of the levels via V_{ab} into eigenstates, $|U\rangle$ and $|L\rangle$, (denoting upper and lower eigenstates, respectively) of $H_0 + V_{ab}$ introduces extra non-zero terms into the expression for $\nabla^2 S_L$ and for the inertial parameter. The latter includes the crossing contributions already analyzed in references [9] and [10], but not then recognized as effects so closely associated with compressibility.

First we outline the procedure for obtaining an approximate expression for the velocity potential, S . We assume that a complex function, $\psi = u + iv$, is calculated to some approximation. Then by equation (10), the corresponding velocity potential S is given by

$$\left(-\frac{im}{\hbar}\right)S = \frac{1}{2} \ln(\psi/\psi^*) \quad (\text{II-3})$$

$$= \frac{1}{2} \ln \frac{u+iv}{u-iv} \quad (\text{II-4})$$

$$= i \tan^{-1}(v/u). \quad (\text{II-5})$$

One notes here that the approximation of $\tan^{-1}(v/u) \approx v/u$ in (II-4) is tempting, if $\dot{\alpha}$ is small, since $v \rightarrow 0$ as $\dot{\alpha} \rightarrow 0$. But this approximation is dangerous if u has any nodes, since in that case the resulting S may have singularities whose successful management is difficult to guarantee. This is the difficulty referred to in footnote (4). If u has no nodes, then the theorem of Wick [14] applies, and his conclusion follows: that the inertial parameter is precisely equal to the irrotational value (II-2). Such questions will be discussed in more detail elsewhere.

To contrast the coupled and uncoupled cases we adopt the following convenient notation. Stationary eigenstates of H_0 are denoted by u_a, u_b, \dots and the time-dependent eigenstates by $\psi_a = u_a + iv_a, \dots$. When a finite coupling, V_{ab} , exists between the two states, the resulting stationary eigenstates are labelled $u_L = Au_a + Bu_b$ and $u_U = Bu_b - Au_a$. The corresponding mixed time-dependent eigenstate is denoted by $\psi_L = \chi_L + i\omega_L$, to emphasize the fact that it will generally contain other terms, in addition to those present in $\psi_L^{(0)} = A\psi_a + B\psi_b = u_L + iv_L$.

In particular, to leading order in $\partial/\partial\tau = \dot{\alpha} \partial/\partial\alpha$,

$$\psi_L = u_L + i\omega_L \quad (\text{II-6})$$

$$= A\psi_a + B\psi_b + i\hbar \frac{\langle u_U | \partial/\partial t | u_L \rangle}{\epsilon_U - \epsilon_L} u_U \quad (\text{II-7})$$

is the approximate wave function for the lower state. (II-7) exhibits a third term over and above the two terms corresponding to ψ_a and ψ_b .

The effect of this extra term upon S can most easily be understood in contrast to the simplest uncoupled case specified by assumptions (II-1) and (II-2), which are realized when the ratios,

$$v_a/u_a = v_b/u_b = \tan \gamma \quad (\text{II-8})$$

are equal for the crossing states. (This equality is actually realized in the quadrupole shape deformation of a simple harmonic oscillator system, [15].) In such a case, one would obtain by considering $\ln(\psi_a/\psi_a^*)$, or $\ln(\psi_b/\psi_b^*)$ the same velocity potential for levels a and b,

$$S_a = -\frac{\hbar}{m} \gamma = S_b. \quad (\text{II-9})$$

The result that the velocity potential is the same for all levels is consistent with the assumption (II-1), and the uniqueness of solutions to (II-1) for specified boundary conditions.

Moreover, the same velocity potential would be obtained from any linear combination, $A\psi_a + B\psi_b$, of ψ_a and ψ_b and in particular for the linear combination given by omitting the third term of (II-7). One concludes that, in this simple case, omission of the third term leads again to (II-9).

We can now inspect the effect of including the third term of (II-7),

$$i\hbar \frac{\langle u_U | \partial / \partial t | u_U \rangle}{\epsilon_U - \epsilon_L} u_U = i\Gamma u_U \quad (\text{II-10})$$

From (II-3), we can see that the new velocity potential is

$$S_L = -\frac{\hbar}{2im} \ln \frac{(Au_a + Bu_b) + i(Av_a + Bv_b) + i\Gamma u_U}{(Au_a + Bu_b) - i(Av_a + Bv_b) - i\Gamma u_U} \quad (\text{II-11})$$

$$= -\frac{\hbar}{2im} \ln \frac{\{(Au_a + Bu_b) + i(Av_a + Bv_b)\} \exp(i\delta)}{\{(Au_a + Bu_b) - i(Av_a + Bv_b)\} \exp(-i\delta)} \quad (\text{II-12})$$

$$= S_a - \frac{\hbar}{m} \delta \quad (\text{II-13})$$

where

$$\delta = \tan^{-1} \left\{ \frac{\Gamma u_U u_L}{u_L^2 + v_L^2 + \Gamma u_U v_L} \right\}. \quad (\text{II-14})$$

This result, plus the observation that δ is certainly not a constant in space, guarantees that,

$$\nabla^2 S_L \neq 0 \quad (\text{II-15})$$

by virtue of the fact that $\nabla^2 S_a = 0$, and by the uniqueness of solutions to Laplace's equation with specified boundary conditions. Thus we reach our first conclusion: that at a level crossing, the velocity potential for ψ_L describes compressible flow, even when each of the flow patterns of the two uncoupled levels is incompressible.

To see the effect of the third term on the collective kinetic energy, we evaluate the expression (I-14) with $u_0 + iv_1$ replaced by (II-7). Then one finds

$$T_c = \hbar \langle v_L | \partial / \partial t | u_L \rangle + \frac{|\langle u_0 | \hbar \partial / \partial t | u_L \rangle|^2}{\epsilon_U - \epsilon_L} \quad (\text{II-16})$$

where the second term arises from presence of (II-10) in (II-7). It is precisely this term which contributes on the average some 10^3 times the irrotational inertia for a typical quadrupole distortion of an independent particle system, and some 40 times the irrotational value when the smoothing effects of pairing are considered [10]. In short, the additional term arising from deviations from incompressible flow at crossings provides the dominant contribution to the nuclear inertia. This, it seems, supports the suspicion that the failure to allow compressibility in a nuclear structure theory is a serious deficiency.

Note Added in Proof: Dr. Charles Critchfield has pointed out to us a paper by E. Madelung (Z. Phys. 40 (1926) 322) in which Eqs (13) and (14) and their fluid dynamical interpretation are derived and discussed in the context of the one-electron problem.

REFERENCES

- [1] WEIZSACKER, C.F., von, Z. Phys. 77 (1932) 1.
- [2] BOHR, N., Nature 137 (1936) 344; BOHR, N., KALCKAR, F., K. Dan. Vidensk. Selsk. Mat-Fys. Medd. 14 (1937) 10.
- [3] HOFSTADTER, R., Rev. Mod. Phys. 28 (1956) 214.
- [4] BRUECKNER, K.A., GAMMEL, J.L., Phys. Rev. 109 (1958) 1023.
- [5] SCHIRMER, J., KNAACK, S., SÜSSMAN, G., Nucl. Phys. A199 (1973) 31. See also WIECZOREK, R., et al., Paper IAEA-SM-174/02, these Proceedings, Vol. 1.
- [6] SWIATECKI, W.J., in Reactions Induced by Heavy Ions (Proc. Conf. Heidelberg, 1969), North Holland, Amsterdam (1970) 720; SWIATECKI, W.J., BJØRNHOLM, S., Phys. Reports 4 (1972) 325.
- [7] HILL, D.L., WHEELER, J.A., Phys. Rev. 89 (1953) 1106 (cf. Figure 8, p. 1123).
- [8] GROSS, E.P., Nucl. Phys. 14 (1959) 389.
- [9] GRIFFIN, J.J., in Physics and Chemistry of Fission, (Proc. Symp. Vienna, 1969), IAEA, Vienna (1969) 3.
- [10] GRIFFIN, J.J., Nucl. Phys. A170 (1971) 395.
- [11] INGLIS, D.R., Phys. Rev. 96 (1954) 1059, 103 (1956) 1786.
- [12] BOHR, A., MOTTELSON, B.R., K. Dan. Vidensk. Selsk., Mat.-Fys. Medd. 30 (1955) 1.
- [13] ROCKMORE, R.M., Phys. Rev. 116 (1959) 469; AMADO, R.D., BRUECKNER, K.A., Phys. Rev. 115 (1959) 778; MIGDAL, A.B., Nucl. Phys. 13 (1959) 655 (cf. pp. 661 and 662).
- [14] WICK, G., Phys. Rev. 73 (1948) 51.

DISCUSSION

L. WILETS: There is an old theorem which states that a nodeless wave function leads to irrotational flow. Does your theory exhibit this effect? Also, is your velocity field the same as other (hydrodynamic) definitions?

J.J. GRIFFIN: Yes. Wick's theorem for a nodeless wave function is consistent with our formalism. However, the rigid body value of the rotational moment in the nuclear independent particle system results only when the deformation is taken to be equal to the equilibrium value. For

a single nucleon in the nodeless wave function, this equilibrium shape is spherical and its collective rotation is not well defined. Thus, Wick's theorem does not directly confront the paradox posed by the rigid moment of inertia. Perhaps Mr. Kan would like to comment on this.

K.-K. KAN: One should remember that the irrotational velocity field exhibited by Wick is a quantity in the rotating frame. It is well known, at least classically, that in transforming back to the space-fixed frame, we get an additional rotational term

$$\vec{v}_{sp} = \vec{v}_{rot} + \vec{\omega} \times \vec{r}$$

Investigation of this kind of transformation in our "quantal" fluid may help to resolve the paradox.

L.G. MORETTO: In listening to the presentation of this paper, it occurred to me that pairing is extremely important in determining the inertial masses, especially insofar as the barrier penetrability is concerned. In a least-action trajectory calculation of the Pauli type, one should include the gap parameter as a collective variable. The resulting pairing least-action path (for which I would propose the acronym (LEAP)) may very well correspond to a substantially larger gap parameter due to the very large gain in superfluidity and to a significant decrease in inertia.

H.C. PAULI: I agree with you that the pairing gap is a collective parameter, like a deformation, and that the variation of the trajectory in "pairing space" should be included. Perhaps this will even be easy to perform technically. At the moment it is difficult to estimate the changes in the action integral. Personally, I believe that the inclusion of this dimension would create effects as large as those due to surface pairing.

J.J. GRIFFIN: Pairing happens to affect the ground state in the low-lying spectra very much. There may be four or five other such variables in the nucleus which are not so obvious to us, meaning that we can calculate the ground state without including them. I think this question opens up a vast realm of possibilities for hidden coordinates; coordinates not equal to p or x or not obvious functions of p or x , which might really play a tremendously important role in the end in determining dynamical nuclear structure.

What seems to me to be most important about understanding the inertial parameters is that the single-particle wave functions in the process of being rearranged make the dominant contribution to the inertial parameter. Pairing reduces that from a factor of 1000 to a factor of 10 but I consider the more important underlying conceptual item to be the rearrangement of the single-particle wave functions. Therefore I look to the independent-particle limit to be the more informative one, even though it does not give the quantitatively correct results. It is the pure, more pristine, philosophical case, if you like.

UNIFIED THEORY OF LOW-ENERGY FISSION AND FISSION MODELS*

W. NÖRENBERG

Institut für Theoretische Physik der Universität
and

Max-Planck-Institut für Kernphysik,
Heidelberg, Federal Republic of Germany

Abstract

UNIFIED THEORY OF LOW-ENERGY FISSION AND FISSION MODELS.

An S-Matrix formulation of the induced fission $P + T \rightarrow C \rightarrow F_1 + F_2$ is presented by introducing scattering states $|c e_c^{(+)}\rangle$ of the target-projectile system, bound states $|\lambda\rangle$ of the compound system C and fissioning states $|f e_f^{(-)}\rangle$ of pairs of fragments F_1 and F_2 . The states $|c e_c^{(+)}\rangle$, $|\lambda\rangle$ and $|f e_f^{(-)}\rangle$ are conveniently defined within an extended generator coordinate method by $|\Phi\rangle \approx \sum_{\alpha} \int d\rho \phi_{\alpha}(\rho) |\alpha, \rho\rangle$. Here, in addition to the integral over

the generator coordinate(s) ρ , a sum over a limited number of adiabatic states α is included. The sum and integral is limited to appropriate subspaces $\{c\}$, $\{\lambda\}$ and $\{f\}$. Near or below the fission threshold the subspaces are defined as follows: $\{c\}$ includes the adiabatic states $|\alpha, \rho\rangle$ around the ground state deformation in the first valley with a light particle in the continuum, $\{\lambda\}$ is restricted to bound states in the first and second valley and $\{f\}$ consists of adiabatic states beyond the second saddle point. Within this approach the threshold dependence of the fission cross-section is discussed and the model Hamiltonian for the description of gross, intermediate and fine-structure resonances in the total fission cross-section is obtained.

Whereas in low-energy fission the dependence of the total fission cross-section is mainly determined by the structure of the compound states, there are many fission phenomena (e.g. mass yields, charge and spin distributions between the fragments, total kinetic energies and excitation energies of the fragments) which are strongly influenced by the properties of the fissioning states $|f e_f^{(-)}\rangle$. Assume that there is a specific adiabatic state populated at the (second) saddle point. The fission phenomena are mainly determined by the coupling of this specific state to other adiabatic states. This coupling is considered in the level-crossing model and found to be strong between collective states and weak between non-collective states. A useful hierarchy of the adiabatic states is introduced which leads to the definition of fission bands. In the picture of this hierarchy, the static scission point model, the adiabatic model, the diabatic model of Kelson and Griffin, the statistical model of Fong and the thermodynamical model or quasi-equilibrium model is discussed.

1. INTRODUCTION

Nearly 35 years have passed now since Hahn and Straßmann [1] discovered nuclear fission. In the meantime plenty of experimental data have been compiled and partly described by models which have been developed for specific phenomena. We have reached a point where it seems to be useful to study all these specific models in the framework of a unified theory. The first step in this direction has been done already by Hill and Wheeler [2] several years ago. Such a general description of nuclear fission is particularly important in order to unify the language not only for the fission process but also, more generally, for heavy-ion

* Work supported by the Bundesministerium für Bildung und Wissenschaft.

reactions. The aim of this paper is to pick up the idea of Hill and Wheeler and formulate a unified description of fission. Thereby, we hope to give a guide for using our knowledge on fission in the collision of very heavy nuclei and vice versa.

2. UNIFIED THEORY

Let us study the induced fission process

$$P+T \rightarrow C \rightarrow F_1+F_2 \quad \text{or} \quad T(P,f) \quad (2.1)$$

where the projectile P is absorbed by the target. The excited compound nucleus C fissions into two excited fragments F_1 and F_2 of comparable size. We restrict the discussion to two particles in the outgoing channels in order to avoid the three-body problem.

2.1. S-matrix formulation

The channels are suitably defined by the total angular momentum J , M , the total parity Π and the channel indices

$$c \equiv A_p, Z_p, v_p; A_T, Z_T, v_T; (J_p J_T) J_c L_c \quad (2.1.1)$$

for the projectile-target channels and

$$f \equiv A_1, Z_1, v_1; A_2, Z_2, v_2; (J_1 J_2) J_f L_f \quad (2.1.2)$$

for the fission channels. The stationary scattering solution at the energy E is given by [3,4]

$$|\Psi_{J\mathbb{M},c}^{(+)}\rangle = \lim_{\eta \rightarrow +0} \frac{i\eta}{E - H + i\eta} |cJ\mathbb{M}\rangle \quad (2.1.3)$$

where H is the total Hamiltonian of the system. The wave function $|cJ\mathbb{M}\rangle$ is the free spherical wave solution in the incoming channel c . The S-matrix elements $S_{fc}^{J\Pi}$ are given by the ratio of the outgoing amplitude in the channel f over the incoming amplitude in the channel c . The S-matrix elements $S_{fc}^{J\Pi}$ contain the complete information about the fission process. The various cross-sections

can be obtained from these matrix elements in the usual way [4,5]. A particularly simple expression is obtained for the total cross-section for fission by unpolarized particles, namely

$$\sigma_{fc}^{\text{unpol.}} = \frac{\pi}{K_c^2} \sum_{J \Pi} \frac{2J+1}{(2J_p+1)(2J_T+1)} \sum_{J_c L_c J_f L_f} |S_{fc}^{J \Pi}|^2 \quad (2.1.4)$$

where K_c is the wave number in the incoming channel c .

The scattering solution (2.1.3) can be calculated approximately in a truncated Hilbert space with projection operator P . The following derivation of the S -matrix is closely related to the description given by Fano [6] and Weidenmüller [7]. We approximate the scattering solution (2.1.3) for a given total angular momentum and parity by

$$\begin{aligned} |\psi_c^{(+)}\rangle &= \sum_{\lambda} \alpha_{\lambda} |\lambda\rangle + \sum_{c'} \int_{E_{oc'}} d\epsilon_c \beta_{c'}(\epsilon_c) |c', \epsilon_c^{(+)}\rangle \\ &\quad + \sum_f \int_{E_{of}} d\epsilon_f \gamma_f(\epsilon_f) |f, \epsilon_f^{(-)}\rangle \end{aligned} \quad (2.1.5)$$

where we use a basis of three classes of wave functions:

- (i) The states $|\lambda\rangle$ are bound states of the compound system.
- (ii) The states $|c', \epsilon_c^{(+)}\rangle$ are scattering states with thresholds $E_{oc'}$, containing one light particle in the continuum and the target in a bound state. Asymptotically $|c', \epsilon_c^{(+)}\rangle$ consists of an incoming and outgoing wave in the channel c' and only outgoing waves in all other channels $c'' \neq c'$.
- (iii) The states $|f, \epsilon_f^{(-)}\rangle$ are scattering states of the fragments F_1, F_2 which are later referred to as fissioning states. Asymptotically they consist of outgoing and incoming waves in channel f and only incoming waves in all other channels $f' \neq f$.

Inserting the expansion (2.1.5) for the scattering solution into eq. (2.1.3) written in the form

$$(E - PHP + i\eta) |\psi_c^{(+)}\rangle = i\eta |c, \epsilon_c^{(+)}\rangle$$

where $|c, J\pi M\rangle$ has been replaced by the corresponding scattering state $|c, \epsilon_c^{(+)}\rangle$, ref. [3], we obtain a coupled set of equations for α_λ , $\beta_{c'}(\epsilon_c)$ and $\gamma_f(\epsilon_f)$. This set of coupled equations is solved by neglecting the continuum-continuum interaction [6,7] i.e. $\langle f, \epsilon_f^{(-)} | H | c', \epsilon_{c'}^{(+)} \rangle = 0$. This is a good approximation because the scattering states $|c', \epsilon_{c'}^{(+)}\rangle$ and the fissioning states $|f, \epsilon_f^{(-)}\rangle$ have rather different shapes. If $|c', \epsilon_{c'}^{(+)}\rangle$ and $|f, \epsilon_f^{(-)}\rangle$ are normalized to δ -functions in the energy, the resulting S-matrix is given by

$$S_{fc} = -2\pi i \sum_{\lambda} \langle f | H | c \rangle \alpha_{\lambda}^{(-)} | H | \lambda \rangle \alpha_{\lambda} \quad (2.1.6)$$

where α_{λ} is determined by the set of coupled equations

$$\sum_{\lambda'} \{ (E - \epsilon_{\lambda}) \delta_{\lambda\lambda'} - \sum_c G_{\lambda\lambda'}^{c'}(E) + \sum_f G_{\lambda\lambda'}^f(E) \} \alpha_{\lambda'} = \langle \lambda | H | c \rangle \epsilon_c^{(+)} \quad (2.1.7)$$

with ($j = c^{(+)}$ or $f^{(-)}$)

$$G_{\lambda\lambda'}^j(E) \equiv \lim_{\eta \rightarrow +0} \int_{E_{oj}}^{\infty} d\epsilon_j \frac{\langle \lambda | H | j \epsilon_j \rangle \langle j \epsilon_j | H | \lambda \rangle}{E - \epsilon_j + i\eta} \quad (2.1.8)$$

$$\equiv F_{\lambda\lambda'}^j(E) + \frac{i}{2} \Gamma_{\lambda\lambda'}^j(E)$$

with $F_{\lambda\lambda'}^j(E)$ and $\Gamma_{\lambda\lambda'}^j(E)$ real. A particularly simple solution is obtained if the energy dependence of the matrix elements $\langle \lambda | H | f \epsilon_f^{(-)} \rangle$ and $\langle \lambda | H | c', \epsilon_{c'}^{(+)} \rangle$ and the nondiagonal terms of $G_{\lambda\lambda'}^j(E)$ are negligible. Then the S-matrix is given by

$$S_{fc} = -2\pi i \sum_{\lambda} \frac{\langle f | H | c \rangle \epsilon_c^{(-)} \langle \lambda | H | c \rangle \epsilon_c^{(+)}}{E - E_{\lambda}' + \frac{1}{2} i \Gamma_{\lambda}} \quad (2.1.9)$$

with the shifted resonance energies $E_{\lambda}' = E_{\lambda} + \sum_c F_{\lambda\lambda}^{c'} + \sum_f F_{\lambda\lambda}^f$

and the widths $\Gamma_{\lambda} = 2\pi \{ \sum_c |\langle \lambda | H | c' \epsilon_{c'}^{(+)} \rangle|^2 + \sum_f |\langle \lambda | H | f \epsilon_f^{(-)} \rangle|^2 \}$.

For non-overlapping resonances the unpolarized cross-section at a resonance E'_λ is, according to eq. (2.1.4),

$$\sigma_{fc}^{\text{unpol.}} = \frac{4\pi^2}{K_c^2} \frac{2J+1}{(2J_p+1)(2J_T+1)} \frac{\Gamma_\lambda^f \Gamma_\lambda^c}{(E-E'_\lambda)^2 + \frac{1}{4}\Gamma_\lambda^2} \quad (2.1.10)$$

with $\Gamma_\lambda^f = 2\pi \sum_{fL_f} |\langle \lambda | H | f E^{(-)} \rangle|^2$ and $\Gamma_\lambda^c = 2\pi \sum_{cL_c} |\langle \lambda | H | c E^{(+)} \rangle|^2$.

In order to discuss the fine, intermediate and gross structure of the resonances, observed in the fission cross-section, one has to specify the basis states, particularly the compound states, in some detail.

2.2. Basis functions

According to Griffin and Wheeler [8] we look for wave functions of the form

$$|\Phi\rangle = \sum_{\alpha} \int d\rho \phi_{\alpha}(\rho) |\alpha\rho\rangle \quad (2.2.1)$$

where $|\alpha, \rho\rangle$ are some appropriate states depending on a set of quantum numbers α and a continuous variable ρ , the generator coordinate. We like to call these states $|\alpha, \rho\rangle$ adiabatic states which could be constructed from a deformed single-particle potential with some residual interaction (e.g. pairing interaction) or from deformed Hartree-Fock (HF) calculations or related self-consistent methods. The various approximations, i.e. the amount of residual interaction taken into account or the ansatz for the wave function (HF, HF-Bogolyubov, RPA), lead to different adiabatic states reaching from shell-model states (sometimes called diabatic states) to collective RPA states. The 'true' adiabatic states are defined by exactly solving the Schrödinger equation with the total Hamiltonian under the constraint of given deformations. Inserting the expansion (2.2.1) into the Schrödinger equation one obtains in a given subset of the adiabatic states the coupled set of integral equations

$$\sum_{\alpha} \int d\rho \{ \langle \alpha' \rho' | H | \alpha \rho \rangle - \epsilon \langle \alpha' \rho' | \alpha \rho \rangle \} \phi_{\alpha}(\rho) = 0 \quad (2.2.2)$$

which determines the weight functions $\phi_\alpha(\rho)$. Eq. (2.2.1) can be transformed approximately, e.g. by a moment expansion [9] or by relating the overlap integrals to derivatives of Gaussian-type functions [9,10], into a coupled set of differential equations of the form

$$\{T_{\text{coll}}(\rho) + V_\alpha(\rho) - \epsilon\}\phi_\alpha(\rho) = \sum_{\alpha' \neq \alpha} C_{\alpha\alpha'}(\rho)\phi_{\alpha'}(\rho) \quad (2.2.3)$$

where the collective energy $T_{\text{coll}}(\rho)$ is a second-order differential operator, $V_\alpha(\rho)$ is a collective potential and $C_{\alpha\alpha'}(\rho)$ is in general a differential coupling operator.

In dealing with the fission process, the generator coordinate is a deformation parameter or more generally a set of deformation parameters $\rho \equiv \rho_1, \rho_2, \dots$. The ground state energy $V_0(\rho)$ as function of the deformation ρ has been calculated successfully in recent years by Strutinsky's method [11-15]. Excited states ($\alpha \neq 0$) can be built upon the HF or HFB ground state by introducing particle-hole or quasi-particle states. A schematic picture of the adiabatic energies $V_\alpha(\rho)$ is shown in Fig. 1. According to this picture we can divide the Hilbert space, which is already truncated to avoid over-completeness, into four subspaces:

- (i) The subspace $\{c\}$ consists of all adiabatic states in the compound region I (first valley) with a light particle in the continuum.
- (ii) The subspace $\{\lambda_I\}$ consists of all bound adiabatic states in the compound region I (first valley).
- (iii) The subspace $\{\lambda_{II}\}$ consists of all bound adiabatic states in the compound region II (second valley).
- (iv) The subspace $\{f\}$ consists of all bound adiabatic states in the fission region.

We can now define the basis states $|c', \epsilon_c^{(+)}\rangle$, $|f, \epsilon_f^{(-)}\rangle$, $|\lambda_I\rangle$ or $|\lambda_{II}\rangle$ by eqs. (2.2.1) and (2.2.3) in the subspaces $\{c\}$, $\{f\}$, $\{\lambda_I\}$ and $\{\lambda_{II}\}$, respectively. The boundary conditions between the regions, indicated in Fig. 1, couple the solutions in the different subspaces. It has been shown [9] that this coupling can be taken into account approximately by introducing artificially

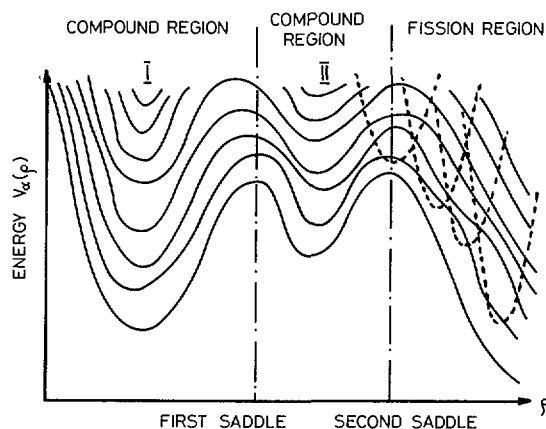


FIG.1. Schematic picture of adiabatic states. The definition of the adiabatic states, given in the text, does not forbid level crossings. Some shell-model (or HF) configurations are indicated by dashed lines.

the boundary conditions $\phi_\alpha(\rho(\text{boundary})) = 0$, $(d\phi_\alpha/d\rho)_{\rho(\text{boundary})} = 0$ and at the same time taking an effective Hamiltonian H_{eff} which couples the states across the barrier. Let us briefly discuss in the following subsection the phenomena connected with H_{eff} and the compound states.

2.3. Threshold behaviour and resonances

Let us assume that one of the two barriers is much higher than the other and that we are dealing with fission at energies near this barrier. If the second barrier is higher we cannot distinguish between λ_I and λ_{II} states any more. If the first barrier is higher we have no λ_{II} states near threshold energies. In both cases only one sort of compound states λ is left over. According to eq. (2.1.10) the mean fission cross-section, averaged over an energy interval which is large compared to the distance D_λ of the compound states λ , is given by

$$\langle \sigma_{fc}^{\text{unpol.}} \rangle \propto \frac{\langle \Gamma_\lambda^f \rangle}{D_\lambda} = \frac{1}{2\pi} |T|^2 \quad (2.3.1)$$

where Γ_λ^f is the mean value of the squared coupling matrix element $2\pi |\langle fE^{(-)} | H_{\text{eff}} | \lambda \rangle|^2$ and T is the transmission coefficient through

the barrier. The energy dependence of this transmission coefficient determines the threshold behaviour of the fission cross-section. The lowest threshold is due to the adiabatic ground state $\alpha = 0$. For an inverted harmonic oscillator, Hill and Wheeler [2] have obtained

$$|T|^2 = \{1 - \exp(2\pi \frac{E_s - E}{\hbar\omega})\}^{-1} \quad (2.3.2)$$

where E_s is the barrier height and $\hbar\omega$ the oscillator energy.

Let us briefly discuss the nature of gross, intermediate and fine structure in the fission cross-section. According to our treatment in subsection 2.2, the total Hamiltonian is approximated by

$$H \approx H_C + H_I + H_{II} + H_f + H_{CI} + H_{I II} + H_{II f} \quad (2.3.3)$$

The energy dependence of the fission cross-section below or near to both barriers can be studied in analogy to subsection 2.1. The Hamiltonian (2.3.3) has been treated in detail several times [9,16]. The result can be summarized as follows (Fig.2): Fine structure resonances are due to compound states $|\lambda_I\rangle$ in the first valley. Intermediate structure resonances are due to compound states $|\lambda_{II}\rangle$ in the second well. The energy distances between intermediate resonances are much larger than between the fine structure resonances, because of the lower level density in the

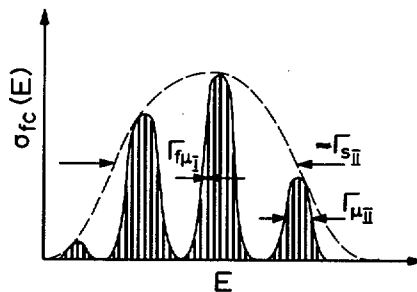


FIG.2. Gross structure (Γ_{SII}), intermediate structure ($\Gamma_{\mu II}$) and fine structure ($\Gamma_{\mu I}$) resonances in the fission cross-section.

shallower second well. The gross structure is due to a doorway mechanism for the states: Collective vibrational states carry the total coupling across the barriers. If the spreading width of these doorway states are smaller than the distance to neighbouring doorway states, gross structures due to these doorway states are observed in the fission cross-section.

3. FISSION MODELS

We have seen in section 2 that the energy dependence of the fission cross-section is determined by the structure of the barrier. Other information about fission phenomena, like mass and charge distribution, kinetic and excitation energies of the formed fragments are contained in the fissioning states $|fE^{(-)}\rangle$ introduced above. A rigorous calculation of $|fE^{(-)}\rangle$ according to eq. (2.2.3) is far beyond our abilities to solve exactly. Therefore quite simple models which are feasible numerically have been introduced to get a feeling about what is happening in the fission process between the saddle and the scission point. In order to discuss all these models in a common language, it is necessary first to study the adiabatic states $|\alpha\rangle$ somewhat closer and to define a hierarchy of these states.

3.1. Hierarchy of adiabatic states

Consider the problem of level crossing, as shown in Fig. 3, which has been treated by Landau, Zener and Stueckelberg in a time-dependent quasi-classical approximation [17] . Suppose that

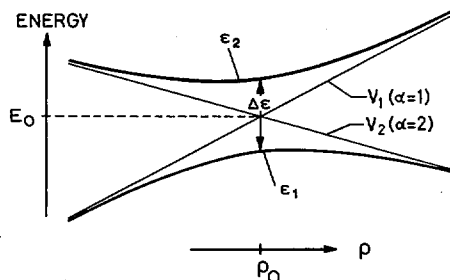


FIG.3. Crossing of the adiabatic levels $\alpha=1$ and $\alpha=2$.

there are only two adiabatic states, $\alpha = 1$ and 2, which have to be taken into account and assume that the coupled eqs. (2.2.3) have the following form

$$\frac{\hbar^2}{2M_\alpha} \frac{d^2 \phi_\alpha}{d\rho^2} + [\epsilon - V_\alpha(\rho)] \phi_\alpha(\rho) = V_{\alpha\alpha'} \phi_{\alpha'}(\rho) \quad (3.1.1)$$

with $\alpha, \alpha' = 1$ and 2, and M_α , $V_{\alpha\alpha'}$, independent of ρ . In a moment expansion of the integral eq. (2.2.2) one obtains [9]

$$\frac{\hbar^2}{2M_\alpha} = \frac{V_\alpha(\rho) I_{\alpha\alpha}^{(0)}(\rho) - H_{\alpha\alpha}^{(0)}(\rho)}{I_{\alpha\alpha}^{(0)}(\rho)},$$

$$V_\alpha(\rho) = \frac{H_{\alpha\alpha}^{(0)}(\rho)}{I_{\alpha\alpha}^{(0)}(\rho)}, \quad V_{\alpha\alpha'} = \frac{H_{\alpha\alpha'}^{(0)}(\rho)}{I_{\alpha\alpha'}^{(0)}(\rho)} \quad (3.1.2)$$

where $H_{\alpha\alpha'}^{(n)}$ and $I_{\alpha\alpha'}^{(n)}$ are the n -th moments in $\rho - \rho'$ of the energy and norm overlap of eq. (2.2.2). Inserting the ansatz

$$\phi_\alpha(\rho) = \psi_\alpha(\rho) \exp\{-i \int_{\rho_0}^{\rho} \kappa(\xi) d\xi\} \quad (3.1.3)$$

with $\kappa(\rho) \equiv \sqrt{\frac{1}{2} [K_1^2(\rho) + K_2^2(\rho)]}$ and $\hbar^2 K_\alpha^2(\rho) = 2M_\alpha (E - V_\alpha(\rho))$, eliminating $\psi_2(\rho)$, we obtain a fourth order differential equation for $\psi_1(\rho)$ which reduces to

$$\frac{d^2}{dx^2} \psi_1(x) + [|G|^2 + x^2 + i] \psi_1(x) = 0 \quad (3.1.4)$$

$$\text{with } |G|^2 = \frac{2|V_{12}|^2}{\hbar^2 \kappa(\rho_0) |\gamma|}, \quad x = \sqrt{\frac{M_1 M_2 \gamma}{2\hbar^2 \kappa(\rho_0)}} (\rho - \rho_0)$$

and $\gamma = \frac{K_1^2(\rho) - K_2^2(\rho)}{2(\rho - \rho_0)} \frac{\hbar^2}{M_1 M_2}$ for sufficiently large energies, i.e.

$|\kappa| \gg q$ and $\hbar^2 q \kappa^2 \gg M_1 M_2 \gamma$ where q denotes a characteristic wave number of $\psi_1(x)$. The same eq. (3.1.4) has been obtained in the

time-dependent quasi-classical description [2,17] . If for $x \rightarrow -\infty$ we have an incoming wave with $|\psi_1|^2 = 1$ in the adiabatic state 1 and nothing in the adiabatic state 2, the result for $x \rightarrow \infty$ is

$$|\psi_1(x \rightarrow \infty)|^2 = \exp(-\pi|G|^2) \quad (3.1.5)$$

$$|\psi_2(x \rightarrow \infty)|^2 = 1 - \exp(-\pi|G|^2)$$

i.e., the probability that the system remains in the same adiabatic state is $\exp(-\pi|G|^2)$.

For $|G|^2 \ll 1$ the system does not feel anything from the second adiabatic state and completely stays in the initial one. In the opposite case, $|G|^2 \gg 1$, the system is, after the crossing, completely in the other state. If this is true it is useful for the following discussion to redefine the adiabatic states by diagonalizing the interaction V_{12} in the old adiabatic states which then transform into new adiabatic states with adiabatic energies indicated in Fig. 3 by thick lines. Note that these new adiabatic states are usually referred to as 'the' adiabatic states. Table I gives some information about the coupling of different kinds of states.

TABLE I. CHARACTERISTIC VALUES FOR THE CROSSING OF DIFFERENT ADIABATIC STATES

Crossing of	$ V_{12} $ (MeV)	γ (MeV/fm)	$ G ^2$	$\exp(-\pi G ^2)$
collective (p,h) states	1	1	1/2	0.2
non-collective (p,h) states	0.1	4	0.001	1.0

The variable ρ is taken to be the distance between the centres of two interacting fragments. Taking $M_1 = M_2 = M$ to be the reduced mass of the interacting fragments, we have calculated for $E-V(\rho) = 4$ MeV the coupling constants $|G|$ for collective and non-collective particle-hole states. According to the values given in the table, we expect in general strong coupling between collective states only and a considerably weaker coupling between collective and non-collective states. The coupling between non-collective states is negligibly small.

In the light of this discussion it is reasonable to introduce the following hierarchy of adiabatic states. Let us denote with K a collective excitation for a given deformation ρ . This collective excitation may consist of several individual collective vibrations. With n we want to denote a non-collective excitation which in general also consists of several individual non-collective excitations. Then an adiabatic state $\alpha \equiv (n, K)$ consists of a collective and a non-collective excitation. Now we can define a hierarchy with respect to a specific adiabatic state $\alpha_0 \equiv (n_0, K_0)$: To the first hierarchy belong all adiabatic states (n_0, K) which differ in the collective excitation k only. The rest of the states then belong to the second hierarchy. Because of the axial symmetry of the fissioning system and the smallness of the Coriolis coupling, the component Λ of the total angular momentum along the symmetry axis is a rather good quantum number and practically conserved during the descent from saddle to scission [18]. Therefore, adiabatic states with different Λ are treated as states of different non-collective excitations.

In this instructive picture of hierarchies we can qualitatively discuss the fission process between saddle and scission. Suppose that the compound system starts at the saddle point in a definite adiabatic state $\alpha_0 \equiv (n_0, K_0)$. During the descent towards the scission point, the system strongly couples to all other collective states. Let us call all these strongly coupled states with the same non-collective excitation n a fission band, because they play with respect to fission a role similar to the states in a rotational band with respect to electromagnetic perturbation (radiation, Coulomb excitation). Because of the strong coupling between the adiabatic states of a fission band,

the motion in the fission direction is strongly damped. A considerably weaker coupling is expected between different fission bands $n \neq n_0$. But it is not clear if this coupling can be neglected completely. At the scission point we expect the compound system to be in an excited state which mainly consists of collective excitations built on the non-collective excitation n_0 . We are now at the stage where we can discuss various fission models which have been introduced in the literature.

3.2. Static scission point models

As stated above the compound system is expected to be in highly excited states when reaching the scission point. These highly excited states can be understood as collective and non-collective states built on the ground state. Certain properties of these highly excited states can be expected, at least in the mean over such states, to be the same as for the adiabatic ground state. This is probably the reason why static calculations for the scission point configuration have been successfully applied for describing certain fission phenomena. Static scission-point calculations have been frequently performed within the framework of the liquid-drop model [19] . Shell-model calculations have been performed in the Nilsson model without [20] and with [21] Strutinsky renormalization of the total binding energies. Taking also the nuclear interaction between the fragments into account, charge distributions [22] and moments of inertia [23] have been calculated for ^{236}U . For ^{240}Pu and ^{242}Pu level schemes, equilibrium deformations of the fragments, total energies and charge distributions have been studied [24] . The results have supported the existence of a barrier at scission [25] .

3.3. Statistical model of Fong

If one assumes strong coupling between all adiabatic states, i.e. strong coupling also between different fission bands, during the descent from saddle to scission, it is reasonable [26] that all states available for a given energy are populated with equal probability. By this assumption all fission phenomena are determined by the level densities of the fragments at the scission point. We know today that a complete statistical equilibrium is

in contradiction to the observed angular anisotropy of fission fragments in low-energy fission [18] . Such statistical considerations are probably useful for very high excitation energies only.

3.4. Adiabatic model

This model is obtained if one restricts the basis $|\alpha\rho\rangle$ to the lowest (adiabatic) state as a function of one or a set ρ of collective variables. In such an approach one completely neglects the coupling to non-collective and collective degrees which are not taken explicitly into account. For a review see e.g. Nix [27] A successful study on spontaneous fission half-lives has been performed by Ledergerber and Pauli [28] within such an adiabatic model. Obviously, excitation of collective states are strongly suppressed in a tunneling process. Therefore it is in fact reasonable to calculate fission half-lives without taking the coupling to additional collective degrees into account. This is no longer justified for the motion at positive energies where, as discussed above, the coupling to collective states is expected to be strong.

3.5. Diabatic model of Kelson and Griffin

In contrast to the adiabatic model, Kelson [29] and Griffin [30] assume that the compound system moves not on the lowest adiabatic potential surface but rather on potential surfaces corresponding to specific shell-model or HF configurations. According to our discussion on the coupling between non-collective particle-hole or quasi-particle excitations it is reasonable to assume that the system stays in the same state also when crossing with other states occur. Kelson and Griffin go a step further by taking the (diabatic) shell-model or the HF configurations as the adiabatic states $|\alpha\rho\rangle$, thereby neglecting completely effects from pairing. The system is then assumed to stick to a definite adiabatic or rather diabatic state. These diabatic states are illustrated in Fig. 1 by dashed lines. In a sense these diabatic states play the same role as the non-collective excitations n in our discussion of hierarchies of adiabatic states α . There are the additional collective degrees which in Griffins model correspond to the collective variables ρ in the potential surface. Thus in

this diabatic model of Griffin a hierarchy of the degrees of freedom has been incorporated which is somewhat analogous to the hierarchy of adiabatic states introduced above. The collective degrees are allowed to be strongly coupled within a multidimensional collective model whereas no coupling is assumed between the diabatic states. The only difference to our hierarchy is the fact that we assume the (adiabatic) ground state to be a collective state (at least with pairing correlations) whereas Griffin assumes the ground state to be dissolved into its non-collective components, the lowest diabatic states.

3.6. Thermodynamic or semi-equilibrium model

According to the discussion about the hierarchies of adiabatic states, we expect strong coupling within a fission band. In a fission reaction one gets into the interesting region between saddle and scission point via a certain state $\alpha_0 \equiv (n_0, K_0)$. The thermodynamic or semi-equilibrium model [9,31] is defined by assuming

- (i) that the coupling within the fission band n_0 is so strong as to achieve at scission a statistical equilibrium among all members of the fission band
- (ii) that the coupling to other fission bands $n \neq n_0$ is negligible.

The number of collective degrees of freedom is expected to be about 10 to 15. Even though this number is rather small, the population probability of a given state ν in a certain degree of freedom f is very well approximated by the Boltzmann factor

$$P_{fv}^{(n)} \propto \exp \{-\beta_{\text{coll}}^{(n)} \epsilon_{fv}^{(n)}\} \quad (3.6.1)$$

where $\epsilon_{fv}^{(n)}$ is the energy of the level ν and $K_B \beta_{\text{coll}}^{(n)} = 1/T_{\text{coll}}^{(n)}$, with K_B the Boltzmann constant, is the inverse collective temperature characterizing the statistical equilibrium in the fission band n . The applicability of eq. (3.6.1) is demonstrated in Fig. 4 for only four oscillators of equal energy. In the case of $f = 10$ the differences become smaller than 5%.

The Boltzmann factor (3.6.1) immediately allows one to calculate e.g., the element distribution in fission. We prefer to consider

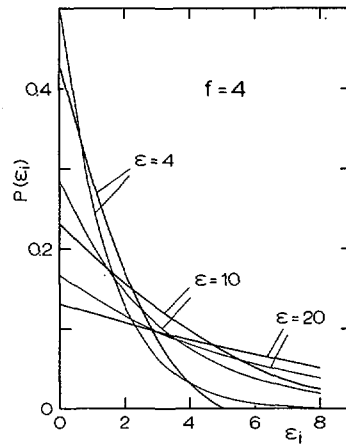


FIG. 4. Comparison between exact population probability $P(\epsilon_i)$ (thick curves) and the Boltzmann factor (thin curves) for a model of four equal oscillators of energy $\hbar\omega$ for different total energies $E = \epsilon\hbar\omega$.

the element distribution $P(Z_1, Z_2)$ instead of the mass distribution $P(A_1, A_2)$ because the fragment charges are already rather good quantum numbers at scission [24] . Thus, the element distribution in fission is given by

$$P^{(n)}(Z_1, Z_2) \propto \exp\{-\beta_{\text{coll}}^{(n)} \epsilon_{Z_1 Z_2}^{(n)}\} \quad (3.6.2)$$

for the fission band n , where $\epsilon_{Z_1 Z_2}^{(n)}$ is the adiabatic energy $V_n(\rho(\text{scission}); Z_1, Z_2)$ at the scission point. For a scission barrier one has to take a mean value of the valley and the barrier energy [24] . For fission near threshold, only the ground-state fission band is excited. Therefore, the element distribution is completely determined by the adiabatic ground-state energies at scission as a function of the fragment sizes, measured by Z_1 and Z_2 . A fit [24] to the experimental distribution for ^{240}Pu gives $K_B T_{\text{coll}} = 2.3 \text{ MeV}$ which is consistent with fits of the energy dependence of symmetric to asymmetric fission yields [9, 31] .

Let us illustrate the temperature dependence, e.g., for the spin distribution of fission fragments. This spin distribution has

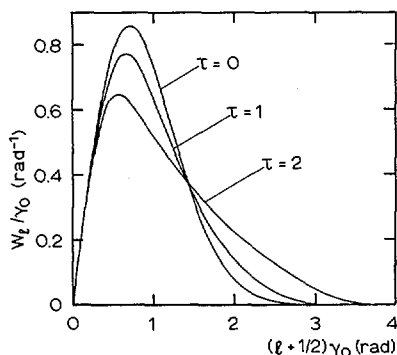


FIG. 5. Spin distribution of a deformed fragment for different values of the temperature $\tau = K_B T_{\text{coll}} / \hbar \omega_b$. Typical values are $\hbar \omega_b = 1.5$ MeV, $\gamma_0 = 0.145$ (from Ref. [32]).

been calculated for $T_{\text{coll}} = 0$ in ref. [32]. The temperature-dependent spin distribution is given by

$$P^{(0)}(l) \propto \sum_v a_v(l) \exp \{-\beta_{\text{coll}}^{(0)} \epsilon_{bv}^{(0)}\} \quad (3.6.3)$$

where, according to ref. [32], $a_v(l)$ denotes the spin distribution for a given bending-mode state v and $\epsilon_{bv}^{(0)}$ is the corresponding energy. The resulting distribution is shown for three different temperatures in Fig. 5. Further studies within the framework of this thermodynamic or semi-equilibrium model are in progress [33].

3.7. Friction in the adiabatic model

It is well known [34] how to introduce an imaginary potential in the Schrödinger equation for a scattering state within the elastic channel. But since in fission we are not only interested in the elastic channel but in properties of all adiabatic states excited in the fission process, we need more than the reduction of flux in the elastic channel.

In classical mechanics one treats the coupling to other degrees of freedom by a friction term which is proportional to the

velocity of the particle under consideration. In a straightforward way, one could think of introducing into the Schrödinger equation an analogous friction term proportional to the momentum of the collective motion. As in the optical model, it is no problem that the Hamiltonian is no longer time-reversal invariant. But this procedure is dangerous because of the following reason: As is obvious from the coupled set of differential eqs. (2.2.3), the friction term should effectively take into account the excitation of different adiabatic states. But in this case it is in general no longer possible to describe the system by a single wave function only. Therefore it is in general self-contradictory to introduce such a friction term in the Schrödinger equation. Doing so one implies that the system is at any given ρ in a single adiabatic state only. This can be true if and only if there is one specific (diabatic) state through which the system runs, as assumed by Griffin. But if this is so, it is advantageous to think about this diabatic state from the beginning instead of starting from the adiabatic model.

4. CONCLUSION

It has been demonstrated that the description introduced in this paper is useful to interpret fission models on a unified basis showing the limitations and advantages of the various concepts. Up to now we cannot distinguish between these models because we did not succeed in obtaining, from the existing fission experiments, sufficient information about the fission mechanism between the saddle and the scission point. We hope that additional and maybe more clear information about this problem can be obtained from the near-future heavy-ion experiments. It is expected that the unified description and the given concept of hierarchies of adiabatic states will be a useful tool for the understanding of these heavy-ion experiments and in turn of the fission process.

R E F E R E N C E S

- [1] HAHN, O., STRASSMANN, F., Naturwiss. 27 (1939) 11 and 89.
- [2] HILL, D.L., WHEELER, J.A., Phys. Rev. 89 (1953) 1102.
- [3] BRENIG, W., HAAG, R., Fortschr. Physik 7 (1959) 183.

- [4] GOLDBERGER, M.L., WATSON, K.M., Collision Theory, Wiley, New York (1964).
- [5] LEMMER, R.H., Rep. Progr. Phys. 29 (1966) 131.
- [6] FANO, U., Phys. Rev. 124 (1961) 1866.
- [7] WEIDENMÜLLER, H.A., Nucl. Phys. 75 (1966) 189;
MAHAUX, C., WEIDENMÜLLER, H.A., Shell Model Approach to Nuclear Reactions, North-Holland, Amsterdam (1969).
- [8] GRIFFIN, J.J., WHEELER, J.A., Phys. Rev. 108 (1957) 185.
- [9] NÖRENBERG, W., Habilitationsschrift, Universität Heidelberg (1970), unpublished.
- [10] NÖRENBERG, W., Z. Physik 260 (1973) 165.
- [11] STRUTINSKY, V.M. Nucl. Phys. A95 (1967) 420 and A 122 (1968) 1.
- [12] BRACK, M., DAMGAARD, J., PAULI, H.C., STENHOLM-JENSEN, A., STRUTINSKY, V.M., WONG, C.Y., Rev. Mod. Phys. 44 (1972) 320; PAULI, H.C., Phys. Reports 7C (1973) 35.
- [13] ANDERSON, B.L., DICKMANN, F., DIETRICH, K., Nucl. Phys. A159 (1970) 337.
- [14] SCHARNWEBER, D., GREINER, W., MOSEL, U., Nucl. Phys. A164 (1971) 257.
- [15] BOLSTERLI, M., FISET, E.O., NIX, J.R., NORTON, J.L., Phys. Rev. C5 (1972) 1050.
- [16] LYNN, J.E., in Physics and Chemistry of Fission, IAEA, Vienna (1969) p. 249 and AERE - R 5891 Harwell (1968);
WEIGMANN, H., Z. Physik 214 (1968) 7.
- [17] LANDAU, L., Sov. Phys. 2 (1932) 46; ZENER, C., Proc. Roy. Soc. (London), A137 (1932) 696;
STUECKELBERG, E.C.G., Helv. Phys. Acta 5 (1932) 370.
- [18] BOHR, A., Int. Conf. peaceful Uses atom. Energy (Proc. Conf. Geneva, 1955) 2, UN, New York (1956) 151;
BJØRNHOLM, S., STRUTINSKY, V.M., Nucl. Phys. A136 (1969) 1.
- [19] VANDENBOSCH, R., Nucl. Phys. 46 (1963) 129; FERGUSON, J.M., READ, P.A., Phys. Rev. 150 (1966) 1018;
SCHMITT, H.W., Arkiv Fysik 36 (1967) 633; TERRELL, J., in Physics and Chemistry of Fission, IAEA, Vienna (1965)

- vol. II, p. 3; ARMBRUSTER, P., Nucl. Phys. A140 (1970) 385;
 RASMUSSEN, J.A., NÖRENBERG, W., MANG, H.J., Nucl. Phys. A136
 (1969) 465.
- [20] IGNATYUK, A.V., Yadern. Fiz. 7 (1968) 1043; transl. Sov. J. Nucl.
 Phys. 7 (1968) 626.
- [21] DICKMANN, F., DIETRICH, K., Nucl. Phys. A129 (1969) 241.
- [22] NÖRENBERG, W., Phys. Lett. 19 (1965) 589 and Z. Physik
197 (1966) 246.
- [23] RÖSCH, N., Z. Physik 215 (1968) 368.
- [24] NÖRENBERG, W., Phys. Rev. C5 (1972) 2020.
- [25] NÖRENBERG, W., Phys. Lett. 31B (1970) 621.
- [26] FONG, P., Phys. Rev. 89 (1953) 332, 102 (1956) 434,
122 (1961) 1542, 1543, 135 B (1964) 1338.
- [27] NIX, J.R., Los Alamos preprint, LA-DC-72-769 (1972).
- [28] LEDERGERBER, T., PAULI, H.C., Nucl. Phys. 207 (1973) 1.
- [29] KELSON, I., Phys. Rev. Lett. 20 (1968) 867.
- [30] GRIFFIN, J.J., in Physics and Chemistry of Fission, IAEA,
 Vienna (1969), p. 3; Nucl. Phys. A170 (1971) 395.
- [31] NÖRENBERG, W., in Physics and Chemistry of Fission, IAEA,
 Vienna (1969), p. 51.
- [32] RASMUSSEN, J.O., NÖRENBERG, W., MANG, H.J., Nucl. Phys. A136
 (1969) 465.
- [33] NÖRENBERG, W., Abstract IAEA-SM-174/23, these Proceedings, Vol.2.
- [34] FESHBACH, H., Ann. Phys. (N.Y.) 5 (1958) 357 and 19 (1962) 287

DISCUSSION

H.J. KRAPPE: If you assume statistical equilibrium between the collective degrees of freedom all the way down from saddle to scission, I wonder what the characteristic time of the collective degrees of freedom has to be compared to the time scale of the fission motion. What is the relaxation time of the collective degrees of freedom, which you would derive from your coupling strength?

W. NÖRENBERG: In the semi-equilibrium model we do not assume that a statistical equilibrium is obtained all the way down to the scission point. The assumption is that, due to the strong coupling between saddle

and scission, the members of a fission band are populated with equal probability. The relaxation time was not very well defined in the level crossing diagram discussed here, but on the basis of this diagram I expect the effective relaxation time for the coupling of collective states to be of the order of 10^{-22} sec.

M.G. MUSTAFA: In your calculations, what is the exact excitation energy of a compound fissioning nucleus (^{236}U or any other actinides) at the point where the mass distribution shifts from asymmetry to complete symmetry?

W. NÖRENBERG: According to Refs [9, 31] of the paper, the ratio ξ of symmetric to asymmetric fission yield is given by

$$\xi(E^*) \propto \exp \{ \kappa E^* / (2\Delta) \}$$

where E^* is the excitation energy above the barrier and Δ the pairing gap. The constant κ turns out to be ≈ 0.44 . If e.g. $\xi(0) \approx 10^{-3}$, then $\xi = 1$ is obtained for $E^* \approx 50$ to 60 MeV.

THE ASYMMETRIC TWO-CENTRE SHELL MODEL AND MASS DISTRIBUTIONS IN FISSION*

J. MARUHN, W. GREINER,
Institut für Theoretische Physik
der Universität Frankfurt,
Frankfurt am Main

P. LICHTNER, D. DRECHSEL
Institut für Kernphysik, Mainz,
Federal Republic of Germany

Abstract

THE ASYMMETRIC TWO-CENTRE SHELL MODEL AND MASS DISTRIBUTIONS IN FISSION.

The two-centre shell model is introduced which can describe nuclear shapes occurring during the fission process. The parametrization allows quadrupole as well as mass-asymmetric distortions of the fissioning nucleus. Potential energy surfaces are calculated by the macroscopic-microscopic method according to Strutinsky. The parameters are then regarded as dynamical collective coordinates and the model is used for generating mass parameters in the cranking model approximation. The Schrödinger equation for movement in the mass-asymmetric degree of freedom is solved numerically for the zero-point vibrations, which are then interpreted as the main component determining the fragment mass yield in spontaneous fission. Calculated mass distributions are compared to experiment.

Semi-empirical shell model calculations employing the shell correction method have been quite successful in explaining the preference of nuclei in the actinide region for asymmetric fission and are even able to reproduce the experimental values of the most favourable heavy-to-light fragment ratios [1,2].

These ratios were determined either from the location of the asymmetrically deformed minima in the potential energy surface without any dynamical considerations, or by a minimization of the WKB penetration probability.

However, both of these methods neglect the fact that there are dynamical fluctuations around these preferred mass asymmetries which contribute to the spread of the final mass yield curve around the peak. There will be collective vibrations of the type illustrated in fig. 1 which correspond to oscillations

* Work supported by the Bundesministerium für Forschung und Technologie and by the Gesellschaft für Schwerionenforschung (GSI).

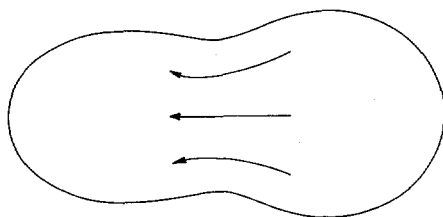


FIG.1. Type of mass flow which gives rise to mass asymmetry fluctuations in a fissioning nucleus, described by the collective coordinate ξ .

in the mass asymmetry. We introduce a collective coordinate ξ to describe this kind of motion by the definition

$$\xi = (A_1 - A_2) / (A_1 + A_2) \quad (1)$$

where A_1 and A_2 are the masses of the two nascent fragments. Evidently it is not possible to define A_1 and A_2 unambiguously as long as the fragments are connected and parts of the mass located near the neck could be assigned to either fragment. However, as the size of the neck decreases, this ambiguity becomes smaller until all definitions of A_1 and A_2 converge at the scission point, where A_1 and A_2 are completely determined. The meaning of ξ as a coordinate describing collective motion is lost after the scission point, since the masses of the fragments cannot change anymore once they have left the nuclear interaction range. This problem is unimportant for nuclear fission where one is interested in the pre-scission behaviour only, but for describing heavy-ion reactions with a ξ -like coordinate it may become advantageous to extend the definition of ξ to that region by introducing a singular mass parameter.

The behaviour of the ξ -vibrations during the fission process may be understood in the following way: Near the ground state deformation ξ describes an octupole vibration around a symmetric shape with admixtures from all the higher odd multipoles. As the nucleus goes along the fission path and through the second barrier, however, asymmetric deformation will begin according to refs. [1-3] and the vibrational wave function $\psi(\xi)$ will have its maximum at a non-zero value of ξ . For fission

well below threshold this will occur during tunneling so that motion in the fission degree of freedom is extremely slow compared to the ξ -vibrations and the adiabatic approximation will be valid. After that, the nucleus goes down the Coulomb slope very rapidly, but as calculations of Mustafa et al.[3] show that there is very little interaction between the ξ -vibrations and the fission mode, the adiabatic approximation will continue to hold for some time. Only when the neck between the fragments decreases rapidly, motion in ξ will be inhibited and, finally, frozen at the scission point. So we may expect the probability for a certain mass division ξ to be correlated to the amplitude $|\psi_R(\xi)|^2$ of the ξ -vibrational wave function at some point R on the fission path located in a region of weak dependence of $\psi_R(\xi)$ on R near the scission point.

For the practical calculations, an asymmetric two-centre shell model as described in ref. [4] was used. It allows for five free parameters explained as follows:

λ : overall length of the nucleus in units of the diameter of the corresponding spherical nucleus. λ is used as the coordinate R describing the fission path.

β_1, β_2 : β -deformations of the fragments.

ϵ : determines the neck size.

ξ : as defined in eq. 1 with A_1 and A_2 determined from the fragment volumes.

The variables ϵ, β_1 , and β_2 were not treated as independent coordinates, but rather as functions of λ and ξ obtained by searching for minimal total energy for fixed values of λ and ξ . It turned out that the behaviour of the fragments with respect to β -deformations is decisive for obtaining asymmetric minima in the potential energy surface. So the coupling of ξ - and β -vibrations will certainly have to be investigated in a more complete treatment.

Restriction to the two coordinates λ and ξ yields the following classical Hamiltonian:

$$H = \frac{1}{2} B_{\lambda\lambda} \dot{\lambda}^2 + B_{\lambda\xi} \dot{\lambda} \dot{\xi} + \frac{1}{2} B_{\xi\xi} \dot{\xi}^2 + V(\lambda, \xi) \quad (2)$$

where $V(\lambda, \xi)$ is the potential energy calculated according to the Strutinsky prescription and the mass parameters $B_{x_i x_j}$ are given by the cranking formula

$$B_{x_i x_j} = 2\hbar^2 \sum_k \frac{\langle 0 | \partial / \partial x_i | k \rangle \langle k | \partial / \partial x_j | 0 \rangle}{E_k - E_0} \quad (3)$$

with pairing included in the BCS-treatment. x_i and x_j correspond to either λ or ξ . The Hamiltonian of eq. 2 can be quantized in a straightforward manner [5-6] and the corresponding Schrödinger equation could be solved at least in principle, yielding a wave function that describes the evolution of asymmetry during the fission process.

Practically, however, even with the simplifications already made, this still is very complicated numerically, since the mass parameters and the potential have to be calculated numerically and at a large number of points in the (λ, ξ) -plane. So to get a first glance at the results one may expect with the model, we assumed extreme adiabaticity, i.e. that the wave function in ξ is confined to the relatively lowest state for each value of λ . This ground state can be obtained from the Schrödinger equation

$$\left[-\frac{\hbar^2}{2\sqrt{B}} \frac{\partial}{\partial \xi} \frac{1}{\sqrt{B}} \frac{\partial}{\partial \xi} + V(\lambda, \xi) \right] \psi_\lambda(\xi) = E_\lambda \psi_\lambda(\xi) \quad (4)$$

where $B = B_{\xi\xi}$ and λ enters only as a parameter. The coupling mass $B_{\lambda\xi}$ could be neglected since $B_{\lambda\xi}^2 \ll B_{\lambda\lambda} B_{\xi\xi}$ was found to hold. This assumption should be true at least for sub-threshold fission, where little excitation in collective degrees of freedom is expected until tunneling has been completed. The descent down the Coulomb slope may of course excite some higher states in ξ , but this has to be neglected here. Calculations by Geilikman et al. [7], however, seem to support the validity of this approximation. Calculations were carried out for the systems ^{236}U and ^{226}Ra .

For ^{236}U two values of λ were chosen, viz. $\lambda=1.65$ and $\lambda=1.8$. The shapes yielding lowest energy for these fixed values of λ are shown in fig.2.

For $\lambda=1.65$ the system is close to the point where tunneling is completed (less than 0.5 MeV difference in energy to the

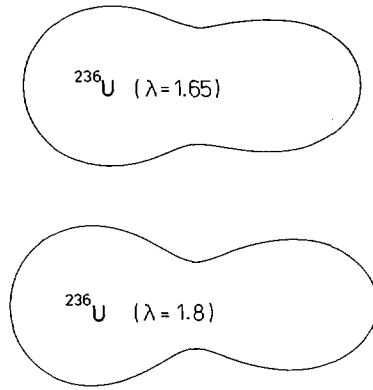


FIG. 2. Shapes corresponding to minimum energies of a ^{236}U nucleus at elongations of $\lambda = 1.65$ and 1.8 .

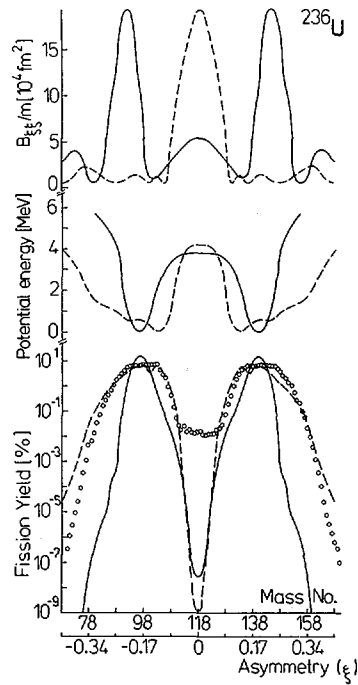


FIG. 3. Potential energy, mass parameter $B_{\xi\xi}$, and amplitude of the collective wave function as a function of ξ for ^{236}U at an elongation of $\lambda = 1.65$ and $\lambda = 1.8$. The wave function has been plotted in such a normalization that it can be compared directly to the experimental mass yield indicated by circles. Dashed lines correspond to $\lambda = 1.65$ and full lines to $\lambda = 1.8$.

ground state). The potential and mass parameters are exhibited in fig.3. To facilitate comparison with experimental mass distributions, the wave function was multiplied by a normalizing factor to convert it into a yield per mass number in percent $Y(A_1)$ calculated as the probability for the mass number of one of the fragments to be inside an interval of length one around a specified number A_1 :

$$Y(A_1) = |\psi_\lambda(\xi = \xi(A_1))|^2 \cdot 2/(A_1 + A_2) \cdot |B(\lambda, \xi)|^{1/2} \quad (5)$$

The wave function itself was obtained from a finite difference method for solving the Schrödinger equation (4). The factor $B^{1/2}$ appears because of the different volume element in ξ -space arising through quantization (see e.g. ref. [8]). It was found that the wave function itself does not depend on the detailed behaviour of the mass parameter and only the yield shows some wiggles caused exclusively by the volume element. The wiggles are not physical anyway, since the mass parameter was calculated only for values of ξ lying 0.05 units apart, so that the smooth curve drawn is the result of interpolation. Thus, only the overall behaviour of the theoretical mass yield and not its fine structure should be considered when comparing with experiment.

Comparing the results for $\lambda = 1.65$ with those for $\lambda = 1.8$, it is seen that the potential becomes steeper around the minima and causes the wave function to become more concentrated at the peaks. The experimental data, taken from ref. [9], are somewhere in between and apparently even this simple calculation is able to give an order-of-magnitude estimate for the spread. It should be kept in mind, however, that experiment is for neutron-induced fission, whereas the theory at its present stage describes only spontaneous fission.

It is not very difficult to generalize the theory to small excitation energies. The higher states of the ξ -oscillator can be calculated and occupied according to a temperature distribution. Evidently this will make the peak broader and fill in the middle of the distribution, as the higher states have a broader spread in ξ -space. Such calculations are being done at present.

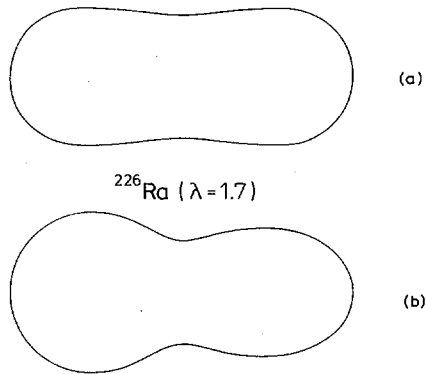


FIG. 4. Shapes corresponding to the two ξ -values of minimum energy for ^{226}Ra at $\lambda = 1.7$. (a) corresponds to the symmetric minimum and (b) to the asymmetric.

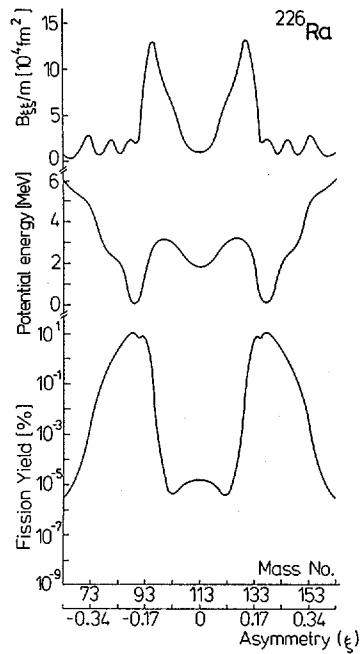


FIG. 5. Same as Fig. 3 for ^{226}Ra at $\lambda = 1.7$. Experimental results are not plotted and only one value of λ was used.

The nuclides in the Radium region provide an interesting test for any theory of asymmetric fission because of their triple-peaked mass yield. We have calculated a wave function for $\lambda = 1.7$ and find three minima in the potential. The results are shown in figs. 4 and 5, showing the shapes at the symmetric and asymmetric minima and, as for Uranium, the potential, mass parameter and wave function. The nuclide treated is ^{226}Ra .

Even for ground state fission a third peak is obtained near symmetric mass division. It can be expected that this peak will become more prominent for higher excitation energies, the region where experimental mass yields have been measured. We have not included experimental data, since they are obtained at too-large excitation energies.

Drawing a conclusion from these results, it may be said that the model is able to explain experimental mass yields in their gross behaviour but not yet in better quantitative agreement. On the other hand, there is not a single fit parameter in the calculations and there are some crucial improvements that can be made to overcome the crudest approximations. One of these is the inclusion of the higher states of the ξ -oscillator to describe induced fission.

The next generalization could consist in the next-order adiabatic approximation including motion in λ of the form

$$\phi(\lambda, \xi) = \sum_{\nu} a_{\nu}(\lambda) \cdot \psi_{\nu}(\xi) \quad (6)$$

with λ treated as a time-dependent parameter. Such calculations should give some knowledge about the development of asymmetry during the fission process.

We cannot expect to describe any details of the mass yield until the coupling to the β -vibrations in the fragments has been investigated. But even without that, it would be sufficient to describe the gross behavior of the mass yield for a larger number of nuclides and the results for uranium certainly seem to encourage us.

REFERENCES

- [1] MÖLLER, P., Nucl. Phys. A192 (1972) 529.
- [2] PAULI, H.C., LEDERGERBER, T., BRACK, M., Phys. Lett. 34B (1971) 265.
- [3] MUSTAFA, M.G., MOSEL, U., SCHMITT, H.W., Phys. Rev. C7 (1973) 1519.
- [4] MARUHN, J., GREINER, W., Z. Phys. 251 (1972) 431.
- [5] PAULI, W., in Handbuch der Physik, 24 Springer, Berlin (1933) 120.

- [6] PODOLSKY, B., Phys. Rev. 32 (1928) 812.
- [7] GEILIKMAN, B. T., ZIMINA, O. V., Yad. Fiz. 15 (1972) 457.
- [8] EISENBERG, J., GREINER, W., Nuclear Models, Ch. 6, North Holland, Amsterdam (1971).
- [9] WEINBERG, A. M., WIGNER, E., The Physical Theory of Neutron Chain Reactors, University of Chicago Press, Chicago (1959).

DISCUSSION

H. J. KRAPPE: Does the cranking formula yield an infinite mass parameter for the asymmetry degree of freedom at the scission point?

J. MARUHN: The problem of how the asymmetry mass parameter behaves near the scission point is being investigated with a view to possible application in heavy-ion calculations. Problems occurring in that respect are: (a) the coordinate ξ should become discrete when mass flow between the fragments is interrupted; and (b) the adiabatic assumption breaks down, since even for very close distances between the fragments the mass exchange is extremely slow owing to the need for the nucleons to tunnel through the separating potential barrier. Both these arguments make it improbable that the simple cranking formula will produce the desired result at and beyond the scission point without more serious modifications. The problem of infinite mass, however, is more of mathematical interest, since physically it is simply caused by the fact that ξ is no longer a meaningful collective coordinate in this region.

H. J. KRAPPE: All applications of the cranking formula to tunnelling processes are connected with a fundamental problem. The cranking model yields classical equations of motion for the collective variables considered as classical observables. In order to treat the tunnelling process, one has to quantize these equations of motion. The assumption that this can be done by the usual canonical quantization prescription is by no means trivial, especially in the multidimensional case. This ambiguity was the reason for the whole discussion after Pauli's paper¹ on the applicability of the least-action trajectory and whether the potential energy to be used in the Schrödinger equation for the collective motion should be different from that derived from constrained Hartree-Fock calculations. I think this problem ought to be investigated in simple models in order to clarify the principles involved.

Z. FRAENKEL: Have you tried to reproduce the mass distribution of ²⁰⁹Bi or any other nucleus lighter than ²²⁶Ra?

J. MARUHN: Not yet, but we are considering using such a system for future calculations.

D. C. HOFFMAN: Have you performed these calculations for the fermium isotopes where the trend from asymmetric to symmetric fission has been experimentally established for spontaneous fission?

J. MARUHN: No, we have not done this yet either, but we are quite confident because calculations by Mustafa, Mosel and Schmitt, who use a very similar shell model, have shown such a trend in the potential energy surfaces for the fermium isotopes. According to our experience the potential is the main factor determining the mass yield, while the mass parameter causes only small deviations, so that the effect should not disappear when a full dynamic treatment is performed.

¹ PAULI, H. C., LEDERGERBER, T., Paper IAEA-SM-174/206, these Proceedings, Vol. 1.

S. BJØRNHOLM: How do you choose the value of λ at which you evaluate the mass distributions?

J. MARUHN: λ is chosen so that the nucleus is in the region where its kinetic energy is positive and, on the other hand, it has not accelerated too much, that is to say, in the region just behind the point where tunnelling terminates. Obviously this is not completely adequate and we hope to do coupled-channel calculations following the evolution of mass asymmetry all the way down from the barrier to scission.

CHAIRMEN OF SESSIONS

Session I	J. R. HUIZENGA	United States of America
Session II	J. J. GRIFFIN	United States of America
Session III	S. BJØRNHOLM	Denmark
Session IV	Z. FRAENKEL	Israel
Session V	H. J. SPECHT	Federal Republic of Germany

SECRETARIAT

Scientific Secretary	S. L. WHETSTONE	Division of Research and Laboratories, IAEA
Administrative Secretary	C. DE MOL VAN OTTERLOO	Division of External Relations, IAEA
Editor	F. MAUTNER MARKHOF	Division of Publications, IAEA
Records Officer	P. B. SMITH	Division of Languages, IAEA

HOW TO ORDER IAEA PUBLICATIONS

Exclusive sales agents for IAEA publications, to whom all orders and inquiries should be addressed, have been appointed in the following countries:

UNITED KINGDOM	Her Majesty's Stationery Office, P.O. Box 569, London SE1 9NH
UNITED STATES OF AMERICA	UNIPUB, Inc., P.O. Box 433, New York, N.Y. 10016

In the following countries IAEA publications may be purchased from the sales agents or booksellers listed or through your major local booksellers. Payment can be made in local currency or with UNESCO coupons.

ARGENTINA	Comisión Nacional de Energía Atómica, Avenida del Libertador 8250, Buenos Aires
AUSTRALIA	Hunter Publications, 58 A Gipps Street, Collingwood, Victoria 3066
BELGIUM	Office International de Librairie, 30, avenue Marnix, B-1050 Brussels
CANADA	Information Canada, 171 Slater Street, Ottawa, Ont. K 1 A 0S 9
C.S.S.R.	S.N.T.L., Spálená 51, CS-11000 Prague
FRANCE	Alfa, Publishers, Hurbanovo námestie 6, CS-80000 Bratislava
	Office International de Documentation et Librairie, 48, rue Gay-Lussac, F-75005 Paris
HUNGARY	Kultura, Hungarian Trading Company for Books and Newspapers, P.O. Box 149, H-1011 Budapest 62
INDIA	Oxford Book and Stationery Comp., 17, Park Street, Calcutta 16
ISRAEL	Heiliger and Co., 3, Nathan Strauss Str., Jerusalem
ITALY	Libreria Scientifica, Dott. de Biasio Lucio "aeiou", Via Meravigli 16, I-20123 Milan
JAPAN	Maruzen Company, Ltd., P.O.Box 5050, 100-31 Tokyo International
NETHERLANDS	Marinus Nijhoff N.V., Lange Voorhout 9-11, P.O. Box 269, The Hague
PAKISTAN	Mirza Book Agency, 65, The Mall, P.O.Box 729, Lahore-3
POLAND	Ars Polona, Centrala Handlu Zagranicznego, Krakowskie Przedmiescie 7, Warsaw
ROMANIA	Cartimex, 3-5 13 Decembrie Street, P.O.Box 134-135, Bucarest
SOUTH AFRICA	Van Schaik's Bookstore, P.O.Box 724, Pretoria
	Universitas Books (Pty) Ltd., P.O.Box 1557, Pretoria
SPAIN	Nautrónica, S.A., Pérez Ayuso 16, Madrid-2
SWEDEN	C.E. Kritzes Kungl. Hovbokhandel, Fredsgatan 2, S-10307 Stockholm
U.S.S.R.	Mezhdunarodnaya Kniga, Smolenskaya-Sennaya 32-34, Moscow G-200
YUGOSLAVIA	Jugoslovenska Knjiga, Terazije 27, YU-11000 Belgrade

Orders from countries where sales agents have not yet been appointed and requests for information should be addressed directly to:



Publishing Section,
International Atomic Energy Agency,
Kärntner Ring 11, P.O.Box 590, A-1011 Vienna, Austria

INTERNATIONAL
ATOMIC ENERGY AGENCY
VIENNA, 1974

PRICE: US \$26.00

Austrian Schillings 510,-
(£11.60; F.Fr. 130,-; DM 70,-)

SUBJECT GROUP: III

Physics/
Nuclear Physics, Reactor Physics, Fission